Analysing the function and dysfunction of TLDc proteins in neurological disorders

Eboni Mae Valentine Bucknor



Doctor of Philosophy: Michaelmas Term 2022

Neurological Disorders

MRC Harwell Institute

St Catherine's College

Department of Physiology, Anatomy and Genetics

University of Oxford

Supervisors: Associate Professor Peter Oliver

Dr Silvia Corrochano

Associate Professor Simon Butt



Analysing the function and dysfunction of TLDc proteins in neurological disorders

Eboni M.V. Bucknor, St Catherine's College, University of Oxford

Submitted for the degree of Doctor of Philosophy, Michaelmas Term, 2022

Abstract

Neurological disorders affect 1 in 6 individuals and are responsible for approximately 17% of deaths worldwide, demonstrating a significant burden on global public health care. Oxidative stress, neuroinflammation and neurodegeneration are common pathological features observed across neurological disorders, including amyotrophic lateral sclerosis (ALS) and epilepsy; yet, how these pathways contribute to cellular dysfunction and selective neuronal vulnerability remains unclear. Determining critical modulators in these pathways will help identify novel therapeutic targets for effective broad-spectrum treatment of neurological disorders.

The TLDc domain-containing protein oxidation resistance 1 (OXR1) has been suggested to play a protective role in the neuronal cell response to oxidative stress. Recently, homozygous loss-of-function disease mutations in *OXR1* have been described, causing childhood ataxia, cerebellar degeneration and seizures. Interestingly, *Oxr1* knockout (KO) mice also present with cerebellar neurodegeneration, ataxia and early postnatal death; yet, the rapid onset of symptoms means that the significance of *Oxr1* loss-of-function outside of the cerebellum warrants further investigation. The aim of this thesis was to characterise the role of Oxr1 in the adult mouse brain and elucidate the molecular mechanisms that may underlie the observed neuropathology in *Oxr1* KO mice.

Transcriptomics of presymptomatic *Oxr1* KO cerebellum revealed that upregulation of neuroinflammatory and lysosomal genes precedes cell death in KO mice. Similar to that of *OXR1*-deficient patient cells, an increase in lysosomal number, alongside enhanced autophagic flux, is also observed in primary cells derived from KO mice. These data suggest

that *Oxr1* plays a fundamental role in modulating neuroinflammation and the autophagy-lysosomal pathway. Next, to sustain essential developmental expression of *Oxr1* and study potentially later-onset phenotypes in the adult mouse, a tamoxifen-inducible ubiquitous *Oxr1* KO model was generated, disrupting all isoforms of the gene. This established that a robust global knockdown of *Oxr1* in the adult mouse leads to a surprisingly severe motor and neurological phenotype, with histopathological analysis revealing significant neuroinflammation, as well as localised cell death in the cerebellum and olfactory bulb. These data demonstrate a critical role for *Oxr1* in the adult mouse brain.

Finally, it has been established that transgenic overexpression of *Oxr1* is protective in cellular and mouse models of ALS, yet the molecular mechanism underlying these protective properties is unclear. Additionally, whether the neuroinflammatory response observed in *Oxr1* KO mouse models is driven by the cell-intrinsic defects in neuronal cells lacking *Oxr1* was unknown. Interestingly, crossing the *Oxr1* constitutive KO line with neuron-specific *Oxr1* overexpressing transgenic mice was sufficient to restore wild-type gene expression profiles of neuroinflammatory and lysosomal markers, and rescued the severe KO phenotype. This suggests that cell-autonomous neuronal dysfunction instigates neuroinflammation in this mouse model. Subsequently, a proteomics approach was adopted in order to determine putative Oxr1 transgene interacting partners that may confer the observed neuroprotective properties in a "gain-of-function" manner. This identified 29 candidate proteins with critical functions in the CNS. Overall, this thesis has shed light on the importance of *Oxr1* in neuroinflammatory and autophagy-lysosomal processes, including an essential, non-developmental role for the gene.

Declaration

I, Eboni M. V. Bucknor (E.M.V.B), hereby declare that all work presented in thesis is my own, unless otherwise stated, and was funded by MRC/UKRI. To the best of my knowledge, this thesis contains no material previously published by any other person except where due acknowledgement has been made. Significant contributions are outlined here in brief. Dr Daniel Rial (Oliver Group, MRC Harwell) carried out multielectrode array (MEA) recordings. Associate Professor Peter Oliver kindly prepared samples for transmission electron microscopy (TEM); subsequently, Dr Erinn Johnson performed TEM (Dunn's School of Pathology, University of Oxford). All other contributions to data acquisition are stated clearly in methods, appropriate figure legends and/or corresponding body of text.

Acknowledgements

Words can hardly express the overwhelming feeling of gratitude I have for those that have played an invaluable role during my D.Phil – it has not been an easy journey. First and foremost, I would like to thank my supervisor, Associate Professor Peter Oliver, for his guidance and immense support throughout my scientific development. His mentorship and patience have allowed to me to grow as an individual and build resilience in the face of adversity. I would also like to thank my co-supervisors, Dr Silvia Corrochano and Associate Professor Simon Butt, for their pastoral care and guidance.

I would also like to thank the members of the Oliver group over the course of my D.Phil journey: Dr Silvia Corrochano, Dr Enrico Castroflorio, Dr Daniel Rial, Dr Tania Soares, Anna Parsons and Dominic Simpson. I am truly appreciative of Silvia and Enrico allowing me to shadow them and improve on my molecular and cellular techniques in the lab. Thank you, Daniel, for all your help with the electrophysiology data and discussions surrounding my phenotyping data. Dear Tania, thank you for your kindness and incredible help in the lab, but also for being an amazing friend. Your input and advice in the latter stages of my studies really helped give me the last bit of motivation and momentum over the finish line. I am immensely grateful for all of the Mary Lyon Centre staff involved in looking after my difficult mouse lines over the course of my project. Ward 6 members, especially Simon Gillard, Liz Joynson, Eddie Chambers and Simona Oliveri, have always been on hand to provide guidance and assistance, to which I am extremely thankful for.

Needless to say, the MRC Harwell student community over the years has undoubtedly kept me going through a number of difficult hurdles that we have faced. I am grateful for the support, light-hearted lunch breaks, shared protocols and reagents! In particular, the 'Neuro Bay Baes' have seen it all – the laughter, tears, naps and celebrations. A special mention goes to my esteemed colleague and best friend, Zai – I could not have done this without you! Thank you for always being there for me on the rainy days, but also to celebrate the fun times. I would also like to give a special thanks to Rainn and Dom for your continued support and inspiration in and outside of the lab.

My role as Junior Dean at St Catherine's College has been an incredibly valuable experience in providing student support and helping to reduce stigma surrounding mental health conversations within the university. Thank you to Richard and Heidi for being incredible mentors and providing a support system during this role. I have had the pleasure of working with an incredible team of Junior Deans during my time at St Catz – a huge shout

out goes to the dream team: Alessandro, Isavella, Pierfrancesco and Pierre, who are not only fantastic colleagues, but also amazing and caring friends. A special mention also goes to Leigh, Ian and Julien for always making me laugh, dance and knowing how to put a smile on my face. Thank you to the Catz MCR friends and wider community for embracing me and for all the fun memories we have made!

I am forever grateful to Linacre College and the community that was fostered there. I spent my formative D.Phil years as a Linacrite and will forever be one in my heart. Linacre provided me with a home away from home, as well as friendships that will last a life time. My partner in wine, crime and all things fine in life – Gerardo – you have been my rock throughout this journey. DJ Ash-win – for always having the best tunes and cracking (bad) jokes. To my dear friends Mala, Ruta, Emma and so many other cherished people that have contributed to my incredible Oxford experience.

To my St Clement's Gang/Hursty People – Thomas, Alice, Bailey, Karel, Katie, Katelyn – the most incredible housemates during my time in Oxford. Our time together, house parties and dinners are unmatched and I look forward to more of our adventures! My angels from the North, Hollie and Mimi, have been some of my biggest enthusiasts during my time in Oxford. They have provided some of the best times and lasting memories with our antics as a troublesome trio. I am so glad that chance brought us together in the Linacre Common Room and that we have fostered a lifetime bond. In the words of the Spice Girls, 'Friendship never ends'. Georgia, Caitlin and Alina - I cannot thank you enough for your patience, encouragement, hype and for always believing in me: SWAG (Smart Women Achieving Greatness). I also cannot express enough appreciation for my Edinburgh BioBae, lab and dance partner, Sarah.



I wouldn't have made it this far without the love and backing from my family who mean the absolute world to me. My dear younger siblings, Onyx, Kole, Nero, Caeus, Caethan and Jaya; I hope I have shown you that the world is your oyster and that you deserve the best in life. I am proud of you all and hope you continue to reach for the stars! Finally, this thesis is dedicated to my parents, Helen and Shaun, and my grandparents, Nana & Grandad Bucknor, Nana Teresa and, in particular, Grandad Geoff, who sadly passed away in January 2022. Their endless support and encouragement to reach my goals is the reason I have made it to this monumental milestone. I hope I will continue to make you all proud. They truly are my biggest supporters in life – thank you!

Table of Contents

Abstract **2**

Declaration **4**

Acknowledgements **5**

Table of Contents **7**

List of Figures **11**

List of Tables **15**

List of Abbreviations **16**

Chapter 1 : Introduction **21**

1.1 Introduction to Neurological Disorders *21*
1.1.1 Current Landscape of Neurological Disorders 21
1.1.2 Epilepsy and Seizure Disorders 23
1.1.3 Ataxia 26
1.1.4 Comorbidities in Neurological Disorders 27

1.2 Examples of disease modulators relevant to neurological function *30*
1.2.1 Oxidative Stress 30
1.2.2 Neuroinflammation 33
1.2.3 Disruption of autophagy-lysosomal pathways in the CNS 38

1.3 Tre2/Bub2/Cdc16 (TBC), lysine motif (LysM), domain catalytic (TLDc) protein family *40*
1.3.1 Oxidation resistance 1 (*Oxr1*) 44
1.3.2 Nuclear receptor coactivator 7 (*Ncoa7*) 55
1.3.3 TBC1 domain family member 24 (*Tbc1d24*) 56
1.3.4 mTOR-associated protein, enhancer-of-akt-1-7 (*mEAK-7)* 58
1.3.5 Chromosome 20 open reading frame 118 (*C20Orf118*) 59

1.4 Summary of the TLDc protein family *60*

1.5 Thesis Aims *61*
1.5.1 Chapter 3 Aims 61
1.5.2 Chapter 4 Aims 62
1.5.3 Chapter 5 Aims 62

Chapter 2 : Materials and Methods **65**

2.1 Mouse Strains and Husbandry *65*
2.1.1 *Oxr1*$^{tm1d/tm1d}$ 66
2.1.2 *Oxr1*$^{tm1c/tm1c}$*/UBC-Cre* 66
2.1.3 *Oxr1*$^{tm1d/tm1d}$*/Oxr1-Prnp* 66

2.2 Animal Procedures and Phenotyping *67*
2.2.1 Tamoxifen Dosing 67
2.2.2 Phenotyping sample sizes for each experimental group 67
2.2.3 Phenotyping – Open Field Activity 67
2.2.4 Phenotyping – Accelerating Rotarod Performance Test 68

2.3 Tissue Collection and Immunohistochemistry *68*
2.3.1 Perfused Tissue 68
2.3.2 Fresh Frozen Tissue 68
2.3.3 Immunohistochemistry 69

2.4 Terminal deoxynucleotidyl transferase dUTP nick end labelling (TUNEL) *70*

2.5 Primary Cell Isolation, Culture and Treatment *71*
2.5.1 Genotyping for primary cell culture 71
2.5.2 Primary Ear Fibroblast Culture 72
2.5.3 Primary Cortical Neuron Culture 72
2.5.4 Primary Cell Treatment 73

2.6 Immunocytochemistry *74*

2.7 Lysotracker Live Cell Imaging *75*

2.8 DQ-Red BSA Trafficking Assay *76*

2.9 Multielectrode Array (MEA) Recordings *77*

2.10 Flow Cytometry *78*

2.11 RNA Extraction, cDNA synthesis and qPCR *78*

2.12 Bulk RNA Sequencing *80*

2.13 Protein Extraction, SDS-PAGE and Western Blotting *82*
2.13.1 Protein Extraction 82
2.13.2 SDS-PAGE and Western Blotting 82

2.14 Immunoprecipitation and Mass Spectrometry *83*

2.15 Transmission Electron Microscopy (TEM) *84*

2.16 Data Analysis and Statistics *84*

Chapter 3 : Investigating the molecular mechanisms of *Oxr1* 86

3.1. Introduction *86*
3.1.1. Constitutive loss of *OXR1* causes early-onset and rapid progressive neurodegeneration in loss-of-function patients and Oxr1 knockout mouse model 86
3.1.2. Molecular pathways underpinning disease pathogenesis in *OXR1*-deficient models are unclear 86
3.1.3. Chapter 3 Aims 90

3.2. Results *91*
3.2.1. Pre-symptomatic RNA-Seq data reveals approximately 200 significantly dysregulated genes in Oxr1 knockout cerebellar tissue 91
3.2.2. Gene Ontology and Pathway analysis predict a role for Oxr1 in modulating neuroinflammation and lysosomal function 96
3.2.3. Loss of *Oxr1* induces disruption of neuroinflammatory processes at both pre-symptomatic and disease stage time points. 100
3.2.4. Lysosomal function and autophagy are perturbed *in vivo* in the absence of Oxr1 expression 103
3.2.5. Accumulation of lysosomes but no difference in autophagic flux is observed in primary fibroblasts derived from P22 *Oxr1* knockout mice 109
3.2.6. Increased autophagic degradative activity is observed in primary cortical neurons lacking expression of *Oxr1* 113
3.2.7. Loss of *Oxr1* leads to increased lysosomal biogenesis and active autophagy in primary cortical neurons. 116
3.2.8. Transmission electron microscopy of *Oxr1* knockout cerebellum reveals aberrant ultrastructural features at an early pathological time point 119
3.2.9. *Oxr1* knockout primary cortical neurons demonstrate no difference in electrical activity 121

3.3. Discussion *128*
3.3.1 LoF-*OXR1* patients and *Oxr1* knockout mice share overlapping pathological features with lysosomal storage disorders 128
3.3.2 Limitations of using bulk RNA-seq on cerebellar tissue from *Oxr1* knockout mice 134
3.3.3 Predicted role for Oxr1 in protein-lipid binding 136

3.3.4 Challenges of characterising electrophysiology phenotypes in constitutive *Oxr1* knockout mice ……138
3.3.5 Oxr1 as a synaptic protein 141
3.3.6 Concluding remarks 144

Chapter 4 : Characterisation of a conditionally-induced adult knockout of *Oxr1* 146

4.1 Introduction 146
4.1.1 *Oxr1* plays a critical role in neurodevelopment..... 146
4.1.2 Use of conditional-ready *Oxr1* allele ($Oxr1^{tm1c/tm1c}$) to study role of Oxr1 in brain regions outside of the cerebellum in mice..... 151
4.1.3 Tamoxifen-Inducible Ubiquitous Cre System *in vivo* 153
4.1.4 Chapter 4 Aims 156

4.2 Results..... 157
4.2.1 Pilot study to establish tamoxifen dosing protocol for knockdown of Oxr1 protein 157
4.2.2 Oxr1 knockdown is robust in Hom/Cre^{+} treated with tamoxifen, generating an adult knockout of Oxr1. … 164
4.2.3 Hom/Cre^{+} mice fail to regain weight effectively following tamoxifen treatment, losing up to 15% of their body weight. 169
4.2.4 Loss of Oxr1 in adult mice leads to impaired short-term habituation and an anxiety-related phenotype in open field 172
4.2.5 Loss of Oxr1 in adult mice leads to motor function deficits 4 weeks post-tamoxifen treatment. ……179
4.2.6 Deletion of Oxr1 in the adult mouse leads to highly localised cell death in the cerebellar granule cells and the glomerular layer of the olfactory bulb 181
4.2.7 Loss of Oxr1 in the adult mouse brain induces a strong neuroinflammatory response..... 185
4.2.8 Loss of *Oxr1* in adult mouse cerebellum leads to increased autophagy 190

4.3 Discussion 192
4.3.1 Characterisation of a ubiquitous adult-induced knockout of *Oxr1* identified an essential role for Oxr1 in the adult mouse 192
4.3.2 Conditional-ready *Oxr1* allele as a tool to study the role of *Oxr1* in brain regions outside of the cerebellum in mice 197
4.3.3 Selective neuronal vulnerability in adult-induced *Oxr1* knockout mice..... 201
4.3.4 Oxr1 protein turnover rate in different brain regions and Cre-mosaicism effect *in vivo* 203
4.3.5 Studying reversible phenotypes *in vivo* 205
4.3.6 Concluding Remarks 208

Chapter 5 : *Oxr1* neuronal over-expression rescue of constitutive *Oxr1* knockout ($Oxr1^{tm1d/tm1d}$/*Prnp-Oxr1)* 210

5.1 Introduction 210
5.1.1. Differential expression of *OXR1* in neurological disorders 210
5.1.2. Overexpression of *Oxr1* is protective against OS-induced apoptosis *in vitro* 211
5.1.3. Exogenous expression of *Oxr1* rescues aberrant cellular pathology induced by ALS-associated mutant proteins *in vitro* ……..212
5.1.4. Tg(*Prnp-Oxr1*) transgenic mice: a model to investigate the neuroprotective function of *Oxr1 in vivo* ……215
5.1.5. Transgenic neuronal expression of *Oxr1* delays disease progression in ALS mouse models 216
5.1.6. Transcriptomic analysis of spinal cord tissue from ALS-mouse model with transgenic neuronal expression of *Oxr1* identified putative functional rescue pathways 218
5.1.7. A role for *Oxr1* in neuronal and non-neuronal cell types? 222
5.1.8. Chapter 5 Aims 224

5.2 Results..... 226
5.2.1. *Prnp-Oxr1* expression is sufficient to protect against neurological phenotypes and early lethality observed in constitutive *Oxr1* knockout mice 226
5.2.2. *Prnp-Oxr1-HA* transgene is localised to neurons and is robustly expressed in the mouse brain..228

5.2.3. Neuron-specific overexpression of *Oxr1* is protective against cerebellar granule cell death in constitutive *Oxr1* knockout mice at P22 ... 231
5.2.4. Neuronal overexpression of *Oxr1* is protective against neuroinflammation in 'rescue' mice ... 233
5.2.5. *Prnp-Oxr1* transgenic expression 'rescues' lysosomal gene expression, yet no significant differences in autophagic turnover were observed in Hom/Tg mice ... 239
5.2.6. Downregulation of *Ctsd* is observed in the cerebellum of Hom/Tg mice at 8 months ... 242
5.2.7. Exploring the potential 'gain of function' mechanism of the Prnp-Oxr1-HA transgene using a proteomics approach ... 245

5.3 Discussion ... 258
5.3.1 Neuron-specific overexpression of Oxr1 is sufficient to protect against ubiquitous loss of the protein at P22 ... 258
5.3.2 Putative Prnp-Oxr1 interaction partners in P22 Hom/Tg cerebellar tissue in the context of other proteomic data – potential functional clues? ... 261
5.3.3 Limitations of proteomics approach ... 263
5.3.4 OXR1 as a future therapeutic target in TDP-43 proteinopathies ... 265
5.3.5 Neuron-specific vs ubiquitous *Oxr1* overexpression: practicalities for therapeutic intervention ... 266
5.3.6 Concluding Remarks ... 268

Chapter 6 : Final Discussion ... 270

6.1 Summary of main findings ... 270

6.2 Oxr1 mouse models: relevance to human patients? ... 271
6.2.1. Patients with bi-allelic loss-of-function mutations in *OXR1* (LoF-*OXR1*) ... 271
6.2.2. Subtle neurological phenotypes are also observed in patients with mutations in *OXR1* ... 276

6.3 TLDc proteins in vivo: modulators of v-ATPase assembly and function ... 279
6.3.1 TLDc proteins interact with v-ATPase subunits *in vivo* ... 279
6.3.2 *Oxr1* and autolysosomal function ... 280

6.4 Role of Oxr1 in neuroinflammation and glial cell types ... 282
6.4.1. *Oxr1* modulates neuroinflammation *in vivo* ... 282
6.4.2. A role for *Oxr1* in glial cells: future work *in vivo* ... 283
6.4.3. A role for *Oxr1* in glial cells: future work *in vitro* ... 286

6.5 TLDc protein redundancy in vivo ... 290

6.6 OXR1 as a therapeutic target ... 294
6.6.1 *OXR1* as a therapeutic target for neurological disorders ... 294
6.6.2 *OXR1* as a therapeutic target in non-neurological disorders ... 296
6.6.3 Gene therapy prospects for LoF-*OXR1* patients: future directions ... 297
6.6.4 Endogenous upregulation of *OXR1* as a possible alternative to gene therapy: future directions ... 299

6.7 Concluding Remarks ... 301

Appendix ... 303

References ... 322

List of Figures

Figure 1.1| Comparative estimated global burden of different neurological disorders on patient quality of life and healthcare systems by measures of DALYs and number of deaths. 22

Figure 1.2| Schematic diagram of TLDc protein isoforms in mice 41

Figure 1.3| Pathogenic mutations in well characterised TLDc proteins cause a range of neurological disorders and clinical features 42

Figure 1.4|Schematic illustration of OXR1 genomic DNA sequence and published pathogenic mutations in OXR1 47

Figure 1.5| Human (Homo Sapiens) OXR1 genomic DNA and validated protein-coding transcripts 53

Figure 1.6| Mouse (Mus Musculus) Oxr1 genomic DNA and validated protein-coding transcripts 54

Figure 2.1| Schematic diagram of original Oxr1 knockout-first (tm1a) gene trap cassette and derived *tm1b*, *tm1c* and *tm1d* alleles 65

Figure 2.2| RNA-seq analysis workflow provided by Cambridge Genomic Services 81

Figure 3.1| Volcano plot of microarray transcriptomic data from wild type and Oxr1 knockout cerebellar tissue at P18 89

Figure 3.2| Volcano plot depicting RNA Sequencing data 93

Figure 3.3| Graphic representation showing a comparison of P18 microarray data and P19 RNA-Sequencing data 95

Figure 3.4| Gene Ontology (GO) Term Analysis of differentially expressed genes in P19 Oxr1 knockout cerebellar tissue 96

Figure 3.5| Reactome and Kyoto Encyclopedia of Genes and Genomes (KEGG) pathway analysis of differentially expressed genes in P19 Oxr1 knockout cerebellar tissue 98

Figure 3.6| Western blot and histopathology to investigate markers of neuroinflammation in Oxr1 knockout tissue 102

Figure 3.7|GOrilla enrichment cellular component analysis of differentially expressed genes in Oxr1 knockout cerebellar tissue at P19 103

Figure 3.8| Western blot analysis of endosomal and autophagy-lysosomal markers in wild type and Oxr1 knockout cortical tissue at P22 105

Figure 3.9| Western blot analysis of different markers of endosomal and autophagy-lysosomal function in wild type and Oxr1 knockout cerebellar tissue taken at P22 107

Figure 3.10| Western blot analysis of Sequestosome 1 (p62) in P22 wild type and Oxr1 knockout forebrain and cerebellar tissue 108

Figure 3.11| Western blotting of autophagic turnover markers in primary fibroblasts 110

Figure 3.12| LysoTracker labelling and quantification of primary fibroblasts 112

Figure 3.13| Western blotting of autophagic turnover markers in 14 DIV primary cortical neurons 114

Figure 3.14| Immunostaining of p62 in primary cortical neurons 115

Figure 3.15 |DQ-Red BSA trafficking assay using wild type and Oxr1 knockout primary cortical neurons... 117

Figure 3.16| Ultrastructure visualisation of P19 cerebellar tissue from wild type and Oxr1 knockout mice. 120

Figure 3.17|Neuronal spike activity characterisation of wild type and Oxr1 knockout primary cortical neurons using Multielectrode Array recordings 123

Figure 3.18|Measuring burst activity of wild type and Oxr1 knockout primary cortical neurons using Multielectrode Array recordings following electrical stimulation 125

Figure 3.19| Multielectrode Array recordings determining synchronised network burst activity of wild type and Oxr1 knockout primary cortical neurons following electrical stimulation 127

Figure 3.20| Overlapping differentially expressed genes in RNA sequencing data from Oxr1 knockout cerebellum exhibiting early signs of pathology and transcriptomics from two mouse models of lysosomal storage disorders ($Npc1^{-/-}$, $Grn^{-/-}$) 129

Figure 3.21| STRING APOE-TREM2 protein-protein interactions..... 138

Figure 4.1| Expression of OXR1 in the human brain and cerebellum at different developmental stages.... 149

Figure 4.2| Expression of Oxr1 in the mouse brain and cerebellum at different developmental stages 150

Figure 4.3| Schematic diagram demonstrating generation of conditional $Oxr1^{tm1c/tm1c}$ allele and targeted exons for deletion, disrupting all isoforms of Oxr1 151

Figure 4.4| Schematic diagram of Cre-mediated disruption of Oxr1 isoforms 152

Figure 4.5| Schematic diagram of targeted gene disruption using the Cre-ERT2 Tamoxifen Inducible System 155

Figure 4.6| Punnett squares depicting expected genotypes from outlined breeding crosses and genotype distribution percentages for pilot cohort to study loss of Oxr1 in adult mice..... 158

Figure 4.7| Breeding of conditional Oxr1 knockout-ready mouse line for pilot study to investigate loss of Oxr1 in adult mice. 159

Figure 4.8| Western blot to detect Oxr1-FL in CNS tissue, 2 and 4 weeks post-tamoxifen treatment in Hom/Cre^{+} and Hom/Cre^{-} dosed mice 160

Figure 4.9| Western blot and quantification of Oxr1-FL in a range of tissues taken from Hom/Cre^{+} and Hom/Cre^{-} mice to verify global knockdown of Oxr1 161

Figure 4.10| Longitudinal study to investigate loss of Oxr1 in the adult mouse..... 164

Figure 4.11| Schematic breeding plan to generate experimental cohorts to investigate the role of Oxr1 in the adult mouse 164

Figure 4.12| Western blot for Oxr1-FL expression in brain and cerebellar tissue, 4 weeks post-tamoxifen treatment..... 166

Figure 4.13| Longitudinal record of bodyweight in adult-induced Oxr1 knockout and representative control mice with percent change in body weight relative to pre-tamoxifen treatment 171

Figure 4.14| Total distance travelled and mean velocity in the whole arena measured pre-tamoxifen, 2 weeks and 4 weeks post-tamoxifen treatment 174

Figure 4.15| Open field centre parameters measured in Hom/Cre^{+} and Hom/Cre^{-} tamoxifen-treated mice 175

Figure 4.16| Distance travelled over 5 minute bins in the whole arena and centre of the arena pre-tamoxifen, 2 weeks and 4 weeks post-tamoxifen treatment 178

Figure 4.17| Accelerated rotarod performance assessing motor function in adult Oxr1 knockout mice across longitudinal study 181

Figure 4.18| TUNEL staining in cerebellum and olfactory bulb of adult Oxr1 knockout and representative control mice 4 weeks post-tamoxifen treatment 184

Figure 4.19| Immunohistochemistry to quantify Iba1-positive cells in sagittal brain sections of adult Oxr1 knockout and representative control mice 188

Figure 4.20|Sagittal brain section immunofluorescence to visualise presence of reactive astrocytes in different brain regions of adult Oxr1 knockout and representative control mice. 189

Figure 4.21| Western blotting of autophagic turnover markers on cerebellar tissue from end-stage adult Oxr1 knockout mice 191

Figure 5.1| Schematic diagram of Prnp-Oxr1 transgenic construct 215

Figure 5.2| Venn diagram depicting overlapping genes 'rescued' in SOD1^{G93A}/Tg compared to differential expressed genes in constitutive Oxr1 knockout mice 219

Figure 5.3| Transcriptome analysis of Oxr1 expression in different cell types of the cortex in both human and mouse brain 222

Figure 5.4| Schematic breeding plan and progeny of Oxr1$^{tm1d/wt}$ crossed with Oxr1$^{tm1d/wt}$/Prnp-Oxr1^{+} mice to generate experimental cohorts 227

Figure 5.5| Representative immunofluorescence to detect neuron-specific expression of Prnp-Oxr1-FL-HA transgene 228

Figure 5.6| Expression analysis of Oxr1 isoforms in brain and cerebellum using qRT-PCR and Western blotting 230

Figure 5.7| Terminal deoxynucleotidyl transferase dUTP nick-end labelling (TUNEL) on sagittal cerebellar sections to label apoptotic cell death in WT, Hom, WT/Tg and 'rescue' Hom/Tg mice at P22 . 232

Figure 5.8| Representative anti-Gfap immunofluorescence images of sagittal brain sections from P22 mice, focussing on the cerebellum 234

Figure 5.9| Representative anti-Gfap immunofluorescence images of the cortex and hippocampus in sagittal brain sections from P22 mice 236

Figure 5.10| Expression levels of inflammatory markers in P22 cerebellar tissue 238

Figure 5.11| Expression analysis of lysosomal enzymes and representative Western blot of autophagic turnover markers in P22 cerebellar tissue 241

Figure 5.12| Expression levels of Oxr1-FL, lysosome and inflammatory markers in cerebellar tissue from Het/Tg and Hom/Tg 'rescue' mice at 8 months. 244

Figure 5.13| anti-HA co-immunoprecipitation Western blots and SDS-polyacrylamide (SDS-PAGE) gel images to show bands excised and processed for mass spectrometry 248

Figure 6.1| Auditory brainstem responses (ABR) and click box of wild type and constitutive Oxr1 knockout mice at P22 277

Figure 6.2| Comparing Oxr1 and Ncoa7 expression in different cell types in human and mouse brain 292

List of Tables

Table 1-1| Table of known OXR1 pathogenic mutations **48**

Table 2-1| Sample size of female Oxr1$^{tm1c/tm1c}$/UBC-Cre mice used in phenotyping pipelines **67**

Table 2-2| Antibodies used for immunohistochemistry **69**

Table 2-3| Oxr1 genotyping primers **71**

Table 2-4| Thermocycler settings for Red Taq polymerase genotyping reactions **71**

Table 2-5| Antibodies used in immunocytochemistry **74**

Table 2-6| Table of qPCR primers used **79**

Table 2-7| Table of Antibodies used for Western Blot **83**

Table 3-1| Top 20 significantly differentially expressed genes ranked by false discovery rate (FDR) (adjusted p-value). **94**

Table 3-2| Reactome and KEGG predicted functional interaction networks and associated differentially expressed genes. **99**

Table 3-3| Table of overlapping differentially expressed genes in Oxr1 knockout mice, Npc1$^{-/-}$ and Grn$^{-/-}$ lysosomal storage disorder mouse models **132**

Table 3-4| Gene ontology functional enrichment analysis of 9 overlapping genes observed between Oxr1 knockout mice, Npc1$^{-/-}$ and Grn$^{-/-}$ lysosomal storage disorder mouse models **133**

Table 4-1| Table of genotypes and dose groups generated for this study and reasons for use **168**

Table 5-1| 21 overlapping genes identified when comparing 48/63 annotated 'rescued' genes (SOD1^{G93A} vs WT, SOD1^{G93A}/Tg vs WT) with differentially expressed genes in constitutive Oxr1 knockout mice. **221**

Table 5-2| List of proteins identified through anti-HA pulldown and mass spectrometry in the cortex and cerebellum of Prnp-Oxr1-HA transgene positive and negative protein lysates **249**

Table 5-3| Putative Prnp-Oxr1-HA protein binding partners only identified in anti-HA pulldown of P22 Hom/Tg cerebellar protein extracts **255**

Table 6-1| Comparing clinical features of loss-of-function *OXR1* patients and *Oxr1* knockout mouse models **273**

List of Abbreviations

8-OHdG	8-hydroxydeoxyguanosine
AD	Alzheimer's disease
ADHD	Attention deficit hyperactive disorder
AI	Anti-inflammatory
ALS	Amyotrophic lateral sclerosis
AO	Antioxidant
APL	Autophagy-lysosomal pathways
APOE	Apolipoprotein E
ASD	Autism Spectrum Disorder
ASDs	Anti-seizure drugs
Baf	Bafilomycin A1
BMI	Body mass index
BP	Biological processes
BZDs	Benzodiazepines
C20ORF118	Chromosome 20 Open Reading Frame 118
CA1	Cornu Ammonis 1
CA3	Cornu Ammonis 3
CC	Cellular component
CGC	Cerebellar granule cells
CGCL	Cerebellar granule cell layer
CMT	Charcot-Marie-Tooth disease
CNS	Central nervous system
CSF	Cerebrospinal fluid
DALYs	Disability adjusted life years
DEGs	Differentially expressed genes
DEXA	Dual-energy X-ray absorption
DIV	Days *in vitro*
DMSO	Dimethyl sulfoxide
DOORS	Deafness, onychodystrophy, osteodystrophy, intellectual disability and seizures
DQ-BSA	Dye quenched-bovine serum albumin
E	Embyronic day

EEG	Electroencephalography
ENU	N-ethyl-N-nitrosourea
ERbd	Estrogen receptor binding domain
ERT2	Tamoxifen-inducible estrogen receptor
FDR	False discovery rate
FITC	Fluorescein isothiocyanate
FTLD/FTD	Frontotemporal Lobe Degeneration/Frontotemporal Dementia
FTX	Frataxin
GABA	γ-Aminobutyric acid
GO	Gene ontology
GPX	Glutathione peroxidase
GRAM	Glycosyltransferases, Rab-like GTPase Activators, Myotubularins
HD	Huntington's disease
Hom	Homozygous knockout
IL	Interleukin
iPSC	Induced pluripotent stem cells
KEGG	Kyoto Encyclopedia of Genes and Genomes
KO	Knockout
LC3	Microtubule-associated protein light chain 3
LDAM	Lipid droplet accumulating microglia
LoF	Loss of function
LSD	Lysosomal storage disorder
LysM	Lysin motif
MEA	Multielectrode array
mEAK-7	MTOR Associated Protein, Eak-7 Homolog
MES	2-(N-morpholino) ethane sulfonic acid
MF	Molecular function
MOPS	3-(N-morpholino) propane sulfonic acid
MPTP	1-methyl-4-phenyl-1,2,3,6-tetrahydropyridine
MRI	Magnetic resonance imaging
Mtd	Mustard
mTOR	Mammalian target of rapamycin
NCL	Neuronal ceroid lipofuscinosis

NCOA7	Nuclear Receptor Coactivator 7
ND	Neurological disorders
NMDA	N-methyl-D-aspartate
NO	Nitric Oxide
NPC1	Niemann-Pick disease, type C1/NPC Intracellular Cholesterol Transporter 1
Nrf2	Nuclear factor-erythroid factor 2-related factor 2
O/N	Overnight
OS	Oxidative stress
OXR1	Oxidation resistance 1
P	Postnatal day
p62/SQSTM1	Sequestosome 1
PD	Parkinson's disease
PPT	Palmitoyl-protein thioesterases
PRMT5	Protein arginine methyltransferase 5
PT	Post-tamoxifen treatment
PTZ	Pentylenetetrazol
Rap	Rapamycin
RNA-Seq	RNA Sequencing
ROS	Reactive oxygen species
SCA	Spinal cerebellar atrophy
SCI	Spinal cord injury
SCN1A	Sodium channel protein type 1 subunit alpha
scRNAseq	single cell RNA sequencing
SE	Status Epilepticus
SLI	specific language impairment
SNHL	sensorineural hearing loss
SOD1	Superoxide dismutase 1
TBC	Tre2/Bub2/Cdc16
TBC1D24	TBC1 domain family member 24
TBI	Traumatic brain injury
TEM	Transmission electron microscopy
TLDc	Tre2/Bub2/Cdc16 (TBC), lysin motif (LysM), domain catalytic
TLE	Temporal lobe epilepsy

TNF-α	Tumour necrosis factor alpha
TREM2	Triggering receptor expressed on myeloid cells 2
TUNEL	Terminal deoxynucleotidyl transferase dUTP nick end labeling
UBC	Human ubiquitin C (UBC) promoter
UN	United Nations
v-ATPase	V-type proton (H+) ATPase
WHO	World Health Organisation
WT	Wild type
XLMTM	X-linked myotubular myopathy

INTRODUCTION

Chapter 1 : Introduction

1.1 Introduction to Neurological Disorders

1.1.1 Current Landscape of Neurological Disorders

'Neurological disorders' (NDs) is an umbrella term for a disorder or disease of the central nervous system (CNS), of which over 600 have been identified (Groft et al., 2017). The World Health Organisation (WHO) determined that NDs affect 1 in 6 people and are responsible for ~17% of global deaths recorded, rendering them a leading cause of death worldwide, second only to cancer (Feigin et al., 2020; GBD Neurology Collaborators., 2019; World Health Organization., 2006), presenting a significant global disease burden and valid case for prioritisation in healthcare and development of therapeutic strategies.

Aging has been shown to significantly increase the risk of developing NDs (Hou et al., 2019). Current United Nations (UN) projections predict the average global life expectancy from birth to be 77 years by 2050, a stark 5.51% increase from current 2022 data, which is only expected to continue to rise with the advancement of modern medicine and development of therapeutic interventions (Macrotrends, 2022). These estimations clearly demonstrate an aging population, placing more individuals at risk of developing NDs and experiencing a reduced quality of life, strengthening the need to search for increased prevention and treatment options to ease the global socioeconomic health care burden (Birbeck et al., 2015; Hou et al., 2019).

Dysfunction of the CNS can lead to multiple clinical outcomes, making NDs a heterogeneous group of conditions (World Health Organization., 2006). Within those diagnosed with a ND, neurodegenerative disorders, such as Parkinson's disease (PD) and Alzheimer's disease (AD) which disproportionately affect the elderly, alongside epilepsy and stroke, are some of the most prevalent worldwide (Beghi, 2020; Landgrave-Gomez et al., 2015; Murphy & Werring, 2020; Salman, 2018; World Health Organization., 2006). A

"Global Burden of Disease Study" demonstrated that stroke and dementia bare the largest burden on healthcare systems in disability-adjusted life-years (DALYs), as well as carrying the highest risk of mortality compared to other NDs (**Figure 1.1**) (Feigin et al., 2020; GBD Neurology Collaborators., 2019). Nevertheless, understanding a spectrum of neurological conditions can aide our understanding of associated risk factors and disease manifestation.

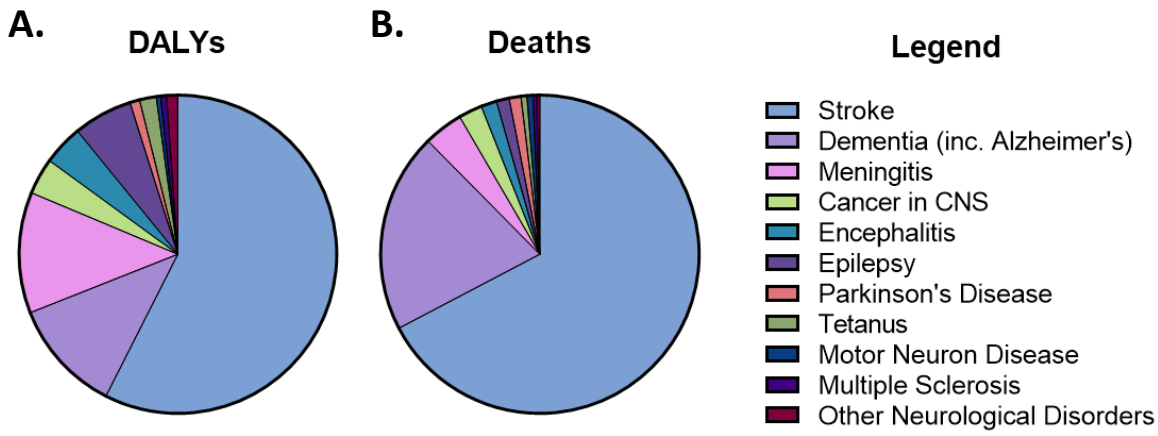

***Figure 1.1*| Comparative estimated global burden of different neurological disorders on patient quality of life and healthcare systems by measures of DALYs and number of deaths.** Pie charts depicting relative proportions of (A) disability-adjusted life-years (DALYs) and (B) deaths in patients affected by prevalent neurological disorders listed in the legend, demonstrating that stroke and dementia carry the most significant disease burden and risk of mortality. Data extracted from (GBD Neurology Collaborators., 2019) and (Feigin et al., 2020; World Health Organization., 2006) (excluding data relating to headaches and migraines).

1.1.2 Epilepsy and Seizure Disorders

Epilepsy is characterised by periods of spontaneous and irregular electrical activity in the brain, known as seizures, which are typically classified as either focal, generalised or of an unknown seizure type (Perucca et al., 2020). Epilepsy affects over 50 million people worldwide (Buckinx et al., 2021; WHO, 2022) and poses significant challenges to an individual's life with increased incidences of premature death, such as Sudden Unexpected Death in Epilepsy (SUDEP) (Maguire et al., 2020; WHO, 2022). In the case of both genetic and acquired epilepsies, there is a significant need to understand varying aetiologies when exploring potential pharmacological and therapeutic targets (Eastman et al., 2020; Terrone et al., 2020). In order to decrease neuronal excitation and inhibit seizure episodes, a number of anti-seizure drugs (ASDs), such as benzodiazepines (BZDs) and Lamotragine, target ion channel activity and neurotransmitter release as their mode of action (Cheung et al., 1992; Kumar et al., 2012; Machado et al., 2011; Rudolph et al., 1999). This is evident in acute treatment of status epilepticus (SE), whereby intravenous administration of Lorazepam (a BZD) produces an anticonvulsant effect (Prasad et al., 2014); the proposed mechanism of action of Lorazepam in the CNS is that it increases the release of inhibitory neurotransmitter γ-Aminobutyric acid (GABA) by binding to postsynaptic ligand-gated chloride channel $GABA_A$ receptors (Rudolph et al., 1999). In turn, this decreases the post-synaptic action potential, therefore reducing neuronal firing and seizure activity in epileptic patients (Greenfield, 2013; Rudolph et al., 1999; Sperk et al., 2004). Despite the effectiveness of approved ASDs, the current incidence of refractory epilepsy prominently lies at up to 40% within the population of seizure disorder patients (Sultana et al., 2021). This demonstrates a need to explore modulators of seizure induction and interictal events as novel therapeutic targets, further aiding our understanding of epileptogenesis (Kirchner et al., 2020; Terrone et al., 2020).

1.1.2.1. Reactive oxygen species and neuroinflammation in epileptogenesis

Reactive oxygen species (ROS) [discussed in **1.2.1**] are potent neurotoxic mediators of epilepsy, particularly in their intricate, mutually reinforcing association with neuroinflammation by simultaneously driving neuronal injury, excitotoxicity and subsequently lowering the seizure threshold (Eastman et al., 2020; Terrone et al., 2020; Vezzani & Granata, 2005). Increased concentrations of 8-hydroxydeoxyguanosine (8-OHdG), a marker of oxidative damage, ROS such as malondialdehyde (MDA) and nitric oxide (NO), alongside increased levels of pro-inflammatory cytokines, e.g. TNF-α, IL-6, and IL-1β, have been identified in biological fluid samples from patients with a range of epileptic disorders, including SE, temporal lobe epilepsy (TLE) and drug-resistant epilepsies (Ethemoglu et al., 2018; Fukuda et al., 2008; Kalita et al., 2019; Vezzani & Granata, 2005; Xia et al., 2018). Collectively, this suggests that chronic inflammation and oxidative stress (OS) in the CNS actively contribute to the persistence of seizure activity and could be effective pathways to target in therapeutic studies.

Compounds with known antioxidant (AO) and anti-inflammatory (AI) properties have been shown to modulate seizure susceptibility in rodent epilepsy models, reducing neurological deficits and biomarkers of seizure activity (Ambrogini et al., 2018; Golechha et al., 2011; Terrone et al., 2020). In a pentylenetetrazol (PTZ)-treated rat model of chronic epilepsy, Kaur *et al.* (2015) demonstrated that supplementation of curcumin, an active compound in turmeric with AO and AI properties, alongside seizure induction resulted in attenuated hippocampal and cortical gliosis, reduced expression of pro-inflammatory cytokines and reduced cognitive deficits compared to PTZ-only treated animals (Kaur et al., 2015), highlighting clinically relevant disease modifications. Increasing curcumin bioavailability is being explored as a therapeutic adjuvant target in combating subsets of epilepsy (Moezi et al., 2021). Ongoing clinical trials involving treating patients with

cannabidiol (CBD), a substance shown to exhibit effective AO and AI properties [reviewed in (Atalay et al., 2019)], reported reduced seizure occurrence compared to placebo control patients in known drug-resistant seizure disorders, such as Lennox-Gastaut and Dravet syndromes (Lattanzi et al., 2019) and Tuberous Sclerosis Complex (Thiele et al., 2021). Overall, the intricate crosstalk between OS and neuroinflammatory response in the CNS make them considerable hallmarks in pathogenesis of epilepsy and further highlights them as prominent therapeutic targets to be investigated in tandem in a range of complex NDs.

1.1.3 Ataxia

Ataxia, a collective term for poor balance, lack of coordination and limited muscle control, is a common clinical feature in conditions such as Spinocerebellar ataxias (SCAs), Friedreich's ataxia (FA) and Wilson's disease (Groft et al., 2017; Salman, 2018). This movement disorder is typically associated with cerebellar damage, but can present with other symptoms such as scoliosis and heart defects (Kemp et al., 2016; Tsirikos & Smith, 2012). Hereditary ataxia is an inherited, monogenic form of the disorder that is caused by deleterious mutations in genes such as calpain-1 (*CAPN1*), interferon related developmental regulator 1 (*IFDR1*), voltage-gated $Ca_V2.1$ (P/Q-type) Ca^{2+} channel α_{1A} subunit (*CACNA1A*) and β-III spectrin (*SPTBN2*) (Lin et al., 2018; Lise et al., 2012; Martinez-Monseny et al., 2021). Alternatively, ataxia can also be acquired as a symptom of other neurological disorders, sporadic mutations or exogenous insults, such as traumatic brain injury (TBI), infection or excessive alcohol intake (Klockgether, 2010; Salman, 2018; Sarva & Shanker, 2014).

The distinct mechanistic aetiology of ataxia and cerebellar damage differs between subtypes of the disorder, making it difficult to produce a generic disease modifying therapy. Intrinsically, this may be due to death of cerebellar cell types, such as Purkinje or cerebellar granule cells (CGCs) (Kemp et al., 2016; Wang et al., 2016). For example, deleterious mutations in *CAPN1* lead to impaired cerebellar development by failed degradation of PH domain and leucine-rich repeat protein phosphatase 1 (PHLPP1), which in turn leads to reduced Akt activity, thus contributing to a pro-apoptotic environment in CGCs (Lafon-Cazal et al., 2002; Wang et al., 2016). Additionally, factors such as perturbed metal homeostasis, OS and impaired autophagy in the cerebellum have also been inextricably linked to selective neuronal vulnerability and disease manifestation in other forms of ataxia (Marcelo et al., 2021; Squadrone et al., 2018; Wang et al., 2016).

Currently, a cure for genetic or sporadic ataxia has not been identified, therefore a combination of speech therapy, physiotherapy and medication is utilised to alleviate symptoms and manage this neurological condition (Sarva & Shanker, 2014). Marcelo *et al.* (2021) demonstrated that administration of cordycepin, a drug compound that mediates the activation of autophagy via the adenosine monophosphate-activated protein kinase (AMPK) pathway (Marcelo et al., 2019), rescues the reported autophagic impairment therefore promoting the degradation of mutant ataxin-2 aggregates (Marcelo et al., 2021). Overall, a reduction in protein aggregation, neuroinflammation and neuronal apoptosis was observed in a cordycepin-treated mouse model of SCA type 2, therefore identifying autophagy as a prospective mechanistic target for treatment of SCA patients (Marcelo et al., 2021). Similarly, pharmacological prospects targeting Purkinje cell function and survival are improving for symptomatic intervention through activation of the Akt signal transduction pathway (Wang et al., 2016).

1.1.4 Comorbidities in Neurological Disorders

Shared genetic aetiology, histopathogenesis, overlapping symptoms and risk factors all contribute to the co-occurrence of a number of different NDs (Chowdhury et al., 2021). Some examples of frequent comorbid neurological conditions include, but are not limited to: epilepsy and neurodevelopmental disorders, such as autism spectrum disorder (ASD) and attention deficit hyperactivity disorder (ADHD) (Bozzi et al., 2012; Brainstorm Consortium. et al., 2018); amyotrophic lateral sclerosis (ALS) and frontotemporal dementia (FTD)(Chowdhury et al., 2021; Neumann et al., 2006); and PD with Gaucher's disease and Lewy body disease (LBD) (Chowdhury et al., 2021; Shachar et al., 2011). The complex, heterogeneous nature of these disorders only increase the prevalence of neurological comorbidities, which has been shown to significantly contribute to greater disability-

adjusted life years (DALYs), health care burden, alongside increased mortality (GBD Neurology Collaborators., 2019).

Monogenic disruptions often present with clinical heterogeneity and comorbidities. In an example of two distinct neurodegenerative conditions, Niemann-Pick disease types and Parkinson's Disease (PD), mutations in lysosomal degradative enzyme sphingomyelin phosphodiesterase 1 (*SMPD1*) present an increased risk factor for the co-occurrence of both disorders, likely caused by disruptions of the lysosomal pathway in the CNS in the absence of functional SMPD1 (Alcalay et al., 2019; Dagan et al., 2015). Pathogenic mutations in *SPMD1* have been found to cause systemic endolysosomal accumulation of sphingomyelin and lipids and progressive neurodegenerative phenotypes in Niemann-Pick Disease patients (Deshpande et al., 2021; Platt, 2014). To investigate *SMPD1* as a genetic risk factor for PD, Alcalay *et al.* (2019) employed RNA interference to knockdown expression and reduce acid sphingomyelinase (ASMase) activity in HeLa cells which resulted in a 3-fold increase of α-synuclein expression and impaired lysosomal trafficking of ASMase. Notably, a more than 8-fold increase in α-synuclein aggregation, a pathogenic hallmark of PD (Alcalay et al., 2019; Mendoza-Velasquez et al., 2019), outlining how amorphic mutations in *SMPD1* may increase PD-like pathology and disease progression. Of note, the exact genotype-phenotype correlation and variable penetrance of *SMPD1* mutations has not been fully established (Alcalay et al., 2019; Zampieri et al., 2016), yet converges the observed disease pathogenesis of Niemann-Pick Disease and PD on to perturbed lysosomal dysfunction.

Interestingly, a spectrum of amorphic mutations in *CACNA1A* have been shown to have aetiological associations with different forms of ataxia, such as episodic and SCA, impaired cognitive function, alongside a predisposition to the development of epilepsy (Gur-Hartman et al., 2021; Martinez-Monseny et al., 2021). *CACNA1A* is expressed at the

presynaptic terminal of both excitatory and inhibitory neurons across the CNS, with robust expression in cerebellar Purkinje neurons, but also across the cerebral cortex (Westenbroek et al., 1995). In mice, conditional deletion of *Cacna1a* in cortical cell types causes a seizure phenotype, notably with the absence of ataxia (Bomben et al., 2016; Rossignol et al., 2013). Yet, delayed Purkinje cell depletion of *Cacna1a* was sufficient to cause both ataxia and seizure onset (Mark et al., 2011), thus highlighting the importance of spatial gene expression and implications in disease pathogenesis and emerging comorbidities.

It must be noted that many NDs exhibit overlapping symptomology as a result of the dysregulation of common pathways, such as oxidative stress, neuroinflammation and autophagy-lysosomal function (Eastman et al., 2020; Kregel & Zhang, 2007; Murphy & Werring, 2020; Zenuni et al., 2021), it is reasonable to hypothesise that identifying novel neuroprotective therapeutic targets ameliorating these disease modulators would advance strategies to prevent neurological disease onset and/or progression.

1.2 Examples of disease modulators relevant to neurological function

1.2.1 Oxidative Stress

Reactive oxygen species (ROS) are oxygen-derived free radicals that exist naturally in cells as a by-product cellular metabolism, including mitochondrial respiration (Cobley et al., 2018; Hajam et al., 2022). Endogenous ROS play a vital role in maintaining the intracellular environment, in conjunction with acting as secondary messengers in signal transduction pathways and as an immune system defence mechanism against pathogenic insults (Cobley et al., 2018; Hajam et al., 2022). Disruption of such pathways can have severe consequences *in vivo*, particularly in the CNS.

The brain is a highly energy expensive organ leading to high production levels of ROS, such as hydrogen peroxide (H_2O_2), superoxide anion radical ($O_2^{\bullet -}$) and hydroxyl free radicals ($HO^{\bullet}$)(Cobley et al., 2018; Wang & Michaelis, 2010); elevated ROS production, exogenous ROS-generating insults and diminished antioxidant capacity can lead to imbalances in ROS homeostasis, subsequently leading to oxidative stress (OS). ROS play an essential role in numerous aspects of neuronal function, including neuronal polarity, synaptic transmission and plasticity (Cobley et al., 2018; Dennery, 2007); however, mature neurons of the CNS are critically vulnerable to OS-induced damage, as their post-mitotic state prevents proliferation and expansion in response to damage (Kole et al., 2013). Downstream effects of OS include disruptions in cellular signalling, leading to lipid peroxidation of membranes, oxidative modification of proteins, DNA damage and ultimately cell death (Kregel & Zhang, 2007).

Biomarkers of OS have been identified at presymptomatic, symptomatic and post-mortem time points in ND patient samples, compared to healthy controls. For example, blood samples from Huntington Disease (HD) patients showed increased concentrations of peroxidised lipids and 8-hydroxy-2'-deoxyguanosine (8-OHdG), an indicator of oxidative

DNA damage (Tang et al., 2020). An OS blood plasma biomarker study conducted by Klepac *et al.* (2007) revealed that HD and asymptomatic HD patients both presented with increased plasma lipid peroxidation and decreased concentrations of Glutathione (GSH), an antioxidant marker, compared to healthy controls. As OS biomarkers are observed in asymptomatic HD patients prior to significant neuronal cell loss, this suggests that early pathological changes can be detected in plasma of at-risk individuals prior to manifestation of clinical symptoms and that OS biomarkers may not just be a secondary effect of increased cell death (Klepac et al., 2007). Further to this, 8-OHdG and other biomarkers of OS have been identified in the serum and cerebral spinal fluid (CSF) in AD, ALS and PD patients, as well as in post-mortem brain tissue (Gmitterova et al., 2009; Hou et al., 2019; Kalita et al., 2019; Tam et al., 2019; Tang et al., 2020; Zenuni et al., 2021). Similarly, in cases of refractory epilepsy, the overall oxidative stress index in blood serum samples was significantly higher than patients with well-controlled epilepsy or healthy controls (Ethemoglu et al., 2018). Overall, this heavily implicates OS in the onset, progression and severity of a range of NDs.

Endogenous antioxidant mechanisms include enzymatic antioxidants, such as superoxide dismutases (SOD) and glutathione peroxidases (GPX) that directly catalyse the reduction of free radicals, whereas non-enzymatic antioxidant molecules, including Glutathione (GSH) and vitamins, scavenge ROS or act as cofactors in the neutralisation of free radicals (Cobley et al., 2018; Wang & Michaelis, 2010). Mutations reducing or abolishing the dismutase activity of superoxide dismutase 1 (SOD1) or inducing mislocalisation have been linked to both familial and sporadic forms of ALS (Berdynski et al., 2022). Other perturbations of ROS homeostasis, such as glutamate toxicity and mitochondrial impairment, all contribute to the onset of OS and pathogenesis of NDs (Cobley et al., 2018).

Overall, the endogenous antioxidant defence capacity of the brain is relatively low given its high metabolic activity and subsequent ROS production, leaving the brain critically vulnerable to OS (Cobley et al., 2018). Activation of nuclear factor erythroid 2–related factor (Nrf2) is currently being explored as a target for pharmacological upregulation to boost antioxidant defence in the CNS which, thus far, has proven to be effective in clinical trials treating Friedrich's Ataxia (Lynch et al., 2019). Brains of Nrf2-deficient mice showed clear vulnerability and oxidative damage in high ROS-producing brain regions, including CA3 region of the hippocampus (Rojo et al., 2017). Transcriptional activation of endogenous antioxidant defence mechanisms are initiated upon binding of Nfr2 to antioxidant response elements (ARE) that are situated in the promoter regions of antioxidant coding genes, such as *SOD1*, *GPX* and *catalase* (Buendia et al., 2016; Kensler et al., 2007). Furthermore, Nrf2-ARE activation has also been shown to act on cytoprotective genes involved in the unfolded protein response (UPR), which could prove beneficial in the clearance of protein aggregates often observed in neurodegenerative conditions (Pajares et al., 2017). As well as OS, Nrf2-ARE has also been shown to be regulated by other important ND modulators, such as neuroinflammation and autophagy (Ichimura et al., 2013; Jain et al., 2010).

Supplementation of naturally biosynthesised antioxidants are being explored as viable treatment options, such as in cases of patients with ataxia, mouse models of epilepsy and a PD rat model, but has been met with a number of limitations, such as not achieving therapeutic concentrations *in vivo* and failed statistical significance in patient symptom improvement at the phase III, randomized, double-blind placebo-controlled clinical trial stage (Golechha et al., 2011; Lynch et al., 2010; Park et al., 2020; Sarva & Shanker, 2014). Further to this, pharmacological mimics of enzymatic antioxidants has been shown to attenuate symptoms and disease progression; this has been observed in a MPTP-mouse

model of PD treated with AEOL11207, a metalloporphyrin with dismutase activity (Liang et al., 2007). These cases exemplify the importance of understanding how to maintain ROS homeostasis in relation to the development and progression of NDs.

1.2.2 Neuroinflammation

Another example of a disease-modifying process is neuroinflammation, an immune response in the CNS proven to be both protective and deleterious in NDs (Geloso et al., 2017; Hewett et al., 2012; Rama Rao & Kielian, 2015; Sofroniew & Vinters, 2010; Terrone et al., 2020). Glial cells are CNS immune cells that are critical in both neurodevelopment and adult brain homeostasis, playing key roles in synaptic formation and pruning, as well as modulating neurotransmission and maintaining the blood brain barrier (Casali & Reed-Geaghan, 2021; Sofroniew & Vinters, 2010; Vainchtein & Molofsky, 2020). Indeed, astrocytes and microglia, two examples of glial cell types, predominantly function to maintain cellular homeostasis and protect against neuronal injury by responding to damage-associated molecular patterns (DAMPs)(Piccinini & Midwood, 2010). Both glial cell types express Toll-like receptors (TLRs) which can recognise DAMPs released by apoptotic cells and transiently induce a proinflammatory signalling cascade through secretion of neurotrophic factors and cytokines, including interleukin-6 (IL-6), IL-1 and IL-1β, and infiltration of other neuroimmune cells (Heidari et al., 2022; Sofroniew & Vinters, 2010). However, chronic activation of these pathways can trigger a reactive state in astrocytes and microglia, contributing to a neurotoxic, self-propagating cycle of neuroinflammation (Liddelow et al., 2017), therefore, it is unsurprising that glial cell activation is a prominent feature in ND patients and rodent models of these disorders.

A consensus statement released by Nature Neuroscience called for a need for the field to redefine how glial cell reactivity is referred to and characterised in ND models to reflect their functional diversity and dynamics at varying stages of immune response and disease progression (Escartin et al., 2021). More recently, a number of studies in humans and mice have employed single-cell RNA-sequencing (scRNA-seq) resulting in identification and characterisation of distinct transcriptomic signatures of putative intermediate and transitional glial profiles beyond the classically defined homeostatic state and proinflammatory and anti-inflammatory-like phenotypes (Gerrits et al., 2021; Habib et al., 2020; Hasel et al., 2021; Liddelow et al., 2017; Mendiola et al., 2020; Pettas et al., 2022). For example, Gerrits *et al.* (2021) identified 13 sub-clusters of microglial transcriptomic profiles when comparing scRNA-seq when comparing grey matter tissue from AD patient and control samples; interestingly, AD-associated microglial transcriptomic clusters could be further categorised dependent on the presence of amyloid-β (Aβ) or tau pathology (Gerrits et al., 2021). Thus, it remains essential to characterise the glial reactivity profiles in NDs and understand the balance between a pro and anti-inflammatory response.

Understanding morphological changes of microglia and astrocytes in disease neuropathology and in response to different stimuli is one angle currently being explored to stratify phenotypic differences in glial cells; with developments of artificial intelligence platforms and machine learning, alongside integration of high-resolution microscopy, this allows for high-throughput, unbiased glial phenotypic profiling as a means for understanding glial morphology dynamics in NDs (Choi et al., 2022; Escartin et al., 2021; Kugler et al., 2023; Leyh et al., 2021). One such example is an open-source, 'multi-dimensional data analysis platform' developed by Kugler *et al.*, referred to as 'GliaMorph' (Kugler et al., 2023). Kugler *et al.* (2023) piloted the platform by investigating Müller glia cell morphology in the zebrafish retina and later found that the image analysis pipeline

could be extended in to additional experimental models, such as in a mouse model of glaucoma. Similarly, five different microglial morphologies (categorised as ramified, amoeboid, rod, activated and hyper-ramified) could be distinguished when applying automated image analysis to investigate microglial activation in the retina of aging mice (Choi et al., 2022). These advances in computational analysis will revolutionise the way in which immunohistochemistry informs us of glial cell phenotype classification, reactivity profiles and how this relates to their differing functions *in vivo.*

In the context of characterising neuroinflammatory pathology through immunohistochemistry (IHC), ionized calcium-binding adapter molecule 1 (Iba1) and glial fibrillary acidic protein (Gfap) are typically used as markers of activated microglia and astrocytes, respectively (Ben Haim et al., 2015; Wendimu & Hooks, 2022). However, in order to distinguish between their protective or pathological states, additional markers are recommended to be employed. For example, Cluster of differentiation 68 (CD68), a microglial lysosomal protein, is widely considered a marker of phagocytic activity and has been shown to be increased in the frontal cortex of AD patients compared to healthy controls in a number of studies (Hopperton et al., 2018). When characterising astrocyte reactivity, Liddelow *et al.* (2017) defined a population of 'neurotoxic' astrocytes with reduced phagocytic capabilities and hypertrophic morphology that were $GFAP^+$/complement component 3 (*C3*)-positive in the prefrontal cortex of post-mortem AD brain tissue; however, 40% of all reactive $GFAP^+$ astrocytes detected were $C3^-$ suggesting a subpopulation of astrocytes that may be functioning in a different capacity to the identified neurotoxic $GFAP^+$ astrocytes (Liddelow et al., 2017). Overall, a multipronged approach to define glial cell profiles will refine how we classify complex neuroinflammatory processes, by integrating parameters such as '-omics' data, IHC and morphology (Escartin et al., 2021).

Physiological levels of inflammatory mediators are essential to CNS development and function (Bourgognon & Cavanagh, 2020). For example, loss of cytokines IL-6 and tumour necrosis factor alpha (TNFα) results in a significant learning and memory impairment in mice (Baune et al., 2008; Braida et al., 2004). Baune *et al.* (2008) hypothesised that physiological levels of TNFα promotes synaptic plasticity. Conversely, chronic astrocytic expression of IL-6 in the cerebrum results in neuroinflammation, seizures, ataxia and neurodegeneration in mice (Campbell et al., 1993). This highlights the importance of mediating cytokine production, as well as the likely role of neuron-glial cross talk in neuroinflammation and neurodegeneration (Bernaus et al., 2020).

As outlined previously, aging is tightly correlated with an increased risk of developing NDs (Hou et al., 2019). Interestingly, overlapping microglial transcriptomic signatures have been identified in post-mortem brain tissue from aged-individuals and those with neurodegenerative conditions such as AD and PD, indicating a reactive primed state in the CNS (Mukherjee et al., 2019). Upregulation of the Triggering Receptor Expressed on Myeloid Cells 2-Apolipoprotein E (*TREM2-APOE*) pathway has been heavily implicated in the transition of homeostatic microglia to a microglial neurodegenerative phenotype, as identified in mouse models of ALS and AD (Krasemann et al., 2017). For example, the more recently coined term, disease associated microglia (DAM) has been used to describe a sub-population of microglia that exhibited enhanced phagocytosis to clear debris such as Aβ plaques, and increased lipid metabolism, suggesting a protective activation phenotype in NDs and aging (Keren-Shaul et al., 2017; Pettas et al., 2022; Sobue et al., 2021). Interestingly, variants of both *APOE* and *TREM2* have been associated with an increased risk of developing a number of NDs, including AD, PD and FTD, a pathway which DAM are suggested to rely on (Atagi et al., 2015; Keren-Shaul et al., 2017; Krasemann et al., 2017), suggesting perturbations of this pathway can cause or accelerate

neurodegeneration. Conversely, the presence of lipid-laden microglia shown by colocalised of $Iba1^{+}$/$BODIPY^{+}$ immunostaining, referred to as lipid droplet accumulation microglia (LDAM), demonstrate impaired phagocytosis and hyperactivation of a proinflammatory response through increased secretion of proinflammatory cytokines, such as TNF-α and IL-1β, therefore are thought to elicit a pathological proinflammatory microglial phenotype (Marschallinger et al., 2020).

Overall, it is important to consider that neuroinflammatory responses in NDs are dynamic and context-dependent. Whilst glial cells hold a critical function in maintaining brain homeostasis, it is clear that dysregulation and shifts in the capability of astrocytes and microglia to adopt protective and pathological cellular phenotypes in response to stimuli may contribute to disease progression. Understanding how neuroinflammatory profiles change through the progression of different NDs will be pertinent to harness aspects of glial cell function and immunomodulation as a therapeutic strategy (Bernaus et al., 2020; Vainchtein & Molofsky, 2020).

1.2.3 Disruption of autophagy-lysosomal pathways in the CNS

A number of processes that are critical to neuronal cells converge on to aspects of lysosomal function and subsequent maintenance of intracellular protein and organelle homeostasis (Bonam et al., 2019; Lie & Nixon, 2019). For example, endolysosomal (Repnik et al., 2013) and autophagy-lysosomal (APL) pathways (Abounit et al., 2012; Lee, 2012; Lie & Nixon, 2019) have been identified as key players in the regulation of neuronal maturation and migration, axonal transport, and synaptic transmission (Bressan et al., 2020; Soukup et al., 2016; Tammineni et al., 2017); dysregulation of these neuronal processes have all been implicated in a range of NDs (Lie & Nixon, 2019).

Disruption of APL pathways has been shown to have detrimental effects in the CNS, particularly in driving neuroinflammation and neurodegeneration (Bonam et al., 2019; Lee, 2012), yet the exact mechanisms linking APL dysfunction, neurodegeneration and other features of NDs are still not entirely understood. Pathogenic mutations in APL-associated proteins, or those that cause disruption to physiological autophagic turnover, have been reported to give rise to an array of NDs, including lysosomal storage disorders (LSDs), Alzheimer's Disease and Parkinson's Disease (PD) (Dagan et al., 2015; Lee, 2012; Lie & Nixon, 2019; Shachar et al., 2011; Siintola et al., 2006; Varvagiannis et al., 2018).

Mutations in lysosomal hydrolytic enzymes have been linked to a number of neurodegenerative disorders. Cathepsins are lysosomal proteases that play a critical degradative role, whereby aberrant function can lead to toxic accumulation of cellular proteins and proteinaceous aggregates that are detrimental to neuronal function and survival (Bonam et al., 2019). This is evident in reports of patients with pathogenic mutations in Cathepsin D (*CTSD*), where aberrant accumulation of granular osmiophilic deposits is observed in CNS cell types, resulting in an LSD known as neuronal ceroid lipofuscinosis (NCL) (Siintola et al., 2006; Steinfeld et al., 2006; Varvagiannis et al., 2018).

Alongside neurodegeneration, patients also present with multisystemic features and comorbidities, including ataxia, seizures and respiratory failure (Siintola et al., 2006; Steinfeld et al., 2006). Niemann-Pick Diseases (NPDs) are LSDs characterised by abnormal cellular accumulation of cholesterol and lipids typically caused by mutations in proteins required for normal trafficking or recycling in APL pathways, for example NPC Intracellular Cholesterol Transporter 1 and 2 (NPC1/NPC2) (Alam et al., 2012; Fancello et al., 2009) and Progranulin (*GRN*) (Evers et al., 2017), as well as mutations in lysosomal lipases, such as *SMPD1* (Dagan et al., 2015).

In addition to previously attributed proteins necessary for APL function, activity of the V-type proton (H^+) ATPase (v-ATPase) is essential for vesicular acidification that provides the correct luminal environment for degradative activity (Mindell, 2012). Compounds that inhibit v-ATPase function, such as bafilomycin and archazolid, directly impair maturation of cathepsins and proteolytic activity in lysosomal compartments (Bowman & Bowman, 2002; Jessop et al., 2017; Kubisch et al., 2014). Missense mutations in highly conserved regions of *ATP6V1A,* a gene encoding the A subunit of the v-ATPase complex, have been shown to disrupt lysosomal homeostasis and impede neuronal development *in vitro*, by means of aberrant lysosomal acidification, thus affecting neurite outgrowth and synaptic connectivity downstream (Fassio et al., 2018). Additionally, loss of v-ATPase assembly chaperone, Vacuolar ATPase Assembly Factor (VMA21) leads to diminished v-ATPase activity and decreased lysosomal acidification; VMA21-deficiency has been linked to myopathies (Cannata Serio et al., 2020; Ramachandran et al., 2013). Taken together, these mutations demonstrate that disruption of the assembly, stability or activity of the multimeric enzymatic v-ATPase complex can have detrimental effects in the CNS, identifying the v-ATPase as a therapeutic target in NDs (Eaton, Merkulova, et al., 2021).

1.3 Tre2/Bub2/Cdc16 (TBC), lysine motif (LysM), domain catalytic (TLDc) protein family

Overall, the described disease modulators of CNS function significantly impact and contribute to the global ND disease burden. Therefore, exploitation of endogenous neuroprotective factors or mechanisms that may ameliorate disease onset or progression by targeting underlying, overlapping pathogenic pathways warrants further attention. Since 2002, the Tre2/Bub2/Cdc16 (TBC), lysine motif (LysM), domain catalytic (TLDc) family has gained traction as candidate neuroprotective proteins that are now starting to be harnessed to modulate neuronal sensitivity to OS (Doerks et al., 2002; Durand et al., 2007; Finelli et al., 2016; Volkert & Crowley, 2020).

Doerks *et al.* (2002) used sequence alignment to identify the TLDc domain, consisting of approximately 220 amino acids, in eukaryotic genomes as diverse as *Arabidopsis thaliana*, *Drosophila melanogaster* and *Homo sapiens* (Doerks et al., 2002). Although 30 different TLDc proteins are predicted to exist across different species, five members were identified in mammals (Doerks et al., 2002; Durand et al., 2007; Finelli et al., 2016). This includes oxidation resistance 1 (Oxr1) and nuclear receptor coactivator 7 (Ncoa7), both which have full-length and short isoforms, TBC1 domain family member 24 (Tbc1d24), mTOR associated protein, eak-7 homologue (mEAK7, previously known as Kiaa1609) and lastly, chromosome 20 open reading frame 118 (C20Orf118), all sharing the highly conserved C-terminal TLDc domain (**Figure 1.2**) (Finelli et al., 2016).

Although expression of all TLDc genes has been detected in the brain, *Oxr1*, *Ncoa7* and *Tbc1d24* are highly expressed in the developing mouse embryo and adult CNS in both neuronal and non-neuronal cell types (**Figure 1.3A**) (Finelli et al., 2016; Schaum et al., 2019). Robust expression of these TLDc genes is observed in the cortex and hippocampus, with notable expression of *Oxr1* in the CA3 hippocampal region, olfactory bulb and cerebellum, discretely in the granule cell layer (GCL) (Finelli et al., 2016). Similarly in the

cerebellum, *Tbc1d24* is also expressed in the GCL, whereas *Ncoa7* expression is confined to Purkinje cells (Castroflorio et al., 2021; Finelli et al., 2016).

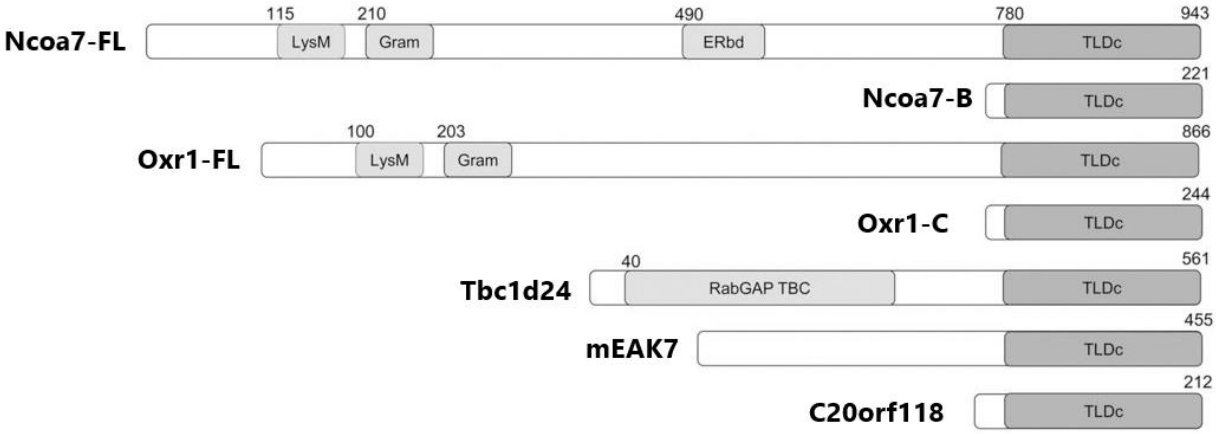

***Figure 1.2*| Schematic diagram of TLDc protein isoforms in mice**

Depiction of main TLDc protein isoforms in the mouse with annotated domains and position indicated by amino acid number. LysM: lysin motif, GRAM: GRAM domain, ERbd: estrogen receptor binding domain, TLDc: Tre2/Bub2/Cdc16 (TBC), lysin motif (LysM), domain catalytic. Diagram taken from (Finelli et al., 2016).

Thus far, a number of studies have identified mutations in TLDc protein family members with a number of overlapping neurological symptoms observed, including developmental delay, ataxia and seizures (**Figure 1.3B**) (Balestrini et al., 2016; Chen et al., 2017; Doan et al., 2019; Lin et al., 2022; Wang et al., 2019). The intersecting clinical features of patients with deleterious mutations in TLDc proteins highlight their critical role in neuronal development and function *in vivo*, therefore warranting further investigation in to their molecular mechanisms and properties.

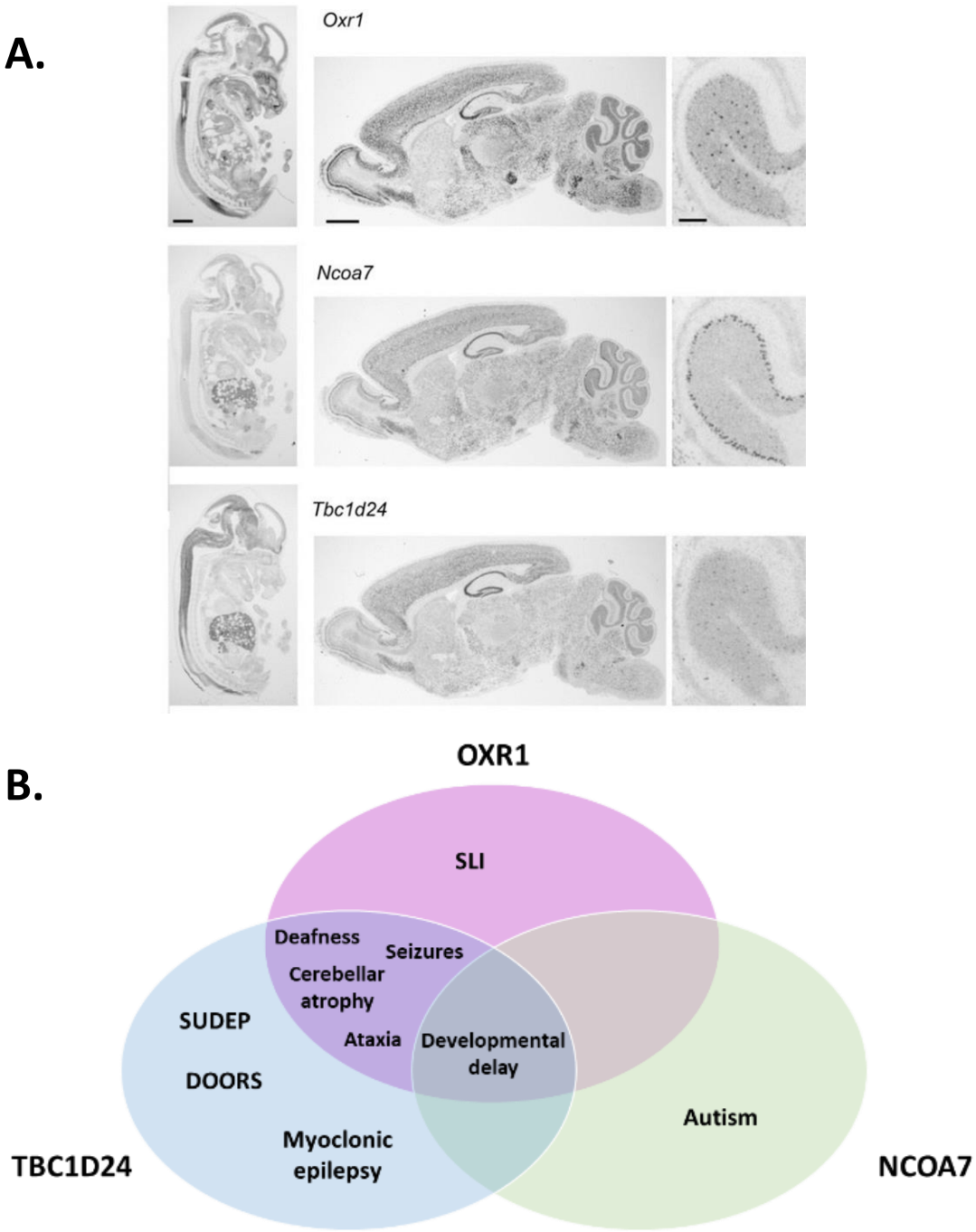

***Figure 1.3*| Pathogenic mutations in well characterised TLDc proteins cause a range of neurological disorders and clinical features**

(**A**) *In situ* hybridisation of *Oxr1, Ncoa7* and *Tbc1d24* expression at three developmental stages in male wild-type mice using riboprobes that detect all isoforms of each of these TLDc domain gene family members. The left panels depict the developing embryo at E14.5 (Scale bar: 1 mm), the middle panels illustrate a sagittal section of the adult brain (Scale bar: 1 mm), with the right panels showing a magnified image of the adult cerebellum (Scale bar: 200 µm). Figure adapted from Finelli *et al.* (2016). (**B**) Venn diagram illustrating overlapping clinical features of known pathological mutations in OXR1, TBC1D24 and NCOA7. SLI: specific language impairment, SUDEP: sudden unexpected death in epilepsy, DOORS: deafness, onychodystrophy, osteodystrophy and intellectual disability. (Balestrini et al., 2016; Chen et al., 2017; Doan et al., 2019; Li et al., 2022; Lin et al., 2022; Mucha et al., 2017; Wang et al., 2019).

Cultured *bel* CGCs showed a significant reduction in sensitivity to H_2O_2 treatment when transfected with *Oxr1-C,* suggesting that the TLDc domain is likely responsible for neuronal protection against OS (Oliver et al., 2011). The functional importance of the TLDc domain *in vivo* has been proven in both Drosophila and mice. Expression of the shortest isoforms of OXR1 and NCOA7, which are predominantly TLDc-domain containing, can rescue the neurological phenotype and lethality observed in Drosophila lacking expression of *mustard* (*mtd*), the fly homolog of *OXR1* (Wang et al., 2019; Wang et al., 2012), further highlighting striking evolutionary conservation of sequence and function. Interestingly, mice with a targeted deletion of the full-length isoform of Oxr1, *Oxr1-FL,* show no signs of ataxia, neurodegeneration or *bel* pathology, confirming that expression of the short *Oxr1-C* isoform alone is sufficient to protect against neuron sensitivity to OS (Oliver et al., 2011).

The crystal structure of the TLDc domain has been resolved from zebrafish (Blaise et al., 2012), Drosophila (Luthy et al., 2019) and, more recently, human recombinant protein (Arnaud-Arnould et al., 2021) and have been used for mapping of pathological human mutations in a bid to establish structure-function relationships (Arnaud-Arnould et al., 2021; Finelli, Aprile, et al., 2019; Luthy et al., 2019). Mapping TBC1D24 epilepsy-causing mutations on to the Drosophila TLDc crystal structure identified amino acids critical to domain integrity and stability (Luthy et al., 2019). Indeed, disruption of structurally conserved amino acids have been linked to a number of NDs. Excitingly, the TLDc domain has been shown to be a direct interactor of other protein complexes and motifs that elicit critical cellular functions (Finelli & Oliver, 2017), such as the (H+)V-ATPase (Eaton, Brown, et al., 2021), therefore mutations that disrupt these interactions are likely to contribute to the pleiotropic nature of TLDc protein-associated NDs (Finelli et al., 2016; Svistunova et al., 2019; Yang et al., 2020).

1.3.1 Oxidation resistance 1 (*Oxr1*)

The role of TLDc proteins in OS response was first revealed in a functional genomic screen using a strain of *Escherichia coli* (*E. coli*) that was susceptible to oxidative DNA damage (Volkert et al., 2000). Subsequent transformation of this DNA-repair deficient *E.coli* strain with an array of human cDNA library clones identified a gene with oxidation protection and anti-mutator properties, known as *Oxr1* (Volkert et al., 2000). Further sequence alignment demonstrated that Oxr1 is highly conserved across eukaryotic organisms (Durand et al., 2007; Finelli et al., 2016; Volkert et al., 2000). Following on from uncovering the role of Oxr1 in OS defence, Oliver *et al.* (2011) characterised the role of Oxr1 in mammalian systems and uncovered its importance to CNS development and function.

1.3.1.1. *Bella:* mouse model of early onset rapid progressive neurodegeneration

The significance of Oxr1 to neuronal cell death was discovered via characterisation of the spontaneous *bella* (*bel*) mouse mutant (Oliver et al., 2011). A large-scale N-ethyl-N-nitrosourea (ENU) mutagenesis screen for neurological phenotypes relevant to human NDs identified the *bel* mutant that displayed progressive ataxia, oxidative DNA damage, apoptotic cell death in the cerebellar GCL and a shortened lifespan (P24 – P26) (Acevedo-Arozena et al., 2008; Oliver et al., 2011). From P18/19, *bel* mice display an unsteady gait and fail to thrive; prior to this time point, *bel* mice are phenotypically indistinguishable from control littermates (Finelli, Paramo, et al., 2019; Oliver et al., 2011). Histopathological analysis of CNS tissue revealed the onset of apoptosis in CGCs with significant selective cerebellar GCL degeneration observed by P22-24, in concordance with increased severity of gait abnormalities and ataxic symptoms observed in *bel* mice (Finelli, Paramo, et al., 2019; Oliver et al., 2011). Molecular analysis identified a 193.5 kb deletion including the entire *Oxr1* locus and adjacent gene, actin binding Rho activating protein (*Abra*) (Oliver et

al., 2011). Ubiquitous transgenic *Oxr1-FL* expression rescued the *bel* mutant, determining *Oxr1* as the causative gene of the observed phenotype (Oliver et al., 2011). Importantly, constitutive knockout of *Oxr1* in an independent mouse model targeting all isoforms (see **1.3.1.5**) recapitulates the *bel* phenotype and histopathology (Finelli et al., 2016; K. X. Liu et al., 2015) confirming that *Oxr1* is essential for neuronal cell response to oxidative stress *in vivo*.

Histopathology and transcriptomics of *bel* mutants revealed upregulation of inflammatory and lysosomal markers in the cerebellum at a presymptomatic time point (P18) (K. X. Liu et al., 2015)(unpublished observations). Further to this, it is evident that *Oxr1* expression levels determine neuronal sensitivity to OS, particularly in CGCs. In the absence of *Oxr1* expression, neurodegeneration is limited to the GCL of the cerebellum suggesting this particular neuronal population is potentially more susceptible to OS (Oliver et al., 2011). *In vitro* studies further demonstrate selective vulnerability of *Oxr1*-deficient CGCs to exogenous OS-inducing treatment, compared to wild type CGCs and primary cortical neurons; conversely, overexpression of *Oxr1* reduced neuronal sensitivity to OS (Oliver et al., 2011). Owing to the rapid onset of symptoms in the *bel* mutant, the function of *Oxr1* in brain regions outside of the cerebellum and in the adult mouse is yet to be determined.

1.3.1.2. Pathogenic variants in *OXR1* cause neurological phenotypes

Recently, whole exome sequencing of patients presenting with neurological symptoms detected a number of disease-causing mutations in *OXR1* resulting in neurological phenotypes (**Figure 1.4**), including early onset clinical manifestation of hypotonia, movement disorders, cerebellar atrophy and seizures (**Table 1-1**) (Lin et al., 2022; Wang et al., 2019). Crucially, bi-allelic loss of function *OXR1* (LoF-*OXR1*) mutations in the TLDc domain result in complete absence of the protein, leading to a human *OXR1*

'knockout' with a number of overlapping symptoms identified in *Oxr1* knockout mice (Lin et al., 2022; Oliver et al., 2011; Wang et al., 2019). As sourced from gnomAD within MARRVEL (Model organism Aggregated Resources for Rare Variant ExpLoration), the expected number of predicted LOF single nucleotide variants (SNVs) in OXR1 was 45.7, whereas the observed number of SNVs was 9 (Wang et al., 2017). Wang *et al.* (2019) reported the LOF observed/expected (o/e) ratio to be 0.20; given that this value is below the confidence interval of o/e ≤ 0.35, this suggests that *OXR1* is intolerant to LOF mutations and that these mutations are rare in the population (Harrison et al., 2019; Wang et al., 2017; Wang et al., 2019).

OXR1 has also been identified as a susceptibility locus for specific language impairment (SLI), a childhood neurodevelopmental disorder (Chen et al., 2017). Exome sequencing of patient cohorts with severe SLI detected a heterozygous nonsense mutation in the unique first exon of *OXR1-D*, a short isoform of OXR1, preceding the TLDc domain (Chen et al., 2017) (**Figure 1.4**). This suggests that haploinsufficiency of shorter *OXR1* isoforms can also lead to a neurological phenotype in humans, alluding to isoform-specific functions.

A number of pathogenic mutations in *TBC1D24* cause both dominant and recessive forms of hearing loss, with and without additional neurological features (Azaiez et al., 2014; Balestrini et al., 2016; Campeau et al., 2014; Mucha et al., 2017). Interestingly, only very recently a 4 year old proband presented with severe sensorineural hearing loss (SNHL) as well as cerebellar arterial abnormalities; next-generation sequencing of the proband and family members with signs of hearing loss determined the causative gene variant to be a missense mutation in a highly evolutionarily conserved amino acid of OXR1 (c.233A>G, p.Lys78Arg); the proband was homozygous for this mutation, whereas unaffected family members were heterozygous carriers (Li et al., 2022).

Overall, these recent data highlight the critical role of *OXR1* in neurological function; the interesting overlap of clinical features of pathogenic mutations in other TLDc proteins suggest that this highly conserved protein family share similar functions within the CNS.

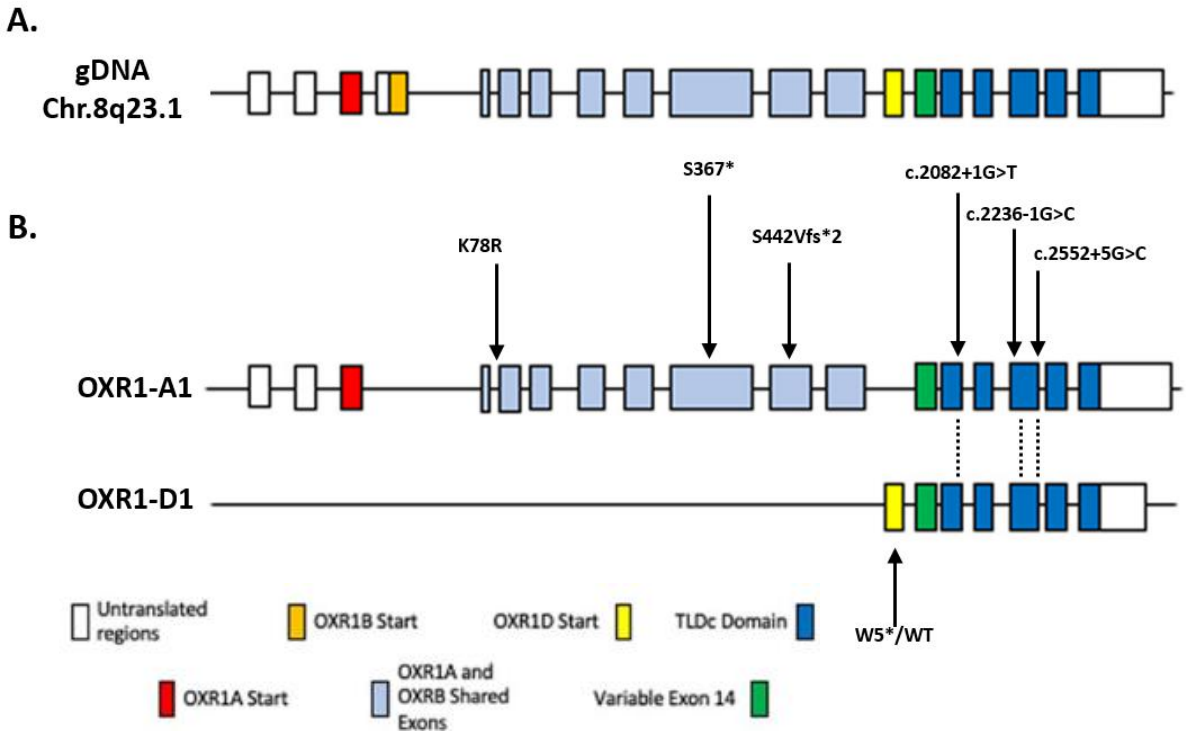

***Figure 1.4*|Schematic illustration of *OXR1* genomic DNA sequence and published pathogenic mutations in OXR1**

(A) Schematic diagram of coding and non-coding exons of human *OXR1*, located on chromosome 8q23.1. (B) Illustration of published human *OXR1* mutations spanning the main full-length and short isoforms (Chen et al., 2017; Lin et al., 2022; Wang et al., 2019).

Table 1-1| Table of known *OXR1* pathogenic mutations

Mutation	Protein level	Developmental delay (inc. motor)	Growth impairment	SLI	Intellectual disability	Dyslexia	Hypotonia	Scoliosis	Epilepsy/Seizures	Cerebellar atrophy	Ataxia	Hearing loss	References
S367*/ c.2082+1G>T (splice donor)	ND	X	X	X	X		X	X	X	X			(Wang et al., 2019)
S442Vfs*2	Protein knockout in patient fibroblasts	X	X	X	X		X		X	X			(Wang et al., 2019)
c.2236-1G>C (spice acceptor)	Protein knockout in patient fibroblasts	X	X	X	X		(X)	(X)	X	X	X		(Wang et al., 2019)
c.2552+5G>C, (splice donor) (*OXR1*$^{\Delta Ex18}$)	Protein knockout in patient lymphoblasts	X	X	X	X		X		X	X	X		(Lin et al., 2022)
c.233A>G p.K78R	ND											X	(Li et al., 2022)
W5*/WT (OXR1-D)	ND			X		X							(Chen et al., 2017)

1.3.1.3. Transcriptional role of *Oxr1*

Oxr1 is essential for cellular resistance to oxidative stress, however the molecular mechanisms conferring this protection are unknown. As the TLDc domain holds no proven catalytic activity (Blaise et al., 2012; Oliver et al., 2011), it has since been proposed that TLDc proteins operate by regulating the expression of ROS detoxifying enzymes (Jaramillo-Gutierrez et al., 2010; Yang et al., 2014) and reducing protein S-nitrosylation (Finelli et al., 2016). Elliott and Volkert (2004) demonstrated that *OXR1* expression can be induced by OS or heat stress. In addition, there is accruing evidence for the role of *Oxr1* as a transcriptional regulator of antioxidant defence genes (Volkert & Crowley, 2020). Localisation of Oxr1 to the cytoplasm and mitochondria has been established in yeast, H_2O_2-treated primary CGCs from mice, as well as in human cell lines (Elliott & Volkert, 2004; Oliver et al., 2011), yet a number of studies also detect Oxr1 in the nucleus (Fischer et al., 2001; Natoli et al., 2008; Yang et al., 2020), pertinent to its potential role as a transcriptional regulator.

In mice, a brain-specific isoform of Oxr1 (Oxr1-A) has been found to interact and activate protein arginine methyltransferase 5 (PRMT5) and PRMT1 which catalyses histone arginine methylation, a process that has been implicated in transcriptional regulation and signal transduction (Finelli et al., 2015; Litt et al., 2009; Yang et al., 2020). Two studies have suggested that OXR1 regulates the expression of glutathione peroxidase (Gpx) and catalase ROS-detoxifying enzymes through the Jun Kinase (JNK) pathway (Jaramillo-Gutierrez et al., 2010; Su et al., 2017). Further to this, depletion of *OXR1* in H_2O_2-treated HeLa cells lead to significant downregulation of *GPX2* and *HO-1,* as well as upregulation of the p53 pro-apoptotic pathway (Yang et al., 2015; Yang et al., 2014), suggesting that Oxr1 is involved in the downstream regulation of transcriptional networks that may confer resistance to OS and cellular survival.

Recent zebrafish studies have corroborated a role for Oxr1 in transcriptional regulation of OS-related genes; loss of *oxr1a* or *oxr1b, OXR1* paralogs, revealed impaired antioxidant gene signalling (Xu et al., 2020; Xu et al., 2021). RNA sequencing of *oxr1a*$^{-/-}$ mutant zebrafish revealed differential expression of genes relating to transcription factors, signal transduction and early response to OS (Xu et al., 2020). These also data identified significant downregulation of glutathione peroxidase genes (*Gpx1b, Gpx4a, Gpx7*) (Xu et al., 2020). Similarly, *oxr1b*-deficient zebrafish failed to exhibit upregulation of antioxidant genes, such as *Sod1* and *Gpx4a*, as well as increased apoptosis and a reduced life span when OS was induced via H_2O_2-treatment, demonstrating enhanced OS sensitivity in the absence of *oxr1b* (Xu et al., 2021). The authors hypothesised that *oxr1a/oxr1b* confer OS resistance in zebrafish through transcription regulation of antioxidant and early stress response genes to prevent OS-induced apoptotic events (Xu et al., 2020; Xu et al., 2021).

1.3.1.4. Neuroprotective function of *Oxr1*

Loss of *Oxr1* has deleterious consequences to CNS function and neuronal cell viability, particularly CGCs and rod photoreceptors (Natoli et al., 2008; Oliver et al., 2011) highlighting the neuroprotective role of Oxr1. *In vitro*, 80% knockdown of *Oxr1* using siRNA resulted in significant cell death under OS-induced conditions (Oliver et al., 2011). Further to this, elevated levels of microRNAs (miRNAs) that suppress expression of *OXR1* have been identified in different NDs where oxidative damage and apoptosis are observed, suggesting they are detrimental in disease progression, yet why these miRNAs are induced is unknown (Jiang et al., 2019; N. Li et al., 2017; Mo et al., 2019; Yang et al., 2018).

It is clear that downregulation of *OXR1* is detrimental to neuronal survival, however upregulation of *OXR1* has proven to be neuroprotective in a number of NDs. OXR1 protein was found to be upregulated in spinal cord tissue from ALS patients, as well as in a

transgenic hSOD1^{G93A} ALS mouse model at a presymptomatic time point (Oliver et al., 2011). Neuronal overexpression of *Oxr1* improves neuropathology and motor function in hSOD1^{G93A} and TDP-43^{M337V} mouse models of ALS (K. X. Liu et al., 2015; Williamson et al., 2019). Given that neuronal upregulation of *Oxr1* expression delays disease onset, alongside extending the lifespan of the hSOD1^{G93A} model, it is likely that *Oxr1* functions to protect against OS-induced pathology at presymptomatic time points (K. X. Liu et al., 2015; Oliver et al., 2011). Interestingly, *OXR1* was found to be substantially downregulated in the substantia nigra pars compacta (SNc) of post-mortem PD tissue; this region contains a subpopulation of dopaminergic neurons that exhibit selective vulnerability in the onset of PD (Wang & Michaelis, 2010), and other brain tissue post-mortem (Stamper et al., 2008; Zhang et al., 2005), as well as in brain tissue from a 1-methyl-4-phenyl-1,2,3,6-tetrahydropyridine (MPTP)-PD mouse model (Jiang et al., 2019). However, Jiang *et al.* (2019) used the MPTP-PD mouse to further demonstrate that upregulation of *OXR1* expression using lentivirus injection alleviated behavioural phenotypes and reduced apoptosis in the SNc (Jiang et al., 2019). Taken together, this evidence identifies *OXR1* as an important determinant in disease pathogenesis, suggesting modulating its expression may prove beneficial in the case of NDs and OS-induced pathology.

1.3.1.5. *OXR1* isoform diversity

A majority of the existing literature does not differentiate between different OXR1 isoforms beyond long and short forms, however it is clear that *OXR1* is expressed as multiple transcripts resulting in isoform diversity (Volkert & Crowley, 2020) (**Figure 1.5**; **Figure 1.6**). Short isoforms of OXR1 (OXR1-D in humans and Oxr1-C in mouse) have a unique first coding exon followed by the TLDc domain, whereas long/full-length isoforms also contain a lysine motif (LysM) and GRAM domain which may contribute to isoform-specific functions in different cell types and tissue (Finelli et al., 2016; Mitchell et al., 2019). To date, there are 17 putative protein-coding human *OXR1* transcripts listed on the National Centre for Biotechnology Information (NCBI)(Sayers et al., 2022), of which 6 have been validated *in vivo* (Volkert & Crowley, 2020). Interestingly, intermediate OXR1 isoforms were also found to be upregulated in spinal cord biopsies from ALS patients, yet the functional relevance of the different isoforms has not been clarified (Oliver et al., 2011). *Oxr1* expression has also been identified in tissues outside of the CNS, including in the heart, liver and testes, but the tissue specific roles are yet to be fully elucidated (Finelli et al., 2016).

Thus far, section **1.3** has highlighted a number of roles of *Oxr1 in vitro* and *in vivo*, which this thesis aims to further characterise. Evidently, Oxr1 is critical in the CNS of both mice and humans, supporting the importance of understanding the mechanisms of how *OXR1* contributes to human health and disease going forward. As the TLDc protein family members bare a number of similarities in structure and function, their characteristics have been broadly summarised in the following sections.

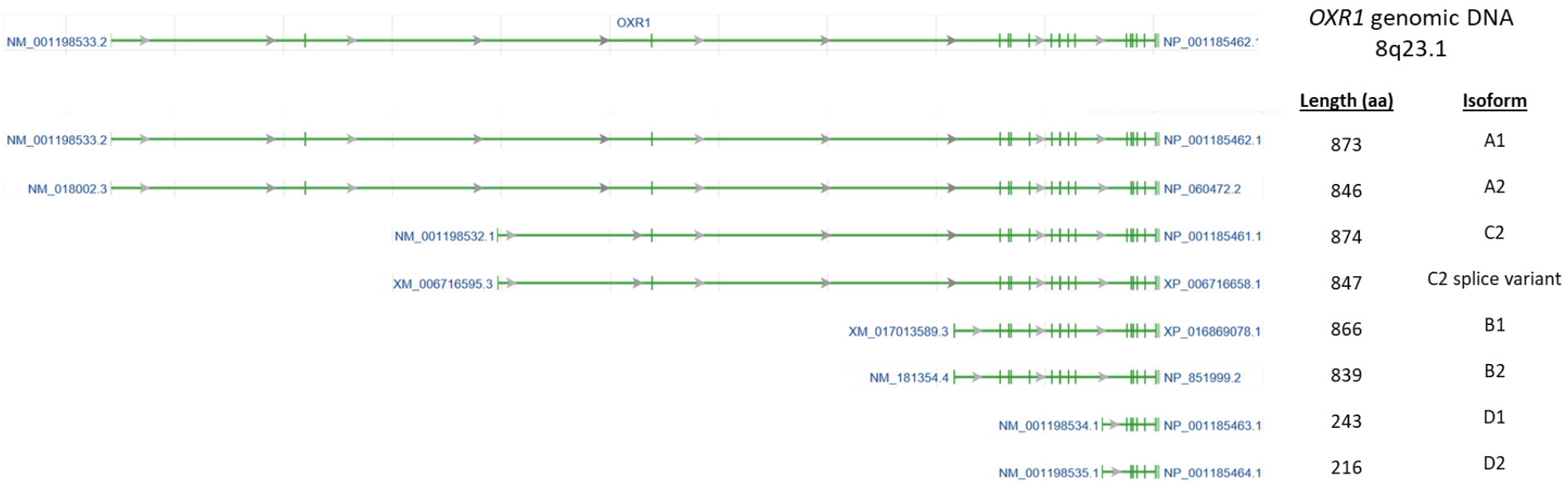

Figure 1.5| Human (*Homo Sapiens*) *OXR1* genomic DNA and validated protein-coding transcripts

Validated protein-coding human OXR1 isoforms and protein length (amino acids), cross-referenced to protein nomenclature in recent literature (Lin et al., 2022; Volkert & Crowley, 2020; Wang et al., 2019; Yang et al., 2014); based on RefSeq (NCBI Reference Sequence Database) annotations with accession numbers.

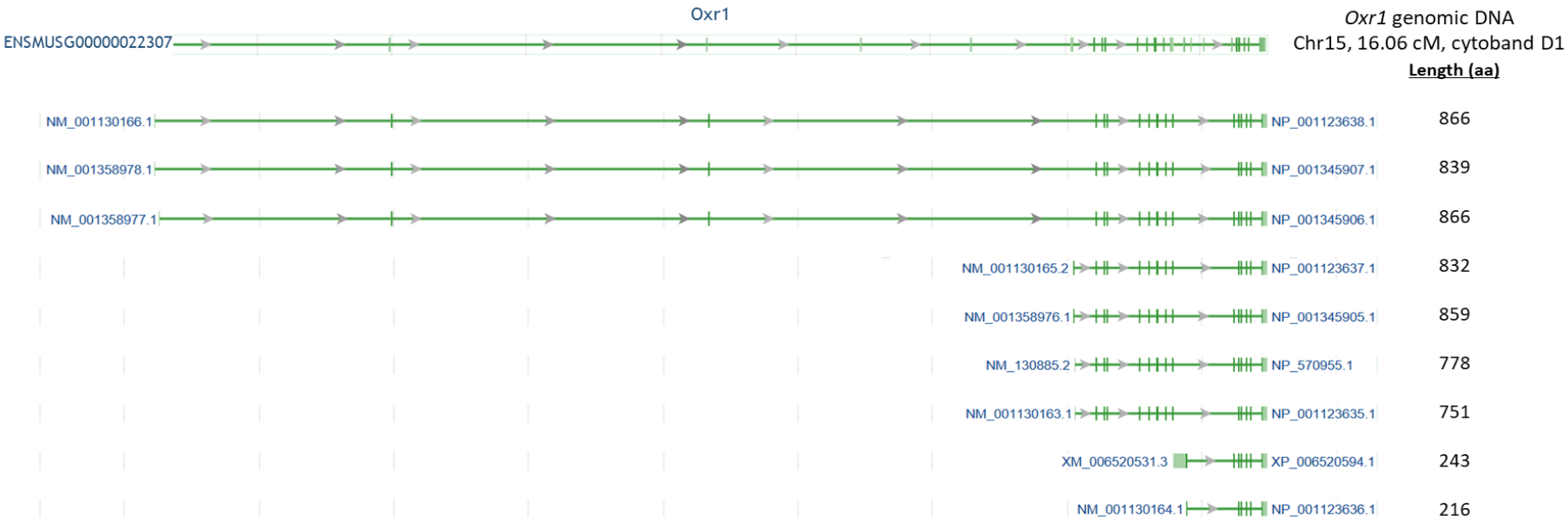

***Figure 1.6*| Mouse (*Mus Musculus*) *Oxr1* genomic DNA and validated protein-coding transcripts**

Validated protein-coding mouse Oxr1 isoforms and protein length (amino acids) based on RefSeq (NCBI Reference Sequence Database) annotations with accession numbers. Oxr1A (Yang et al., 2020): NM_001130166; XM_011245478, Oxr1-FL (Oliver et al., 2011): NM_130885; Oxr1-C (Oliver et al., 2011): NM_001130164.

1.3.2 Nuclear receptor coactivator 7 (*Ncoa7*)

Owing to the fact that NCOA7 shares a number of structural and functional characteristics with OXR1, it is predicted to have arisen through gene duplication (Durand et al., 2007). Similar to *OXR1*, *NCOA7* is expressed as multiple isoforms, more notably as a long (*NCOA7-FL*) and short isoform (*NCOA7-B*) (**Figure 1.2**) that is suggested to have an independent function to its full length counterpart (Finelli et al., 2016; Shao et al., 2002; Shkolnik et al., 2008); high expression levels of *NCOA7* isoforms have also been identified in the kidney (Finelli et al., 2016; Shao et al., 2002).

In addition to the LysM, GRAM and TLDc domain, shared features with OXR1-FL, NCOA7-FL also possesses an estrogen receptor binding domain (ERbd) which provides the ability to bind estrogen receptor alpha, as well as transcription factors and nuclear receptors, identifying NCOA7-FL as a potential transcriptional regulator (Finelli & Oliver, 2017). More recently, NCOA7 has been highlighted to play a key role in neurodevelopment and is considered a susceptibility locus for autism spectrum disorder (ASD) (Castroflorio et al., 2021; Doan et al., 2019; Mahfouz et al., 2015). Exome sequencing identified homozygous LoF mutations in NCOA7-FL in a family with ASD (Doan et al., 2019). Similarly, behavioural phenotyping of mice with complete genetic disruption of the *Ncoa7* locus demonstrated increased anxiety and decreased sociability, which are considered to be ASD-related behaviours (Castroflorio et al., 2021).

Neurons derived from *Ncoa7*-deficient mice exhibit clear endolysosomal dysfunction which may underlie the neurodevelopmental effects observed both *in vitro* and *in vivo* (Castroflorio et al., 2021). Outside of the CNS, *Ncoa7* plays a key role in facilitating urine acidification through its modulatory role in v-ATPase assembly and function in the kidney (Castroflorio et al., 2021; Merkulova et al., 2018). Alterations in urine pH levels are a known biomarker of renal dysfunction (Aslan et al., 2020); genetic

disruption of the entire *Ncoa7* locus in mice resulted in decreased urine acidity (Castroflorio et al., 2021). Similarly, urinalysis of mice lacking expression of *Ncoa7-FL* demonstrated significantly increased pH levels, alongside aberrant size and morphology of intercalated cells in the kidney (Merkulova et al., 2018).

Ncoa7-B, also known as *NCOA7-AS* (alternative start) in human data, structurally consists of the highly conserved TLDc domain and preceded by a unique short coding exon (Finelli et al., 2016; Yu et al., 2015). The adjacent promoter site shares sequence similarity to that of type 1 interferon (IFN) stimulated response elements, facilitating transcriptional activation following IFN-β-1b or lipopolysaccharide (LPS)-treatment via the JAK-STAT pathway, alluding to a role for Ncoa7-B in the immune response (Yu et al., 2015). In support of this, *NCOA7-AS* overexpressing cells demonstrated a more than 2-fold reduction in endosome-mediated viral entry events when challenged with viral infection *in vitro*, thus identifying Ncoa7-B as a putative antiviral protein (Doyle et al., 2018). Taken together, the *NCOA7* locus appears to play a pivotal role in oxidative stress response and v-ATPase functionality, as well as in transcriptional regulation, immune response and viral-mediated endocytosis (Castroflorio et al., 2021; Doyle et al., 2018; Eaton, Brown, et al., 2021). These studies show overlapping, as well as independent, functions for both full length and short isoforms of NCOA7.

1.3.3 TBC1 domain family member 24 (*Tbc1d24*)

The pleiotropic effects of disease-associated mutations in TBC1D24 demonstrate a complex role for this TLDc protein *in vivo*, particularly in CNS function (Balestrini et al., 2016; Finelli, Aprile, et al., 2019). Patients with deleterious mutations in TBC1D24 present with a number of overlapping clinical features to LoF-OXR1 patients, including intellectual disability, cerebellar atrophy and seizures (Balestrini et al., 2016; Chen et al., 2017; Finelli

& Oliver, 2017; Lin et al., 2022; Mucha et al., 2017; Wang et al., 2019). Moreover, a complex range of NDs, including Familial Infantile Myoclonic Epilepsy (FIME) (Falace et al., 2010), deafness, onychodystrophy, osteodystrophy, intellectual disability, and seizures (DOORS) syndrome and non-syndromic hearing loss are caused by mutations (> 80 reported) in TBC1D24 (Azaiez et al., 2014; Campeau et al., 2014). Epilepsy-inducing TBC1D24 mutations have been identified across the protein sequence, including a number that have been identified in the TLDc domain; these pathogenic mutations are predominantly autosomal recessive or compound heterozygous (Balestrini et al., 2016; Mucha et al., 2017; Ngoh et al., 2017)

As well as containing the TLDc domain, Tbc1d24 also possesses a Tre2–Bub2–Cdc16 (TBC) domain which has been shown to modulate ADP ribosylation factor (ARF) 6 activity during neuronal migration (Falace et al., 2014). Loss of *skywalker* (*sky*), the *Drosophila* TBC1D24 orthologue, has been shown to increase the pool of synaptic vesicles and subsequent neurotransmission (Uytterhoeven et al., 2011). Building on from this evidence, a role for *Tbc1d24* in mammalian synaptic vesicle trafficking and neuronal survival was established; haploinsufficiency of *Tbc1d24* was sufficient to cause endosomal and synaptic defects in mice (Finelli, Aprile, et al., 2019). Importantly, Tbc1d24 is found at both pre- and postsynaptic terminals, alluding to a role for Tbc1d24 in synaptic function (Lin et al., 2020; Pandya et al., 2017; Uytterhoeven et al., 2011). Despite clues from studies in the mouse and fly, there is no obvious correlation between genotype and phenotype in TBC1D24-associated disorders (Balestrini et al., 2016).

1.3.4 mTOR-associated protein, enhancer-of-akt-1-7 (*mEAK-7)*

Earlier studies suggested *KIAA1609* to be the human orthologue of *Eak-7*, which is implicated in stress resistance in *C. elegans* (Alam et al., 2010; Williams et al., 2010). More recent molecular characterisation in mammalian systems lead to the more functionally relevant name, mTOR-associated protein/mammalian enhancer-of-akt-1-7 (*mEAK-7*) (Nguyen et al., 2018). Three functional domains have been identified in mEAK-7: an N-myristoylation motif, TLDc domain and an mTOR-binding (MTB) domain (Nguyen et al., 2018).

Myristoylation helps target proteins to membranes by the increased hydrophobicity from the addition of a lipid moiety (Maurer-Stroh et al., 2002). Mutating the N-myristoylation motif of mEAK-7 showed mislocalisation of the protein from the lysosome, and in part the plasma membrane, to the cytoplasm, confirming its requirement for anchorage to the lysosome and association with the plasma membrane (Nguyen et al., 2018). mTOR signalling is an important regulator of many cellular processes including survival and proliferation (Laplante & Sabatini, 2009). Nguyen *et al.* (2018) demonstrated that mEAK-7 stimulates cell proliferation through interaction with mTOR through the MTB domain and subsequent activation of S6K2, which has been implicated in transcriptional regulation and cell survival (Pardo & Seckl, 2013).

Notably, a human coding missense mutation in the TLDc domain (T354M) has been associated with specific language impairment (SLI) (personal communication). The SLI Consortium screened for novel loci that may be involved in the development of speech and language abilities, which identified 16q and 19q (Consortium, 2002). Interestingly, mEAK-7 is located on the long arm of human chromosome 16 (16q24.1), however the potential functional significance of this variant has not been investigated.

1.3.5 Chromosome 20 open reading frame 118 (*C20Orf118*)

To date, little is known about the function of *C20Orf118 in vivo*. In both human and mouse brain, expression of *C20Orf118* remains virtually undetectable throughout embryonic and postnatal development (Cardoso-Moreira et al., 2019; Finelli et al., 2016). Similarly, *C20Orf118* expression in embryonic human and mouse cerebellum, as well as postnatally in human cerebellum, is almost untraceable; a slight increase in expression is observed in mouse cerebellum between P14-P63, however only a maximum of 3 reads per kilobase of transcript per million reads mapped (RPKM) were detected in this developmental timeframe (Cardoso-Moreira et al., 2019; Finelli et al., 2016).

Limited gene ontology (GO) annotations have been assigned to *C20Orf118* owing to the limited research focusing on this gene. *C20Orf118* is predicted to act in the nucleus and play a role in cellular response to oxidative stress, although a specific molecular function has not been ascribed (Cunningham et al., 2022). Interestingly, overexpression of *C20Orf118* in arsenite treated Neuro2a (N2a) cells resulted in a non-significant decrease in levels of oxidative stress, suggesting a limited neuroprotective capacity compared to other members of the TLDc family (Finelli et al., 2016). In *Nile Tilapia*, RNA sequencing (RNA-Seq) of multiple tissues, including brain, identified differential expression of TLDc2 transcripts, an orthologue of *C20Orf118,* in hypoxia challenged fish which further suggests a role for this gene in oxidative stress response (H. L. Li et al., 2017).

More recently, the TLDc domain from C20Orf118 was shown to interact with the B1 subunit of V-ATPase using kidney lysate; when overexpressed in HEK293T cells, C20Orf118 also co-immunoprecipated with the B1 subunit of V-ATPase, although the functional significance of this is not known (Eaton, Brown, et al., 2021).

1.4 Summary of the TLDc protein family

It is evident that TLDc proteins possess overlapping functions in the CNS, but also hold important independent functions beyond response to OS (Finelli & Oliver, 2017). As disruption of TLDc protein expression produces pleiotropic effects, this indicates that the protein family plays a critical role in a number of cellular mechanisms. However, it is particularly interesting that there are specific clinical features in common between OXR1 and TBC1D24 loss-of-function mutations, such as seizures and neurodegeneration (**Figure 1.3**) (Balestrini et al., 2016; Lin et al., 2022; Wang et al., 2019). In addition, there has begun to be some converging evidence for v-ATPase interaction as being a key feature of TLDc protein functionality (Eaton, Brown, et al., 2021).

It is worth noting that loss of *OXR1* is deleterious in both human and mouse, yet loss of its close homolog *NCOA7* is tolerated *in vivo* (Castroflorio et al., 2021; Doan et al., 2019; Durand et al., 2007; Lin et al., 2022; Merkulova et al., 2018; Oliver et al., 2011; Wang et al., 2019). Interestingly, *Oxr1* and *Ncoa7* double knockout mice are not viable, however heterozygous expression of either gene was sufficient to rescue viability, suggesting an element of functional compensation of these TLDc genes (Castroflorio et al., 2021). This highlights the importance in understanding the overlapping mechanisms between TLDc proteins and how these properties can be exploited *in vivo.*

1.5 Thesis Aims

The increasing global burden of NDs calls for the need to understand the course of disrupted pathways in disease onset and progression in order to identify broadly applicable novel therapeutic targets. From the current literature, the TLDc protein family stand as potentially viable therapeutic candidates, given their ability to confer neuroprotection against OS in vitro and in vivo. Overexpression of *Oxr1* has already been shown to modulate neuroinflammation, as reflected by reduced reactive glial neuropathology and expression of neuroinflammatory genes, as well as decreased neuronal cell death in a number of mouse models of neurodegeneration, yet the exact overarching neuroprotective mechanisms remain unknown. This thesis endeavours to further characterise the role of Oxr1 in vitro and in vivo using a combination of cellular and mouse models to understand which pathways Oxr1 and other TLDc proteins may act in, as described below:

1.5.1 Chapter 3 Aims

The reported clinical presentations and cerebellar pathology of LoF-*OXR1* patients demonstrate a fundamental overlap with features of constitutive *Oxr1* knockout mice, yet the cause of this disease aetiology and region-specific neurodegeneration is unknown. Thus, the constitutive *Oxr1* knockout mouse model serves as a valuable tool to identify fundamental molecular pathways that may underpin cellular dysfunction and neuronal cell death *in vivo*. In this chapter, bulk RNA-sequencing analysis of pre/early-symptomatic cerebellar tissue was employed to determine differentially expressed genes and potentially dysregulated pathways in *Oxr1*-deficient mice. These candidate pathways were further explored at the protein level in both tissue and primary cells, alongside the utilisation of *in vitro* cellular assays to determine the role of *Oxr1* in lysosome biology and overall neuronal function.

1.5.2 Chapter 4 Aims

Constitutive loss of *OXR1* in both humans and mice results in juvenile onset ataxia, neurodegeneration and premature death, demonstrating that OXR1 is required for normal neurological function. The severity of the phenotypes precludes the study of Oxr1 in the adult mouse, including potential behavioural effects and susceptibility of non-cerebellar cell types to neurodegeneration. Therefore, to determine the effects of Oxr1 depletion in the adult mouse, a tamoxifen-inducible, conditional-ready *Oxr1* knockout mouse line was used to sustain critical developmental expression of *Oxr1* prior to inducing ubiquitous loss of Oxr1 in the adult mouse. Following adult-induced knockdown of Oxr1, behavioural changes and neuropathological effects, focusing on neuroinflammation and cell death, were investigated to assess the pathophysiological consequences of loss of Oxr1 in adulthood.

1.5.3 Chapter 5 Aims

Significant neuroinflammation is observed across *Oxr1* knockout mouse models. Given that *Oxr1* is expressed in both neuronal and non-neuronal cell types, it is unknown whether neuroinflammation is activated in a cell-autonomous fashion in *Oxr1*-deficient glial cells or if neuronal dysfunction likely instigates a neuroinflammatory response in *Oxr1* knockout mice. Therefore, transgenic *Oxr1* expression, driven by the mouse prion promoter (*Oxr1*-transgene) to confer neuronal specificity, was employed to determine whether neuron-specific expression of *Oxr1* is sufficient to compensate for ubiquitous loss of the protein and negate neuroinflammation *in vivo* in *Oxr1*-null mice. A combination of gene expression analysis and histopathology was then used to ascertain whether *Oxr1*-transgene expression could 'rescue' known pathways that are dysregulated in *Oxr1* knockout mice.

Additionally, neuron-specific overexpression of *Oxr1* reduces neuroinflammation in ALS mouse models, though the neuroprotective mechanism is unknown. This chapter aimed to investigate the *Oxr1*-transgene mechanism of action; brain lysates from *Oxr1*-transgene expressing mice were subjected to proteomic analysis, with the aim of identifying putative interaction partners that may confer the neuroprotective properties of *Oxr1*-transgene in a "gain-of-function" manner. In summary, these experiments set out to advance our understanding of *Oxr1* in different cell types, as well as exploring the therapeutic capacity of overexpressing *Oxr1* in neurons.

MATERIALS AND METHODS

Chapter 2 : Materials and Methods

2.1 Mouse Strains and Husbandry

All breeding and animal procedures were performed under project licence 18/0001 with local ethical approval, compliant with the Animals Scientific Procedures Act 1986 and in accordance to UK Home Office regulations. All colonies were bred and maintained on a C57BL/6J background in the Mary Lyon Centre. Genotyping was performed by the Genotyping and Mutation Screen (GEMS) core facility at MRC Harwell. Mice were housed in individually ventilated cages (IVCs) with *ad libitum* access to food and water. IVCs were limited to a maximum of 5 mice per cage and kept on a 12 hour on:off light cycle. Conditional ready *Oxr1*^{tm1c} allele and *Oxr1*^{tm1d} knockout allele were derived from the original *Oxr1* knockout-first (*tm1a*) gene trap cassette, as described by (Skarnes et al., 2011) (**Figure 2.1**), inserted in to the TLDc domain which targets deletion of all isoforms of Oxr1.

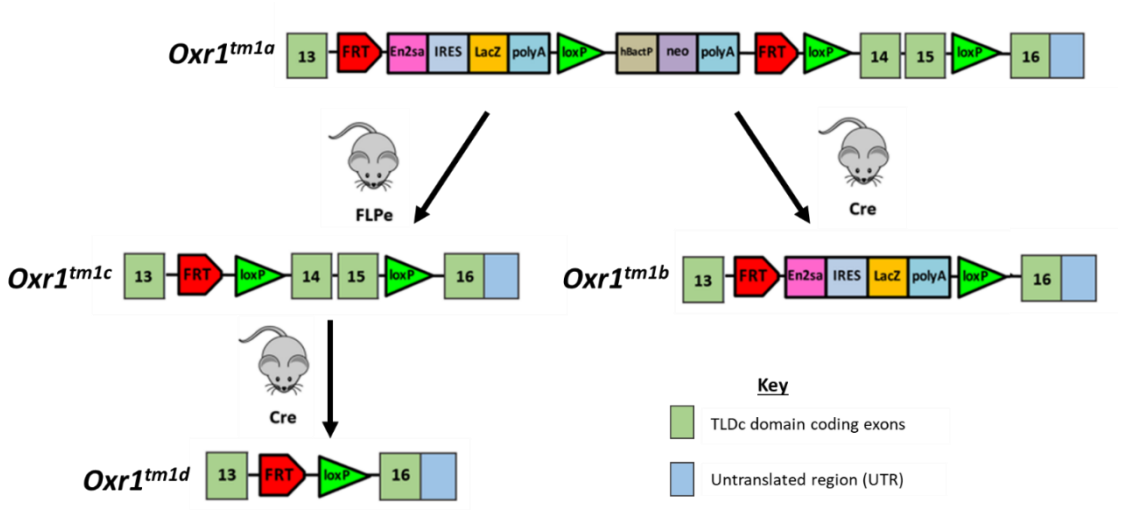

***Figure 2.1*| Schematic diagram of original *Oxr1* knockout-first (*tm1a*) gene trap cassette and derived *tm1b, tm1c* and *tm1d* alleles**

FLPe: enhanced flippase, FRT: FLPe recognition target sites, En2sa: mouse *engrailed 2* exon 2 splice acceptor, IRES: internal ribosome entry site, LacZ: *lacZ* reporter gene, polyA: SV40 poly-adenylation signal, neo: neomycin resistance gene, LoxP: Locus of X-over P1 Cre recombinase target sites and hBactP: autonomous human β-actin promoter. Numbered boxes correspond to TLDc domain coding exons. Diagram adapted from (Skarnes et al., 2011; Williamson, 2019).

2.1.1 *Oxr1$^{tm1d/tm1d}$*

Constitutive *Oxr1* knockout mice (*Oxr1$^{tm1d/tm1d}$*) were bred as described in (Finelli, Paramo, et al., 2019). In summary, *Oxr1^{tm1c}* (described in **2.1.2**) were crossed to a ubiquitous Cre-recombinase expressing mouse line, excising critical exons and inducing a premature stop codon, thus generating the tm1d deletion allele. For removal of the Cre recombinase transgene, these mice were backcrossed to C57BL6/J for at least 10 generations and successively, heterozygous *Oxr1^{tm1d}* mice were intercrossed to produce homozygous *Oxr1$^{tm1d/tm1d}$* knockout mice.

2.1.2 *Oxr1$^{tm1c/tm1c}$/UBC-Cre*

Oxr1^{tm1a} mice were crossed to a ubiquitous FlpE recombinase expressing mouse line to generate a conditional-ready *Oxr1^{tm1c}* allele. Subsequently, *Oxr1^{tm1c}* lines were crossed to tamoxifen inducible B6.Cg-Tg(UBC-cre/ERT2)1Ejb/J Cre line (Ruzankina et al., 2007) to generate *Oxr1^{tm1c}/UBC-Cre* experimental cohorts.

2.1.3 *Oxr1$^{tm1d/tm1d}$/Oxr1-Prnp*

As outlined in K. X. Liu et al. (2015), HA-tagged Oxr1-FL cDNA expression was driven under a prion protein *Prnp* promoter (Borchelt et al., 1996) to confer neuron-specific overexpression of *Oxr1* (*Prnp-Oxr1*). Heterozygous *Oxr1^{tm1d}* mice were crossed with heterozygous *Oxr1^{tm1d}* mice that were also hemizygous for the *Prnp-Oxr1* transgene, to produce experimental cohorts on a C57BL/6J background.

2.2 Animal Procedures and Phenotyping

2.2.1 Tamoxifen Dosing

Tamoxifen (Sigma) was dissolved to a concentration of 20 mg/mL in autoclaved corn oil (Sigma) (2% ethanol) at 42˚C, and then stored at 4˚C in the dark. *Oxr1*$^{tm1c/tm1c}$*/UBC-Cre* experimental cohort mice were dosed at 200 mg/kg for 5 consecutive days by oral gavage and left to recover for at least 14 days.

2.2.2 Phenotyping sample sizes for each experimental group

***Table 2-1*| Sample size of female *Oxr1*$^{tm1c/tm1c}$*/UBC-Cre* mice used in phenotyping pipelines**

Genotype	Simplified Genotype	Tamoxifen	n Number
Oxr1$^{tm1c/tm1c}$*/UBIQC-Cre*$^{+}$	Hom Cre +	Dose	12
		No Dose	9
Oxr1$^{tm1c/tm1c}$*/UBIQC-Cre*$^{-}$	Hom Cre -	Dose	11
		No Dose	11
Oxr1$^{tm1c/wt}$*/UBIQC-Cre*$^{+}$	Het Cre +	Dose	9
		No Dose	11
Oxr1$^{tm1c/wt}$*/UBIQC-Cre*$^{-}$	Het Cre -	Dose	10
		No Dose	10

2.2.3 Phenotyping – Open Field Activity

Female *Oxr1*$^{tm1c/tm1c}$*/UBC-Cre* experimental cohort mice were subjected to open field activity assessment to investigate locomotion and behaviour in a novel environment. At least 20 minutes prior to the start of the test, mice were taken to the phenotyping room to acclimatise and the apparatus was set up and cleaned with 70% ethanol. Mice were placed individually in opaque Plexiglas square arenas (44 x 44 cm) in a small testing room, with a minimum of 2 and a maximum of 4 mice tested per trial. Lighting was set to 150 – 200 lux and the animals were video tracked via overhead camera for 20 minutes. All arenas were cleaned with 70% ethanol in between trials. Data was recorded and analysed using Ethovision XT software (Noldus, Netherlands), with the arena divided in to zones; centre

(11x11cm box in the centre), periphery (8 cm region from edge of arena) and remaining in-between zone and whole arena (Walsh & Cummins, 1976).

2.2.4 Phenotyping – Accelerating Rotarod Performance Test

Female *Oxr1*$^{tm1c/tm1c}$*/UBC-Cre* experimental cohort mice were subjected to an accelerating rotarod performance test at three time points. The device (Ugo Basile) was set to accelerate from 4-40 rpm over 300 seconds. Mice were placed on a foam padded rod, opposing the direction of rotation. A rotarod session consisted of 1 trial each day, on 3 consecutive days. The trial ended and the time was taken when a mouse exceeded one passive rotation or fell from the rod (latency to fall) for the 3 trials at each time point. Average time of three trials was calculated.

2.3 Tissue Collection and Immunohistochemistry

2.3.1 Perfused Tissue

To obtain perfused tissue, mice were sacrificed by lethal intraperitoneal injection of pentobarbitone, followed by transcardial perfusion and fixation with 4% paraformaldehyde (PFA) (Performed by P.L.O and Necropsy at MRC Harwell). Brains were dissected out and post fixed in 10% neutral buffered formalin and then cryoprotected in 30% sucrose at 4˚C. Brains were set in 2-3% agarose and vibratome (Leica) sectioned at 30 µm. Sections were stored in PBS with 0.01% sodium azide at 4˚C.

2.3.2 Fresh Frozen Tissue

Mice were culled by cervical dislocation and decapitated. Prior to storage at -80˚C, tissue was dissected out of the carcass and rapidly frozen on dry ice. Tissue for cryosectioning was embedded in OCT matrix (Fisher Scientific) and set on dry ice. Using an Epredia™

Cryostat (Fisher Scientific) tissue was cut to 12 µm per section. Following this, sections were mounted on to Superfrost Plus slides (Thermo Fisher) and stored at -80˚C.

2.3.3 Immunohistochemistry

Free floating sections were washed with PBS and blocked in 10% normal goat serum (NGS), 0.1% Triton X-100 for 1 hr at room temperature. Sections were incubated with primary antibodies, rocking overnight at 4˚C. Next, the sections were washed with PBS and incubated with AlexaFluor secondary antibodies (Invitrogen) for 1hr at room temperature. Sections were then washed again in PBS, mounted on Superfrost Plus slides (Thermo Fisher) and left to dry. Prior to imaging, slides were then sealed with ProLong™ Diamond Antifade Mountant with DAPI (ThermoFisher). All antibodies were diluted in 3% NGS, 0.1% Triton X-100. Antibodies used for immunohistochemistry are listed in **Table 2-2**.

***Table 2-2*| Antibodies used for immunohistochemistry**

Antibody	Supplier	Catalogue Number	Dilution
Anti-Mouse	Thermo Fisher Scientific	A-11005	1:1500
Anti-Rabbit	Thermo Fisher Scientific	A-11008	1:1500
Gfap	Sigma Aldrich	AB5804	1:1000
HA	Abcam	ab9110	1:1000
Iba1	FUJIFILM Wako Pure Chemical Corporation	019-19741	1:1000
NeuN	Sigma Aldrich	MAB377	1:500

2.4 Terminal deoxynucleotidyl transferase dUTP nick end labelling (TUNEL)

Brains embedded in frozen OCT were cut to 12µm using a cryostat and mounted on to Superfrost Plus slides (Thermo Fisher). Terminal deoxynucleotidyl transferase dUTP nick end labelling (TUNEL) was carried out using the *in situ* cell death detection kit, Fluorescein (Roche) following the manufacturer's protocol. Slides were mounted using ProLong™ Gold Antifade Mountant with DAPI (Thermo Fisher) and 1 mm glass coverslips. Imaging was carried out using a Zeiss LSM 700 inverted confocal microscope (Carl Zeiss AG) and analysed using Zen Black.

2.5 Primary Cell Isolation, Culture and Treatment

2.5.1 Genotyping for primary cell culture

Tail clips (~2mm) were obtained from culled P1 or P22 pups and incubated in tail lysis buffer (10 mM Tris pH 8.0, 100 mM NaCl, 10 mM EDTA pH 8.0, 0.2% SDS) supplemented with Proteinase K (Sigma) and incubated at 37˚C overnight (O/N). Subsequently, 5M NaCl was added to the tail digest and vortexed until homogeneously cloudy. Following this, the solution was centrifuged at 10'000 rpm for 5 minutes and supernatant was transferred to a new eppendorf. Equal volume of 100% ethanol was added to the supernatant and gently inverted to precipitate out the DNA, prior to pelleting through additional centrifugation. The pelleted DNA was washed with 70% ethanol and subsequently left to air dry before resuspension in double distilled water (ddH_2O). A genotyping REDTaq® Ready Mix PCR Reaction (Sigma) master mix was prepared with the isolated DNA as per manufacturer's instructions, using genotyping primers for *Oxr1* wild-type (*Oxr1*^{tm1a}) and knockout (*Oxr1*^{tm1d}) alleles as listed in **Table 2-3**. The master mix was run in a thermocycler (BioRad) using parameters outlined in **Table 2-4**. PCR products were separated by size using agarose (1.5% [w/v]) gel electrophoresis to determine genotype.

***Table 2-3*| Oxr1 genotyping primers**

***Oxr1* allele**	**Forward/Reverse**	**Primer Sequence (5'- 3')**
***Oxr1*^{tm1a}**	**F**	TGGAATATCCAGTCTCACCTCA
	R	CAGAGCACAGAAGCGTCTCA
***Oxr1*^{tm1d}**	**F**	AAGGCGCATAACGATACCAC
	R	ACTGATGGCGAGCTCAGACC

***Table 2-4*| Thermocycler settings for Red Taq polymerase genotyping reactions**

	Temperature (°C)	**Time**
	94	2 mins
X 37 Cycles	94	20 secs
	56	30 secs
	72	1 min 30 secs
	72	7 mins
	10	∞

2.5.2 Primary Ear Fibroblast Culture

Oxr1$^{wt/wt}$ and *Oxr1*$^{tm1d/tm1d}$ were culled by cervical dislocation at P22 and genotyping was performed as described in **2.5.1.** Ears were dissected and placed in 70% ethanol for 10 minutes, then placed in a petri dish to remove excess hair and air dry. Following a PBS and complete Roswell Park Memorial Institute (RPMI) 1640 Medium (Gibco) (10% FBS + 1mM Glutamax + 25 mM HEPES) wash, ears were finely chopped and digested in filtered Pronase (Merck Millipore) and Collagenase D (Roche) for 90 minutes at 37°C. Digested ears were passed through a 70 µm cell strainer (Corning), pestled and washed in complete RPMI. Cells were pelleted by centrifugation, PBS washed, resuspended in complete RPMI with Normacin (Invivogen) and cultured in T-75 flasks (SLS) overnight. RPMI media was then replaced with complete Dulbecco's Modified Eagle Medium (DMEM) (10% FBS, 5% Glutamax, 1% Penicillin-Streptomycin (P/S)) and cells were grown to confluency prior to passaging to T-175 flasks (SLS).

2.5.3 Primary Cortical Neuron Culture

Primary cortical neurons were prepared from P1 *Oxr1*$^{wt/wt}$ and *Oxr1*$^{tm1d/tm1d}$ pups. Pups were culled by decapitation, then cerebral cortices were dissected out and meninges removed. Genotyping was performed as described in **2.5.1.** Cortices were dissociated by enzymatic digestion in 0.25% Trypsin (Gibco) with DNAse (0.8 mg/mL) for 15 mins at 37°C. Trypsin activity was inhibited using Neurobasal A (NBA) (Gibco) with 20% FBS (Gibco) and gently triturated into a single cell suspension. The suspension was passed through a 40 µm cell strainer (VWR international) and washed through with NBA. Cells were pelleted by centrifuging for 5 minutes at 300g and the supernatant was aspirated. Following resuspension of the cell pellet in complete NBA (NBA, 1% Glutamax, 2% B27, 5 µg/mL Gentamicin), the cell suspension was passed through a 40 µm cell strainer. Cells were counted using the Countess II Automated Cell Counter (ThermoFisher) protocol and plated

at a density of 200 cells/mm^2 per coverslip or 500'000 cells/well in a 6 well plate (Greiner Bio-One). Prior to seeding, coverslips or wells were coated with poly-D-Lysine (Gibco) and a neuron feeder layer (DMEM, 10% FBS, 1% P/S). Cortical neuron cultures were maintained *in vitro* by performing half-volume media replacement complete NBA media every 3-4 days.

2.5.4 Primary Cell Treatment

Primary fibroblasts were treated to a final well concentration of either 0.1% dimethyl sulfoxide (DMSO)(ThermoFisher), 20 nM Rapamycin (Merck) for 24 hours or 50 nM Bafilomycin (VWR international) for 6 hours, prior to sample collection. Primary cortical neurons were treated to a final well concentration of either 0.1% DMSO, 10 nM Rapamycin for 24 hours or 25 nM Bafilomycin for 6 hours, prior to sample collection. Concentrations for neuron treatment were derived from Guedes-Dias et al. (2015).

2.6 Immunocytochemistry

Cells were fixed using 4% paraformaldehyde (PFA) (Santa Cruz) in PBS for 20 minutes at room temperature then washed x3 PBS. Cells were blocked in 10% normal goat serum (NGS) in PBS with 0.5% Triton X-100 (PBS-Tx) and incubated with primary antibodies in 3% NGS in PBS-Tx O/N at 4˚C. Coverslips were washed with PBS before AlexaFluor secondary antibody (Invitrogen) incubation for 2 hr at RT in the dark. Coverslips were washed and mounted in ProLong™ Diamond Antifade Mountant with DAPI (Thermo Fisher) and imaged using a Zeiss inverted confocal microscope. Antibodies are listed in **Table 2-5**.

***Table 2-5*| Antibodies used in immunocytochemistry**

Antibody	Supplier	Catalogue Number	Dilution
Anti-Mouse	Thermo Fisher Scientific	A-11005	1:1500
Anti-Rabbit	Thermo Fisher Scientific	A-11008	1:1500
Anti-Rat	Thermo Fisher Scientific	A-21247	1:1500
Lamp1	Santa Cruz	1D4B/sc-19992	1:1000
LC3A/B	Cell Signalling Technologies	4108S	1:500
NeuN	Sigma Aldrich	MAB377	1:500
SQSTM1/p62	Abcam	ab56416	1:500

2.7 Lysotracker Live Cell Imaging

Fibroblasts were seeded in CELLVIEW Cell Culture Slides (Greiner Bio-One) at a density of 10’000 cells in 100 µl of media per well and left to adhere overnight. The following day, LysoTracker® Red DND-99 (ThermoFisher) stock was used at a working concentration of 100 nM in Eagle's Minimum Essential Medium (EMEM) media (Gibco), supplemented with 10% FBS and 1% Glutamax. NucBlue™ Live ReadyProbes™ Reagent (Hoechst 33342) was used at 2 drops per mL. Cells were incubated in Lysotracker working solution for 15 mins at 37°C, then washed and imaged immediately in imaging solution (FlouroBrite, 1% Glutamax, 25 mM HEPES). Live cell imaging was performed on three biological replicates per genotype with a Zeiss LSM 700 confocal microscope (Carl Zeiss AG) fitted with a 37°C and 5% CO_2 chamber and images were acquired within 20 minutes to avoid signal leaching. Images were taken at 40x using Z-series stacks of at least 4 slices (1024x1024). Quantitative analysis was performed using FIJI software by compressing a maximum intensity projection image and counting LysoTracker positive puncta relative to cell area.

2.8 DQ-Red BSA Trafficking Assay

Primary cortical neurons were isolated as described in **2.5.3** and seeded in PDL and feeder layer coated PhenoPlate 96 well imaging plates (PerkinElmer) at a density of 10'000 cells/well. DQ™ Red BSA (ThermoFisher) trafficking assay was carried out as described in (Carling et al., 2022) with the help of William McGuiness (University of Oxford) using chloroquine-treated neurons as an experimental control. This was conducted in the Wade-Martins Group (University of Oxford). In summary, 14 DIV neurons were incubated with 35 µg/mL DQ™ Red BSA and NucBlue™ Live ReadyProbes™ (Hoechst 33342, ThermoFisher) for 5 hours at 37°C with 5% CO_2. Prior to imaging, cells were washed with Dulbecco's phosphate-buffered saline (DPBS) and incubated with Hank's Balanced Salt Solution (HBSS) and NeuroFluor™ NeuO (Stem Cell Technologies) at a working concentration of 0.1 µM. Images were acquired using the OperaPhenix (Perkin Elmer, USA) with laser configurations as described by (Carling et al., 2022). Harmony software (Perkin Elmer) was used for downstream image analysis to measure number of puncta, size and fluorescent intensity, selecting for NeuO-positive cells (analysed with William McGuiness).

2.9 Multielectrode Array (MEA) Recordings

Primary cortical neurons were cultured as described in **2.5.3** and seeded in PDL and feeder layer coated Multiwell-MEA plates (Multi Channel Systems) at a density of 3000 cells/mm^2 in complete NBA. All parameters and recordings were set and performed by Dr Daniel Rial. Electrophysiological activity was recorded using the MEA-2100 multi-well system (MultiChannel Systems, Boston, USA) equipped with the Multiwell-Analyzer v 1.8.7.0 software for post-recording analysis. Each plate consisted of 24 wells (Model 24W300/30G-288 V.232), each containing 12 electrodes of 30 µm diameter each, 300 µm apart. Electrode number 9 was assigned as the stimulating electrode. All MEA recordings were conducted at DIV 14 at 37°C in culture medium without perfusion, as described in (Fan et al., 2019). The total period of recording was 150 seconds, where different levels of current (1, 10, 25 or 50 uA) were injected from 60 s to 120 s period (inter-stimulus interval 250 ms). Total period (150 s) was used for analysis. Spikes were detected at 20000 Hz sampling rate. Butterworth order 4 low pass filter with a cut-off frequency of 3500 Hz and an order 2 high-pass filter with a cut-off frequency of 10 Hz were applied to data acquisition. Spike count was defined as plus or minus 5 standard deviations from baseline in amplitude. A burst was defined as 5 active electrode units within 5 ms. A network burst was defined as 5 consecutive connected active electrode units within 5 ms of analysis. Bicuculline (10 uM) was added to culture solution 5 minutes before recording.

2.10 Flow Cytometry

Primary fibroblasts were harvested at confluency and samples were transferred to 5 mL round-bottomed FACS tubes (FisherScientific) at 1'000'000 cells/tube. Cells were pelleted and washed with PBS twice and then incubated with LysoTracker® Green DND-26 (ThermoFisher) at a working concentration of 200 nM in PBS for 10 minutes at room temperature, shielded from light. Following this, cells were centrifuged at 1500 rpm for 5 minutes, supernatant discarded, then washed and resuspended in FACS buffer (10% BSA, 5 mM EDTA in PBS) with Sytox Blue DNA stain (ThermoFisher). Samples were run using the BD FACSCanto™ II system and FlowJo_V10 software (BD Biosciences) was used for data analysis. This experiment was performed to collect preliminary data only (1 technical replicate).

2.11 RNA Extraction, cDNA synthesis and qPCR

Total RNA was extracted from cerebellar tissue using the Maxwell® RSC Instrument and simplyRNA Tissue Kit (Promega) as per manufacturer's instructions. RNA quantification and integrity was established using Nanodrop (Thermo Fisher) and Bioanalyzer (Agilent). cDNA was synthesised using 2 µg RNA per reaction and the High-Capacity cDNA Reverse Transcription Kit (Applied Biosystems). 20 µl reactions were set up in triplicates with 20 ng cDNA, 360 nM F + R primers and 10 µL Fast SYBR™ Green Master Mix (ThermoFisher) per well in MicroAmp™ Fast Optical 96-Well Reaction Plate (ThermoFisher), sealed with MicroAmp™ Optical Adhesive Film (ThermoFisher) and run on a 7500 Fast Real-Time System PCR machine (Applied Biosystem). The amplification reaction protocol was established as: 1 cycle at 95°C for 20 secs; 40 cycles at 95°C for 3 secs and 60°C for 30 secs. A melt dissociation curve was established to determine that only one PCR product was amplified (heating ramp from 55 to 95°C). All reactions were normalised to internal control

housekeeping genes glyceraldehyde 3-phosphate dehydrogenase (*Gapdh*), 40S ribosomal protein S16 (*S16*) and peptidylprolyl isomerase A (*Ppia*) and fold changes were calculated using ΔΔ Ct method and expressed relative to a control genotype. Primers used in qPCR experiments are listed in **Table 2-6**.

***Table 2-6*| Table of qPCR primers used**

Gene	Forward Sequence (5' - 3')	Reverse Sequence (5' - 3')
C1qa	AAAGGCAATCCAGGCAATATCA	TGGTTCTGGTATGGACTCTCC
Ctsd	GCTTCCGGTCTTTGACAACCT	CACCAAGCATTAGTTCTCCTCC
Cd68	TGCCTGACAAGGGACACTTC	TGGTGGCTTACACAGTGGAC
Gapdh	CGGCCGCATCTTCTTGTG	CCGACCTTCACCATTTTGTCTAC
Gfap	GCAGAAGCTCCAAGATGAAACC	CGAACTTCCTCCTCATAGATCTTC
HexB	AATGGTCAGCCGTGGAATAG	CATAGCTGGAATGCTGTAGACG
Laptm5	GATGCCGTACCTCAGGATGG	CTCCCGGTTCTTGACCACG
Ly86	TATACTATGCCGGCCCTGTC	GGGTCCCCTGAGATTGAGTT
Oxr1 C	CCATAAATACACTCTGGTAGTGTC	TTTGGTCGGAAAGATTCAGG
Oxr1 FL	CAGTCGTGACTGGACAGGTTT	ATGGGCTACATCTGGAGTCG
Ppia	AGTTTTTTATCTGCACTGCCAAGA	CCTTCCCAAAGACCACATGCT
S16	TTCTGGGCAAGAGCGATT	GATGGACTGTCGGATGGCA
Tbc1d24	GGAGATGAGAGACATTTGGTCC	GCTTGCCTCCGAATTTAGTC
Tgfβ	TGAGTGGCTGTCTTTTGACG	GGTTCATGTCATGGATGGTG
Trem2	CTGGAACCGTCACCATCACTC	CGAAACTCGATGACTCCTCGG

2.12 Bulk RNA Sequencing

Total RNA was extracted from *Oxr1*$^{wt/wt}$ and *Oxr1*$^{tm1d/tm1d}$ whole cerebellar tissue at P19 using the Maxwell® RSC Instrument (Promega) with DNase treatment. Bioanalyzer RNA 6000 Nano assay (Agilent) was used to assess RNA integrity and quantity and run on the Bioanalyzer 2100 system (Agilent Technologies, CA, USA). Samples were sent to Cambridge Genomic Services (University of Cambridge, U.K.) for sequencing library preparation and next-generation sequencing. Downstream analysis to detect differential gene expression was performed by Cambridge Genomic Services. TruSeq Stranded Total RNA library preparation kit (Illumina) was used to generate sequencing libraries and index coding, as per manufacturer's instructions. Cluster generation of index-coded samples was performed on PE Cluster Kit cBot-HS (Illumina) using the cBot Cluster Generation System (Illumina) and single-end sequencing was carried out with the NextSeq500 platform (Illumina). 31 to 40 million reads per sample was achieved.

Figure 2.2 summarises the employed analysis workflow and was kindly provided by Cambridge Genomic Services. In brief, quality control of raw data was performed using FastQC software (v0.11.4) and reads were trimmed using TrimGalore (v0.5.0). Spliced Transcripts Alignment to a Reference (STAR) (v2.7.1) was utilised to map reads to Ensembl Mus_musculus GRCm38 (release 99) reference genome. HTSeq (v.0.6.1) software was applied to calculate the number of reads that map to reference genome. Principal Component Analysis (PCA) plots and heat maps were used to assess sample clustering and were based on normalised and rlog transformed counts obtained with DESeq2 (v.1.24.1, R version 3.6.1). Pairwise differential gene expression analysis was performed between genotypes using counted reads and edgeR (v3.26.5, R v.3.6.1); the Benjamini-Hochberg method was used to adjust p-values for multiple testing of the FDR. Genes with false discovery rate (FDR) values of FDR≤0.05, and more stringently as FDR≤0.01, were assigned

as differentially expressed genes (DEGs). Full data analysis report available upon request. Subsequent Gene Ontology (GO) enrichment analysis of DEGs (FDR≤0.01) was performed using ordered queries in g:Profiler and *GOrilla* (Gene Ontology enRIchment anaLysis and visuaLizAtion tool).

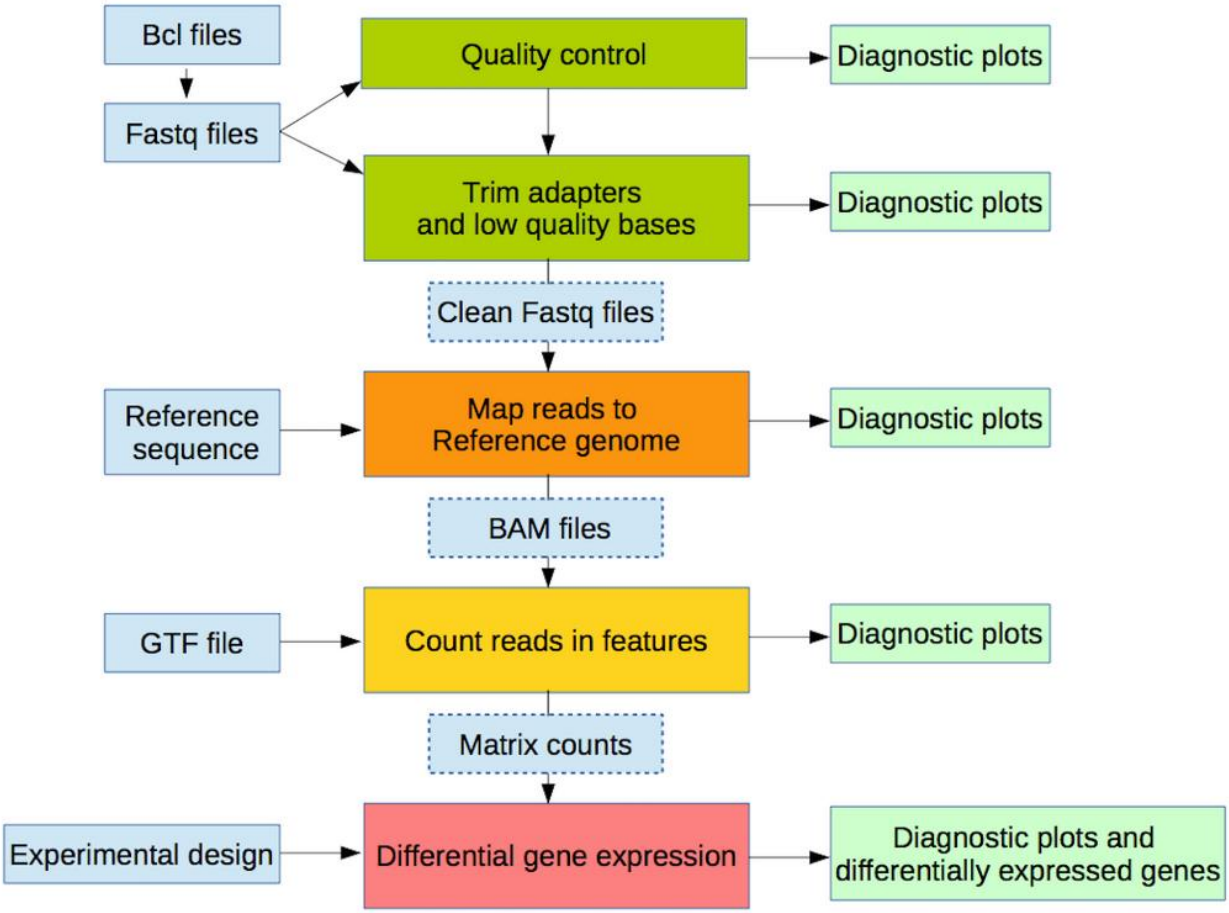

***Figure 2.2*| RNA-seq analysis workflow provided by Cambridge Genomic Services**

2.13 Protein Extraction, SDS-PAGE and Western Blotting

2.13.1 Protein Extraction

From tissue: Tissue samples were cut in to small pieces and placed in to BioPulverizer Lysing Matrix D tubes (MP Biomedicals) with cold radioimmunoprecipitation assay buffer with cOmplete™ Mini EDTA-free protease and phosphatase inhibitors (Roche) (RIPA+PPI). Samples were homogenised for 2 x 15 secs in a MP Biomedicals™ FastPrep-24™ Instrument (Fisher Scientific), spun down for 10 mins, 13'000 rpm at 4˚C. Supernatant was aliquoted and stored at -80 ˚C.

From cells: Cells were scraped and collected in cold RIPA+PPI buffer. Lysates were incubated on a wheel at 4˚C for 30 minutes and spun down for 10 mins, 13'000 rpm at 4˚C. Supernatant was aliquoted and stored at -80 ˚C.

2.13.2 SDS-PAGE and Western Blotting

Protein samples were thawed on ice and quantified using the DC Protein Assay (Bio-Rad) method and bovine serum albumin (BSA) protein standards. Samples were mixed with 5X NuPAGE loading dye (ThermoFisher) and 10X NuPAGE reducing agent (ThermoFisher), then heat denatured. Samples were run on NuPAGE Bis-Tris gels (ThermoFisher) for ~50 minutes at 200V in MOPS or MES buffer (ThermoFisher), followed by dry transfer using an iBlot Gel Transfer system (Invitrogen). As standard, nitrocellulose iBlot Transfer Stacks (Invitrogen) were used; polyvinylidene difluoride (PVDF) iBlot Transfer Stacks (Invitrogen) were used for the detection of lower molecular weight proteins. Membranes were blocked in 4% milk in PBS + 0.1% Tween (PBS-T). Primary antibodies were incubated rocking O/N at 4˚C. Membranes were then washed in PBS-T and incubated rocking with IRDye secondary antibodies (LiCor Biosciences) for 1 hour at RT. Membranes were washed x2 in PBS-T and once in PBS before drying. Membranes were imaged using LI-COR Odyssey® CLx and

analysed using Image Studio Lite Version 5.2 Software (LiCor Biosciences). All antibodies used are listed in **Table 2-7**.

***Table 2-7*| Table of Antibodies used for Western Blot**

Antibody	Supplier	Catalogue Number	Dilution
β-actin	Sigma Aldrich	A2066	1:3000
Anti-Mouse	LI-COR Biosciences	926–68,070	1:10000
Anti-Rabbit	LI-COR Biosciences	926–32,211	1:10000
Lamp1	Abcam	ab24170	1:500
LC3A/B	Cell Signalling Technologies	4108S	1:1000
Oxr1	Proteintech	13514-1-AP	1:1000
Rab7	Abcam	ab137029	1:1000
SQSTM1/p62	Abcam	ab56416	1:1000
α-Tubulin	Santa Cruz Biotechnology	T9026	1:3000

2.14 Immunoprecipitation and Mass Spectrometry

Tissue samples were lysed using NP40 lysis buffer and pre-cleared using mouse IgG-Agarose (Sigma) ahead of immunoprecipitation (IP). Pre-cleared lysates were incubated and immunoprecipated using EZview Red Anti-HA Affinity Gel (Sigma) and listed protocol. After washing the bead pellet, bound proteins were eluted in sample buffer and gel beads were removed by heat denaturation and centrifugation. Lysate and IP samples were 4-12% Bis-Tris gel in MOPs and stained with Coomassie Blue prior candidate interactor band excision. Western blotting was also performed as described in **2.13.2,** using anti-HA (mouse, 1:20000) (Sigma). Protein lysate preparation was prepared by Associate Professor Peter Oliver. IP, SDS-PAGE and gel band preparation were kindly performed by Helen Hilton (Protein Core, MRC Harwell). Selected bands were prepared and sent for mass spectrometry analysis at the Functional Genomics and Proteomics Facility, University of Birmingham. Full details are outlined in (Lee, 2021). In short, tandem mass spectrometry was performed using a Q-Exactive HF hybrid quadrupole-orbitrap mass spectrometer via a nano-flow LC system with reverse phase column for protein/peptide identification.

2.15 Transmission Electron Microscopy (TEM)

For TEM preparations, *Oxr1*$^{w/wt}$ and *Oxr1*$^{tm1d/tm1d}$ littermates (n = 3) were perfused at P19 with saline and then 2.5% glutaraldehyde + 2% PFA in 0.1M sodium cacodylate buffer. Cerebella were cut in to 1 mm cubed blocks from the midline using a brain blade matrix. This was carried out by Associate Professor Peter Oliver. The remaining processing was carried out as described in (Castroflorio et al., 2021). Images were acquired using a FEI Tecnai T12 TEM at 100 kV and an ORIUS SC1000 CCD camera (Gatan). Image acquisition was performed by Dr Errin Johnson (Dunn's School of Pathology, University of Oxford).

2.16 Data Analysis and Statistics

FIJI (Fiji Is Just ImageJ) Windows (64-bit) and ZEISS ZEN (Black and Blue editions) microscopy Software were used to process and analyse confocal microscopy images. Western Blot images were analysed using Licor Image Studio^{TM} Lite Quantification Software. All numerical data were analysed using GraphPad Prism version 9.0 (GraphPad Software, Inc) and appropriate statistical analysis and post-hoc test were applied (ns ≥ 0.05, * ≤ 0.05, **≤0.01, *** ≤ 0.001, **** ≤ 0.0001). Data are represented as mean ± SEM, unless otherwise stated in figure legends. Broadly, an unpaired Student's t-test was used for two normally distributed data sets and one or two-way ANOVA was applied to normally distributed data sets with more than two experimental groups. Alternative analyses are stated in figure legends where used.

RESULTS I

Chapter 3 : Investigating the molecular mechanisms of *Oxr1*

3.1. Introduction

3.1.1. Constitutive loss of *OXR1* causes early-onset and rapid progressive neurodegeneration in loss-of-function patients and Oxr1 knockout mouse model

Oliver *et al.* (2011) established that *bella*, a mouse model lacking the entire *Oxr1* locus and a second adjacent gene (*Abra*), showed progressive ataxia, cerebellar neurodegeneration and early postnatal death. Finelli *et al.* (2016) reaffirmed that constitutive *Oxr1* knockout mice (*Oxr1*$^{tm1d/tm1d}$) replicated this phenotype. Of late, patients with bi-allelic loss-of-function (LoF) mutations in *OXR1* (LoF-*OXR1*) have been reported to cause cerebellar-specific pathology, ataxia and seizures in childhood, thus sharing a number of overlapping early postnatal features to *Oxr1* knockout mouse models (Lin et al., 2022; Oliver et al., 2011; Wang et al., 2019). These shared disease characteristics point towards conserved OXR1 function between humans and mice, therefore utilising *Oxr1*-deleted mouse models may further our understanding of the pathophysiology driving cellular dysfunction and phenotypic onset in the absence of *OXR1* expression.

3.1.2. Molecular pathways underpinning disease pathogenesis in *OXR1*-deficient models are unclear

Early studies identified *OXR1* as a critical defence factor against oxidative stress (OS) in eukaryotic organisms (Elliott & Volkert, 2004; Volkert et al., 2000); several reports have further supported the finding that depletion of *OXR1* in mammalian cells increases their sensitivity to OS, such as exogenous H_2O_2 treatment, inducing apoptosis via the p53 signalling axis (Lin et al., 2022; Oliver et al., 2011; Yang et al., 2015; X. Zhang et al., 2018). As post-mitotic cells, neurons are particularly vulnerable to OS due to their high rate of

energy consumption leading to increased ROS generation and hold limited antioxidant defence mechanisms compared to other cell types (Cobley et al., 2018; Wang & Michaelis, 2010). In particular, wild type cerebellar granule cells (CGCs) show distinct selective neuronal vulnerability to OS-related insults (X. Wang et al., 2009), thus it was hypothesised that OS underpins the observed cerebellar pathology and neurological phenotype.

Interestingly, *OXR1*-deficient lymphoblasts and iPSC-derived neurons from LoF-OXR1 patients also demonstrated increased sensitivity to OS-challenges and cell death, although this was coupled with dysregulation in other pathways, such as autophagy and mitochondrial function (Lin et al., 2022); conversely, *OXR1*-deficient fibroblasts did not exhibit significant signs of, nor increased susceptibility to, OS (Wang et al., 2019). Furthermore, biomarkers of OS were not identified in LoF-*OXR1* patient blood counts or cerebrospinal fluid analysis (Lin et al., 2022; Wang et al., 2019), suggesting that OS is not the primary cause of the observed neuropathology. In the *Oxr1* knockout mouse, OS pathology was limited to oxidative DNA damage at the late disease stage in the cerebellar granule cell (Oliver et al., 2011); however, the cause of the distinctive pathology was still unclear.

Using a combination of both LoF-*OXR1* patient-derived fibroblasts and neuronal knockdown in Drosophila of the *OXR1* fly homolog, *mustard* (*mtd*), through RNA interference (RNAi), the authors revealed distinct lysosomal abnormalities (Wang et al., 2019). LysoTracker is commonly used basic dye that labels acidic organelles, such as lysosomes (Bjorkoy et al., 2005; Mindell, 2012). LysoTracker staining of patient-derived fibroblasts showed significant accumulation of lysosomal compartments compared to control individuals (Wang et al., 2019). In addition to this, Drosophila lacking neuronal expression of *mtd* displayed an increasing number of abnormal lysosomal structures in *mtd*-deficient R7 photoreceptors, strongly suggesting a role for *OXR1* in lysosomal function

(Wang et al., 2019). Whether this lysosomal pathway disruption is a cause or a consequence of disease pathology is yet to be determined.

In order to begin to identify pre-symptomatic pathways that might instigate neurodegeneration, a microarray transcriptomics approach was taken using P18 whole cerebellar tissue from wild type and *Oxr1* knockout (*Oxr1*$^{tm1d/tm1d}$) mice. This method identified 20 differentially expressed genes (DEGs) that reached statistical significance, all of which were upregulated in *Oxr1*$^{tm1d/tm1d}$ cerebellar tissue (**Figure 3.1**) (Svistunova, 2020). Functional enrichment analysis of these data revealed that a subset of DEGs, such as chemokine (C-X3-C motif) receptor 1 (*Cx3cr1*) and TYRO protein tyrosine kinase binding protein (*Tyrobp*), are implicated in the regulation of neuron apoptotic processes, negative regulation of long-term synaptic potentiation and microglial cell activation (Svistunova, 2020). Moreover, DEGs were enriched in pathways relating to the innate immune response, including complement component 1q chains (*C1qa, C1qb, C1qc*), lymphocyte antigen 86 (*Ly86*) and chemokine (C-C motif) ligand 3 (*Ccl3*) (Svistunova, 2020). Lysosomal enzymes were also found to be significantly upregulated (Svistunova, 2020). This study is limited by the use of whole cerebellar tissue and does not consider post-transcriptional events, yet it was somewhat surprising that suggested pathways from previous transcriptomic studies of *OXR1*-depleted cells did not overlap (Svistunova, 2020; Yang et al., 2015). Overall, the microarray analysis of presymptomatic *Oxr1* knockout cerebellar tissue suggested that neuroinflammation and lysosomal dysfunction likely precede OS and neurodegeneration, identifying these processes as possible disease-modifying pathways.

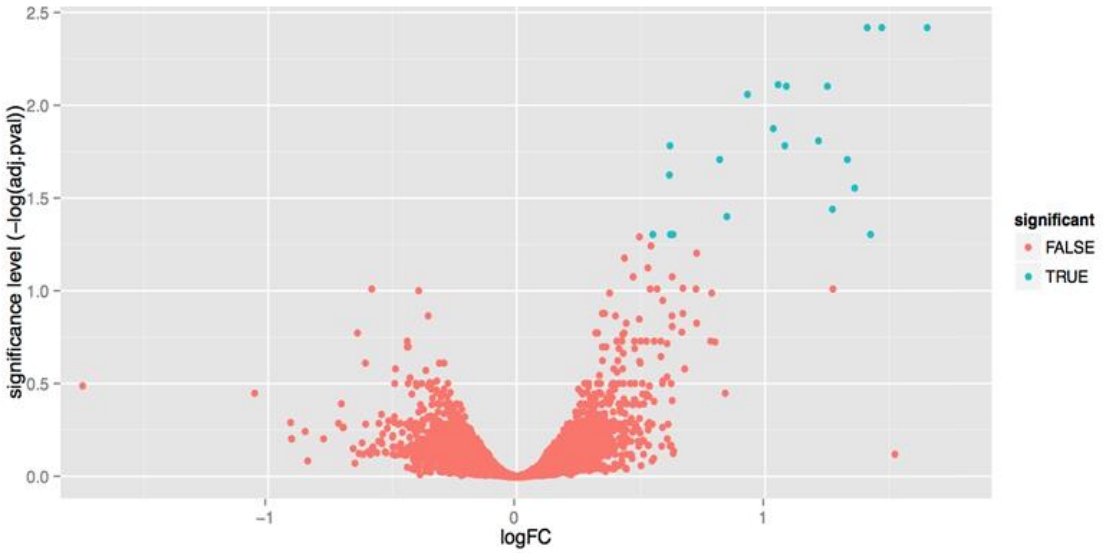

***Figure 3.1*| Volcano plot of microarray transcriptomic data from wild type and *Oxr1* knockout cerebellar tissue at P18**

Volcano plot of microarray data illustrating 20 significantly upregulated genes in *Oxr1* knockout (KO) cerebellar tissue compared to wild type (WT) tissue. Taken from (Svistunova, 2020). Data are presented as log2 fold change (FC) of normalised WT vs KO expression per gene, plotted against significance level of differential expression. Genes that are expressed over 1.5-fold in KO mice versus wild-type with a <0.05 adjusted p-value are considered as significantly up-regulated (TRUE, blue).

- - significantly upregulated transcripts in *Oxr1* KO cerebellum compared to WT (TRUE)
- - non-significant transcripts (FALSE)

3.1.3. Chapter 3 Aims

Since overlapping pathological features are present in mice and human patients lacking *OXR1*, it is likely that there are shared underlying molecular pathways. Therefore, this chapter aimed to further characterise the role of Oxr1 *in vivo* and *in vitro* by studying key pathways that are disrupted in the absence of *Oxr1* expression, using the *Oxr1* constitutive knockout mouse model (*Oxr1*$^{tm1d/tm1d}$). Importantly, clues from *OXR1*-deficient cells imply that OXR1 plays a role in lysosome biology. Further to this, microarray data suggested that neuroinflammatory process and lysosomal dysfunction precede OS and neurodegeneration; however, this method carries a number of limitations, including potentially low specificity and sensitivity (Rao et al., 2018). Therefore, RNA-seq was utilised for a more sensitive transcriptomic analysis of *Oxr1* knockout (Hom) cerebellar tissue, with the aim of identifying more dysregulated pathways in the absence of *Oxr1* expression that may underpin pathological features observed in *Oxr1* knockout mice and LoF-*OXR1* patients. From this, the role of *Oxr1* in these enriched pathways was explored using a combination of histopathology, protein analysis and *in vitro* cellular assays.

3.2. Results

3.2.1. Pre-symptomatic RNA-Seq data reveals approximately 200 significantly dysregulated genes in Oxr1 knockout cerebellar tissue

This chapter aimed to characterise the molecular mechanisms underpinning cerebellar dysfunction and disease progression in constitutive *Oxr1* knockout mice. In an attempt to uncover cellular pathways dysregulated prior to cell death, an unbiased transcriptomic approach was taken, whereby total cerebellar RNA was isolated from 5 pairs of male matched littermates, with 3 additional wild-type (WT) mice from the litters (WT, n=8; Hom, n=5) and sent for bulk RNA Sequencing (RNA-Seq) at the Cambridge Genomic Services (University of Cambridge). At P19, Hom mice exhibit an abnormal gait and loss of balance demonstrating the onset of ataxia, yet significant oxidative DNA damage and cell death are not observed in the cerebellum (Finelli, Paramo, et al., 2019; Oliver et al., 2011). Therefore, P19 was chosen to avoid aberrant gene expression from apoptotic cells observed in end-stage disease pathology in constitutive *Oxr1* knockout mice (Oliver et al., 2011). Furthermore, compared to the cerebellar microarray data collected from age and sex-matched P18 male mice (Svistunova, 2020), this additional day of disease progression may provide more functional clues in understanding the molecular role of *Oxr1*. While there have been no reported sex differences in *Oxr1* knockout mice thus far, this RNA-Seq study utilized male mice to enable a comparison with the previously acquired microarray data.

Initial data quality control, filtering and subsequent analyses revealed 458 significant DEGs in Hom cerebellar tissue with an adjusted-p value (q) ≤0.05, of which 270 genes were found to be upregulated (**Figure 3.2**). When applying more stringent parameters of q≤0.01, this identified 197 DEGs (139 upregulated, 58 downregulated) (**Appendix. 1**). The top 20 highly significant DEGs based on false discovery rate (FDR) values

were all upregulated in Hom cerebellar tissue and each associated with neuroinflammation or lysosomal function (**Table 3.1**).

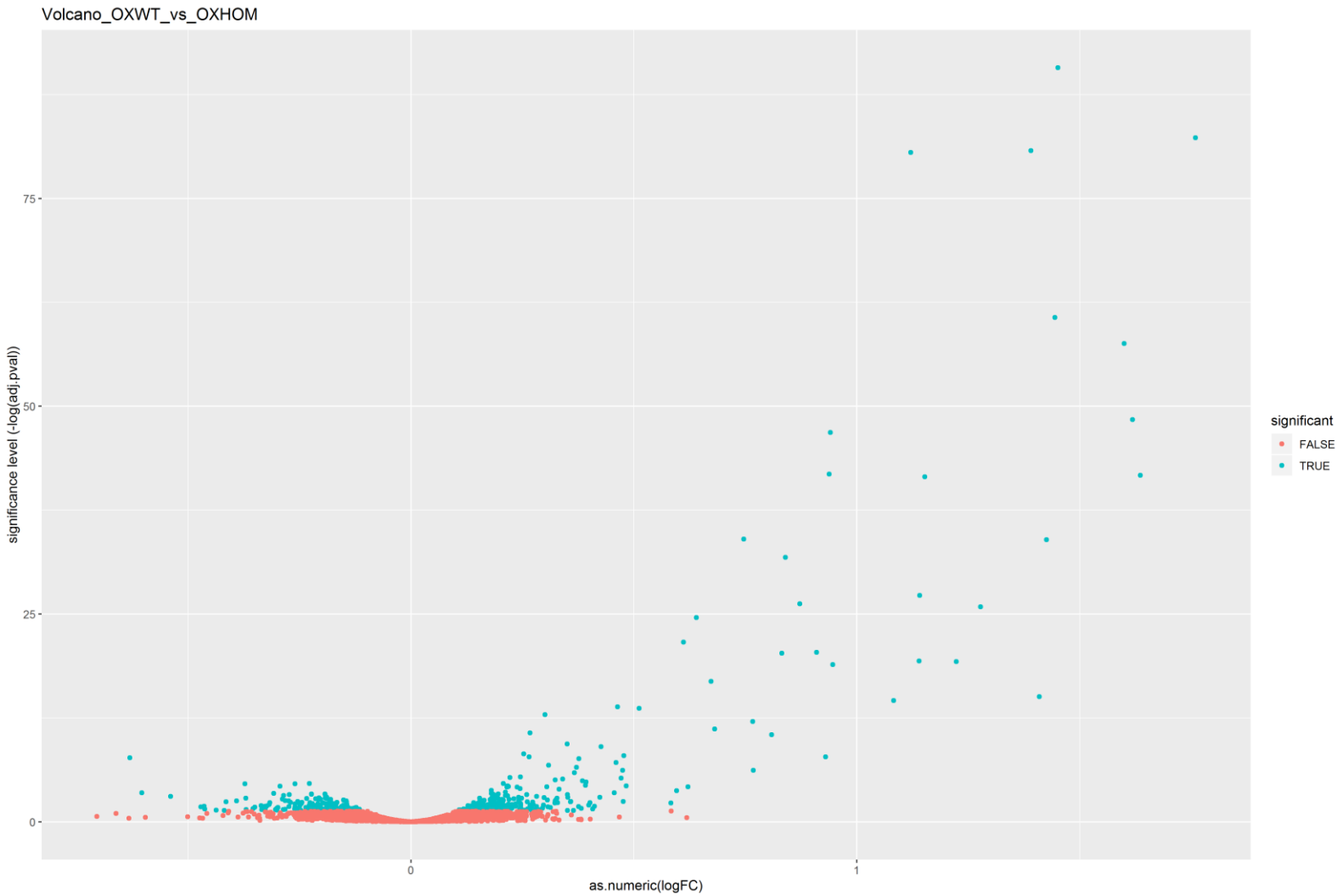

***Figure 3.2*| Volcano plot depicting RNA Sequencing data**

Volcano plot of RNA Sequencing data illustrating differentially expressed genes in *Oxr1* knockout (KO) cerebellar tissue compared to wild type (WT) tissue.
• - genes that are significantly differentially expressed • - genes that are not significantly differentially expressed

Table 3-1 **| Top 20 significantly differentially expressed genes ranked by false discovery rate (FDR) (adjusted p-value).**

Genes highlighted in green indicate a role in neuroinflammatory processes; blue indicates a role in lysosomal function.

Ranking	Gene Symbol	Gene	Log_2FC	FDR
1	*C1qa*	Complement component 1, q subcomponent, alpha polypeptide	1.45	1.9E-91
2	*Mpeg1*	Macrophage expressed gene 1	1.76	5.0E-83
3	*C1qb*	Complement component 1, q subcomponent, beta polypeptide	1.39	1.8E-81
4	*Hexb*	Hexosaminidase B	1.12	2.9E-81
5	*C1qc*	Complement component 1, q subcomponent, C chain	1.44	2.2E-61
6	*Tyrobp*	TYRO protein tyrosine kinase binding protein	1.60	2.8E-58
7	*Fcrls*	Fc receptor-like S, scavenger receptor	1.62	4.2E-49
8	*Ctss*	Cathepsin S	0.94	1.4E-47
9	*Cx3cr1*	Chemokine (C-X3-C motif) receptor 1	0.94	1.5E-42
10	*Cd68*	CD68 antigen	1.64	2.1E-42
11	*Laptm5*	Lysosomal-associated protein transmembrane 5	1.15	3.0E-42
12	*Plek*	Pleckstrin	0.75	9.6E-35
13	*Ly86*	Lymphocyte antigen 86	1.43	1.1E-34
14	*Ctsz*	Cathepsin Z	0.84	1.5E-32
15	*Lyz2*	Lysozyme 2	1.14	5.7E-28
16	*Gfap*	Glial fibrillary acidic protein	0.87	5.8E-27
17	*Trem2*	Triggering receptor expressed on myeloid cells 2	1.28	1.3E-26
18	*Ctsd*	Cathepsin D	0.64	2.6E-25
19	*B2m*	Beta-2 microglobulin	0.61	2.5E-22
20	*Olfml3*	Olfactomedin-like 3	0.91	4.2E-21

Next, this list of 20 genes was compared to microarray data from P18 cerebellar tissue determined to be significantly differentially expressed based on p-value (p≤0.05), which also identified 20 genes. This comparison found 14 overlapping genes between the data (**Figure 3.3**), further affirming the presence of neuroinflammatory and lysosomal dysfunction in *Oxr1* knockout cerebellum. For example, complement C1q genes (*C1qa*, *C1qb* and *Clqc*) are essential components of the classical complement activation system in the innate immune response (Fouet et al., 2021; Schartz & Tenner, 2020); these three genes were present in both DEG lists. Similarly, genes encoding lysosomal enzymes cathepsins D, S, Z (*Ctsd*, *Ctss* and *Ctsz*) and hexosaminidase subunit beta (*Hexb*) that degrade target substrates within lysosomes were also found to be highly upregulated in these data (Bonam et al., 2019; Kuil et al., 2019).

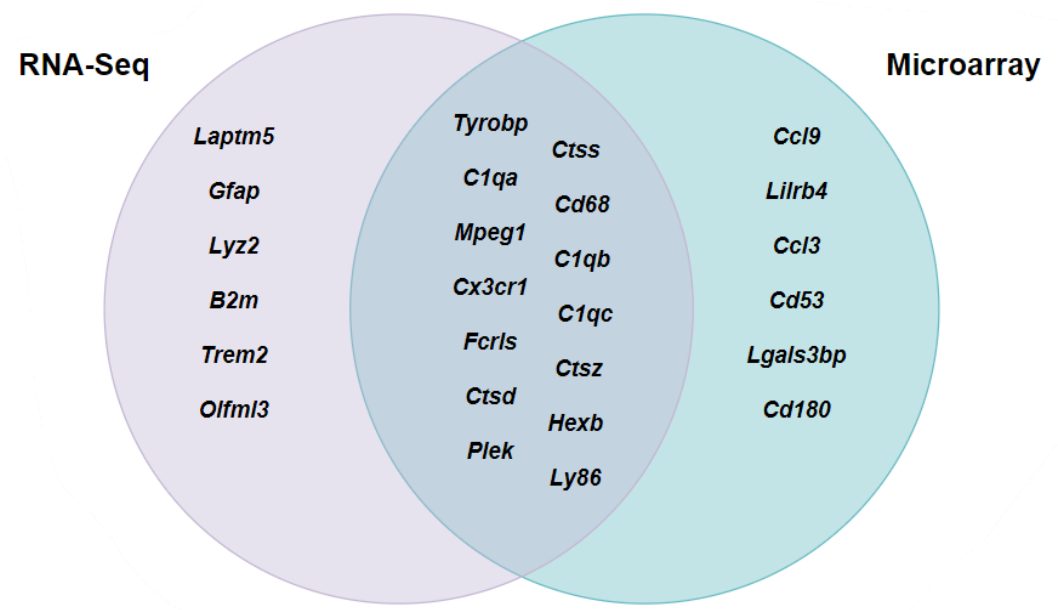

***Figure 3.3*| Graphic representation showing a comparison of P18 microarray data and P19 RNA-Sequencing data**

Venn diagram depicting overlap of the 20 most significant differentially expressed genes identified at P18 by microarray and P19 by RNA sequencing of cerebellar tissue from wild type and *Oxr1* knockout mice. P18 microarray data was collected from male littermate pairs of n=4 WT and Hom mice. P19 microarray data was collected from 5 male littermate pairs of WT and Hom mice, as well as an additional 3 male WT littermate controls (WT, n=8; Hom, n=5).

3.2.2. Gene Ontology and Pathway analysis predict a role for Oxr1 in modulating neuroinflammation and lysosomal function

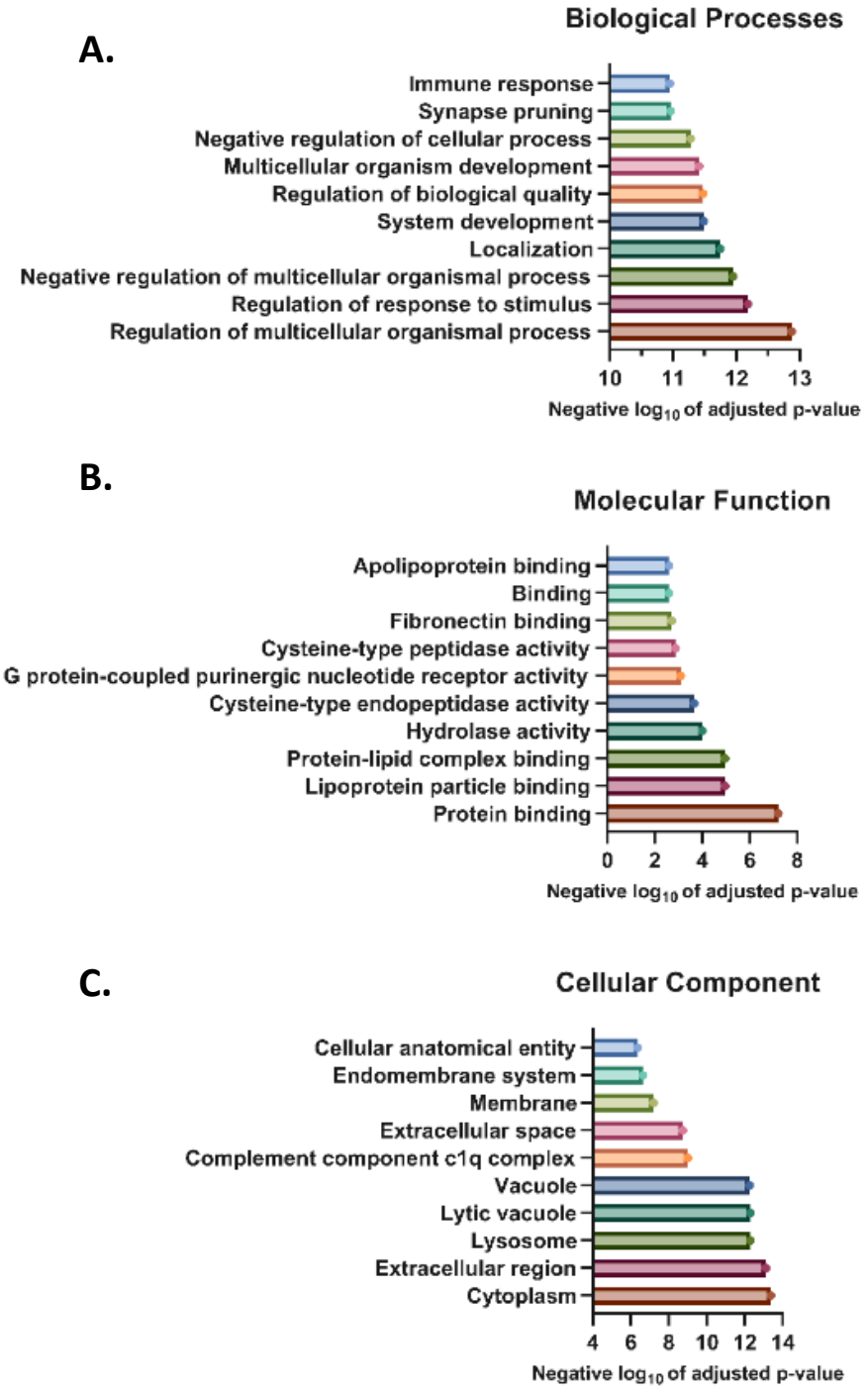

***Figure 3.4*| Gene Ontology (GO) Term Analysis of differentially expressed genes in P19 *Oxr1* knockout cerebellar tissue**

GO classification of the RNASeq data using a q-value ranked list to perform an ordered query. Results are presented as negative $\log_{10}$ scale of adjusted enrichment p-values and summarised by the categories (A) Biological Processes, (B) Molecular Function and (C) Cellular Component.

Gene Ontology (GO) analysis was subsequently conducted using a ranked list of the 197 statistically significant (q≤0.01) DEGs in an attempt to identify molecular pathways that are dysregulated in *Oxr1* knockout cerebellar tissue. This significance threshold was chosen to heighten confidence values, whilst maintaining hypothesis-free functional enrichment pathway analysis. An overview of the top ten enriched terms for biological processes (**Figure 3.4A**), molecular function (**Figure 3.4B**) and cellular component (**Figure 3.4C**) are presented.

Biological process GO terms demonstrated a potential role for *Oxr1* in the immune response, synapse pruning and CNS development (**Figure 3.4A**). Common themes identified in GO molecular function enrichment analysis implied a critical role for Oxr1 in protein binding, protein-lipid binding, as well as hydrolase activity (**Figure 3.4B**). Cellular component analysis showed that a majority of functional changes occur in the cytoplasm, extracellular region and in the lysosome (**Figure 3.4C**). Assessing affected biological networks using Reactome and Kyoto Encyclopedia of Genes and Genomes (KEGG) pathway databases showed that these transcriptional profiles largely mapped to the (innate) immune system and lysosomal pathway (**Figure 3.5**)(Fabregat et al., 2017; Kanehisa et al., 2017), which further supports the notion of inflammatory and lysosomal dysfunction in this mouse model.

Table 3-2 presents the DEGs involved the predicted dysregulated pathways, a number of which are in the top 20 significant DEGs (**Table 3-1**). Further annotations predicted that loss of *Oxr1* affects interactions with transcription regulatory motifs in DNA, the microglia pathogen phagocytosis pathway, as well as correlations to human disease and abnormal phenotypes, including decreased serum complement factor I and complement deficiency (**Appendix. 2**).

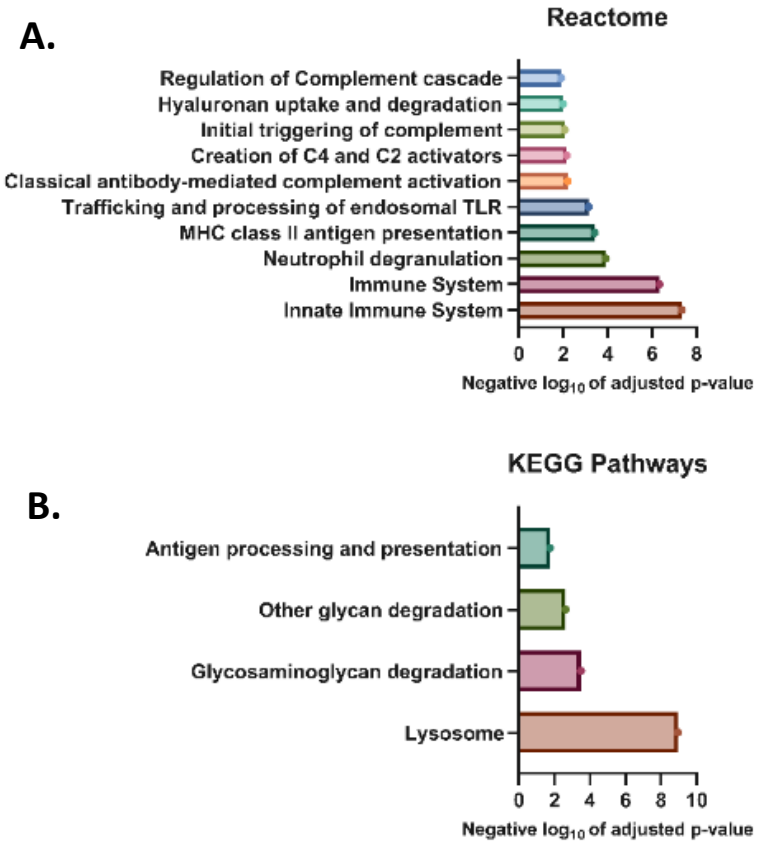

***Figure 3.5*| Reactome and Kyoto Encyclopedia of Genes and Genomes (KEGG) pathway analysis of differentially expressed genes in P19 *Oxr1* knockout cerebellar tissue**

(A) Reactome and (B) KEGG pathway functional enrichment using a q-value ranked list to perform an ordered query. Results are presented as negative $\log_{10}$ scale of adjusted enrichment p-values.

Separate GO analysis of upregulated and downregulated DEGs in Hom cerebellar tissue demonstrated that majority of impacted pathways are driven by upregulated genes (**Appendix. 3**). Moreover, when investigating significantly downregulated genes, molecular functional annotation predicted primary active transmembrane transporter activity pathways to be disrupted ($q=1.985\times10^{-2}$) (*Mt-Nd6, Atp2b4, Abca7, Abcc8*).

In summary, RNA-Seq analysis of pre-symptomatic Hom cerebellar tissue demonstrated that neuroinflammatory and lysosomal pathways are dysregulated prior to significant pathological features in the absence of *Oxr1* expression. Therefore, the role of *Oxr1* in these pathways warrants further investigation.

Table 3-2| **Reactome and KEGG predicted functional interaction networks and associated differentially expressed genes.**

Pathway	Genes	Adjusted p value
Reactome		
Innate Immune System	*C1qa, C1qb, Hexb, C1qc, Tyrobp, Ctss, Cd68, Ly86, Ctsz, Lyz2, Trem2, Ctsd, B2m, C4b, Grn, Gusb, Ctsl, Nckap1l, Lgmn*	4.55E-08
Immune System	*C1qa, C1qb, Hexb, C1qc, Tyrobp, Ctss, Cd68, Ly86, Ctsz, Lyz2, Trem2, Ctsd, B2m, C4b, Csf1r, Lag3, Grn, Gusb, Ctsl ,Inpp5d, Nckap1l, Lgmn*	4.66E-07
Neutrophil degranulation	*Hexb, Tyrobp ,Ctss, Cd68, Ctsz, Lyz2, Ctsd, B2m, Grn, Gusb, Nckap1l, Ctsa, Ctsc, Gns*	1.25E-04
MHC class II antigen presentation	*Ctss, Ctsd ,Lag3, Ctsl, Lgmn, Ctsa, Ctsc*	3.85E-04
Trafficking and processing of endosomal TLR	*Ctss, Ctsl, Lgmn, Ctsb*	7.34E-04
Classical antibody-mediated complement activation	*C1qa, C1qb, C1qc*	6.34E-03
Creation of C4 and C2 activators	*C1qa, C1qb, C1qc*	7.24E-03
Initial triggering of complement	*C1qa, C1qb, C1qc*	8.63E-03
Hyaluronan uptake and degradation	*Hexb, Gusb, Hexa*	1.03E-02
Regulation of Complement cascade	*C1qa, C1qb, C1qc*	1.25E-02
KEGG Pathways		
Lysosome	*Hexb, Ctss, Cd68, Ctsz, Ctsd, Gusb, Ctsl, Lgmn, Ctsa, Ctsc, Gns, Hexa*	1.11E-09
Glycosaminoglycan degradation	*Hexb, Gusb, Gns, Hexa, Arsb*	3.23E-04
Other glycan degradation	*Hexb, Hexa, Man2b1, Man2b2*	2.32E-03
Antigen processing and presentation	*Ctss ,B2m, Ctsl, Lgmn*	1.82E-02

3.2.3. Loss of *Oxr1* induces disruption of neuroinflammatory processes at both pre-symptomatic and disease stage time points.

RNA-Seq data from P19 cerebellar tissue demonstrated that loss of *Oxr1* leads to differentially expression of genes implicated in neuroinflammatory processes prior to cell death observed in constitutive knockout mice (Oliver et al., 2011). Gene Ontology enrichment analysis and visualization tool (GOrilla) was utilised to contextualise and envisage significant relationships between enriched GO terms of biological processes from these set of ranked data (Eden et al., 2007; Eden et al., 2009). Hierarchical clustering of these annotations and predicted pathways confirmed that the most significantly enriched terms relate to the immune response, more specifically classical compliment pathway activation and microglial cell activation (**Appendix. 4**).

Given that glial fibrillary acidic protein (*Gfap*), a marker of reactive astrocytes and astrogliosis, is a highly ranked DEG (q=5.8E-27), it was hypothesised that a significant increase may be detected at the protein level in Hom cerebellar tissue. Western blotting, using anti-Gfap, was carried to compare protein levels in pre-symptomatic and end-stage tissue. No difference was observed in *Oxr1* knockout cerebellar tissue at P18 ($p = 0.537$) **(Figure 3.6A)**, however an increase in Gfap was detected at P22 ($p = 0.0167$) **(Figure 3.6B).** This demonstrates that gene dysregulation may occur prior to an increased presence of reactive astrocytes during disease progression.

Numerous functional enrichment analyses have suggested a role for Oxr1 in microglial cell activation, therefore immunohistochemistry (IHC) was carried out to investigate levels of activated microglia in P22 tissue. Ionized calcium-binding adapter molecule 1 (*Iba1/Aif1*) was chosen as a marker of activated microglia/microgliosis (Juckel et al., 2011); interestingly, *Iba1* was not found to be differentially expressed at P19 by transcriptomics. However, by IHC at P22, a strikingly increased number of Iba1 positive

cells were identified in the cerebellum (**Figure 3.6C**). In other regions across the brain, including the cortex and hippocampus, there are no observable increases in the number of immunopositive cells in *Oxr1* knockout tissue (**Figure 3.6C**).

Thus far, these data indicate that loss of *Oxr1* leads to upregulation of neuroinflammatory genes prior to neuronal degeneration; subsequently, reactive astrocytes and activated microglia are observed in the cerebellum at a symptomatic time point (P22), suggesting that loss of *Oxr1* induces a rapid neuroinflammatory response and that neuroinflammation occurs prior to cell death in *Oxr1* knockout mice (Oliver et al., 2011).

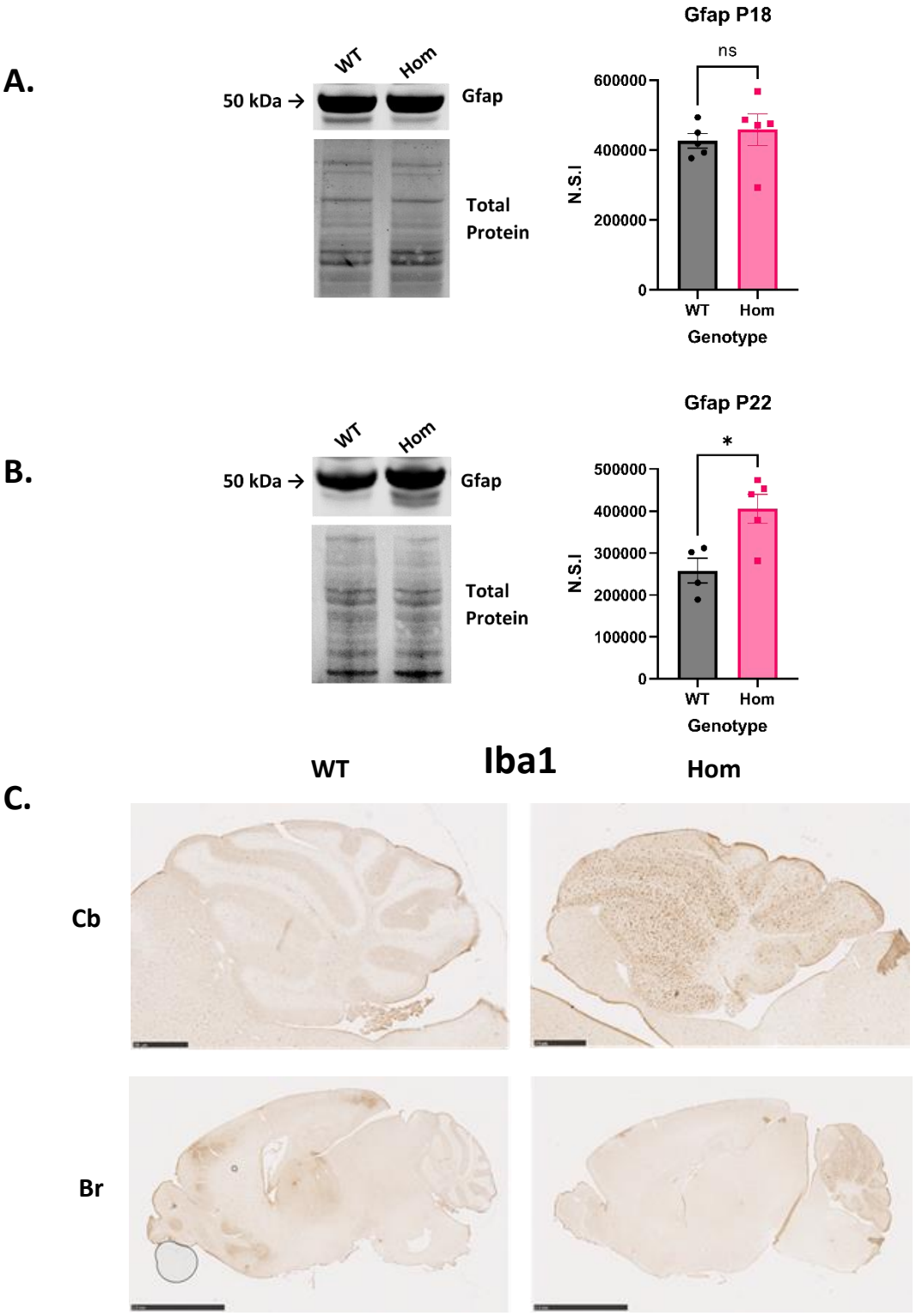

***Figure 3.6*| Western blot and histopathology to investigate markers of neuroinflammation in *Oxr1* knockout tissue**

Representative Western blot images and quantification of Gfap expression at (A) P18 and (B) P22 in protein lysates extracted from WT and Hom cerebellar tissue. Experiment performed by Dr Silvia Corrochano; Data analysis by E.M.V.B. Gfap signal normalised to total protein. NSI =normalised signal intensity. Data are presented as mean ± SEM, unpaired t-test, *= $p<0.05$. (n = 4-5) (C) Anti-Iba1 DAB immunohistochemistry on P22 WT and Hom tissue. Experiment and image acquisition performed by Dr Peter Oliver. Scale bar cerebellum = 500 µm; Scale bar whole brain = 2.5 mm. Cb = cerebellum; Br = whole brain.

3.2.4. Lysosomal function and autophagy are perturbed *in vivo* in the absence of Oxr1 expression

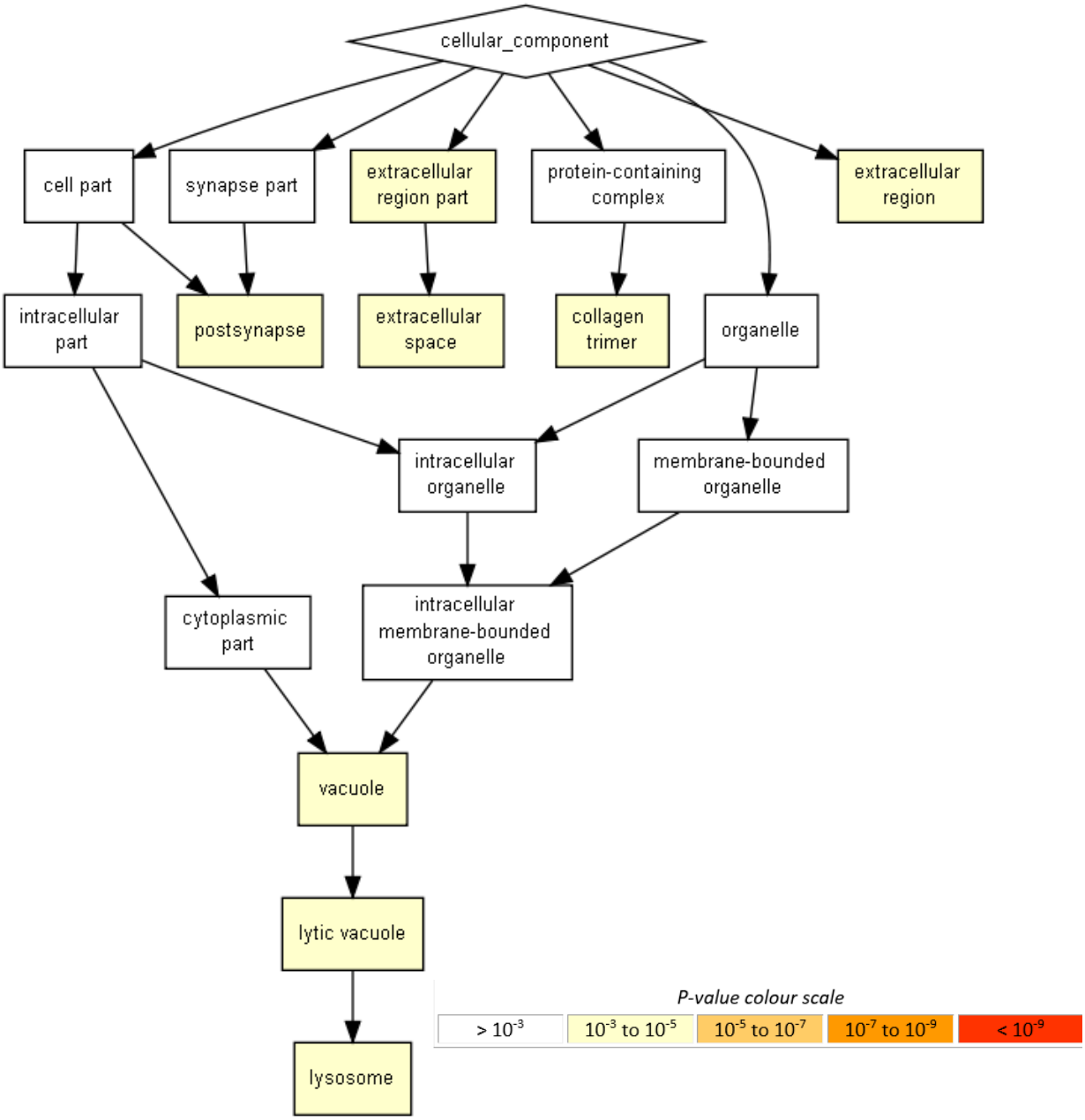

***Figure 3.7*|GOrilla enrichment cellular component analysis of differentially expressed genes in *Oxr1* knockout cerebellar tissue at P19**

Cellular component GOrila analysis identified a significant number of DEGs to be overrepresented in the lysosome. GOrilla database was last updated on March 6th 2022 at time of writing.

A number of the top 20 DEGs at P19 related to lysosome function (*Hexb, Ctss, Ctsz, Ctsd*) in Hom cerebellar tissue (**Table 3.1**). GOrilla graphical representation of cellular component annotations predicts that that the observed cellular dysfunction may occur in the lysosome (**Figure 3.7**) (Eden et al., 2007; Eden et al., 2009).

Lysosomes play a critical catabolic role in endosomal trafficking and autophagy (Abounit et al., 2012; Jacomin et al., 2016; Lee, 2012; Watts, 2022). In the endocytic pathway, lysosomes fuse with late endosomes that contain degradation-destined and recycling cargo including membrane receptors, such as Toll-like receptors (TLRs) (Barton & Kagan, 2009; Jacomin et al., 2016; Repnik et al., 2013). Autophagy relies on the fusion of mature autophagosomes containing cytoplasmic cellular components targeted for digestion with lysosomes to form autophagolysosome (autolysosome) (Abounit et al., 2012; Lee, 2012). In both degradation pathways, lysosomal fusion releases acid hydrolases to break down target cargo, thus forming crucial parts of the lysosomal degradation pathways (Repnik et al., 2013; Sakamaki & Ryan, 2017). For example, β-hexosaminidase (HexB) acts as a glycosyl hydrolase, degrading fatty substrates, whereas cathepsins (e.g. Ctsd, Ctsd and Ctsz) harbour proteolytic properties (Kuil et al., 2019; Lie & Nixon, 2019; Steinfeld et al., 2006). Given these genes were significantly differentially expressed in RNA-Seq data, the effect of loss of *Oxr1* on key autolysosomal pathways was examined at the protein level *in vivo* to assess if function is perturbed, such as measuring autophagic protein turnover (Guedes-Dias et al., 2015; Jacomin et al., 2016).

Western blots were carried out on brain and cerebellar protein extracts from WT and Hom tissue at P22 (**Figure 3.8A,B** and **Figure 3.9A,B**). No significant differences were identified in levels of Rab7, a marker of late endosome formation and maturation, suggesting that this pathway is not significantly altered in the brain and cerebellum of *Oxr1* knockout mice (**Figure 3.8C** and **Figure 3.9C**) (Vanlandingham & Ceresa, 2009). In Hom cerebellar tissue, a significant variance in the standard error of the mean (SEM) is found (WT=16.34 vs Hom=65.30, p=0.0477) which may be caused by varying stages of disease progression in Hom mice, although an increased sample size is needed to confirm this (**Figure 3.9C**).

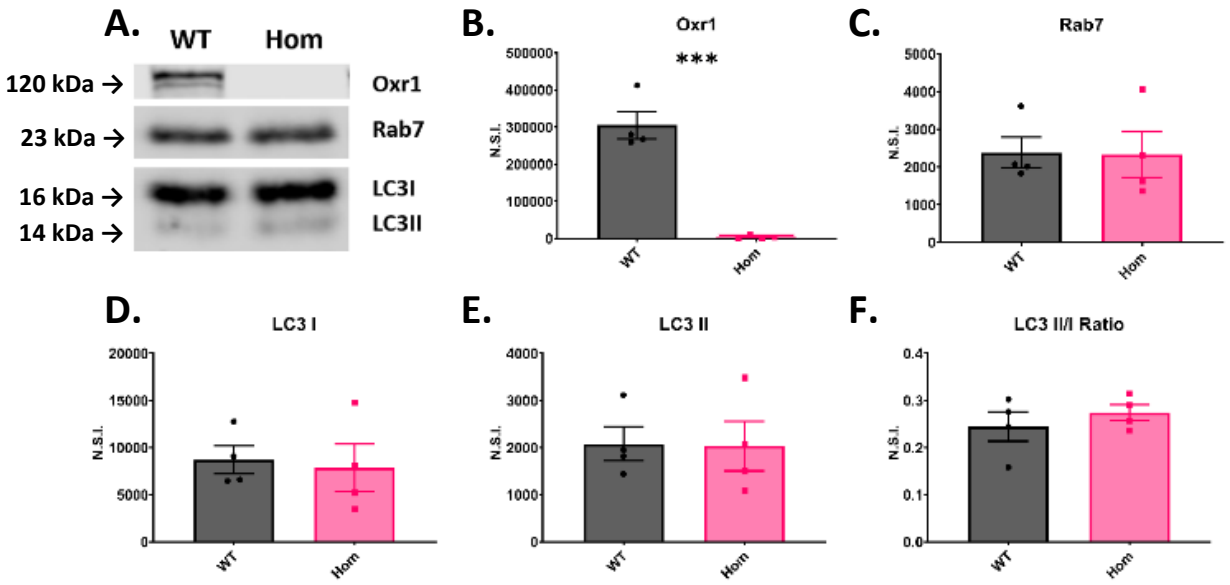

***Figure 3.8*| Western blot analysis of endosomal and autophagy-lysosomal markers in wild type and *Oxr1* knockout cortical tissue at P22**

(A) Representative western blot image and quantification of (B) Oxr1, (C) Rab7, (D) LC3I, (E) LC3II and (F) LC3II/I ratio from protein extracts of WT and Hom cortical tissue taken at P22. All protein signal was normalised to total protein. NSI = normalised signal intensity. Data are presented as ±SEM, unpaired t-test, p values * ≤ 0.05, **≤0.01, *** ≤ 0.001. n=4

In order to investigate the role of Oxr1 in autophagy, levels of microtubule-associated protein light chain 3 (LC3) were investigated in both WT and Hom tissue at P22. LC3 is a highly regarded marker of autophagy, owing to its role in autophagosome formation (Abounit et al., 2012; Yoshii & Mizushima, 2017). C-terminal cleavage of LC3 propeptide forms cytosolic LC3I; subsequent lipidation of LC3I with phosphatidylethanolamine forms membrane-bound LC3II, marking autophagosomes. This conversion reaction and levels of LC3II are quantified to provide insight in to the number of autophagosomes and autophagic flux (Yoshii & Mizushima, 2017).

Cerebral tissue was first analysed to determine if disruption of the autophagy-lysosomal pathway occurs in the absence of neuroinflammatory histopathology. In P22 brain tissue, no significant differences were observed in the pools of LC3I and LC3II by Western blot (**Figure 3.8D** and **E**). Further to this, when quantifying the LC3-II/I ratio, no difference was observed in Hom tissue compared to WT at P22, which suggests that loss of Oxr1 does not cause alterations to autophagic flux at this time point in cerebral tissue (**Figure 3.8F**). Next, LC3 protein levels were assessed in P22 cerebellar tissue. Western blot analysis of LC3-I, levels of the lipidated form LC3II, as well as LC3-II/I ratio, showed no robust difference in detected protein levels in P22 Hom cerebellar tissue by unpaired t-test (**Figure 3.9D, E and F**). Taken together, these data indicate no difference in the levels of autophagy marker LC3 in *Oxr1* knockout whole brain and cerebellar tissue at P22.

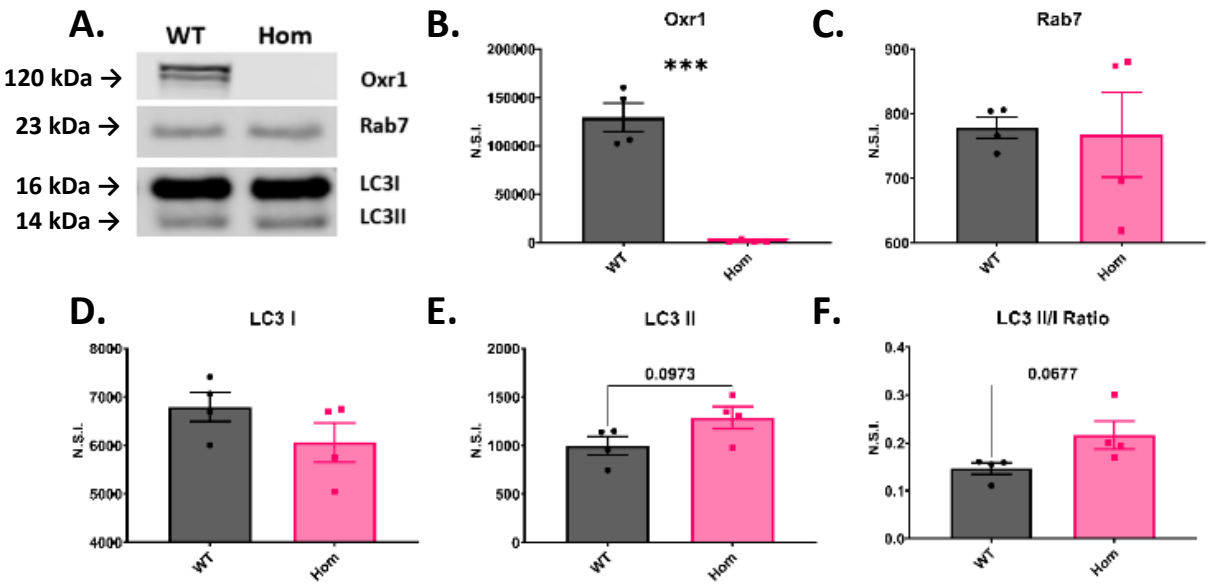

***Figure 3.9*| Western blot analysis of different markers of endosomal and autophagy-lysosomal function in wild type and *Oxr1* knockout cerebellar tissue taken at P22**

(A) Representative western blot image and quantification of (B) Oxr1, (C) Rab7, (D) LC3I, (E) LC3II and (F) LC3II/I ratio from protein extracts of WT and Hom cerebellar tissue taken at P22. All protein signal was normalised to total protein. NSI = normalised signal intensity. Data are presented as ±SEM, unpaired t-test, p values * ≤ 0.05, **≤0.01, *** ≤ 0.001. n=4

Sequestosome 1 (Sqstm1/p62) is degraded in an autophagy-dependent manner and thus used as an indicator of autophagic activity (Pankiv et al., 2007; Yoshii & Mizushima, 2017). It is worth noting that differential expression of this gene was not identified in the RNA-Seq data set (q<0.01). At the protein level, no significant change in p62 expression was observed in both brain and cerebellar tissue at P22 (**Figure 3.10A** and **B**). Overall, despite GO analysis of RNA-Seq data alluding to autolysosomal dysfunction in this mouse model, this could not be confirmed at the protein level through these selected markers of autophagy in bulk tissue analysis.

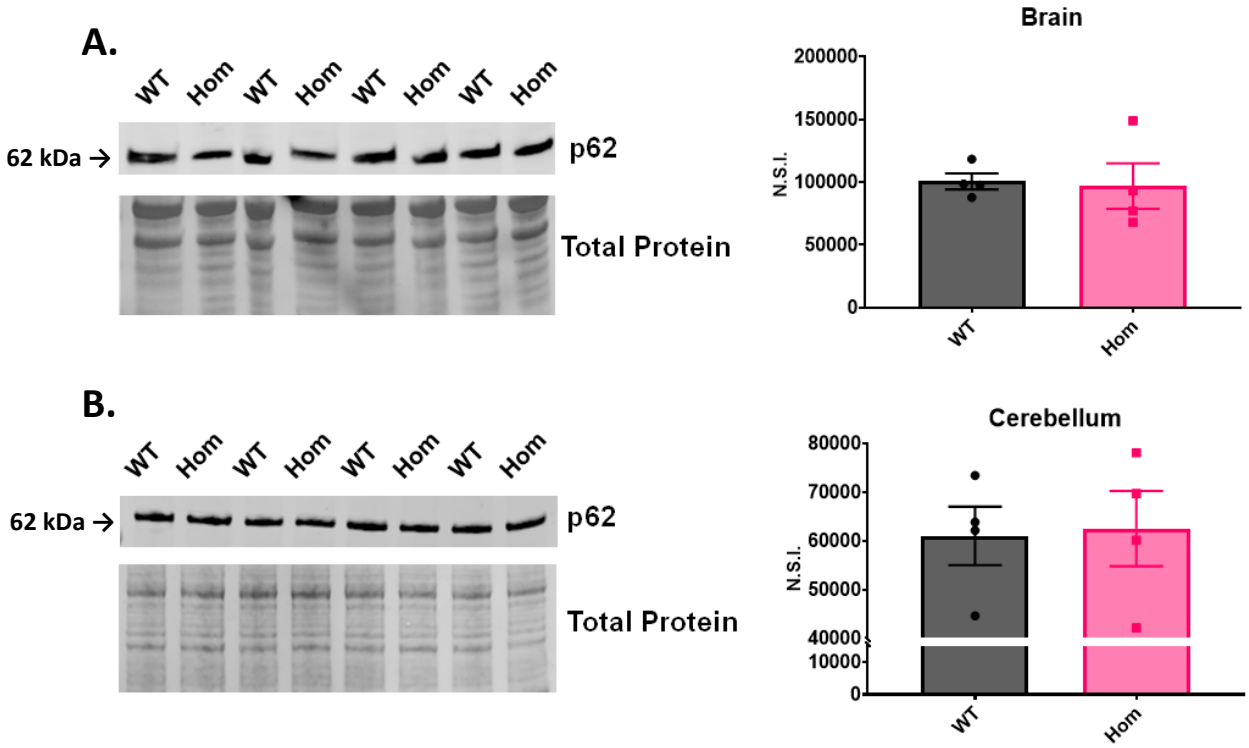

***Figure 3.10*| Western blot analysis of Sequestosome 1 (p62) in P22 wild type and *Oxr1* knockout forebrain and cerebellar tissue**

Representative western blot images and quantification of p62 in (A) forebrain and (B) cerebellar protein extracts from P22 WT and Hom tissue, normalised to total protein. NSI = normalised signal intensity. Data is presented as ±SEM, unpaired t-test, n=4.

3.2.5. Accumulation of lysosomes but no difference in autophagic flux is observed in primary fibroblasts derived from P22 *Oxr1* knockout mice

The vulnerability of *Oxr1*-deficient primary granule cells to apoptosis was demonstrated when exposed to peroxide treatment (Oliver et al., 2011), therefore exogenous insults or augmentation of a molecular pathway may be required to reveal a cellular phenotype. Hence, to further characterise the role of Oxr1 in autophagy, an *in vitro* approach was subsequently adopted using primary cells isolated from WT and Hom mice. As lysosomal abnormalities are observed in fibroblasts derived from LoF-OXR1 patients (Wang et al., 2019), primary fibroblasts were generated from P22 WT and Hom mice and used to perform initial characterisation of lysosomal molecular phenotypes in the absence of Oxr1 (Wang et al., 2019). Fibroblasts were treated with bafilomycin, which prevents acidification of lysosomes and autophagosome-lysosome fusion by blocking V-ATPase activity, thus inhibiting autophagy (Redmann et al., 2017). Dimethyl sulfoxide (DMSO) was used as a solvent for bafilomycin and thus used as a control for drug treatment. Cells were harvested following DMSO and bafilomycin treatment, then protein was extracted to perform western blotting for markers of autophagy (**Figure 3.11A**).

Two-way ANOVA confirmed that bafilomycin treatment had a statistically significant effect ($p<0.0001$) in this experiment, but genotype demonstrated no effect. Šídák's multiple comparisons test showed no significant differences in levels of p62 and LC3 quantifications between WT and Hom fibroblasts when treated with either DMSO or bafilomycin (**Figure 3.11B**). Thus, no robust differences in autophagic flux were observed in this set of experiments.

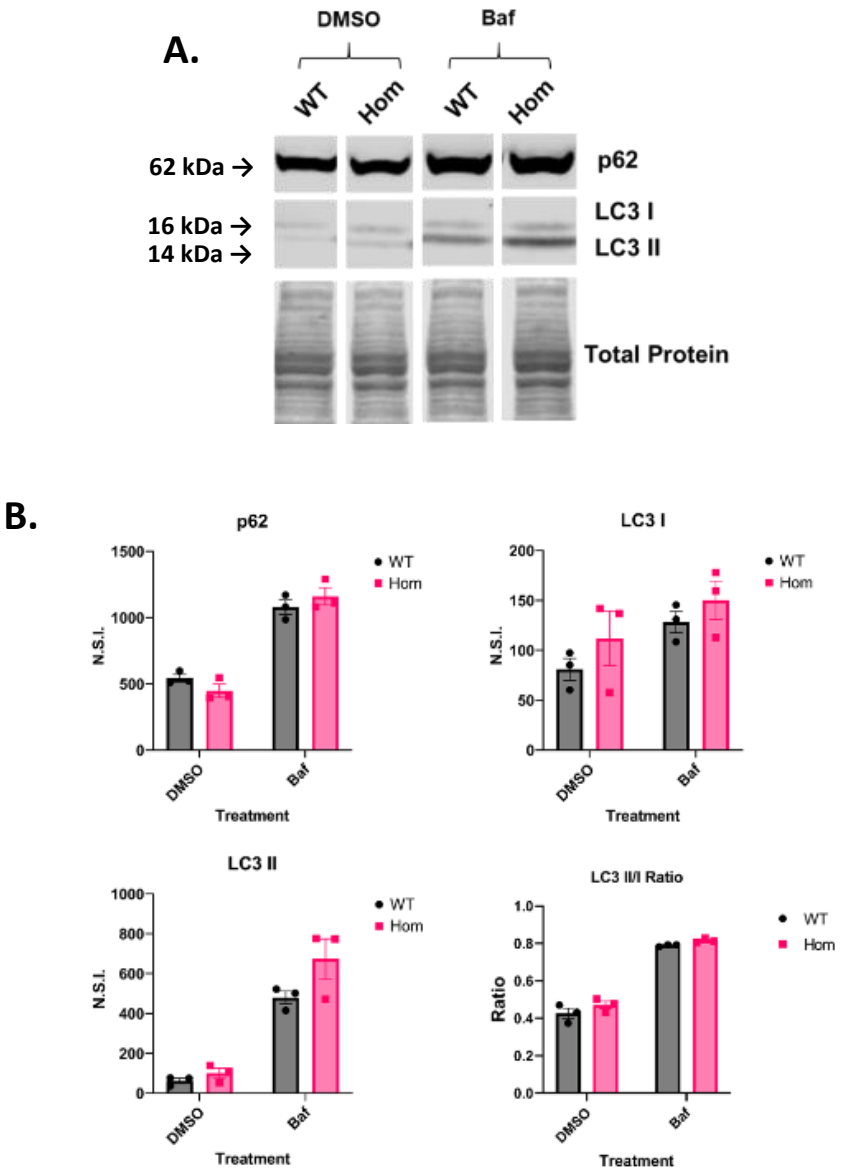

Figure 3.11| **Western blotting of autophagic turnover markers in primary fibroblasts**

(A) Representative western blot and (B) relative quantification of p62, LC3I, LC3II and LC3II/I in WT and Hom primary fibroblasts incubated with 0.1% DMSO solvent or 50 nM bafilomycin A1 (BAF) for 6 hours. Signal intensity normalised to total protein. Two-way ANOVA followed by Šídák's multiple comparisons test. n = 3 biological replicates.

Next, a combination of live cell imaging and flow cytometry on WT and Hom fibroblasts incubated with LysoTracker was employed to further characterise the role of *Oxr1* in lysosomal function *in vitro* (**Figure 3.12**). LysoTracker is a pH sensitive dye that is used as a marker of acidic organelles, predominantly lysosomes, in loaded cells (Guerrini et al., 2022). Quantification of labelled fibroblasts identified a significant increase in the number of LysoTracker-positive puncta in Hom fibroblasts (**Figure 3.12A** and **B**). Similarly, flow cytometry demonstrated an increase in the number of acidic organelles in *Oxr1* knockout fibroblasts, although this did not reach statistical significance (**Figure 3.12G**). It is worth noting that no changes in fluorescent intensity or particle size were found, suggesting that increased loading or enlargement of lysosomes is not found in Hom fibroblasts (**Figure 3.12C** and **D**). Intercellular localisation of lysosomes has been defined as an indicator of cytoplasmic pH and autophagy, with perinuclear clustering indicating increased acidification and autophagy induction (Li et al., 2016; Uusi-Rauva et al., 2012). In fibroblasts, no changes to lysosomal localisation were identified between WT and Hom cells (**Figure 3.12E** and **F**). Overall, although these data did not show any significant difference in lysosomal clustering, analysis of live cell imaging and flow cytometry of LysoTracker loaded cells suggest that loss of *Oxr1* likely leads to an increase in the number of lysosomes in fibroblasts.

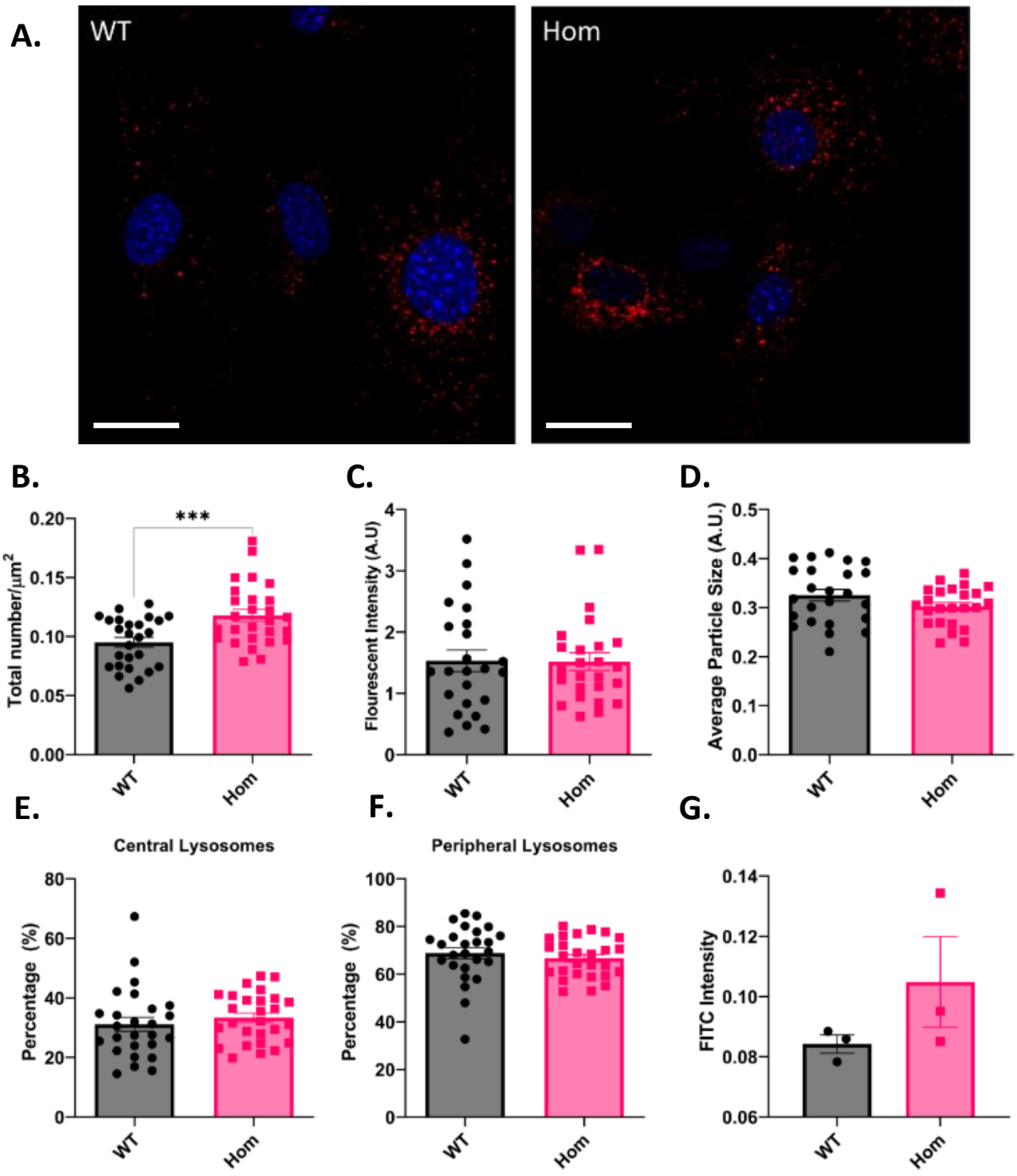

***Figure 3.12*| LysoTracker labelling and quantification of primary fibroblasts**

(A) Representative immunofluorescence of WT and Hom primary fibroblasts incubated with Lysotracker. Scale bar = 20 µm. Relative quantification of (B) total number of lysosomes, (C) fluorescent intensity and (D) average particle size in arbitrary units (A.U.). Calculated percentage of lysosomes localised to the (E) centre and (F) periphery of cells. (F) Fluorescein isothiocyanate (FITC) intensity quantified through flow cytometry. All data is presented as ±SEM, unpaired t-test, p value = *** ≤ 0.001, n = 3 biological replicates.

3.2.6. Increased autophagic degradative activity is observed in primary cortical neurons lacking expression of *Oxr1*

Previous experiments have indicated increased autophagic flux in cortical and cerebellar tissue taken from end-stage constitutive *Oxr1* knockout mice; this dysfunction has further been identified in primary *Oxr1* knockout fibroblasts. Aberrant lysosome trafficking and induction of autophagy in neurons is tightly linked to neurodegenerative disease pathogenesis (Lee, 2012; Lie & Nixon, 2019), therefore primary cortical neurons were isolated from WT and Hom P1 pups and cultured until 14 DIV before *in vitro* lysosomal molecular phenotyping was carried out.

In DMSO-treated primary cortical neurons, a reduction in p62 was detected in Hom cells, although this did not reach statistical significance (**Figure 3.13**). Although no difference was identified in levels of LC3I and LC3II, a small but non-significant increase in LC3II/I ratio was observed in Hom neurons, overall suggesting increased autophagic flux in *Oxr1*-knockout cells (**Figure 3.13**). Inhibition of autophagy through bafilomycin treatment showed a significant increase in p62, LC3II and LC3II/I ratio in both WT and Hom neurons (**Figure 3.13**). An increase in LC3I levels were observed in bafilomycin treated WT neurons but not in Hom cells (**Figure 3.13**). These data initially suggest an elevated autophagic turnover in Hom primary cortical neurons. Treatment of WT and Hom cells with rapamycin, an inducer of autophagy, lead to significant decrease in p62, confirming that loss of Oxr1 does not inhibit initiation of autophagy *in vitro* (**Figure 3.13**) (Guedes-Dias et al., 2015).

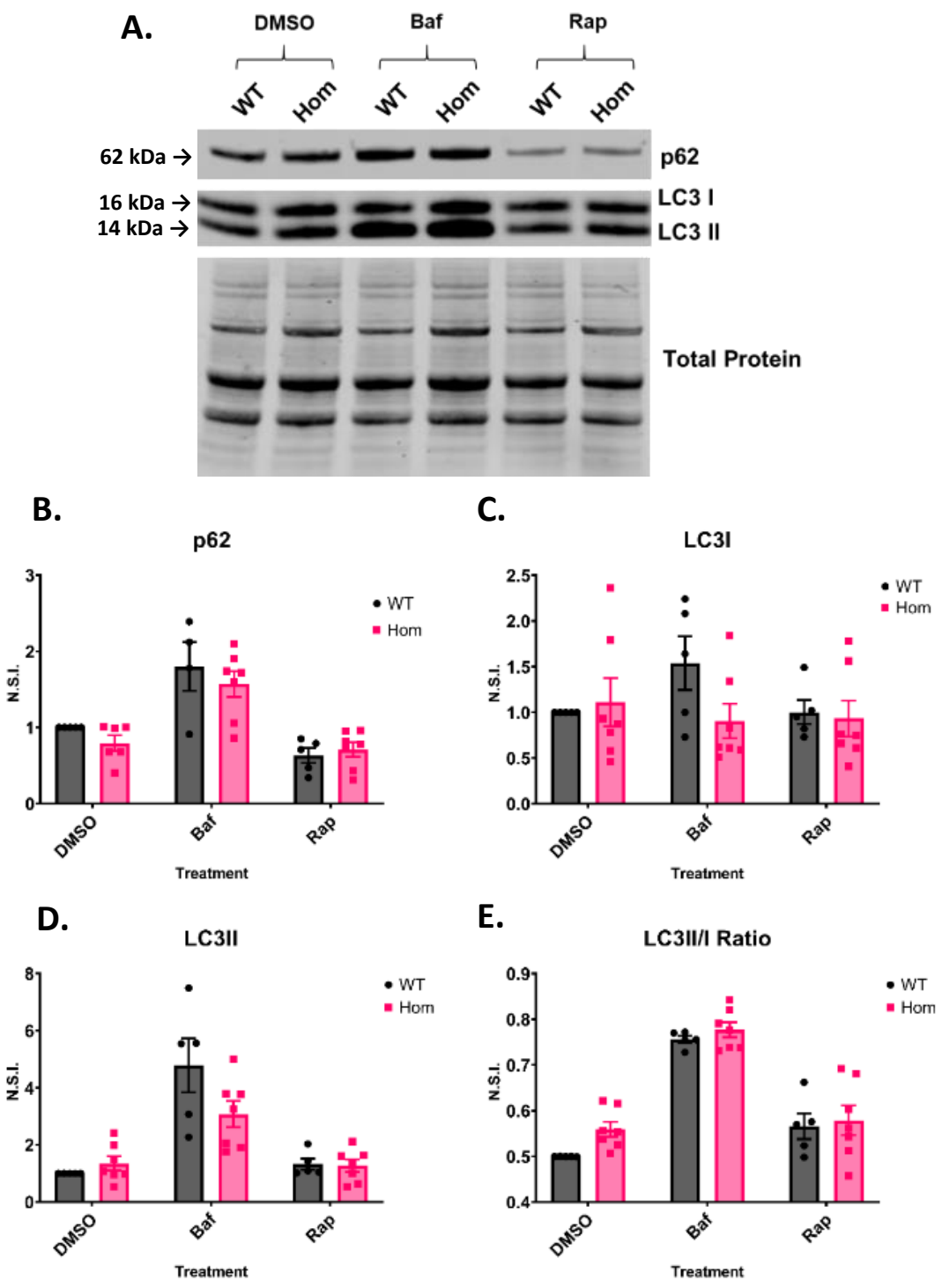

***Figure 3.13*| Western blotting of autophagic turnover markers in 14 DIV primary cortical neurons**

(A) Representative western blot and (B) relative quantification of p62, LC3I, LC3II and LC3II/I in WT and Hom primary cortical neurons incubated with 0.1% DMSO solvent, 25 nM bafilomycin A1 (BAF) for 6 hours or 10 nM rapamycin (RAP) for 24 hours. Signal intensity normalised to total protein. n= 5-7 neuronal preps from independent litters

Next, PFA-fixed DMSO and bafilomycin A1-treated WT and Hom cortical neurons were immunostained for autophagy substrate protein p62 and $p62^{+}$ puncta were assessed by confocal imaging (**Figure 3.14**). This experiment was conducted in order investigate p62 accumulation following bafilomycin A1-mediated blocking of autophagy as an indirect readout of autophagic flux (Yoshii & Mizushima, 2017). Although Two-way ANOVA shows that treatment of bafilomycin A1 has an effect in WT and Hom cells (P=0.0083), genotype has no effect between cell treatments (P=0.7362) in the raw intensity of p62 immunofluorescence in primary cortical neurons (**Figure 3.14**). From these data, no robust difference in autophagic flux is detected in *Oxr1*-deficient primary cortical neurons.

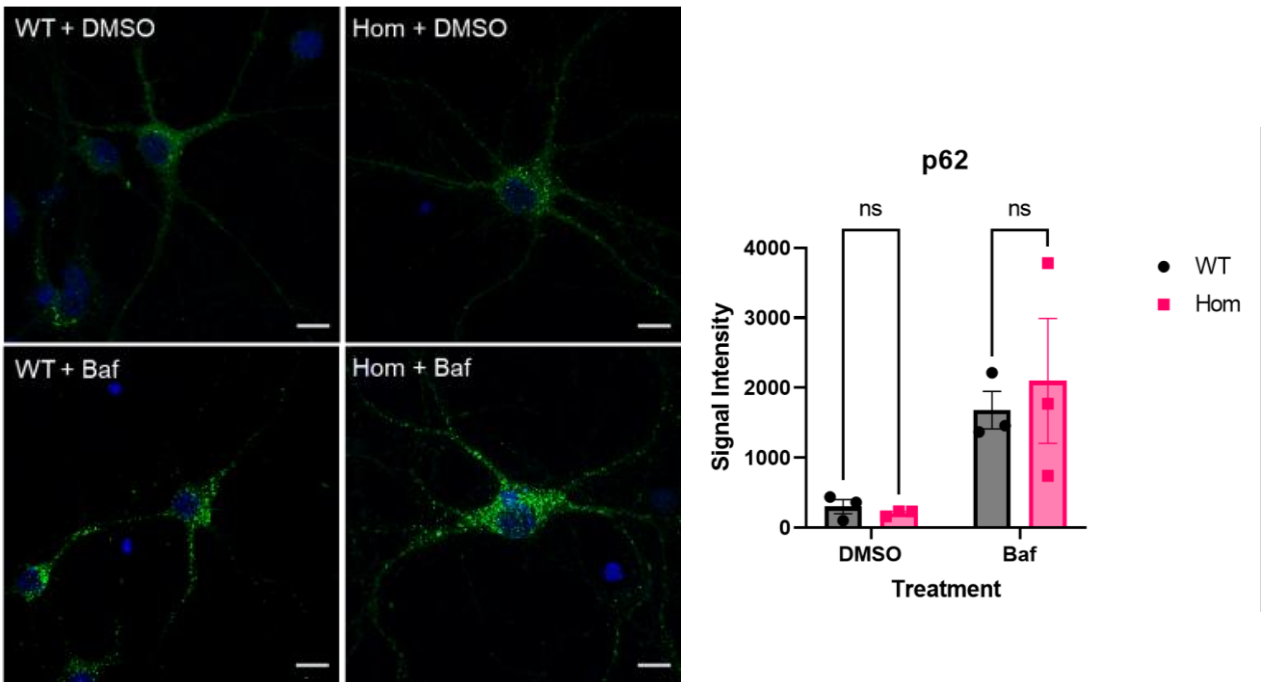

***Figure 3.14*| Immunostaining of p62 in primary cortical neurons**

Representative immunofluorescence and quantification of p62 in WT and Hom primary cortical neurons treated with 0.1% DMSO solvent or 25 nM bafilomycin A1 (BAF) for 6 hours. DAPI: Blue, p62: Green. Scale bar = 10 µM. n = 3 independent cultures. Two-way ANOVA of raw intensity, followed by Šídák's multiple comparisons test (DMSO – WT vs Hom Adjusted P = 0.9887; Baf – WT vs Hom, Adjusted P = 0.7933). Analysed with Dr Tania Soares.

3.2.7. Loss of *Oxr1* leads to increased lysosomal biogenesis and active autophagy in primary cortical neurons.

Taken together, data from cerebellar tissue transcriptomics, *in vitro* live cell imaging and protein expression allude to some disruption of normal lysosomal activity in the absence of *Oxr1* expression. In an attempt to begin to quantify this effect functionally, dye quenched-bovine serum albumin (DQ-BSA) trafficking assay was performed on 14 DIV primary cortical neurons isolated from WT and Hom P1 pups. Cells were treated with DQ-BSA for 5 hours before imaging using the Opera Phenix confocal imaging system. This microscopy-based high-content screening system was utilised in order to rapidly acquire live-cell images in an unbiased, systematic manner. Autolysosomes internalise the DQ-BSA and subsequent proteolysis by active proteases releases the self-quenching system and produces fluorescent peptides (Carling et al., 2022; Frost et al., 2017). From this, we can infer that an increase in fluorescent signal correlates to increased autophagic activity. In order to assess the ability of this assay to monitor active autolysosomes and subsequent autophagic processes, DQ-BSA fluorescent intensity in neurons was assessed in the absence and presence of an inhibitor of autophagy, chloroquine (CQ) (Redmann et al., 2017). Untreated neurons yielded a high fluorescent signal indicating efficient proteolysis of the DQ-BSA substrate, whereas fluorescence could not be detected in CQ-treated neurons, thus demonstrating a system to successfully assess autophagy (data not shown).

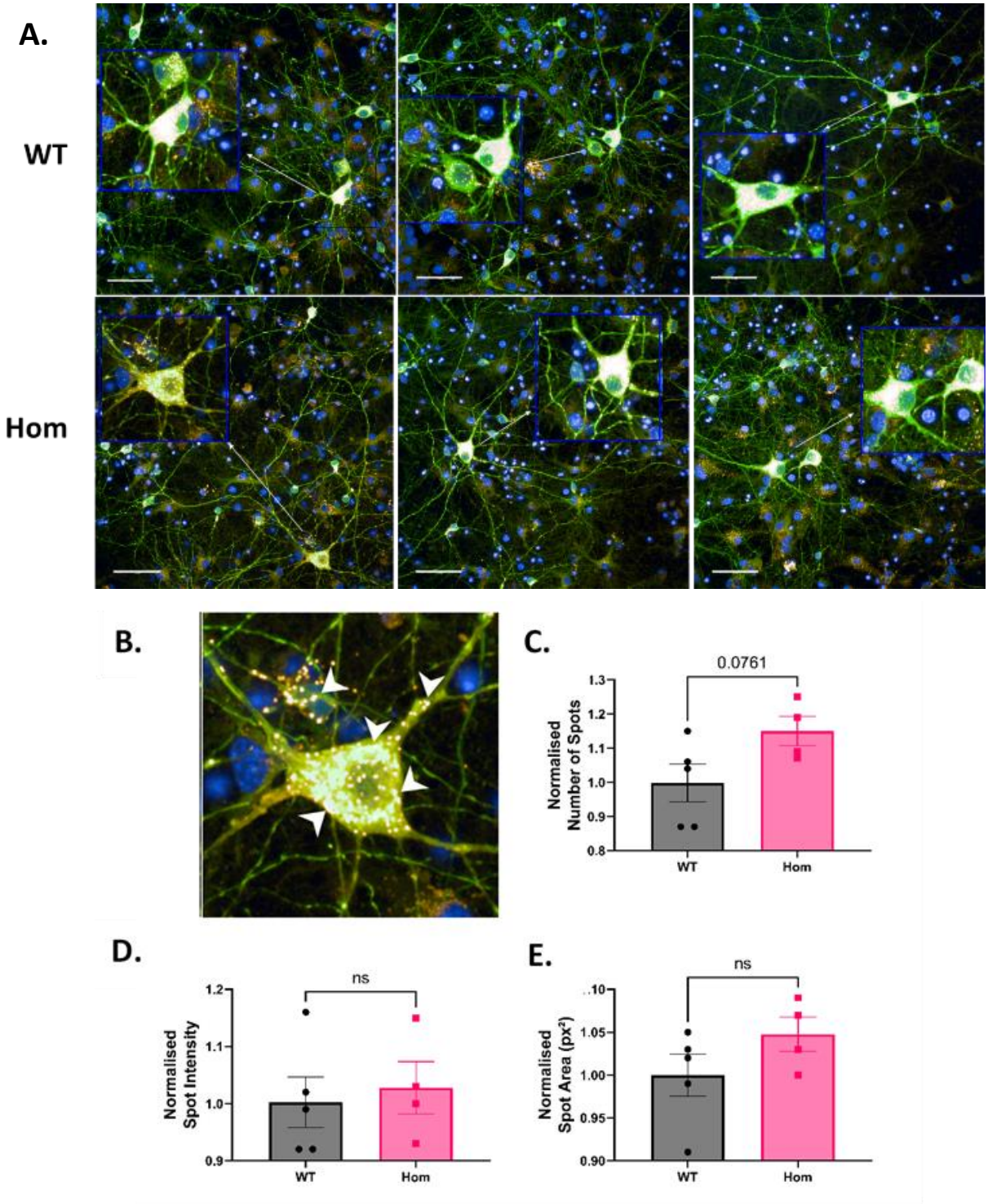

Figure 3.15 **|DQ-Red BSA trafficking assay using wild type and *Oxr1* knockout primary cortical neurons**

(**A**) Representative images from DQ-Red BSA treated WT and Hom primary cortical neurons at DIV14 and (**B**) example image labelling fluorescent puncta. Normalised quantification of (**C**) spot number, (**D**) spot intensity and (**E**) spot area. All values are normalised and expressed relative to average WT value. Data analysed by unpaired t-test and presented as mean ± SEM. Represented images contain inset images with blue border magnified by a factor of 2. Scale bar: 50 µm. Blue – DAPI, Green – NeuO, Red – DQ-BSA. WT n=5, Hom n=4. Images were processed in Harmony by William McGuinness and data subsequently analysed by E.M.V.B. ns: data not statistically significant.

DQ-BSA assay data were collected from WT and Hom treated at 14 DIV and subsequently processed using the Harmony image analysis software that quantifies relative fluorescent intensity emitted from cleaved DQ-BSA peptides in individual cells; a neuronal-selection marker, NeuO, was used to ensure quantification of neurons *in vitro* (**Figure 3.15A**). This analysis suggests a potential increase in number of lysosomes in Hom neurons, indicated by a non-significant increase in number of puncta (**Figure 3.15B**) observed compared to WT [p=0.0761] (**Figure 3.15C**). A small increase in puncta intensity and area was observed in Hom neurons, although these data did not reach statistical significance (**Figure 3.15D** and **E**). This suggests that *Oxr1*-deficient cortical neurons have an increased rate of autophagy and contain larger autolysosomes. Taken together, these data suggest that loss of Oxr1 may influence lysosomal biogenesis and increases autophagosome cargo loading.

3.2.8. Transmission electron microscopy of *Oxr1* knockout cerebellum reveals aberrant ultrastructural features at an early pathological time point

As the apparent differences in lysosomal gene expression and functional assays are at the limit of detection in the various experimental systems used, an additional screening method was to apply ultrastructural analysis of Hom cerebellar tissue to identify organelle disruption would provide further clues as to the consequences of Oxr1 deletion. Transmission electron microscopy (TEM) was employed from mid-sagittal cerebellar tissue was taken from WT and Hom littermates (n=3) at P19 (Oliver et al., 2011). These samples were processed and then subsequently imaged by Dr Errin Johnson at the Dunn School Bioimaging Facility (University of Oxford).

Dr Johnson was blind to genotype during image acquisition, yet could correctly identify the mutant samples owing to the presence of multiple abnormal morphological features and organelle structure in Hom tissue when compared to that of WT littermate controls (**Figure 3.16**). For example, enlarged synaptic vesicles are observed compared to WT mice (**Figure 3.16A**). This molecular phenotype has been associated with impaired synaptic vesicle trafficking and turnover (Banks et al., 2020; Shimizu et al., 2003). Additionally, increased aberrant membranous compartments, known as myelin figures, as well as accumulation of lipid droplets, were identified in Hom tissue (**Figure 3.16B**) (Mao et al., 2019). Formation of myelin figures have been linked with autophagy induction (Martinet et al., 2004), whereas accumulation of lipid droplets, particularly in microglia, is a hall mark of neurodegeneration (Farmer et al., 2020; Simpson & Oliver, 2020). Overall, TEM demonstrated gross abnormal pathology in P19 Hom cerebellar tissue; larger numbers of images and sections would be required for full quantification of pathological features.

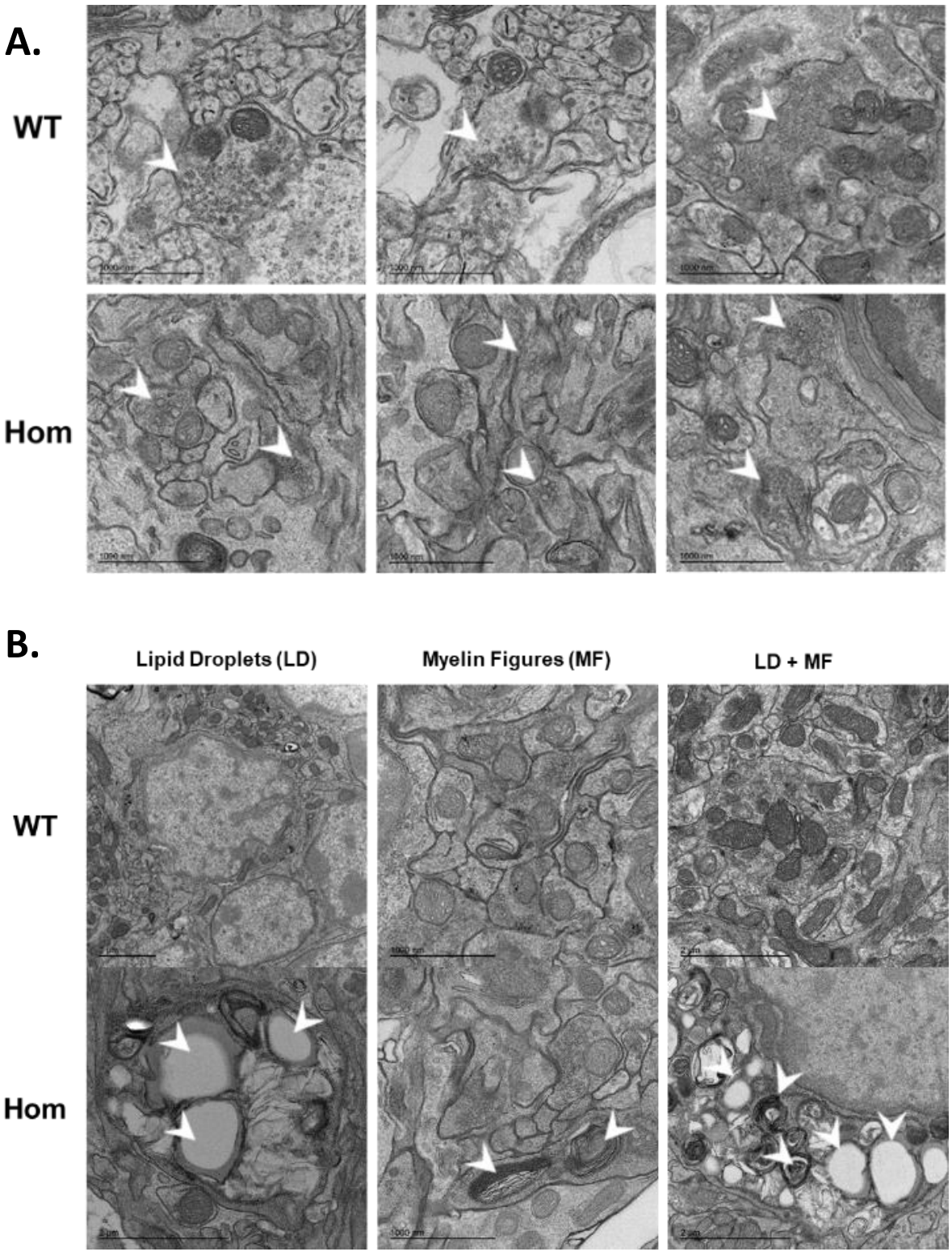

***Figure 3.16*| Ultrastructure visualisation of P19 cerebellar tissue from wild type and *Oxr1* knockout mice.**

Representative transmission electron micrographs of WT and Hom cerebellar tissue, with arrows drawing attention to (A) enlarged vesicles, (B) lipid droplet accumulation and myelin figures in Hom cerebellar tissue, WT and Hom littermate pairs (n=3).

3.2.9. *Oxr1* knockout primary cortical neurons demonstrate no difference in electrical activity

Oxr1 knockout mice and LoF-OXR1 patients have overlapping pathological features, including early-onset ataxia and cerebellar degeneration; epilepsy is a prominent clinical phenotype of LoF-OXR1 patients; however, this has not been observed in *Oxr1* knockout mice (Lin et al., 2022; Oliver et al., 2011; Wang et al., 2019). Acute onset of symptoms and rapid degeneration of the mouse model may possibly mask seizure events (Oliver et al., 2011). The early death in constitutive *Oxr1* knockout mice makes it difficult to evaluate epileptogenesis and seizure events *in vivo* using the routine method of electroencephalography (EEG), therefore assessing neuronal dysfunction *in vitro* was essential.

Multielectrode array (MEA) is an excellent technique to assess neuronal dysfunction and seizure susceptibility *in vitro*, therefore this technique was performed on *Oxr1*-knockout derived primary cortical neurons to preliminarily investigate electrophysiological properties, including neuronal activity, connectivity and cross talk (Fan et al., 2019). Bicuculline, $GABA_A$ receptor antagonist, is known to enhance neuronal excitability and induce seizure-like events (Gu et al., 2018; Olsen, 2018). A sharp increase in spike count was observed when primary wild-type cortical neuron cultures were injected with Bicuculline (10 μM), validating that the MEA set up was sufficient to detect neuronal activity (**Appendix. 5**).

Primary cortical neurons were isolated from WT and Hom pups at P1 and plated in PDL-coated Multichannel Systems Multiwell-MEA plates; all MEA recordings were taken at 14 DIV. The following MEA data were analysed using unpaired nonparametric Mann-Whitney tests with false discovery rate (FDR) correction by Benjamini, Krieger, and Yekutieli two-stage set up procedures, unless stated otherwise. Random spiking events

represents unsynchronised action potentials and is a general marker for neuronal activity and electrophysiological properties (Carlson & Carin, 2019; Lewicki, 1998). When WT and Hom neurons were stimulated with 25 and 50 µA, Hom cells displayed an overall lower spike count [25 µA, p= 0.07][50 µA, p=0.06] and spike rate [25 µA, p= 0.07][50 µA, p=0.06] compared to WT suggesting a reduction in spontaneous firing rate (**Figure 3.17A, Figure 3.17B**), although these parameters do not remain close to significance when FDR corrected.

It is important to note that a significant reduction [p= 0.0084] is observed between number of spike counts at 1 µA compared to 10 µA in Hom neurons when analysed by 2-Way ANOVA followed by FDR correction, however when comparing main row effects an overall significant reduction is observed at 10 µA (**Figure 3.17A**). This demonstrates an unexpected reduction of neuronal activity in both genotypes, creating limitations regarding comparisons to this discrete data set.

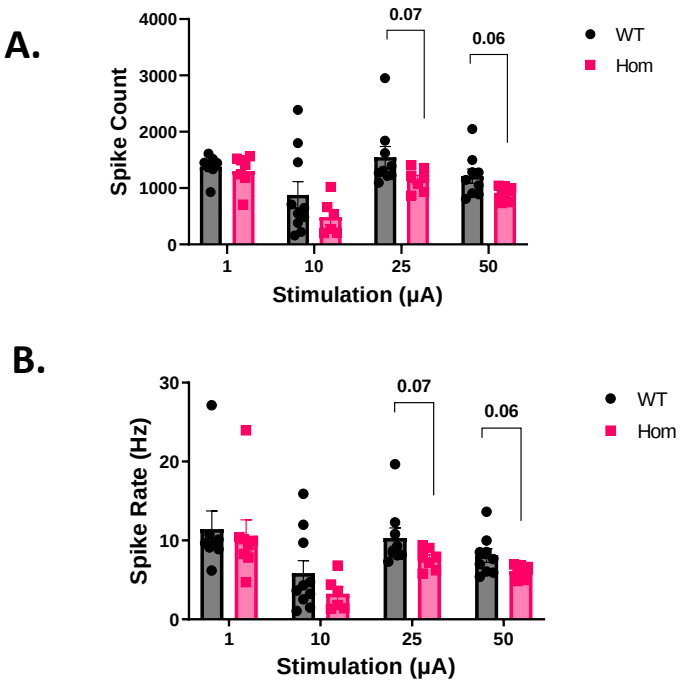

***Figure 3.17*|Neuronal spike activity characterisation of wild type and *Oxr1* knockout primary cortical neurons using Multielectrode Array recordings**

Quantification of MEA recordings on WT and Hom primary cortical cultures using parameters of (A) spike count and (B) spike rate (Hz) following electrical stimulation of 1, 10 , 25 and 50 µA. Unpaired nonparametric Mann-Whitney tests with false discovery rate (FDR) correction by Benjamini, Krieger, and Yekutieli two-stage set up procedures.

Bursting activity is a measure of a singular neuron firing at high frequency during a short period of time and is important for synchronous firing and synaptic plasticity (Negri et al., 2020; Winnubst et al., 2015). Bursts were defined at a frequency of at least 10 spikes/10 ms as an ictal sequence. Within each stimulation event, Hom neurons exhibit fewer burst counts and shorter burst durations, although statistical significance is not reached within these parameters (**Figure 3.18A** and **B**). A significant reduction of burst spike counts is observed in Hom neurons stimulated with 25 μA [p=0.031], but this statistical analysis did not survive FDR correction (**Figure 3.18C**). No significant differences were found between WT and Hom neurons in burst spike rate or percentage spikes in bursts within each stimulation episode (**Figure 3.18D, Figure 3.18E**), indicating no substantial changes in propensity to burst. Finally, Hom neurons demonstrate a slight increase in time between burst activity when stimulated by 10 and 50 μA; no differences are observed at 1 and 25 μA (**Figure 3.18F**). Overall, these burst data indicate a marginal reduction in Hom intrinsic neuronal dynamic activity.

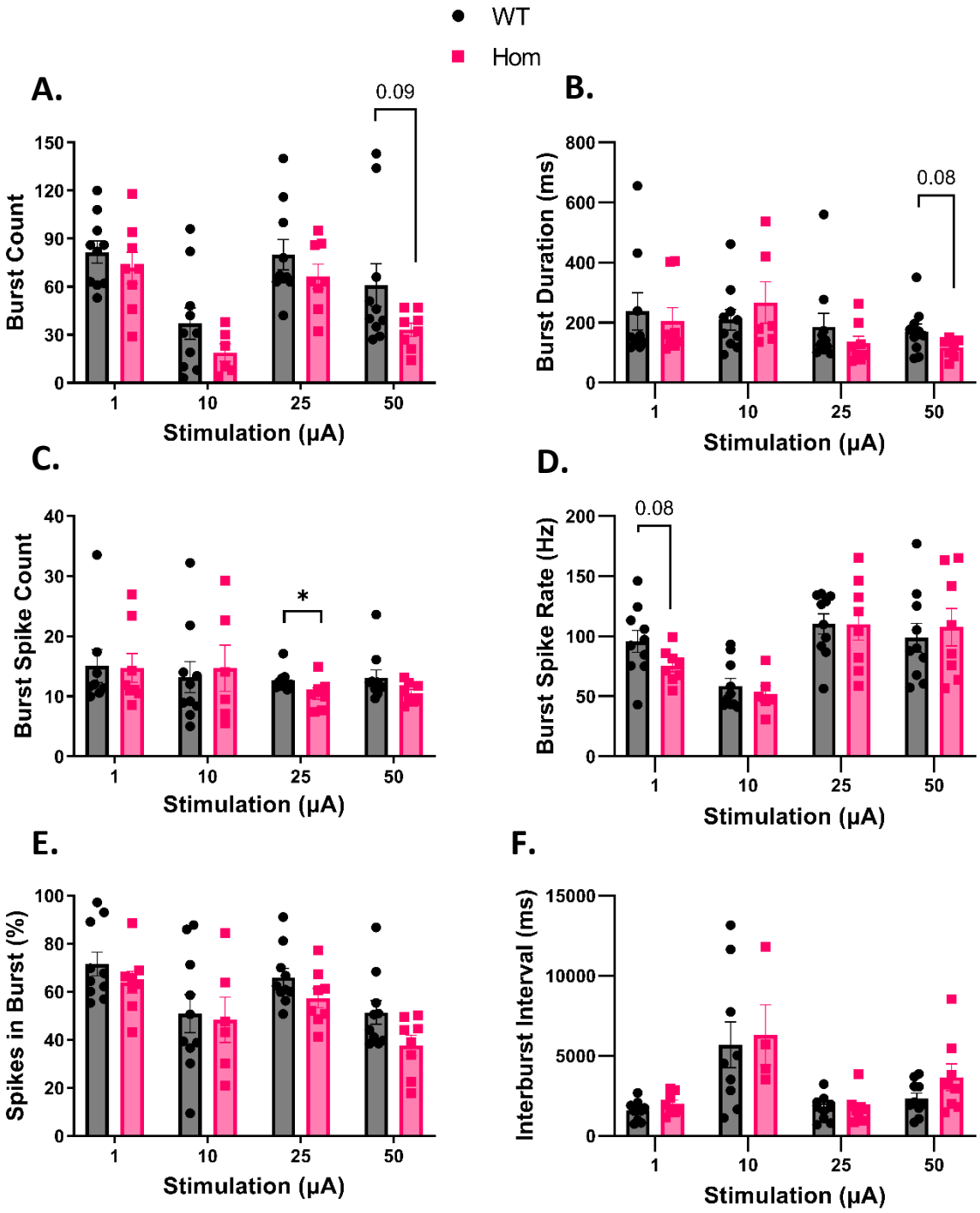

***Figure 3.18*|Measuring burst activity of wild type and Oxr1 knockout primary cortical neurons using Multielectrode Array recordings following electrical stimulation**

Quantification of MEA recordings on WT and Hom primary cortical cultures using parameters of (A) burst count, (B) burst duration (ms), (C) burst spike count, (D) burst spike rate (Hz), (E) spikes in burst (%) and (F) interburst interval (ms) following electrical stimulation of 1, 10 , 25 and 50 µA. Unpaired nonparametric Mann-Whitney tests with false discovery rate (FDR) correction by Benjamini, Krieger, and Yekutieli two-stage set up procedures.

Networks bursts are defined as a number of neurons firing in synchrony and are more indicative of epileptiform activity (Biffi et al., 2013; Engel et al., 2013). Network burst patterns were defined as a minimum of 5 separate cellular units collectively bursting. No overt differences in network burst counts were identified, although a non-significant reduction in overall number of Hom network bursts recorded is observed under 50 μA stimulation (**Figure 3.19A**). A low number of network bursts were recorded under 10 μA stimulation, an unsurprising discovery given the previously established trend of lower general activity in this group. A general decrease in network burst duration (**Figure 3.19B**) and network spike burst count (**Figure 3.19C**) is observed in Hom neurons, although statistical significance was not reached in these parameters. Conversely, a non-significant increase is observed in spike rate of Hom neurons at 1, 25 and 50 μA (**Figure 3.19D**). Network interburst intervals seemingly increase in Hom neurons when stimulated with 50 mA, however, this is not observed when neurons were stimulated with lower current compared to WT neurons (**Figure 3.19E**).

In summary, *Oxr1*-knockout derived cortical neurons do not display any clear differing electrophysiological properties compared to wild type neurons in the reviewed parameters. Overall, increasing electrical stimulation did not affect intrinsic neuronal excitability of wild type and homozygous *Oxr1* knockouts differently under these conditions, although general trends in reduced spontaneous firing, fewer network bursts and reduced synchronicity at higher currents is alluded to, suggesting fewer ictogenic events but no clear evidence of increased seizure susceptibility *in vitro*.

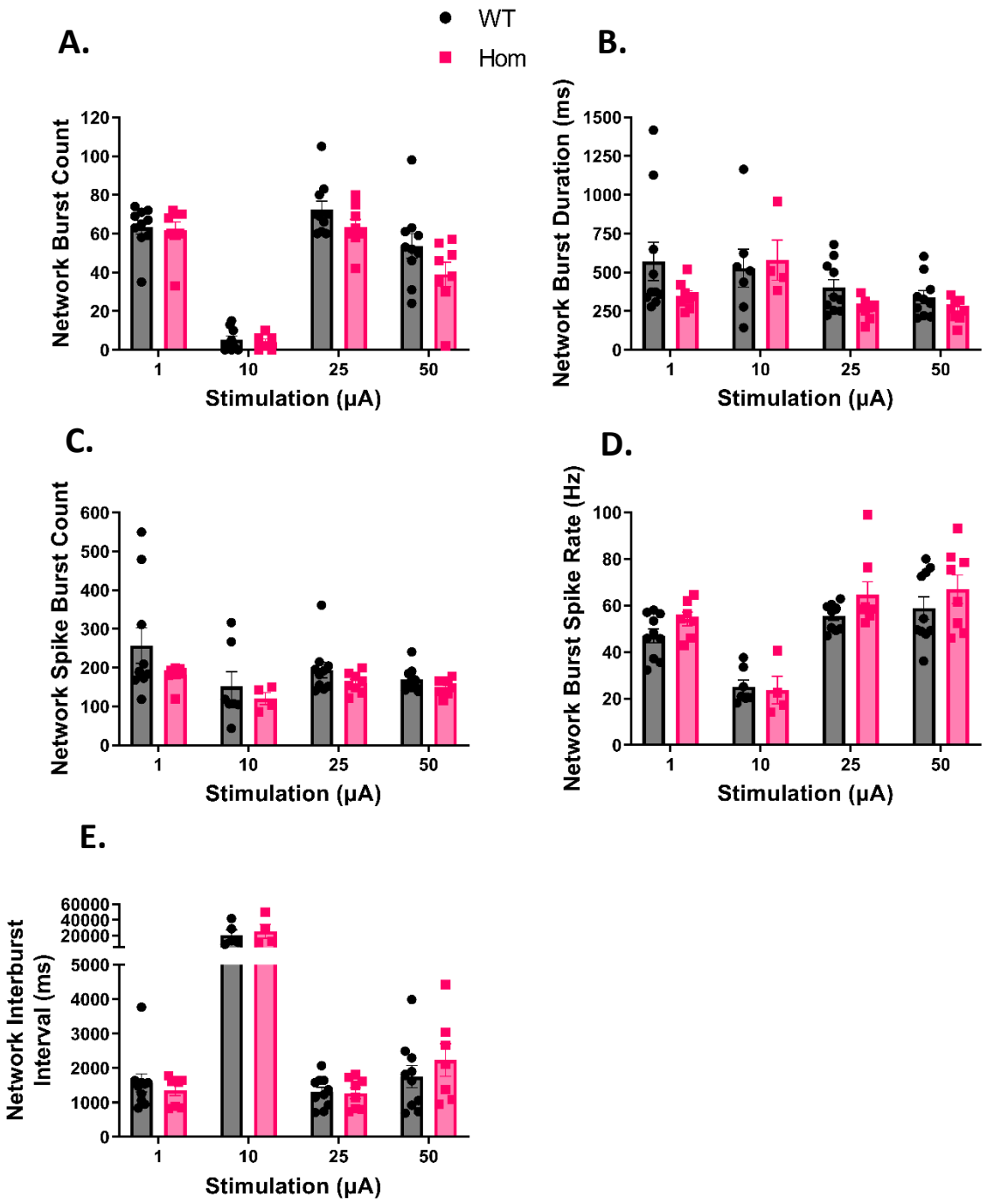

***Figure 3.19*| Multielectrode Array recordings determining synchronised network burst activity of wild type and *Oxr1* knockout primary cortical neurons following electrical stimulation**

Quantification of MEA recordings on WT and Hom primary cortical cultures using parameters of (A) network burst count, (B) network burst duration (ms), (C) network spike burst count, (D) network burst spike rate (Hz) and (E) network burst spike rate (Hz) following electrical stimulation of 1, 10 , 25 and 50 µA. Unpaired nonparametric Mann-Whitney tests with false discovery rate (FDR) correction by Benjamini, Krieger, and Yekutieli two-stage set up procedures

3.3. Discussion

3.3.1 LoF-*OXR1* patients and *Oxr1* knockout mice share overlapping pathological features with lysosomal storage disorders

Recently, deleterious mutations in the TLDc domain of *OXR1* have been identified; these patients emulate features observed in constitutive *Oxr1* knockout mice, including motor dysfunction and cerebellar degeneration (Lin et al., 2022; Wang et al., 2019). This demonstrates that expression of *OXR1* is essential for cerebellar function in both humans and mice. Data presented in this chapter demonstrate that Oxr1 is a multifaceted protein that likely plays additional critical functions beyond conferring neuroprotection against OS (Oliver et al., 2011).

Here, pre-symptomatic bulk RNA-Seq data identified 197 significant DEGs that are predominantly upregulated in cerebellar tissue from *Oxr1* knockout mice at P19; the profiles pointed clearly to an upregulation of neuroinflammatory and lysosomal-associated genes (**Table 3-1**; **Appendix. 1**). Interestingly, *Oxr1* KO cerebellar data contains a high degree of overlap with transcriptomic studies in other neurodegenerative mouse models, including those related to lysosomal storage disorders (LSDs) where neurodegenerative pathology is featured (Alam et al., 2012; Evers et al., 2017). Two in particular are: i) Loss-of-function mutations in Niemann-Pick disease, type C1/NPC Intracellular Cholesterol Transporter 1 (NPC1), a cholesterol trafficking protein, cause cerebellar ataxia, aberrant endolysosomal storage of cholesterol and cerebellar Purkinje cell death (Alam et al., 2012; Cougnoux et al., 2020); and ii) Granulin (*GRN*) encodes for progranulin (PGRN), a protein that is targeted and cleaved in lysosomes for downstream functions such as growth factor regulation (Townley et al., 2018). Mutations in *GRN* have been linked to neuronal ceroid lipofuscinosis (NCL) and frontotemporal lobar degeneration (FTLD) (Evers et al., 2017; Townley et al., 2018). Of note, the pathology in *Npc1* null mice is confined to the Purkinje

cell layer, with no CGC death, while in the *Grn1* mutant, neuropathology is characterised in frontotemporal lobes (Ghoshal et al., 2012; Townley et al., 2018).

Transcriptomic analysis has been performed on *Npc1* (*Npc1*$^{-/-}$) and *Grn* (*Grn*$^{-/-}$) knockout mice in order to elucidate disease-causing mechanisms in these LSD mouse models (Alam et al., 2012; Evers et al., 2017). Alam *et al.* (2012) subjected total RNA from whole brains of *Npc1*$^{-/-}$ and littermate controls to microarray transcriptomic analysis at several time points to represent different stages of disease progression. 186 DEGs were identified in common across the 6 different time points (115 upregulated, 71 downregulated) (Alam et al., 2012). Evers *et al.* (2017) employed RNA-seq to assess differential gene expression in whole brain RNA from presymptomatic *Grn*$^{-/-}$ mice compared to control animals, identifying 254 DEGs (59 upregulated, 195 downregulated).

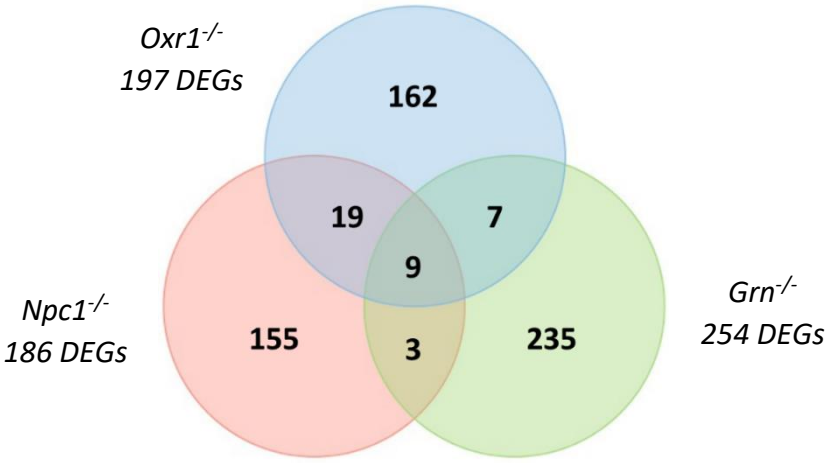

***Figure 3.20*| Overlapping differentially expressed genes in RNA sequencing data from *Oxr1* knockout cerebellum exhibiting early signs of pathology and transcriptomics from two mouse models of lysosomal storage disorders (*Npc1*$^{-/-}$, *Grn*$^{-/-}$)**

Venn diagram of overlapping differentially expressed genes (DEGs) when comparing RNA-sequencing data from *Oxr1* knockout cerebellum, *Npc1*$^{-/-}$ and *Grn*$^{-/-}$ mouse models of lysosomal storage disorders (Alam et al., 2012; Evers et al., 2017). *Oxr1* DEGs (q<0.01) as listed in **Appendix 1.** 186 DEGs identified in microarray of total RNA from whole brain of *Npc1*$^{-/-}$ mice across disease progression (20–84 days) with 1.5 fold change or higher (p<0.05) (Alam et al., 2012). 254 DEGs identified by mRNA sequencing of total RNA from whole brain of 7 month old presymptomatic *Grn*$^{-/-}$ mice (compared to wild type only) with 1.5 fold change or higher (Evers et al., 2017).

These data were taken and compared to pre-symptomatic *Oxr1* knockout cerebellar transcriptomic data obtained in this Chapter; interestingly, a distinct overlap of dysregulated genes between the datasets is observed (**Figure 3.20**) (**Table 3-3**). Nine genes (*C4b, Cd68, Ctsd, Ctss, Gfap, Lyz2, Trem2, Man2b1* and *Tyrobp*) were found to be significantly differentially expressed in all three mutants (**Table 3-3**) and GO functional enrichment suggests a role for these genes in the inflammatory response (microglial cell activation), response to stress and dysregulation is predicted to occur in the lysosome (**Table 3-4**).

An additional 19 genes were identified in common between *Oxr1* knockout and *Npc1*$^{-/-}$ mice, a number of which are the most differentially expressed in *Oxr1* knockout cerebellum (**Table 3-3**) (Alam et al., 2012). These DEGs showed enrichment for molecular functions such as hydrolase activity and carbohydrate binding, involvement in biological processes including microglial cell activation and astrocyte development, and cellular component enrichment of the extracellular space, lysosome and complement component C1q complex. Functional enrichment analysis of the 7 genes overlapping between *Oxr1* knockout and *Grn*$^{-/-}$ mice did not result in any significant annotations (**Table 3-3**). Comparing these sets of data has highlighted a number of overlapping perturbed pathways in pre-symptomatic *Oxr1* knockout cerebellum and LSD mouse models, demonstrating a clear interplay between neuroinflammation and lysosome function in the pathophysiology of NDs.

Earlier published transcriptomic studies of Oxr1-depletion have pointed towards a role in p53 regulation; analysis of *OXR1*-deficient HeLa cells treated with H_2O_2 showed differential expression of genes implicated in the OS response and the p53 signalling pathway leading to apoptosis (Yang et al., 2015). Further to this, *Oxr1A* knockout in zebrafish also presented dysregulation in the p53 signalling pathway, stress response and

inflammatory response genes in the altered transcriptome (Xu et al., 2020), demonstrating differing transcriptomic profiles to *Oxr1* knockout cerebellar tissue.

More recently, RNA-Seq profiling has been described from homozygous LoF-OXR1 patient-derived iPSCs subjected to neuronal differentiation (Lin et al., 2022). Although the authors did not specify the intended neuronal subtype identity, immunostaining at DIV20 of the neural differentiation protocol of *OXR1*-deficient cells using markers for mature neurons, specifically microtubule-associated protein 2 (MAP2) and neuron-specific class III beta-tubulin (Tuj1), revealed a decrease in fluorescent intensity compared to neuronal cells derived from healthy control iPSCs (Lin et al., 2022). This suggests that loss of *OXR1* perturbs neuronal differentiation and neuron fate commitment *in vitro* (Lin et al., 2022). RNA-Seq at DIV20 revealed 6758 DEGs (3334 upregulated, 3424 downregulated; significant at adjusted-p value < 0.05) in *OXR1*-deficient iPSC-derived 'neurons' when compared to control cells, with an enrichment for genes involved in stress responses and neuronal death, but underrepresentation of genes determining neuron projection (FDR<0.05) (Lin et al., 2022). Of note, Lin *et al.* (2022) used iPSCs derived from only a single patient and a single healthy control, and there were additionally 4723 DEGs (2318 upregulated, 2405 downregulated; significant at adjusted-p value < 0.05) at the undifferentiated iPSC stage between the two genotypes. Furthermore, the healthy control iPSC line was obtained from a cell bank (Coriell Institute) and derived from an unrelated individual, introducing genetic variability as a confounding factor in this study. In order to overcome this limitation, genome editing of homozygous LoF-OXR1 patient-derived iPSCs could be conducted to 'correct' the pathogenic *OXR1* mutation, thus generating isogenic control iPSCs for further characterisation of the effect of LoF variants in *OXR1* (Bassett, 2017; Steyer et al., 2018).

Cerebellar RNA-seq data presented in this Chapter studies Oxr1 loss-of-function in the context of whole cerebellar tissue with a full complement of cell types, in contrast to

previous studies using immortal cell lines or iPSC-derived neuronal cells (Lin et al., 2022; Yang et al., 2015). Indeed, the *in vivo* neuroinflammatory response could not be recapitulated in iPSC and 3D brain organoid models that were limited to neuronal cell types (Lin et al., 2022); as such, it is unclear how these data can be extrapolated to the context of a mammalian brain.

***Table 3-3*| Table of overlapping differentially expressed genes in *Oxr1* knockout mice, *Npc1*$^{-/-}$ and Grn$^{-/-}$ lysosomal storage disorder mouse models**
Genes listed in bold are ranked in the 20 most significant differentially expressed genes in *Oxr1* knockout cerebellum at P19.

Gene Symbol	Gene	*Oxr1*	*Npc1*	*Grn*
Adgre1	Adhesion G protein-coupled receptor E1	✓	✓	
B2m	Beta-2 microglobulin	✓	✓	
Ctsb	Cathepsin B	✓	✓	
Ctsd	Cathepsin D	✓	✓	✓
Ctss	Cathepsin S	✓	✓	✓
Ctsz	Cathepsin Z	✓	✓	
Cd68	CD68 antigen	✓	✓	✓
C1qa	Complement component 1, q subcomponent, alpha polypeptide	✓	✓	
C1qb	Complement component 1, q subcomponent, beta polypeptide	✓	✓	
C1qc	Complement component 1, q subcomponent, C chain	✓	✓	
C4b	Complement component 4B	✓	✓	✓
Dync2h1	Dynein cytoplasmic 2 heavy chain 1	✓		✓
Fcgr3	Fc receptor, igg, low affinity III	✓	✓	
Fcrls	Fc receptor-like S, scavenger receptor	✓	✓	
Ftl1	Ferritin light polypeptide 1	✓		✓
Gfap	Glial fibrillary acidic protein	✓	✓	✓
Gusb	Glucuronidase, beta	✓	✓	
Gpnmb	Glycoprotein NMB		✓	✓
Grn	Granulin	✓	✓	✓
H2-D1	H2-D1 histocompatibility 2, D region locus 1		✓	✓
Hexb	Hexosaminidase B	✓	✓	
Lgals9	Lectin, galactose binding, soluble 9	✓	✓	
Lgals3bp	Lectin, galactoside-binding, soluble, 3 binding protein	✓	✓	
Luzp2	Leucine zipper protein 2	✓		✓
Ly86	Lymphocyte antigen 86	✓	✓	
Laptm5	Lysosomal-associated protein transmembrane 5	✓	✓	
Lyz2	Lysozyme 2	✓	✓	✓

Mpeg1	Macrophage expressed gene 1	✓	✓	
Man2b1	Mannosidase 2, alpha B1	✓	✓	✓
Mbnl2	Muscleblind like splicing factor 2	✓		✓
Pcnp	PEST proteolytic signal containing nuclear protein	✓		✓
Plek	Pleckstrin	✓	✓	
Plp1	Proteolipid protein (myelin) 1		✓	✓
Rps21	Ribosomal protein S21	✓		✓
Serpina3n	Serine (or cysteine) peptidase inhibitor, clade A, member 3N	✓	✓	
Trem2	Triggering receptor expressed on myeloid cells 2	✓	✓	✓
Tyrobp	TYRO protein tyrosine kinase binding protein	✓	✓	✓
Usp9x	Ubiquitin specific peptidase 9, X chromosome	✓		✓
Ucp2	Uncoupling protein 2 (mitochondrial, proton carrier)	✓	✓	

***Table 3-4*| Gene ontology functional enrichment analysis of 9 overlapping genes observed between *Oxr1* knockout mice, *Npc1*$^{-/-}$ and Grn$^{-/-}$ lysosomal storage disorder mouse models**

BP: Biological Processes, CC: Cellular Compartment

Gene Ontology	Term Name	Adjusted p value	Associated Genes
BP	Microglial Cell Activation Involved In Immune Response	0.001068978	*Tyrobp, Trem2*
BP	Inflammatory Response	0.001929487	*Tyrobp, C4b, Ctss, Cd68, Trem2*
BP	Defense Response	0.006085432	*Tyrobp, C4b, Ctss, Cd68, Lyz2, Trem2*
BP	Response To Stress	0.048487984	*Tyrobp, C4b, Ctss, Gfap, Cd68, Lyz2, Trem2*
CC	Lysosome	5.68695E-05	*Man2b1, Ctss, Gfap, Ctsd, Cd68*
CC	Extracellular Region	0.010903254	*C4b, Man2b1, Ctss, Ctsd, Lyz2, Trem2*
CC	Lysosomal Membrane	0.011142519	*Gfap, Ctsd, Cd68*

3.3.2 Limitations of using bulk RNA-seq on cerebellar tissue from *Oxr1* knockout mice

Total cerebellar RNA was isolated from wild type and *Oxr1* knockout mice at P19 and subsequently analysed to generate this RNA-seq dataset. Thus, these values are the average differential expression of each gene without distinguishing between different cell types that may reveal specific aspects of gene dysregulation driving CGC death. Nevertheless, CGCs are highly enriched in the cerebellum, accounting for approximately 99% of the neuronal cell population in this brain region (Consalez et al., 2020). Niemann-Pick Disease Type C (NPC) mouse models feature specific loss of cerebellar Purkinje neurons and neuroinflammation, yet the reason for this distinct Purkinje cell degeneration was largely uncharacterised, though Purkinje neuronal dysfunction was hypothesised to be cell autonomous (Alam et al., 2012; Lopez et al., 2011; Sarna et al., 2003).

In order to determine whether constitutive loss of *Npc1* was causing cell type-specific cerebellar pathology, single cell RNA sequencing (scRNA-seq) was conducted on both pre-symptomatic and symptomatic *Npc1*$^{-/-}$ cerebellar tissue (Cougnoux et al., 2020). These data identified overlapping transcriptomic profiles in Purkinje cells and other cerebellar neuronal populations; for example, *Apoe, Ctsd* and *Lyz2* were found to be significantly upregulated in Purkinje cell types in *Npc*$^{-/-}$ symptomatic cerebellar tissue, but also in basket neurons and unipolar brush cells (Cougnoux et al., 2020). Interestingly, DEGs were only detected in microglial and endothelial populations at an asymptomatic time point, suggesting microglial activation precedes neuronal dysfunction (Cougnoux et al., 2020). Furthermore, the non-neuronal cell transcriptomic profile largely overlaps with that of Purkinje neurons and other cerebellar neuronal cell types at a symptomatic time point in *Npc1*$^{-/-}$mice, thus these data did not shed light on reasons for selective neuronal vulnerability of Purkinje neurons in this mouse model (Cougnoux et al., 2020). In the context of performing scRNA-seq on pre-symptomatic *Oxr1* knockout cerebellar tissue, it

is possible that this method would not identify CGC-specific intrinsic pathways contributing to the observed degeneration.

Although RNA-sequencing provides transcriptome-wide analysis of molecular dysregulation, it is not representative of the dynamic cellular interactome and perturbations of molecular pathways at the protein level (Tasaki et al., 2022). For example, an increase in autophagic flux is observed in cells and tissue lacking expression of *Oxr1*, indicated by protein levels of p62 and lipidated LC3. Notably, their encoding genes were not found to be differentially expressed in *Oxr1* knockout cerebellum at P19. Furthermore, it is now understood that loss of the *Oxr1-A* brain-expressed isoform leads to a significant reduction in histone H3 arginine 2 methylation due to the absence of Oxr1A-PRMT5 protein-protein interactions (Yang et al., 2020); importantly, epigenetic modifications, perturbations of protein-protein interactions and post-translational modifications are not detected by this technique. Taking this in to consideration, RNA-seq is a gold-standard method for transcriptional profiling (Rao et al., 2018), however a combination of proteomic and other molecular techniques are likely required to further characterise the role of *Oxr1* in cerebellar pathology.

3.3.3 Predicted role for Oxr1 in protein-lipid binding

GO molecular function enrichment analysis of significant DEGs (q<0.01) found in pre-symptomatic *Oxr1* knockout cerebellum predicted a likely role for Oxr1 in lipoprotein particle binding, protein-lipid complex binding, as well as apolipoprotein binding (**Figure 3.4B**). Intriguingly, full-length Oxr1 isoforms contain a GRAM (Glycosyltransferases, Rab-like GTPase Activators, Myotubularins) domain in the N-terminal half of the protein (Finelli et al., 2016). GRAM domain-containing proteins are typically membrane-associated and may harbour lipid-binding signalling properties (Aalinkeel & Mahajan, 2016). Mutations in the GRAM domain of Myotubularin-related proteins, lipid phosphatases, have been shown to cause NDs, X-linked myotubular myopathy (XLMTM) and Charcot-Marie-Tooth (CMT) disease (Herman et al., 2002; Tersar et al., 2007). A number of overlapping clinical phenotypes are observed between XLMTM patients and LoF-OXR1 patients, including hypotonia, seizures and scoliosis, suggesting loss of Oxr1-FL and subsequent lack of GRAM domain contributes to observed symptomology (Cahill et al., 2007; Herman et al., 2002; Lin et al., 2022; McEntagart et al., 2002; Wang et al., 2019).

Male mice lacking *Oxr1A*, a brain specific full-length mouse Oxr1 isoform, but other *Oxr1* isoforms are still expressed, present with hepatic steatosis at 12 months of age; liver concentrations of cholesterol remained unaltered, where as a significant increase in triglyceride levels were observed (Yang et al., 2020). Indeed, liver transcriptomes from mice lacking expression of a brain specific isoform of *Oxr1* demonstrated a role for Oxr1 in fatty acid metabolism, immune response and apoptotic processes (Yang et al., 2020). TEM of P19 cerebellar tissue from constitutive *Oxr1* knockout mice demonstrated an accumulation of lipid droplets. Taken together, this predicts a role for Oxr1 in lipid/fatty acid metabolism, possibly through lipid binding via GRAM domain interactions.

DEGs in P19 RNA-Seq data that were assigned to protein-lipid binding GO terms were *Trem2 (*Triggering Receptor Expressed on Myeloid cells 2, FC=2.42*), Lpl* (Lipoprotein Lipase, FC=2.66)*, Abca1 (*ATP Binding Cassette Subfamily A Member 1 FC=1.20*), Ldlr (*Low-density lipoprotein receptor, FC=1.28)*, Apoe (*Apolipoprotein E, FC=1.12*)* and *Stab1* (Stabilin 1, FC=1.28) (**Appendix. 1**). The APOE-TREM2 pathway in microglia plays a crucial role in the innate immune response and has been heavily implicated in in Alzheimer's disease (AD), by modulating microglial homeostasis (Atagi et al., 2015)(**Figure 3.21**). Alterations on this axis are associated with a neurodegenerative 'phenotypic-switch' to a disease-associated signature including upregulation of *Hexb, Cx3Cr1* and *Olfml3* (Krasemann et al., 2017). It is possible that loss of Oxr1 triggers a microglial phenotypic switch by lipid-protein binding interactions in the cerebellum.

Low-density lipoprotein (LDL) has also been identified as a TREM2 ligand (Yeh et al., 2016); interestingly, upregulation of *LDLR,* which is significantly overexpressed in the cerebellum of *Oxr1* knockout mice (*Ldlr*), has been shown to aid sequestration of free cholesterol, facilitating regulation of LDL uptake and maintenance of LDL-cholesterol plasma levels of *in vivo* (Huang et al., 2010; Issandou et al., 2004). TYRO protein tyrosine kinase binding protein (TYROBP) also binds TREM2 and plays a downstream role in activation of the complement cascade and immune response (Haure-Mirande et al., 2019). Finally, TREM2 interactions facilitate the clearance of apoptotic neurons and extracellular debris (Atagi et al., 2015; Casali & Reed-Geaghan, 2021); given that cerebellar granule cells are apoptotic at disease end-stage in *Oxr1* knockout mice, it is possible that the Apoe-Trem2 pathway is activated to mitigate the effects of cerebellar granule cell dysfunction (Oliver et al., 2011).

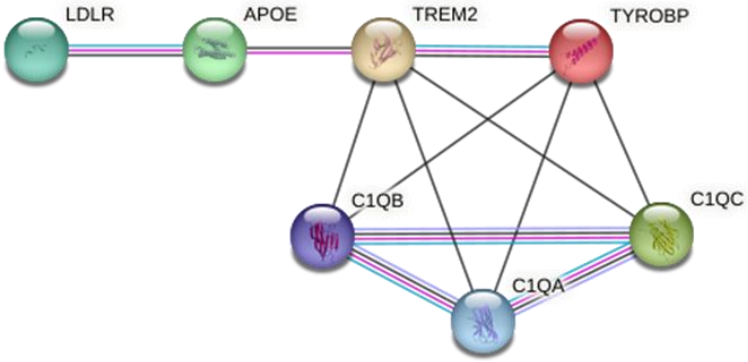

***Figure 3.21*| STRING APOE-TREM2 protein-protein interactions**

Visual representation of APOE-TREM2 protein interactions extracted from STRING database. LDLR: Low-density lipoprotein receptor, APOE: Apolipoprotein E, TREM2: Triggering Receptor Expressed on Myeloid cells 2, TYROBP: TYRO protein tyrosine kinase binding protein, C1QA/C1QB/C1QC: Complement C1q subcomponent subunit A/B/C.

3.3.4 Challenges of characterising electrophysiology phenotypes in constitutive *Oxr1* knockout mice

A key clinical phenotype observed in LoF-OXR1 patients is early-onset epilepsy; overt myoclonic/tonic seizures are not observed in *bella* mice, however this has not been assessed quantitatively over 24 hours and subtle events may be masked by the gait abnormalities and ataxia (Lin et al., 2022; Oliver et al., 2011; Wang et al., 2019). Electroencephalography (EEG) is the gold standard method to measure neuronal activity in humans, as well as in adult rodent models of NDs (Maheshwari, 2020; Shellhaas, 2015; Srinivasan & Nunez, 2012; Vogler et al., 2017). Although technically challenging, there are reports of performing EEG on early postnatal mice (Chini et al., 2019; Gataullina et al., 2016; Rensing et al., 2018; Zanelli et al., 2014); de Camp *et al.* (2017) carried out EEG electrode implantation and recordings as early as P0/P1, yet there are still major caveats associated with neonatal EEG recordings, such as high signal background issues, logistical implantation and stability of electrodes, as well as pup-dam dependence (Gataullina et al.,

2016; Odabaee et al., 2014; Rensing et al., 2018). As such, this outlines a number of difficulties in obtaining EEG recordings from constitutive *Oxr1* knockout mice due to their early lethality (Oliver et al., 2011).

In this Chapter, an *in vitro* approach was adopted to begin characterising the electrophysiological properties of primary neurons derived from constitutive *Oxr1* knockout mice. At 14 DIV, MEA recordings from primary cortical neurons demonstrated that loss of *Oxr1* did not cause significant alterations in neuronal activity *in vitro*, although an overall trend in reduced neuronal activity was observed (**3.2.9**). In iPSC-derived neuronal cellular models of epileptic disorders, reported MEA characteristic features of a seizure-like profile include elevated spontaneous firing activity, coupled with a significant increase in burst frequency and spike rate, outlining a hyper excitability seizure phenotype *in vitro* (Nadadhur et al., 2019; Que et al., 2021; Quraishi et al., 2019). In light of this characterisation, *Oxr1* cortical knockout neurons show a non-significant decrease in spontaneous firing, burst frequency, as well as reduced network burst activity, suggesting limited differences in cell-intrinsic excitability between wild type and *Oxr1* knockout cortical neurons and absence of a 'typical' seizure phenotype in this cellular model. Further to this, significant differences in network burst intervals were not observed between the two genotypes, therefore it appears that loss of *Oxr1* in cortical neurons does not cause perturbations in synchronicity *in vitro* (Quraishi et al., 2019).

Interestingly, the observed electrophysiological properties of *Oxr1*-deficient cortical neurons overlap, in part, with an iPSC model of Kleefstra syndrome. Pathogenic mutations in Euchromatic Histone Lysine Methyltransferase 1 (*EHMT1*) causes Kleefstra syndrome which, similar to LoF-OXR1 patients, features intellectual disability and developmental delay (Frega et al., 2019; Lin et al., 2022; Wang et al., 2019). Frega *et al.* (2019) conducted MEA recordings on iPSC patient-derived excitatory neurons which

revealed increased interburst intervals, as well as decreased spontaneous firing and bursting activity. From this, it could be hypothesised that *Oxr1* knockout cortical neurons may display elements of neuronal network dysfunction *in vitro*.

Impaired neurodevelopmental processes, such as neuronal migration and maturation, have also been implicated in epileptogenesis (Bozzi et al., 2012). Pathogenic mutations in SCN1A (Sodium channel protein type 1 subunit alpha) have been found to impair neuron maturation and reduce neuronal excitability in patient iPSCs-derived neurons *in vitro*, thus increasing susceptibility to febrile seizures (Scalise et al., 2022). This can lead to aberrant neuronal connectivity and subsequent emergence of a seizure phenotype (Engel et al., 2013; Goldberg & Coulter, 2013). Interestingly, 3D cerebral organoids derived from LoF-OXR1 patient iPSCs demonstrated impaired neurogenesis, maturation and migration through dysregulation of PRMT-mediated histone modifications (Lin et al., 2022). Taken together, the suggested role of *Oxr1* in neuronal maturation and migration may result in the observed reduction in neuronal activity of *Oxr1* knockout-derived primary cortical neurons and onset of epilepsy in LoF-OXR1 patients, although distinct cortical malformations have not been described in humans or mice (Lin et al., 2022; Oliver et al., 2011; Wang et al., 2019). In order to challenge this hypothesis, Sholl analysis and longitudinal MEA could be employed to assess neuronal maturation, synaptic connectivity and electrical activity *in vitro* of primary cortical neurons (Bird & Cuntz, 2019; Negri et al., 2020).

Thus far, the underlying seizure aetiology in human LoF-OXR1 patients is unclear, yet studying the role of *Oxr1* in epileptogenesis and synaptic dysfunction using *Oxr1* knockout models is very much in its infancy due to the described limitations. There are also some critical constraints to the design of this study. This includes the absence of glial cells *in vitro* and amalgamation of excitatory and inhibitory cortical neurons used in the MEA

recordings, both of which have been demonstrated to influence overall electrophysiological properties detected using this method (McCready et al., 2022; Nadadhur et al., 2019). Given the observed neuroinflammatory response in constitutive *Oxr1* knockout mice, it may be more appropriate to investigate neuronal dysfunction and putative *in vitro* seizure phenotypes using co-cultures.

3.3.5 Oxr1 as a synaptic protein

Synaptic dysfunction is unequivocally linked to epileptogenesis (Bozzi et al., 2012; Calcagnotto et al., 2005). Using primary cortical and hippocampal neurons isolated from a mouse model of *Tbc1d24* haploinsufficiency, Finelli, Aprile, et al. (2019) demonstrated that Tbc1d24 plays a critical role in endocytosis, synaptic vesicle trafficking and regulating neurotransmission. Similarly, proteomic studies in humans and mice have also identified Oxr1 as a synaptic protein (Bayes et al., 2012; Gonzalez-Lozano et al., 2020; Roy et al., 2018). Attempts to elucidate the endogenous subcellular localisation of Oxr1 have been impeded by lack of specific Oxr1 antibodies suitable for immunostaining, therefore studies have employed transgenic overexpression of HA-tagged Oxr1 which may not be representative of the native protein. Nevertheless, Wang *et al.* (2019) demonstrated that OXR1 localised to lamina neuron synapses in the medulla of *mtd*-knockout Drosophila overexpressing HA-tagged *OXR1*. Previous immunocytochemistry revealed that Oxr1-FL-HA colocalises with the Golgi apparatus and synaptic boutons in primary cerebellar granule cell cultures, further supporting the possible role of Oxr1 in synaptic function and synaptic vesicle trafficking (Svistunova, 2020).

Palmitoylation is a posttranslational modification whereby lipid motifs are covalent added to proteins; intriguingly this process typically occurs at synapses and plays an important role in membrane trafficking and synaptic function (Sapir et al., 2019; Zareba-

Koziol et al., 2018). Mutations in depalmitoylation enzymes PPT1/PPT2 (Palmitoyl-protein thioesterases) have be found to cause neuronal ceroid lipofuscinosis (NCL), a neurodegenerative disorder associated with defects in lysosomal function that can result in brain atrophy, intellectual disability and epilepsy (Gupta et al., 2001; Sapir et al., 2019). A systematic review of current palmitoylation databases, such as Swiss Palm, compared to PPT1 KO data identified Oxr1 as a putative substrate of PPT1 but the functional relevance of this remains to be determined (Gorenberg et al., 2022).

Preliminary TEM analysis of P19 *Oxr1*-knockout cerebellum revealed enlarged pre-synaptic vesicles, although additional quantitative analysis would require further images. Interestingly, increased synaptic vesicle size has been correlated to neurotransmitter loading (Budzinski et al., 2009; Daniels et al., 2004). Loss of Rab5, a regulator of endosomal trafficking, leads to increased synaptic vesicle size and defects in synaptic transmission in Drosophila photoreceptors (Shimizu et al., 2003). To investigate the contents of these putatively enlarged vesicles observed in TEM, purification of synaptic vesicles from wild type and constitutive *Oxr1* knockout cerebellar and cortical tissue followed by quantitative proteomic analysis could be employed (Chantranupong et al., 2020; Takamori et al., 2006; Wittig et al., 2021).

Interestingly, the v-ATPase holoenzyme is essential for establishing a proton gradient for synaptic vesicle neurotransmitter loading (Eaton, Merkulova, et al., 2021; Forgac, 2007). Recently, Oxr1 and other TLDc proteins have been implicated in regulating the reversible disassembly of the v-ATPase holoenzyme (**6.3.1**), therefore it could be that loss of *Oxr1* impairs normal intravesicular acidification of synaptic vesicles (Eaton, Brown, et al., 2021; Eaton, Merkulova, et al., 2021; Khan et al., 2022). Bodzeta *et al.* (2017) observed a significant reduction in synaptic vesicle release upon pharmacological induction of v-ATPase assembly. Thus far, Khan *et al.* (2022) proposed a role for Oxr1 in regulating

the disassembly of the v-ATPase holoenzyme; as such, it could be inferred that loss of Oxr1 leads to an increase in assembled v-ATPase complexes at the synaptic vesicle membrane, subsequently impairing synaptic transmission *in vitro* (Bodzeta et al., 2017). MEA recordings of *Oxr1* knockout primary cortical neurons demonstrated a reduction in neuronal activity is observed, therefore it is possible that loss of Oxr1 at excitatory synapses disrupts release of neurotransmitters, such as glutamate (Bozzi et al., 2012). Yet, single cell RNA-seq data of the human brain indicates that *OXR1* is expressed in both excitatory and inhibitory neurons, therefore characterising the role of Oxr1 in these different neuronal cell types and in establishing excitatory/inhibitory networks is required (Human Protein Atlas)(Karlsson et al., 2021). Furthermore, determining how TLDc proteins regulate v-ATPase assembly and function will be crucial in understanding their role in synaptic dysfunction; nevertheless, these data provide increasing evidence that disruption of Oxr1 and other TLDc proteins leads to synaptopathies.

3.3.6 Concluding remarks

This chapter has demonstrated that constitutive loss of *Oxr1* in the mouse leads to a robust neuroinflammatory response in the cerebellum at P22, as well as autolysosomal dysfunction in cerebellar tissue and *Oxr1* knockout-derived primary cells. Significant differential expression of genes implicated in inflammatory and lysosomal pathways is observed in pre/early-symptomatic *Oxr1* knockout cerebellar tissue. Given that the observed gene dysregulation occurs prior to the emergence of apoptotic cerebellar granule cells and the ataxic phenotype displayed by disease end-stage *Oxr1* knockout mice, this implicates these pathways as disease-driving mechanisms in the absence of *Oxr1* expression.

Moreover, there are many overlapping features between LoF-*OXR1* patients and constitutive *Oxr1* knockout mice, including early-onset cerebellar-specific pathology, neurodegeneration and evident pathogenic disruption of lysosomal pathways. This demonstrates that *OXR1* is required for neurological function in both humans and mice. Conversely, inflammation has not been described in LoF-O*XR1* patients and typical seizure phenotypes have not been characterised in *Oxr1*-deleted mice or *in vitro*. This stresses a high level of conserved function between *OXR1* in both species, however some critical differences are still observed. Nevertheless, this constitutive *Oxr1* knockout mouse model remains a useful tool to study the molecular role of *OXR1* and implications in human disease.

RESULTS II

Chapter 4 : Characterisation of a conditionally-induced adult knockout of *Oxr1*

4.1 Introduction

4.1.1 *Oxr1* plays a critical role in neurodevelopment

Disruption of autolysosomal functions and inflammatory processes in CNS development have been linked to early-onset neurological pathologies, including seizures and neurodegeneration (Alam et al., 2012; Bozzi et al., 2012; Fassio et al., 2018; Gupta et al., 2001; Kim et al., 2015; Siintola et al., 2006). For example, in humans, deleterious mutations in key lysosomal proteolytic enzyme cathepsin D (CTSD) have been reported to cause neonatal seizures, as well as cerebral and cerebellar atrophy (Hersheson et al., 2014; Varvagiannis et al., 2018). Evidently in mice, neuron-specific knockout of autophagy-related 5 (*Atg5*) resulted in early-onset motor dysfunction and neurodegeneration from P21, with apparent swelling of Purkinje cells and apoptotic CGCs by 6 weeks of age (Hara et al., 2006), thus suggesting that autolysosomal processes are essential for neuronal function and survival during development.

Further to this, inflammatory insults and immune system stimulation *in utero* leads to impaired neurogenesis and neurobehavioral defects in mice (Hester et al., 2018; Kwon et al., 2022; Moller et al., 2015); for example, exposing developing embryos to lipopolysaccharide (LPS), a pathological stimuli, lead to an overall reduction in hippocampal neurogenesis and CGC density by P28 (Hester et al., 2018). Interestingly, downregulation of interleukin-6 (IL-6) was observed in serum from children with both Autism Spectrum Disorder (ASD) and epilepsy, preliminary identifying cytokines as risk factors for aberrant neurodevelopment (Inga Jacome et al., 2016). Taken together, this delineates a clear role for autolysosomal and neuroimmune function during embryonic and early postnatal CNS development in both human and rodent brains to establish neuronal circuitry and cell

survival (Kole et al., 2013); excitingly, **Chapter 3** has established a putative role for Oxr1 in autolysosomal function and modulating neuroinflammation *in vivo* and is pertinent to CGC survival.

Given that early CNS development is an energy demanding period, the increased metabolic requirements render this process critically vulnerable to oxidative stress (OS) (Rice & Barone, 2000). Indeed, reactive oxygen species (ROS) are natural by-products of metabolism, but also play a critical role as signal transducers during development, thus adequate redox regulation and the preservation of ROS homeostasis is essential during neurodevelopment (Dennery, 2007; Rice & Barone, 2000; Wang & Michaelis, 2010).

Elevated OS in neurodevelopment has broadly been associated with neurological disorders, such as ASD (Morimoto et al., 2020), epilepsy (Aguiar et al., 2012) and schizophrenia (Moller et al., 2015). For example, exposing rat pups to OS *in utero* leads to elevated concentrations of pro-oxidation markers and reduced antioxidant capacity (Rains et al., 2021). At P21, increased brain and plasma lipid peroxidation resulted in impaired locomotor activity and cognitive behaviour, indicating tight negative correlation between levels of OS and neurological impairment (Rains et al., 2021). In mice, inducing perinatal hyperoxia resulted in impaired hippocampal development and cognitive ability in early adulthood (Abbah et al., 2022). Ultimately, this illustrates the need for endogenous protective mechanisms to modulate OS in early neurodevelopment.

Oxr1 has previously been described to be neuroprotective both *in vitro* and *in vivo*, and is expressed in the brain embryonically, postnatally, as well as in adulthood in both humans and mice (**Figure 4.1**; **Figure 4.2**)(Cardoso-Moreira et al., 2019; Finelli et al., 2016; Oliver et al., 2011). In both organisms, embryonic expression of *Oxr1* is relatively low, however a stark increase is observed in postnatal brain and cerebellum (**Figure 4.1**; **Figure 4.2**). Patients with bi-allelic loss-of-function (LoF) mutations in OXR1 present with a

combination of seizures, ataxia and cerebellar atrophy, alongside thinning of the corpus callosum (Lin et al., 2022; Wang et al., 2019). Considering that the onset of symptoms is typically in childhood, it is interesting to note that a sharp increase in cerebellar expression of *OXR1* is observed between the new-born stage and 4 years age, with a decline in expression following this period; *OXR1* expression continues to gradually increase in the brain (forebrain) from birth until approximately 30 years (**Figure 4.1**). Exome sequencing of individuals affected by specific language impairment (SLI) identified a premature stop codon variant in the short isoform of OXR1 (Chen et al., 2017). LoF-OXR1 patients have also been reported to have developmental delay, intellectual disability and speech impairments (Lin et al., 2022; Wang et al., 2019). Together, this offers *OXR1* as a susceptibility locus for the development of SLI and other neurological impairments, supporting the importance of OXR1 in neurodevelopment.

Similarly, constitutive knockout of *Oxr1* results in early-onset progressive cerebellar ataxia, localised neurodegeneration of CGCs and juvenile lethality at P22-26 (Finelli et al., 2016; Oliver et al., 2011). Of note, significant oxidative DNA damage and OS-induced cell death is observed at P24 (Oliver et al., 2011), while an exponential increase is observed in expression of *Oxr1* between P3-P28 in mouse brain and cerebellum (**Figure 4.2**); a time frame in which we observe the onset of the ascribed phenotype in *Oxr1* knockout mice.

Overall, this strongly implicates Oxr1 as a critical factor in early murine postnatal development, particularly for cerebellar function (Oliver et al., 2011). Owing to the rapid onset of symptoms and discrete regional neurodegeneration observed in knockout mice, the function of *Oxr1* in brain regions outside of the cerebellum, as well as beyond early postnatal time points, was still undetermined (Oliver et al., 2011).

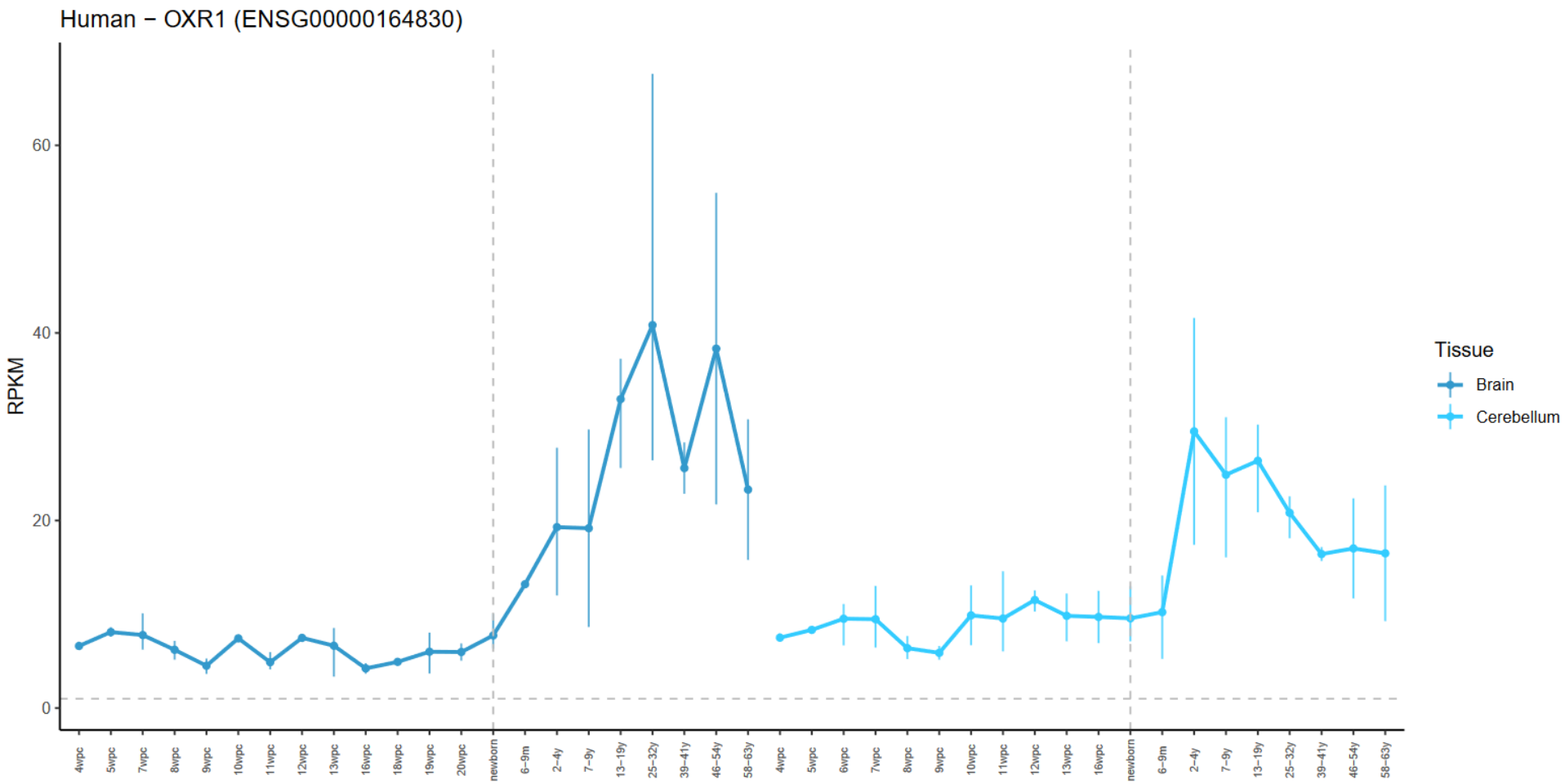

***Figure 4.1*| Expression of OXR1 in the human brain and cerebellum at different developmental stages**

Human gene expression profile of OXR1 in the developing brain (forebrain/cerebrum) and cerebellum (hindbrain/cerebellum), from 4 weeks post-conception (wpc) until 63 years.

RPKM – Reads per kilobase of transcript, per million mapped reads.

Transcriptomic data and figure from (Cardoso-Moreira et al., 2019; Chen et al., 2017).

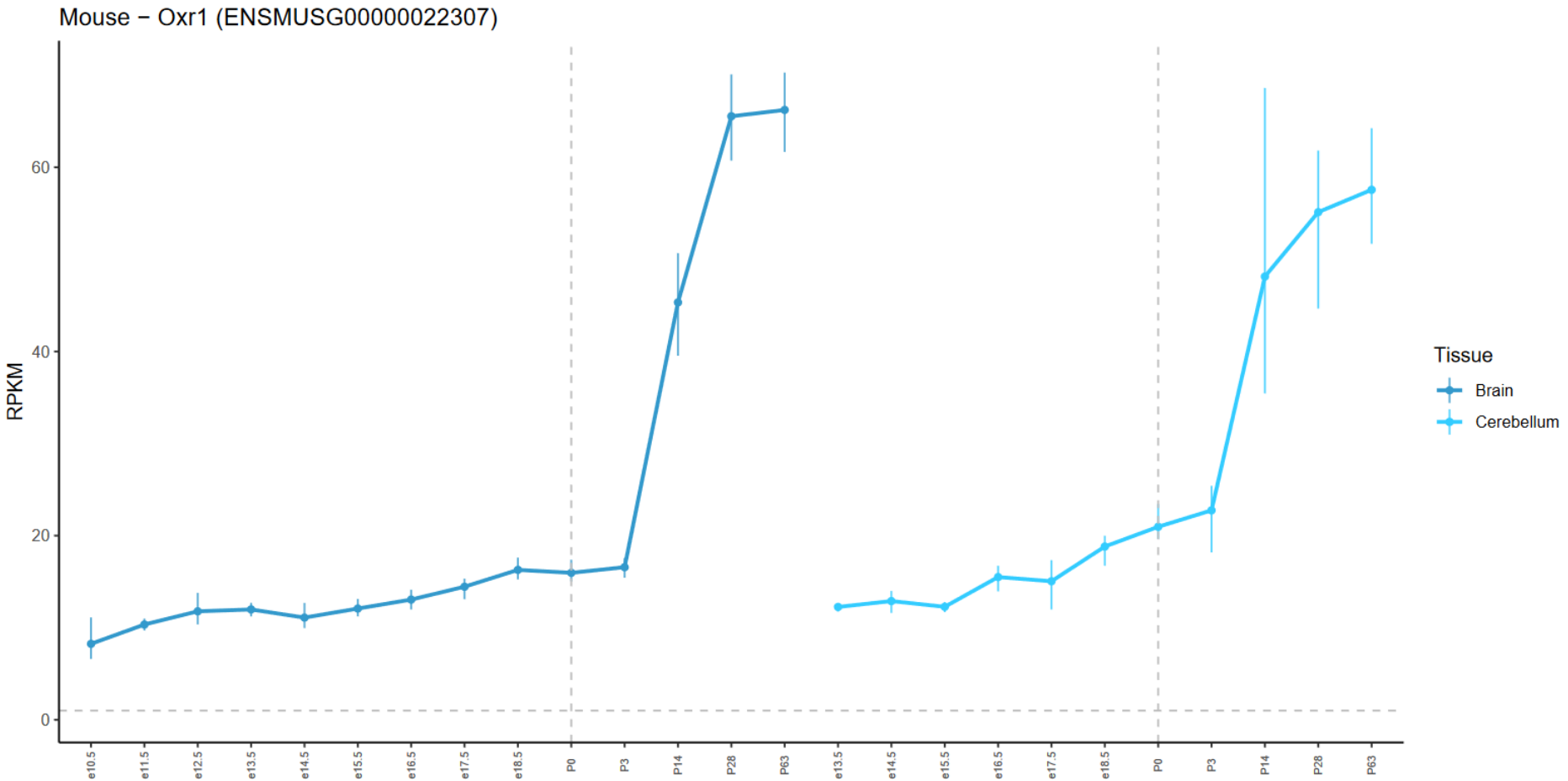

***Figure 4.2*| Expression of Oxr1 in the mouse brain and cerebellum at different developmental stages**

Mouse gene expression profile of Oxr1 in the developing brain (forebrain/cerebrum) and cerebellum (hindbrain/cerebellum) from embryonic day/stage (e) 10.5 until postnatal day (P) 63.

RPKM – Reads per kilobase of transcript, per million mapped reads.

Transcriptomic data and figure from (Cardoso-Moreira et al., 2019).

4.1.2 Use of conditional-ready *Oxr1* allele (*Oxr1*$^{tm1c/tm1c}$) to study role of Oxr1 in brain regions outside of the cerebellum in mice

Cre-driver lines, in combination with conditional loss-of-function alleles, can be utilised in order to create temporal and spatial deletions of a target gene (Adams & van der Weyden, 2008; Morozov et al., 2003). A custom knockout-first conditional allele (*Oxr1*$^{tm1a/tm1a}$) was initially generated as described by Skarnes et al. (2011) and subsequently, a conditional-ready line was derived through FLP-FRT site directed recombination (**Figure 4.3**)(Finelli et al., 2016).

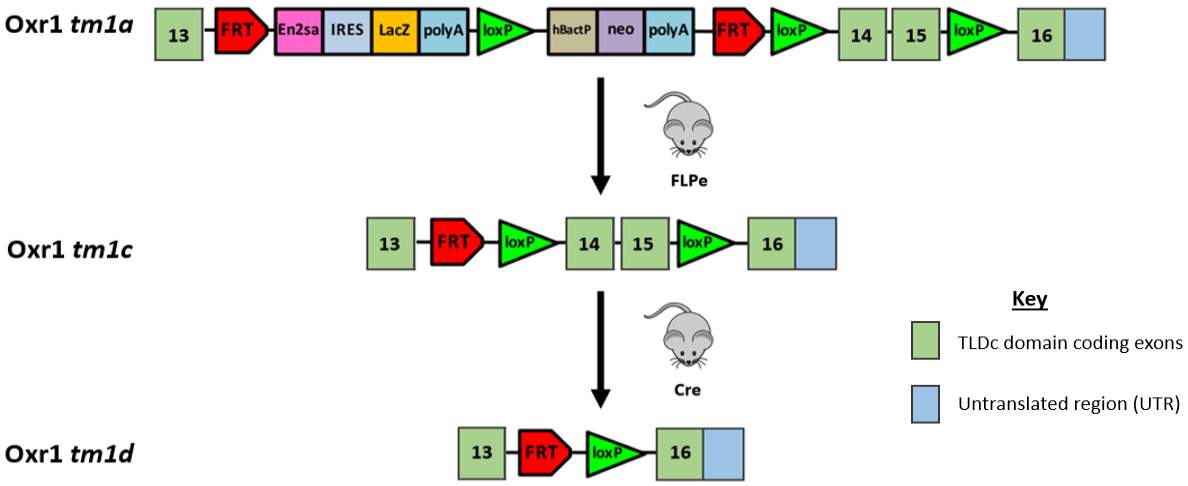

***Figure 4.3*| Schematic diagram demonstrating generation of conditional *Oxr1*$^{tm1c/tm1c}$ allele and targeted exons for deletion, disrupting all isoforms of Oxr1**

Schematic diagram of conversions from 'knock-out first allele (*Oxr1*$^{tm1a/+}$*, tm1a*)' to 'conditional ready allele (*Oxr1*$^{tm1c/+}$*, tm1c*)' to 'knockout allele (*Oxr1*$^{tm1d/+}$*, tm1d*)'. *Oxr1* 'knock-out first' (*tm1a*) allele from the Wellcome Trust Sanger Institute (*Oxr1*$^{tm1a(EUCOMM)Wtsi}$) ablates *Oxr1* via the gene trapping method described in Skarnes et al. (2011). By crossing *tm1a* mice with a β-actin driven enhanced Flippase (FLPe) mouse line, flippase recombinase target sites recombine which excises the IRES-lacZ gene trapping element and floxed promoter-driven neo cassette, thus generating the conditional-ready *tm1c* allele. Subsequently, *tm1c* mice can be crossed to various Cre-driver lines to generate targeted Oxr1 deletions. Upon expression of Cre recombinase, loxP sites flanking critical exons 14 and 15 recombine, introducing a frameshift mutation and early stop codon resulting in the null *tm1d* allele.

FLPe: enhanced flippase, FRT: FLPe recognition target sites, En2sa: mouse *engrailed 2* exon 2 splice acceptor, IRES: internal ribosome entry site, LacZ: *lacZ* reporter gene, polyA: SV40 poly-adenylation signal, neo: neomycin resistance gene, LoxP: Locus of X-over P1 Cre recombinase target sites and hBactP: autonomous human β-actin promoter. Numbered boxes correspond to TLDc domain coding exons. Diagram adapted from (Williamson, 2019).

In the conditional-ready allele, the critical TLDc domain exons 14 and 15, present in all Oxr1 isoforms, are flanked by LoxP target sites. Cre-mediated recombination deletes these exons, thereby introducing a frameshift mutation and early stop codon. This, in turn, produces a truncated protein product that is subsequently degraded, generating a true null allele (**Figure 4.4**). Constitutive Cre-driven deletion of *Oxr1* using this conditional-ready line (*Oxr1*$^{tm1c/tm1c}$) resulted in the identical phenotype to the original *bella* mutant, thus confirming its validity to ablate expression of all Oxr1 isoforms (**Figure 4.3**; **Figure 4.4**) (Finelli et al., 2016; Oliver et al., 2011). Previous members of the Oliver lab have employed this conditional-ready mouse model and crossed it to a number of Cre-driver lines. This allowed for the spatially controlled Cre-mediated deletion of *Oxr1*, providing novel insights in to the role of *Oxr1* outside of the cerebellum (discussed in **4.3.2**).

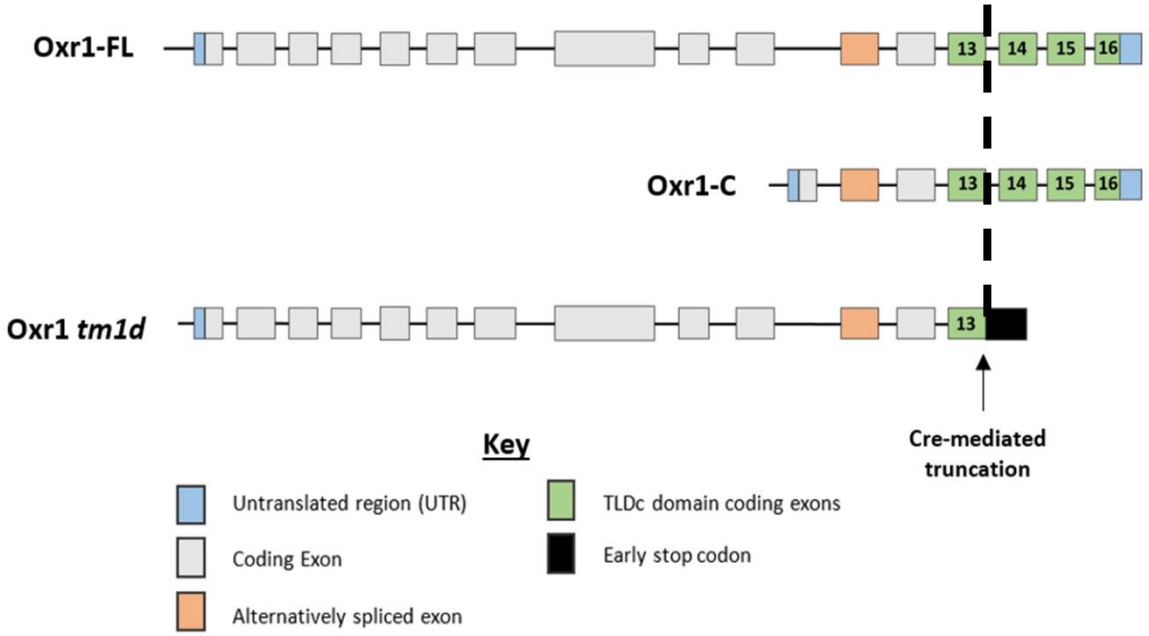

***Figure 4.4*| Schematic diagram of Cre-mediated disruption of Oxr1 isoforms**
Exon structure of Oxr1-FL and Oxr1-C isoforms, with exons 13-16 encoding the TLDc domain (not to scale). As described in **Figure 4.3**, exons 14 and 15 are targeted for deletion in the *tm1c* allele in the presence of Cre. Following Cre-mediated recombination activity, exons 14 and 15 are excised, which introduces a frameshift mutation leading to an early stop codon and subsequently truncated protein isoforms, resulting in a true null. Numbered boxes correspond to TLDc domain coding exons. Diagram adapted from (Williamson, 2019).

4.1.3 Tamoxifen-Inducible Ubiquitous Cre System *in vivo*

Recent studies have demonstrated the value of using inducible knockout systems to circumvent early lethality or discover novel functions in adulthood, independent of developmental roles. For example, constitutive knockout of *Zinc-finger homeobox 3 (Zfhx3)*, an essential developmental gene required for the establishment of circadian rhythms, results in early lethality and the adult-associated function was previously unknown (Sun et al., 2012). Wilcox et al. (2017) later revealed that expression of *Zfhx3* is necessary to maintain circadian rhythms in adult mice, by employing the UBC-Cre-ERT2 transgenic mouse model to avoid the reported pre-weaning mortality and sustain critical developmental expression of *Zfhx3* (Sun et al., 2012; Wilcox et al., 2017).

The UBC-Cre-ERT2 transgenic mouse model is a useful tool to study the adult-associated function of a target gene. Temporal control of Cre recombinase activity *in vivo* is achieved by fusing Cre-recombinase to a mutated oestrogen receptor (ERT2). This Cre-ERT2 fusion protein is sequestered in the cytoplasm and remains inactive in the presence of endogenous oestrogen (Feil et al., 1997). Tamoxifen is metabolised to 4-hydroxytamoxifen (4-OHT) in the liver, which is a ligand and activator of the Cre-ERT2 complex (Donocoff et al., 2020). Hence, administration of tamoxifen initiates Cre-ERT2 nuclear translocation, allowing recombination activity to occur at LoxP sites. The subsequent Cre-mediated recombination results in the targeted gene disruption, thereby demonstrating a tamoxifen-inducible system (Adams & van der Weyden, 2008; Ruzankina et al., 2007) (**Figure 4.5**). Oral gavage or intra-peritoneal (IP) injection are the preferred tamoxifen delivery procedures, as they ensure more accurate and efficient weight-dependent dosing compared to mixing with diet or drinking water (Turner et al., 2011; Whitfield et al., 2015). When active, Cre recombinase is driven by the human ubiquitin C (UBC) promoter which has been shown to confer high levels of ubiquitous transgene

expression *in vivo* (Schorpp et al., 1996). In summary, the UBC-Cre-ERT2 transgenic mouse model provides a tamoxifen inducible system with the ability to instigate a ubiquitous knockout of a target gene at a specific time point *in vivo*, allowing for the study of a target gene in the adult mouse whilst excluding any developmental effects (Adams & van der Weyden, 2008).

Cre-driver lines have shown to be largely successful in generating specifically localised genetic manipulation, however it has to be noted that there can be non-specific off-target Cre expression (Alvarez-Aznar et al., 2020; Vooijs et al., 2001) or in the instance of Cre-ERT2, expression of Cre in the absence of tamoxifen via spontaneous Cre-LoxP recombination events (Kristianto et al., 2017)**.** This point highlights the importance of validating the Cre line and characterising the expression pattern in embryonic and postnatal tissue (Alvarez-Aznar et al., 2020). The UBC-Cre line has been previously been validated and characterised using the R26R reporter line, pre and post-tamoxifen treatment (Soriano, 1999; Wilcox, 2019).

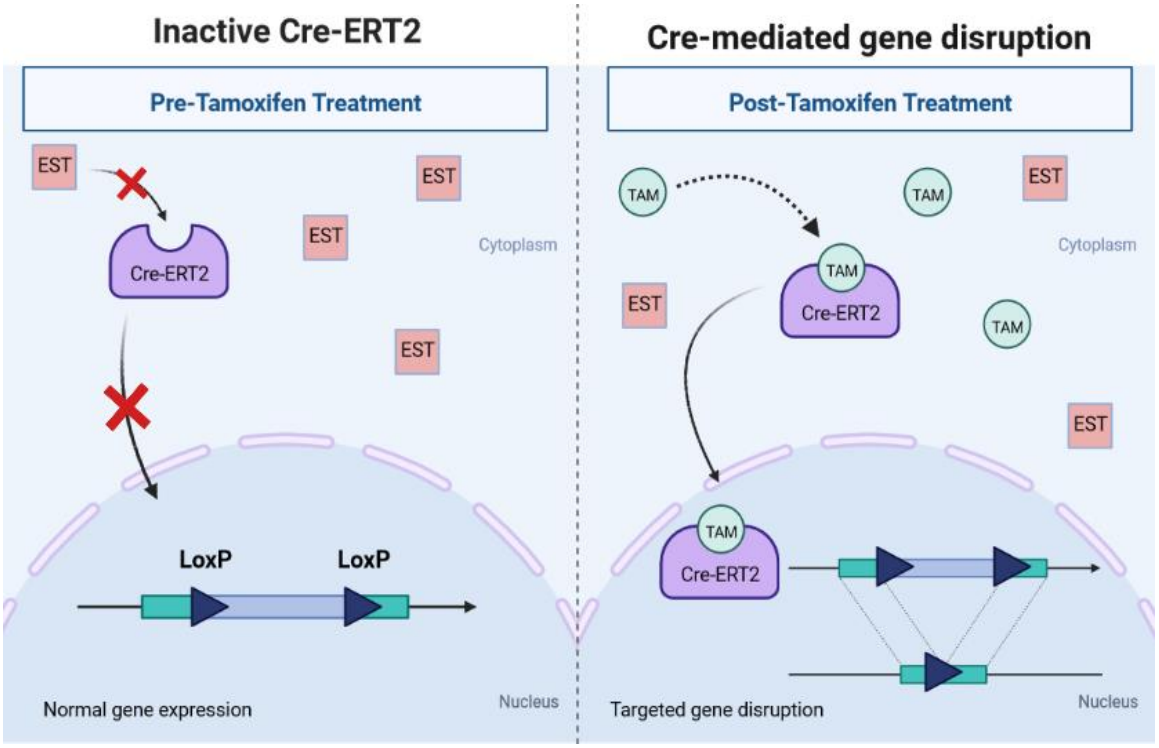

***Figure 4.5*| Schematic diagram of targeted gene disruption using the Cre-ERT2 Tamoxifen Inducible System**

In the absence of tamoxifen (TAM), Cre-ERT2 is sequestered in the cytoplasm, rendering the protein complex inactive. As the ERT2 is mutated, it cannot recognise endogenous estrogen (EST). Upon addition of tamoxifen, the Cre-complex translocates in to the nucleus and induces LoxP site recombination. This initiates targeted gene disruption. Image created with BioRender.com.

4.1.4 Chapter 4 Aims

The early-onset phenotype and neuropathology in both humans and mice establishes Oxr1 as an essential factor in neurodevelopment and cerebellar function (Lin et al., 2022; Oliver et al., 2011; Wang et al., 2019). In addition, the role of *Oxr1* in discrete brain regions is currently being characterised through the use of the conditional-ready *Oxr1* allele (*Oxr1*$^{tm1c/tm1c}$) and region-specific Cre-driver lines (see **4.3.2** for more detail), yet the specific significance of Oxr1 in adulthood is uncharacterised, owing to the limited lifespan of complete LOF-OXR1 patients and early postnatal death of *Oxr1* knockout mice (Lin et al., 2022; Oliver et al., 2011; Wang et al., 2019).

The aim of this chapter was to examine the effects of ubiquitous loss of Oxr1 in the adult mouse, particularly in the CNS. By crossing conditional-ready *Oxr1*$^{tm1c/tm1c}$ mice with a tamoxifen-inducible ubiquitous Cre line (UBC/ERT2-Cre), critical development expression of *Oxr1* is sustained before inducing global gene disruption in adult mice (Ruzankina et al., 2007), thus evading early-postnatal mortality. This provides a novel paradigm to investigate if adult-specific loss of *Oxr1* is detrimental to other cellular populations outside of the cerebellum and establish a role for *Oxr1* beyond neurodevelopment.

4.2 Results

4.2.1 Pilot study to establish tamoxifen dosing protocol for knockdown of Oxr1 protein

Given the known severity of constitutive *Oxr1* knockout mice (Oliver et al., 2011), a pilot study was conducted in order to determine whether global loss of Oxr1 in adult mice causes an overt neurological phenotype. Female mice, heterozygous for the conditional-ready *Oxr1* allele (*Oxr1*$^{tm1c/wt}$) were crossed with male mice expressing UBC-Cre-ERT2 (Cre^{+}) (**Figure 4.6A**). This produced *Oxr1*$^{tm1c/wt}$/Cre^{+} progeny, whereby males were bred to female *Oxr1*$^{tm1c/wt}$ mice that did not possess Cre (*Oxr1*$^{tm1c/wt}$/Cre^{-}) (**Figure 4.6B**). In turn, this resulted in homozygous conditional knockout-ready mice, with and without UBC-Cre-ERT2 (*Oxr1*$^{tm1c/tm1c}$/Cre^{+} and *Oxr1*$^{tm1c/tm1c}$/Cre^{-}) (**Figure 4.7A**).

Oxr1$^{tm1c/tm1c}$/Cre^{+} and *Oxr1*$^{tm1c/tm1c}$/Cre^{-} (hereafter abbreviated as Hom/Cre^{+} and Hom/Cre^{-} respectively) were administered with tamoxifen at 200 mg/kg for 5 consecutive days by oral gavage and then monitored in their home cage. Following tamoxifen treatment, Hom/Cre^{+} mice undergo Cre-mediated targeted gene disruption (**Figure 4.5**), whereby critical exons 14 and 15 are excised through loxP recombination, disrupting all Oxr1 isoforms and generating a knockdown of Oxr1 expression in adulthood (**Figure 4.7B**). Owing to the absence of UBC-Cre-ERT2, expression of Oxr1 is expected remain uninterrupted in Hom/Cre^{-} mice treated with tamoxifen. As this was a new genetic intervention in mice, a small-scale pilot study was carried out to ascertain whether there would be any unexpected adverse effects.

Initially, all mice appeared phenotypically normal; however, preliminary home-cage observations later identified the emergence of an acute neurological phenotype in Hom/Cre^{+} mice, 4 weeks post-tamoxifen treatment (PT). Strikingly, Hom/Cre^{+} developed a severe ataxic gait, displayed seizure-like behaviour and rapidly began to lose weight at this time point.

A.

♀ $Oxr1^{tm1c/wt}/Cre^{-}$

♂ $Oxr1^{wt/wt}/Cre^{+}$	$Oxr1^{tm1c}/Cre^{-}$	$Oxr1^{tm1c}/Cre^{-}$	$Oxr1^{wt}/Cre^{-}$	$Oxr1^{wt}/Cre^{-}$
$Oxr1^{wt}/Cre^{+}$	$Oxr1^{tm1c/wt}/Cre^{+}$	$Oxr1^{tm1c/wt}/Cre^{+}$	$Oxr1^{wt/wt}/Cre^{+}$	$Oxr1^{wt/wt}/Cre^{+}$
$Oxr1^{wt}/Cre^{+}$	$Oxr1^{tm1c/wt}/Cre^{+}$	$Oxr1^{tm1c/wt}/Cre^{+}$	$Oxr1^{wt/wt}/Cre^{+}$	$Oxr1^{wt/wt}/Cre^{+}$
$Oxr1^{wt}/Cre^{-}$	$Oxr1^{tm1c/wt}/Cre^{-}$	$Oxr1^{tm1c/wt}/Cre^{-}$	$Oxr1^{wt/wt}/Cre^{-}$	$Oxr1^{wt/wt}/Cre^{-}$
$Oxr1^{wt}/Cre^{-}$	$Oxr1^{tm1c/wt}/Cre^{-}$	$Oxr1^{tm1c/wt}/Cre^{-}$	$Oxr1^{wt/wt}/Cre^{-}$	$Oxr1^{wt/wt}/Cre^{-}$

Genotype	Expected percentage of offspring
$Oxr1^{tm1c/wt}/Cre^{+}$	25%
$Oxr1^{tm1c/wt}/Cre^{-}$	25%
$Oxr1^{wt/wt}/Cre^{+}$	25%
$Oxr1^{wt/wt}/Cre^{-}$	25%

B.

♀ $Oxr1^{tm1c/wt}/Cre^{-}$

♂ $Oxr1^{tm1c/wt}/Cre^{+}$	$Oxr1^{tm1c}/Cre^{-}$	$Oxr1^{tm1c}/Cre^{-}$	$Oxr1^{wt}/Cre^{-}$	$Oxr1^{wt}/Cre^{-}$
$Oxr1^{tm1c}/Cre^{+}$	$Oxr1^{tm1c/.tm1c}/Cre^{+}$	$Oxr1^{tm1c/.tm1c}/Cre^{+}$	$Oxr1^{tm1c/wt}/Cre^{+}$	$Oxr1^{tm1c/wt}/Cre^{+}$
$Oxr1^{tm1c}/Cre^{-}$	$Oxr1^{tm1c/.tm1c}/Cre^{-}$	$Oxr1^{tm1c/.tm1c}/Cre^{-}$	$Oxr1^{tm1c/wt}/Cre^{-}$	$Oxr1^{tm1c/wt}/Cre^{-}$
$Oxr1^{wt}/Cre^{+}$	$Oxr1^{tm1c/wt}/Cre^{+}$	$Oxr1^{tm1c/wt}/Cre^{+}$	$Oxr1^{wt/wt}/Cre^{+}$	$Oxr1^{wt/wt}/Cre^{+}$
$Oxr1^{wt}/Cre^{-}$	$Oxr1^{tm1c/wt}/Cre^{-}$	$Oxr1^{tm1c/wt}/Cre^{-}$	$Oxr1^{wt/wt}/Cre^{-}$	$Oxr1^{wt/wt}/Cre^{-}$

Genotype	Expected percentage of offspring
$Oxr1^{tm1c/.tm1c}/Cre^{+}$	12.5%
$Oxr1^{tm1c/.tm1c}/Cre^{-}$	12.5%
$Oxr1^{tm1c/wt}/Cre^{+}$	25%
$Oxr1^{tm1c/wt}/Cre^{-}$	25%
$Oxr1^{wt/wt}/Cre^{+}$	12.5%
$Oxr1^{wt/wt}/Cre^{-}$	12.5%

***Figure 4.6*| Punnett squares depicting expected genotypes from outlined breeding crosses and genotype distribution percentages for pilot cohort to study loss of Oxr1 in adult mice**
Expected inheritance pattern when inter-crossing (A) female $Oxr1^{tm1c/wt}/Cre^{-}$ mice with male $Oxr1^{wt/wt}/Cre^{+}$ mice and (B) female $Oxr1^{tm1c/wt}/Cre^{-}$ with male $Oxr1^{tm1c/wt}/Cre^{+}$ mice.

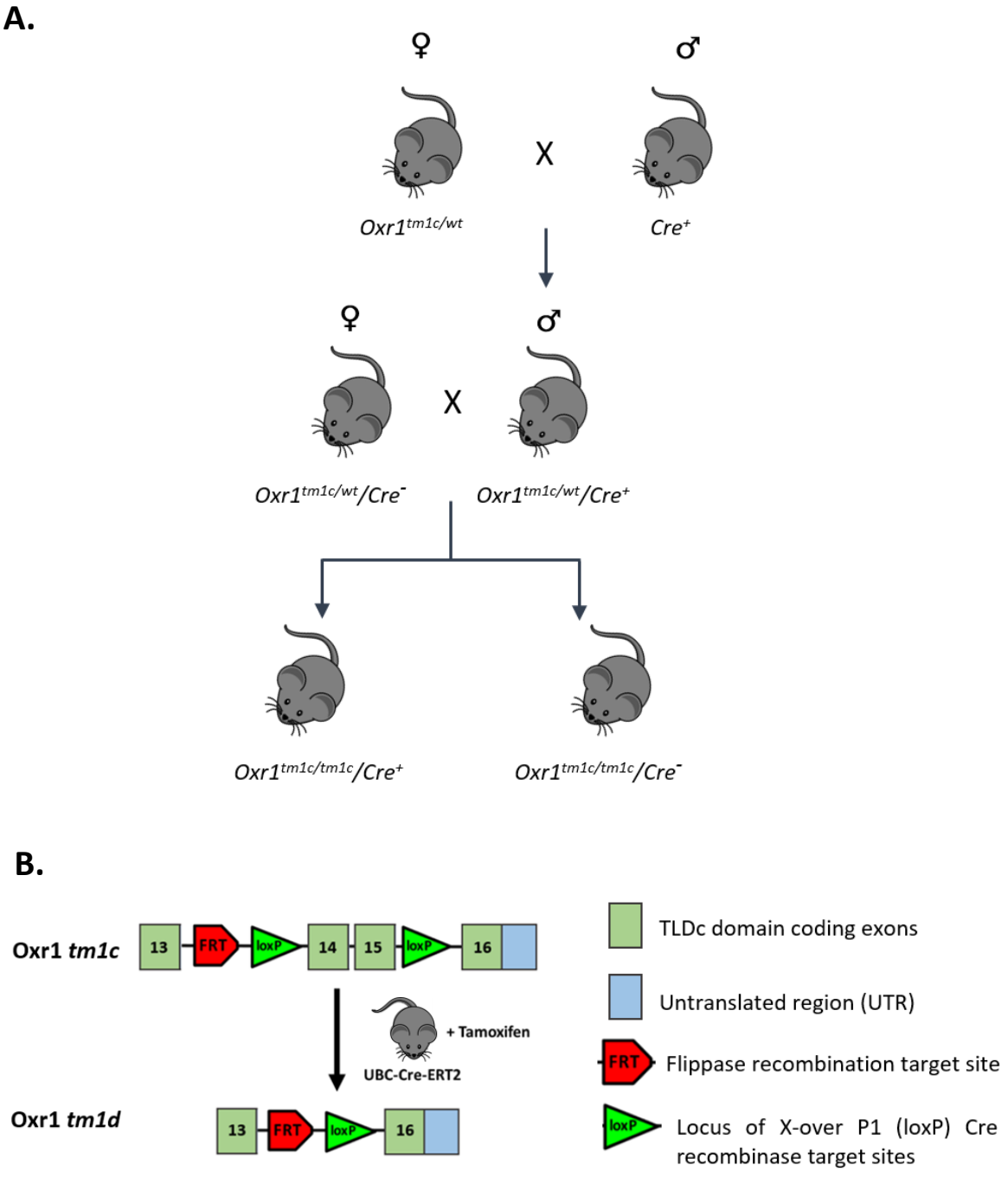

***Figure 4.7*| Breeding of conditional *Oxr1* knockout-ready mouse line for pilot study to investigate loss of Oxr1 in adult mice.**

(A) Simplified breeding scheme to depict generation of homozygous conditional knockout-ready mouse line (*Oxr1*$^{tm1c/tm1c}$/Cre^{+}) and representative control (*Oxr1*$^{tm1c/tm1c}$/Cre^{-}). Cre^{+} indicates hemizygosity, whereby + indicates presence of Cre and – represents no Cre. Female *Oxr1*^{tm1c} mice were used. Cre was paternally inherited. (Note, additional genotypes produced are outlined in **Figure 4.6** but not included in this simplified schematic). (B) Upon addition of tamoxifen, Cre recombinase activity is initiated. This converts the *Oxr1* conditional *tm1c* allele in to the knockout *tm1d* allele through loxP site recombination, thus generating an *Oxr1* knockout.

In light of this, cerebellar tissue was dissected from Hom/Cre$^+$ and Hom/Cre$^-$ at 2- and 4-weeks PT; forebrain (brain) and spinal cord tissue was also taken at 4 weeks PT. Concurrently, protein was extracted from these samples and analysed by western blot to examine levels of Oxr1. In Hom/Cre$^+$ cerebellar tissue, a ~4-fold reduction of all full-length Oxr1 (Oxr1-FL) isoforms is observed 2 weeks PT, with almost complete loss of the protein by 4 weeks PT in the cerebellum, cortex and spinal cord (**Figure 4.8**), thus confirming successful protein knockdown in CNS tissue. Oxr1 expression is sustained in the cerebellum, cortex and spinal cord of Hom/Cre$^-$ control mice (**Figure 4.8**).

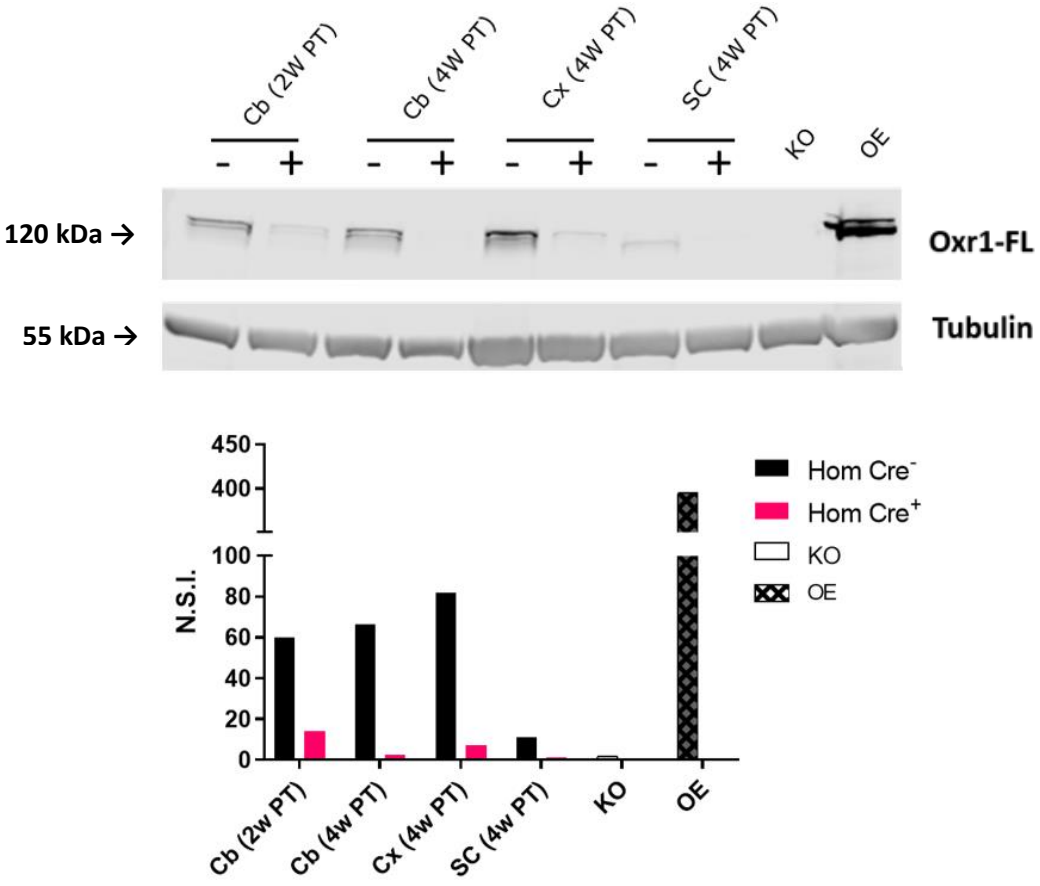

***Figure 4.8*| Western blot to detect Oxr1-FL in CNS tissue, 2 and 4 weeks post-tamoxifen treatment in Hom/Cre$^+$ and Hom/Cre$^-$ dosed mice**

Western blot and corresponding quantification of Oxr1-FL expression in cerebellar tissue (Cb) 2 weeks post tamoxifen treatment (2W PT) and at 4 weeks post tamoxifen treatment (4W PT) in cerebellar, forebrain (Cx) and spinal cord (SC) tissue from Hom/Cre$^-$ (-) and Hom/Cre$^+$ (+) mice. Two Oxr1 bands represent two long isoforms of the protein, both lost 4 weeks after tamoxifen treatment. Oxr1 expression was verified against tissue from Oxr1 knockout (KO) and over-expresser (OE) mice. N.S.I.: Normalised signal intensity of Oxr1 relative to loading control, α-tubulin. All Oxr1 bands were included in quantification values. (n=1 per genotype and time point)

As UBC-Cre is ubiquitously expressed, knockdown of Oxr1 was verified in additional tissues outside of the CNS, 4 weeks PT. Loss of Oxr1 was also observed in the thymus, spleen, hind limb muscle, liver and heart (**Figure 4.9**), confirming that UBC-Cre activity is sufficient to induce global knockdown of Oxr1. In agreement with previous findings, Oxr1-FL is not detected in kidney (Li, Li, et al., 2014). Of note, these data also demonstrate the varying distribution of Oxr1-FL isoforms in the different tissues, all of which are regulated by the *Oxr1*^{tm1c} allele and a knockdown in expression is also observed following tamoxifen treatment; for example, the distribution of Oxr1-FL in the spinal cord is distinct from that in the brain (**Figure 4.9**).

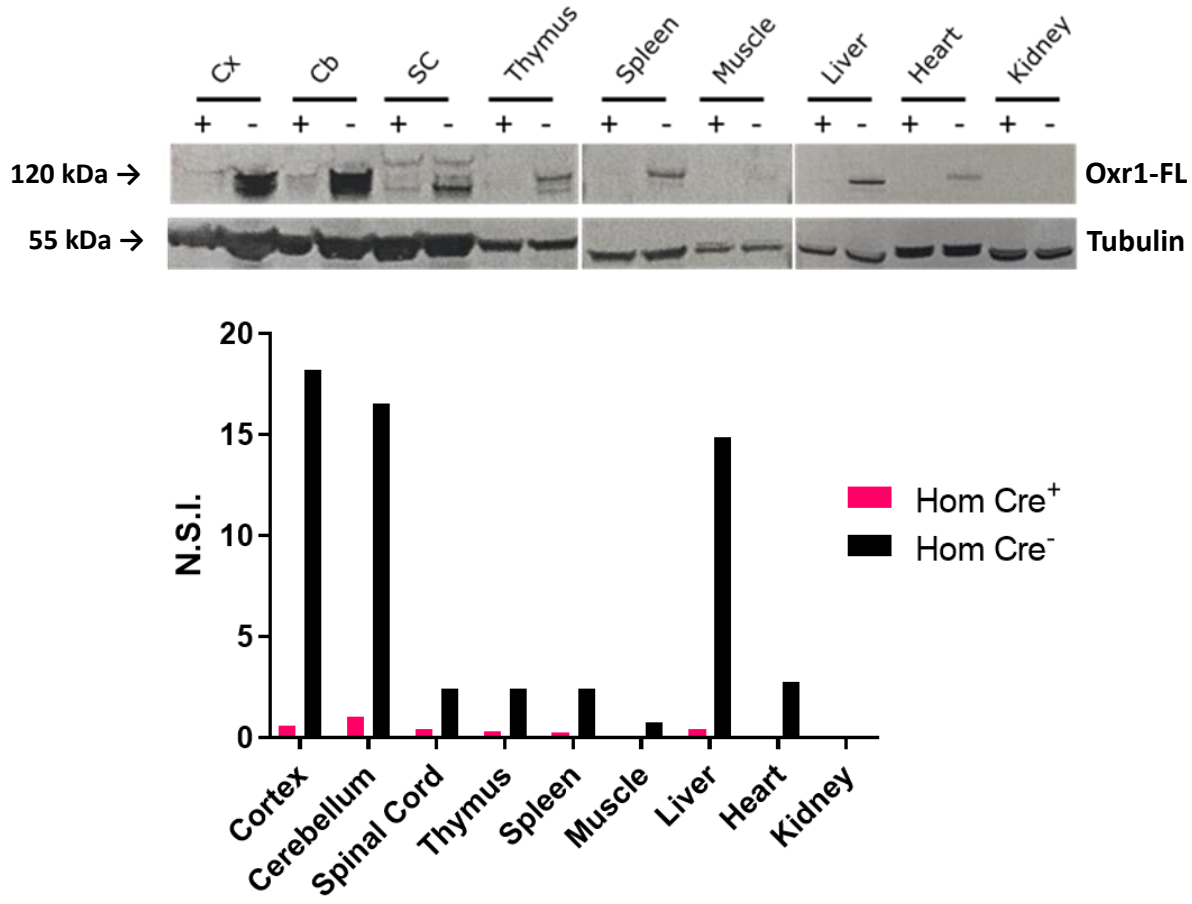

***Figure 4.9*| Western blot and quantification of Oxr1-FL in a range of tissues taken from Hom/Cre^{+} and Hom/Cre^{-} mice to verify global knockdown of Oxr1**

Western blot and corresponding quantification of Oxr1 expression in the cortex (Cx), cerebellum (Cb), spinal cord (SC), thymus, spleen, muscle, liver, heart and kidney, 4 weeks post-tamoxifen treatment. N.S.I.: Normalised signal intensity of Oxr1 relative to loading control, α-tubulin. All Oxr1 bands were included in quantification values. (n=1 per genotype)

In summary, this pilot study established that 5 consecutive days of tamoxifen treatment in Hom/Cre^{+} mice at 200 mg/kg was sufficient to induce a robust knockdown of Oxr1 in adult mice. At 2 weeks PT, tamoxifen-dosed Hom/Cre^{+} and Hom/Cre^{-} appear phenotypically unaffected through general observations, yet a substantial knockdown of Oxr1 was observed in Hom/Cre^{+} cerebellar tissue. At 4 weeks PT, Oxr1 is virtually undetectable in Hom/Cre^{+} tissue, suggesting that loss of Oxr1 in adult mice likely contributes to the severe neurological phenotype. Importantly, protein expression remained stable in tamoxifen-treated Hom/Cre^{-} mice. Owing to welfare concerns surrounding significant weight loss and seizure-like episodes, 4 weeks PT was determined as the experimental endpoint. Building on this preliminary data, a longitudinal study was designed with the aim of characterising the effects of depleting Oxr1 in the adult mouse (**Figure 4.10**). Of note, in between tamoxifen treatment and 2 week PT behavioural testing, only weekly weighing, general cage changing and observational welfare checks occurred in the interim. This was to allow time for the mice to recover from any tamoxifen treatment-induced stress, as well as allowing time for Oxr1 protein turnover *in vivo.*

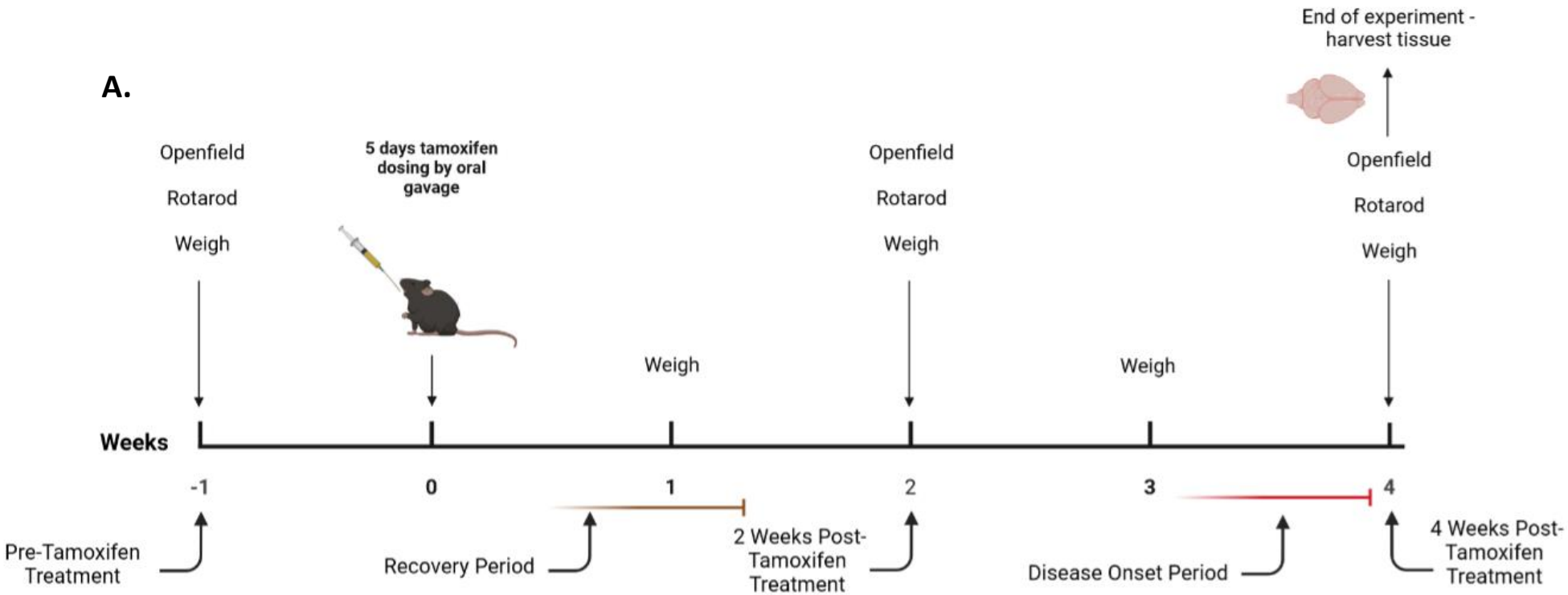

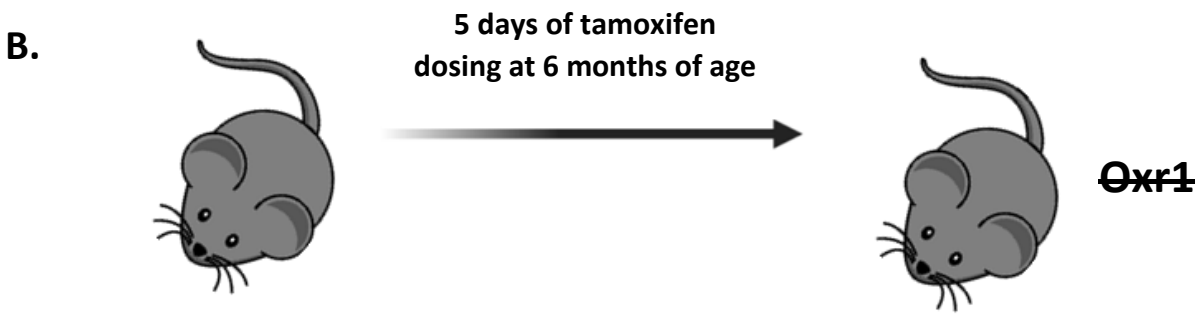

***Oxr1*$^{tm1c/tm1c}$/Cre^{+} (Hom/Cre^{+})**

Normal expression of Oxr1 in all tissues

Ubiquitous knockdown

Adult knockout of Oxr1

***Figure 4.10*| Longitudinal study to investigate loss of Oxr1 in the adult mouse**

(**A**) Short phenotyping schedule conducting over the course of 6 weeks. All mice were weighed weekly. Pre-tamoxifen treatment (week -1), mice underwent open field and Rotarod behavioural testing. The "dosed" groups were subsequently administered tamoxifen by oral gavage for 5 days (week 0) and left to recover for two weeks (recovery period). Open field and Rotarod behavioural testing were performed again 2 and 4 weeks post-tamoxifen treatment. At the end of the study, tissue was harvested and processed for further analysis. It is important to note that only females were used in the longitudinal study, but both sex groups were used for histopathological analysis. This study was carried out over multiple cohorts. Image (**A**) created with BioRender.com. (**B**) Simplified schematic representation of inducing ubiquitous adult knockout of *Oxr1,* following 5 days of tamoxifen treatment at 6 months of age.

4.2.2 Oxr1 knockdown is robust in Hom/Cre^{+} treated with tamoxifen, generating an adult knockout of Oxr1.

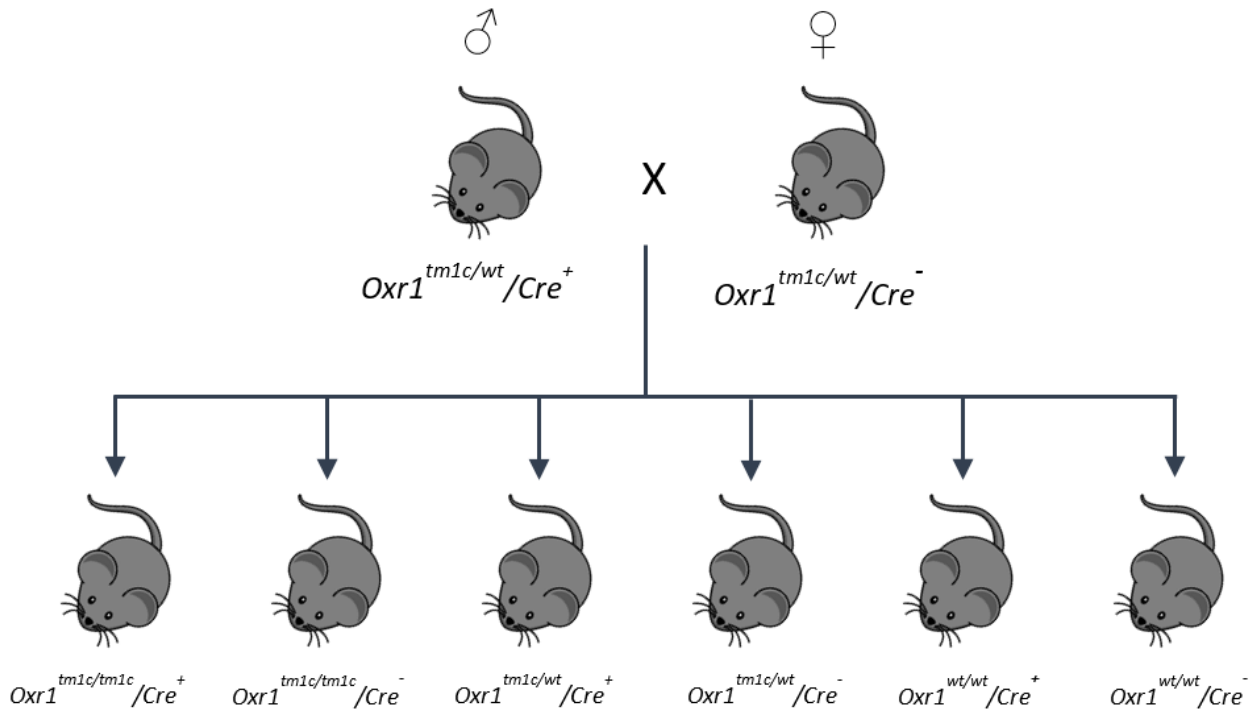

***Figure 4.11*| Schematic breeding plan to generate experimental cohorts to investigate the role of *Oxr1* in the adult mouse**

Oxr1$^{tm1c/wt}$*/Cre*$^{+}$ (Het/Cre^{+}) males were crossed to *Oxr1*$^{tm1c/wt}$*/Cre*$^{-}$ (Het/Cre^{-}) females to produce six genotype groups; *Oxr1*$^{tm1c/tm1c}$/Cre^{+}, *Oxr1*$^{tm1c/tm1c}$/Cre^{-}, *Oxr1*$^{tm1c/wt}$/Cre^{+}, *Oxr1*$^{tm1c/wt}$/Cre^{-}, *Oxr1*$^{wt/wt}$/Cre^{+} and *Oxr1*$^{wt/wt}$/Cre^{-} of Mendelian inheritance patterns (1:1:2:2:1:1, respectively).

Following on from the pilot study, male *Oxr1*$^{tm1c/wt}$/Cre^{+} mice were generated, as shown in **Figure 4.7A**, and subsequently crossed with female *Oxr1*$^{tm1c/wt}$/Cre^{-} mice to yield experimental cohorts (**Figure 4.6B**). The following genotypes were generated by this breeding strategy: *Oxr1*$^{tm1c/tm1c}$/Cre^{+} (Hom/Cre^{+}), *Oxr1*$^{tm1c/tm1c}$/Cre^{-} (Hom/Cre^{-}), *Oxr1*$^{tm1c/wt}$/Cre^{+} (Het/Cre^{+}), *Oxr1*$^{tm1c/wt}$/Cre^{-} (Het/Cre^{-}), *Oxr1*$^{wt/wt}$/Cre^{+} (WT/Cre^{+}) and *Oxr1*$^{wt/wt}$/Cre^{-} (WT/Cre^{-}) (**Figure 4.11**). Next, each genotype was split in to two groups: treated with tamoxifen (Dosed, D) and untreated controls (No Dose, ND).

To examine Oxr1 expression at 4 weeks PT in each genotype and dose group, whole brains were harvested at this time point and western blots were carried out on brain and cerebellar protein extracts (**Figure 4.12A, Figure 4.12B**). In Hom/Cre^{+} dosed brain tissue, a ~9 fold reduction in Oxr1 is observed compared to 'No Dose' Hom/Cre^{+} control group (**Appendix. 6A**). A marked ~50 fold decrease in Hom/Cre^{+} dosed cerebellar tissue is found when compared to Hom/Cre^{+} not treated with tamoxifen (**Appendix. 6B**). In comparison to 'No Dose' control counterparts, a ~2 fold drop is found in brain tissue of Het/Cre^{+} dosed mice (**Figure 4.12A**, **Appendix. 6A**), however this was anticipated due to the presence of one *Oxr1* conditional-ready *tm1c* allele. Tamoxifen-induced Cre activity would create a null allele, leaving only one wild type *Oxr1* allele and resulting in an overall reduction of protein. Oxr1 expression remains stable in all other control genotypes and dose groups.

In contrast to Hom/Cre^{-} mice at 4 weeks PT, Oxr1 expression in significantly diminished ~9 fold in brain [$p<0.0001$] (**Figure 4.12C, Figure 4.12D**) and ~23 fold cerebellar tissue [$p=0.0389$] (**Figure 4.12E, Figure 4.12F**) of Hom/Cre^{+} mice when both genotypes are treated with tamoxifen. Collectively, this demonstrates that a robust, almost complete knockdown of Oxr1 is only observed in Hom/Cre^{+} mice dosed with tamoxifen in this experiment.

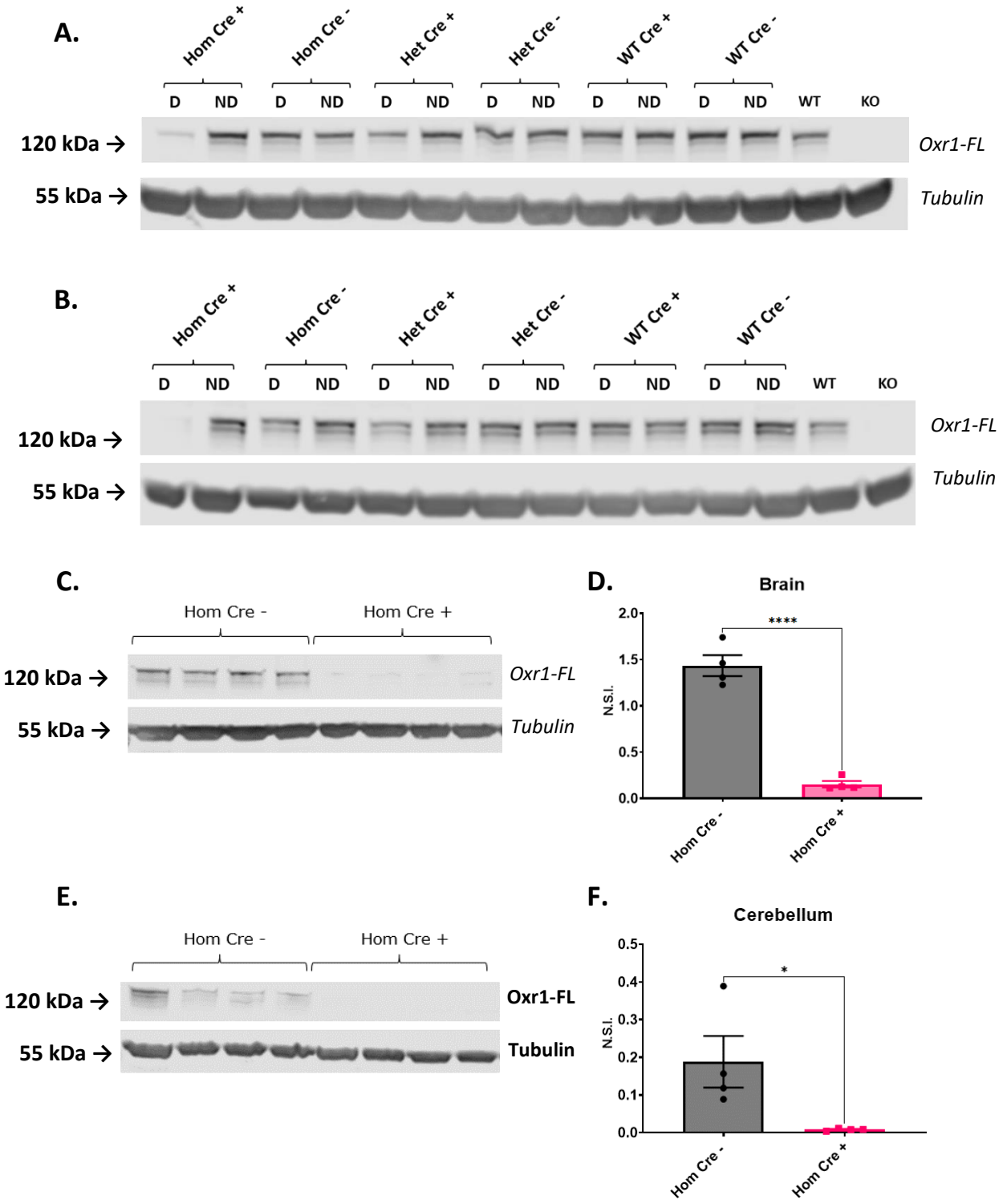

***Figure 4.12*| Western blot for Oxr1-FL expression in brain and cerebellar tissue, 4 weeks post-tamoxifen treatment.**

(**A-B**) Western blots showing knockdown of Oxr1 in Hom/Cre^{+} dosed mouse (**A**) brain and (**B**) cerebellum. Oxr1 levels remain stable in control genotype and dose groups. Normalised quantification shown in **Appendix. *6***. Representative western blots and normalised quantification of Oxr1 in (**C**,**D**) brain and (**E**,**F**) cerebellar tissue with loading control, α-tubulin, in Hom/Cre^{-} and Hom/Cre^{+} animals treated with tamoxifen. N.S.I.: normalised signal intensity of Oxr1 relative to α-tubulin. Normalised quantification presented as mean ± SEM, unpaired t-test, *p<0.05, ****p<0.0001. D – Dosed with tamoxifen, ND – not dosed with tamoxifen, WT – wild type, KO – constitutive *Oxr1* knockout

When using a tamoxifen inducible Cre-driver line, several experimental controls need to be included to negate effects of different variables when making conclusions (Schmidt-Supprian & Rajewsky, 2007). Although no off-target effects have been described when using the 'knockout-first' conditional allele, it is important to control for *Oxr1* locus disruption and insertion of the transgene cassette (Finelli, Paramo, et al., 2019; Finelli et al., 2016; Skarnes et al., 2011). Second to this, UBC-Cre-ERT2 transgene has been found to have integrated in to the NADPH-dependent diflavin oxidoreductase 1 (*Ndor1*) locus, therefore it is paramount to determine that any observed phenotype is not a result of transgene genomic disruption or Cre-mediated toxicity (Goodwin et al., 2019; Schmidt-Supprian & Rajewsky, 2007).

It is worth noting that tamoxifen treatment has been reported to alter numerous behavioural aspects in mice, including memory impairment and increased anxiety (Chen et al., 2002; X. Li et al., 2020). Consecutive days of oral-gavage is also known to induce stress and oesophageal trauma in rodents (Brown et al., 2000; Jones et al., 2016). Induction of Cre-activity by tamoxifen in itself can cause unexpected effects *in vivo*. For example, crossing a lymphoma mouse model ($p53^{-/-}$) to UBC-Cre-ERT2 expressing mice and subsequent treatment of tamoxifen triggers apoptosis and tumour regression (Li, Choi, et al., 2014).

It is noteworthy that Wilcox (2019) demonstrated that when UBC-Cre-ERT2 expressing mice were crossed with a LacZ reporter line, some residual Cre-activity could be detected through X-Gal staining in E18.5 cortex as well as in the cortex of adult mouse brain prior to any tamoxifen treatment, although the use of experimental controls described in **Table 4-1** were used to negate potential effects of spontaneous Cre activity. A summary of controls can be found in **Table 4-1**. Owing to genotype availability, Cre positive and

negative *tm1c* heterozygous mice were used as baseline controls to assess behavioural and neuropathological in adult *Oxr1* knockout mice.

Table 4-1|Table of genotypes and dose groups generated for this study and reasons for use

Genotype	Shorthand	Dose Group	Reason for inclusion
Oxr1$^{tm1c/tm1c}$/Cre^{+}	Hom/Cre^{+}	Dosed	Experimental group – Adult induced Oxr1 knockout
		No Dose	Control for effect of Cre without induction by tamoxifen. Spontaneous recombination activity
Oxr1$^{tm1c/tm1c}$/Cre^{-}	Hom/Cre^{-}	Dosed	Control for tamoxifen dosing effects
		No Dose	Control for disruption of gene trap cassette insertion
Oxr1$^{tm1c/wt}$/Cre^{+}	Het/Cre^{+}	Dosed	Control for presence of Cre and tamoxifen induction on *tm1c* heterozygous background
		No Dose	Control for presence of Cre in genome on *tm1c* heterozygous background
Oxr1$^{tm1c/wt}$/Cre^{-}	Het/Cre^{-}	Dosed	Control for tamoxifen dosing effects in *tm1c* heterozygous animals
		No Dose	Baseline *tm1c* heterozygous control
Oxr1$^{wt/wt}$/Cre^{+}	WT/Cre^{+}	Dosed	Control for presence of Cre and tamoxifen induction
		No Dose	Control for presence of Cre in genome
Oxr1$^{wt/wt}$/Cre^{-}	WT/Cre^{-}	Dosed	Control for tamoxifen dosing effects in wild-type animals
		No Dose	Baseline wild-type control

4.2.3 Hom/Cre$^+$ mice fail to regain weight effectively following tamoxifen treatment, losing up to 15% of their body weight.

From P14, *bella* mice fail to gain weight as efficiently littermate controls (Oliver et al., 2011). Tamoxifen has also been reported to induce acute lipoatrophy, leading to significant weight loss in dosed mice (Ye et al., 2015). Taking this in to consideration, mice were weighed weekly, as demonstrated in **Figure 4.10**; tamoxifen-treated mice were weighed daily during the 5 day dosing period to ensure accurate dosing concentrations (200 mg/kg) and monitor adverse weight changes. All tamoxifen-treated mice lose weight significantly [$p<0.0001$] between Week -1 (pre-tamoxifen treatment) and Week 1 (one week PT) (**Appendix. 7**), indicating that tamoxifen treatment induces weight loss, irrespective of genotype. For simplicity and ease of viewing, only Hom/Cre$^+$ 'No Dose' representative control animals are shown in the following figures; collective data can be found in **Appendix. 8**.

A two-way repeated measures ANOVA identified no significant differences in mean body weight between groups at each time point (**Appendix. 9**), although the interaction between time and dosing group was statistically significant [$p<0.0001$]. By 4 weeks PT, Hom/Cre$^+$ Dosed animals showed a significant decrease in body weight compared to their initial weight at Week -1 [$p=0.035$], whereas Hom/Cre$^+$ No Dose animals gain weight gradually over the same time period (**Figure 4.13A**) (**Appendix. 10**). Hom/Cre$^+$ Dosed fail to gain weight back effectively following tamoxifen treatment compared to control mice treated with tamoxifen (**Appendix. 9** and **Appendix. 10**). When evaluating the percentage change in weight, further statistical analysis revealed a significant difference between changes observed in Hom/Cre$^+$ Dosed mice compared to No Dose controls, from 1 week PT (**Figure 4.13B**).

Collectively, this demonstrates that tamoxifen treatment affects body weight in mice, causing significant weight loss in all dosed animals. In parallel, loss of Oxr1 in adult mice results in failure to gain weight during disease progression, suggesting that a reduction in Oxr1 affects body weight in adult mice.

A.

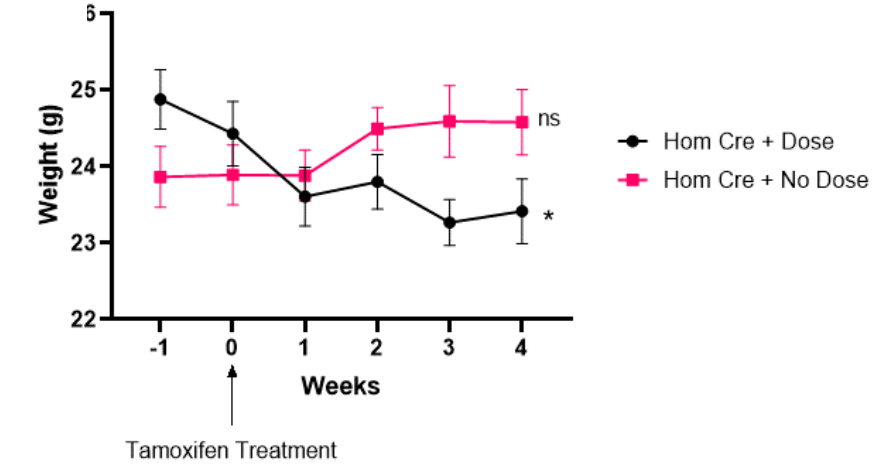

	Hom/Cre$^+$ Dosed			
Week	Mean Weight (g)	SEM	n	(Compared to Week -1) Adjusted p-value:
0	24.43	0.42	14	0.1867
1	23.61	0.39	14	0.0002
2	23.80	0.36	14	0.0003
3	23.27	0.30	14	<0.0001
4	23.42	0.42	14	0.035

	Hom/Cre$^+$ No Dose			
Week	Mean Weight (g)	SEM	n	(Compared to Week -1) Adjusted p-value:
0	23.89	0.39	9	>0.9999
1	23.88	0.33	9	>0.9999
2	24.50	0.28	9	0.2
3	24.59	0.47	9	0.4576
4	24.58	0.43	9	0.5967

B.

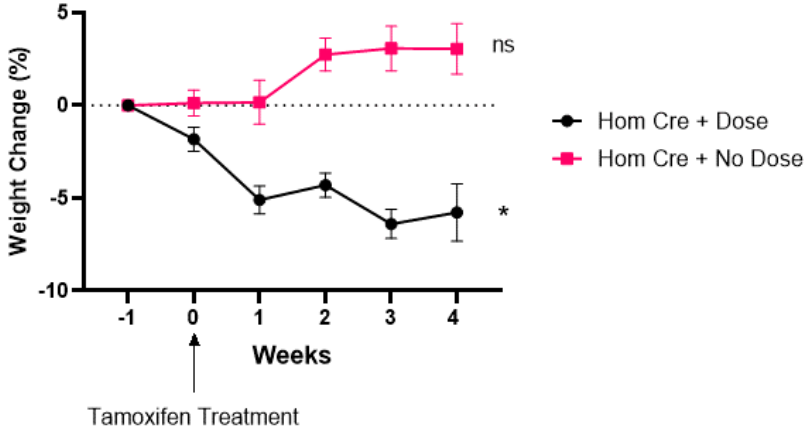

	Hom/Cre$^+$ Dosed			Hom/Cre$^+$ No Dose			
Week	Weight Change (%)	SEM	n	Weight Change (%)	SEM	n	Hom/Cre+ Dosed vs No Dose Adjusted p-value:
0	-1.82	0.65	14	0.13	0.69	9	0.2856
1	-5.09	0.75	14	0.17	1.18	9	0.0123
2	-4.30	0.65	14	2.74	0.89	9	<0.0001
3	-6.39	0.78	14	3.08	1.21	9	<0.0001
4	-5.77	1.55	14	3.06	1.36	9	0.002

***Figure 4.13*| Longitudinal record of bodyweight in adult-induced Oxr1 knockout and representative control mice with percent change in body weight relative to pre-tamoxifen treatment**

(A) Weekly recorded bodyweight (g) of female Hom/Cre$^+$ Dose and Hom/Cre$^+$ No Dose mice and statistical significance (adjusted p-value) at each time point compared to week -1 (pre-tamoxifen treatment) for each group. (B) Percentage (%) change in bodyweight and statistical comparison between groups at each time point. Hom/Cre$^+$ Dose: n=14, Hom/Cre$^+$ No Dose: n=9. All data are presented as ± SEM. Data were analysed by two-way repeated measures ANOVA, with Sidak's multiple comparisons test. Ns: not significant, p value * ≤ 0.05. Significant adjusted p-values are highlighted in red.

4.2.4 Loss of Oxr1 in adult mice leads to impaired short-term habituation and an anxiety-related phenotype in open field

Given the severity and rapid onset of the phenotype in this experiment, the window for longitudinal behavioural testing was short. Therefore, only a limited number of tests were chosen to provide some behavioural insights into the effect of loss of Oxr1 in adult mice. The open field test is a short paradigm that has been established to help characterise general activity and anxiety-related phenotypes in response to a novel environment in models of neurological disorders (Gerber et al., 2012; Kraeuter et al., 2019; Rial et al., 2014; Seibenhener & Wooten, 2015; Silverman et al., 2013). Here, open field was performed pre-tamoxifen treatment, as well as 2 and 4 weeks PT. Behavioural performance in the open field is notably affected by handling and exposure to other behavioural tests, therefore it was executed before rotarod testing to limit external variability at each time point (McIlwain et al., 2001).

In order to assess general activity of each genotype and dose group, total distance travelled in the whole arena (**Appendix. 11**), as well as specifically in the centre (**Appendix. 12**) and peripheral area (**Appendix. 13**), was measured and compared between all groups at each time point. When comparing Hom/Cre^{+} Dosed and Hom/Cre^{-} No Dose, a significant difference was identified in the total distance travelled in the periphery [p=0.0183], 4 weeks PT (**Appendix. 13**); all other comparisons were not significant between experimental groups at each separate time point. Importantly, no significant variability was found between experimental control groups in each of these parameters, therefore a representative control, Hom/Cre^{-} Dosed, was used for more in-depth analysis of behaviour. When evaluating the changes in activity between experimental groups over time either a two-way repeated measure- ANOVA or Mixed Effects Analysis were performed, followed by appropriate multiple comparison testing.

Overall, no significant differences were observed between Hom/Cre$^+$ and Hom/Cre$^-$ mice treated with tamoxifen at each time point (Pre-Tamoxifen, 2W PT and 4W PT), although time was found to have a significant interaction effect ($p<0.0001$) as both genotypes displayed overall reduced activity at 2W and 4W PT compared to the pre-tamoxifen treatment time point; the interaction between time point and genotype was also statistically significant ($p=0.0171$) (**Figure 4.14A**). Furthermore, differences in mean velocity in the whole arena was not significant between tamoxifen-treated Hom/Cre$^+$ and Hom/Cre$^-$ mice; additionally, time was a significant source of variation ($p<0.0001$) (**Figure 4.14B**). These initial results indicate that Hom/Cre$^+$ mice display similar levels of general activity in the period prior to- and following tamoxifen treatment compared to representative control Hom/Cre$^-$ control mice, suggesting that loss of *Oxr1* in adult mice does not induce significant differences in locomotor activity. Furthermore, comparable mean velocity in the whole arena at each time point suggests that adult-induced *Oxr1* knockout mice do not exhibit features of hypo- or hyperactivity by 4W PT.

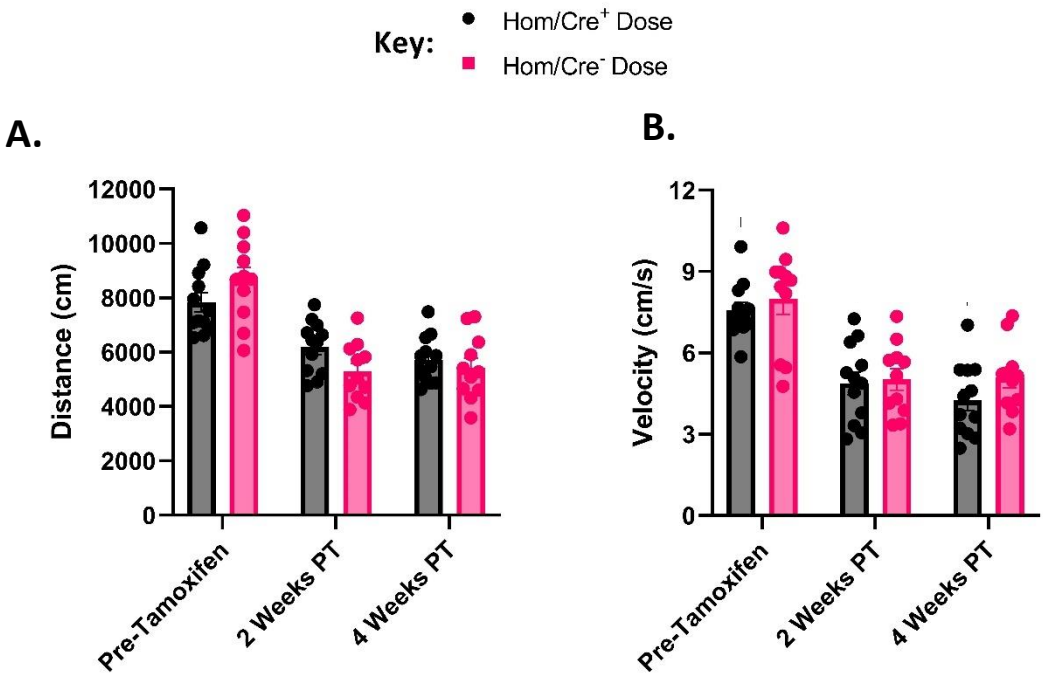

***Figure 4.14*| Total distance travelled and mean velocity in the whole arena measured pre-tamoxifen, 2 weeks and 4 weeks post-tamoxifen treatment**

(A) Total distance travelled (cm) and (B) mean velocity (cm/s) in the whole arena across 20 minute recordings, comparing female Hom/Cre^{+} Dose and Hom/Cre^{-} Dose experimental groups pre-tamoxifen, 2 weeks post-tamoxifen (PT) and 4 weeks PT. All data are presented as ± SEM. Two-way repeated measures ANOVA followed by Sidak's multiple comparisons. Genotypes compared at each time point. n= 9-12 per genotype.

Neuropsychiatric disorders, including anxiety, are a common comorbid feature in NDs and impaired cognition (Brainstorm Consortium. et al., 2018). Thigmotaxis is inherent mouse behaviour, therefore the centre of the open field arena is considered anxiety-inducing and mice typically spend more time in the periphery, infrequently entering the centre zone to explore a novel environment (Kraeuter et al., 2019). Similarly, mice also exhibit some exploratory behaviour, therefore time spent in the centre zone can be an indicator of increased exploratory drive and reduced anxiety (Kraeuter et al., 2019). Thus, to characterise if loss of *Oxr1* in the adult mouse leads to behavioural alterations or anxiety-related phenotypes, centre parameters were measured (**Figure 4.15**).

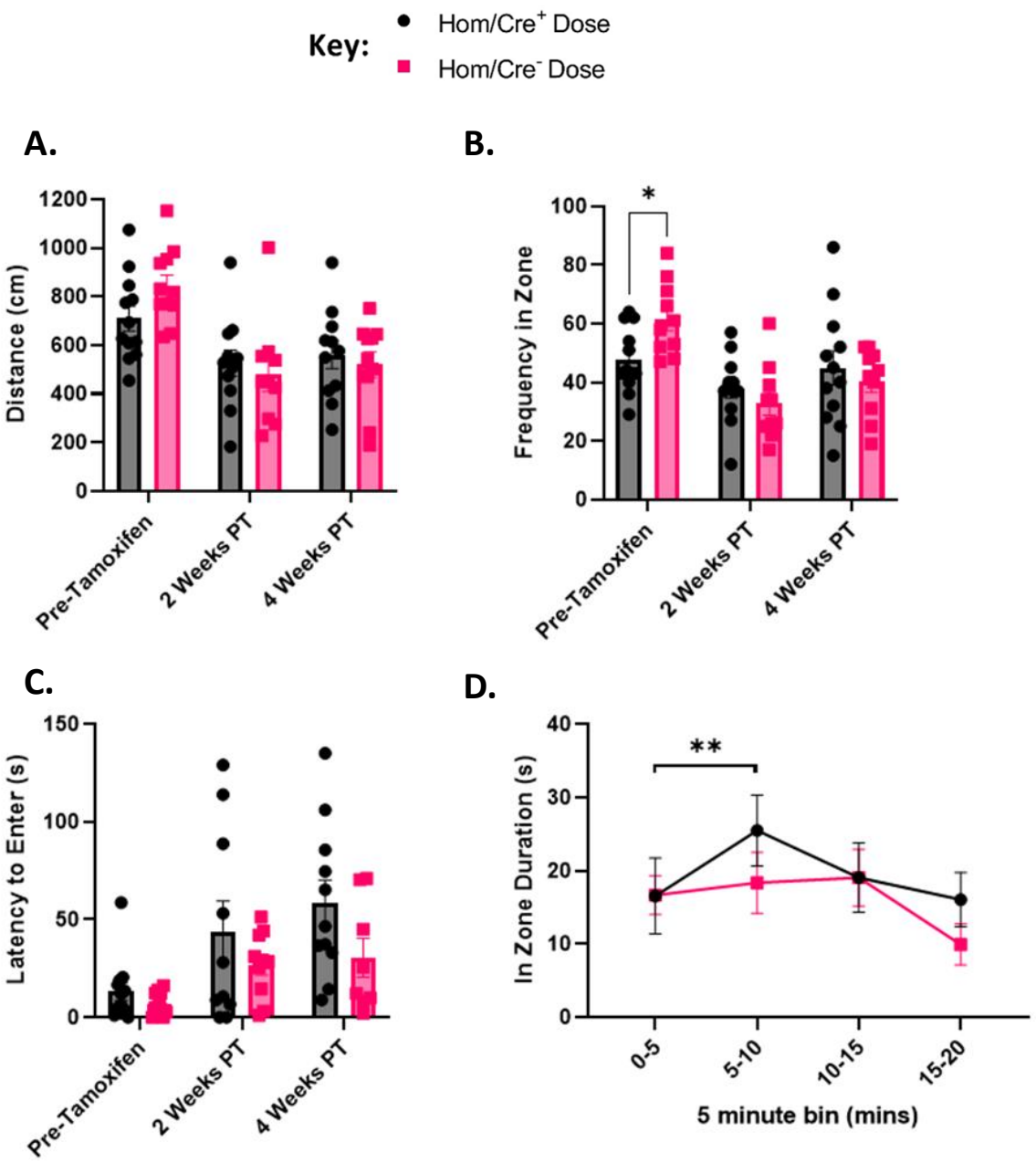

***Figure 4.15*| Open field centre parameters measured in Hom/Cre$^+$ and Hom/Cre$^-$ tamoxifen-treated mice**

(A) Total distance travelled (cm), (B) frequency in zone (centre) and (C) latency to enter centre zone (s) measurements, comparing female Hom/Cre$^+$ Dose and Hom/Cre$^-$ Dose experimental groups pre-tamoxifen, 2 weeks post-tamoxifen (PT) and 4 weeks PT. (D) In zone (centre) frequency (s) in 5 minute bins across 20 mins at 4 weeks PT. All data are presented as mean ± SEM. Two-way repeated measures ANOVA or mixed effects model followed by Sidak's multiple comparisons. p values * ≤ 0.05, **≤0.01. n= 9-12 per genotype.

Similar to observations in the whole arena, both tamoxifen-treated Hom/Cre^{+} and Hom/Cre^{-} mice show reduced overall activity in the centre at 2W and 4W PT when compared to pre-tamoxifen total distance travelled, although significant differences were not observed between genotypes at each time point (**Figure 4.15A**); this could indicate an element of spatial learning and memory of a familiar environment in both experimental groups. When comparing the frequency of entries to the centre at each time point, an inexplicable difference is observed at the pre-tamoxifen treatment, whereby Hom/Cre^{-} mice enter the centre more frequently ($p = 0.0375$) (**Figure 4.15B**). In centre zone frequency is not significant at 2W and 4W PT time points between the two experimental groups, although Hom/Cre^{+} dosed mice show a non-significant trend of increased frequency of entries to the centre, 4W PT (**Figure 4.15B**). Although these results are not significant, they initially suggest that loss of *Oxr1* may lead to an anxiety-related phenotype in open field.

When compared to pre-tamoxifen data, Hom/Cre^{+} show no significant differences at 2W PT, although their latency to first enter significantly increases by 4W PT ($p=0.0190$). Hom/Cre^{-} dosed mice show a significant difference in latency to enter the centre at 2W PT when compared to pre-tamoxifen ($p=0.0075$) however, significance is lost at 4W PT (**Figure 4.15C**). Following on from these data, in zone duration was analysed across 5 minute bins to further assess anxiety-related behaviour during the 20 minute recording period, 4W PT. Although, Hom/Cre^{+} dosed mice exhibit an increased latency to first enter the centre, the time spent in this zone within the first 5 minutes is comparable to Hom/Cre^{-} dosed control mice. Interestingly, Hom/Cre^{+} dosed mice spend significantly more time in the centre during the 5-10 minute period ($p=0.010$), compared to the first five minutes of the open field test (**Figure 4.15D**), thus, possibly indicating short-term spatial memory deficits in this group; no significant changes of in zone duration of Hom/Cre^{-} dosed mice is observed over

the 20 minute period (**Figure 4.15D**). Of note, cumulative in zone duration was not significant between Hom/Cre^{+} and Hom/Cre^{-} dosed mice at each time point (data not shown).

As an initial assessment of spatial memory and habituation phenotypes, distance travelled in the whole arena and centre was analysed in 5 minute time bins across the 20 minute recording period, pre-tamoxifen, 2W and 4W PT (**Figure 4.16**). Overall, the reduction observed in distance travelled in the whole arena and centre zone at 2W and 4W PT may indicate that long-term habituation is unaffected in Hom/Cre^{+} and Hom/Cre^{-} tamoxifen-treated mice. Interestingly, distance travelled across the 20 minute recordings was significantly increased in the whole arena in the 5-10 and 10-15 minute time frames in Hom/Cre^{+} dosed mice compared to control Hom/Cre^{-} dosed mice, 2W PT (**Figure 4.16A**). Similarly in the centre, Hom/Cre^{+} dosed mice show increased distance travelled in this zone between the 5-20 minute time period, compared to control mice at both 2W and 4W PT (**Figure 4.16B**); this is observed in contrast to their gradual reduction in activity across the 20 minute recording period exhibited pre-tamoxifen treatment. Taken together, these open field data preliminarily suggest that tamoxifen-dosed Hom/Cre^{+} mice show short-term habituation deficits at both 2W and 4W PT within the 20 minute recordings, although long-term habituation appears intact when comparing 2W and 4W PT data to the pre-tamoxifen time point.

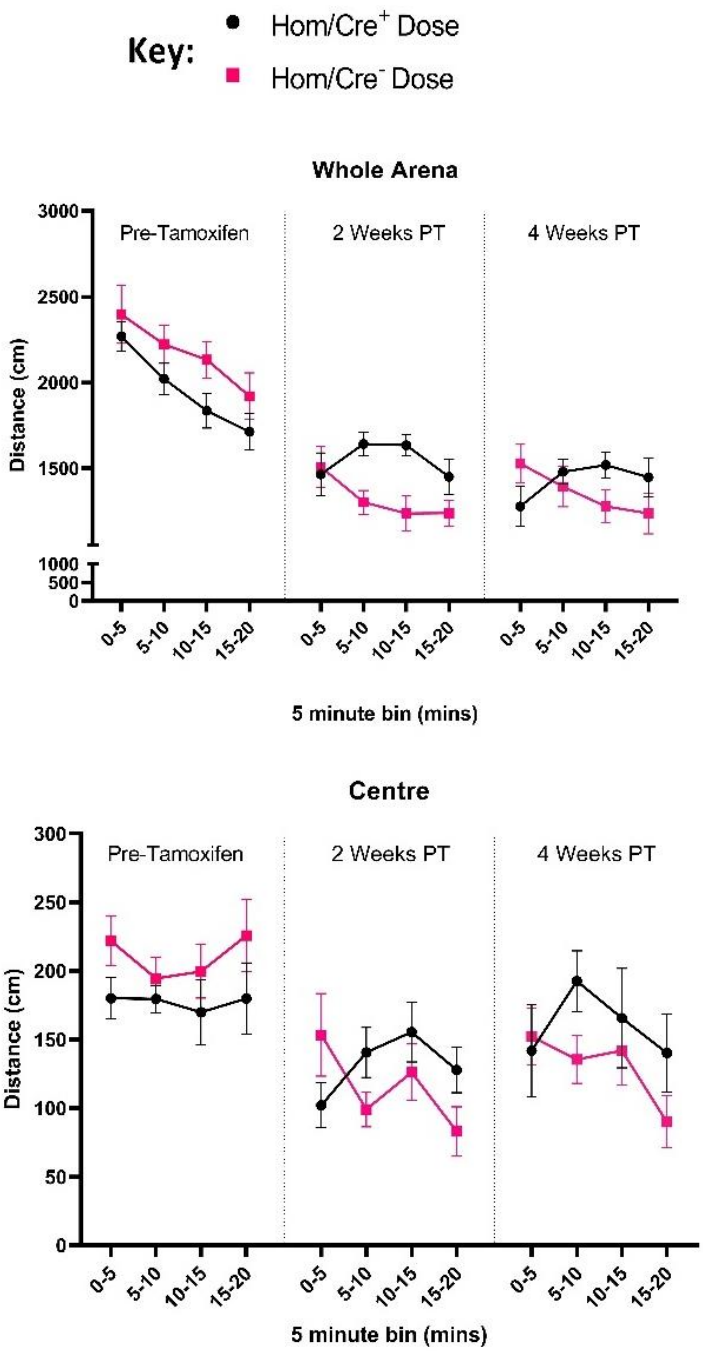

***Figure 4.16*| Distance travelled over 5 minute bins in the whole arena and centre of the arena pre-tamoxifen, 2 weeks and 4 weeks post-tamoxifen treatment**

Distance travelled (cm) in (A) whole arena and (B) in centre zone, comparing female Hom/Cre^{+} Dose and Hom/Cre^{-} Dose experimental groups pre-tamoxifen, 2 weeks post-tamoxifen (PT) and 4 weeks PT. All data are presented as mean ± SEM. Two-way repeated measures ANOVA or mixed effects model followed by Sidak's multiple comparisons. n= 9-12 per genotype.

4.2.5 Loss of Oxr1 in adult mice leads to motor function deficits 4 weeks post-tamoxifen treatment.

To establish whether loss of Oxr1 affects motor function in adult mice, that might relate to cerebellar function and pathology, accelerating rotarod was undertaken pre-tamoxifen treatment, 2 weeks PT and 4 weeks PT (**Figure 4.17A**). Prior to tamoxifen treatment, Hom/Cre$^-$ Dosed group showed a significantly shorter latency to fall time, compared to Hom/Cre$^+$ No Dose [p=0.0472] and Het/Cre$^-$ Dosed [p=0.0219] groups; all other differences between groups were not significant (**Figure 4.17B**). There was no difference identified between latency to fall times amongst groups 2 weeks PT (**Figure 4.17C**); however, when assessing latency to fall at 4 weeks PT, Hom/Cre$^+$ Dosed animals exhibited significantly impaired performance compared to all other groups [p <0.001] (**Figure 4.17D**). Mixed-effects analysis, followed by Tukey's multiple comparisons test, comparing individual group performances over time demonstrated a stark decrease in latency to fall in Hom/Cre$^+$ Dosed at 4 weeks PT when compared to their pre-tamoxifen [p=0.0028] and 2 week PT performance [p=0.0001](**Figure 4.17E**), implying that loss of Oxr1 affects motor function. No significant differences were observed in all other control groups. As Het/Cre$^+$ Dosed mice display no significant differences over time, this suggests that at least one functional Oxr1 allele is required for normal motor function.

A.

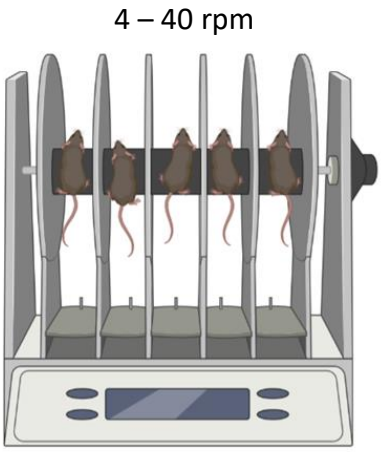
4 – 40 rpm

B.

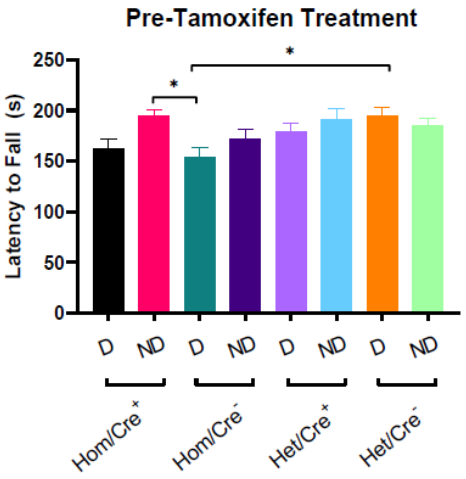
Pre-Tamoxifen Treatment
Latency to Fall (s)
250
200
150
100
50
0
*
*
D
ND
D
ND
D
ND
D
ND
Hom/Cre+
Hom/Cre-
Het/Cre+
Het/Cre-

C.

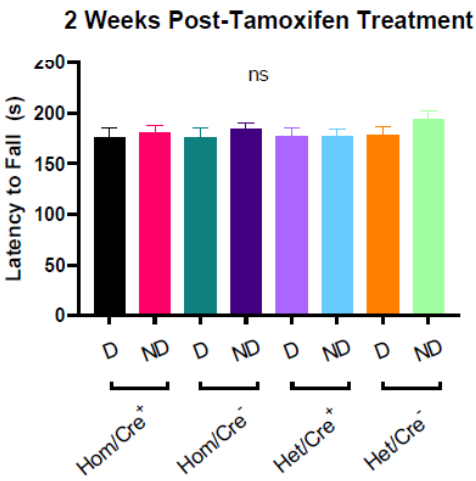
2 Weeks Post-Tamoxifen Treatment
Latency to Fall (s)
250
200
150
100
50
0
ns
D
ND
D
ND
D
ND
D
ND
Hom/Cre+
Hom/Cre-
Het/Cre+
Het/Cre-

D.

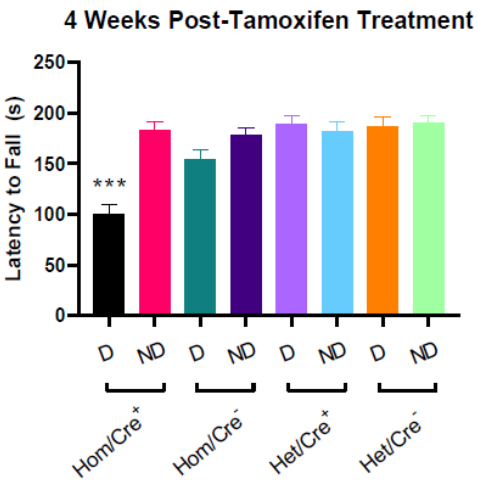
4 Weeks Post-Tamoxifen Treatment
Latency to Fall (s)
250
200
150
100
50
0
***
D
ND
D
ND
D
ND
D
ND
Hom/Cre+
Hom/Cre-
Het/Cre+
Het/Cre-

E.

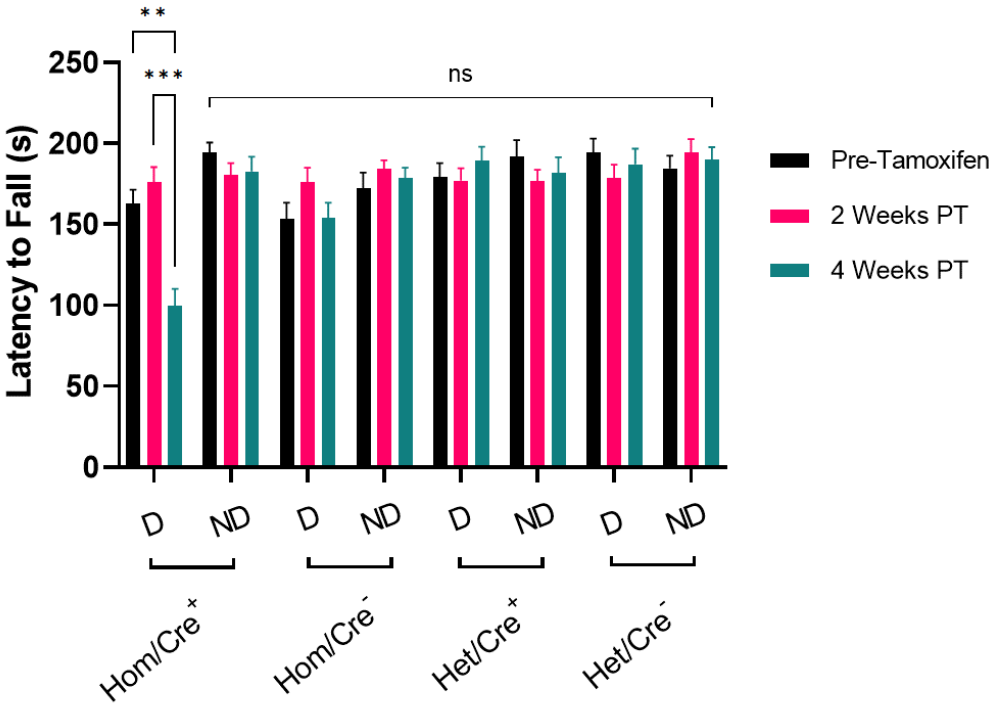
Latency to Fall (s)
250
200
150
100
50
0
**
***
ns
D
ND
D
ND
D
ND
D
ND
Hom/Cre+
Hom/Cre-
Het/Cre+
Het/Cre-
Pre-Tamoxifen
2 Weeks PT
4 Weeks PT

***Figure 4.17*| Accelerated rotarod performance assessing motor function in adult *Oxr1* knockout mice across longitudinal study**

(A) Illustration of accelerating rotarod performance test apparatus used. Average latency to fall (s) of female mice in each genotype and dose group across three trials on consecutive days (B) pre-tamoxifen treatment, (C) 2 weeks post-tamoxifen treatment and (D) 4 weeks post-tamoxifen treatment. Statistical significance was analysed by one-way ANOVA followed by Tukey's multiple comparisons test. (E) Analysis of group rotarod performance over longitudinal study measuring average latency to fall. Statistical significance was analysed by mixed-effects analysis, followed by Tukey's multiple comparisons test. PT: post-tamoxifen treatment, D: dosed with tamoxifen, ND: not dosed with tamoxifen. All data presented as mean ± SEM. Ns: not significant, *p<0.05, **p<0.01, ***p<0.001. n= 9-12 per genotype.

4.2.6 Deletion of Oxr1 in the adult mouse leads to highly localised cell death in the cerebellar granule cells and the glomerular layer of the olfactory bulb

Oxr1-deficiency increases cellular susceptibility to OS-induced cell death, *in vitro* and *in vivo* (Matsui et al., 2020; Oliver et al., 2011; Yang et al., 2014); importantly, cerebellar neurodegeneration is a key feature in both LoF-OXR1 patients and constitutive *Oxr1* knockout mouse model (Lin et al., 2022; Oliver et al., 2011; Wang et al., 2019). As previously described, in-cage observations documented that tamoxifen-treated Hom/Cre^{+} mice developed a severe ataxic gait, similar to the *bel* mutant (Oliver et al., 2011), and seizure-like behaviour, four weeks after dosing. Signs of 'seizure-like behaviour' included abnormal jerking movements and repetitive grooming behaviour (personal observations). Moreover, tamoxifen-treated Hom/Cre^{+} mice collectively demonstrated a reduction in latency to fall, demonstrating a diminished rotarod performance at this time point. Given that ataxia and motor impairment is linked to cerebellar neurodegeneration (Salman, 2018), neuropathological analysis was conducted at 4W PT to determine if neuronal apoptosis is also observed in this mouse model.

Terminal deoxynucleotidyl transferase dUTP nick end labelling (TUNEL) was carried out on fresh-frozen brain sections from tamoxifen-treated Hom/Cre^{+} and Hom/Cre^{-} mice to identify the presence of any apoptotic, TUNEL-positive cells; this revealed highly localised apoptosis in the CGCL of Hom/Cre^{+} mice 4W PT (**Figure 4.18A**). No cell death was observed in representative control Hom/Cre^{-} dosed mice at this time point. Interestingly, TUNEL-positive cells were also observed in the glomerular layer of the olfactory bulb in tamoxifen-treated Hom/Cre^{+} mice, whereas no regional TUNEL staining was observed in representative control mice (**Figure 4.18B**).

A.

TUNEL DAPI

Hom/Cre^{+}

Hom/Cre^{-}

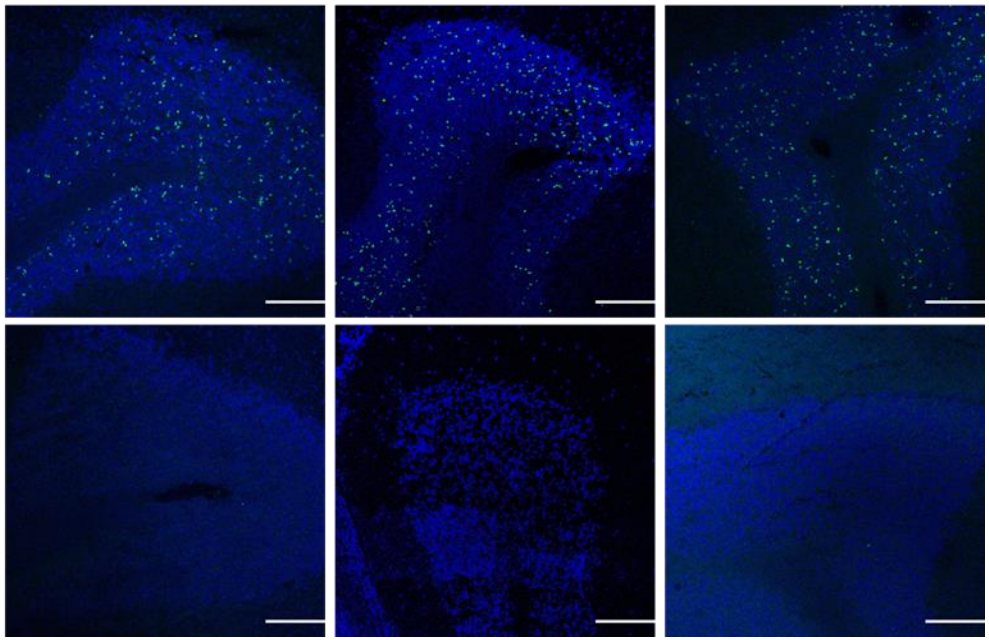

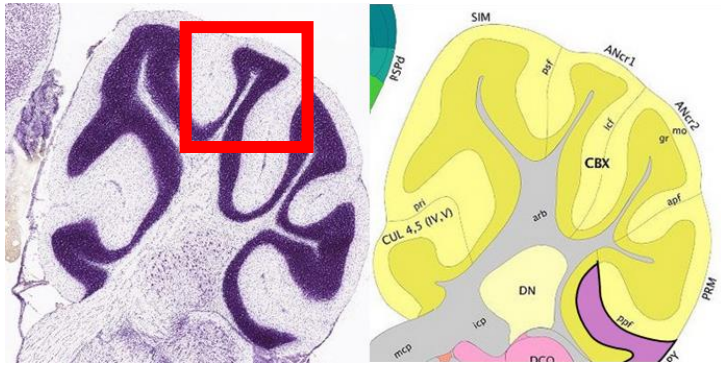

B.

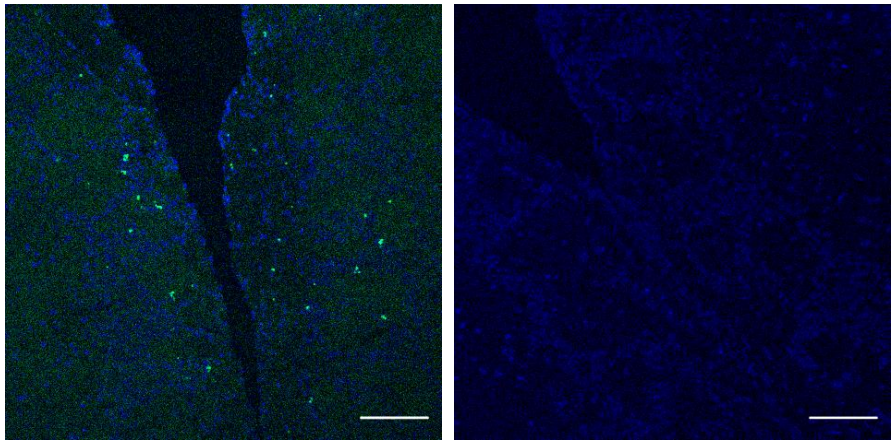

Hom/Cre^{+} Hom/Cre^{-}

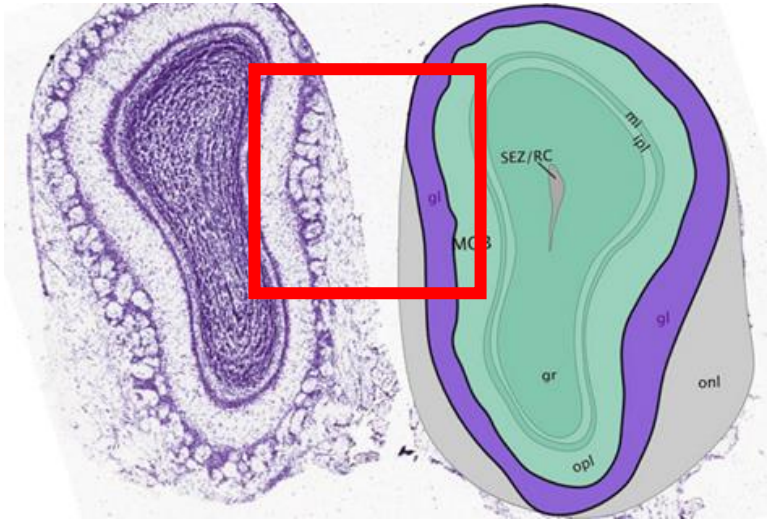

***Figure 4.18*| TUNEL staining in cerebellum and olfactory bulb of adult *Oxr1* knockout and representative control mice 4 weeks post-tamoxifen treatment**

Representative images of terminal deoxynucleotidyl transferase dUTP nick end labelling (TUNEL) of apoptotic cells localised to the (A) granule cell layer of the cerebellum and (B) glomerular layer of the olfactory bulb in Hom/Cre^{+} dosed mice compared to a representative control Hom/Cre^{-} dosed mice, 4 weeks post-tamoxifen treatment. Allen Brain Atlas P56 reference images to depict representative regions of confocal images. n=4 Green: TUNEL, Blue: DAPI. Scale bar: 100 µm

Cell death was not observed in any additional brain regions or in other control groups (data not shown). These data demonstrate that loss of Oxr1 in the adult mouse causes apoptotic cell death in the CGCL and the glomerular layer of the olfactory bulb, highlighting selective vulnerability of these cell types to the loss of Oxr1 in adult mice.

4.2.7 Loss of Oxr1 in the adult mouse brain induces a strong neuroinflammatory response

Thus far, previous research has indicated that is Oxr1 is likely to possess an immunomodulatory function, whereby over-expression can delay or prevent neuroinflammation *in vivo*, while RNA-Seq identified significant upregulation of neuroinflammatory markers in pre-symptomatic cerebellum from *Oxr1*$^{tm1d/tm1d}$ mice, ionized calcium-binding adapter molecule 1 (Iba1) and glial fibrillary acidic protein (Gfap)(**Chapter 3**) (Finelli et al., 2015; Li, Li, et al., 2014; K. X. Liu et al., 2015; Wang et al., 2012; Williamson et al., 2019). From this evidence, and considering the cell death pattern at 4W PT, it was hypothesised that loss of Oxr1 in adult mice would result in neuroinflammation, particularly in the cerebellum and olfactory bulb.

Neuroinflammation was assessed at 4 weeks PT in Hom/Cre^{+} Dosed animals, compared to representative controls Hom/Cre^{+} No Dose and Het/Cre^{+} Dosed groups, by immunostaining whole brain sagittal sections with anti-Iba1 and anti-Gfap, markers of activated microglia and astrogliosis respectively (**Figure 4.19**; **Figure 4.20**). Representative controls were used as all control groups exhibited no phenotypic differences or cell death pathology. Moreover, a strong neuroinflammatory response was not observed in any other control groups (data not shown). *Oxr1* is expressed across the brain, with notable expression in the cerebellum, cortex, hippocampus and olfactory bulb (Finelli et al., 2016), therefore these regions were chosen to investigate neuroinflammatory susceptibility to loss of Oxr1 in adult mice.

Anti-Iba1 immunohistochemistry revealed significant levels of activated microglia in the cerebellum [p<0.0001] (**Figure 4.19B)**, olfactory bulb [p=0.0197] (**Figure 4.19C)**, motor cortex [p=0.0002] (**Figure 4.19D)** and hippocampus [p=0.0019] (**Figure 4.19E)** in adult knockout mice, when compared to Het/Cre^{+} Dosed controls. Additionally, a significant difference was identified between numbers of immune-positive cells in Hom/Cre^{+} Dosed and Hom/Cre^{+} No Dose controls in the cerebellum [p=0.0033] (**Figure 4.19B)** and hippocampus [p=0.0026] (**Figure 4.19E)**.

Similarly, preliminary anti-Gfap staining revealed strong astrogliosis in the GCL of the cerebellum, olfactory bulb and hippocampus of Hom/Cre^{+} Dosed mice; no differences in presence of reactive astrocytes are observed in the somatomotor cortex when comparing Hom/Cre^{+} Dosed mice to representative control groups (**Figure 4.20**). Together, these initial studies indicate that Oxr1 plays a critical role in modulating neuroinflammation across the brain in adult mice.

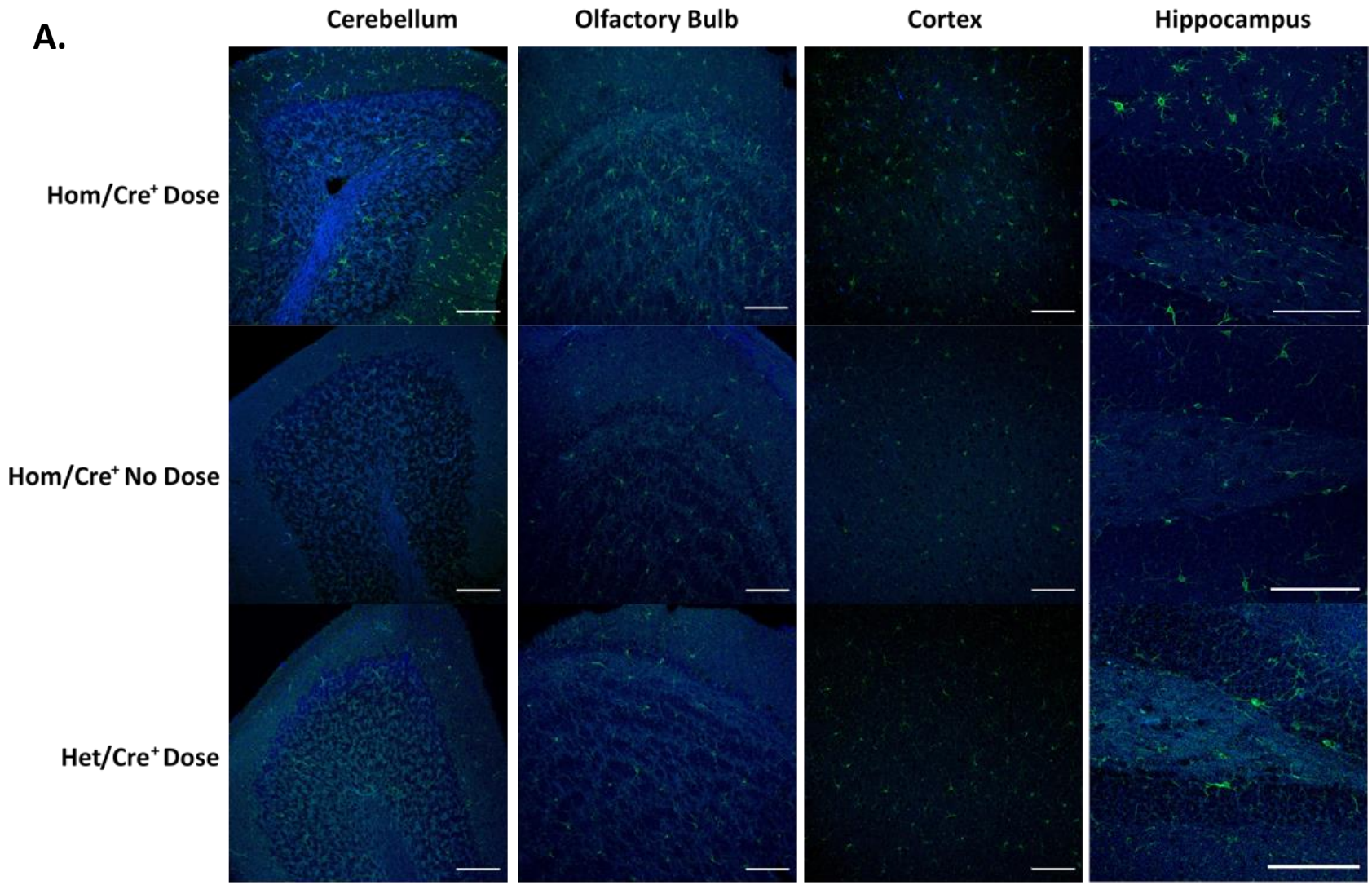

**** Figure continued on next page ****

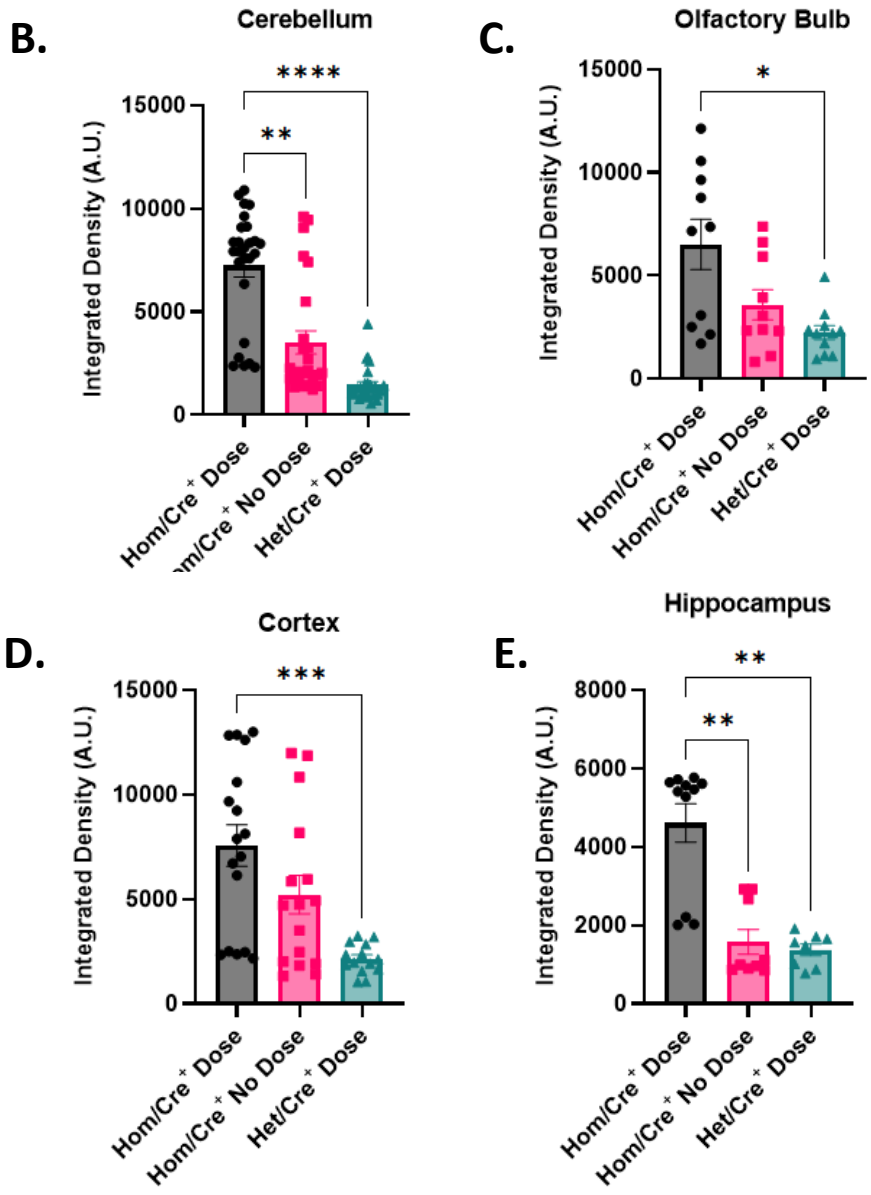

***Figure 4.19*| Immunohistochemistry to quantify Iba1-positive cells in sagittal brain sections of adult *Oxr1* knockout and representative control mice**

Representative immunostaining (A) and quantification of integrated density in arbitrary units (A.U.) for Iba1 in the (B) cerebellum, (C) olfactory bulb, (D) cortex and (E) hippocampus of Hom/Cre$^+$ dosed mice and representative control genotypes, Hom/Cre$^+$ No Dose and Het/Cre$^+$ Dosed. All tissue was taken at the 4 week post-tamoxifen treatment time point. Scale bar: 100 µm for all panels. Green: Iba1, Blue: DAPI. Images acquired using the Inverted Zeiss LSM 710 confocal. Data is presented as ±SEM. Kruskal-Wallis test followed by Dunn's multiple comparisons test. p values * ≤ 0.05, **≤0.01, *** ≤ 0.001, **** ≤ 0.0001.

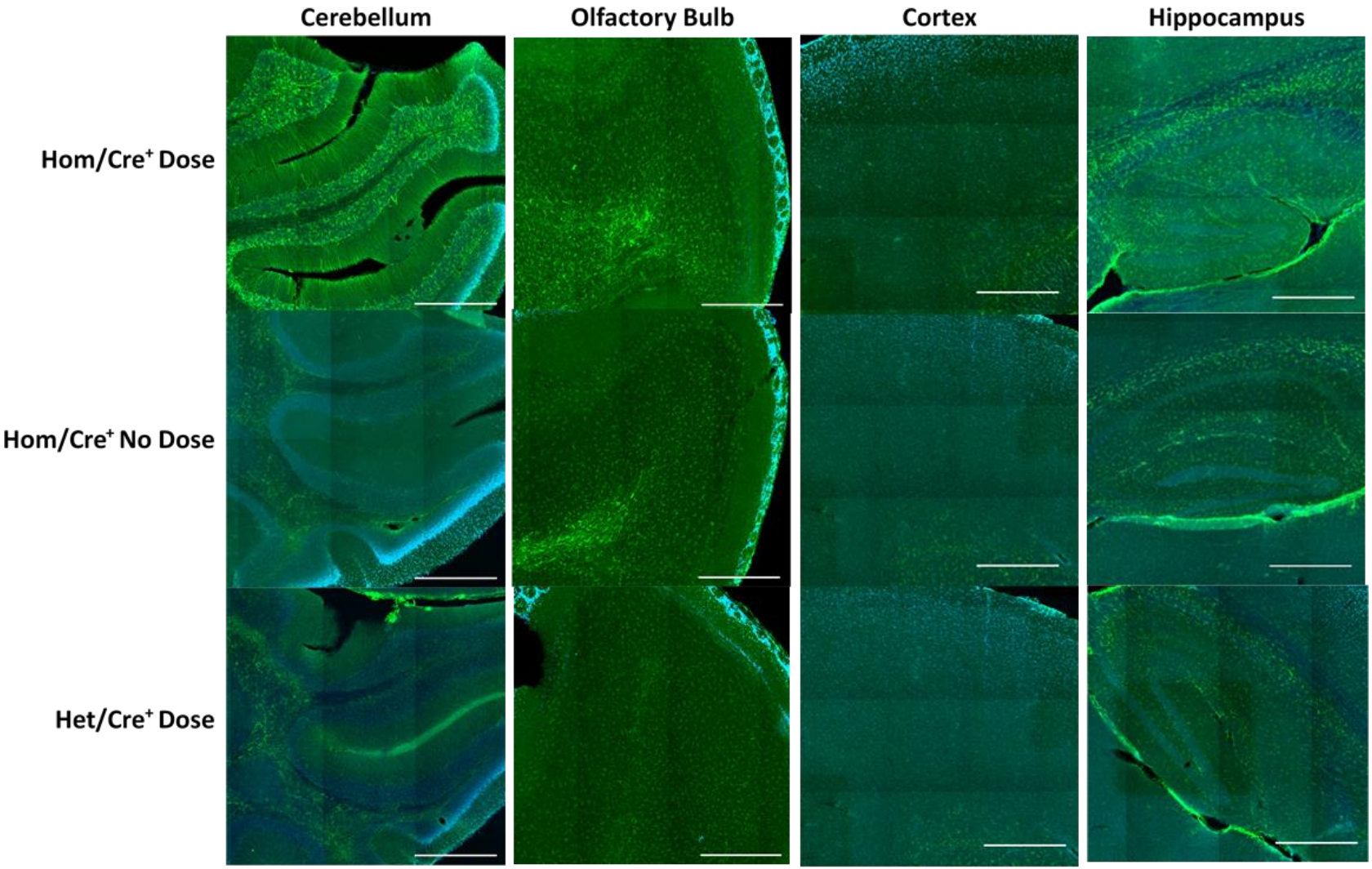

***Figure 4.20*|Sagittal brain section immunofluorescence to visualise presence of reactive astrocytes in different brain regions of adult *Oxr1* knockout and representative control mice.**

Representative immunostaining for Gfap and DAPI in the cerebellum, olfactory bulb, cortex and hippocampus of Hom/Cre$^+$ dosed mice and representative control genotypes, Hom/Cre$^+$ No Dose and Het/Cre$^+$ Dosed. All tissue was taken at the 4 week post-tamoxifen treatment time point. Scale bar: 500 µm for all panels. Green: Gfap, Blue: DAPI. Images acquired using the ZEISS Axioscan 7 slide scanner. n=3-4

4.2.8 Loss of *Oxr1* in adult mouse cerebellum leads to increased autophagy

Results discussed in **Chapter 3** suggested the importance of Oxr1 in autophagy. As adult *Oxr1* knockout mice exhibit strong neuropathology in the cerebellum, similar to observations found in *Oxr1*$^{tm1d/tm1d}$ mice, end-stage cerebellar tissue was analysed by western blot to assess whether autophagy was also perturbed in Hom/Cre^{+} dosed mice (**Figure 4.21A**). Whilst a significant increase in LC3-II was observed in Hom/Cre^{+} dosed mice [p=0.0398] (**Figure 4.21D**), the protein levels of p62 and LC3-I were not significantly different in adult knockout whole cerebellar tissue compared to control animals, as observed by Western blot analysis (**Figure 4.21B, C**). Similarly, when comparing the overall ratio of LC3II/I, no significant difference was identified (**Figure 4.21E**). Taken together, these results suggest dysregulation of autophagy in the cerebellum of *Oxr1*-depleted adult mice, similar to constitutive *Oxr1* knockout mice. Given that there is an observed increase in LC3-II levels, but not p62 or LC3-I, this suggests that lysosomal function or LC3-II^{+} autophagosome-lysosome fusion could be impaired in this mouse model (Abounit et al., 2012).

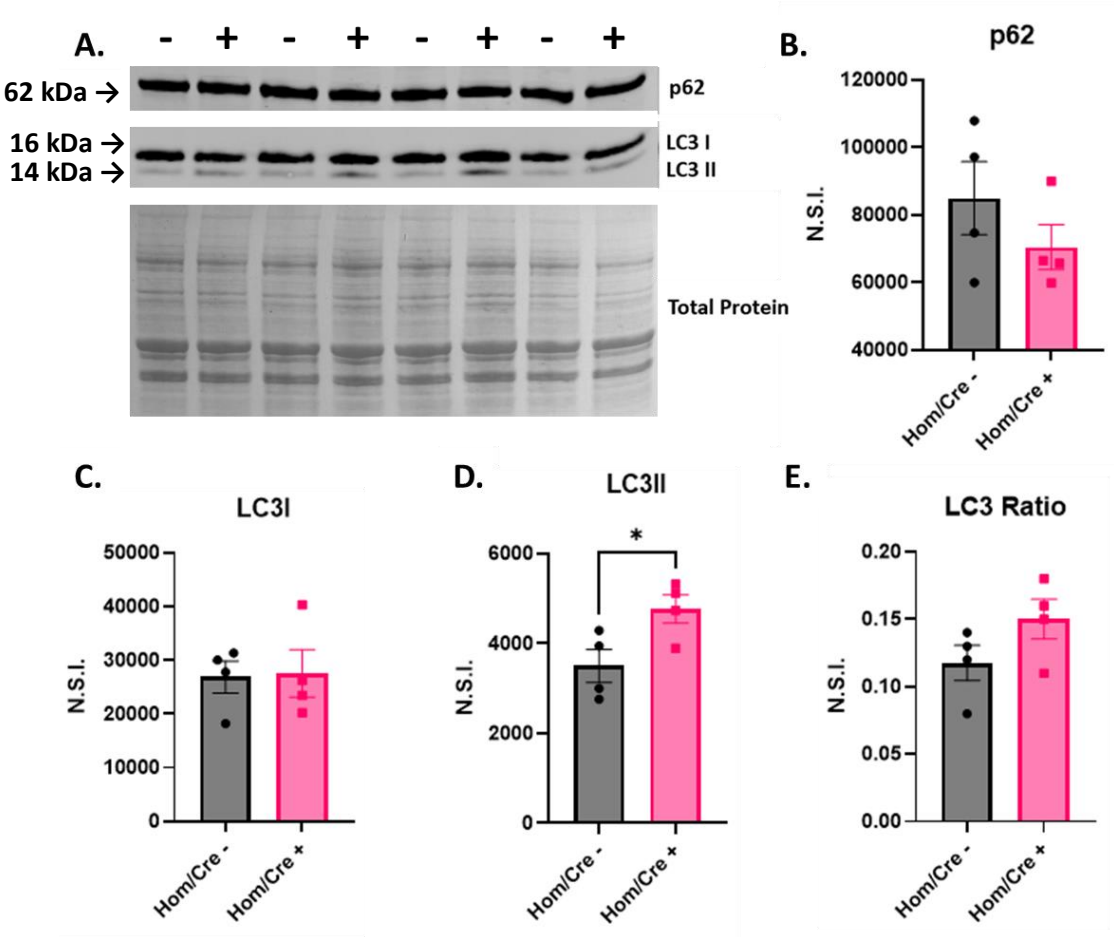

***Figure 4.21*| Western blotting of autophagic turnover markers on cerebellar tissue from end-stage adult *Oxr1* knockout mice**

(**A**) Representative western blot and relative quantification of (**B**) p62, (**C**) LC3I, (**D**) LC3II and (**E**) LC3II/I ratio autophagic flux markers in cerebellar tissue taken from Hom/Cre^{-} (-) and Hom/Cre^{+} (+) 4 weeks post-tamoxifen treatment. Normalised to total protein. N.S.I.: Normalised signal intensity. Unpaired t-test, p value = * ≤ 0.05, n=4.

4.3 Discussion

Evidently, *OXR1* expression is required during embryonic and early postnatal development in both human and mice, particularly for proper neurological function. LoF-OXR1 patients present with neurological clinical features from birth or in early childhood (Lin et al., 2022; Wang et al., 2019); likewise, mice lacking *Oxr1* do not survive beyond P26 (Oliver et al., 2011). To that effect, little is known regarding the role of Oxr1 in adulthood, yet it is robustly expressed in the forebrain and cerebellum beyond these early developmental time points (Cardoso-Moreira et al., 2019; Finelli et al., 2016); previously, a distinct role of Oxr1 in adulthood had not been described. This chapter has established that ubiquitous loss of Oxr1 in the adult mouse has detrimental effects in the CNS. Surprisingly, tamoxifen-induced knockout of *Oxr1* in adulthood resulted in a severe neurological phenotype, similar to that observed in the *bel* mice, with ataxia but also seizure-like episodes 4 weeks PT (Oliver et al., 2011)(personal observations). Behavioural characterisation and histopathology of this mouse line demonstrated, for the first time, that Oxr1 is essential in the adult mouse brain.

4.3.1 Characterisation of a ubiquitous adult-induced knockout of *Oxr1* identified an essential role for Oxr1 in the adult mouse

Constitutive *Oxr1* null mutant mice fail to gain weight as efficiently from P14 compared to their littermate controls (Oliver et al., 2011); similarly, weight loss is tightly correlated with disease progression in *Npc1*-deficient LSD mouse models (Ahmad et al., 2005; Williams et al., 2014). In concurrence with this data, the body weight of a number of LoF-OXR1 patients was reported to be below the 10th percentile for each of their reported ages (Wang et al., 2019). Interestingly, following tamoxifen dosing, adult *Oxr1* knockout mice are unable to effectively regain weight compared to tamoxifen-treated control mice and significantly lose weight during disease progression. Low body mass index (BMI) and

metabolic dysfunction are considered significant risk factors in the severity of a number of NDs, such as PD, ALS and Dementia (Astell-Burt et al., 2021; Capecci et al., 2013; Dardiotis et al., 2018), thus identifying weight and metabolism as confounding factors in progressive neurodegeneration.

It has been widely reported that tamoxifen treatment can induce substantial weight loss through acute lipoatrophy (Geiser et al., 2012; L. Liu et al., 2015; Ye et al., 2015), therefore it is unsurprising that weight loss is observed in all tamoxifen treated mice, yet there are apparent systematic metabolic alterations in adult mice lacking expression of *Oxr1*. Further to this, a significant reduction in body weight is also observed in the early postnatal developmental stages of brain-specific isoform *Oxr1* knockout (*Oxr1A*$^{-/-}$) mice (Yang et al., 2020). Together, these data suggest that Oxr1 plays a role in metabolism and determining weight, however metabolic phenotyping was beyond the scope of this thesis. It would be insightful to perform body composition analysis on these cohorts through EchoMRI or dual energy X-ray absorptiometry (DEXA), in the period from tamoxifen-induced weight loss to disease onset, establishing if there is differential composition of fat and lean mass between the different genotypes (Brommage, 2003; Mystkowski et al., 2000).

In addition to significant weight loss, Hom/Cre^{+} mice dosed with tamoxifen displayed a severe ataxic gait and seizure-like activity within four weeks of tamoxifen-treatment, thus determining an abrupt experimental endpoint. This defined a narrow window of opportunity to characterise the effects of ubiquitous loss of Oxr1 in the adult mouse, despite initially sustaining the critical global, developmental expression of *Oxr1* (Oliver et al., 2011). As a result of this, only a limited behavioural assessment could be performed prior to adult *Oxr1* knockout mice reaching the humane endpoint in disease progression. In spite of this challenge, the ability to follow the progressive deterioration

and behavioural changes associated with adult-induced loss of *Oxr1* in the same animals from pre-tamoxifen treatment to the end of the study is a critical benefit of an inducible knockout system (Mercado-Ayon et al., 2022; Wilcox et al., 2017).

Hippocampal dysfunction has been linked to memory and learning deficits (Abbah et al., 2022; Bygrave et al., 2019; Nakazawa et al., 2002; Papp et al., 2007), key clinical features in patients with neurodegenerative pathology (Hou et al., 2019). Intellectual disability, which often encompasses cognitive impairment and poor memory, has also been reported in LoF-OXR1 patients (Groft et al., 2017; Lin et al., 2022; Wang et al., 2019). Surprisingly, both adult *Oxr1* knockout mice and representative control animals demonstrate a reduction in general activity, as indicated by a decrease in total distance travelled at 2W and 4W PT compared to the pre-tamoxifen time point. This trend has been also observed when comparing the locomotor activity of mice naïve to phenotyping, to those that had been through a test battery pipeline (McIlwain et al., 2001). Likewise, a study on wild type C57BL/6J behaviour using repeated open field trials found overall activity to be largely reduced in the second and third open field trials, indicating memory of a familiar environment and intersession habituation (Bolivar et al., 2000). In a PD mouse model, *parkin*$^{-/-}$ mice showed a significant increase in total difference travelled between the first and second open field trial, which is not observed in Oxr1-depleted adult mice, whereas wild type mice exhibited a typical habituation response (Rial et al., 2014). From this evidence, it is likely that long-term habituation and memory are not affected in adult *Oxr1* knockout mice.

Conversely, intra-session analysis of open field data implied impaired short-term habituation and an anxiety-related phenotype in adult *Oxr1* knockout mice, at both 2W and 4W PT, thus suggesting that depletion of Ox1 leads to cognitive impairment, prior to exhibiting a motor phenotype. Additional behavioural tests, such as Y-maze, contextual

fear conditioning and light/dark box, would be needed to further assess memory impairments and anxiety related phenotypes (Bygrave et al., 2019; Castroflorio et al., 2021; Lin et al., 2020; Rial et al., 2014). This initial data alludes to perturbed hippocampal function in adult *Oxr1* knockout mice, in the absence of cell death in this region; importantly, an increase in microgliosis and reactive astrocytes are found in the hippocampus. Strikingly, conditional deletion of *Oxr1* in CA3 region of the hippocampus (see **4.3.2**) leads to spatial memory impairments (unpublished data). Further to this, these mice also spend more time in the centre of the open field arena, as well as in centre of the elevated plus-maze, suggesting that loss of Oxr1 has an anxiolytic effect in CA3-specific *Oxr1* knockout mice (unpublished data). In parallel to adult *Oxr1* inducible knockout mice, hippocampal histopathology of CA3-*Oxr1* knockout mice did not indicate neurodegeneration, though a strong localised neuroinflammatory response was observed in the CA3 region (unpublished data). Taken together, this suggests that loss of Oxr1 may disrupt hippocampus-dependent short-term memory formation, as well as leading to neuroinflammation in the hippocampus.

Motor dysfunction and gait abnormalities are a prominent clinical feature in NDs, such as PD, LSDs and ataxia disorders (Fancello et al., 2009; Marcelo et al., 2021; Sarva & Shanker, 2014; Shachar et al., 2011). Post-mortem analysis of Oxr1 expression demonstrated a substantial protein knockdown in the cerebellum at 2W PT, yet a motor phenotype was only observed 4W PT. Adult *Oxr1* knockout mice present with a severe ataxic gait and an overall reduced latency to fall in rotarod, compared to experimental control groups at 4W PT, suggesting motor dysfunction in this mouse model. Crucially, western blot at 4W PT indicated the absence of Oxr1 in cerebellar tissue, with only residual expression in the cerebral cortex, alongside apoptotic CGCs, suggesting that impaired motor function correlates to almost complete knockdown of Oxr1 in the brain and

neurodegeneration, highlighting the importance of Oxr1 protein dosage *in vivo* (see **4.3.4**). Although the gait abnormalities and motor impairment are extremely apparent in this mouse model, broad neurological screens that include short tests, e.g. wire suspension test, could be performed to provide a more extensive quantitative assessment of motor function in ND mouse models (McIlwain et al., 2001).

Notably, cell death is observed in the CGCL and olfactory bulb, as well as a neuroinflammatory response across the brain at 4W PT. Therefore, significant loss of *Oxr1* in the adult mouse induces cerebellar degeneration and neuroinflammation that is likely responsible for the severe progressive motor phenotype. Further to this, levels of autophagy-related proteins, p62 and LC3, were suggestive of increased autophagic turnover in cerebellar tissue from end-stage adult *Oxr1* knockout mice. Given that upregulation of lysosome-associated genes precedes cerebellar degeneration in constitutive *Oxr1* knockout mice, it is likely that autolysosomal dysfunction is also a key driver of disease pathogenesis in this mouse model.

4.3.2 Conditional-ready *Oxr1* allele as a tool to study the role of *Oxr1* in brain regions outside of the cerebellum in mice

Crossing conditional-ready *Oxr1* mice to the tamoxifen-inducible UBC/ERT2-Cre line revealed apoptosis in CGCs and additionally, the glomerular layer of the olfactory bulb in *Oxr1*-depleted adult mice. In contrast to CGCs, cell death was not previously observed in the olfactory bulb of *bel* mice, thus the adult-induced *Oxr1* knockout mouse model identified a novel selective neuronal vulnerability that may have been masked by the early mortality in constitutive *Oxr1* knockout mice (Oliver et al., 2011). This establishes the conditional-ready *Oxr1* allele as an essential tool in uncovering a role for *Oxr1* in cell survival in brain regions outside of the cerebellum, which can be used in conjunction with region-specific Cre-driver lines (Heffner et al., 2012).

Indeed, *Oxr1* is robustly expressed in the CGCL and olfactory bulb; *Oxr1* is most highly expressed in CA3 field of the hippocampus, yet cell death is not observed in constitutive or adult-deletion *Oxr1* mouse models (Finelli et al., 2016; Oliver et al., 2011). Intriguingly, differential vulnerability has been identified between CA1 and CA3 regions of the hippocampus in response to OS challenges. CA1-derived neurons show increased vulnerability to OS insults and ischemia, resulting in higher levels of apoptosis compared to CA3 pyramidal neurons *in vitro* and *in vivo* (Medvedeva et al., 2017; Wilde et al., 1997). Surprisingly, CA3 neurons are more susceptible to degeneration following limbic seizures, but exhibit limited degeneration following ischemia (Medvedeva et al., 2017; Wilde et al., 1997). Given the contrasting responses between the two cell types and significant expression of *Oxr1* in the CA3-region of the hippocampus (Finelli et al., 2016), *Oxr1* could be a confounding neuroprotective factor against OS-related insults in the hippocampus. To determine if discrete loss of *Oxr1* is detrimental to CA3 neuronal viability, a CA3-specific *Oxr1* knockout was generated by crossing conditional-ready *Oxr1* mice with a Grik4-Cre expressing line (Nakazawa et al., 2002). Loss of Oxr1 in the CA3 region of the hippocampus

lead to highly localised microgliosis and region-related phenotypes (Papp et al., 2007), although cell death was not observed (unpublished data). These mice exhibited short-term memory deficits, hyperactivity and reduced anxiety (unpublished data) which revealed the importance of hippocampal *Oxr1* expression in determining behaviour and modulating localised neuroinflammation *in vivo*. Notably, short-term habituation deficits and an anxiety-related phenotype was observed in adult *Oxr1* knockout mice.

One of the common clinical phenotypes in LoF-OXR1 patients is epilepsy, where there is likely involvement of the cerebral cortex (Lin et al., 2022; March, 1998; Wang et al., 2019). Conversely, constitutive *Oxr1* knockout mice did not appear to develop spontaneous seizures, with no marked neuroinflammation or cell death observed in the neocortex of the P22 mouse (Oliver et al., 2011). Together, this indicates that the role of Oxr1 in the cortex warrants further investigation (Alonso-Nanclares et al., 2005; Calcagnotto et al., 2005; Pfisterer et al., 2020). Calcium/calmodulin-dependent protein kinase type II α chain (CamKIIα) is an enzyme that is highly expressed in the forebrain and CA1 pyramidal hippocampal and be detected as early as P0 in the mouse (Dragatsis & Zeitlin, 2000; Mayford et al., 1996; Miller & Kennedy, 1986). Crossing conditional-ready *Oxr1* mice with CamKIIα-Cre expressing mice generated a cortical knockout allowing for the study of the role of Oxr1 in the forebrain (Choi et al., 2014; Dragatsis & Zeitlin, 2000; Tsien et al., 1996). Preliminary pathological studies indicated that cortical deletion of Oxr1 reduces the overall thickness of the cerebral cortex and corpus callosum, as well as inducing neuroinflammation (unpublished data); of note, thinning of the corpus callosum has been identified in LoF-OXR1 patients (Lin et al., 2022). Interestingly, gene ontology (GO) analysis of differentially expressed genes in LoF-OXR1 patient iPSCs that underwent neurodifferentiation demonstrated down regulation of genes that play a role in cell migration and axon guidance, critical processes required for corpus callosum formation (Lin

et al., 2022; Wegiel et al., 2018). Lin *et al.* (2022) hypothesised that perturbed axon guidance in the absence of *OXR1* may attribute to the thinner corpus callosum observed in these LoF-OXR1 patients. Corpus callosum malformation has not been identified in *bella* mice (Oliver et al., 2011); given that corpus callosum formation and maturation continues in to early adulthood in mice yet constitutive *Oxr1* knockout mice early-onset cerebellar degeneration and shortened lifespan (P24-26), it could be hypothesised that this pathological phenotype may only be possible to observe in forebrain-specific *Oxr1* knockout mice that survive beyond this early postnatal timepoint. Neural progenitor cell proliferation and survival in embryogenesis and postnatal life have been suggested to be key contributing factors in determining the size of the adult brain (Laporte et al., 2017). Neurogenesis is a highly dynamic process inevitably generating ROS which, in the absence of *Oxr1* in cortex, could inflict OS and trigger atypical apoptosis contributing to the reduced cortical size exhibited in the mice (Chui et al., 2020; Guo et al., 2010; Tsatmali et al., 2006). More recently, a study found that transient depletion of microglia prevented cortical thinning in a kainic acid-induced mouse model of epilepsy, implicating microglial activation in modulating cortical thickness, although seizure frequency was not attenuated in the model (Altmann et al., 2022).

Furthermore, an increased number of Iba1-positive cells was observed in the cortex of both adult-induced and forebrain-specific *Oxr1* conditional knockout mouse models, suggesting microglial activation. Seizure-like behaviour was observed in adult *Oxr1* knockout mice, though not fully characterised, yet no visible seizures were observed in mice lacking expression of *Oxr1* in the cortex. Neuroinflammation, and its dynamic interplay with ROS, are critical factors underpinning epileptogenesis and lowering the seizure threshold (Campbell et al., 1993; Eastman et al., 2020; Parsons et al., 2022; Vezzani & Granata, 2005). There is also increasing evidence that alongside post-seizure

inflammatory responses, microglial activation precedes the first seizure event (Vezzani & Granata, 2005). Intriguingly, increasing microglial mTOR signalling, through selective deletion of tuberous sclerosis complex 1 (*Tsc1*) specifically in microglia, lead to increased microglial proliferation, altered morphology and a spontaneous seizure phenotype in mice (Zhao et al., 2018). Expression profiling of these microglia identified significant upregulation of phagocytosis-related and lysosomal genes, such as *HexA*, cathepsins and v-ATPase subunits, with the absence of a proinflammatory transcriptome (Zhao et al., 2018). Therefore, one hypothesis deduced from this evidence is that loss of *Oxr1* in the cerebral cortex induces microglial reactivity and may increase seizure susceptibility *in vivo.* To assess alterations in seizure threshold in *Oxr1*-deficient mouse models, exposure to seizure evoking stimuli, such as kainic acid or auditory tones, in conjunction with EEG could be employed in these adult mice (Chabrol et al., 2010; Maheshwari, 2020; Vogt et al., 2011).

These collective data highlight the value of using the *Oxr1*$^{tm1c/tm1c}$ mouse line for *in vivo* studies of region/tissue-specific effects in the absence of *Oxr1*. A key limitation lies in the absence of inflammatory markers in cerebrospinal fluid from LoF-OXR1 patients (Lin et al., 2022), particularly as it appears to be a key disease-modulator in Oxr1-deficient mouse models. This challenges the validity of the model in relation to LoF-OXR1 patients (**See Chapter 6**). Nevertheless, these models offer an opportunity to study other behavioural and pathological paradigms relevant to OXR1-deficient patients, particularly those that were previously unknown due to the early mortality of constitutive *Oxr1* knockout mice (Oliver et al., 2011).

4.3.3 Selective neuronal vulnerability in adult-induced *Oxr1* knockout mice

In addition to CGC death, global, temporal control of *Oxr1* gene disruption in the adult mouse revealed surprising, selective neuronal vulnerability in the olfactory bulb, with evident apoptosis in the olfactory glomeruli in adult-induced *Oxr1* knockout mice. Olfactory system impairment is a hallmark characteristic of several NDDs, including Alzheimer's and Parkinson's disease, but also in epilepsy (Khurshid et al., 2019; Navarro et al., 2020; Ruan et al., 2012). Seizures are a persistent feature in LOF-OXR1 patients and in addition to this, seizure-like behaviour was observed in adult-induced *Oxr1* knockout mice (Lin et al., 2022; Wang et al., 2019). Interestingly, cells of the glomerular layer of the olfactory bulb are identified as highly ROS-producing, both postnatally and into adulthood (Tsatmali et al., 2006). Further to this, differential expression of *Oxr1* was identified through spatial transcriptomics of olfactory bulb tissue from a transgenic Alzheimer's disease (AD) mouse model; *Oxr1* was found to be upregulated in AD models where olfaction was also impaired and increased neuroinflammation was identified (Navarro et al., 2020). Therefore, it is possible that upregulation of Oxr1 occurs to mediate OS-induced neuroinflammation and neurodegeneration in the olfactory bulb of AD mice. To evaluate this hypothesis, selective deletion of *Oxr1* in the olfactory bulb, using T-Box transcription factor 21 (*Tbx21*) or cholecystokinin (*Cck*) Cre-driver lines, could be employed to determine if loss of *Oxr1* exacerbates olfactory pathology and impaired sensory phenotype in this AD mouse model (Koldaeva et al., 2021).

Significant neuroinflammation was also identified in the olfactory bulb of adult-induced *Oxr1* knockout mice. Given the neuroprotective capacity of Oxr1 against OS-mediated neurodegeneration, it is likely that a build-up of ROS contributes to selective vulnerability of this cell type (Finelli et al., 2016; Oliver et al., 2011). In order to determine if the cell death observed in the glomerular layer affects olfactory function, a buried food

phenotyping test can be performed pre- and post-tamoxifen treatment of Hom/Cre^{+} mice, although the severity of motor phenotype may mask impaired olfactory function (Yang & Crawley, 2009). It is worth noting that loss of olfactory senses has not been reported in LOF-OXR1 patients (Lin et al., 2022; Wang et al., 2019).

Olfactory dysfunction is simultaneously observed in a number of neurodegenerative mouse models, including those citing cerebellar pathology. An example is ATP/GTP-Binding Protein 1 (*Agtpbp1*) null mice, also known as Purkinje cell degeneration (*pcd*) mice (Berezniuk et al., 2010; Chakrabarti et al., 2009). Purkinje cell loss is apparent from P15, whereas degeneration in the olfactory bulb did not arise until 13 weeks of age (Mullen et al., 1976); given the limited life span of constitutive *Oxr1* knockout mice, whether olfactory atrophy would present at a later time point cannot be determined (Oliver et al., 2011).

Similar to adult-induced *Oxr1* knockout mice, reduced p62 and increased LC3-II/LC3- I ratio was observed in cerebellar protein lysate from *pcd*-deficient mice indicating induction of autophagy (Chakrabarti et al., 2009), yet increased autophagy was also observed in brain regions that do not undergo cell death (Berezniuk et al., 2010). Thus, this indicates selective vulnerability of Purkinje cells to autophagic dysfunction in the pathogenesis of neurodegeneration in *pcd*-deficient mice, yet the reasons for olfactory bulb degeneration are still largely undescribed (Berezniuk et al., 2010; J. Li et al., 2020). Baltanas *et al.* (2013) found that cerebellar expression of *Agtpbp1* was 5-fold more than in the olfactory bulb of wild type mice between P15 and P25, a notable period of Purkinje cell degeneration in *pcd*-deficient mice (Mullen et al., 1976), providing a possible reason for their acute postnatal selective cerebellar vulnerability to loss of Agtpbp1. Furthermore, regional glial environment has been cited as a critical factor in maintaining CNS homeostasis and preventing neurodegeneration *in vivo* (Wang & Michaelis, 2010).

Interestingly, differential glial responses in the cerebellum and olfactory bulb have been reported in *pcd*-deficient mouse models (Baltanas et al., 2013), highlighting glial cells as potential confounding factors in disease aetiology of *pcd*-mice.

Why CGCs, and now olfactory glomeruli, exhibit distinct selective vulnerability to loss of Oxr1 in adult mice is still unknown. *In situ* hybridisation identified overlapping robust co-expression of *Oxr1, Ncoa7* and *Tbc1d24* in the cortex and hippocampus in wild type mice, where no cell death is evident in both constitutive and adult-induced *Oxr1* knockout mice (Castroflorio et al., 2021; Finelli et al., 2016; Oliver et al., 2011). Crucially, *Oxr1* is highly expressed in both CGCL and olfactory bulb; *Tbc1d24* is also expressed in the CGCL, although not in abundance, yet *Ncoa7* expression is highly restricted to Purkinje cells in the cerebellum (Castroflorio et al., 2021; Finelli et al., 2016). It is possible that, in the absence of Oxr1, expression of other TLDc proteins is sufficient to prevent or delay neurodegeneration in brain regions such as the cortex, highlighting that TLDc proteins may be functionally redundant in certain cell types; absence of *Ncoa7* and low levels of *Tbc1d24* expression may contribute to selective vulnerability observed in CGCs and olfactory glomeruli.

4.3.4 Oxr1 protein turnover rate in different brain regions and Cre-mosaicism effect *in vivo*

At 4 weeks PT, western blotting identified a clear difference in Oxr1 protein turnover rates between non-cerebellar and cerebellar brain tissue (**Figure 4.12**). At this time point, it is evident that almost complete knockdown of Oxr1 is present in the cerebellum 4W PT, whereas residual Oxr1 protein can still be detected in forebrain tissue, one indication that protein degradation is occurring at a faster rate in cerebellar tissue. *In vivo* metabolic pulse assays revealed that Oxr1 turnover rate is slower in cortical tissue (6.93 days) than in the cerebellum (6.19 days) (Fornasiero et al., 2018). Further to this, Oxr1

exhibits a faster turnover rate in primary hippocampal neuronal cultures (4.33 days) compared to mixed neuron-glial cultures (4.86 days) (Dorrbaum et al., 2018). Given the indication that Oxr1 can modulate neuroinflammation, it would have been interesting know differences in protein turnover rates in neuronal and glial populations independently, however this was not reported (Dorrbaum et al., 2018; Fornasiero et al., 2018). Protein turnover naturally occurs at tissue and cell-specific rates (Dorrbaum et al., 2018; Fornasiero et al., 2018), a limitation to consider when discussing selective vulnerability of neuronal populations induced by loss of Oxr1. In cell culture, 80% knockdown of Oxr1 was needed to result in significant cell death under OS conditions (Oliver et al., 2011); these data are consistent with the hypothesis that a significant knockdown level is needed *in vivo* to observe a visible phenotype.

With the aim of generating a ubiquitous knockout mouse model, the stochastic nature of efficient Cre-mediated recombination in individual cells within different tissues is a key limitation of this tamoxifen-inducible system (Heffner et al., 2012). For instance, Ruzankina et al. (2007) observed mosaicism of Cre-recombination events across different tissues in a tamoxifen-induced ubiquitous knockout of essential developmental gene, *ATM-and Rad3-related* protein kinase (*ATR)* (Ruzankina et al., 2007). Southern blotting demonstrated an apparent variability in the efficacy of gene deletion across different tissues, although recombination was still deemed efficient (>70%) three days after the final dose of tamoxifen (Ruzankina et al., 2007). Similarly, more efficient recombination events were observed in the kidney compared to the spleen in a tamoxifen-induced postnatal knockdown of insulin-like growth factor type 1 receptor (*IGF1R*) (Lopez et al., 2015). These findings outline difficulties in controlling for the efficacy of recombination events across different tissues and cell types. However, the nature of temporal knockdown across an

experimental cohort is still a valuable tool to assess protein dosage and phenotypic outcome.

4.3.5 Studying reversible phenotypes *in vivo*

Gene therapy is currently being explored as a therapeutic strategy for both developmental and adult-onset NDs (Pena et al., 2020). As it stands, these approaches are mostly effective in the slowing or delaying of disease progression, but not in reversing or ameliorating neurodegenerative pathology given the extremely limited capacity of adult neurogenesis and regeneration (Kole et al., 2013; Ming & Song, 2011). Therefore, it is important to consider the feasibility of rescuing symptomatic disease pathology, particularly where there are already profound neurological deficits and neurodegeneration (Pena et al., 2020).

This adult-inducible *Oxr1* knockout mouse model recapitulates the severe neurological phenotype and pathology observed in *bel* mice (Oliver et al., 2011), alongside novel findings of cell death in the olfactory bulb and seizure-like events. In addition to sharing clinical features observed in LoF-OXR1 patients, a critical advantage of this inducible system is the ability to study the adult-associated effects of *Oxr1*-depletion ubiquitously and in discrete cell types, alongside assessing the potential to reverse neurological phenotypes and disease-related pathophysiology upon restoration of *Oxr1* expression.

Friedreich's ataxia (FRDA) is an ND typically characterised by an ataxic gait, as well as selective atrophy in the cerebellum and spinal cord (Kemp et al., 2016). Following adult-induced depletion of *frataxin* (*fxn*), a known causative gene of FRDA, restoring expression of *Fxn* lead to a rescue of neurological phenotypes in mice, with reversal of gait abnormalities, grip strength comparable to control animals and improved survival (Chandran et al., 2017). Conversely in a more recent adult-inducible study, reintroducing

Fxn expression using an adeno-associated virus (AAV)-vector rescued the levels of cerebellar synaptic markers, such as vesicular glutamate transporter 1 (VGLUT1), yet effects on behaviour and pathology were negligible (Mercado-Ayon et al., 2022). Overall, this attributed part of the phenotype to doxycycline treatment when inducing Fxn knockdown (Chandran et al., 2017; Mercado-Ayon et al., 2022), demonstrating the importance of considering potential toxic dosing effects when using drug-inducible gene knockout systems.

Remarkably, reinnervation of neuromuscular junctions has been observed through suppressing expression of mutant neurofilament-light subunit in a symptomatic mouse model of Charcot–Marie–Tooth (CMT) disease (Dequen et al., 2010). These mice also demonstrated a significant rescue of motor deficits, highlighting a case of reversible neuropathology and behaviour *in vivo* (Dequen et al., 2010). Constitutive deletion of sodium channel protein type 1 subunit alpha (*Scna1*) causes early-onset epilepsy, yet reintroducing *Scna1* after the onset of seizures rescued the epileptic phenotype in both early postnatal and adult mice (Valassina et al., 2022), thus outlining that epilepsy may not lead to irreversible pathology in some patients; this is of particular relevance to the seizure phenotype observed in LoF-OXR1 patients (Lin et al., 2022; Wang et al., 2019).

Interestingly, downregulation of Oxr1 was observed in whole brain tissue from MPTP-induced PD mice, however, subsequent lentiviral injection of *OXR1* in symptomatic PD mice ameliorated behavioural deficits and improved disease pathology (Jiang et al., 2019). Re-establishing *Oxr1* expression alleviated the severe motor phenotype and reduced OS-induced neurodegeneration in the substantia nigra pars compacta in this PD mouse model (Jiang et al., 2019), thus demonstrating the therapeutic potential of restoring *Oxr1* expression *in vivo* to mitigate neuronal injury. This is a crucial therapeutic aspect given

that downregulation of *OXR1* has also been observed in the cortex of patients with PD with dementia (Stamper et al., 2008).

More broadly, neuroinflammation, perturbed lysosomal function and neurodegeneration are a few common features of the constitutive and adult *Oxr1* knockout mouse models (Oliver et al., 2011). Pertinently, there is some overlapping pathophysiology with LoF-OXR1 patients (Chen et al., 2017; Lin et al., 2022; Wang et al., 2019), as well as other NDs, including FRDA, Spinocerebellar ataxia (SCA) and lysosomal storage disorders (LSDs) (Fancello et al., 2009; Kemp et al., 2016; Marcelo et al., 2021); thus, the adult-induced *Oxr1* knockout and subsequent disease progression serve as a valuable model to test the reversal potential of severe cerebellar neuropathology and associated-behavioural phenotypes through restoring or upregulating expression of *Oxr1*.

4.3.6 Concluding Remarks

Ultimately, this chapter has demonstrated that Oxr1 expression is required in the adult mouse to sustain CGC survival, as well as maintain cellular viability in the olfactory bulb. Given the surprising and significant overlapping phenotype and neuropathology between constitutive and adult-induced *Oxr1* knockout mice, this suggests that there are fundamental functional aspects of the gene that are independent of neurodevelopment in the mouse and that cannot be compensated for by other TLDc proteins. Utilisation of the conditional-ready *Oxr1* allele crossed to different Cre-driver lines, including the tamoxifen-inducible UBC-Cre-ERT2 line, circumvents early-lethality observed in constitutive *Oxr1* knockout mice and provides an additional tool to investigate the contextual role of Oxr1 and other paradigms associated with loss-of-function mutations observed in OXR1, such as seizure susceptibility and cognitive impairment.

RESULTS III

Chapter 5 : *Oxr1* neuronal over-expression rescue of constitutive *Oxr1* knockout (*Oxr1*$^{tm1d/tm1d}$*/Prnp-Oxr1)*

5.1 Introduction

5.1.1. Differential expression of *OXR1* in neurological disorders

Oxidative stress (OS) underpins the manifestation and progression of a number of neurological disorders (NDs), such as Amyotrophic Lateral Sclerosis (ALS) (Barber & Shaw, 2010; K. X. Liu et al., 2015; Tam et al., 2019), Parkinson's disease (PD) (Dias et al., 2013; Gmitterova et al., 2009) and epilepsy (Eastman et al., 2020; Terrone et al., 2020); as such, endogenous cellular protective mechanisms that function to regulate OS-associated cellular damage warrant further investigation. Analysis of ND patient tissue samples have increasingly shown *OXR1* to be differentially expressed at varying stages of disease progression, supporting the argument for the role of dysregulated OS response as a factor in this process.

Increased OXR1 expression has been identified in spinal cord biopsies from end-stage ALS patients via western blot (Oliver et al., 2011). Tam *et al.* (2019) used post-mortem cortical samples to distinguish OS as one of three distinct molecular profiles in ALS patients. Cortical transcriptomic profiling from sporadic ALS patients categorised oxidative phosphorylation as the most enriched pathway in this subset compared to control samples (Tam et al., 2019). Specifically, *OXR1* and *thioredoxin (TXN)*, hallmark genes of the OS response, were found to be upregulated in the frontal and motor cortex (Tam et al., 2019). A metabolomics study in searching for blood biomarkers of Huntington's Disease (HD) demonstrated that *OXR1* was significantly overexpressed at both pre-symptomatic and symptomatic stages of the disease (Christodoulou et al., 2020). Spatial transcriptomic analysis of an Alzheimer's Disease (AD) mouse model identified upregulation of *Oxr1* in external plexiform layer and mitral cell layer of the olfactory bulb (Navarro et al., 2020).

Conversely, PD without Dementia patients exhibited a 3-fold downregulation of *OXR1* in neurons of the posterior cingulate cortex (Stamper et al., 2008). Similarly, a two-fold decrease in *OXR1* was observed in PD patients with Dementia (Stamper et al., 2008), suggesting a reduced capacity to respond to oxidative stress and promoting neurodegeneration and disease progression. Together, these data identify *OXR1* dysregulation as a potential diagnostic biomarker in a range of NDs, thus understanding the role of *OXR1* in disease pathogenesis is essential.

5.1.2. Overexpression of *Oxr1* is protective against OS-induced apoptosis *in vitro*

In the years following the initial discovery of *Oxr1* and the TLDc family, neuroprotection against OS was identified as a shared functional characteristic of these proteins (Durand et al., 2007; Finelli et al., 2016; Oliver et al., 2011; Volkert et al., 2000). Oliver *et al.* (2011) were the first group to characterise the putative neuroprotective properties using *in vitro* techniques in mammalian systems. Lentiviral expression of either of the main isoforms of *Oxr1*, *Oxr1-FL* or *Oxr1-C*, in wild type and *Oxr1* knockout primary CGCs treated with hydrogen peroxide (H_2O_2) lead to a robust reduction in apoptosis in both genotypes (Oliver et al., 2011). Likewise, exogenous expression of these two *Oxr1* isoforms significantly improved cell viability in arsenite-treated Neuro-2a (N2a) cells, a mouse neuroblastoma cell line, further demonstrating a strong neuroprotective response to OS *in vitro* (Finelli et al., 2016). In a more recent example, stable overexpression of *OXR1* in a photoreceptor-like cell line improved neuronal cell viability under OS conditions (Sahu et al., 2021). Taken together, these examples support the hypothesis that overexpression of *Oxr1* confers neuroprotection against OS-related insults *in vitro*.

5.1.3. Exogenous expression of *Oxr1* rescues aberrant cellular pathology induced by ALS-associated mutant proteins *in vitro*

Further evidence for the utility of *OXR1* as a protective factor in disease has come from several studies that have highlighted the beneficial influence of the protein in models of ALS. Finelli *et al.* (2015) conducted an unbiased proteomic screen to identify novel binding partners of Oxr1 isoforms under OS conditions. The aim of this experiment was to reveal functional clues to determine how Oxr1 may confer neuroprotection *in vitro* and *in vivo*; co-immunoprecipitation was performed using N2a cells overexpressing either tagged Oxr1-FL or Oxr1-C, with and without induction of OS, followed by mass spectrometry of putative binding partners (Finelli et al., 2015). Surprisingly, this proteomic screen revealed that Oxr1-FL has the ability to bind to Fused in sarcoma (Fus), whereas Oxr1-C binds to both Fus and Transactive response (TAR) DNA binding protein 43 (Tdp-43) under OS conditions *in vitro;* this was further validated by co-immunoprecipitation with tagged Fus and Tdp-43 constructs (Finelli et al., 2015), confirming the direct interactions between Oxr1 isoforms and two ALS-associated proteins.

FUS and *TDP-43* are two of the leading causative genes of ALS (Andersen & Al-Chalabi, 2011; Kawaguchi et al., 2020; Van Deerlin et al., 2008). Both FUS and TDP-43 are part of the heterogeneous nuclear ribonucleoprotein family, functioning as RNA/DNA binding proteins involved in RNA splicing, RNA metabolism and general transcription regulation (Lagier-Tourenne et al., 2010; Van Deerlin et al., 2008). Aberrant nuclear-cytoplasmic translocation and cytoplasmic mislocalisation of these proteins is heavily associated with ALS pathology (Lagier-Tourenne et al., 2010; Vance et al., 2009); the presence of TDP-43-positive cytoplasmic inclusions and altered stress granule formation are well characterised features in ALS histopathology, as well as in frontotemporal dementia (FTD) (Arai et al., 2006; Van Deerlin et al., 2008). As mentioned previously, OXR1

was found to be upregulated in spinal cord tissue procured from end-stage ALS patients; these patients were defined as sporadic ALS cases and non-superoxide dismutase (SOD)-related in genetic origin (Oliver et al., 2011). Taken together with data from the proteomic screening, it was inferred that OXR1 could possibly modulate ALS cellular pathology through direct protein-protein interactions *in vitro*.

In order to test this hypothesis, Finelli *et al.* (2015) modelled Tdp and Fus ALS-associated mutations and initially assessed for altered binding affinity to Oxr1 isoforms *in vitro*. These data identified a subset of mutations in Fus (P157L) and Tdp-43 (A321G and D169G) that showed a significant reduction in binding affinity to Oxr1-C (Finelli et al., 2015). In OS conditions, substantial knockdown of all *OXR1* isoforms increased cytoplasmic aggregation of exogenous wild type and mutant Fus and Tdp-43 proteins in HeLa cells; counter to this, overexpression of *Oxr1-C* reduced the tendency of these proteins to form cytoplasmic inclusions in HeLa cells, as well as rescuing observed splicing defects and mitochondrial dysfunction, known ALS-associated cellular pathologies, in motor neuron-like cells (Arai et al., 2006; Finelli et al., 2015; Vance et al., 2009). However, it must be noted that overexpression of *Oxr1-C* did not rescue ALS-associated cellular pathology in cells transfected with mutant Fus and Tdp-43 proteins that previously showed significantly reduced binding affinity to Oxr1-C (Finelli et al., 2015).

In summary, these data demonstrated that Oxr1 isoforms bind to ALS-associated proteins, Fus and Tdp-43, under OS *in vitro* (Finelli et al., 2015). Robust direct protein interactions were shown to ameliorate ALS-associated cellular pathology *in vitro*, whereas overexpression of *Oxr1-C* failed to restore aberrant cellular phenotypes caused by Fus and Tdp-43 mutations that reduced binding affinity to Oxr1 (Finelli et al., 2015). This suggests that Oxr1 has the potential to modulate disease pathogenesis *in vivo*. Given that OS is a

pivotal feature in ALS pathogenesis (Barber & Shaw, 2010; Tam et al., 2019), it is possible that overexpression of *Oxr1* may confer neuroprotection in a subset of ALS mouse models.

5.1.4. Tg(*Prnp-Oxr1*) transgenic mice: a model to investigate the neuroprotective function of *Oxr1 in vivo*

In order to investigate the neuroprotective function of overexpressing *Oxr1 in vivo,* K. X. Liu et al. (2015) generated a transgenic mouse model, where *Oxr1-FL* cDNA was driven by a mouse prion protein (*Prnp*) promoter to confer neuron-specific expression (Borchelt et al., 1996). The *Oxr1-FL* transgene also contained a C-terminal HA-tag for further experimental validation (**Figure 5.1**). Hemizygous transgenic mice (Tg(Prnp-Oxr1)/+) demonstrated stable, neuron-specific expression of *Oxr1* in the CNS and embryonic, postnatal and adult mouse tissue at up to 5-fold more than physiological levels (K. X. Liu et al., 2015). Additionally, the transgenic mice displayed no overt histopathological or phenotypic differences to their littermate controls (Liu et al., 2015), indicating that overexpression of *Oxr1-FL* is safe and tolerated *in vivo*, an important point when considering future therapeutic applications. Subsequently, Tg(Prnp-Oxr1)/+ mice have been crossed to mouse models of neurodegenerative disorders to determine whether neuronal overexpression of *Oxr1* is sufficient to protect against selective vulnerability of different neuron populations and modify disease progression *in vivo*.

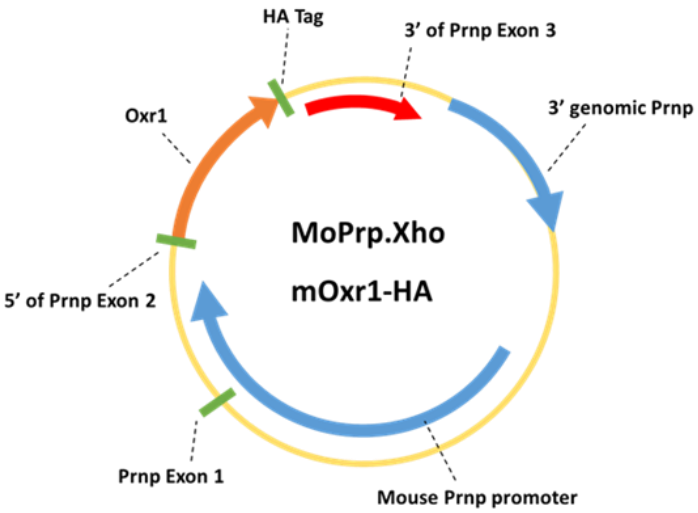

***Figure 5.1*| Schematic diagram of *Prnp-Oxr1* transgenic construct**

The cDNA sequence of C-terminally HA-tagged *Oxr1-FL* (NM_130885) was cloned in to the MoPrp.Xho expression vector containing necessary *Prnp* genomic sequences to drive neuron-specific expression of the transgene (Borchelt et al., 1996; K. X. Liu et al., 2015; Oliver et al., 2011). Diagram adapted from (Liu, 2014).

5.1.5. Transgenic neuronal expression of *Oxr1* delays disease progression in ALS mouse models

Transgenic neuronal expression of *Oxr1* (*Prnp-Oxr1*) has been shown to modify two independent ALS mouse models *in vivo*, delaying the progressive neuromuscular-associated phenotypes and aberrant cellular pathology (K. X. Liu et al., 2015; Williamson et al., 2019). *Prnp-Oxr1* overexpression increased survival rate, improved motor neuron viability and delayed disease onset in a hSOD1^{G93A} mouse model of ALS (K. X. Liu et al., 2015). Williamson *et al.* (2019) also investigated the neuroprotective effects of *Prnp-Oxr1* by crossing this mouse line to mice carrying a human bacterial artificial chromosome (BAC) expressing wild type or mutant hTDP-43^{M337V}, an ALS-linked mutation (Finelli et al., 2015). This study found that neuron-specific overexpression of *Oxr1* improved muscle innervation and neuromuscular junction pathology, as well as rescuing motor function deficits in the hTDP-43^{M337V} ALS mouse model (Williamson et al., 2019). Strikingly, neuroinflammation is significantly decreased in both ALS mouse models expressing the *Prnp-Oxr1* transgene (K. X. Liu et al., 2015; Williamson et al., 2019), suggesting that neuronal overexpression of *Oxr1* modulates neuroinflammatory phenotypes *in vivo*.

Previous *in vitro* studies demonstrated that only Oxr1-C binds to Tdp-43, yet hTDP-43 was co-immunoprecipitated with Oxr1-C, Oxr1-FL and Prnp-Oxr1-HA expressing *Oxr1-FL in vivo* (Finelli et al., 2015; Williamson et al., 2019). *In vitro* studies using primary motor neurons derived from wild type hTDP-43 and hTDP-43^{M337V} pups showed aberrant cytoplasmic localisation and aggregation of TDP-43 in *TDP-43^{M337V}* expressing cells only; primary motor neurons derived from hTDP-43^{M337V} pups with transgenic neuronal overexpression of *Oxr1* exhibited improved nuclear localisation levels of mutant TDP-43 up to 20-fold (Williamson et al., 2019), corroborating previous data observed in earlier *in vitro* studies (Finelli et al., 2015).

Taken together, these studies highlight that overexpression of *Oxr1* isoforms is sufficient to rescue ALS-associated phenotypes, histopathology and aberrant cellular features *in vitro* and, crucially, *in vivo* (Finelli et al., 2015; K. X. Liu et al., 2015; Williamson et al., 2019). This demonstrates the therapeutic potential of upregulating expression of *OXR1* in ALS patients, but also in other NDs where OS and neuroinflammation are key pathological features. In order to assess applicability to a range of NDs, it remains paramount to understand the molecular mechanisms of the *Prnp-Oxr1* transgene *in vivo*.

5.1.6. Transcriptomic analysis of spinal cord tissue from ALS-mouse model with transgenic neuronal expression of *Oxr1* identified putative functional rescue pathways

Conclusively, the neuroprotective ability of overexpressing *Oxr1* has been demonstrated in multiple independent cellular and mouse models, yet the functional protective mechanism of the *Prnp-Oxr1* transgene remains to be elucidated (Finelli et al., 2015; K. X. Liu et al., 2015; Williamson et al., 2019). In order to identify candidate molecular pathways that *Prnp-Oxr1* may act on, K. X. Liu et al. (2015) isolated RNA from the lumbar spinal cord of wild type mice and mice expressing the *Prnp-Oxr1* transgene, as well as from a hSOD1^{G93A} ALS mouse model (SOD1^{G93A}) and SOD1^{G93A} mice expressing the *Prnp-Oxr1* transgene (SOD1^{G93A}/Tg) at an early symptomatic time point (P90); subsequently, microarray analysis was performed to reveal differentially expressed genes (DEGs) between the different genotypes (K. X. Liu et al., 2015). This transcriptomic approach demonstrated that *Prnp-Oxr1* transgene expression alone does not influence the transcriptional profile of the spinal cord, however when comparing SOD1^{G93A} and SOD1^{G93A}/Tg expression data relative to wild type mice, transgenic neuronal *Oxr1* overexpression in SOD1^{G93A}/Tg tissue 'rescued' 63 DEGs identified in SOD1^{G93A} (K. X. Liu et al., 2015). Gene ontology (GO) enrichment analysis of these data demonstrated rescue of genes in molecular pathways, such as cell to cell signalling and interaction, immune cell trafficking and lipid metabolism (K. X. Liu et al., 2015), thus suggesting that *Prnp-Oxr1* confers neuroprotection in the SOD1^{G93A} ALS mouse model through acting on these pathways *in vivo*.

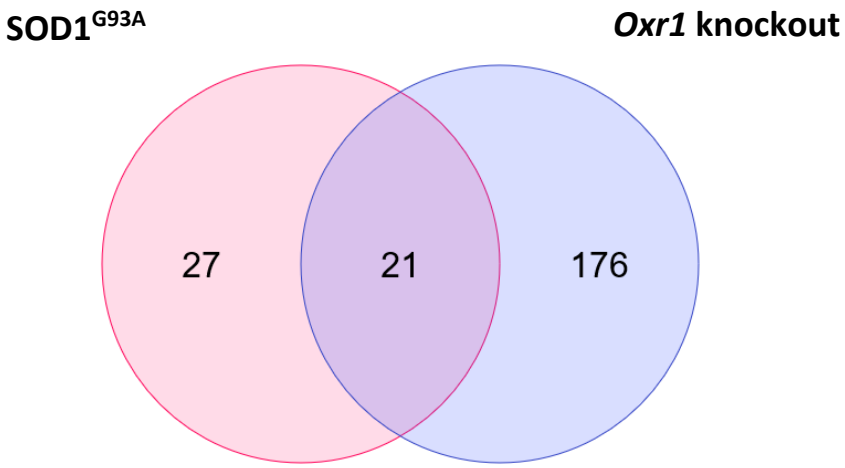

***Figure 5.2*| Venn diagram depicting overlapping genes 'rescued' in SOD1^{G93A}/Tg compared to differential expressed genes in constitutive *Oxr1* knockout mice**

Overlapping genes when comparing 48 annotated differential expressed genes in SOD1^{G93A} that are 'rescued' in SOD1^{G93A}/Tg mice and 197 significantly differentially expressed genes in early symptomatic P19 cerebellar tissue from constitutive *Oxr1* knockout mice.

When comparing SOD1^{G93A} DEGs 'rescued' by transgenic neuronal overexpression of *Oxr1* (48 out of 63 were annotated) with DEGs (q≤0.01) in P19 constitutive *Oxr1* constitutive knockout cerebellar tissue (**Chapter 3**), 21 overlapping genes were identified (**Figure 5.2**). **Table 5-1** lists the 21 overlapping genes in these sets of data, all of which were significantly upregulated. Interestingly, 14 of these genes were also ranked in the 20 most statistically significant DEGs in *Oxr1* knockout cerebellum at P19, such as *C1qa*, *Trem2* and *Hexb*, which indicated lysosomal and neuroinflammatory dysfunction in *Oxr1*-deleted mice (**Chapter 3**). Notably, all subunits of the complement component 1q complex (*C1qa, C1qb* and *C1qc*) are found to be upregulated in both mouse models (**Table 5-1**), suggesting that expression of *Oxr1* may suppress activation of the classical complement pathway (Schartz & Tenner, 2020).

GO functional enrichment analysis of these overlapping genes identified recognised roles in known biological pathways, including microglial pathogen phagocytosis pathway and the innate immune system, further implicating endogenous *Oxr1* and *Prnp-Oxr1* in modulating inflammatory phenotypes *in vivo.* Although neuroinflammation is evidently delayed by neuron-specific overexpression of *Oxr1* in both $SOD1^{G93A}$ and $TDP\text{-}43^{M337V}$ mouse models of ALS, the pathways that underlie these neuroprotective properties are still unclear (K. X. Liu et al., 2015; Williamson et al., 2019).

***Table 5-1*| 21 overlapping genes identified when comparing 48/63 annotated 'rescued' genes (SOD1^{G93A} vs WT, SOD1^{G93A}/Tg vs WT) with differentially expressed genes in constitutive *Oxr1* knockout mice.**

Reported fold changes (↑ upregulated) in microarray data comparing P90 SOD1^{G93A} vs WT spinal cord tissues and RNA-seq data comparing P19 *Oxr1*$^{tm1d/tm1d}$ vs WT cerebellar tissue. Genes listed in bold are ranked in the 20 most significant differentially expressed genes in *Oxr1* knockout cerebellum at P19.

		Fold Change ↑	
Gene Symbol	**Gene**	**SOD1^{G93A}**	***Oxr1*$^{tm1d/tm1d}$**
Lyz2	Lysozyme 2	2.0	2.2
Fcrls	Fc receptor-like S, scavenger receptor	1.9	3.1
Cd68	CD68 antigen	1.9	3.1
C4b	Complement component 4B	1.8	1.8
Serpina3n	Serine (or cysteine) peptidase inhibitor	1.8	1.5
Mpeg1	Macrophage expressed gene 1	1.7	3.4
Ly86	Lymphocyte antigen 86	1.7	2.7
C1qb	Complement C1q B chain	1.6	2.6
C1qc	Complement C1q C chain	1.6	2.7
Lgals3bp	Galectin 3 binding protein	1.5	1.4
Olfml3	Olfactomedin-like3	1.4	1.9
Abca1	ATP binding cassette subfamily A member 1	1.4	1.2
Grn	Granulin	1.4	1.4
Tyrobp	TYRO protein tyrosine kinase-binding protein	1.4	3.0
C1qa	Complement C1q A chain	1.4	2.7
Ctsz	Cathepsin Z	1.4	1.8
Ctss	Cathepsin S	1.4	1.9
Anxa3	Annexin A3	1.4	2.6
Hpgds	Hematopoietic prostaglandin D synthase	1.4	2.2
Trem2	Triggering receptor expressed on myeloid 2	1.4	2.4
Hexb	Hexosaminidase B	1.3	2.2

5.1.7. A role for *Oxr1* in neuronal and non-neuronal cell types?

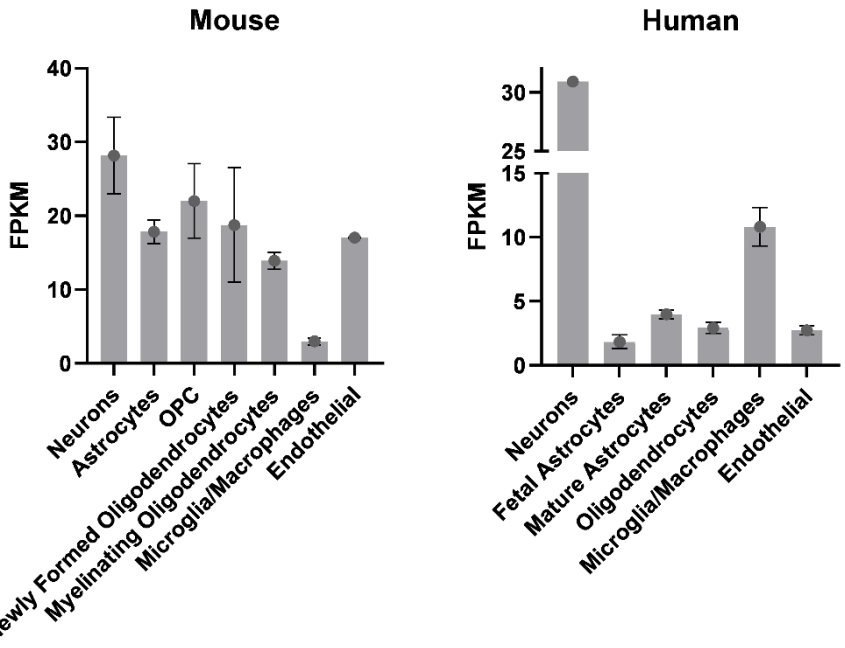

***Figure 5.3*| Transcriptome analysis of Oxr1 expression in different cell types of the cortex in both human and mouse brain**

Oxr1 expression data in neurons and non-neuronal cell types in cortical tissue from (A) mouse and (B) human brain RNA sequencing data. Gene expression presented as fragments per kilobase of exon per million mapped fragments (FPKM). Mouse data source: (Zhang et al., 2014). Human data source: (Zhang et al., 2016).

In humans, LoF-OXR1 mutations lead to cerebellar atrophy (Lin et al., 2022; Wang et al., 2019). Constitutive loss of *Oxr1* in mice results in substantial neuroinflammation and selective apoptosis of CGCs (Oliver et al., 2011)(**Chapter 3**); alongside marked neuroinflammation and death of CGCs, induced loss of *Oxr1* in adult mice also resulted in selective vulnerability of olfactory glomeruli (Chapter 4). In concordance with previous *in vitro* studies, this demonstrated that loss of *Oxr1* is detrimental to neuronal cell survival, *in vivo* (Finelli et al., 2016; Oliver et al., 2011), but whether expression of *Oxr1* is required in glial cells is unknown.

Previously, *in situ* hybridisation confirmed that *Oxr1* isoforms are highly expressed throughout the developing embryo and adult mouse brain; qRT-PCR distinguished between the two main isoforms of *Oxr1,* demonstrating that both *Oxr1-FL* and *Oxr1-C* are robustly expressed in the brain, cerebellum and spinal cord of adult wild type mice (Finelli et al., 2016). Interestingly, transcriptomic analysis of cortical tissue from both mouse and human brains demonstrated that *Oxr1* is expressed abundantly in neurons (**Figure 5.3**); however, it is important to note that expression is also observed in glial cell types, such as astrocytes and microglia, although this analysis did not discriminate between different *Oxr1* isoforms (Zhang et al., 2014; Zhang et al., 2016). The functional importance of *Oxr1* in non-neuronal cell types of the CNS has not been characterised.

Oliver *et al.* (2011) demonstrated that ubiquitous expression of *Oxr1* was sufficient to rescue the phenotype and neuropathology observed in *bella* mice. Previous studies investigating the protective role of neuronal over-expression of *Oxr1 in vivo* identified a significant delay in brain and spinal neuroinflammatory phenotypes in ALS mouse models; of note, *Oxr1* was still endogenously expressed (K. X. Liu et al., 2015; Williamson et al., 2019). The hypothesis drawn from these data is that *Prnp-Oxr1* modulates neuroinflammation *in vivo*, yet whether *Oxr1* expression constrained to neurons is sufficient to counteract *Oxr1*-deficient neuroinflammatory pathology at a symptomatic time point (P22) or if *Oxr1* expression is required in non-neuronal cell types was still unknown.

5.1.8. Chapter 5 Aims

A key experimental control in the SOD1^{G93A}/Oxr1 rescue study was the transcriptomics of wild type spinal cord samples with and without the presence of the Oxr1-FL-HA transgene. Although the over-expression of *Oxr1* was evident in transgenic mice, as expected, no other differentially expressed genes reached statistical significance (K. X. Liu et al., 2015). As such, these data did not provide clues as to the potential 'gain-of-function' properties related to neuroprotection and the apparent anti-inflammatory action of Oxr1, despite clear evidence that neuronal *Oxr1* over-expression is well-tolerated *in vivo*. Additionally, ubiquitous loss of *Oxr1* results in cerebellar degeneration and severe ataxia, preceded by a striking neuroinflammatory response (Chapters 3 and 4). Together, these data suggest Oxr1 plays an important role in regulating or gating inflammation in the brain, however the function and timing of this protein in these complex signalling pathways is not known.

In the original *bella* study, a β-actin (ubiquitous) transgenic over-expressing Oxr1-FL-HA model was generated, using the same cDNA construct as the neuronal Tg(Prnp-Oxr1)/+ line. This was crossed to the *bella* mutant where two genes, *Abra* and *Oxr1,* were deleted. Importantly, the ubiquitous Oxr1 transgene was able to completely rescue the homozygous *bella* phenotype, demonstrating that loss of *Oxr1* alone was causing the neurodegeneration and ataxia (Oliver et al., 2011). Thus, these data effectively served as a 'gene replacement' experiment that was not cell-type specific.

Here, given the notable CNS expression of *Oxr1* in both neuronal and non-neuronal cell types (Finelli et al., 2015)(**Figure 5.3**), importance lies in understanding whether specifically neuronal overexpression of *Oxr1*, as used in the successful *in vivo* protective studies of ALS, influences other cell types and has impact on the pathology observed in the constitutive *Oxr1* knockout. Therefore, this chapter aimed to establish if neuron-specific

upregulation of *Oxr1* is sufficient to protect against ubiquitous loss of the protein. In addition, in an attempt to ascertain potential 'gain-of-function' roles for the same Oxr1 transgene, protein binding partner studies in the brain were carried out in the context of both wild-type and *Oxr1* knockout backgrounds.

5.2 Results

5.2.1. *Prnp-Oxr1* expression is sufficient to protect against neurological phenotypes and early lethality observed in constitutive *Oxr1* knockout mice

In order to determine whether neuronal overexpression of the *Oxr1-FL* transgene is protective against ubiquitous loss of the protein, the *Prnp-Oxr1* transgenic mouse line was employed and crossed to mice carrying a constitutive *Oxr1* knockout allele ($Oxr1^{tm1d}$) (Finelli, Paramo, et al., 2019; K. X. Liu et al., 2015; Williamson et al., 2019). As previously stated, expression of *Oxr1-FL* cDNA with a C-terminal HA tag is driven by the mouse *Prnp* promoter (**Figure 5.1**) (Borchelt et al., 1996; Liu, 2014). Heterozygous mice for the $Oxr1^{tm1d}$ allele ($Oxr1^{tm1d/wt}$, Het) were initially crossed to mice with hemizygous expression of the *Prnp-Oxr1* transgene (*Prnp-Oxr1*$^{+}$,Tg) to generate heterozygous $Oxr1^{tm1d/wt}$ mice carrying the transgene $Oxr1^{tm1d/wt}$/*Prnp-Oxr1*$^{+}$, Het/Tg). Subsequently, experimental cohorts were generated by intercrossing Het and Het/Tg mice (**Figure 5.4A**). The progeny of this cross predominately used in this chapter were <u>WT</u> ($Oxr1^{wt/wt}$/ *Prnp-Oxr1*$^{-}$, WT/WT), <u>Hom</u> ($Oxr1^{tm1d/tm1d}$/*Prnp-Oxr1*$^{-}$, Hom/WT), constitutive *Oxr1* knockout mice, <u>WT/Tg</u> ($Oxr1^{wt/wt}$/*Prnp-Oxr1*$^{+}$), a control for transgene expression over a wild type background and finally <u>Hom/Tg</u> ($Oxr1^{tm1d/tm1d}$/*Prnp-Oxr1*$^{+}$), the hypothetical 'rescue' model (**Figure 5.4B**). Het and Het/Tg mice were also progeny from this cross.

The litters from this intercross were genotyped at P14 and monitored for adverse effects. Onset of ataxia occurred from approximately P19 in Hom mice and rapidly deteriorated to disease end-stage, as previously characterised by Oliver *et al.* (2011). Surprisingly, Hom/Tg mice were visibly indistinguishable from WT and WT/Tg littermate controls, with no apparent gait abnormalities or growth defects. A small cohort of Hom/Tg 'rescue' mice and littermate controls were aged to 8 months old, but ataxia or other neurological phenotypes did not emerge within this timeframe. These initial observations

imply that *Prnp-Oxr1* expression is sufficient to protect against ataxia and early mortality observed in constitutive *Oxr1* knockout mice (Oliver et al., 2011).

A.

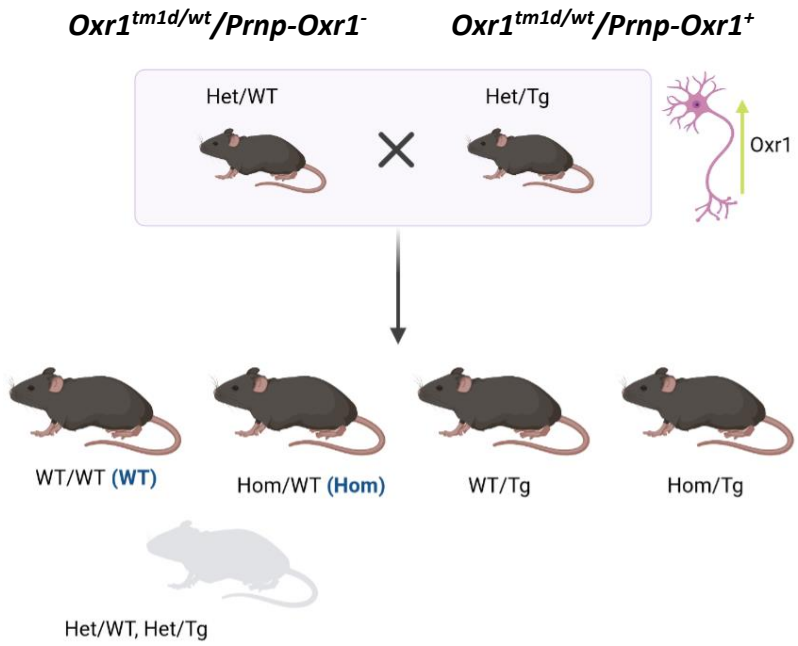

B.

Genotype	Expected percentage of offspring	Experimental use
WT	12.5%	Wild type
Hom	12.5%	Constitutive *Oxr1* knockout
WT/Tg	12.5%	Transgene control
Hom/Tg	12.5%	Hypothetical rescue
Het	25%	Aging littermates
Het/Tg	25%	

***Figure 5.4*| Schematic breeding plan and progeny of *Oxr1*$^{tm1d/wt}$ crossed with *Oxr1*$^{tm1d/wt}$*/Prnp-Oxr1*$^{+}$ mice to generate experimental cohorts**

(A) Offspring from Het x Het/Tg intercross. (B) Table of expected percentage of offspring from Het/WT and Het/Tg intercross with reasons for experimental use.

5.2.2. *Prnp-Oxr1-HA* transgene is localised to neurons and is robustly expressed in the mouse brain

As controls for the *Prnp-Oxr1* transgene expression, immunostaining, qRT-PCR and Western blotting was carried out. Multiple antibodies against Oxr1 are not effective (previously demonstrated using 'true null' models, unpublished observations), therefore it was essential to verify that *Prnp-Oxr1* expression was neuron specific. WT and WT/Tg sagittal brain sections were co-stained with anti-HA and neuronal marker, NeuN (Mullen et al., 1992). In agreement with K. X. Liu et al. (2015), HA-positive cells co-localised with NeuN-positive cells in WT/Tg samples, whereas no anti-HA signal was detected in WT samples, confirming that *Prnp-Oxr1-HA* expression is neuron specific and strongly detected in the cytoplasm (**Figure 5.5**).

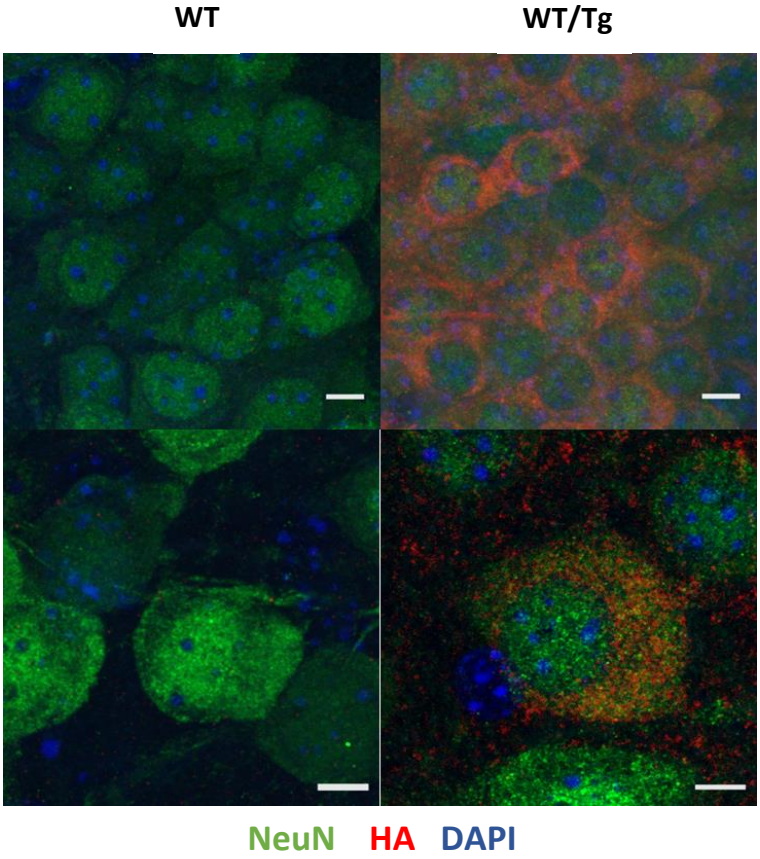

***Figure 5.5*| Representative immunofluorescence to detect neuron-specific expression of Prnp-Oxr1-FL-HA transgene**

Co-staining in the cortex of NeuN and anti-HA in sagittal brain sections from WT and WT/Tg mice. NeuN was used to label neurons, anti-HA was used as a proxy to label Prnp-Oxr1. NeuN: Green, anti-HA: Red, DAPI: Blue. Scale bars: 5 µm

Next, brain tissue from mice of all four main genotypes was analysed at P22, the disease end-stage time point of Hom mice. The expression of *Oxr1-FL*, which includes *Prnp-Oxr1*, and *Oxr1-C* isoforms was quantified through qRT-PCR; as the qRT-PCR primers for *Oxr1* transcripts are located upstream of the *Oxr1*^{tm1d} mutation in the TLDc domain, i.e. removal of two exons and subsequent truncation of the protein, *Oxr1-FL* and *Oxr1-C* transcripts is detected in the cerebellum of all genotypes (**Figure 5.6A** and **B**)**.** Unsurprisingly, significantly higher levels of *Oxr1-FL* expression in WT/Tg and Hom/Tg samples were detected demonstrating transcription of the cDNA transgene (**Figure 5.6A** and **B**). Intriguingly, a slight increase in *Oxr1-C* expression is observed in WT/Tg, suggesting that the *Prnp-Oxr1* transgene may induce a self-regulatory feedback loop however, this was not explored further (**Figure 5.6B**).

Western blotting demonstrated that endogenous Oxr1-FL protein isoforms are not present in both brain and cerebellar tissue, indicating that the detected transcripts are not translated in to stable protein isoforms (**Figure 5.6C** and **D**). The Oxr1-FL antibody (Proteintech, 13514-1-AP) used targets an epitope towards the N-terminus of the FL protein and several Oxr1-FL isoforms are detected in WT and WT/Tg samples; this reflects the known isoforms in the mouse (**Figure 1.6**) (**Figure 5.6C** and **D**). As expected, the HA-tagged transgene, representing the shortest of the FL isoforms, is expressed robustly in WT/Tg and Hom/Tg brain and cerebellum (**Figure 5.6C** and **D**). Taken together, these data confirm successful expression of *Prnp-Oxr1 in vivo*.

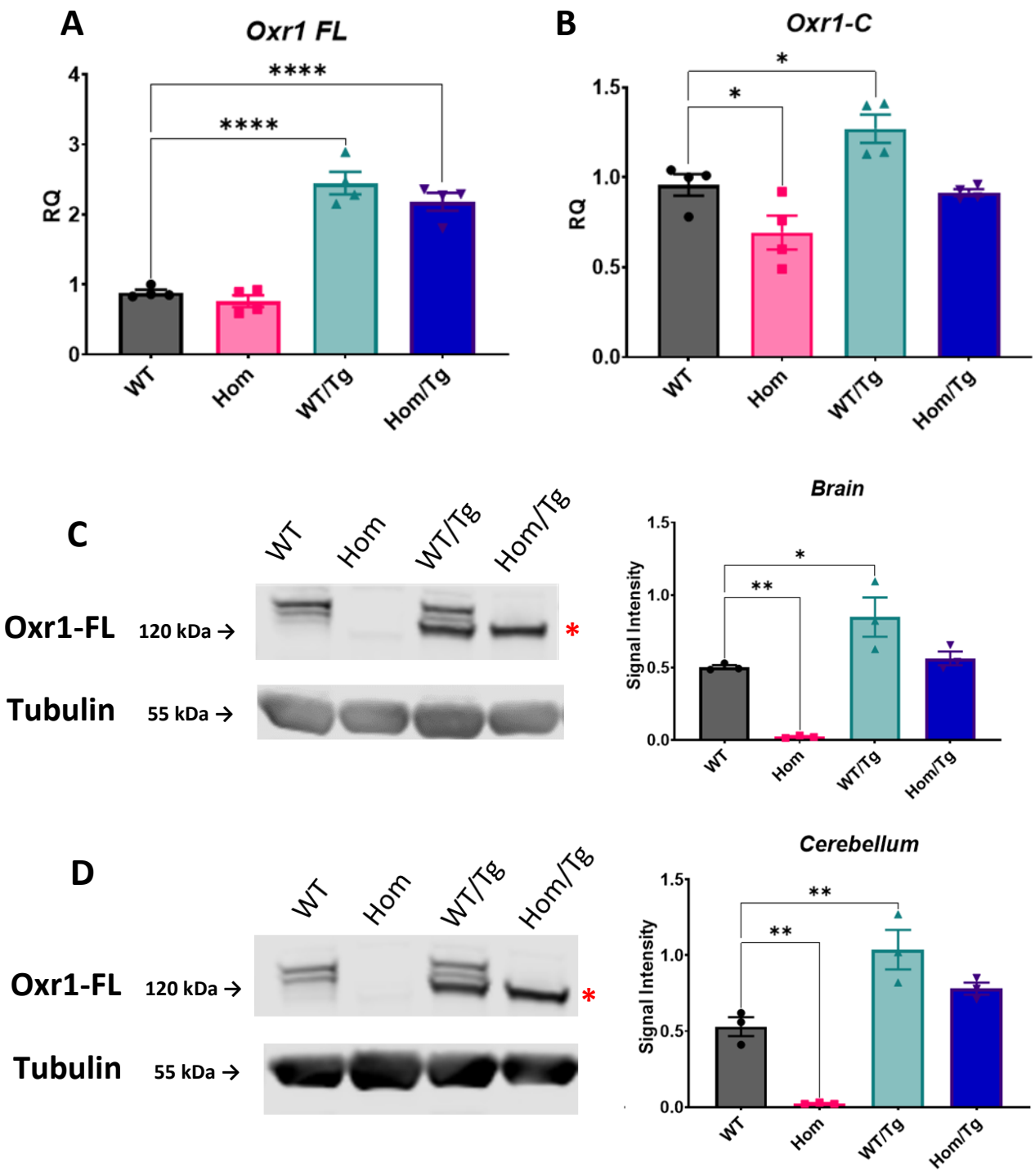

***Figure 5.6*| Expression analysis of Oxr1 isoforms in brain and cerebellum using qRT-PCR and Western blotting**

qRT-PCR analysis of (A) *Oxr1-FL*, *Prnp-Oxr1* and (B) *Oxr1-C* transcripts in cerebellar tissue from all genotypes. Western blot and quantification of Oxr1-FL isoforms, including Prnp-Oxr1, in brain and cerebellar tissue from WT, Hom, WT/Tg and Hom/Tg mice at P22. Oxr1-FL quantification normalised to α-Tubulin; all full-length isoforms included in quantification. Red asterisks (*) indicate HA-tagged Oxr1 transgene. Statistical significance analysed by ordinary one-way ANOVA, followed by Dunn's multiple comparison's test, relative to WT. *p<0.05, **p<0.01, ***p<0.001, ****p<0.0001. n=3-4 per genotype.

5.2.3. Neuron-specific overexpression of *Oxr1* is protective against cerebellar granule cell death in constitutive *Oxr1* knockout mice at P22

As described in **5.2.1**, Hom/Tg mice did not develop a severe ataxic gait by P22 compared to Hom mice, thus demonstrating that *Prnp-Oxr1* expression rescues this neurological phenotype. The key pathology exhibited in *bella* mice and subsequent *Oxr1* knockout mouse models is early apoptotic cell death of CGCs (Oliver et al., 2011). This highly localised neurodegeneration significantly contributes to the impaired motor function and ataxia observed in these models. Similarly in Chapter 4, ubiquitous loss of *Oxr1* in adult mice also results in a very similar pattern of CGCL degeneration to *bella* mutants; additionally, apoptotic cells in the glomerular layer of the olfactory bulb are also present.

Given that CGCL degeneration influences the ataxic phenotype in *Oxr1* knockout mouse models, yet ataxia was not observed in Hom/Tg, terminal deoxynucleotidyl transferase dUTP nick-end labelling (TUNEL) was carried out on sagittal brain sections to establish if *Prnp-Oxr1* transgenic expression is sufficient to modulate cell death at P22. TUNEL-positive cells were only observed in the CGCL of Hom mice; WT, WT/Tg and surprisingly Hom/Tg mice showed no cell death pathology in the CGCL (**Figure 5.7**) or any other brain regions at P22 (data not shown). These qualitative data demonstrate that Hom/Tg mice show a rescue of neurodegenerative pathology, suggesting that neuronal overexpression of *Oxr1* is sufficient to prevent cerebellar degeneration at P22 in Hom mice.

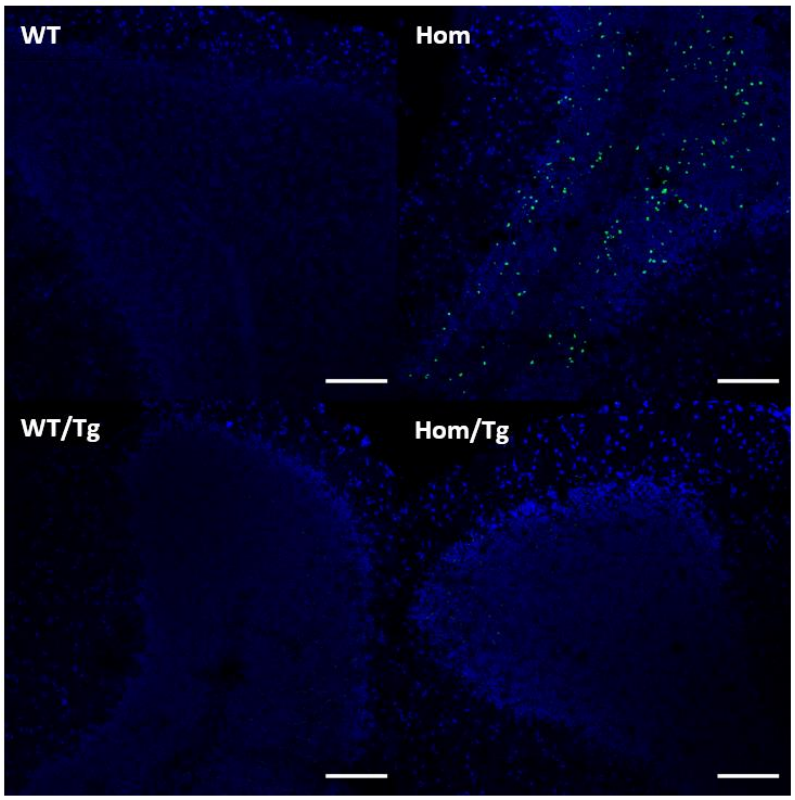

***Figure 5.7*| Terminal deoxynucleotidyl transferase dUTP nick-end labelling (TUNEL) on sagittal cerebellar sections to label apoptotic cell death in WT, Hom, WT/Tg and 'rescue' Hom/Tg mice at P22**

Representative TUNEL immuno-labelling on cerebellar tissue (from n=3-4), focusing on the granule cell layer, from all genotypes at P22. Green: TUNEL, Blue: DAPI. Scale bar: 100 µm.

5.2.4. Neuronal overexpression of *Oxr1* is protective against neuroinflammation in 'rescue' mice

Neuroinflammation is a key pathogenic feature in mouse models of constitutive or induced loss of *Oxr1* (Chapter 3 and 4). More broadly, neuroinflammation is a critical disease modulator in NDs, such as PD, ALS and epilepsy (Geloso et al., 2017; Heidari et al., 2022; Rama Rao & Kielian, 2015; Terrone et al., 2020). RNA-seq identified significant upregulation of glial fibrillary acidic protein (*Gfap*) in early symptomatic P19 cerebellar tissue from Hom mice; subsequently, immunofluorescent staining revealed astrogliosis in the cerebellum of Hom mice at P22 (Chapter 3). Intriguingly, *Gfap* expression has also been shown to be inversely correlated with levels of *Oxr1* under hypoxic conditions in the retina *in vivo* (Natoli et al., 2008), further suggesting that Oxr1 plays a role in modulating levels of inflammation.

To test if neuron-specific overexpression of *Oxr1*, notably in the absence of expression of all *Oxr1* isoforms in non-neuronal cell types, is sufficient to reduce or prevent astrocyte reactivity observed in Hom mice (Chapter 3), immunofluorescent staining of astrocyte marker, Gfap, was carried out on sagittal brain sections from mice of all genotypes at P22. A qualitative increase in Gfap-positive astrocytes was only observed in the cerebellum of Hom, indicating the presence of reactive astrocytes compared to WT, WT/Tg and remarkably, Hom/Tg mice (**Figure 5.8A**). However, one-way ANOVA followed by Tukey's multiple comparison test correction revealed no difference in quantified integrated fluorescent density between genotypes in this small sample size (n=3-4) (**Figure 5.8B**). Although in Chapter 3, Western Blot analysis of P22 cerebellar tissue demonstrated a significant increase in GFAP expression in Hom mice compared to WT, this result was not reproduced by immunofluorescent quantification of GFAP in the cerebellum. Therefore, it would have been beneficial to increase the sample size in this experiment to achieve

appropriate statistical power and simultaneously conduct Western blot analysis of GFAP expression in all genotypes before concluding how *Prnp-Oxr1* transgene expression effects the cerebellar neuroinflammatory phenotype previously reported in Hom mice at P22.

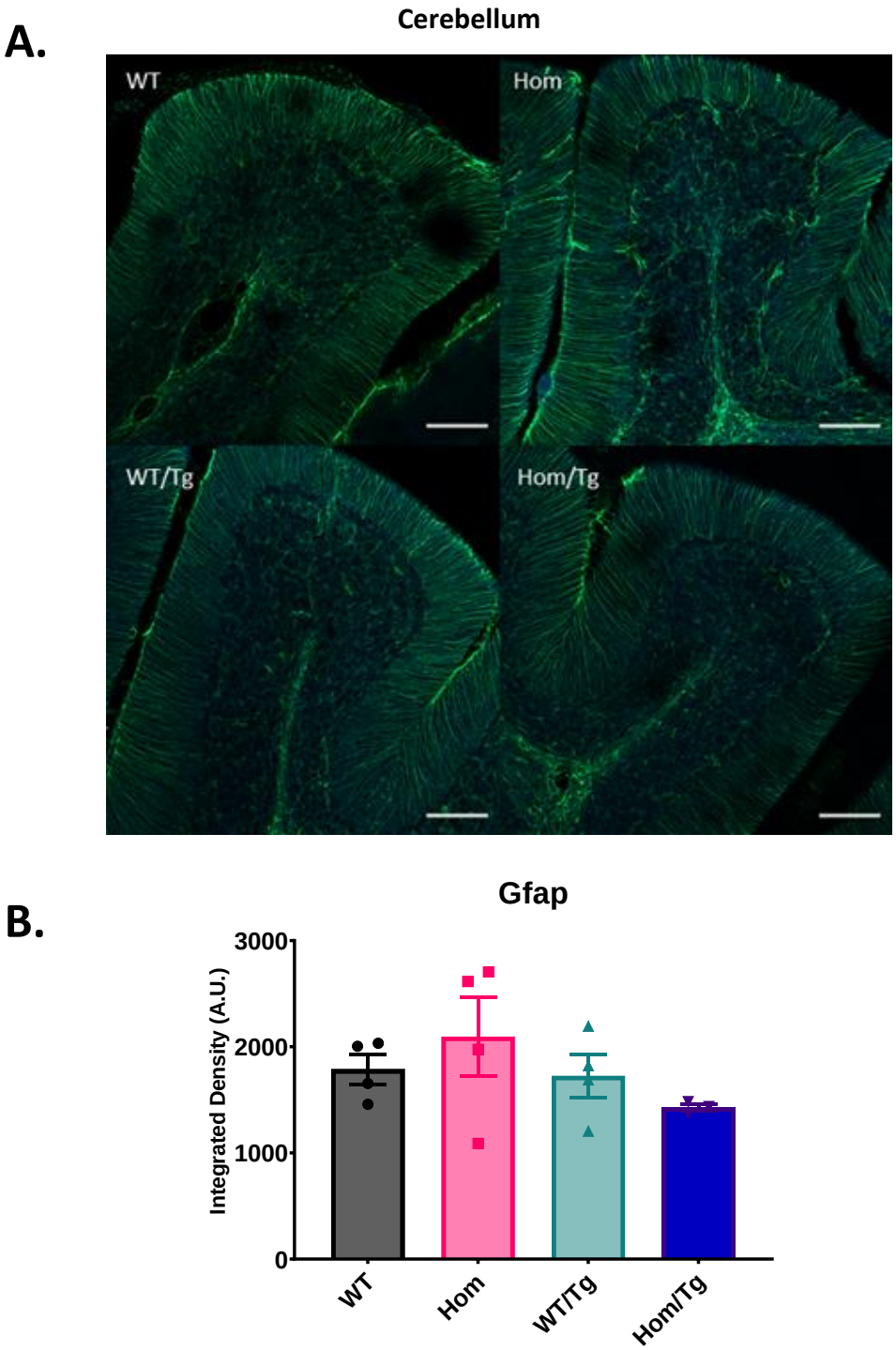

***Figure 5.8*| Representative anti-Gfap immunofluorescence images of sagittal brain sections from P22 mice, focussing on the cerebellum**

Anti-Gfap immunostaining on sagittal brain sections from WT, Hom, WT/Tg and Hom/Tg mice at P22 and quantification of integrated density in arbitrary units (A.U.). Scale bar: 100 µm. Blue: DAPI, Green: anti-Gfap. Representative images from n=3-4 of each genotype. Statistical significance analysed by ordinary one-way ANOVA, followed by Tukey's multiple comparison's test – not significant.

In order to confirm that the *Prnp-Oxr1* transgene does not induce aberrant inflammatory phenotypes *in vivo*, additional brain regions were analysed. Astrogliosis in the cortex of *bella* mice has not previously been reported (Oliver et al., 2011). In agreement with these data, no differences in Gfap-positive cells were observed between all genotypes (**Figure 5.9A**). Initial qualitative histopathological analysis of the hippocampus indicated increased Gfap-positive astrocytes in Hom mice at P22, compared to WT and WT/Tg mice; a reduction in signal intensity is observed in Hom/Tg mice, although further quantitative analysis is needed (**Figure 5.9B**).

Overall, these data indicate that neuron-specific overexpression of *Oxr1* does not induce neuroinflammation *in vivo*, but from immunohistopathology of the cerebellum, it cannot be concluded how *Prnp-Oxr1* affects the population of GFAP-positive astrocytes *in vivo*.

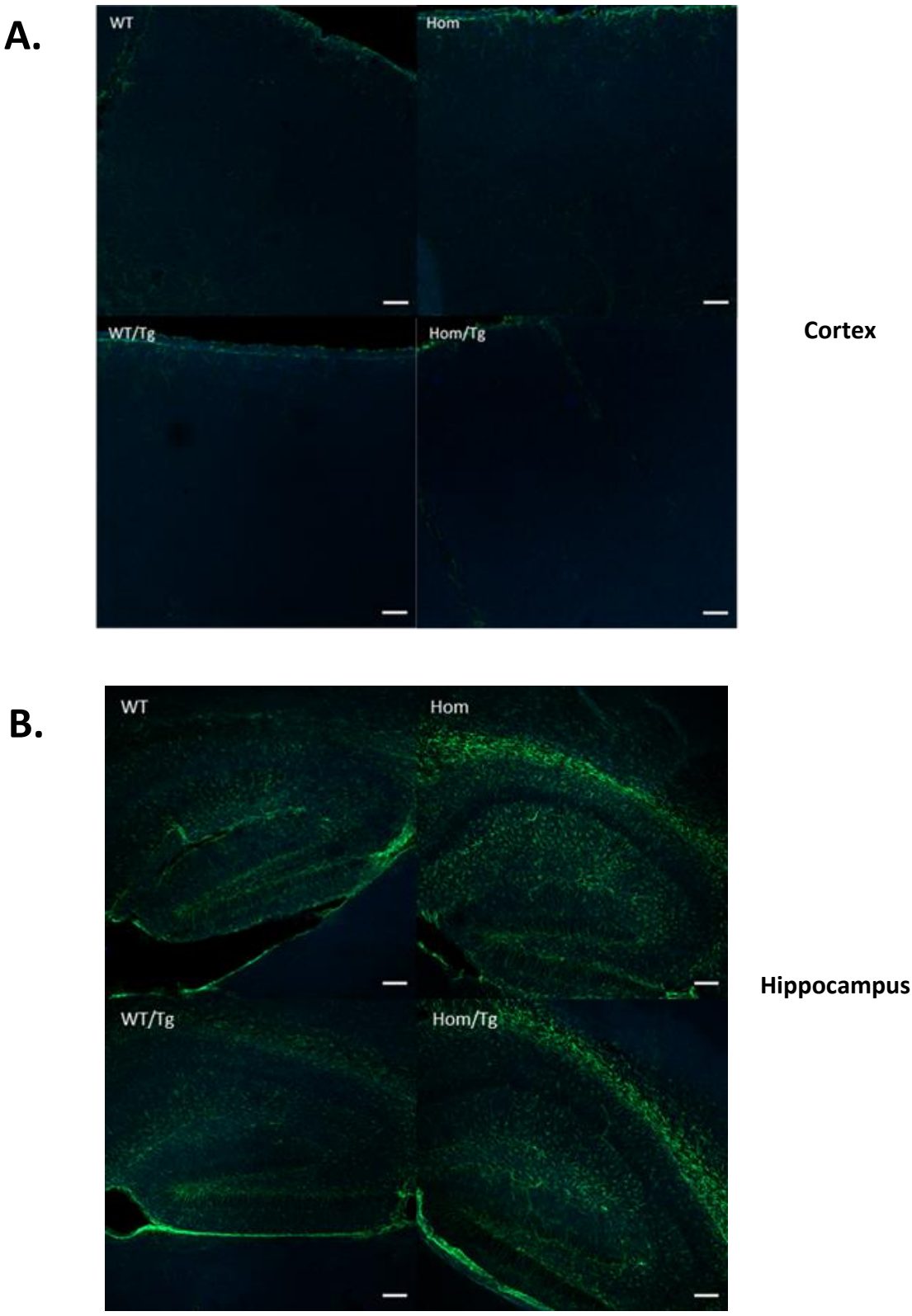

***Figure 5.9*| Representative anti-Gfap immunofluorescence images of the cortex and hippocampus in sagittal brain sections from P22 mice**

Anti-Gfap immunostaining on sagittal brain sections from WT, Hom, WT/Tg and Hom/Tg mice at P22, with a focus on the (A) cortex and (B) hippocampus. Scale bar: 100 µm. Blue: DAPI, Green: anti-Gfap. Representative images from n=3-4 of each genotype.

Chapter 3 established that differential expression of neuroinflammatory genes precedes cerebellar degeneration in constitutive *Oxr1* knockout mice. Insofar, this Chapter has demonstrated that *Prnp-Oxr1* transgene expression is protective against CGC death in Hom/Tg mice at P22, however the effect of the transgene on the neuroinflammatory response observed in P22 Hom mice is unclear at the protein level. Therefore, the expression profiles of key inflammatory markers, including *Gfap* and microglia-associated genes *Iba1* and *Trem2*, were analysed in order to determine if *Prnp-Oxr1* effects gene expression of these markers in the cerebellum. Neuroinflammatory markers were selected from the list of the 20 most significantly DEGs identified in RNA-seq of Hom cerebellar tissue at P19 (**Chapter 3**).

Total cerebellar RNA was isolated from mice of all genotypes at P22; following this, cDNA was synthesised and qRT-PCR was conducted to measure levels of inflammatory markers in Hom, WT/Tg and Hom/Tg mice relative to WT. One-way ANOVAs, followed by Tukey's multiple comparisons test, verified that selected markers, *C1qa*, *Cd68*, *Laptm5*, *Gfap, Iba1, Ly86, Tgf-β* and *Trem2,* were significantly upregulated in Hom cerebellar tissue compared to WT at P22 ($p<0.05$ – $p<0.0001$) (**Figure 5.10**). Comparing expression of each gene in WT/Tg to WT revealed no significant differences, further confirming that the *Prnp-Oxr1* transgene alone does not affect transcriptional regulation of these key neuroinflammatory markers in the cerebellum (**Figure 5.10**). Finally, all 8 inflammatory marker genes were 'rescued' in Hom/Tg cerebellum at P22, showing no significant differences in expression levels compared to WT mice (**Figure 5.10**). Overall, these data provide evidence to support the hypothesis that *Prnp-Oxr1* transgenic expression negates the cerebellar transcriptional neuroinflammatory signature observed in Hom mice at P22 in the absence of all *Oxr1* isoforms in non-neuronal cell types *in vivo*.

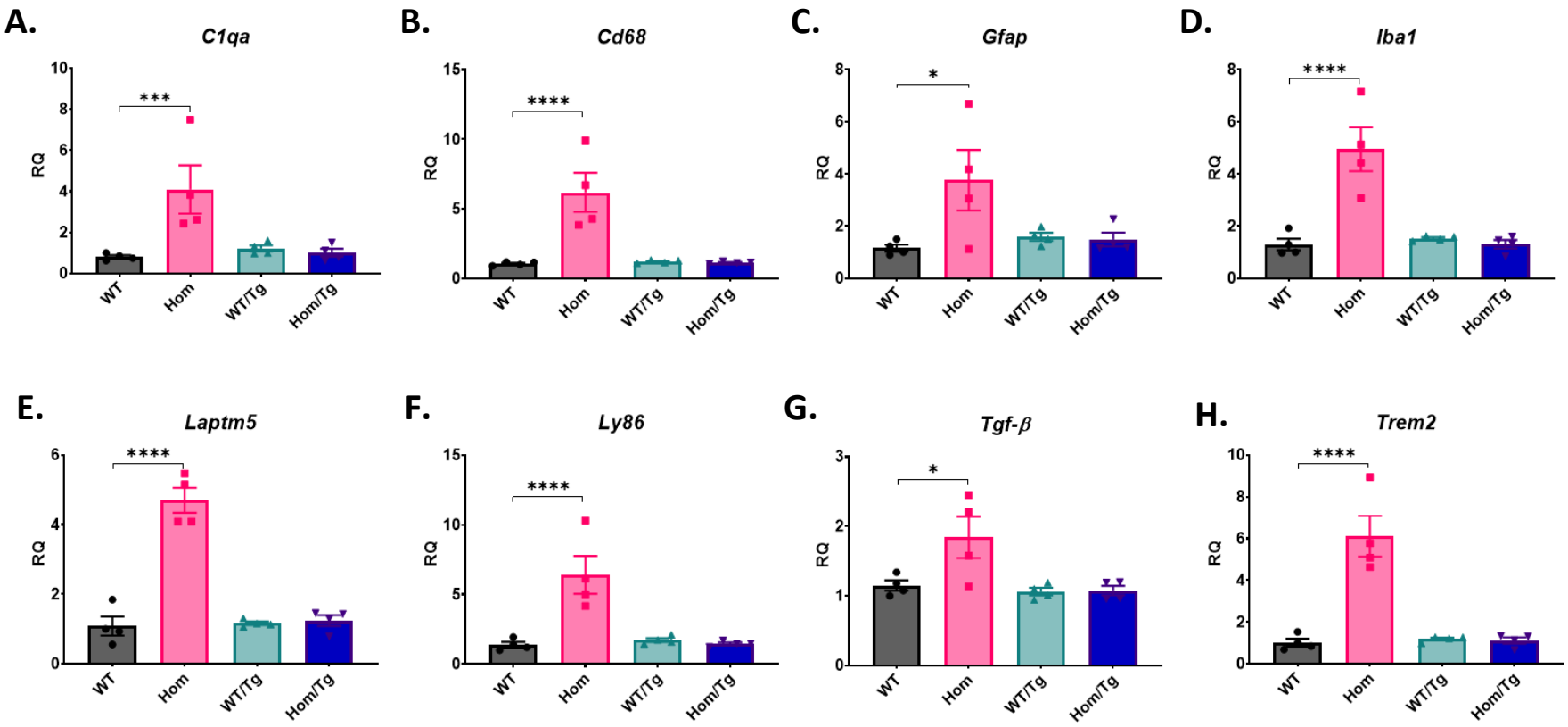

***Figure 5.10*| Expression levels of inflammatory markers in P22 cerebellar tissue**

qRT-PCR analysis of inflammatory markers (A) *C1qa*, (B) *Cd68*, (C) *Gfap*, (D) *Iba1*, (E) *Laptm5*, (F) *Ly86,* (G) *Tgf-β* and (H) *Trem2* in Hom, WT/Tg, Hom/Tg expressed relative to WT sample. Data presented as mean ± SEM and analysed by one-way ANOVA, followed by Tukey's multiple comparison test, relative to WT. *p<0.05, **p<0.01, ***p<0.001, ****p<0.0001. n=4 per genotype.

5.2.5. *Prnp-Oxr1* transgenic expression 'rescues' lysosomal gene expression, yet no significant differences in autophagic turnover were observed in Hom/Tg mice

Constitutive loss of *Oxr1* leads to disruption of the autolysosomal pathway in the cerebellum, as well as in primary cortical neurons and fibroblasts derived from *Oxr1* knockout mice (**Chapter 3**); furthermore, staining LoF-OXR1 patient fibroblasts with LysoTracker showed a significant increase in number of lysosomes (Wang et al., 2019), indicating lysosomal dysfunction in both *Oxr1*-deficient mouse models and human patients. *Ctsd* and *Hexb*, both genes that encode degradative enzymes in the lysosome (Lie & Nixon, 2019), were identified as significantly upregulated in P19 cerebellar RNA-seq data. Given that key markers of neuroinflammation were 'rescued' in Hom/Tg at P22, expression levels of *Ctsd* and *Hexb* in P22 cerebellar tissue of each genotype were analysed to determine in neuronal overexpression of *Oxr1* protects against dysregulation of these lysosomal enzymes at the RNA level.

As to be expected, qRT-PCR revealed significant upregulation of *Ctsd* ($p<0.0001$) and *HexB* ($p=0.0002$) (**Figure 5.11A** and **B**) in Hom cerebellar tissue compared to WT mice at P22. Interestingly, cerebellar expression of *Ctsd* and *Hexb* was not significant in WT/Tg or 'rescue' Hom/Tg tissue when compared to WT (**Figure 5.11A** and **B**). A more than 2-fold decrease in expression of these lysosomal enzymes is observed in Hom/Tg mice when compared to Hom tissue. These data imply that the *Prnp-Oxr1* transgene is able to prevent dysregulated expression of lysosomal enzymes that is typically induced in Hom mice, therefore supports the hypothesis that loss of *Oxr1* induces neuropathogenic alterations in the autolysosomal pathway.

Given the hypothesised role of *Oxr1* in autolysosomal dysfunction in the cerebellum, perturbations in autophagic flux were investigated at the protein level in this 'rescue' transgenic mouse model. Western blotting (**Figure 5.11C)** using protein extracts from P22 cerebellar tissue did not identify significant differences in levels of p62 or ratio of LC3II/I in Hom/Tg mice compared to WT, Hom and WT/Tg mice (**Figure 5.11D** and **E**). From these data alone, it is unclear how *Oxr1* and, in turn, *Prnp-Oxr1* influence autophagic flux *in vivo.*

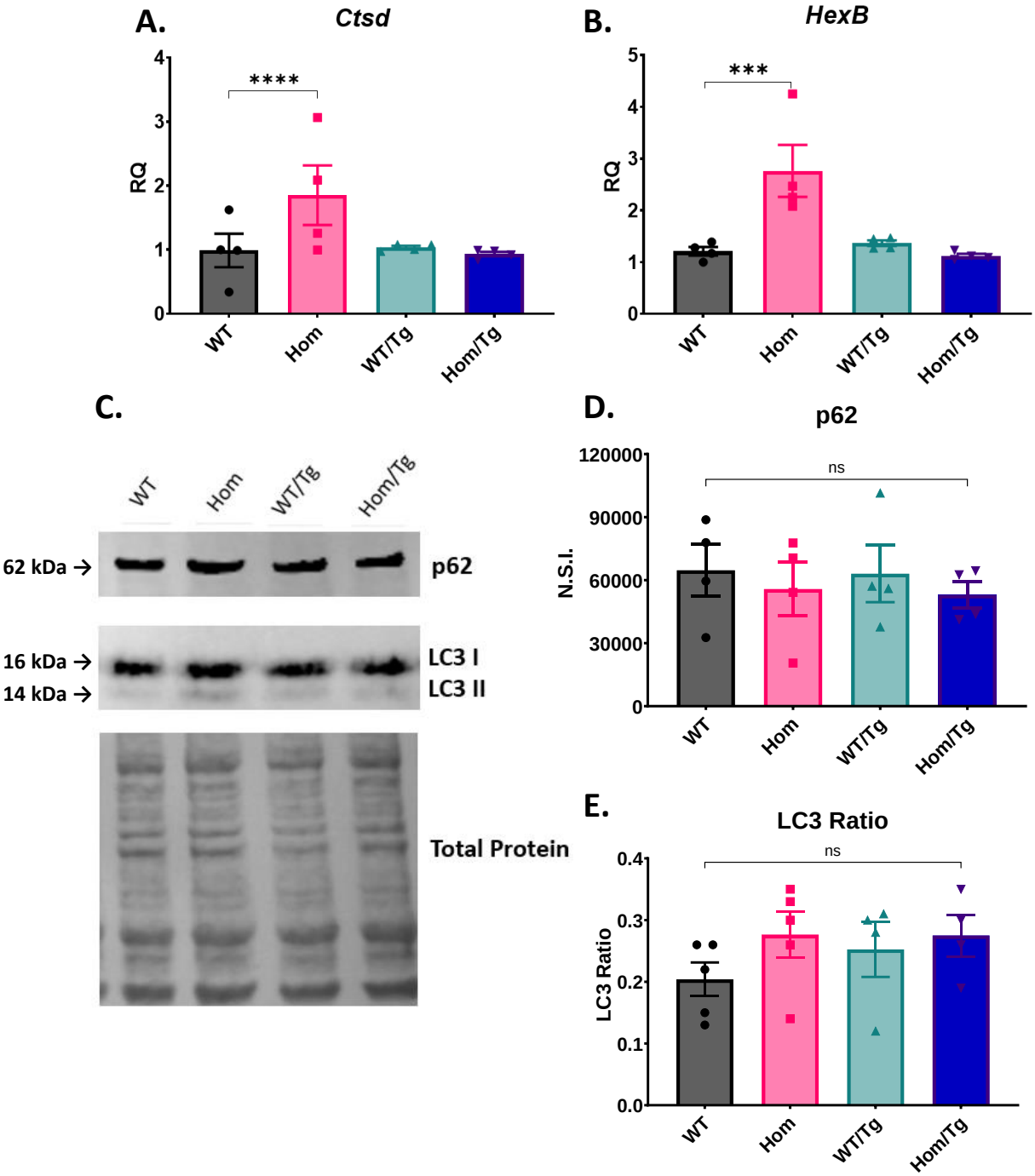

***Figure 5.11*| Expression analysis of lysosomal enzymes and representative Western blot of autophagic turnover markers in P22 cerebellar tissue**

qRT-PCR analysis of lysosomal enzymes (A) *Ctsd* and (B) *Hexb* in P22 cerebellar tissue from in Hom, WT/Tg, Hom/Tg expressed relative to WT sample. (C) Representative Western blot and quantitative analysis of autophagy markers (D) p62 and (E) LC3 ratio, normalised to total protein. Data presented as mean ± SEM and analysed by one-way ANOVA, followed by Tukey's multiple comparison test, relative to WT. *p<0.05, **p<0.01, ***p<0.001, ****p<0.0001. n=4-5 per genotype. RQ: Relative quantification; N.S.I: Normalised signal intensity.

5.2.6. Downregulation of *Ctsd* is observed in the cerebellum of Hom/Tg mice at 8 months

Oliver *et al.* (2011) established that Oxr1 expression is essential to life in the mouse; loss of this protein results in paralysis and early death (P22-24); similarly, **Chapter 4** established that Oxr1 is required in the adult mouse brain to negate neuroinflammation and autophagic dysfunction in the cerebellum, as well as cell death in the olfactory bulb and CGCL. Neuron-specific overexpression of *Oxr1* has been shown to protect against dysregulation of lysosomal and inflammatory genes (**5.2.4**); given that increased neuroinflammation is observed in aging brains (Mukherjee et al., 2019), it is possible that Hom/Tg mice would be more vulnerable to age-related pathology and for aging to exacerbate a neurological phenotype.

To determine whether mice with neuronal overexpression of *Oxr1* on an *Oxr1* null background were more susceptible to aberrant gene expression in lysosomal and neuroinflammatory pathways at 8 months, qRT-PCR was carried out on cerebellar tissue harvested from Hom/Tg and representative control Het/Tg mice. *Oxr1-FL* expression was examined initially; relative to control Het/Tg animals, a reduction in *Oxr1-FL* expression is observed in Hom/Tg cerebellum (**Figure 5.12A**). This was expected considering that Het/Tg representative controls have one wild type *Oxr1* allele expressed alongside neuronal transgene expression.

Autolysosomal dysfunction is heavily associated with the onset of NDs and neurodegenerative conditions (Hou et al., 2019; Kuil et al., 2019; Lie & Nixon, 2019; Steinfeld et al., 2006) and importantly, *Prnp-Oxr1* expression 'rescues' dysregulation of lysosomal markers, *HexB* and *Ctsd,* on a ubiquitous *Oxr1* null background at P22. When comparing expression of *HexB* in Hom/Tg and Het/Tg mice, differential expression is not observed, suggesting that the *Prnp-Oxr1* transgene sustains protection against dysregulation of *HexB* when expressed in constitutive *Oxr1* knockout (**Figure 5.12B**).

Intriguingly, significant downregulation of *Ctsd* (p=0.0114) is observed in Hom/Tg adult mouse cerebellum compared to control tissue (**Figure 5.12C**). This indicates that neuron-specific overexpression of *Oxr1* in ubiquitous *Oxr1* knockout mice delays deregulation of lysosomal enzyme, *Ctsd,* in adult mice. It could be hypothesised that further aging of Hom/Tg mice may result in the emergence of significant neuropathology and/or a neurodegenerative phenotype.

Next, expression of neuroinflammatory markers was quantified in cerebellar tissue from Hom/Tg and Het/Tg at 8 months. Differential expression of *C1qa*, *Cd68*, *Laptm5*, *Gfap*, *Trem2* and *Iba1* was not significant in Hom/Tg mice when compared to Het/Tg control animals (**Figure 5.12D-I**). From these data, it could be inferred that *Prnp-Oxr1* expression in 8 month old Hom/Tg mice does not increase susceptibility to neuroinflammatory pathology.

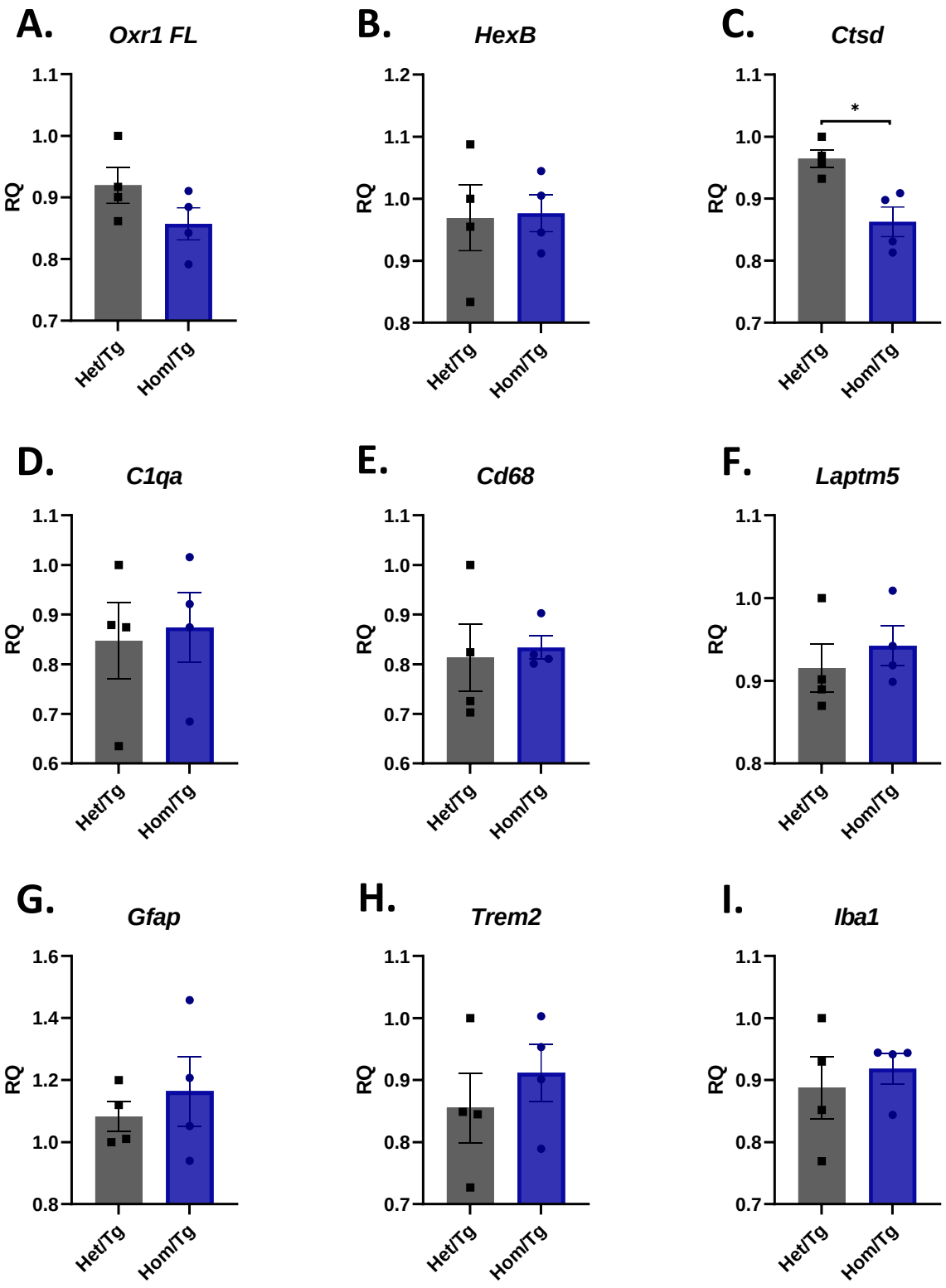

***Figure 5.12*| Expression levels of *Oxr1-FL*, lysosome and inflammatory markers in cerebellar tissue from Het/Tg and Hom/Tg 'rescue' mice at 8 months.**

qRT-PCR analysis of (A) *Oxr1-FL*, lysosome markers (B) *Hexb*, and (C) *Ctsd* and inflammatory markers (D) *C1qa*, (E) *Cd68*, (F) *Laptm5,* (G) *Gfap*, (H) *Trem2* and (I) *Iba1* in Hom/Tg mice expressed relative to a Het/Tg sample. RQ: relative quantification. Data presented as mean ± SEM and analysed by unpaired t-test, p values * ≤ 0.05. n=4

5.2.7. Exploring the potential 'gain of function' mechanism of the Prnp-Oxr1-HA transgene using a proteomics approach

Neuronal overexpression of *Oxr1* has been proven to be protective in number of neurodegenerative models, including the ability to delay the onset of motor symptoms and neuroinflammation in ALS mouse models (K. X. Liu et al., 2015; Williamson et al., 2019). Thus far, transcriptomic analysis of spinal cord from WT and WT/Tg mice at P90 only identified significant differential expression of *Oxr1* from *Prnp-Oxr1* expression in WT/Tg mice (K. X. Liu et al., 2015); as a result, this initial analysis did not shed light on any potential functional mechanisms of *Prnp-Oxr1* expression *in vivo*. Less stringent analysis parameters revealed subtle changes within the spinal cord transcriptome of WT/Tg mice, identifying differential expression of genes involved in biological pathways such as related to cell death and survival, nervous system development and function and lipid metabolism, similar to those found when analysing DEGs identified by RNA-Seq of P19 *Oxr1* knockout cerebellum (**Chapter 3**). This suggests that the *Prnp-Oxr1* transgene may augment the endogenous function of *Oxr1* in neurons.

Of note, it may be that 'gain-of-function' properties of the transgene need to be investigated in context of a disease model. Although K. X. Liu et al. (2015) identified 63 'rescued' genes, such as *HexB* and *C1qa*, in the spinal cord of $SOD1^{G93A}$/Tg mice when compared to $SOD1^{G93A}$ tissue, Williamson (2019) compared the transcriptome in spinal cord from $TDP\text{-}43^{M337V/M337V}$ and $TDP\text{-}43^{M337V/M337V}$/Tg mice at 18 months and surprisingly, did not find any DEGs, despite transgene expression significantly improving muscle pathology, neuroinflammation and motor function in $TDP\text{-}43^{M337V/M337V}$/Tg mice at this time point (Williamson et al., 2019).

Given that Oxr1 isoforms bind to TDP-43 *in vitro* and *in vivo*, as well as rescue cytoplasmic mislocalisation and aggregation of TDP-43, it possible that *Prnp-Oxr1* confers

neuroprotection through protein-binding partners (Finelli et al., 2015; Williamson et al., 2019). In an attempt to understand the neuroprotective mechanisms of *Prnp-Oxr1 in vivo,* a proteomic approach was adopted. Brain and cerebellar protein lysates were taken from mice expressing *Prnp-Oxr1-HA* (WT/Tg, Het/Tg and Hom/Tg) and littermate controls (WT, Het and Hom) at P22; subsequently, immunoprecipitation (IP) was conducted, followed by denaturation of the IP eluent and protein separation by sodium dodecyl-sulfate polyacrylamide gel electrophoresis (SDS-PAGE). Currently, an Oxr1 antibody suitable for IP does not exist, therefore an anti-HA antibody was used to pull down the C-terminally HA-tagged Oxr1 transgene and putative interacting partners.

Anti-HA Western blot analysis of whole lysate and IP samples showed that Oxr1 could be detected in transgene expressing samples (WT/Tg, Het/Tg, Hom/Tg) and not in WT and Het littermate controls (**Figure 5.13A, C** and **D**), demonstrating that Oxr1 was successfully pulled-down by the anti-HA antibody. In order to identify novel protein interactors, transgene-positive samples from the cortex and cerebellum were compared to transgene-negative samples on Coomassie stained SDS-PAGE gels. Regions of interest, whereby by unique bands were present only in transgene positive samples, were isolated by gel excision and subjected to protein identification by mass spectrometry (MS) (**Figure 5.13B** and **E**). IP, SDS-PAGE and gel Coomassie staining was also carried out using protein lysates from Hom and Hom/Tg, however there was insufficient protein concentration to send samples for MS (**Figure 5.13F**).

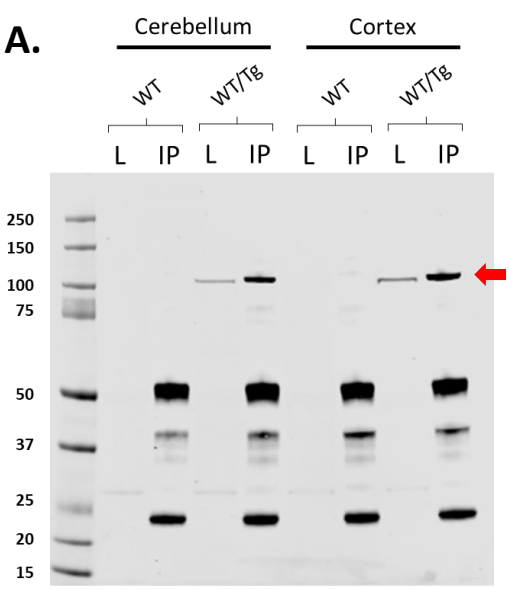
A.
Cerebellum
Cortex
WT
WT/Tg
WT
WT/Tg
L IP L IP L IP L IP
250
150
100
75
50
37
25
20
15

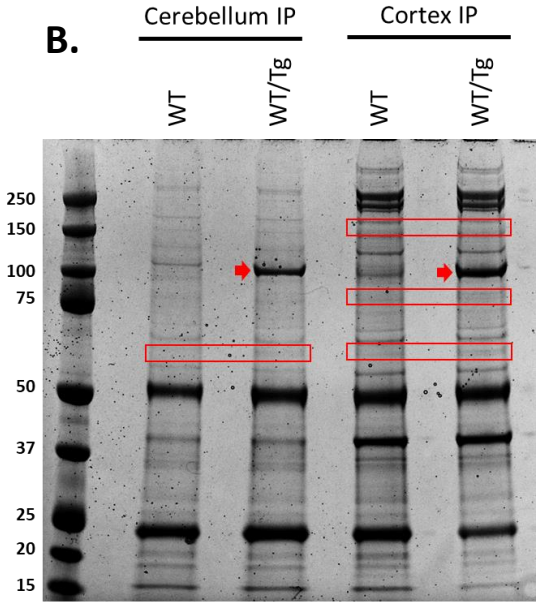
B.
Cerebellum IP
Cortex IP
WT
WT/Tg
WT
WT/Tg
250
150
100
75
50
37
25
20
15

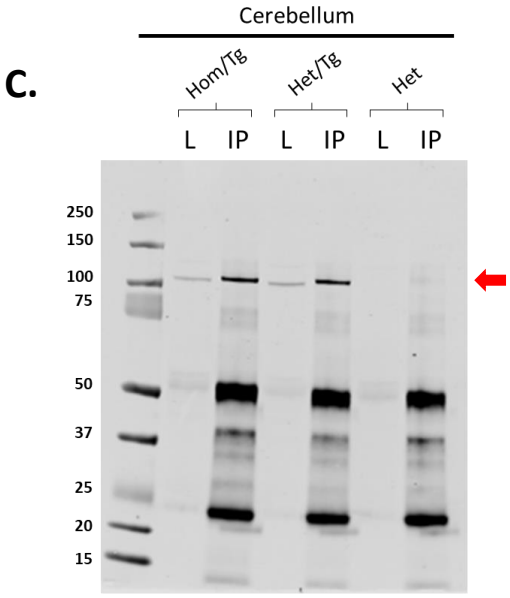
C.
Cerebellum
Hom/Tg
Het/Tg
Het
L IP L IP L IP
250
150
100
75
50
37
25
20
15

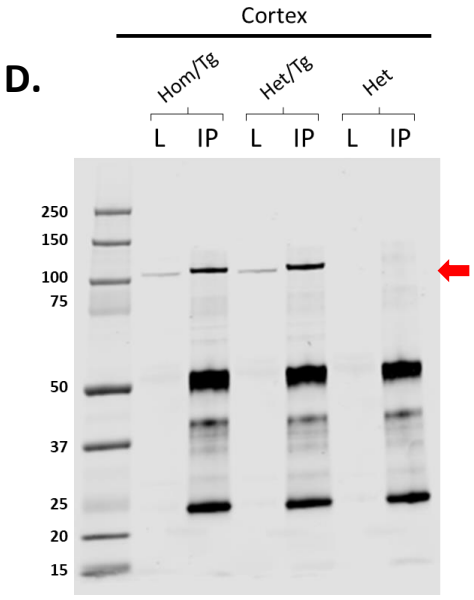
D.
Cortex
Hom/Tg
Het/Tg
Het
L IP L IP L IP
250
150
100
75
50
37
25
20
15

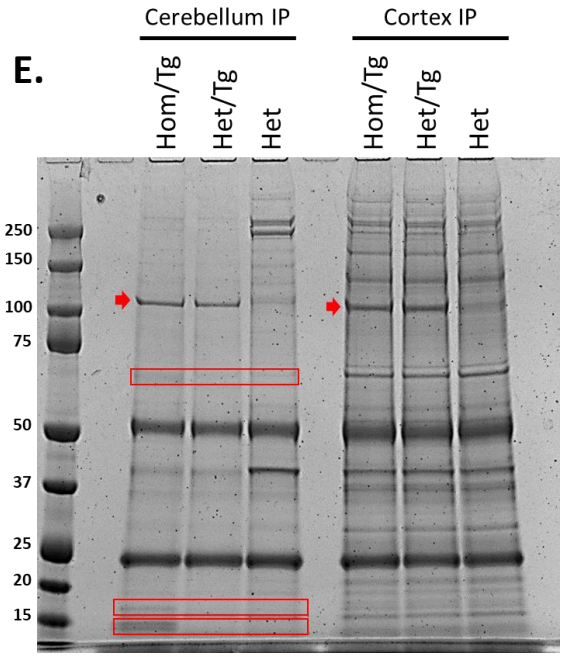
E.
Cerebellum IP
Cortex IP
Hom/Tg
Het/Tg
Het
Hom/Tg
Het/Tg
Het
250
150
100
75
50
37
25
20
15

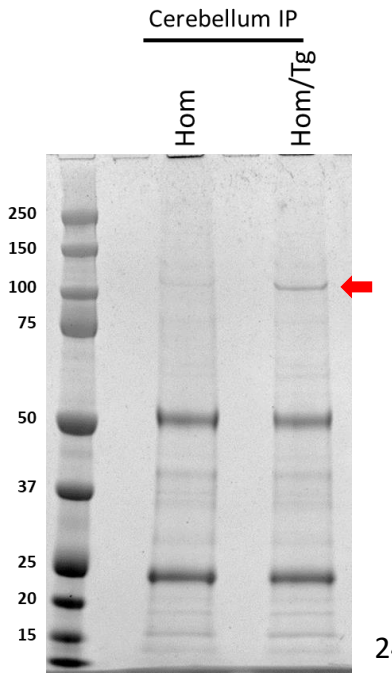
F.
Cerebellum IP
Hom
Hom/Tg
250
150
100
75
50
37
25
20
15

***Figure 5.13*| anti-HA co-immunoprecipitation Western blots and SDS-polyacrylamide (SDS-PAGE) gel images to show bands excised and processed for mass spectrometry**

(A,B) Anti-HA co-immunoprecipitation using protein extract from the cerebellum and cortex of P22 WT and WT/Tg mice with (A) anti-HA Western blot of whole lysate and IP, and (B) image of Coomassie stained SDS-PAGE of IP. (C,D,E) Anti-HA co-immunoprecipitation using protein extract from the (C) cerebellum and (D) cortex of P22 Hom/Tg, Het/Tg and Het mice with (C,D) anti-HA Western blots of whole lysate and IP from (C) cerebellum and (D) cortex. (E) Coomassie stained SDS-PAGE of Hom/Tg, Het/Tg and Het anti-HA IPs. (F) SDS-PAGE image of anti-HA co-IP with Hom and Hom/Tg cerebellar protein extracts. Anti-HA (Ms): 1:20000. Red box: bands of interest excised and processed for peptide identification; Red arrows: indicating Prnp-Oxr1-HA transgene; IP: immunoprecipitation; L: whole lysate.

Protein/peptide identification was carried out at the Functional Genomics and Proteomics Facility, University of Birmingham. In brief, peptide separation was carried out using a reverse-phase nano-flow high performance liquid chromatography (HPLC) *c*olumn (Dionex) coupled to a mass spectrometer and subsequently identified through MS/MS. Initial proteomic analysis and peptide matching to the UniProt database was performed using Proteome Discoverer v. 2.2 at the University of Birmingham, where primary filtering of positive hits was set to a minimum of 2 unique peptides, a maximum of 2 missed cleavages and FDR ≥ 0.01. Stringent filtering of MS data has been shown to be effective in removing false positives from the extensive data set (Damodaran et al., 2007), therefore as an additional filter, only MS hits with at least 10% peptide sequence coverage and a minimum of four peptides matching were included in the list of potential interaction partners (**Table 5-2**).

***Table 5-2*| List of proteins identified through anti-HA pulldown and mass spectrometry in the cortex and cerebellum of Prnp-Oxr1-HA transgene positive and negative protein lysates**

		Cortex		Cerebellum				
UniProt Accession Number	**Protein Name**	**WT**	**WT/Tg**	**WT**	**Het**	**WT/Tg**	**Het/Tg**	**Hom/Tg**
I6L985	Igh protein	X	X	X	X	X	X	X
P02535	Keratin, type I cytoskeletal 10	X	X	X	X		X	X
P01869	Ig gamma-1 chain C region, membrane-bound form	X	X	X	X		X	X
O08553	Dihydropyrimidinase-related protein 2	X	X	X	X		X	X
Q4KMM3	Oxidation resistance protein 1	X	X			X	X	X
Q546G4	Serum albumin	X	X		X		X	X
P56959	RNA-binding protein FUS (Protein pigpen)	X	X		X		X	X
P08551	Neurofilament light polypeptide, NF-L protein)	X	X		X		X	X
B1AQ77	Keratin, type I cytoskeletal 15		X				X	X
Q9JJV2	Profilin-2 (Profilin II)				X		X	X
Q9ERS2	NADH dehydrogenase [ubiquinone] 1 alpha subcomplex subunit 13				X		X	X
Q9CQZ5	NADH dehydrogenase [ubiquinone] 1 alpha subcomplex subunit 6				X		X	X
Q91VB8	Alpha globin 1 (Alpha globin 2)				X		X	X
Q8BMK4	Cytoskeleton-associated protein 4				X		X	X
Q8BMF4	Dihydrolipoyllysine-residue acetyltransferase component of pyruvate dehydrogenase complex				X		X	X
Q61765	Keratin, type I cuticular Ha1				X		X	X
Q5XFY8	Uncharacterized protein				X		X	X
Q58DZ3	60S ribosomal protein L30				X		X	X
Q3V0Z8	Probable ATP-dependent RNA helicase DDX5, (DEAD box protein 5)				X		X	X
Q3THQ5	Stress-induced-phosphoprotein 1 (Hsc70/Hsp90-organizing protein)				X		X	X
P99027	60S acidic ribosomal protein P2				X		X	X
P97861	Keratin, type II cuticular Hb6				X		X	X
P62806	Histone H4				X		X	X
P51880	Fatty acid-binding protein, brain				X		X	X

O08599	Syntaxin-binding protein 1				X		X	X
G5E924	Heterogeneous nuclear ribonucleoprotein L				X		X	X
F7AEH4	40S ribosomal protein S12				X		X	X
A0A411P8U6	Myelin basic protein				X		X	X
Q9QXS6	Drebrin (Developmentally-regulated brain protein)	X	X		X			
Q9Z2T6	Keratin, type II cuticular Hb5						X	X
Q9DAK9	14 kDa phosphohistidine phosphatase						X	X
Q8K2B3	Succinate dehydrogenase [ubiquinone] flavoprotein subunit, mitochondrial						X	X
Q5SX50	Profilin						X	X
Q544F6	Cotl1 protein						X	X
P99024	Tubulin beta-5 chain						X	X
P60867	40S ribosomal protein S20						X	X
P40142	Transketolase, TK, EC 2.2.1.1 (P68)						X	X
Q9D023	Mitochondrial pyruvate carrier 2 (Brain protein 44)				X			X
Q8K0Y2	Keratin, type I cuticular Ha3-I				X			X
Q61649	Alpha-globin mRNA				X			X
Q54AH9	Beta-2-globin				X			X
P62897	Cytochrome c, somatic				X			X
P62317	Small nuclear ribonucleoprotein Sm D2, Sm-D2 (snRNP core protein D2)				X			X
P19783	Cytochrome c oxidase subunit 4 isoform 1, mitochondrial				X			X
P11404	Fatty acid-binding protein, heart				X			X
P05213	Tubulin alpha-1B chain (Alpha-tubulin 2)				X			X
A8DUQ1	Beta-globin				X			X
A0A1W2P7Q9	Myosin light polypeptide 6				X			X
Q9Z0X1	Apoptosis-inducing factor 1, mitochondrial				X		X	
Q9JJF3	Ribosomal oxygenase 1				X		X	
Q9ERD7	Tubulin beta-3 chain				X		X	
Q9EQF6	Dihydropyrimidinase-related protein 5				X		X	
Q925I1	ATPase family AAA domain-containing protein 3 (AAA-ATPase TOB3)				X		X	
Q91VE0	Long-chain fatty acid transport protein 4				X		X	
Q8R326	Paraspeckle component 1 (Paraspeckle protein 1, mPSP1)				X		X	

Q8C854	Myelin expression factor 2, MEF-2, MyEF-2				X		X	
Q7TMK9	Heterogeneous nuclear ribonucleoprotein Q				X		X	
Q61584	Fragile X mental retardation syndrome-related protein 1, mFxr1p				X		X	
Q548L6	Glutamate decarboxylase				X		X	
P68369	Tubulin alpha-1A chain				X		X	
P62245	40S ribosomal protein S15a				X		X	
P16390	Potassium voltage-gated channel subfamily A member 3				X		X	
P16388	Potassium voltage-gated channel subfamily A member 1				X		X	
O70194	Eukaryotic translation initiation factor 3 subunit D				X		X	
A2AVR6	Acyl-coenzyme A thioesterase 11				X		X	
A2AKB9	DDB1- and CUL4-associated factor 10 (WD repeat-containing protein 32)				X		X	
A0A0R4J1N0	Dihydropyrimidinase-related protein 4				X		X	
Q3TVV6	Uncharacterized protein		X			X		
Q71LX8	Heat shock protein 84b	X	X					
Q5SUS9	RNA-binding protein EWS	X	X					
Q02248	Catenin beta-1 (Beta-catenin)	X	X					
P13020	Gelsolin	X	X					
B2RRX1	Actin, beta	X	X					
A3KGU9	Spectrin alpha chain, non-erythrocytic 1	X	X					
A0A571BG39	SRC kinase-signaling inhibitor 1	X	X					
Q3U6B1	Uncharacterized protein			X	X			
Q9D2M8	Ubiquitin-conjugating enzyme E2 variant 2 (Ubc-like protein MMS2)							X
Q9CR61	NADH dehydrogenase [ubiquinone] 1 beta subcomplex subunit 7							X
Q91ZZ3	Beta-synuclein							X
Q91X72	Hemopexin							X
Q8C0M9	Isoaspartyl peptidase/L-asparaginase							X
Q64524	Histone H2B type 2-E (H2B-clustered histone 21) (H2b 613)							X
Q561N5	40S ribosomal protein S18							X
Q542T4	Myelin basic protein							X
Q4VAI2	Low molecular weight phosphotyrosine protein phosphatase							X
Q497I3	Fatty acid binding protein 5, epidermal							X

Q3UDZ1	Uncharacterized protein							X
Q3U9A8	SH3 domain-binding glutamic acid-rich-like protein							X
Q3TLP8	Ras-related C3 botulinum toxin substrate 1							X
Q3TKM9	Actin-related protein 2/3 complex subunit 5							X
Q02257	Junction plakoglobin (Desmoplakin III) (Desmoplakin-3)							X
Q00915	Retinol-binding protein 1 (Cellular retinol-binding protein, CRBP)							X
P70349	Adenosine 5'-monophosphoramidase HINT1							X
P63242	Eukaryotic translation initiation factor 5A-1							X
P54227	Stathmin (Leukemia-associated gene protein)							X
P52480	Pyruvate kinase PKM							X
P32848	Parvalbumin alpha							X
P16045	Galectin-1							X
P07309	Transthyretin (Prealbumin)							X
O70591	Prefoldin subunit 2							X
F8WGL3	Cofilin-1 (Cofilin, non-muscle isoform)							X
B1Q450	Hemoglobin beta chain subunit							X
A7VJ98	Glia maturation factor							X
A0A494BA94	Nucleoside diphosphate kinase							X
A0A023T778	Mago nashi protein (Protein mago nashi homolog 2)							X
Q9WU79	Proline dehydrogenase 1, mitochondrial						X	
Q9CWF2	Tubulin beta-2B chain						X	
Q9CQY2	RNA guanine-N7 methyltransferase activating subunit						X	
Q80TT4	MKIAA0719 protein						X	
Q544D7	AMP-binding domain-containing protein						X	
Q3U900	Dolichyl-diphosphooligosaccharide--protein glycosyltransferase subunit 1						X	
Q3TFG3	RNA helicase, EC 3.6.4.13						X	
P62320	Small nuclear ribonucleoprotein Sm D3						X	
P56480	ATP synthase subunit beta, mitochondrial						X	
P50544	Very long-chain specific acyl-CoA dehydrogenase, mitochondrial						X	
O89086	RNA-binding protein 3 (RNA-binding motif protein 3)						X	
E9PWE8	Dihydropyrimidinase-related protein 3						X	

A8DUK4	Beta-globin (Globin a1)						X	
A0A0A0MQA5	Tubulin alpha chain						X	
A0A068BGR9	NADH dehydrogenase [ubiquinone] 1 alpha subcomplex subunit 7						X	
Q9JI91	Alpha-actinin-2		X					
Q8VCE0	Sodium/potassium-transporting ATPase subunit alpha		X					
Q8K232	Adducin 1 (Alpha)		X					
Q7TPR4	Alpha-actinin-1		X					
Q5SWR1	AP complex subunit beta		X					
P39053	Dynamin-1, EC 3.6.5.5		X					
P17426	AP-2 complex subunit alpha-1		X					
E9Q3E2	Synaptopodin		X					
A1BN54	Alpha actinin 1a		X					
A0A571BG24	LIM and calponin homology domains-containing protein 1		X					
A0A1L1SV25	Alpha-actinin-4		X					
A0A1L1STE4	Interleukin enhancer-binding factor 3		X					

These MS data suggest that Prnp-Oxr1-HA interacts with a broad range of proteins in both the cortex and cerebellum. Proteins identified in both transgene-positive and negative samples, such as Dihydropyrimidinase-related protein 2, Syntaxin-binding protein 1 and Drebrin are likely to be false positives and not candidates for conferring the neuroprotective function of the transgene. As Oxr1 and IgH were the only common interactors in all transgene-positive samples, candidates were systematically assessed to those that were only captured in the 'rescue' sample. 29 potential transgene interaction partners were identified in Hom/Tg cerebellum that may confer the neuroprotective effect seen *in vivo* (**Table 5-3**)**.** Although a few hits are likely to be non-specific interactors, such as Histone H2B type 2-E and 40S ribosomal protein S18 (Mellacheruvu et al., 2013), some proteins have critical functions in the CNS that may contribute to the neuroprotective mechanism of the transgene; **Table 5-3** highlights specific critical functions of each putative transgene interactor leading to a subset of proteins of interest to be explored.

***Table 5-3*| Putative Prnp-Oxr1-HA protein binding partners only identified in anti-HA pulldown of P22 Hom/Tg cerebellar protein extracts**

UniProt Accession Number	Protein Name	Relevant CNS Functions	References
Q9D2M8	Ubiquitin-conjugating enzyme E2 variant 2 (Ubc-like protein MMS2)	Forms part of the E2 ubiquitin-conjugating enzymatic complex (UBC13-MMS2), involved in Lys-63 poly-ubiquitination targeting proteins for non-proteolytic functions – possible signal transduction mechanism. UBC13-MMS2 complex mediates error-free DNA repair (post-replication). Regulation of cell cycle progression.	(Ashley et al., 2002; Ulrich & Jentsch, 2000; Xiao et al., 2000)
Q9CR61	NADH dehydrogenase [ubiquinone] 1 beta subcomplex subunit 7	Non-catalytic component of the mitochondrial Mammalian Complex I. Part of the respiratory electron transport chain that oxidises NADH. Subsequently produces reactive oxygen species as a by-product.	(Nehls et al., 1992; Sharma et al., 2009)
Q91ZZ3	Beta-synuclein	A synaptic phosphoneuroprotein that may facilitate synaptic function, modulate protein aggregation and degradation. Not found in glial cells.	(Hayashi & Carver, 2022; Nakajo et al., 1993)
Q91X72	Hemopexin	Involved in the binding and transportation of heme. Antioxidant functional capacity.	(Hahl et al., 2017; Tolosano & Altruda, 2002)
Q8C0M9	Isoaspartyl peptidase/L-asparaginase	Proteolytic activity. Mediates L-aspartate production which can function as an excitatory neurotransmitter.	(Cantor et al., 2009; Cavallero et al., 2009)
Q64524	Histone H2B type 2-E	Part of the nucleosome. Associated with DNA binding and transcriptional regulation.	(McGinty & Tan, 2015)
Q561N5	40S ribosomal protein S18	Component of the 40S ribosomal subunit. Critical for mRNA decoding and protein synthesis.	(Lafontaine & Tollervey, 2001)
Q542T4	Myelin basic protein	Formation of protective axonal projection layer, myelin sheath.	(Franklin & Ffrench-Constant, 2008)
Q4VAI2	Low molecular weight phosphotyrosine protein phosphatase	Catalyses tyrosine phosphorylated proteins. Suggested importance in signal transduction, cell growth and regulation of cytoskeletal activity.	(Caselli et al., 2016; Park et al., 2002)
Q497I3	Fatty acid binding protein 5, epidermal	Fatty acid binding protein family implicated in lipid metabolism as well as uptake and transport of fatty acids which are an important fuel supply in the CNS.	(Panov et al., 2014)
Q3UDZ1	Uncharacterized protein, Rhog	Rho-related GTP-binding protein. Predicted Rho GTP-binding/GTPase activity. Rho-related activity in the CNS is implicated in numerous critical	(Govek et al., 2005; Huttlin et al., 2010)

		pathways, including neuronal development, cytoskeletal activity and neuritogenesis.	
Q3U9A8	SH3 domain-binding glutamic acid-rich-like protein	SH3 domains notably bind proline-rich sequences and involved in numerous protein-protein interactions. Scaffold protein. Suggested to be involved in CNS development.	(Cesareni et al., 2002; Tong et al., 2016)
Q3TLP8	Ras-related C3 botulinum toxin substrate 1	Activator of JNK pathway. Modulates immune response, subsequent inflammation and apoptosis.	(Hirohama et al., 2020; Kowluru, 2020; Tebar et al., 2020)
Q3TKM9	Actin-related protein 2/3 complex subunit 5	A subunit of the Arp2/3 complex that facilitates actin polymerisation and assembles branched networks, which is important in cell migration, morphology, polarity and neuronal dendrite formation. The actin cytoskeleton is fundamental to numerous cellular processes.	(Hudson & Cooley, 2002; Mullins et al., 1998; Qualmann & Kessels, 2008; Sturner et al., 2019; Zallen et al., 2002)
Q02257	Junction plakoglobin	Common junctional plaque protein, formation of adheren junctions Involved cytoskeleton arrangement dynamics. Important in cell migration and cell signalling. Possible moderator of apoptosis.	(Aktary et al., 2017; Aktary & Pasdar, 2012)
Q00915	Retinol-binding protein 1	Retinol transporter and involved in vitamin A metabolism. Factor in CNS development.	(Ghyselinck et al., 1999; Parenti & Cicirata, 2004)
P70349	Histidine triad nucleotide-binding protein 1, HINT1	Hydrolytic activity of adenosine-5'-monophosphoramidate. Transcription factor regulation in apoptosis. Neuronal regulation of calcium sensing and signalling homeostasis.	(Bieganowski et al., 2002; Linde et al., 2013; Peeters et al., 2017)
P63242	Eukaryotic translation initiation factor 5A-1	Binds to mRNA and assists with translation elongation. Maintains protein homeostasis, mediates cell differentiation and proliferation. Activated with HIF-1α under hypoxic conditions.	(Pelechano & Alepuz, 2017; Tauc et al., 2021; Zanelli et al., 2006)
P54227	Stathmin	Tubulin-binding phosphoprotein, destabilises microtubules. Expressed in early postnatal brain development.	(Charbaut et al., 2001; Koppel et al., 1990)
P52480	Pyruvate kinase	Catalytic activity and involved in glycolysis. Transcriptional regulator by phosphorylation. Potential immunomodulatory effect.	(Alves-Filho & Palsson-McDermott, 2016; Yang & Lu, 2015)
P32848	Parvalbumin alpha	Calcium-binding protein. Part of a GABAergic neuronal sub-population – fast spiking PV+ interneurons. Promotes muscle relaxation post-contraction.	(Hu et al., 2014; Racay et al., 2006)

P16045	Galectin-1	Regulates inflammation and apoptosis. Facilitates neuronal development, neurite outgrowth, synaptic connectivity, axonal regeneration and general cell survival.	(Camby et al., 2006; Law et al., 2020)
P07309	Transthyretin	Binds and transport thyroid proteins and retinol. Neuronal stress biomarker. Ability to bind β-amyloid plaques.	(Buxbaum et al., 2008; Sharma et al., 2019)
O70591	Prefoldin subunit 2	Part of the prefoldin complex that chaperones newly synthesised peptides and mediates correct folding of proteins or reorganisation of misfolded proteins. Maintains protein homeostasis.	(Liang et al., 2020; Tahmaz et al., 2021)
F8WGL3	Cofilin-1	Positively regulates actin filament assembly – actin depolymerisation factor. Affiliated with neuronal migration and synaptic plasticity. Suspected role in neuroinflammation and neurodegeneration.	(Alsegiani & Shah, 2020; Bamburg et al., 1999)
B1Q450	Haemoglobin beta chain subunit	Subunit of red blood cell component, haemoglobin. Haemoglobin carries oxygen throughout the body, particularly to the brain which uses 20% of the total oxygen, promoting neuronal survival and activity.	(Cobley et al., 2018; Rawn & Ouellette, 2018)
A7VJ98	Glia maturation factor	Neurotrophic factor found in neurons and glial cells. Negative regulator of the Arp2/3 complex and antioxidant activity. Proinflammatory.	(Fan et al., 2018; Zaheer et al., 2008)
A0A494BA94	Nucleoside diphosphate kinase	Synthesising nucleoside triphosphates and maintaining cellular nucleotide pools. Linked to promoting signal transduction, cell proliferation and apoptosis.	(Lacombe et al., 2000; Masse et al., 2002; Otero, 2000)
A0A023T778	Mago nashi	Involved in cellular splicing and mRNA processing machinery. Part of the exon-junction complex. Regulator of neural stem cell division.	(Le Hir et al., 2016; Silver et al., 2010; Singh et al., 2013)

5.3 Discussion

Exogenous expression of *Oxr1* has been established as a therapeutic strategy to negate neuronal cell death in mouse models of ALS, PD and Retinitis Pigmentosa (RP) (Jiang et al., 2019; K. X. Liu et al., 2015; Sahu et al., 2021; Williamson et al., 2019), however the neuroprotective mechanisms are still unclear. This chapter aimed to elucidate the protective role of Oxr1 in neurons and determine whether neuron-specific expression of Oxr1 is protective against the phenotypic and histopathological effects seen in *Oxr1*-null mice at P22 (Oliver et al., 2011). Additionally, a proteomics approach was taken in order shed light on the potential neuroprotective mechanisms of the *Prnp-Oxr1* transgene.

5.3.1 Neuron-specific overexpression of Oxr1 is sufficient to protect against ubiquitous loss of the protein at P22

Understanding the intrinsic neuronal features contributing to selective vulnerability has been at the forefront of research in to neurodegenerative disease pathogenesis (Rama Rao & Kielian, 2015; Van Harten et al., 2021; Wang & Michaelis, 2010). Still, the importance of glial cells and neuronal-glial crosstalk in neurodegeneration is gaining traction, supporting hypotheses describing non-cell autonomous mechanisms of neuronal cell death (Bernaus et al., 2020; Garden & La Spada, 2012; Van Harten et al., 2021). For example, in an *in vitro* model of HD neuronal vulnerability, co-culturing wild type cortical and striatal neurons with astrocytes expressing a mutant form of huntingtin (htt) lead to significantly decreased expression of microtubule-associated protein 2 (MAP2), marking early neurodegeneration, when spiked with excitatory neurotransmitter, glutamate (Shin et al., 2005; Wang & Michaelis, 2010). This was observed in contrast to glutamate-treated wild type neurons displaying improved viability when co-cultured with wild type astrocytes, thus serving as an example of glial dysfunction contributing neuronal injury and cell death (Shin et al., 2005).

In the context of loss-of-function *Oxr1* mouse models, cerebellar inflammation and selective degeneration of CGCs are critical neuropathological features (K. X. Liu et al., 2015; Oliver et al., 2011). Interestingly, pre/early-symptomatic transcriptomic analysis identified significant upregulation of neuroinflammatory genes prior to neuronal cell death in constitutive *Oxr1* knockout cerebellar tissue (Chapter 3), suggesting that chronic glial activation and/or dysfunction may drive neuronal injury. Yet, data presented thus far showed that neuronal overexpression of *Oxr1-FL* in the absence of *Oxr1* expression in all other cell type is sufficient to protect against cerebellar degeneration and significant neuroinflammation in *Oxr1* knockout mice and rescues early lethality (Oliver et al., 2011). These data indicate that survival of CGCs is dependent on expression of *Oxr1*, suggesting cell-autonomous cerebellar degeneration and instigation of a neuroinflammatory phenotype from neuronal dysfunction *in vivo*.

A major caveat of this experimental design is that *Oxr1* is not expressed at physiological levels, therefore it is possible that there are compensatory mechanisms of neuronal overexpression of *Oxr1* masking possible glial dysfunction in *Oxr1*-deficient neuroimmune cells. Additionally, although *Prnp-Oxr1* has been well characterised to neuron-specific expression in both the brain and spinal cord (K. X. Liu et al., 2015; Williamson et al., 2019), additional triple immunofluorescent staining of anti-HA, NeuN and glial markers anti-Iba1 or anti-Gfap would confirm the absence of 'leaky' transgene and off-target expression in glial cell types. Overall, this model suggests that glial overexpression of *Oxr1* may not be sufficient to prevent neuronal injury and degeneration in *Oxr1*-deficient neurons. To further test this theory *in vitro*, *Oxr1* knockout CGCs could be co-cultured with either wild type, *Oxr1* knockout or *Oxr1* overexpressing glial cells to assess neuronal sensitivity to cellular stress, such as nutrient starvation or OS-induced conditions (Nguyen et al., 2018; Oliver et al., 2011; Shin et al., 2005).

Given the acute onset of neurological dysfunction and neurodegeneration in the absence of *OXR1* in both humans and mice, it was striking to observe Hom/Tg 'rescue' mice survive beyond P22 (Lin et al., 2022; Oliver et al., 2011; Wang et al., 2019). Neuron-specific overexpression of *Oxr1* has been shown to delay onset, ameliorate symptoms and disease progression in $SOD1^{G93A}$ and $TDP\text{-}43^{M337V}$ mouse models of ALS, nevertheless disease symptomology is not completely abolished (K. X. Liu et al., 2015; Williamson et al., 2019). The authors hypothesised that neuron-specific upregulation of *Oxr1* protects against neuronal degeneration through modulating ROS levels, thus preventing extracellular release of ROS, proinflammatory signals and subsequent glial activation; a possible explanation for the observed neuroinflammatory delay is that mutant glial cells eventually succumb to OS or cellular dysfunction and initiate a neuroinflammatory response (Geloso et al., 2017; K. X. Liu et al., 2015; Simpson & Oliver, 2020; Williamson et al., 2019).

Hom/Tg mice showed restoration of deregulated lysosomal and neuroinflammatory genes at P22, yet a significant decrease in *Ctsd* expression, as well as non-significant increase in neuroinflammatory markers was observed at 8 months, despite absence of an obvious neurological phenotype. Lopez *et al.* (2011) previously demonstrated that both pan-neuronal and Purkinje cell-specific expression of *Npc1* was sufficient to extend life span and reduce inflammation in an NPC mouse model, where cerebellar Purkinje neuron degeneration is a hallmark feature (Lopez et al., 2011). However, Purkinje cell-*Npc1* rescue only delayed severe disease pathogenesis of $Npc1^{-/-}$ mice; similarly, neuronal–*Npc1* mice eventually showed neurological deterioration with age, although the end point was not determined for these animals (Lopez et al., 2011). This model suggests that neuronal overexpression of *Npc1* did not rescue disease onset and neuropathology, but significantly delayed. From these examples, it could be hypothesised that *Prnp*-*Oxr1* delays the onset of aberrant neuropathology in *Oxr1*-deficient mice.

In a cohort of 10 'rescue' mice, qualitative observations revealed seizure-like behaviour of one Hom/Tg mouse at 8 months (P244); this animal displayed a period of hyperactivity, repetitive grooming behaviour and convulsive movements. Whether this is the emergence of a delayed neurological phenotype is yet to be determined, as time constraints determined the primary endpoint to be 8 months. As seizures are part of the clinical symptoms observed in patients with loss-of-function mutations in *OXR1* (Lin et al., 2022; Wang et al., 2019), investigating the levels of *c-Fos* in this model may help identify abnormal neuronal activity indicative of seizures (Ahmadi et al., 2017; Bullitt, 1990). Furthermore, home cage analysis (HCA) can be employed to identify and monitor ictal behavioural characteristics in proposed models of epilepsy (Grieco et al., 2021; Jankovic et al., 2019). As outlined in Chapter 4, microglial-specific loss of tuberous sclerosis complex 1 (*Tsc1*) in mice induces hyper-activation of mTOR signalling, resulting in spontaneous seizures, thus demonstrating a role for aberrant microglial function in epileptogenesis (Zhao et al., 2018). Whether lack of glial cell *Oxr1* expression in adult mice instigates a seizure phenotype remains to be determined.

5.3.2 Putative Prnp-Oxr1 interaction partners in P22 Hom/Tg cerebellar tissue in the context of other proteomic data – potential functional clues?

Unbiased proteomic approaches have previously been employed to identify putative binding partners of Oxr1, under OS-induced conditions *in vitro*, in adult mouse brain and at different disease time points in a $SOD1^{G93A}$ mouse model of ALS (unpublished work)(Finelli et al., 2015; Liu, 2016). Crossing referencing potential interactors of Prnp-Oxr1 identified in **Table 5-2** with anti-HA pull down data from $SOD1^{G93A}$/Tg mice only identified a small number of overlapping candidates. From this, it could be inferred that factors, such as disease pathogenesis and affected brain regions, may drive differential protein-protein interactions (Sen et al., 2009; Thompson et al., 2012), as robust neuroprotection is observed in both mouse models. For example, allelic variant ApoE2 has been suggested to

be a neuroprotective factor against AD through differential binding affinity of protein interactors, such as low-density lipoprotein receptor (LDLR), thus promoting reduced plaque formation and improved efficiency of Aβ clearance (Reiman et al., 2020; Ruiz et al., 2005).

Beta(β)-synuclein was identified as an interaction partner by mass spectrometry in both Hom/Tg cerebellar protein lysate (**Table 5-2**) and at P90 in transgenic mouse brain (Liu, 2014). β-synuclein is a small phosphoneuroprotein typically found at synapses (Nakajo et al., 1993) and is known to have lipid binding properties, regulate metal homeostasis and proteasomal activity, cumulatively contributing to its anti-apoptotic role in neurons (da Costa et al., 2003; Rivers et al., 2008; Snyder et al., 2005). One of its most documented neuroprotective features is suppression of alpha(α)-synuclein aggregation, a pathogenic feature of PD (Brown et al., 2016; Hashimoto et al., 2001; Hayashi & Carver, 2022; Janowska et al., 2015). Exogenous expression of β-synuclein is being explored as an anti-aggregation therapeutic strategy of both α-synuclein deposits and amyloid plaques (Hashimoto et al., 2004; Krassnig et al., 2015). The potential recruitment of β-synuclein by Oxr1 may call upon the aforementioned functions in order to confer neuroprotective properties in NDs, providing further evidence that neuron-specific overexpression of Oxr1 is a highly relevant therapeutic target in α-synucleinopathies, such as PD, Dementia with Lewy Bodies and Multiple System Atrophy (Mendoza-Velasquez et al., 2019), as well as amyloidopathies, such as Alzheimer's disease (Murphy & LeVine, 2010).

Pyruvate kinase (PKM2, P52480) was additionally identified as a putative interaction partner in both P22 Hom/Tg cerebellar tissue (**Table 5-2**) and in $SOD1^{G93A}$/Tg brain at symptomatic time point, P90 (Liu, 2014). PKM2 plays a catalytic role in the last step of glycolysis and simultaneously produces ATP, as well as possessing regulatory functions through kinase activity in prominent molecular pathways, such as the Warburg's vicious

circle (PKM2-STAT3-HIF-1α feedback loop) (Alves-Filho & Palsson-McDermott, 2016; Demaria & Poli, 2012; Yang & Lu, 2015). Signal transducers and activators of transcription 3 (STAT3)-dependent transcriptional regulation via PKM2-dependent phosphorylation has been shown stimulate expression of *Gfap* and cytokine production (Beurel & Jope, 2009). K. X. Liu et al. (2015) have previously demonstrated that neuron-specific overexpression of *Oxr1* reduces phosphorylation and subsequent activation of STAT3 resulting in lower expression of downstream targets, such as *Vimentin* and *SerpinA3N*, that are implicated in neuroinflammation (K. X. Liu et al., 2015). Intriguingly, both Oxr1-FL and -C co-immunoprecipitated with Vimentin under OS conditions induced *in vitro* (Finelli et al., 2015). Taken together, this data further supports the hypothesis that the transgene may ameliorate neuroinflammation via this immunomodulatory pathway.

5.3.3 Limitations of proteomics approach

Although anti-HA immunoprecipitation followed by MS identified several candidate proteins that may ascertain the neuroprotective function of the transgene, it is also important to recognise potential limitations in the chosen method. For example, a validated Oxr1 antibody to pull-down endogenous protein does not currently exist and thus, the *Prnp-Oxr1* transgene was generated with a C-terminal HA-epitope tag to allow for further *in vitro* characterisation (K. X. Liu et al., 2015). Mellacheruvu *et al.* (2013) systematically reviewed native interactors of affinity tags, including HA, which identified a number protein candidates that may be pulled down alongside true interaction partners of the tagged protein of interest (Frankenfield et al., 2022). Notably, a number of these affinity tag background contaminants, such as cytoskeletal proteins and keratin, were identified as potential interactors this study, thereby contributing 'noise' to the dataset (**Table 5-2**) (Frankenfield et al., 2022; Hodge et al., 2013; Mellacheruvu et al., 2013).

Further to this, MS also identifies non-sample derived contamination peptides, further adding to the 'background noise' (Hodge et al., 2013; Nesvizhskii, 2012). Open source databases of common MS contaminants are being generated to enable stringent filtering of data and reduction of false discovery rates; the Contaminant Repository for Affinity Purification (CRAPome) is a prime example of an established pipeline (Mellacheruvu et al., 2013). Applying exclusion lists from relevant databases as further in *silico* analysis may help refine the list of putative transgene interaction partners (Hebert et al., 2018; Hiemstra et al., 2011; Hodge et al., 2013; Nesvizhskii, 2012; Poulos et al., 2020).

Of note, a negative control purification is essential when identifying authentic associated binding partners (Dunham et al., 2012). Although the experiment was conducted in the presence and absence of the transgene, using an *Oxr1* knockout as additional control would have further helped identify non-specific interactors and *bona fide* binding partners of Prnp-Oxr1-HA. Furthermore, the functional hypothesis relies upon the transgene strongly interacting with proteins in order to confer neuroprotection. IP is limited to detecting robust protein-protein interactions and, as a consequence, may not uncover transient or highly dynamic interactions *in vivo* (Dunham et al., 2012). Stabilising transient protein-protein interactions using chemical crosslinking may support the identification of putative transgene binding partners (Wittig et al., 2021).

5.3.4 OXR1 as a future therapeutic target in TDP-43 proteinopathies

Perturbations in protein homeostasis and subsequent protein misfolding and aggregation frequently underlie neurodegenerative disease pathogenesis (Kumar et al., 2016; Tahmaz et al., 2021). For example, TDP-43 cytoplasmic mislocalisation and aggregation is a prominent pathological feature of subsets in ALS, frontotemporal lobar degeneration (FTLD) and other neurodegenerative disorders, defining a class of TDP-43 proteinopathies (Arai et al., 2006; Neumann et al., 2006; Van Deerlin et al., 2008). Thus, modulators of protein homeostasis may prove beneficial as a therapeutic target (Kumar et al., 2016). Both Oxr1-FL and C isoforms display potential holdase activity *in vitro*, as well as modulating the chaperone activity of peroxiredoxin 2 (Prdx2), possibly through direct binding interactions (Svistunova et al., 2019). Therefore, overexpression of *Oxr1* may prove beneficial in dispersing protein aggregates *in vivo,* directly or indirectly.

Although TDP-43 aggregation was not observed in a TDP-43^{M337V} mouse model of ALS, neuronal overexpression of *Oxr1-FL* was found to rescue cytoplasmic mislocalisation of mutant TDP-43 in motor neurons and subsequently improved neuromuscular defects *in vivo* (Williamson et al., 2019). It is important to note that overexpression of *Oxr1-C* mitigated cytoplasmic aggregation of wild type and a subset of mutant Tdp-43 constructs *in vitro* under OS-induced conditions (Finelli et al., 2015). Given that Oxr1-FL, Oxr1-C and Prnp-Oxr1-FL all bind to TDP-43 *in vivo* (Williamson et al., 2019), it is possible neuron-specific overexpression of *Oxr1* may ameliorate TDP-43 aggregation in mouse models of TDP-43 proteinopathies. In order to test this hypothesis, *Prnp-Oxr1* transgenic mice could be crossed to a $(G_4C_2)_{149}$ C9orf72 repeat expansion mouse model of ALS-FTD (Cook et al., 2020) or TDP-43^{N390D} knock-in ALS mouse model (Huang et al., 2020), both of which exhibit TDP-43 aggregation histopathology. Taken together, this highlights a route to explore *OXR1*

as a putative genetic modifier of TDP-43 proteinopathies *in vivo* and how this may translate to other aggregation-prone proteins, such as FUS (Finelli et al., 2015).

5.3.5 Neuron-specific vs ubiquitous *Oxr1* overexpression: practicalities for therapeutic intervention

Transgenic neuronal overexpression of *Oxr1* has been shown to be neuroprotective in two independent mouse models of ALS and more recently in a PD mouse model (K. X. Liu et al., 2015; Williamson et al., 2019)(unpublished work). 1-methyl-4-phenyl-1,2,3,6-tetrahydropyridine (MPTP) is a potent inducer of dopaminergic neuronal cell death in the substantia nigra pars compacta (SNc), thus MPTP-treated mice serve as a valuable PD model (Ballard et al., 1985). Introducing *Oxr1* overexpression by either the *Prnp-Oxr1* transgene or via injection of an *OXR1*-overexpressing lentiviral vector in MPTP-treated mice protected against neuroinflammation and extensive cell death normally seen in the SNc, as well as rescuing the motor phenotype in the PD mouse model (unpublished work)(Jiang et al., 2019). These models further demonstrated the translational benefits of targeting *OXR1* upregulation specifically in the CNS but also ubiquitously.

In order to investigate the therapeutic potential of neuronal gene replacement therapy, constitutive *Oxr1* knockout mice or the tamoxifen-inducible adult *Oxr1* knockout mouse model could be injected with an AAV9 viral vector expressing *Oxr1* under a pan-neuronal promotor; a subsequent survival curve and analysis of neuroinflammatory, autolysosomal and apoptotic markers could be employed to assess the putative neuroprotective effects. AAV-mediated gene therapy constraining *Npc1* expression to neurons improved the lifespan of *Npc1*-deficient mice ~1.5 fold, as well as delayed both motor dysfunction and importantly, Purkinje cell loss (Chandler et al., 2017). Yet, when Chandler *et al.* (2017) employed the expression of *Npc1* under a modified human

elongation factor 1 alpha (EF1α) ubiquitous promoter, survival increased ~2.5 fold compared to *Npc1*$^{-/-}$ mice. Moreover, EF1α-*Npc1* gene delivery had more significant effects on weight, improved mobility and significantly reduced cholesterol storage in the CNS, as well as rescuing systemic pathology, such as cholesterol accumulation in the liver (Chandler et al., 2017). Given that systemic pathology has not been reported in LoF-*OXR1* patients, targeted neuron-specific *OXR1* overexpression may suffice as effective gene replacement therapy (Lin et al., 2022; Wang et al., 2019); yet from these data, targeting ubiquitous upregulation of *OXR1* is likely to have more long-term efficacy in NDs with characterised systemic pathology. The SOD1^{G93A} ALS mouse model could be crossed to a mouse line ubiquitously overexpressing *Oxr1* to compare survival to *SOD1*^{G93A}*/Prnp-Oxr1* mice (K. X. Liu et al., 2015; Oliver et al., 2011).

Targeting endogenous upregulation of short *Oxr1* isoforms is also being considered as an additional therapeutic angle. Surprisingly, mice only expressing *Oxr1-C* did not present with a neurological phenotype or significant neuropathology up to 12 months of age, indicating that the shortest *Oxr1* isoform is functional and sufficient to compensate for loss of other isoforms *in vivo* (Oliver et al., 2011). Parallel work in the Oliver group employed a dual luciferase reporter assay to conduct high throughput screening for pharmacological upregulation of *Oxr1 in vitro* (unpublished work). Stable N2a cell lines driving luminescent signal under highly conserved promoter sequences of *Oxr1-C* or *OXR1-D* were utilised to screen putative therapeutic compounds that act on short *Oxr1* isoform promoters to induce expression (unpublished work); importantly, screening libraries with compounds known to permeate the blood brain barrier were chosen, thus relevant for future *in vivo* applications.

Alternatively, further characterisation of endogenous *OXR1* regulatory elements could allow for *in vivo* transcriptional upregulation using novel approaches, such as

CRISPRa (gene-activating clustered regularly interspaced short palindromic repeats; CRISPR activation) (Becirovic, 2022). This therapeutic strategy has successfully been employed in ND mouse models such as epilepsy, congenital muscular dystrophy (MD) and retinal degeneration (Bohm et al., 2020; Colasante et al., 2020; Kemaladewi et al., 2019). Notably, CRISPRa-targeted upregulation of laminin-α1 in a laminin-α2-deficient MD mouse model significantly improved neuromuscular pathology, as well as alleviating paralysis in symptomatic animals (Kemaladewi et al., 2019), thus showing the therapeutic potential of endogenously upregulating disease-modifying genes *in vivo* to attenuate disease progression.

5.3.6 Concluding Remarks

This chapter has established that the *Prnp-Oxr1* transgene modulates expression of both lysosomal and neuroinflammatory genes *in vivo.* Surprisingly, neuron-specific overexpression of *Oxr1* over an *Oxr1*-null background is sufficient to prevent significant neuroinflammation and OS-induced cell death in CGCs at P22. Though the role of *Oxr1* in glial cells is yet to be fully characterised, these data suggest cell autonomous cerebellar degeneration and that neuronal dysfunction instigates neuroinflammation in *Oxr1* knockout mice. Aging the 'rescue' mice beyond 8 months would establish whether neurological phenotypes, such as ataxia, and neuropathology are significantly delayed or entirely absent and 'rescued'. Protein binding partner studies provided several novel candidate proteins, such as PKM2, which may contribute to the neuroprotective function of Oxr1, though further *in vitro* validation is required. Despite not clarifying the functional mechanisms of transgenic neuronal overexpression of *Oxr1*, data presented in this chapter exemplifies the therapeutic benefits of using overexpression of *Oxr1* constrained to neurons, but also considers the practicalities of ubiquitous upregulation for wider translational applications.

FINAL DISCUSSION

Chapter 6 : Final Discussion

6.1 Summary of main findings

The work presented in this thesis employed two loss-of-function *Oxr1* mouse models in tandem with *in vitro* characterisation of cellular dysfunction to further our understanding surrounding the detrimental neurological effects and neurodegeneration observed in LoF-*OXR1* patients and constitutive *Oxr1* knockout mice (Lin et al., 2022; Oliver et al., 2011; Wang et al., 2019). Additionally, a theoretical 'rescue' mouse model was generated in an attempt to delineate the protective mechanisms of neuronal transgenic expression of *Oxr1-FL,* with the aim of broadening prospects of using *OXR1* as a point of therapeutic intervention in NDs.

Chapter 3 identified significant upregulation of genes implicated in neuroinflammation and lysosomal function in the cerebellar transcriptome of P19 *Oxr1*-deleted mice, a pre/early symptomatic time point, suggesting these pathways underpin neuronal demise in this mouse model. Subsequent *in vitro* analysis demonstrated autolysosomal dysfunction in an *Oxr1*-deficient mammalian animal model for the first time. Chapter 4 utilised a tamoxifen-inducible mouse line to induce ubiquitous loss of *Oxr1* which revealed selective neuronal vulnerability of CGCs and olfactory glomeruli, as well as an essential requirement of *Oxr1* for normal neurological function in adult mice. This model provides additional scope to study parameters that were not feasible in constitutive *Oxr1* knockout mice, such as a role for *Oxr1* in neurobehaviour and putative reversible phenotypes *in vivo*. Finally, Chapter 5 demonstrated that transgenic neuronal overexpression of *Oxr1-FL* was sufficient to 'rescue' the early-onset neurological phenotype, neuroinflammation and cerebellar degeneration in *Oxr1*-null mice, suggesting cell-autonomous neuronal dysfunction is responsible for instigating the neuroinflammatory phenotype observed at P22. Furthermore, *Prnp-Oxr1-FL* expression

was sufficient to significantly delay differential expression of lysosomal and neuroinflammatory genes, although the endpoint for Hom/Tg 'rescue' mice is undetermined. A proteomic approach identified putative transgene interactors that may confer neuroprotection in a range of neurodegenerative mouse models. Building on these data, further work on Oxr1 and other TLDc proteins should not only consider their role in conferring neuroprotection against OS, but also in the context of immunomodulation and lysosome biology, key pathways that are dysregulated in a spectrum of NDs (Bonam et al., 2019; Eastman et al., 2020; Finelli & Oliver, 2017; Rama Rao & Kielian, 2015).

6.2 *Oxr1* mouse models: relevance to human patients?

6.2.1. Patients with bi-allelic loss-of-function mutations in *OXR1* (LoF-*OXR1*)

The significance of *Oxr1* in neurological function was initially discovered in an ENU mutagenesis screen for ataxic mutant mice to model human movement disorders; this preceded reports of pathogenic mutations of *OXR1* in human patients (Acevedo-Arozena et al., 2008; Oliver et al., 2011). Adult deletion of *Oxr1* critically showed that CGC vulnerability to loss of *Oxr1* is independent of developmental processes, as well as exploring emerging behavioural traits in the absence of *Oxr1* expression (Chapter 4). More broadly, disease progression was analogous to that observed in constitutively deleted *Oxr1* knockout mice, implying an overlapping requirement for *Oxr1* in the CNS at these different time points (Chapter 4)(Oliver et al., 2011).

In due course, human LoF mutations ablating expression of all *OXR1* isoforms have been reported; interestingly, these patients share key neuropathological features with constitutive and inducible *Oxr1* knockout mouse models, including rapid-onset ataxia and cerebellar abnormalities (Finelli et al., 2016; Lin et al., 2022; Oliver et al., 2011; Wang et al., 2019). Furthermore, both LoF-*OXR1* patients and constitutive *Oxr1* knockout mice show faltering growth, with the most severe case being a patient that measured in the 0.1 percentile for her weight and height at 13 years of age (Lin et al., 2022; Oliver et al., 2011; Wang et al., 2019). In *Oxr1* knockout mice, failure to thrive is observed from P14 when compared to littermate controls (Oliver et al., 2011). Analogous to this, Chapter 4 demonstrated that tamoxifen-treated mice exhibited weight loss, however inducible adult *Oxr1* knockout mice do not regain weight effectively during the post-dosing period compared to control mice, overall suggesting that loss of *OXR1* is associated with faltering growth in both humans and mice.

The fundamental similarities and differences observed between LoF-*OXR1* patients and *Oxr1* knockout mouse models used in this thesis are summarised in **Table 6-1**. Overall, these mouse models recapitulate hallmark features of LoF-*OXR1* patients; still, the absence of a clear seizure phenotype in the mouse models and lack of a neuroinflammatory response in LoF-*OXR1* patients imply human and mouse specific *OXR1* functions or differing functional compensation mechanisms, possibly through other TLDc proteins *in vivo* (**see 6.5**)(Castroflorio et al., 2021; Finelli & Oliver, 2017).

Table 6-1| Comparing clinical features of loss-of-function *OXR1* patients and *Oxr1* knockout mouse models

+ : presence of features, **-** : absence of features, **?**: uncharacterised observations, N/A: not applicable/not measured/not tested. (Lin et al., 2022; Wang et al., 2019)

	LoF-OXR1 patients	***bella/Oxr1*$^{tm1d/tm1d}$**	**Adult-induced ubiquitous *Oxr1* knockout**
Onset of phenotype	Birth/childhood	Early postnatal (~P19)	Induced - rapid
Cerebellar degeneration	**+**	**+**	**+**
Olfactory dysfunction	N/A	**-**	**+**
Neuroinflammation	CSF analysis normal/no pathology reported	**+**	**+**
Ataxia	**+**	**+**	**+**
Behaviour	Developmental delay, poor motor and social skills	N/A	Motor, memory and anxiety-related phenotype
Seizures	**+**	N/A	**?**
Faltering growth	**+**	**+**	**+**
Low weight/weight loss	**+**	**+**	**+**
Autolysosomal dysfunction	**+**	**+**	**+**
Other findings	Hypotonia, scoliosis, intellectual disability, speech delay	Paralysis	N/A

In addition to the clinical presentation of seizures in LoF-*OXR1* patients, quantitative trait loci mapping in mice identified *Oxr1* as a putative genetic modifier of seizure susceptibility (Lin et al., 2022; Schauwecker, 2013; Wang et al., 2019). Despite the absence of characteristic seizure-like aberrant neural activity and hyper-excitability in MEA recordings on primary cortical neurons derived from *Oxr1* knockout mice (Chapter 3), this cannot be ruled out in *Oxr1*-deficient mice *in vivo* (Lin et al., 2022; Wang et al., 2019). Chapter 3 discussed the impracticalities of performing EEG on constitutive *Oxr1* knockout mice due to their pre-weaning age and early lethality (Oliver et al., 2011). Loss of function mutations spanning *TBC1D24* cause epilepsy, yet *Tbc1d24*-null mice are embryonic lethal, thus were unsuitable to study the role of *Tbc1d24* in epileptogenesis (Balestrini et al., 2016; Falace et al., 2010; Mucha et al., 2017; Tona et al., 2019)(unpublished data). However, the Oliver group employed a conditional-ready *Tbc1d24* mouse line crossed to the same UBC-Cre-ERT2 mice used here to model *Tbc1d24* depletion in adult mice (unpublished data). As seen for the Oxr1 allele, the target Tbc1d24 protein levels decreased over 2-3 weeks; interestingly, EEG recordings demonstrated robust seizure events in the frontal cortex that later became more frequent, ultimately resulting in tonic-clonic seizures 4-5 weeks after tamoxifen dosing (unpublished data). Although not analogous to the constitutive disruption of TBC1D24 in disease, these data demonstrate how the tamoxifen-inducible adult knockout system offers a tractable experimental paradigm to study the role of TLDc proteins in seizure aetiology (unpublished data).

At a cellular level, autophagy dysfunction was highlighted in functional enrichment analysis of DEGs identified through RNA-seq of *OXR1*-deficient neurons differentiated from patient iPSCs (Lin et al., 2022). Thus far, data from Chapter 3 alluded to increase lysosomal biogenesis and induction of active autophagy in primary cells lacking expression of *Oxr1,* given the significant increase in LysoTracker-positive puncta and non-significant increase in fluorescent intensity from cleaved DQ-BSA peptides. Strikingly, increased levels of p62 were observed in *mtd*-deficient Drosophila brains (fly homolog of *Oxr1*), whereas a decrease in p62 was found in primary fibroblasts and cortical neurons derived from constitutive *Oxr1* knockout mice, thus suggesting differing impairments of autophagy in these model organisms (Chapter 3)(Wang et al., 2019). Therefore, further molecular characterisation of the apparent autolysosomal dysfunction is required in LoF-*OXR1* patient-derived cell types to determine the pathogenic effects of increased lysosomal biogenesis and aberrant lysosomal structures and whether these are mirrored in *Oxr1*-deleted primary cells (Lin et al., 2022; Wang et al., 2019). Taken together, this suggests that *Oxr1* knockout mouse models serve as valuable and complimentary, but not fully comparable, tools to investigate cellular dysfunction and cerebellar pathology in the context of *OXR1*-null mutations.

6.2.2. Subtle neurological phenotypes are also observed in patients with mutations in *OXR1*

Deleterious human mutations have also been identified in *OXR1* where the neurological phenotype is more subtle, such as SLI, dyslexia and hearing loss (personal communication) (Chen et al., 2017; Li et al., 2022); note, OXR1 protein levels have not been determined in these patients (**Table 1-1**). Chen *et al.* (2017) identified a novel stop-gain mutation in the first exon of *OXR1-D* in SLI patients; surprisingly, *OXR1-D* haploinsufficiency is sufficient to impair human neurodevelopment, demonstrating isoform specific requirements of TLDc proteins *in vivo* (Chen et al., 2017). Thus far, this has not been modelled *in vivo* or *in vitro*.

Over a third of *TBC1D24* mutations cause various forms of hearing loss, such as DOORS syndrome, as well as both autosomal dominant and recessive non-syndromic deafness (Azaiez et al., 2014; Balestrini et al., 2016; Mucha et al., 2017; Parzefall et al., 2020). Recently, Li *et al.* (2022) reported the first OXR1 mutation (K78R) linked to a dominant form of auditory dysfunction. Prior to this discovery, auditory brainstem responses (ABRs) had been performed on P22 constitutive *Oxr1* knockout mice at MRC Harwell to assess cochlear function and perturbations in central auditory pathways in response to acoustic stimuli (Hardisty-Hughes et al., 2010), yet significant differences were not detected in auditory thresholds compared to wild type mice (**Figure 6.1**).

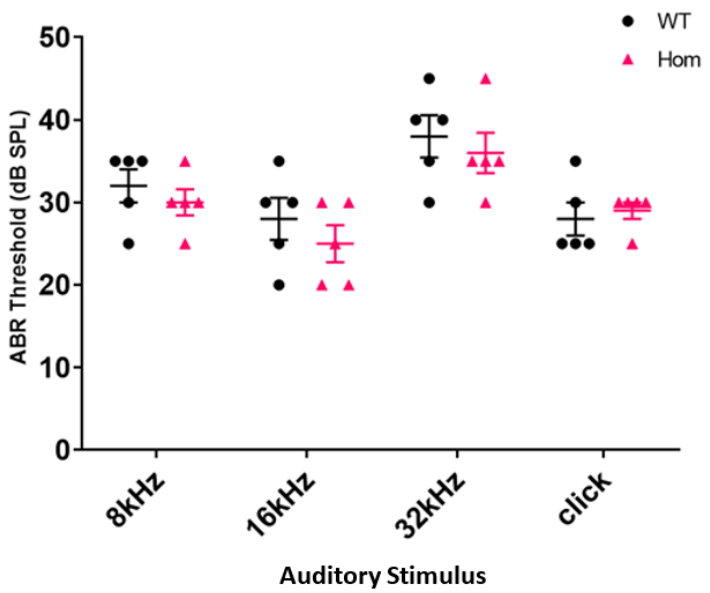

***Figure 6.1*| Auditory brainstem responses (ABR) and click box of wild type and constitutive *Oxr1* knockout mice at P22**

Auditory function assessment of P22 wild type (WT) and constitutive *Oxr1* knockout mice (Hom) at 8, 16 and 32 kHz. dB SPL: decibels of sound pressure level, kHz: kilohertz, n=5 of WT and Hom P22 mice. ABRs performed by Dr. Carlos Aguilar. Unpaired t-tests followed by Holm-Šídák correction.

Recently, whole exome sequencing of non-syndromic hearing loss patient cohorts identified pathogenic mutations in oxysterol binding protein like 2 (OSBPL2), an intracellular lipid receptor (Koh et al., 2022). Similar to constitutive *Oxr1* knockout mice and a *Tbc1d24*-haploinsufficient mouse model, *osbpl2*$^{-/-}$ mice did not exhibit hearing loss (Finelli, Aprile, et al., 2019); yet, mutant human OSBPL2^{Q53R} transgenic knock-in mice lead to cytoplasmic aggregation, autophagic impairment and cochlear degeneration, contributing to profound hearing loss (Koh et al., 2022). Analysis of differential protein binding partners of the mutant and wild type OSBPL2 identified proteins acting in pathways relating to macroautophagy, ubiquitination and endocytic recycling, suggesting novel, yet detrimental, functionality in these processes (Koh et al., 2022). It may be that hearing loss-associated mutant OXR1^{K78R} protein produces a toxic gain-of-function phenotype *in vivo* (Li et al., 2022).

Although the patient presented with deafness at 6 months, the observed early lethality in constitutive *Oxr1*-deleted mice may render this model unsuitable to assess the role of *Oxr1* in the auditory system, particularly as maturation of the auditory pathway is not established until P21 in mice (Carlson & Avraham, 2022; Li et al., 2022; Oliver et al., 2011); to circumvent this caveat, terminal ABRs could be performed on end-stage adult-induced *Oxr1* knockout mice (Hardisty-Hughes et al., 2010). RNA-seq identified robust expression of *Oxr1* in the mouse cochlear, therefore one approach to study the role of *Oxr1* in the auditory system would be to cross conditional-ready *Oxr1*$^{tm1c/tm1c}$ mice to cochlear-specific Cre-driver lines, such as *Myo15-Cre* (Caberlotto et al., 2011; Orvis et al., 2021).

In light of these considerations regarding the role of TLDc proteins in auditory function, it must also be noted that a recent mouse model of a deafness-causing pathogenic variant in *TBC1D24* did not present with auditory dysfunction (Tona et al., 2020). The authors reasoned that differential spatial expression of *TBC1D24* in the inner ear may account for the observed differences in pathology between humans and mice (Tona et al., 2020), highlighting challenges of using mouse models to infer the role of genes in human auditory function [reviewed in (Carlson & Avraham, 2022)].

6.3 TLDc proteins *in vivo*: modulators of v-ATPase assembly and function

6.3.1 TLDc proteins interact with v-ATPase subunits *in vivo*

Recent literature has highlighted a role for TLDc domain-containing proteins in v-ATPase assembly and function through direct protein-protein interactions (Arnaud-Arnould et al., 2021; Eaton, Brown, et al., 2021; Tan et al., 2022). The v-ATPase holoenzyme comprises of membrane-bound (V_0) and cytosolic (V_1) multimeric domains that reversibly disassemble; this dynamic process relies on a number of critical assembly factors to regulate v-ATPase function in maintaining intracellular pH homeostasis and organelle acidification (Forgac, 2007; Mindell, 2012). Crucially, mutations in v-ATPase subunit encoding genes (e.g. *ATP6V1A, ATP6V1B2*) cause a range of neurodevelopmental phenotypes, including epilepsy, intellectual disability, DOORS and hearing loss, implicating v-ATPase assembly and activity in neurological function (Beauregard-Lacroix et al., 2021; Fassio et al., 2018; Inuzuka et al., 2020). Moreover, deleterious mutations in assembly factors, such as v-ATPase assembly integral membrane proteins (e.g. VMA21) and ATPase H+ transporting accessory proteins (ATP6AP1, ATP6AP2), have been linked to impaired lysosomal function and autophagy defects *in vivo*; interestingly, some probands exhibit neurological dysfunction, including ataxia, epilepsy and intellectual disability (Cannata Serio et al., 2020; Eaton, Merkulova, et al., 2021; Ramachandran et al., 2013; Rujano et al., 2017). Given the significant overlap in clinical features between patients with mutations in v-ATPase subunits, assembly factors, and LoF-*OXR1* patients, as well as recent protein interaction data, one could hypothesise that loss of *OXR1* leads to aberrant v-ATPase function.

6.3.2 *Oxr1* and autolysosomal function

In *Oxr1*-deficient cerebellar tissue and primary cells, Western blotting of key autophagy markers, p62 and LC3, suggested increased autophagic flux (Chapter 3 and 4). Further *in vitro* characterisation of the putative autolysosomal phenotype revealed increased lysosomal biogenesis and autophagy degradation using a combination of LysoTracker and DQ-BSA in primary *Oxr1* knockout cells (Chapter 3). Similar to LoF-*OXR1* patient fibroblasts, membranous whirls were identified in constitutive *Oxr1* knockout cerebellar TEM images, thus supporting the hypothesis that loss of *Oxr1* leads to lysosomal dysfunction and impaired autophagy (Chapter 3)(Mao et al., 2019; Wang et al., 2019).

Crucially, consistent with *in vitro* biochemical studies, cryoelectron microscopy (cryo-EM) data demonstrated that Oxr1 binds to the cytosolic V_1 domain and promotes v-ATPase complex disassociation (Eaton, Brown, et al., 2021; Khan et al., 2022). Inferring from these data, loss of *Oxr1* would lead to an aberrant increase in v-ATPase complex assembly and activity, leading to increased v-ATPase-dependent lysosomal acidification and overall decrease in organelle luminal pH (Eaton, Merkulova, et al., 2021; Forgac, 2007; Khan et al., 2022; Mindell, 2012). To assess this directly, LysoSensor staining of primary cells derived from constitutive *Oxr1* knockout mice and LoF-*OXR1* patients would determine whether altered lysosomal acidification is observed in these cellular models to infer how deletion of *Oxr1* influences the dynamics endo-lysosomal function and intracellular trafficking pathways (Fassio et al., 2018).

Khan *et al.* (2022) modelled the role of Oxr1 in v-ATPase complex disassembly *in vitro,* thus whether this is an accurate model of Oxr1 functionality *in vivo* remains to be determined. To evaluate whether loss of *Oxr1* causes increased v-ATPase association *in vivo*, subcellular fractionation of cerebellar tissue and primary neuronal cell types, followed by immunoblotting of v-ATPase subunits could determine differential membrane

association of cytosolic V_1 domains; this method has been successfully employed to demonstrate the role of Ncoa7 in v-ATPase holoenzyme assembly in mouse brain tissue (Castroflorio et al., 2021).

Increased lysosomal biogenesis, coupled with upregulation of lysosomal enzymes, has been described as a compensatory mechanism for impaired lysosomal degradation and autophagy in LSD mouse models (Alam et al., 2012; Brandenstein et al., 2016; Cougnoux et al., 2020; Evers et al., 2017). Although lysosomal enzymes are significantly upregulated in P19 *Oxr1* knockout cerebellar RNA-seq data, the DQ-BSA trafficking assay did not indicate an overall reduced degradative capacity in primary cortical neurons lacking expression of *Oxr1* (Chapter 3). Overall, it is unclear whether lysosomal degradation deficits are present in *Oxr1* mouse models, such as incomplete degradation and atypical cleavage products of proteins or other substrates. Future work should consider conducting cathepsin activity or β-hexosaminidase enzymatic assays to further characterise any putative perturbations of lysosomal enzyme activity, given that there is likely disruption to lysosomal pH in *Oxr1*-deficient cells (Brandenstein et al., 2016; Kubisch et al., 2014).

Perhaps somewhat surprisingly, neuronal overexpression of *Oxr1-FL* in constitutive *Oxr1* knockout mice 'rescues' expression of lysosomal genes, such as *HexB* and lysosomal cathepsins, suggesting restored autolysosomal function *in vivo* (Chapter 5). It is plausible that the *Prnp-Oxr1*-driven protein is sufficient to restore regulation of v-ATPase complex reversible disassembly in neuronal cell types through direct protein-protein interactions with v-ATPase subunits (Eaton, Brown, et al., 2021; Khan et al., 2022). Furthermore, as this interaction is mediated by the TLDc domain, this may explain why expression of *Oxr1-C* is sufficient to prevent a severe neurological phenotype in mice lacking expression of *Oxr1-FL* isoforms (Eaton, Brown, et al., 2021; Oliver et al., 2011; Yang et al., 2020). In contrast to this hypothesis, the Prnp-Oxr1-HA transgene did not pulldown v-ATPase subunits in

"rescue" and control mouse brain lysates, although only a select number of gel protein bands were chosen to send for MS analysis (Chapter 5). However, the putative v-ATPase:Prnp-Oxr1 interaction may not be stable enough to elute under native conditions, therefore crosslinking mass spectrometry could be employed to further study protein-protein interactions *in vivo* (Wittig et al., 2021).

6.4 Role of *Oxr1* in neuroinflammation and glial cell types

6.4.1. *Oxr1* modulates neuroinflammation *in vivo*

Marked neuroinflammation is a key histopathological feature in both disease end-stage constitutive and adult *Oxr1* knockout mouse models (Chapter 3 and 4). Cerebellar RNA-seq transcriptomic analysis established that substantial upregulation of neuroinflammatory markers precedes cell death in constitutive *Oxr1*-deleted mice (Chapter 3), yet Chapter 5 established that this response is likely instigated by neuronal dysfunction *in vivo*. The exact mechanisms by which loss of *Oxr1* in neurons initiates neuroinflammation or how neuronal overexpression of *Oxr1* attenuates a neuroinflammatory response in ND mouse models remains to be defined (Chapter 5) (K. X. Liu et al., 2015; Williamson et al., 2019), though *Oxr1* is thought to regulate inflammatory mediators, such as STAT3 activation, protein arginine methyltransferase 5 (PRMT5) and glucose-6-phosphate isomerase (Gpi1) (Finelli, Paramo, et al., 2019; K. X. Liu et al., 2015; Yang et al., 2020).

Preliminary TEM ultrastructural analysis of P19 *Oxr1* knockout cerebellar tissue identified lipid droplets, possibly in microglia (Chapter 3); in contrast to these observations, TEM of retinae from neuronal *mtd*-knockdown, LoF-*OXR1* patient fibroblasts and *Ncoa7*-deleted primary cortical neurons did not display overt signs of lipid droplet accumulation in these different cell types (Castroflorio et al., 2021; Wang et al., 2019). Lipid-droplet

accumulating microglia (LDAM), and in part astrocytes, are unequivocally linked to neuroinflammation and neurodegeneration (Farmer et al., 2020; Ioannou et al., 2019; Marschallinger et al., 2020; Simpson & Oliver, 2020). This is of particular importance given the observed micro/astrogliosis in *Oxr1* knockout mouse models and RNA-seq GO functional enrichment data theorised a role for *Oxr1* in microglial homeostasis and activation (Chapter 3 and 4).

To clarify the presence of lipid droplets in *Oxr1* knockout mouse brain tissue and possible instigation of neuroinflammation, immunostaining with NeuN, microglia marker Iba1 and an intracellular lipid stain, such as BODIPY, could be carried out (Marschallinger et al., 2020). Moreover, putative perturbations in neuron-glial lipid transport can be explored using a lipid transfer assay on primary neuron and glial co-cultures (Ioannou et al., 2019), particularly as this pathway may contribute to the chronic activation of glial cell types in *Oxr1*-depleted mouse models. If this functional hypothesis is true, LDAM would arise in a non-cell autonomous fashion, given that neuroinflammation is not observed in mice lacking glial expression of *Oxr1* (Chapter 5).

6.4.2. A role for *Oxr1* in glial cells: future work *in vivo*

Surprisingly, neuron-specific overexpression of *Oxr1* is sufficient to negate significant neuroinflammation in constitutive *Oxr1*-deleted mice at P22 (Chapter 5), thus suggesting that cell-autonomous neuronal dysfunction instigates a neuroinflammatory response in *Oxr1*-deficient mouse models (Chapter 3 and 4). Still, glial cells remain integral to neuronal cell function and survival (Wang & Michaelis, 2010). Given the possible induction of upregulation of neuroinflammatory genes in adult 'rescue' mice with only neuron-specific expression of *Oxr1,* the role of *Oxr1* in these cell types should not be ignored (Chapter 5).

Recently, the conditional ready *Oxr1*$^{tm1c/tm1c}$ mouse has been employed to investigate the effects of induced loss of *Oxr1* in glial cells. Aldehyde dehydrogenase 1 family member L1 (*Aldh1l1)* is a folate-metabolising enzyme and has been identified as an astrocyte specific marker (Champion et al., 1994; Yang et al., 2011). *Tmem119*, also known as osteoblast induction factor (*obif*), is a type I transmembrane protein that stimulates differentiation of mesenchymal stem cells and has proven to be a robust marker of microglial populations (Kanamoto et al., 2009; Satoh et al., 2016). Thus, the established *Aldh1l1-CreERT2* and *Tmem119-CreERT2* transgenic lines have been crossed with *Oxr1*$^{tm1c/tm1c}$ mice in order to study the loss of *Oxr1* in astrocytes and microglia, respectively (Kaiser & Feng, 2019; Srinivasan et al., 2016). At as early as 12 weeks, tamoxifen treatment via oral gavage will induce a robust knockdown of Oxr1 in astrocyte and microglial populations. This work will further contribute to the understanding of whether expression of *Oxr1* is critical in immune cells of the CNS in early adulthood and the role *Oxr1* may play in neuronal-glial crosstalk. Currently, phenotypic and histopathological characterisation of these mouse lines has not taken place; of note, an obvious visible phenotype has not been observed (personal communication). Similarly, glial knockdown of *mustard*, the fly homolog of *OXR1*, showed no effect in *Drosophila*, corroborating the lack of observable phenotypes in these mouse models (Wang et al., 2019). This initially suggests that loss of *Oxr1* in glial cells does not lead to detrimental neurological effects in the absence of cell-autonomous neuronal dysfunction (Chapter 5), given that neuronal expression of *Oxr1* in preserved in these models.

The functional role of *Oxr1* in glial cells is relatively uncharacterised, however if loss of *Oxr1* in these cell types impairs glial cell function in response to neuronal damage and exogenous insults, such as seizure induction or immune-challenges, this could lead to increased susceptibility to neurodegeneration (O'Neil et al., 2022; Vogt et al., 2011; Ziegler-

Waldkirch & Meyer-Luehmann, 2018). Neuron-specific loss of *Tuberous sclerosis 1* (*Tsc1*) from the embryonic developmental stage resulted in an early-onset seizure disorder with increase seizure susceptibility, with a median survival of P35 demonstrating a significant mortality rate in the absence of neuronal *Tsc1* expression in mice (Meikle et al., 2007). Taken together, these data delineate an important role for *Tsc1* in neuronal function (Meikle et al., 2007). Interestingly, postnatal loss of *Tsc1* in astrocytes using a tamoxifen-inducible GFAP-CreER transgenic line gave rise to spontaneous seizures detected by EEG in mice dosed with tamoxifen at 2 weeks, but not 6 weeks from birth, alluding to a temporal astrocyte-specific role of *Tsc1* in seizure susceptibility (Zou et al., 2017). However, it must be noted that some Cre activation was observed in neuronal cell types making it difficult to deduce an effect of astrocyte-specific depletion of *Tsc1* and the role of *Tsc1* in astrocyte dysfunction (Zou et al., 2017). Zhao *et al.* (2018) found that induced microglial depletion of *Tsc1* in mice resulted in spontaneous seizures, however microglial specificity of the Cre-driver line was not confirmed (Zhao et al., 2018). By contrast, *Cx3cr1-CreERT2* tamoxifen-induced microglial-specific deletion of *Tsc1* was not sufficient to induce an epileptic phenotype nor lower the seizure threshold when treated with pentylenetetrazol, whilst claiming increased microglial specificity of Cre activity compared to Zhao *et al.* (2018) (B. Zhang et al., 2018). In a mouse model of global cerebral ischemia (GCI), astrocytic depletion of pyruvate kinase (PKM2) using a 'floxed' PKM2 allele and tamoxifen-inducible *Aldh1l1-CreERT2* transgenic line resulted in increased oxidative damage and hippocampal neuronal cell death compared to sham-surgery and GCI-induced control mice (Kang et al., 2023). Overall, increased neuronal vulnerability was observed in the absence of astrocytic PKM2 expression, thus demonstrating an astrocyte-specific role for PKM2 in promoting neuronal health and survival from OS-related insults (Kang et al., 2023). Taken together, these examples demonstrate the critical importance of characterising the glial cell type-specific

role of genes to elucidate their contribution to perturbations in neuronal-glial interactions and selective neuronal vulnerability.

Given that glial cells are integral to ROS production and OS response (Bernaus et al., 2020; Farmer et al., 2020; Ioannou et al., 2019; Marschallinger et al., 2020; Simpson & Oliver, 2020; Zhu et al., 2022), one hypothesis is that loss of *Oxr1* in these cell types could impair the glial cell response to OS-inducing exogenous insults and exacerbate neuronal dysfunction and cell death. In order to further understand the role of *Oxr1* in glial cells *in vivo*, inducible astrocyte and microglial-specific *Oxr1* knockout mice could be subjected to OS-related insults using methods such as GCI induction or treatment with seizure-inducing pentylenetetrazol, as demonstrated by Kang *et al.* (2023) and Zhang et al. (2018), respectively. Subsequent immunohistopathological analysis to quantify neuronal cell death will begin to inform us whether glial cell expression of *Oxr1* plays an essential role in promoting neuronal health and survival in response to oxidative damage.

6.4.3. A role for *Oxr1* in glial cells: future work *in vitro*

As previously introduced, neuroinflammation is a highly complex and dynamic process, where by glial cells can demonstrate neuroprotective properties, pathological functions, as well as transient functional changes in response to environmental cues (Bernaus et al., 2020; Vainchtein & Molofsky, 2020). Furthermore, dysregulation of glial cell reactivity through excessive release of proinflammatory signals or impaired critical functions, such as phagocytosis, can trigger a neurotoxic inflammatory response and subsequent neuronal demise (Krabbe et al., 2013; Marschallinger et al., 2020; Simpson & Oliver, 2020). Therefore, despite constitutive and adult-induced loss of *Oxr1* eliciting neuroinflammation in likely response to cell-autonomous neuronal dysfunction, the reactivity profile of these glial cells and if they contribute to the observed neurodegeneration remains undefined. Similarly, whether the decreased

neuroinflammatory pathology observed when *Oxr1-Prnp* transgenic mice were crossed to both SOD1^{G93A} and TDP-43^{M337V} mouse models of ALS is simply due to reduced neuronal dysfunction is unknown, particularly given that neuronal *Oxr1* expression is protective against OS-induced neurodegeneration (K. X. Liu et al., 2015; Oliver et al., 2011; Williamson et al., 2019); however, K. X. Liu et al. (2015) proposed *Oxr1* to be a direct immunomodulator given that dysregulation of neuroinflammatory genes observed in SOD1^{G93A} were 'rescued' in the absence of neuropathology at day 60.

As glial morphological changes in differing reactivity and functional states become increasingly more defined, characterising this feature will become a more integral part of investigating neuroinflammatory pathology during disease onset and progression (Escartin et al., 2021; Vainchtein & Molofsky, 2020). Thus, serial collection of constitutive *Oxr1* knockout and wildtype littermate control brains between P18 and end-stage P22, combined with semi-automated high-throughput image analysis, will allow for landscape plotting of glial cell response to neurodegeneration observed in the cerebellar granule cells of constitutive *Oxr1* knockout mice (Choi et al., 2022; Kugler et al., 2023; Leyh et al., 2021).

Given that a number of microglia-associated genes, such as *Trem2, Cd68* and *Ctsz*, are significantly upregulated in constitutive *Oxr1* knockout cerebellum at P19 (Chapter 3), how loss of *Oxr1* may impact microglial function warrants exploration. Importantly, lysosomal function is fundamental in effective phagocytosis and degradation of pathological substances (Kreher et al., 2021). Similarly, work presented in this thesis has suggested a putative role for *Oxr1* in the autolysosomal pathway, therefore the role of *Oxr1* in microglial phagocytosis should be investigated. pH-sensitive fluorescently labelled cargo-of-interest could be used to challenge primary microglia isolated from constitutive *Oxr1* knockout mice to explore the role of *Oxr1* in microglia function in response to different stimuli *in vitro*. For example, incubating *Oxr1*-depleted microglia with pHrodo-

labelled synaptosomes could be exploited as a model of synaptic uptake *in vitro* (Sellgren et al., 2019; Sellgren et al., 2017). Given that upregulation of C1q complement pathway genes (*C1qa, C1qb* and *C1qc*) required for synaptic organisation and pruning is observed in P19 *Oxr1* knockout cerebellar tissue (Chapter 3), alongside pathological features suggestive of aberrant synaptic pruning, such as seizures, neurodevelopmental delay and neurodegeneration, identified in LoF-*OXR1* patients, this initial experiment outlines a method to model and measure synapse elimination *in vitro* and how this may contribute to neurological phenotypes in LoF-*OXR1* patients and mouse models (Lin et al., 2022; Schartz & Tenner, 2020; Wang et al., 2019). From these observations, it could be hypothesised that loss of *Oxr1* in microglia causes dysfunctional or increased synaptic pruning. An additional pathological stimulus that could be employed is Aβ in the context of AD pathology; pH-sensitive fluorescently conjugated Aβ species have been generated, where differential microglial engulfment can be detected using techniques such as live cell imaging or flow cytometry, as demonstrated in both mouse and human microglial cell lines by Prakash *et al.* (2021).

Interestingly, Marschallinger *et al.* (2020) have also utilised similar fluorescently-labelled cargo techniques in organotypic brain slices and *in vivo*, both demonstrating significant phagocytic impairment in $BODIPY^{+}$ lipid-laden populations of microglia in aged mice, compared to $BODIPY^{-}$ microglia. TEM conducted in Chapter 3 indicated possible LDAM in P19 cerebellar tissue from *Oxr1* knockout mice, therefore characterising the phagocytic function of lipid-enriched *Oxr1*-deficient microglia *in situ* will aide definition of any functional differences in sub-populations of glial cells in the absence of *Oxr1* expression (Marschallinger et al., 2020). Furthermore, a critical parallel experiment would consist of assessing phagocytic function of LoF-OXR1 patient iPSC-derived microglia-like cells and isogenic controls, given the lack of characterised neuroinflammatory phenotype observed

in these patients, and evaluating whether this process differs between mouse-derived and human glial cells (Bassett, 2017; Sellgren et al., 2017). Overall, the work proposed here would further characterise the hypothesised role of *Oxr1* in immunomodulation and how loss of *Oxr1* may impact glial cell function *in vitro* and *in vivo*. These experiments would inform how future work considers TLDc proteins in the context of neuroinflammation and neurodegeneration.

6.5 TLDc protein redundancy *in vivo*

Increasing lines of evidence allude to TLDc protein functional redundancy, including co-expression patterns, shared function in OS-resistance and overlapping protein interacting partners, such as v-ATPase subunits, Prdx2 and Gpi1 (Eaton, Brown, et al., 2021; Finelli, Paramo, et al., 2019; Finelli et al., 2016; Svistunova et al., 2019). For example, loss of the *Ncoa7* locus is well tolerated *in vivo*, however mice lacking expression of both *Ncoa7* and *Oxr1* are not viable, suggesting an essential functional requirement for at least one of these TLDc paralogs *in vivo* (Castroflorio et al., 2021).

Interestingly, constitutive loss of *Oxr1* did not lead to differential expression of other TLDc genes in the cerebellum (Chapter 3). Similarly, no significant differences were identified in Oxr1 and Tbc1d24 at the protein level in mice lacking expression of all *Ncoa7* isoforms, suggesting that functional compensation does not require induction of TLDc protein expression (Castroflorio et al., 2021). Lack of TLDc protein co-expression and subsequent compensation was hypothesised to underpin the limited tolerance of CGCs, and in part the olfactory bulb, to loss of *Oxr1* in constitutive and adult knockout mice (Chapter 4)(Finelli et al., 2016).

TLDc protein dosage has also been demonstrated to be critical to neurological function. In support of this, adult-inducible *Oxr1* and *Tbc1d24* knockout mouse models display and show very striking phenotypic similarities to the constitutive null alleles after several weeks of reducing protein dosage (Chapter 4, unpublished data) (Oliver et al., 2011; Tona et al., 2019). Importantly, Finelli *et al.* (2016) demonstrated that an approximate 80% knockdown of Oxr1 at the protein level was required to elicit OS-sensitivity in arsenite-treated N2a cells. Consistent with these data, an acute neurological phenotype was only observed in adult *Oxr1* knockout mice at 4 weeks post-tamoxifen treatment, where Oxr1 was virtually undetectable by Western blot in all tissues (Chapter 4). From this, it could be

inferred that there is a critical threshold to *Oxr1*-depletion *in vitro* and *in vivo*; this serves of particular functional relevance to patients where *OXR1* is found to be significantly downregulated in tissue, as observed in PD and pre-eclampsia (Mary et al., 2017; Stamper et al., 2008; Zhang et al., 2005), as well as determining the effects of LoF mutations in TLDc proteins. Still, haploinsufficient *Oxr1* and *Tbc1d24* mouse models are viable, although primary neuronal cell types derived from *Tbc1d24* heterozygous mice display increased OS-sensitivity, impaired endocytosis and neuronal maturation (Finelli, Aprile, et al., 2019; Oliver et al., 2011). Overall, these data suggest that there are elements of functional redundancy within the TLDc protein family and their various isoforms, independent functions are retained which contribute to the observed lethality of *Tbc1d24* and *Oxr1* knockout mouse models, but survival of *Ncoa7* mice. *C20Orf118* and *mEAK-7* are expressed at relatively low levels in the CNS; it may be that these TLDc genes play a more significant role outside of the CNS, though their functional characterisation is very much in its infancy (Finelli & Oliver, 2017; Finelli et al., 2016; Nguyen et al., 2018; Tan et al., 2022)(briefly reviewed in **1.3.4** and **1.3.5**).

Data presented in this thesis have demonstrated a presymptomatic cerebellar transcriptomic signature and disease-stage neuropathology consisting of markers of neuroinflammation, including upregulation of *Iba1, Gfap* and complement subcomponents (*C1q*) in *Oxr1* knockout mouse models (Chapter 3); critically, inflammatory markers were not detected in cells derived from LoF-*OXR1* patients (Lin et al., 2022; Wang et al., 2019). Transcriptomic analysis of purified microglia and astrocytes isolated from human and mouse cortical tissue demonstrated evident disparities in expression of *OXR1* and *NCOA7* between these two organisms (**Figure 6.2**) (Zhang et al., 2014; Zhang et al., 2016). Significantly, *NCOA7* is expressed almost 20-fold more in human microglia than in mouse (**Figure 6.2B**). From this, it could be inferred that *NCOA7* may compensate for loss of *OXR1*

in human microglia, therefore making this cell type more tolerant to non-cell autonomous neuroimmune activation in LoF-*OXR1* patients. Future work could employ a bioinformatics approach to explore the expression of *OXR1, NCOA7* and other TLDc genes in human and mouse cerebellar neuronal and glial cell types across development and early-postnatal time points using recently published single-cell and single-nuclei RNA-seq data sets (Aldinger et al., 2021; Peng et al., 2019; Sepp et al., 2021).

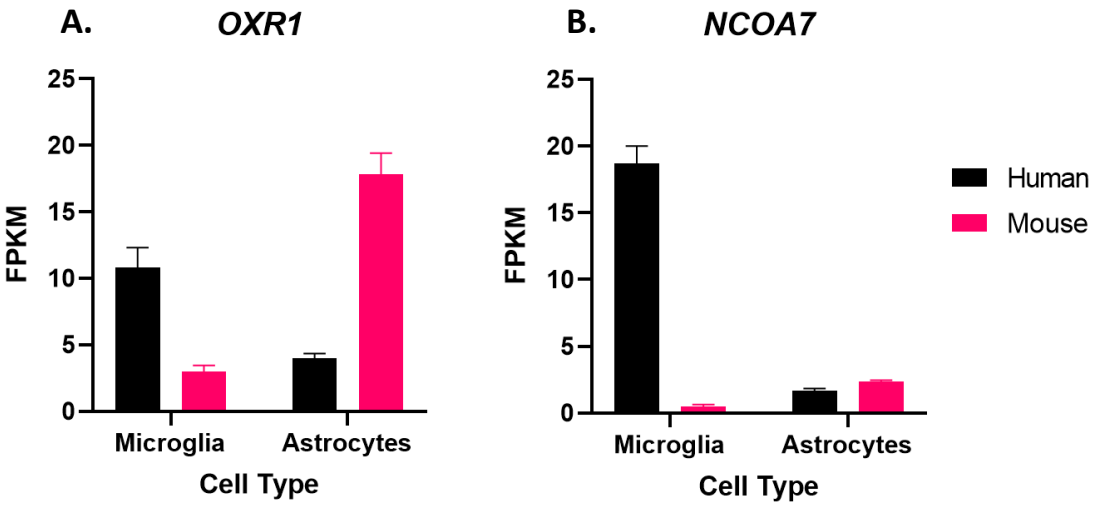

***Figure 6.2*| Comparing *Oxr1* and *Ncoa7* expression in different cell types in human and mouse brain**

Brain RNA-seq data comparing expression of (A) *Oxr1* and (B) *Ncoa7* in neurons, microglia and astrocytes in human cortical tissue and tissue isolated from mouse cerebral cortex. FPKM: fragments per kilobase of exon per million mapped fragments (Zhang et al., 2014; Zhang et al., 2016).

Of interest, neuronal overexpression of *Oxr1* using the same *Prnp*-driven transgenic allele as described in this thesis was sufficient to delay seizure-induced death in a Tbc1d24$^{R360L/R360L}$ mouse model of progressive myoclonus epilepsy with neurodegeneration**,** albeit it only by a few days (unpublished data)(Balestrini et al., 2016). In agreement with these data, antioxidant fed *Drosophila* with impaired Tbc1d24 function showed a delayed seizure and motor phenotype (unpublished data)(Luthy et al., 2019). Taken together, this would suggest that the antioxidant function of Oxr1 can partially compensate for loss of Tbc1d24. Therefore, it is possible that the development of *OXR1*-based therapeutic strategies would also benefit LoF-*TBC1D24* patients in attenuating seizure aetiology.

6.6 *OXR1* as a therapeutic target

6.6.1 *OXR1* as a therapeutic target for neurological disorders

Chapter 5 has already established the putative benefits and possible strategies of employing neuron-specific upregulation of *OXR1.* Other recent studies have also successfully employed overexpression of *OXR1* as a therapeutic strategy in models of CNS dysfunction, including PD (see **5.3.4**), retinal degeneration and spinal cord injury (SCI) (Jiang et al., 2019; Sahu et al., 2021; Zhang et al., 2021). Retinal neuronal cell types, known as photoreceptors, are highly metabolically active and vulnerable to OS, thus OS-mediated retinal degeneration is a key pathological feature in conditions such as retinitis pigmentosa (RP) and diabetic retinopathy (Calderon et al., 2017; Campochiaro & Mir, 2018; Kowluru, 2020). Current therapeutic strategies entail intravitreal injections of anti-vascular endothelial growth factor (anti-VEGF) drugs to slow down disease progression; still, repeated invasive injections are required calling for the development of a more sustainable therapeutic strategy to improve long-term prognosis (Calderon et al., 2017; Miyata et al., 2018). Under hyperoxia, *Oxr1* expression has been found to be essential for photoreceptor viability in OS-challenged mice (Natoli et al., 2008). Concurrently, AAV-mediated *OXR1* gene therapy through sub-retinal injection significantly delayed photoreceptor death by 6 weeks and prolonged retention of visual activity in a mouse model of rapid retinal degeneration (Sahu et al., 2021), ascribing *OXR1* as a potent therapeutic factor.

Although Chapter 5 set out to characterise the neuroprotective properties of transgenic expression of *Prnp-Oxr1*, the exact mechanisms of action remain unclear. Notably, the differences between endogenous and transgenic *Oxr1* localisation and promoter activity are largely undescribed. Previous therapeutic examples focus on harnessing the antioxidant capacity of *OXR1*, particularly in promoting neuronal cell survival (Sahu et al., 2021; Volkert & Crowley, 2020). However, data presented in Chapter

3 and 4 show that loss of *Oxr1* elicits a strong neuroinflammatory response, as well as disrupting autolysosomal function. Of note, LoF-OXR1 patient fibroblasts and *Drosophila* lacking expression of *OXR1* exhibit increased lysosomal numbers and aberrant accumulation of autophagosomal structures (Wang et al., 2019). Reciprocally, neuronal overexpression of *Oxr1* appears to ameliorate lysosomal dysfunction and neuroinflammatory phenotypes *in vivo* (Chapter 5) (K. X. Liu et al., 2015; Williamson et al., 2019), thus further understanding of the role *Oxr1* plays in regulating these pathways will broaden translational prospects of manipulating *OXR1* expression *in vivo*.

6.6.2 *OXR1* as a therapeutic target in non-neurological disorders

Ubiquitous loss of *Oxr1* in the adult mouse leads to a prominent neurological phenotype, as well as neuroinflammatory and neurodegenerative pathology (Chapter 4). Separate to the observed acute weight loss, the systemic effects of Oxr1-depletion were not characterised in this global knockout mouse model, therefore the endogenous role of Oxr1 in tissues outside of the CNS remains to be thoroughly explored (Chapter 4). Despite this limited knowledge, overexpression of *OXR1* outside of the CNS has been employed in an attempt to treat non-neurological disorders (Jin et al., 2022; Li, Li, et al., 2014). One such example is in a mouse model of lupus nephritis (LN), a renal disease. Li, Li, *et al.* (2014) found that intravenous administration of lentiviral-transduced mesenchymal stem cells (MSCs) overexpressing *OXR1* was sufficient to attenuate renal pathology in LN mouse models. Overexpression of *OXR1* reduced renal cell apoptosis, as well as lowering OS markers in the urine and serum of LN mouse models (Li, Li, et al., 2014). Remarkably, transplantation of *OXR1*-expressing MSCs significantly reduced expression of pro-inflammatory markers *IL-1β, IL-6* and *NFκB*, whilst upregulation of antioxidant genes *catalase* and *Gpx1* was observed in the kidneys of MSC-treated LN mice (Li, Li, et al., 2014). *OXR1* has been found to regulate expression of *catalase* and *Gpx1* in mosquitos (Jaramillo-Gutierrez et al., 2010), thus supporting an immunomodulatory and antioxidant role for *OXR1* outside of the CNS. To further characterise the endogenous role of *Oxr1* in other tissues, gene expression analysis of these identified inflammatory and OS markers could be employed to determine whether these pathways are perturbed using tissue taken from the inducible adult *Oxr1* knockout mouse model (Chapter 4). This may provide additional evidence on how *OXR1* may be exploited in treating non-neurological disorders.

6.6.3 Gene therapy prospects for LoF-*OXR1* patients: future directions

Treatment of neurodegenerative conditions is faced with the challenge of post-mitotic neuronal cell death and lack of regenerative capacity within the CNS (Kole et al., 2013; Wang & Michaelis, 2010). As previously described, patients with bi-allelic LoF-OXR1 mutations, disrupting all isoforms, present with early-onset severe neurological symptoms including ataxia, cerebellar atrophy and epilepsy (Lin et al., 2022; Wang et al., 2019); given that symptom-onset typically happens within early childhood, this establishes a narrow window of opportunity for pre/early-symptomatic therapeutic intervention to negate the observed cerebellar atrophy and neurological deficits using strategies such as gene replacement therapy (Pena et al., 2020).

Developments in access to personalised medicine and early genetic screening, such as preimplantation genetic testing and whole genome or exome sequencing at birth, may prove essential in order to successfully intercept disease progression ahead of significant, irreversible neuronal cell death (Berg et al., 2017; Murphy et al., 2020); this would be of particular importance in consanguineous families and where deleterious *OXR1* mutations have been identified in symptomatic siblings (Lin et al., 2022; Wang et al., 2019). Chapter 4 discussed employing the tamoxifen-inducible *Oxr1* knockout mouse model to explore protein dosage and reversible phenotypes *in vivo*, albeit in adult mice. In a recent phase III clinical trial to treat childhood-onset spinal muscular atrophy (SMA) type 1, a single treatment dose of survival motor neuron 1 (*SMN1*) transgene-containing AAV9 viral vector proved efficacious with improved motor function, ventilator-free breathing and increased survival in symptomatic SMA Type 1 patients (Mercuri et al., 2021). Similarly, adrenoleukodystrophy protein (ALDP)-encoding *ABCD1*-gene replacement therapy proved valuable in treating early-disease stage cerebral adrenoleukodystrophy (cALD) patients, showing a 1.7 fold increase in disease progression free survival, compared to untreated

cALD patients, up to 2 years of age (Keam, 2021; Larkin, 2022; Ma et al., 2021). Although, long-term outcomes have not been established in these patients, the overwhelmingly positive evidence highlights gene therapy as a means to improve life span, as well as preliminarily indicating reversible phenotypes observed in early-onset neurodegenerative disorders, similar to LoF-*OXR1* patients.

Complimenting publications effectively exploiting the therapeutic potential of *OXR1* in mouse, using mediums such as AAV-mediated gene delivery and lentiviral transduced mammalian cells expressing *OXR1,* data presented in this thesis supports broadly utilising *OXR1* as a gene replacement strategy (Chapter 5) (Jiang et al., 2019; Jin et al., 2022; Li, Li, et al., 2014)(Discussed more in **5.3.4**). As demonstrated by Western blotting with corresponding behavioural and histopathological analysis, Chapter 4 suggests that a minimal protein threshold of Oxr1 is required *in vivo* to negate a severe neurodegenerative phenotype, though neurological deficits may be present. Still, Chapter 5 and supplemental work conducted by the Oliver group demonstrate that significant overexpression of *Oxr1* is efficacious and does not cause overt pathology (K. X. Liu et al., 2015; Oliver et al., 2011; Williamson et al., 2019). Therefore, driving exogenous *OXR1* expression to achieve a minimal therapeutic dose is unlikely to have toxic effects and invites future *in vivo* applications to be considered.

6.6.4 Endogenous upregulation of *OXR1* as a possible alternative to gene therapy: future directions

In addition to *OXR1* expression being induced by OS and heat (Elliott & Volkert, 2004; Oliver et al., 2011), a study conducted in mosquitos revealed that gene silencing of c-Jun N-terminal kinase (JNK) through RNA interference (RNAi) significantly decreased expression of *OXR1,* as well as ROS detoxification enzymes Catalase (*CAT*) and Glutathione peroxidase (*GPX*), suggesting that JNK acts upstream of *OXR1* (Jaramillo-Gutierrez et al., 2010). Furthermore, gene knockdown by dsRNA of either *OXR1* or *JNK* lead to increased mortality in mosquitos treated with H_2O_2 as an inducer of OS, compared to control H_2O_2-treated mosquitos, suggesting that JNK is required to upregulate *OXR1* in response to OS (Jaramillo-Gutierrez et al., 2010). Similarly in silkworms, administration of a JNK inhibitor (SP600125) increased larvae sensitivity to OS; in parrarel down regulation of *OXR1* transcripts was observed in response to H_2O_2 in the presence of SP600125 further supporting the hypothesis that JNK activity is required to upregulate expression of *OXR1* (Su et al., 2017). From these initial findings, JNK activation appears to be a prospective therapeutic angle for *OXR1* upregulation, however improved spatial learning and memory behavioural phenotypes were observed in an Aβ-induced rat model of AD when treated with SP600125 (Mohammadi et al., 2016). The authors observed that autophagy was elevated in Aβ-treated rats as detected by Western blot of key autophagic markers, such as LC3II/LC3I and Beclin1, in hippocampal tissue lysate; intriguingly, SP600125 treatment in this AD-rat model significantly reduced expression of autophagic markers to levels comparable to that observed in controls animals (Mohammadi et al., 2016). Therefore, they hypothesised that JNK inhibition restored regulation of aberrant autophagy, a pathway that Oxr1 is suggested to play a role in (Chapter 3) (Mohammadi et al., 2016; Wang et al., 2019). Additionally, administration of SP600125 in an MPTP-mouse model of PD was reported to attenuate loss of dopaminergic neurons and reduce motor deficits

observed in MPTP-treated mice (Y. Wang et al., 2009). Yet, both neuronal and injected lentiviral overexpression of *OXR1* show the same therapeutic effect in MPTP-treated mice (unpublished work)(Jiang et al., 2019). Therefore, it would be imperative to understand if SP600125 leads to a reduction of Oxr1 at the mRNA and protein level in these rodent ND models and how the JNK pathway may modulate *OXR1* expression in mammalian models before considering to exploit this pathway as a therapeutic enhancer of *OXR1* expression.

To date, there are no documented compounds that upregulate endogenous *OXR1*. Chapter 5 referenced work conducted in the Oliver group to identify CNS-active compounds that modulate expression of *OXR1,* specifically attempting to target upregulation *in vitro* for downstream *in vivo* applications as an alternative to gene therapy (unpublished work). Identification of lead activating compounds that act on the promoter of *Oxr1-C/OXR1-D* in FDA-approved established compound libraries, such as the BioAscent diversity collection, will be of particular importance in the probing of compounds to validate *in vivo* (Aitken et al., 2017). Following the potential discovery of putative *Oxr1*-enhancing drug molecules and *in vitro* validation, *in vivo* efficacy can be explored using a number of established mouse models where overexpression of *Oxr1* has already been proven to be disease modifying, as observed in models of lupus nephritis, as well as PD and ALS (Jiang et al., 2019; Li, Li, et al., 2014; K. X. Liu et al., 2015; Williamson et al., 2019). Overall, the landscape for OXR1-based therapeutic strategies is in its infancy, but as the field continues to understand the cellular mechanisms of TLDc-domain containing proteins and their functional redundancy, this will only contribute to the development of more targeted and effective disease-modifying treatments.

6.7 Concluding Remarks

In summary, this thesis has offered several novel roles for Oxr1 *in vivo,* as well as highlighting autolysosomal dysfunction in the absence of *Oxr1* expression *in vitro*. Importantly, these data revealed that loss of *Oxr1* in adulthood is detrimental to neurological function, both suggesting an essential role for the gene that is independent of development, and likely cell-autonomous neuronal dysfunction driving neuroinflammation in *Oxr1* knockout mouse models. Although the neuroprotective mechanisms of *Oxr1* remain to be elucidated, overexpression of *Oxr1* is safe and well-tolerated *in vivo*; thus, *OXR1* should be considered as a viable target in the development of novel therapeutics for loss-of-function *OXR1* patients, in neurological disorders, but also potentially outside of the central nervous system. Although LoF-*OXR1* mutations are rare in the population, the serious nature of the clinical outcomes supports the use of gene replacement strategies in the future.

APPENDIX

Appendix

Appendix. 1 | Ranked list of differentially expressed genes with FDR value <0.01 when comparing *Oxr1*$^{tm1d/tm1d}$ to wild type P19 cerebellar tissue through RNA-Seq

Ranking	Gene Symbol	Gene	Log_2FC	FDR
1	*C1qa*	complement component 1, q subcomponent, alpha polypeptide	1.45	1.9E-91
2	*Mpeg1*	macrophage expressed gene 1	1.76	5.0E-83
3	*C1qb*	complement component 1, q subcomponent, beta polypeptide	1.39	1.8E-81
4	*Hexb*	hexosaminidase B	1.12	2.9E-81
5	*C1qc*	complement component 1, q subcomponent, C chain	1.44	2.2E-61
6	*Tyrobp*	TYRO protein tyrosine kinase binding protein	1.60	2.8E-58
7	*Fcrls*	Fc receptor-like S, scavenger receptor	1.62	4.2E-49
8	*Ctss*	cathepsin S	0.94	1.4E-47
9	*Cx3cr1*	chemokine (C-X3-C motif) receptor 1	0.94	1.5E-42
10	*Cd68*	CD68 antigen	1.64	2.1E-42
11	*Laptm5*	lysosomal-associated protein transmembrane 5	1.15	3.0E-42
12	*Plek*	pleckstrin	0.75	9.6E-35
13	*Ly86*	lymphocyte antigen 86	1.43	1.1E-34
14	*Ctsz*	cathepsin Z	0.84	1.5E-32
15	*Lyz2*	lysozyme 2	1.14	5.7E-28
16	*Gfap*	glial fibrillary acidic protein	0.87	5.8E-27
17	*Trem2*	triggering receptor expressed on myeloid cells 2	1.28	1.3E-26
18	*Ctsd*	cathepsin D	0.64	2.6E-25
19	*B2m*	beta-2 microglobulin	0.61	2.5E-22
20	*Olfml3*	olfactomedin-like 3	0.91	4.2E-21
21	*C4b*	complement component 4B (Chido blood group)	0.83	5.1E-21
22	*Hpgds*	hematopoietic prostaglandin D synthase	1.14	4.5E-20
23	*Adgre1*	adhesion G protein-coupled receptor E1	1.22	5.2E-20
24	*Gpr34*	G protein-coupled receptor 34	0.95	1.2E-19
25	*Csf1r*	colony stimulating factor 1 receptor	0.67	1.3E-17
26	*Lpl*	lipoprotein lipase	1.41	9.1E-16
27	*Lag3*	lymphocyte-activation gene 3	1.08	2.6E-15
28	*Grn*	granulin	0.46	1.5E-14
29	*Gusb*	glucuronidase, beta	0.51	2.2E-14
30	*Ctsl*	cathepsin L	0.30	1.3E-13
31	*Inpp5d*	inositol polyphosphate-5-phosphatase D	0.77	8.7E-13
32	*Nckap1l*	NCK associated protein 1 like	0.68	6.6E-12
33	*Lgmn*	legumain	0.27	2.0E-11
34	*P2ry13*	purinergic receptor P2Y, G-protein coupled 13	0.81	3.3E-11
35	*Chpt1*	choline phosphotransferase 1	0.35	4.3E-10
36	*Ucp2*	uncoupling protein 2 (mitochondrial, proton carrier)	0.43	9.4E-10
37	*Ctsa*	cathepsin A	0.25	6.5E-09
38	*Igf1*	insulin-like growth factor 1	0.48	1.1E-08
39	*Cyth4*	cytohesin 4	0.93	1.5E-08
40	*Abca1*	ATP-binding cassette, sub-family A (ABC1), member 1	0.27	1.6E-08
41	*mt-Nd6*	mitochondrially encoded NADH dehydrogenase 6	-0.63	1.9E-08

42	*Igfbp3*	insulin-like growth factor binding protein 3	0.38	2.4E-08
43	*P2ry12*	purinergic receptor P2Y, G-protein coupled 12	0.46	7.6E-08
44	*Cacng5*	calcium channel, voltage-dependent, gamma subunit 5	0.31	1.6E-07
45	*Tceal8*	transcription elongation factor A (SII)-like 8	0.37	2.9E-07
46	*Cd33*	CD33 antigen	0.77	6.3E-07
47	*Ctsc*	cathepsin C	0.47	6.4E-07
48	*Mylip*	myosin regulatory light chain interacting protein	0.37	1.2E-06
49	*Scai*	suppressor of cancer cell invasion	0.25	3.9E-06
50	*Gns*	glucosamine (N-acetyl)-6-sulfatase	0.22	4.7E-06
51	*Unc93b1*	unc-93 homolog B1, TLR signaling regulator	0.47	5.5E-06
52	*Hexa*	hexosaminidase A	0.34	7.3E-06
53	*Lypla1*	lysophospholipase 1	0.32	9.0E-06
54	*Igfbp5*	insulin-like growth factor binding protein 5	0.39	1.2E-05
55	*Sall1*	spalt like transcription factor 1	0.39	1.6E-05
56	*Sybu*	syntabulin (syntaxin-interacting)	-0.23	2.4E-05
57	*Luzp2*	leucine zipper protein 2	0.21	2.4E-05
58	*Anks1*	ankyrin repeat and SAM domain containing 1	-0.26	2.7E-05
59	*Mmp17*	matrix metallopeptidase 17	-0.37	2.7E-05
60	*Tob1*	transducer of ErbB-2.1	0.39	4.0E-05
61	*Paqr8*	progestin and adipoQ receptor family member VIII	0.22	4.8E-05
62	*Rnase4*	ribonuclease, RNase A family 4	0.48	4.8E-05
63	*Sema5b*	sema domain, seven thrombospondin repeats (type 1 and type 1-like), transmembrane domain (TM) and short cytoplasmic domain, (semaphorin) 5B	-0.29	5.1E-05
64	*Zcchc24*	zinc finger, CCHC domain containing 24	0.22	5.5E-05
65	*Fcgr3*	Fc receptor, IgG, low affinity III	0.62	5.9E-05
66	*Gdf10*	growth differentiation factor 10	0.30	6.3E-05
67	*Qk*	quaking, KH domain containing RNA binding	0.22	6.5E-05
68	*Id2*	inhibitor of DNA binding 2	0.24	6.9E-05
69	*Klf3*	Kruppel-like factor 3 (basic)	0.25	1.1E-04
70	*Pmp22*	peripheral myelin protein 22	0.33	1.2E-04
71	*Pabpc1*	poly(A) binding protein, cytoplasmic 1	0.18	1.7E-04
72	*Serpina3n*	serine (or cysteine) peptidase inhibitor, clade A, member 3N	0.60	1.8E-04
73	*Man2b1*	mannosidase 2, alpha B1	0.21	2.8E-04
74	*Lgals3bp*	lectin, galactoside-binding, soluble, 3 binding protein	0.46	3.3E-04
75	*Lars2*	leucyl-tRNA synthetase, mitochondrial	-0.60	3.3E-04
76	*Svep1*	sushi, von Willebrand factor type A, EGF and pentraxin domain containing 1	-0.31	3.7E-04
77	*Aqp4*	aquaporin 4	0.18	3.8E-04
78	*Svop*	SV2 related protein	-0.19	4.4E-04
79	*Gjc3*	gap junction protein, gamma 3	0.18	4.4E-04
80	*Ak3*	adenylate kinase 3	0.20	4.4E-04
81	*Cacna1i*	calcium channel, voltage-dependent, alpha 1I subunit	-0.22	4.6E-04
82	*Ctsb*	cathepsin B	0.18	4.8E-04
83	*Smg1*	SMG1 nonsense mediated mRNA decay associated PI3K related kinase	-0.22	5.1E-04
84	*Ldlr*	low density lipoprotein receptor	0.35	5.2E-04
85	*Ttyh1*	tweety family member 1	0.19	5.2E-04
86	*Gfod2*	glucose-fructose oxidoreductase domain containing 2	-0.27	5.4E-04
87	*Man2b2*	mannosidase 2, alpha B2	0.26	5.6E-04

88	*Uhrf2*	ubiquitin-like, containing PHD and RING finger domains	-0.19	6.0E-04
89	*Plekhg4*	pleckstrin homology domain containing, family G (with RhoGef domain) member 4	-0.29	6.6E-04
90	*Lss*	lanosterol synthase	0.21	6.8E-04
91	*Msi2*	musashi RNA-binding protein 2	0.22	7.6E-04
92	*A830018L16Rik*	RIKEN cDNA A830018L16 gene	0.28	8.6E-04
93	*Gm15564*	predicted gene 15564	-0.54	8.8E-04
94	*Tril*	TLR4 interactor with leucine-rich repeats [	0.19	1.0E-03
95	*Mertk*	MER proto-oncogene tyrosine kinase	0.42	1.1E-03
96	*Ecm2*	extracellular matrix protein 2, female organ and adipocyte specific	0.24	1.1E-03
97	*Ip6k1*	inositol hexaphosphate kinase 1	-0.19	1.1E-03
98	*Entpd1*	ectonucleoside triphosphate diphosphohydrolase 1	0.35	1.2E-03
99	*Anxa3*	annexin A3	0.30	1.3E-03
100	*Disp2*	dispatched RND tramsporter family member 2	-0.19	1.3E-03
101	*Vps13c*	vacuolar protein sorting 13C	-0.21	1.4E-03
102	*Arsb*	arylsulfatase B	0.15	1.5E-03
103	*Sox9*	SRY (sex determining region Y)-box 9	0.33	1.5E-03
104	*Elovl2*	elongation of very long chain fatty acids (FEN1/Elo2, SUR4/Elo3, yeast)-like 2	0.25	1.5E-03
105	*Cotl1*	coactosin-like 1 (Dictyostelium)	0.18	1.5E-03
106	*Col27a1*	collagen, type XXVII, alpha 1	-0.37	1.5E-03
107	*Atp6v1g1*	ATPase, H+ transporting, lysosomal V1 subunit G1	0.20	1.5E-03
108	*Alms1*	ALMS1, centrosome and basal body associated	-0.19	1.6E-03
109	*Armc6*	armadillo repeat containing 6	-0.23	1.6E-03
110	*Pbxip1*	pre B cell leukemia transcription factor interacting protein 1	0.23	1.7E-03
111	*Cntnap4*	contactin associated protein-like 4	-0.21	1.7E-03
112	*Lmbr1l*	limb region 1 like	-0.21	1.7E-03
113	*Atp2b4*	ATPase, Ca++ transporting, plasma membrane 4	-0.21	1.8E-03
114	*Dusp16*	dual specificity phosphatase 16	-0.29	1.8E-03
115	*Urgcp*	upregulator of cell proliferation	-0.20	2.0E-03
116	*Parm1*	prostate androgen-regulated mucin-like protein 1	-0.18	2.0E-03
117	*Mfap3l*	microfibrillar-associated protein 3-like	0.15	2.0E-03
118	*Myorg*	myogenesis regulating glycosidase (putative)	0.22	2.0E-03
119	*Ftl1*	ferritin light polypeptide 1	0.19	2.0E-03
120	*Ednrb*	endothelin receptor type B	0.20	2.0E-03
121	*Emg1*	EMG1 N1-specific pseudouridine methyltransferase	-0.21	2.0E-03
122	*Ptgr2*	prostaglandin reductase 2	0.18	2.2E-03
123	*Eif2ak2*	eukaryotic translation initiation factor 2-alpha kinase 2	0.33	2.2E-03
124	*Usp9x*	ubiquitin specific peptidase 9, X chromosome	-0.15	2.5E-03
125	*Tmem100*	transmembrane protein 100	0.31	2.5E-03
126	*Apoe*	apolipoprotein E	0.16	2.5E-03
127	*Adgrg1*	adhesion G protein-coupled receptor G1	0.21	2.5E-03
128	*Abca7*	ATP-binding cassette, sub-family A (ABC1), member 7	-0.28	2.7E-03
129	*Wipi1*	WD repeat domain, phosphoinositide interacting 1	0.20	3.0E-03
130	*Apba3*	amyloid beta (A4) precursor protein-binding, family A, member 3	-0.27	3.0E-03
131	*Zeb2*	zinc finger E-box binding homeobox 2	0.16	3.0E-03

132	*Cd9*	CD9 antigen	0.32	3.1E-03
133	*Insig1*	insulin induced gene 1	0.24	3.1E-03
134	*Mkks*	McKusick-Kaufman syndrome	-0.39	3.1E-03
135	*Sptbn4*	spectrin beta, non-erythrocytic 4	-0.15	3.1E-03
136	*Kcnip2*	Kv channel-interacting protein 2	0.48	3.5E-03
137	*Ptprt*	protein tyrosine phosphatase, receptor type, T	-0.25	3.5E-03
138	*Capn2*	calpain 2	0.16	3.5E-03
139	*Abcc8*	ATP-binding cassette, sub-family C (CFTR/MRP), member 8	-0.18	3.7E-03
140	*Creg1*	cellular repressor of E1A-stimulated genes 1	0.18	3.7E-03
141	*Stab1*	stabilin 1	0.36	3.7E-03
142	*Lgals9*	lectin, galactose binding, soluble 9	0.36	3.8E-03
143	*Schip1*	schwannomin interacting protein 1	-0.41	3.9E-03
144	*H3f3a*	H3.3 histone A	0.26	3.9E-03
145	*Stard4*	StAR-related lipid transfer (START) domain containing 4	0.27	4.3E-03
146	*Rusc2*	RUN and SH3 domain containing 2	-0.14	4.4E-03
147	*Farp2*	FERM, RhoGEF and pleckstrin domain protein 2	-0.25	4.5E-03
148	*Atg16l2*	autophagy related 16-like 2 (S. cerevisiae)	-0.27	4.5E-03
149	*St5*	DENN domain containing 2B	-0.24	4.6E-03
150	*Taf9b*	TATA-box binding protein associated factor 9B	0.20	4.7E-03
151	*Dync2h1*	dynein cytoplasmic 2 heavy chain 1	-0.17	4.8E-03
152	*Gm35339*	predicted gene, 35339	-0.32	4.8E-03
153	*Hepacam*	hepatocyte cell adhesion molecule	0.14	4.8E-03
154	*Gm2a*	GM2 ganglioside activator protein	0.15	4.8E-03
155	*Uchl1*	ubiquitin carboxy-terminal hydrolase L1	-0.23	4.9E-03
156	*Arhgdib*	Rho, GDP dissociation inhibitor (GDI) beta	0.40	5.0E-03
157	*Kdm5c*	lysine (K)-specific demethylase 5C	-0.20	5.1E-03
158	*Cmtm3*	CKLF-like MARVEL transmembrane domain containing 3	0.33	5.1E-03
159	*Prom2*	prominin 2	0.32	5.4E-03
160	*Slc37a2*	solute carrier family 37 (glycerol-3-phosphate transporter), member 2	0.58	5.4E-03
161	*Pcnp*	PEST proteolytic signal containing nuclear protein	0.19	5.4E-03
162	*Trp53i11*	transformation related protein 53 inducible protein 11	-0.20	5.6E-03
163	*Gpr162*	G protein-coupled receptor 162	-0.18	5.7E-03
164	*Mpv17l*	Mpv17 transgene, kidney disease mutant-like	0.19	5.8E-03
165	*Cnn3*	calponin 3, acidic	0.15	5.9E-03
166	*Ptma*	prothymosin alpha	0.25	6.1E-03
167	*Cul9*	cullin 9	-0.17	6.2E-03
168	*Aldh6a1*	aldehyde dehydrogenase family 6, subfamily A1	0.15	6.2E-03
169	*Rabac1*	Rab acceptor 1 (prenylated)	-0.19	6.4E-03
170	*Huwe1*	HECT, UBA and WWE domain containing 1	-0.19	6.4E-03
171	*Lrrc8b*	leucine rich repeat containing 8 family, member B	0.18	6.4E-03
172	*Lman2l*	lectin, mannose-binding 2-like	-0.25	6.5E-03
173	*Hnrnpdl*	heterogeneous nuclear ribonucleoprotein D-like	0.19	6.5E-03
174	*Rps21*	ribosomal protein S21	-0.22	6.5E-03
175	*Emc4*	ER membrane protein complex subunit 4	-0.21	6.8E-03
176	*Mdga1*	MAM domain containing glycosylphosphatidylinositol anchor 1	-0.26	6.9E-03
177	*Tmcc1*	transmembrane and coiled coil domains 1	-0.17	7.0E-03

178	*Zfp46*	zinc finger protein 46	0.23	7.2E-03
179	*Sdc4*	syndecan 4	0.25	7.3E-03
180	*Serpine2*	serine (or cysteine) peptidase inhibitor, clade E, member 2	0.22	7.6E-03
181	*Sgcb*	sarcoglycan, beta (dystrophin-associated glycoprotein)	0.18	7.9E-03
182	*Klf9*	Kruppel-like factor 9	0.20	7.9E-03
183	*Abhd8*	abhydrolase domain containing 8	-0.14	8.4E-03
184	*Ak4*	adenylate kinase 4	-0.32	8.5E-03
185	*Lactb2*	lactamase, beta 2	0.21	8.5E-03
186	*Ccdc71l*	coiled-coil domain containing 71 like	0.23	8.5E-03
187	*Hspb6*	heat shock protein, alpha-crystallin-related, B6	0.27	8.5E-03
188	*Dazap2*	DAZ associated protein 2	0.16	9.0E-03
189	*Yes1*	YES proto-oncogene 1, Src family tyrosine kinase	0.17	9.1E-03
190	*Zfp36l2*	zinc finger protein 36, C3H type-like 2	0.25	9.4E-03
191	*D630045J12Rik*	RIKEN cDNA D630045J12 gene	-0.20	9.4E-03
192	*Syn2*	synapsin II	-0.15	9.4E-03
193	*F11r*	F11 receptor	0.27	9.5E-03
194	*Mbnl2*	muscleblind like splicing factor 2	0.18	9.5E-03
195	*Tmem198*	transmembrane protein 198	-0.23	9.5E-03
196	*Sox2*	SRY (sex determining region Y)-box 2	0.30	9.6E-03
197	*Arhgap19*	Rho GTPase activating protein 19	0.40	9.7E-03

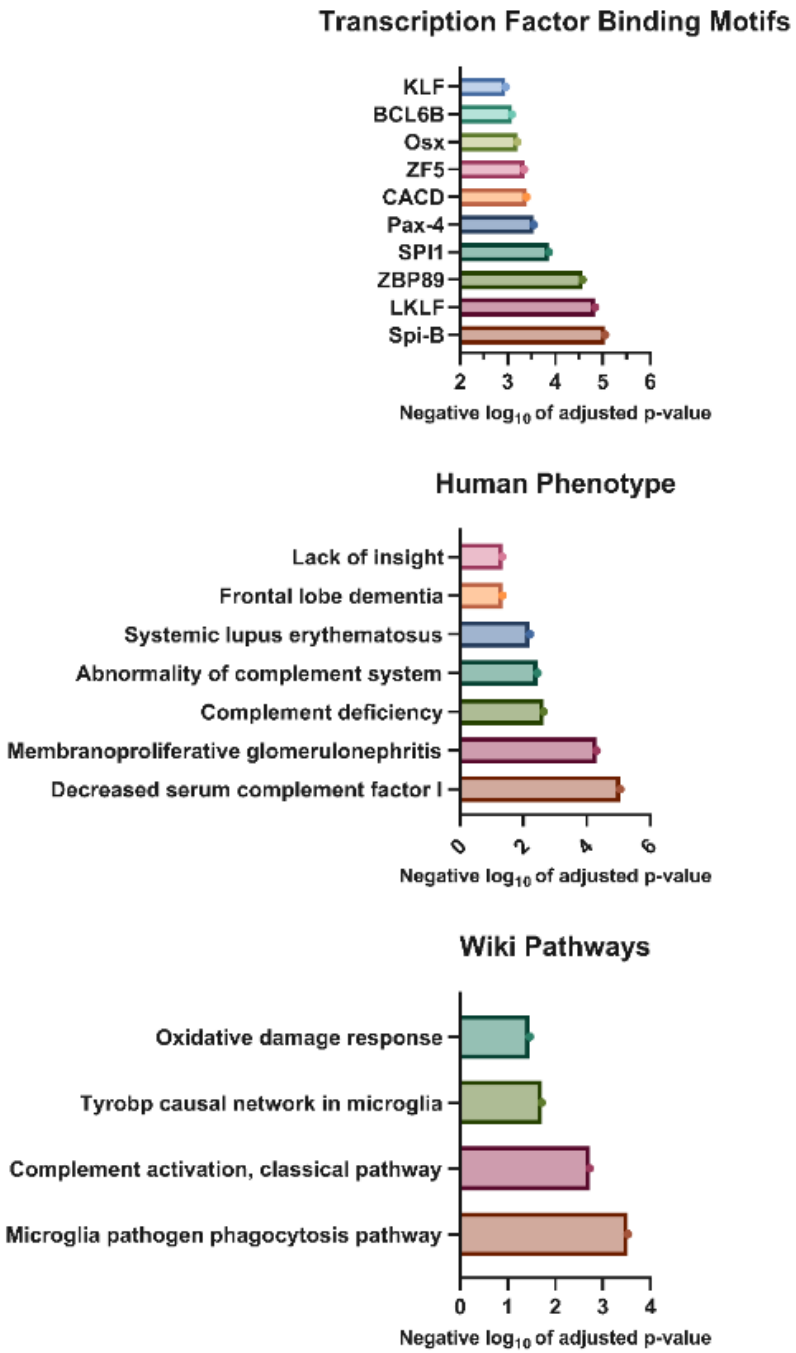

***Appendix. 2*|** Transcription binding factors, Human Phenotype and Wiki Pathways analysis of differentially expressed genes (q≤0.01) in P19 *Oxr1*

***Appendix. 3*|** Table comparing DEGs gene ontology annotations with separate groups of up and down-regulated genes

BP: Biological Processes, MF: Molecular Function, CC: Cellular Component
KEGG: Kyoto Encyclopaedia of Genes and Genomes, REAC: Reactome
TF: Transcription Factor Binding Sites, HP: Human Phenotype, WP: Wiki Pathways

		Combined List	Upregulated	Downregulated
BP	Regulation of multicellular organismal process	1.33E-13	2.07E-12	**X**
	Regulation of response to stimulus	6.56E-13	2.37E-11	**X**
	Negative regulation of multicellular organismal process	1.13E-12	6.46E-11	**X**
	Localization	1.79E-12	2.34E-08	3.73E-02
	System development	3.26E-12	5.65E-09	**X**
	Regulation of biological quality	3.33E-12	3.50E-09	**X**
	Multicellular organism development	3.88E-12	5.27E-08	1.90E-02
	Negative regulation of cellular process	5.28E-12	3.52E-12	**X**
	Synapse pruning	1.09E-11	1.23E-11	**X**
	Immune response	1.12E-11	1.26E-11	**X**
MF	Protein binding	6.19E-08	3.66E-05	
	Lipoprotein particle binding	1.09E-05	2.07E-06	
	Protein-lipid complex binding	1.09E-05	2.07E-06	
	Hydrolase activity, hydrolyzing O-glycosyl compounds	9.79E-05	8.58E-06	**X**
	Cysteine-type endopeptidase activity	2.17E-04	2.24E-04	
	G protein-coupled purinergic nucleotide receptor activity	8.07E-04	7.51E-04	
	Cysteine-type peptidase activity	1.34E-03	7.91E-03	

	Fibronectin binding	1.92E-03	1.78E-03	
	Binding	2.54E-03	2.45E-02	
	Apolipoprotein binding	2.56E-03	2.56E-03	
CC	cytoplasm	4.11E-14	2.14E-09	9.81E-04
	extracellular region	7.65E-14	2.37E-14	**X**
	lysosome	4.89E-13	5.14E-16	**X**
	lytic vacuole	4.89E-13	5.14E-16	**X**
	vacuole	5.62E-13	2.17E-15	**X**
	complement component C1q complex	9.81E-10	9.68E-10	**X**
	extracellular space	1.78E-09	9.05E-11	**X**
	membrane	6.31E-08	1.34E-05	**X**
	endomembrane system	2.33E-07	1.05E-05	**X**
	cellular anatomical entity	4.40E-07	5.51E-05	**X**
KEGG	Lysosome	1.11E-09	1.62E-10	**X**
	Glycosaminoglycan degradation	3.23E-04	1.19E-04	
	Other glycan degradation	2.32E-03	1.24E-03	
	Antigen processing and presentation	1.82E-02	1.66E-02	
REAC	Innate Immune System	4.55E-08	4.25E-08	**X**
	Immune System	4.66E-07	4.35E-07	
	Neutrophil degranulation	1.25E-04	8.86E-05	
	MHC class II antigen presentation	3.85E-04	3.09E-04	
	Trafficking and processing of endosomal TLR	7.34E-04	4.29E-04	
	Classical antibody-mediated complement activation	6.34E-03	5.92E-03	
	Creation of C4 and C2 activators	7.24E-03	6.76E-03	
	Initial triggering of complement	8.63E-03	8.06E-03	

	Hyaluronan uptake and degradation	1.03E-02	9.04E-03	
	Regulation of Complement cascade	1.25E-02	1.16E-02	
WP	Microglia pathogen phagocytosis pathway	2.98E-04	2.79E-04	**X**
	Complement activation, classical pathway	1.89E-03	1.77E-03	
	Tyrobp causal network in microglia	1.92E-02	1.79E-02	
	Oxidative damage response	3.39E-02	3.17E-02	
TF	Factor: Spi-B; motif: AAAAWGMGGAAGTWNSN	8.91E-06	2.62E-06	**X**
	Factor: LKLF; motif: GGGGTGGKSN	1.44E-05	2.03E-04	**X**
	Factor: ZBP89; motif: CCCCKCCCCCNN	2.63E-05	9.30E-04	**X**
	Factor: SPI1; motif: NNAAWGNGGAASTNNNN	1.35E-04	8.40E-05	**X**
	Factor: Pax-4; motif: NNNNNYCACCCB; match class: 1	2.84E-04	1.72E-04	**X**
	Factor: CACD; motif: CCACRCCC	4.01E-04	**X**	**X**
	Factor: ZF5; motif: NRNGNGCGCGCWN	4.49E-04	**X**	4.38E-05
	Factor: Osx; motif: CCNCCCCCNNN	6.25E-04	**X**	**X**
	Factor: BCL6B; motif: NNNNCCGCCCCWNNNN	8.18E-04	**X**	2.80E-02
	Factor: KLF; motif: GGGNGGGG	1.10E-03	8.77E-03	**X**
HP	Decreased serum complement factor I	8.41E-06	7.36E-06	**X**
	Membranoproliferative glomerulonephritis	4.71E-05	4.12E-05	
	Complement deficiency	2.17E-03	1.90E-03	
	Abnormality of complement system	3.39E-03	2.96E-03	
	Systemic lupus erythematosus	5.95E-03	5.20E-03	
	Lack of insight	4.41E-02	3.59E-02	

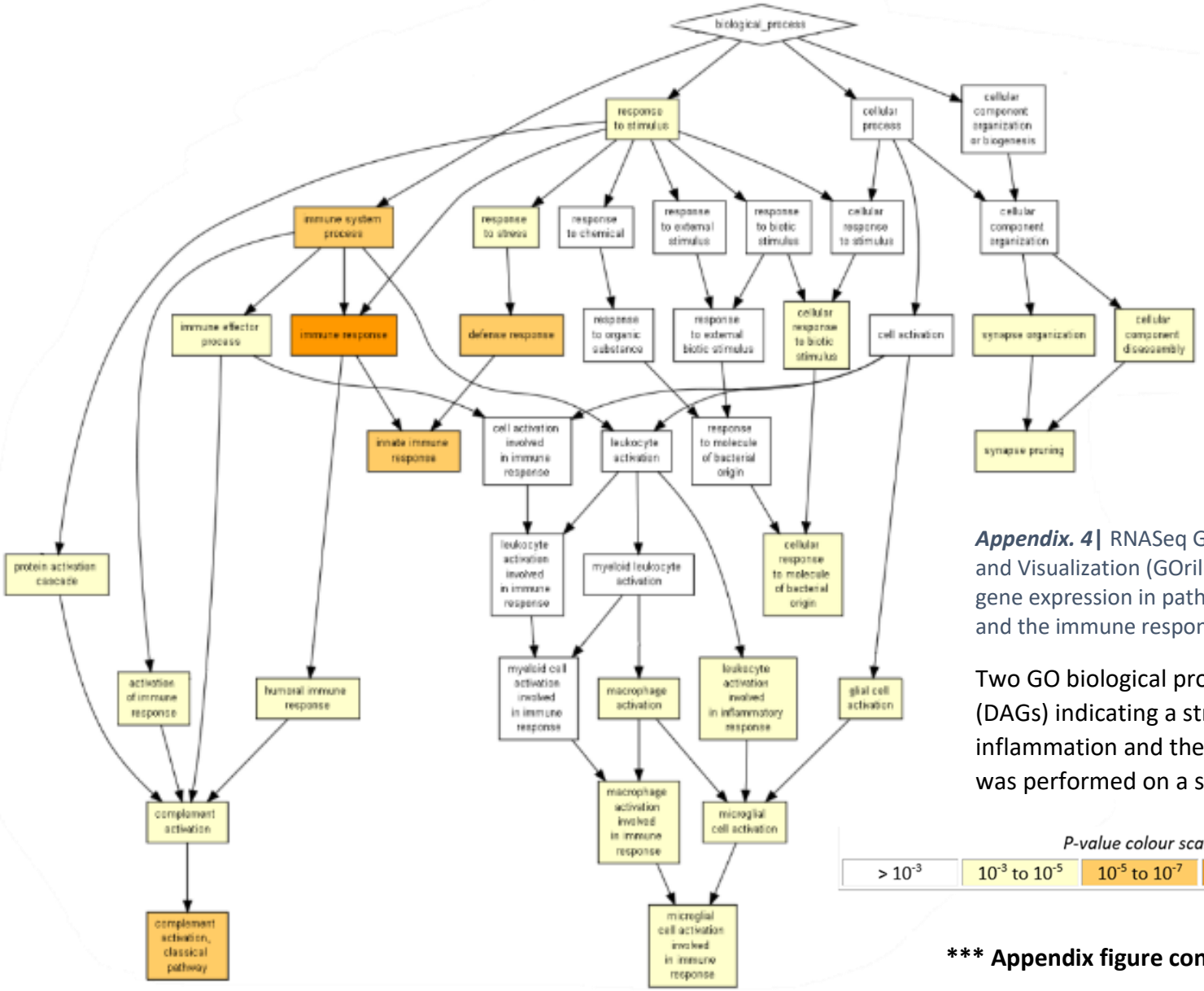

***Appendix. 4*|** RNASeq Gene Ontology Enrichment Analysis and Visualization (GOrilla) shows enrichment of differential gene expression in pathways associated with inflammation and the immune response

Two GO biological process directed acyclic graphs (DAGs) indicating a strong association with inflammation and the immune response. GO analysis was performed on a single ranked list of genes with a

***** Appendix figure continues on to next page *****

Appendix 4 continued.

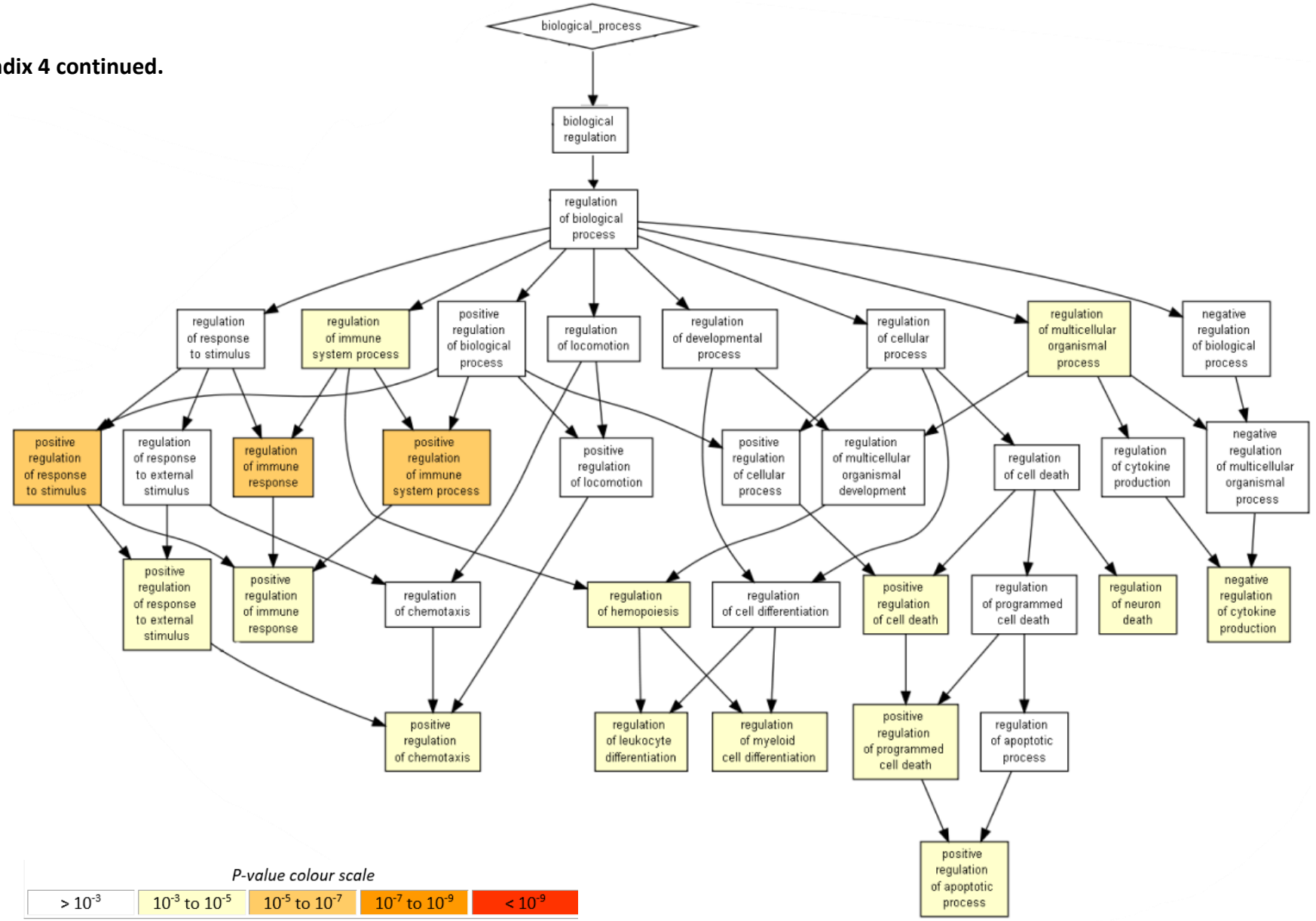

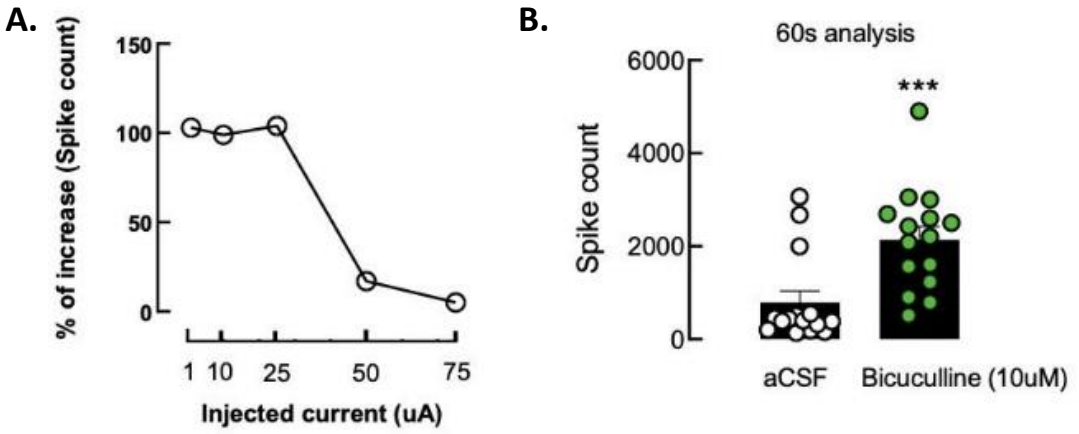

Appendix. 5| Multielectrode Array control experiments for neuronal activity

(A) Percentage increase in spike count activity, comparing before and after injected currents (µA). (B) Graphical representation of neuronal spike count activity under basal culture conditions in artificial cerebrospinal fluid (aCSF) and stimulated with 10 µM Bicuculline. Experiments and figures kindly provided by Dr Daniel Rial.

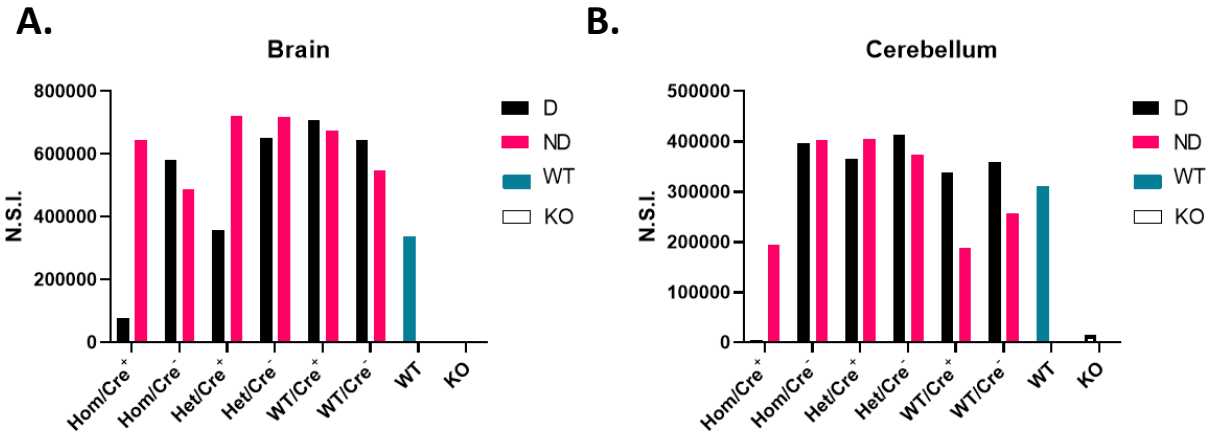

Appendix. 6| Quantification of western blots for Oxr1-FL in brain and cerebellar tissue taken from all genotypes and dose groups, 4 weeks post-tamoxifen treatment

Quantification of Oxr1-FL signal intensity in all genotype and dosing groups normalised to α-tubulin from (A) brain and (B) cerebellar tissue. Wild type (WT) and constitutive *Oxr1* knockout (KO) brain and cerebellar tissue were used as controls. n=1 per genotype and dose group. D:dosed with tamoxifen, ND: no tamoxifen treatment. N.S.I.: normalised signal intensity.

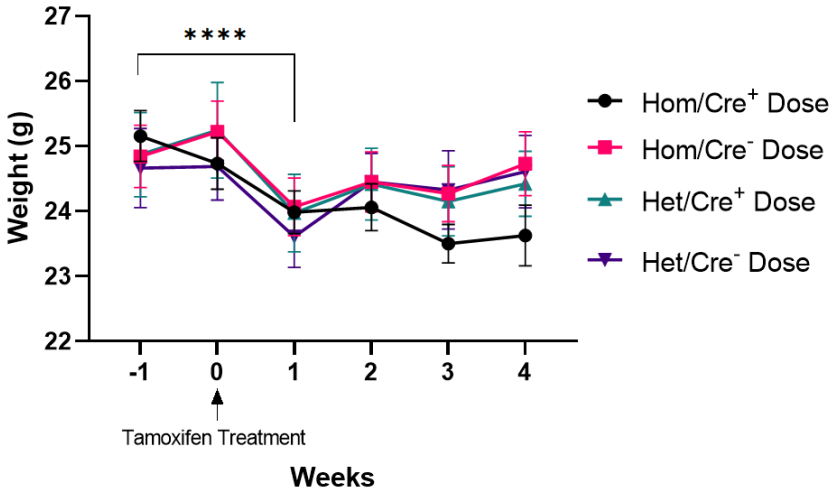

Appendix. 7| Weights of all tamoxifen-treated mice over the longitudinal study

Weekly weight (g) of Hom/Cre$^+$, Hom/Cre$^-$, Het/Cre$^+$ and Het/Cre$^-$ mice all dosed with tamoxifen for 5 consecutive days at "Week 0". Data are mean ± SEM of weight at each time point. Statistical significance was analysed by a repeated measures two-way ANOVA and Sidak multiple comparisons test. Significant time interaction: p value **** ≤0.0001. Comparison of weeks -1 and 1; Hom/Cre$^+$ p= <0.0001, Hom/Cre$^-$ p=0.0002, Het/Cre$^+$ p= 0.0331 and Het/Cre$^-$ p=0.0101.

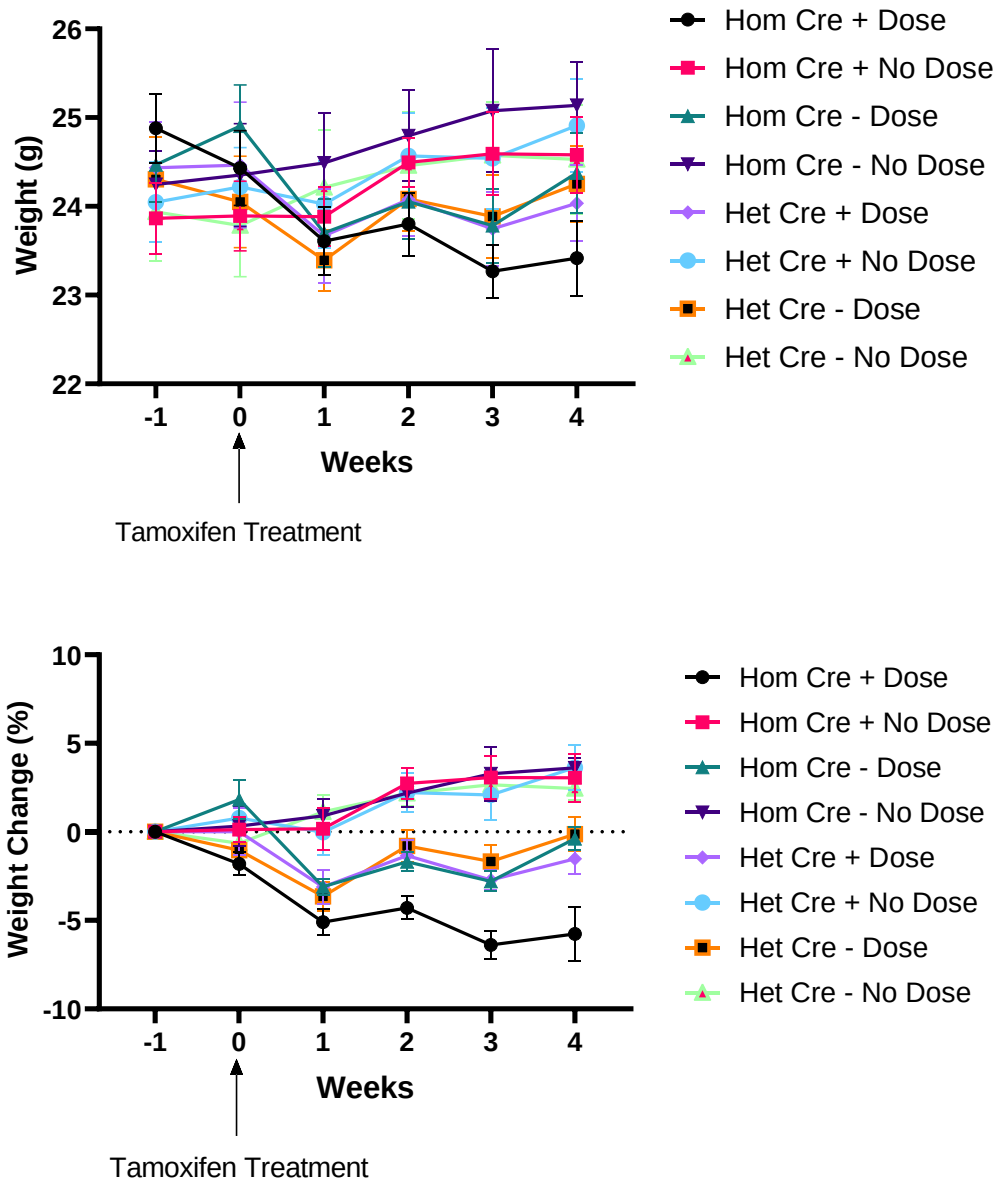

Appendix. 8| Graphical representation of weight (g) and percentage weight change (%) for all genotypes and dose groups.

Tamoxifen treatment regime was performed at Week 0.

	Hom/Cre+ Dosed			Hom/Cre+ No Dose			
Week	Mean Weight (g)	SEM	n	Mean Weight (g)	SEM	n	Hom/Cre+ Dosed vs No Dose Adjusted p-value:
-1	24.88	0.39	14	23.86	0.40	9	0.4029
0	24.43	0.42	14	23.89	0.39	9	0.9309
1	23.61	0.39	14	23.88	0.33	9	0.9954
2	23.80	0.36	14	24.50	0.28	9	0.5877
3	23.27	0.30	14	24.59	0.47	9	0.1734
4	23.42	0.42	14	24.58	0.43	9	0.3391

Appendix. 9| Body weight comparison between experimental groups, Hom/Cre+ Dosed and Hom/Cre+ No Dose mice, at each time point in longitudinal study.

Two-way repeated measures ANOVA with Šídák's multiple comparisons test. SEM: standard error of mean.

	Hom/Cre+ Dosed			
Week	Weight Change (%)	SEM	n	(Compared to Week -1) Adjusted p-value:
0	-1.82	0.65	14	0.076
1	-5.09	0.75	14	<0.0001
2	-4.30	0.65	14	<0.0001
3	-6.39	0.78	14	<0.0001
4	-5.77	1.55	14	0.013

	Hom/Cre+ No Dose			
Week	Weight Change (%)	SEM	n	(Compared to Week -1) Adjusted p-value:
0	0.13	0.69	9	>0.9999
1	0.17	1.18	9	>0.9999
2	2.74	0.89	9	0.0724
3	3.08	1.21	9	0.1621
4	3.06	1.36	9	0.246

Appendix. 10| Percentage weight change compared to initial bodyweight pre-tamoxifen time point (Week -1) in both Hom/Cre+ dosed and representative control Hom/Cre+ No Dose mice

Two-way repeated measures ANOVA with Šídák's multiple comparisons test. SEM: standard error of mean. Significant adjusted p-values highlighted in red.

PRE-TAMOXIFEN

	Hom/Cre$^+$ Dose	Hom/Cre$^+$ No Dose	Hom/Cre$^-$ Dose	Hom/Cre$^-$ No Dose	Het/Cre$^+$ Dose	Het/Cre$^+$ No Dose	Het/Cre$^-$ Dose	Het/Cre$^-$ No Dose
Hom/Cre$^+$ Dose		0.978	0.5561	0.8086	0.9995	0.9968	>0.9999	>0.9999
Hom/Cre$^+$ No Dose	0.978		0.1728	0.9931	0.9997	0.9999	0.9436	0.9969
Hom/Cre$^-$ Dose	0.5561	0.1728		0.1798	0.2877	0.1285	0.931	0.8271
Hom/Cre$^-$ No Dose	0.8086	0.9931	0.1798		0.9416	0.9415	0.748	0.9185
Het/Cre$^+$ Dose	0.9995	0.9997	0.2877	0.9416		>0.9999	0.9926	>0.9999
Het/Cre$^+$ No Dose	0.9968	0.9999	0.1285	0.9415	>0.9999		0.9798	0.9998
Het/Cre$^-$ Dose	>0.9999	0.9436	0.931	0.748	0.9926	0.9798		>0.9999
Het/Cre$^-$ No Dose	>0.9999	0.9969	0.8271	0.9185	>0.9999	0.9998	>0.9999	

2 WEEKS

	Hom/Cre$^+$ Dose	Hom/Cre$^+$ No Dose	Hom/Cre$^-$ Dose	Hom/Cre$^-$ No Dose	Het/Cre$^+$ Dose	Het/Cre$^+$ No Dose	Het/Cre$^-$ Dose	Het/Cre$^-$ No Dose
Hom/Cre$^+$ Dose		0.9462	0.9992	>0.9999	0.9881	>0.9999	0.4783	0.965
Hom/Cre$^+$ No Dose	0.9462		0.8297	0.9186	0.6902	0.9706	0.2562	>0.9999
Hom/Cre$^-$ Dose	0.9992	0.8297		>0.9999	>0.9999	>0.9999	0.954	0.8605
Hom/Cre$^-$ No Dose	>0.9999	0.9186	>0.9999		0.9968	>0.9999	0.6346	0.9419
Het/Cre$^+$ Dose	0.9881	0.6902	>0.9999	0.9968		>0.9999	0.979	0.7196
Het/Cre$^+$ No Dose	>0.9999	0.9706	>0.9999	>0.9999	>0.9999		0.9701	0.9819
Het/Cre$^-$ Dose	0.4783	0.2562	0.954	0.6346	0.979	0.9701		0.2498
Het/Cre$^-$ No Dose	0.965	>0.9999	0.8605	0.9419	0.7196	0.9819	0.2498	

4 WEEKS

	Hom/Cre$^+$ Dose	Hom/Cre$^+$ No Dose	Hom/Cre$^-$ Dose	Hom/Cre$^-$ No Dose	Het/Cre$^+$ Dose	Het/Cre$^+$ No Dose	Het/Cre$^-$ Dose	Het/Cre$^-$ No Dose
Hom/Cre$^+$ Dose		0.9055	0.9456	0.2844	0.7399	0.9683	0.2548	>0.9999
Hom/Cre$^+$ No Dose	0.9055		>0.9999	0.9026	>0.9999	>0.9999	0.8835	0.9961
Hom/Cre$^-$ Dose	0.9456	>0.9999		0.5531	0.9924	>0.9999	0.475	0.9993
Hom/Cre$^-$ No Dose	0.2844	0.9026	0.5531		0.9628	0.6044	>0.9999	0.7732
Het/Cre$^+$ Dose	0.7399	>0.9999	0.9924	0.9628		0.992	0.9523	0.9773
Het/Cre$^+$ No Dose	0.9683	>0.9999	>0.9999	0.6044	0.992		0.5431	0.9997
Het/Cre$^-$ Dose	0.2548	0.8835	0.475	>0.9999	0.9523	0.5431		0.7596
Het/Cre$^-$ No Dose	>0.9999	0.9961	0.9993	0.7732	0.9773	0.9997	0.7596	

Appendix. 11| Comparison of total distance travelled in the whole arena between all genotypes and dose groups, pre-tamoxifen, 2 weeks and 4 weeks post-tamoxifen treatment

Adjusted p-values from two-way ANOVA, followed by Tukey's multiple comparison post-hoc test, comparing each genotype and dose group at pre-tamoxifen, 2 weeks and 4 weeks post-tamoxifen treatment.

PRE-TAMOXIFEN

	Hom/Cre$^+$ Dose	Hom/Cre$^+$ No Dose	Hom/Cre$^-$ Dose	Hom/Cre$^-$ No Dose	Het/Cre$^+$ Dose	Het/Cre$^+$ No Dose	Het/Cre$^-$ Dose	Het/Cre$^-$ No Dose
Hom/Cre$^+$ Dose		0.978	0.5561	0.8086	0.9995	0.9968	>0.9999	>0.9999
Hom/Cre$^+$ No Dose	0.978		0.1728	0.9931	0.9997	0.9999	0.9436	0.9969
Hom/Cre$^-$ Dose	0.5561	0.1728		0.1798	0.2877	0.1285	0.931	0.8271
Hom/Cre$^-$ No Dose	0.8086	0.9931	0.1798		0.9416	0.9415	0.748	0.9185
Het/Cre$^+$ Dose	0.9995	0.9997	0.2877	0.9416		>0.9999	0.9926	>0.9999
Het/Cre$^+$ No Dose	0.9968	0.9999	0.1285	0.9415	>0.9999		0.9798	0.9998
Het/Cre$^-$ Dose	>0.9999	0.9436	0.931	0.748	0.9926	0.9798		>0.9999
Het/Cre$^-$ No Dose	>0.9999	0.9969	0.8271	0.9185	>0.9999	0.9998	>0.9999	

2 WEEKS

	Hom/Cre$^+$ Dose	Hom/Cre$^+$ No Dose	Hom/Cre$^-$ Dose	Hom/Cre$^-$ No Dose	Het/Cre$^+$ Dose	Het/Cre$^+$ No Dose	Het/Cre$^-$ Dose	Het/Cre$^-$ No Dose
Hom/Cre$^+$ Dose		0.9462	0.9992	>0.9999	0.9881	>0.9999	0.4783	0.965
Hom/Cre$^+$ No Dose	0.9462		0.8297	0.9186	0.6902	0.9706	0.2562	>0.9999
Hom/Cre$^-$ Dose	0.9992	0.8297		>0.9999	>0.9999	>0.9999	0.954	0.8605
Hom/Cre$^-$ No Dose	>0.9999	0.9186	>0.9999		0.9968	>0.9999	0.6346	0.9419
Het/Cre$^+$ Dose	0.9881	0.6902	>0.9999	0.9968		>0.9999	0.979	0.7196
Het/Cre$^+$ No Dose	>0.9999	0.9706	>0.9999	>0.9999	>0.9999		0.9701	0.9819
Het/Cre$^-$ Dose	0.4783	0.2562	0.954	0.6346	0.979	0.9701		0.2498
Het/Cre$^-$ No Dose	0.965	>0.9999	0.8605	0.9419	0.7196	0.9819	0.2498	

4 WEEKS

	Hom/Cre$^+$ Dose	Hom/Cre$^+$ No Dose	Hom/Cre$^-$ Dose	Hom/Cre$^-$ No Dose	Het/Cre$^+$ Dose	Het/Cre$^+$ No Dose	Het/Cre$^-$ Dose	Het/Cre$^-$ No Dose
Hom/Cre$^+$ Dose		0.9055	0.9456	0.2844	0.7399	0.9683	0.2548	>0.9999
Hom/Cre$^+$ No Dose	0.9055		>0.9999	0.9026	>0.9999	>0.9999	0.8835	0.9961
Hom/Cre$^-$ Dose	0.9456	>0.9999		0.5531	0.9924	>0.9999	0.475	0.9993
Hom/Cre$^-$ No Dose	0.2844	0.9026	0.5531		0.9628	0.6044	>0.9999	0.7732
Het/Cre$^+$ Dose	0.7399	>0.9999	0.9924	0.9628		0.992	0.9523	0.9773
Het/Cre$^+$ No Dose	0.9683	>0.9999	>0.9999	0.6044	0.992		0.5431	0.9997
Het/Cre$^-$ Dose	0.2548	0.8835	0.475	>0.9999	0.9523	0.5431		0.7596
Het/Cre$^-$ No Dose	>0.9999	0.9961	0.9993	0.7732	0.9773	0.9997	0.7596	

Appendix. 12| Comparison of total distance travelled in the centre between all genotypes and dose groups, pre-tamoxifen, 2 weeks and 4 weeks post-tamoxifen treatment

Adjusted p-values from two-way ANOVA, followed by Tukey's multiple comparison post-hoc test, comparing each genotype and dose group at pre-tamoxifen, 2 weeks and 4 weeks post-tamoxifen treatment.

PRE-TAMOXIFEN

	Hom/Cre$^+$ Dose	Hom/Cre$^+$ No Dose	Hom/Cre$^-$ Dose	Hom/Cre$^-$ No Dose	Het/Cre$^+$ Dose	Het/Cre$^+$ No Dose	Het/Cre$^-$ Dose	Het/Cre$^-$ No Dose
Hom/Cre$^+$ Dose		0.9897	0.9926	0.9955	0.8531	0.8625	0.9997	0.9995
Hom/Cre$^+$ No Dose	0.9897		>0.9999	0.9336	>0.9999	>0.9999	0.9646	0.9996
Hom/Cre$^-$ Dose	0.9926	>0.9999		0.8968	>0.9999	0.991	0.9575	>0.9999
Hom/Cre$^-$ No Dose	0.9955	0.9336	0.8968		0.629	0.6912	>0.9999	0.9617
Het/Cre$^+$ Dose	0.8531	>0.9999	>0.9999	0.629		0.9974	0.7724	0.9986
Het/Cre$^+$ No Dose	0.8625	>0.9999	0.991	0.6912	0.9974		0.7768	0.9767
Het/Cre$^-$ Dose	0.9997	0.9646	0.9575	>0.9999	0.7724	0.7768		0.9889
Het/Cre$^-$ No Dose	0.9995	0.9996	>0.9999	0.9617	0.9986	0.9767	0.9889	

2 WEEKS

	Hom/Cre$^+$ Dose	Hom/Cre$^+$ No Dose	Hom/Cre$^-$ Dose	Hom/Cre$^-$ No Dose	Het/Cre$^+$ Dose	Het/Cre$^+$ No Dose	Het/Cre$^-$ Dose	Het/Cre$^-$ No Dose
Hom/Cre$^+$ Dose		0.9979	0.4079	0.1423	0.3785	>0.9999	0.3277	0.7084
Hom/Cre$^+$ No Dose	0.9979		0.7593	0.3269	0.683	>0.9999	0.5695	0.9514
Hom/Cre$^-$ Dose	0.4079	0.7593		0.9665	>0.9999	0.8122	0.9934	0.9999
Hom/Cre$^-$ No Dose	0.1423	0.3269	0.9665		0.9979	0.4538	>0.9999	0.8793
Het/Cre$^+$ Dose	0.3785	0.683	>0.9999	0.9979		0.7373	0.9998	0.9967
Het/Cre$^+$ No Dose	>0.9999	>0.9999	0.8122	0.4538	0.7373		0.6109	0.9366
Het/Cre$^-$ Dose	0.3277	0.5695	0.9934	>0.9999	0.9998	0.6109		0.9618
Het/Cre$^-$ No Dose	0.7084	0.9514	0.9999	0.8793	0.9967	0.9366	0.9618	

4 WEEKS

	Hom/Cre$^+$ Dose	Hom/Cre$^+$ No Dose	Hom/Cre$^-$ Dose	Hom/Cre$^-$ No Dose	Het/Cre$^+$ Dose	Het/Cre$^+$ No Dose	Het/Cre$^-$ Dose	Het/Cre$^-$ No Dose
Hom/Cre$^+$ Dose		>0.9999	>0.9999	0.0183	0.6911	0.9998	0.9974	0.9839
Hom/Cre$^+$ No Dose	>0.9999		>0.9999	0.266	0.9325	>0.9999	0.9982	0.9944
Hom/Cre$^-$ Dose	>0.9999	>0.9999		0.1523	0.9351	0.9999	0.9996	0.9979
Hom/Cre$^-$ No Dose	0.0183	0.266	0.1523		0.3268	0.2265	0.2755	0.1898
Het/Cre$^+$ Dose	0.6911	0.9325	0.9351	0.3268		0.8719	0.9977	0.9983
Het/Cre$^+$ No Dose	0.9998	>0.9999	0.9999	0.2265	0.8719		0.9901	0.9776
Het/Cre$^-$ Dose	0.9974	0.9982	0.9996	0.2755	0.9977	0.9901		>0.9999
Het/Cre$^-$ No Dose	0.9839	0.9944	0.9979	0.1898	0.9983	0.9776	>0.9999	

Appendix. 13| Comparison of total distance travelled in the periphery between all genotypes and dose groups, pre-tamoxifen, 2 weeks and 4 weeks post-tamoxifen treatment

Adjusted p-values from two-way ANOVA, followed by Tukey's multiple comparison post-hoc test, comparing each genotype and dose group at pre-tamoxifen, 2 weeks and 4 weeks post-tamoxifen treatment. Green highlighted values indicate *p<0.05

REFERENCES

References

Aalinkeel, R., & Mahajan, S. D. (2016). Neuroprotective role of galectin-1 in central nervous system pathophysiology. *Neural Regen Res*, *11*(6), 896-897. https://doi.org/10.4103/1673-5374.184455

Abbah, J., Vacher, C. M., Goldstein, E. Z., Li, Z., Kundu, S., Talbot, B., Bhattacharya, S., Hashimoto-Torii, K., Wang, L., Banerjee, P., Scafidi, J., Smith, N. A., Chew, L. J., & Gallo, V. (2022). Oxidative Stress-Induced Damage to the Developing Hippocampus Is Mediated by GSK3beta. *J Neurosci*, *42*(24), 4812-4827. https://doi.org/10.1523/JNEUROSCI.2389-21.2022

Abounit, K., Scarabelli, T. M., & McCauley, R. B. (2012). Autophagy in mammalian cells. *World J Biol Chem*, *3*(1), 1-6. https://doi.org/10.4331/wjbc.v3.i1.1

Acevedo-Arozena, A., Wells, S., Potter, P., Kelly, M., Cox, R. D., & Brown, S. D. M. (2008). ENU Mutagenesis, a Way Forward to Understand Gene Function. *Annual Review of Genomics and Human Genetics*, *9*(1), 49-69. https://doi.org/10.1146/annurev.genom.9.081307.164224

Adams, D. J., & van der Weyden, L. (2008). Contemporary approaches for modifying the mouse genome. *Physiol Genomics*, *34*(3), 225-238. https://doi.org/10.1152/physiolgenomics.90242.2008

Aguiar, C. C., Almeida, A. B., Araujo, P. V., de Abreu, R. N., Chaves, E. M., do Vale, O. C., Macedo, D. S., Woods, D. J., Fonteles, M. M., & Vasconcelos, S. M. (2012). Oxidative stress and epilepsy: literature review. *Oxid Med Cell Longev*, *2012*, 795259. https://doi.org/10.1155/2012/795259

Ahmad, I., Lope-Piedrafita, S., Bi, X., Hicks, C., Yao, Y., Yu, C., Chaitkin, E., Howison, C. M., Weberg, L., Trouard, T. P., & Erickson, R. P. (2005). Allopregnanolone treatment, both as a single injection or repetitively, delays demyelination and enhances survival of Niemann-Pick C mice. *J Neurosci Res*, *82*(6), 811-821. https://doi.org/10.1002/jnr.20685

Ahmadi, M., Dufour, J. P., Seifritz, E., Mirnajafi-Zadeh, J., & Saab, B. J. (2017). The PTZ kindling mouse model of epilepsy exhibits exploratory drive deficits and aberrant activity amongst VTA dopamine neurons in both familiar and novel space. *Behav Brain Res*, *330*, 1-7. https://doi.org/10.1016/j.bbr.2017.05.025

Aitken, L., Baillie, G., Pannifer, A., Morrison, A., Jones, P. S., Smith, T. K., McElroy, S. P., & Gunn-Moore, F. J. (2017). In Vitro Assay Development and HTS of Small-Molecule Human ABAD/17beta-HSD10 Inhibitors as Therapeutics in Alzheimer's Disease. *SLAS Discov*, *22*(6), 676-685. https://doi.org/10.1177/2472555217697964

Aktary, Z., Alaee, M., & Pasdar, M. (2017). Beyond cell-cell adhesion: Plakoglobin and the regulation of tumorigenesis and metastasis. *Oncotarget*, *8*(19), 32270-32291. https://doi.org/10.18632/oncotarget.15650

Aktary, Z., & Pasdar, M. (2012). Plakoglobin: role in tumorigenesis and metastasis. *Int J Cell Biol*, *2012*, 189521. https://doi.org/10.1155/2012/189521

Alam, H., Williams, T. W., Dumas, K. J., Guo, C., Yoshina, S., Mitani, S., & Hu, P. J. (2010). EAK-7 controls development and life span by regulating nuclear DAF-16/FoxO activity. *Cell Metab*, *12*(1), 30-41. https://doi.org/10.1016/j.cmet.2010.05.004

Alam, M. S., Getz, M., Safeukui, I., Yi, S., Tamez, P., Shin, J., Velazquez, P., & Haldar, K. (2012). Genomic expression analyses reveal lysosomal, innate immunity proteins, as disease correlates in

murine models of a lysosomal storage disorder. *PLoS One*, *7*(10), e48273. https://doi.org/10.1371/journal.pone.0048273

Alcalay, R. N., Mallett, V., Vanderperre, B., Tavassoly, O., Dauvilliers, Y., Wu, R. Y. J., Ruskey, J. A., Leblond, C. S., Ambalavanan, A., Laurent, S. B., Spiegelman, D., Dionne-Laporte, A., Liong, C., Levy, O. A., Fahn, S., Waters, C., Kuo, S. H., Chung, W. K., Ford, B., . . . Gan-Or, Z. (2019). SMPD1 mutations, activity, and alpha-synuclein accumulation in Parkinson's disease. *Mov Disord*, *34*(4), 526-535. https://doi.org/10.1002/mds.27642

Aldinger, K. A., Thomson, Z., Phelps, I. G., Haldipur, P., Deng, M., Timms, A. E., Hirano, M., Santpere, G., Roco, C., Rosenberg, A. B., Lorente-Galdos, B., Gulden, F. O., O'Day, D., Overman, L. M., Lisgo, S. N., Alexandre, P., Sestan, N., Doherty, D., Dobyns, W. B., . . . Millen, K. J. (2021). Spatial and cell type transcriptional landscape of human cerebellar development. *Nat Neurosci*, *24*(8), 1163-1175. https://doi.org/10.1038/s41593-021-00872-y

Alonso-Nanclares, L., Garbelli, R., Sola, R. G., Pastor, J., Tassi, L., Spreafico, R., & DeFelipe, J. (2005). Microanatomy of the dysplastic neocortex from epileptic patients. *Brain*, *128*(Pt 1), 158-173. https://doi.org/10.1093/brain/awh331

Alsegiani, A. S., & Shah, Z. A. (2020). The role of cofilin in age-related neuroinflammation. *Neural Regen Res*, *15*(8), 1451-1459. https://doi.org/10.4103/1673-5374.274330

Altmann, A., Ryten, M., Di Nunzio, M., Ravizza, T., Tolomeo, D., Reynolds, R. H., Somani, A., Bacigaluppi, M., Iori, V., Micotti, E., Di Sapia, R., Cerovic, M., Palma, E., Ruffolo, G., Botia, J. A., Absil, J., Alhusaini, S., Alvim, M. K. M., Auvinen, P., . . . Sisodiya, S. M. (2022). A systems-level analysis highlights microglial activation as a modifying factor in common epilepsies. *Neuropathol Appl Neurobiol*, *48*(1), e12758. https://doi.org/10.1111/nan.12758

Alvarez-Aznar, A., Martinez-Corral, I., Daubel, N., Betsholtz, C., Makinen, T., & Gaengel, K. (2020). Tamoxifen-independent recombination of reporter genes limits lineage tracing and mosaic analysis using CreER(T2) lines. *Transgenic Res*, *29*(1), 53-68. https://doi.org/10.1007/s11248-019-00177-8

Alves-Filho, J. C., & Palsson-McDermott, E. M. (2016). Pyruvate Kinase M2: A Potential Target for Regulating Inflammation. *Front Immunol*, *7*, 145. https://doi.org/10.3389/fimmu.2016.00145

Ambrogini, P., Albertini, M. C., Betti, M., Galati, C., Lattanzi, D., Savelli, D., Di Palma, M., Saccomanno, S., Bartolini, D., Torquato, P., Ruffolo, G., Olivieri, F., Galli, F., Palma, E., Minelli, A., & Cuppini, R. (2018). Neurobiological Correlates of Alpha-Tocopherol Antiepileptogenic Effects and MicroRNA Expression Modulation in a Rat Model of Kainate-Induced Seizures. *Mol Neurobiol*, *55*(10), 7822-7838. https://doi.org/10.1007/s12035-018-0946-7

Andersen, P. M., & Al-Chalabi, A. (2011). Clinical genetics of amyotrophic lateral sclerosis: what do we really know? *Nat Rev Neurol*, *7*(11), 603-615. https://doi.org/10.1038/nrneurol.2011.150

Arai, T., Hasegawa, M., Akiyama, H., Ikeda, K., Nonaka, T., Mori, H., Mann, D., Tsuchiya, K., Yoshida, M., Hashizume, Y., & Oda, T. (2006). TDP-43 is a component of ubiquitin-positive tau-negative inclusions in frontotemporal lobar degeneration and amyotrophic lateral sclerosis. *Biochem Biophys Res Commun*, *351*(3), 602-611. https://doi.org/10.1016/j.bbrc.2006.10.093

Arnaud-Arnould, M., Tauziet, M., Moncorge, O., Goujon, C., & Blaise, M. (2021). Crystal structure of the TLDc domain of human NCOA7-AS. *Acta Crystallogr F Struct Biol Commun*, *77*(Pt 8), 230-237. https://doi.org/10.1107/S2053230X21006853

Ashley, C., Pastushok, L., McKenna, S., Ellison, M. J., & Xiao, W. (2002). Roles of mouse UBC13 in DNA postreplication repair and Lys63-linked ubiquitination. *Gene*, *285*(1-2), 183-191. https://doi.org/10.1016/s0378-1119(02)00409-2

Aslan, G., Afsar, B., Sag, A. A., Camkiran, V., Erden, N., Yilmaz, S., Siriopol, D., Incir, S., You, Z., Garcia, M. L., Covic, A., Cherney, D. Z. I., Johnson, R. J., & Kanbay, M. (2020). The Effect of Urine pH and Urinary Uric Acid Levels on the Development of Contrast Nephropathy. *Kidney Blood Press Res*, *45*(1), 131-141. https://doi.org/10.1159/000504547

Astell-Burt, T., Navakatikyan, M. A., & Feng, X. (2021). Behavioural change, weight loss and risk of dementia: A longitudinal study. *Prev Med*, *145*, 106386. https://doi.org/10.1016/j.ypmed.2020.106386

Atagi, Y., Liu, C. C., Painter, M. M., Chen, X. F., Verbeeck, C., Zheng, H., Li, X., Rademakers, R., Kang, S. S., Xu, H., Younkin, S., Das, P., Fryer, J. D., & Bu, G. (2015). Apolipoprotein E Is a Ligand for Triggering Receptor Expressed on Myeloid Cells 2 (TREM2). *J Biol Chem*, *290*(43), 26043-26050. https://doi.org/10.1074/jbc.M115.679043

Atalay, S., Jarocka-Karpowicz, I., & Skrzydlewska, E. (2019). Antioxidative and Anti-Inflammatory Properties of Cannabidiol. *Antioxidants (Basel)*, *9*(1). https://doi.org/10.3390/antiox9010021

Azaiez, H., Booth, K. T., Bu, F., Huygen, P., Shibata, S. B., Shearer, A. E., Kolbe, D., Meyer, N., Black-Ziegelbein, E. A., & Smith, R. J. (2014). TBC1D24 mutation causes autosomal-dominant nonsyndromic hearing loss. *Hum Mutat*, *35*(7), 819-823. https://doi.org/10.1002/humu.22557

Balestrini, S., Milh, M., Castiglioni, C., Luthy, K., Finelli, M. J., Verstreken, P., Cardon, A., Strazisar, B. G., Holder, J. L., Jr., Lesca, G., Mancardi, M. M., Poulat, A. L., Repetto, G. M., Banka, S., Bilo, L., Birkeland, L. E., Bosch, F., Brockmann, K., Cross, J. H., . . . Sisodiya, S. M. (2016). TBC1D24 genotype-phenotype correlation: Epilepsies and other neurologic features. *Neurology*, *87*(1), 77-85. https://doi.org/10.1212/WNL.0000000000002807

Ballard, P. A., Tetrud, J. W., & Langston, J. W. (1985). Permanent human parkinsonism due to 1-methyl-4-phenyl-1,2,3,6-tetrahydropyridine (MPTP): seven cases. *Neurology*, *35*(7), 949-956. https://doi.org/10.1212/wnl.35.7.949

Baltanas, F. C., Berciano, M. T., Valero, J., Gomez, C., Diaz, D., Alonso, J. R., Lafarga, M., & Weruaga, E. (2013). Differential glial activation during the degeneration of Purkinje cells and mitral cells in the PCD mutant mice. *Glia*, *61*(2), 254-272. https://doi.org/10.1002/glia.22431

Bamburg, J. R., McGough, A., & Ono, S. (1999). Putting a new twist on actin: ADF/cofilins modulate actin dynamics. *Trends Cell Biol*, *9*(9), 364-370. https://doi.org/10.1016/s0962-8924(99)01619-0

Banks, S. M. L., Medeiros, A. T., McQuillan, M., Busch, D. J., Ibarraran-Viniegra, A. S., Sousa, R., Lafer, E. M., & Morgan, J. R. (2020). Hsc70 Ameliorates the Vesicle Recycling Defects Caused by Excess alpha-Synuclein at Synapses. *eNeuro*, *7*(1). https://doi.org/10.1523/ENEURO.0448-19.2020

Barber, S. C., & Shaw, P. J. (2010). Oxidative stress in ALS: key role in motor neuron injury and therapeutic target. *Free Radic Biol Med*, *48*(5), 629-641. https://doi.org/10.1016/j.freeradbiomed.2009.11.018

Barton, G. M., & Kagan, J. C. (2009). A cell biological view of Toll-like receptor function: regulation through compartmentalization. *Nat Rev Immunol*, *9*(8), 535-542. https://doi.org/10.1038/nri2587

Bassett, A. R. (2017). Editing the genome of hiPSC with CRISPR/Cas9: disease models. *Mamm Genome*, *28*(7-8), 348-364. https://doi.org/10.1007/s00335-017-9684-9

Baune, B. T., Wiede, F., Braun, A., Golledge, J., Arolt, V., & Koerner, H. (2008). Cognitive dysfunction in mice deficient for TNF- and its receptors. *Am J Med Genet B Neuropsychiatr Genet*, *147B*(7), 1056-1064. https://doi.org/10.1002/ajmg.b.30712

Bayes, A., Collins, M. O., Croning, M. D., van de Lagemaat, L. N., Choudhary, J. S., & Grant, S. G. (2012). Comparative study of human and mouse postsynaptic proteomes finds high compositional conservation and abundance differences for key synaptic proteins. *PLoS One*, *7*(10), e46683. https://doi.org/10.1371/journal.pone.0046683

Beauregard-Lacroix, E., Pacheco-Cuellar, G., Ajeawung, N. F., Tardif, J., Dieterich, K., Dabir, T., Vind-Kezunovic, D., White, S. M., Zadori, D., Castiglioni, C., Tranebjaerg, L., Torring, P. M., Blair, E., Wisniewska, M., Camurri, M. V., van Bever, Y., Molidperee, S., Taylor, J., Dionne-Laporte, A., . . . Campeau, P. M. (2021). DOORS syndrome and a recurrent truncating ATP6V1B2 variant. *Genet Med*, *23*(1), 149-154. https://doi.org/10.1038/s41436-020-00950-9

Becirovic, E. (2022). Maybe you can turn me on: CRISPRa-based strategies for therapeutic applications. *Cell Mol Life Sci*, *79*(2), 130. https://doi.org/10.1007/s00018-022-04175-8

Beghi, E. (2020). The Epidemiology of Epilepsy. *Neuroepidemiology*, *54*(2), 185-191. https://doi.org/10.1159/000503831

Ben Haim, L., Carrillo-de Sauvage, M. A., Ceyzeriat, K., & Escartin, C. (2015). Elusive roles for reactive astrocytes in neurodegenerative diseases. *Front Cell Neurosci*, *9*, 278. https://doi.org/10.3389/fncel.2015.00278

Berdynski, M., Miszta, P., Safranow, K., Andersen, P. M., Morita, M., Filipek, S., Zekanowski, C., & Kuzma-Kozakiewicz, M. (2022). SOD1 mutations associated with amyotrophic lateral sclerosis analysis of variant severity. *Sci Rep*, *12*(1), 103. https://doi.org/10.1038/s41598-021-03891-8

Berezniuk, I., Sironi, J., Callaway, M. B., Castro, L. M., Hirata, I. Y., Ferro, E. S., & Fricker, L. D. (2010). CCP1/Nna1 functions in protein turnover in mouse brain: Implications for cell death in Purkinje cell degeneration mice. *FASEB J*, *24*(6), 1813-1823. https://doi.org/10.1096/fj.09-147942

Berg, J. S., Agrawal, P. B., Bailey, D. B., Jr., Beggs, A. H., Brenner, S. E., Brower, A. M., Cakici, J. A., Ceyhan-Birsoy, O., Chan, K., Chen, F., Currier, R. J., Dukhovny, D., Green, R. C., Harris-Wai, J., Holm, I. A., Iglesias, B., Joseph, G., Kingsmore, S. F., Koenig, B. A., . . . Wise, A. L. (2017). Newborn Sequencing in Genomic Medicine and Public Health. *Pediatrics*, *139*(2). https://doi.org/10.1542/peds.2016-2252

Bernaus, A., Blanco, S., & Sevilla, A. (2020). Glia Crosstalk in Neuroinflammatory Diseases. *Front Cell Neurosci*, *14*, 209. https://doi.org/10.3389/fncel.2020.00209

Beurel, E., & Jope, R. S. (2009). Lipopolysaccharide-induced interleukin-6 production is controlled by glycogen synthase kinase-3 and STAT3 in the brain. *J Neuroinflammation*, *6*, 9. https://doi.org/10.1186/1742-2094-6-9

Bieganowski, P., Garrison, P. N., Hodawadekar, S. C., Faye, G., Barnes, L. D., & Brenner, C. (2002). Adenosine monophosphoramidase activity of Hint and Hnt1 supports function of Kin28, Ccl1, and Tfb3. *J Biol Chem*, *277*(13), 10852-10860. https://doi.org/10.1074/jbc.M111480200

Biffi, E., Regalia, G., Menegon, A., Ferrigno, G., & Pedrocchi, A. (2013). The influence of neuronal density and maturation on network activity of hippocampal cell cultures: a methodological study. *PLoS One*, *8*(12), e83899. https://doi.org/10.1371/journal.pone.0083899

Birbeck, G. L., Meyer, A. C., & Ogunniyi, A. (2015). Nervous system disorders across the life course in resource-limited settings. *Nature*, *527*(7578), S167-171. https://doi.org/10.1038/nature16031

Bird, A. D., & Cuntz, H. (2019). Dissecting Sholl Analysis into Its Functional Components. *Cell Rep*, *27*(10), 3081-3096 e3085. https://doi.org/10.1016/j.celrep.2019.04.097

Bjorkoy, G., Lamark, T., Brech, A., Outzen, H., Perander, M., Overvatn, A., Stenmark, H., & Johansen, T. (2005). p62/SQSTM1 forms protein aggregates degraded by autophagy and has a protective effect on huntingtin-induced cell death. *J Cell Biol*, *171*(4), 603-614. https://doi.org/10.1083/jcb.200507002

Blaise, M., Alsarraf, H. M., Wong, J. E., Midtgaard, S. R., Laroche, F., Schack, L., Spaink, H., Stougaard, J., & Thirup, S. (2012). Crystal structure of the TLDc domain of oxidation resistance protein 2 from zebrafish. *Proteins*, *80*(6), 1694-1698. https://doi.org/10.1002/prot.24050

Bodzeta, A., Kahms, M., & Klingauf, J. (2017). The Presynaptic v-ATPase Reversibly Disassembles and Thereby Modulates Exocytosis but Is Not Part of the Fusion Machinery. *Cell Rep*, *20*(6), 1348-1359. https://doi.org/10.1016/j.celrep.2017.07.040

Bohm, S., Splith, V., Riedmayr, L. M., Rotzer, R. D., Gasparoni, G., Nordstrom, K. J. V., Wagner, J. E., Hinrichsmeyer, K. S., Walter, J., Wahl-Schott, C., Fenske, S., Biel, M., Michalakis, S., & Becirovic, E. (2020). A gene therapy for inherited blindness using dCas9-VPR-mediated transcriptional activation. *Sci Adv*, *6*(34), eaba5614. https://doi.org/10.1126/sciadv.aba5614

Bolivar, V. J., Caldarone, B. J., Reilly, A. A., & Flaherty, L. (2000). Habituation of activity in an open field: A survey of inbred strains and F1 hybrids. *Behav Genet*, *30*(4), 285-293. https://doi.org/10.1023/a:1026545316455

Bomben, V. C., Aiba, I., Qian, J., Mark, M. D., Herlitze, S., & Noebels, J. L. (2016). Isolated P/Q Calcium Channel Deletion in Layer VI Corticothalamic Neurons Generates Absence Epilepsy. *J Neurosci*, *36*(2), 405-418. https://doi.org/10.1523/JNEUROSCI.2555-15.2016

Bonam, S. R., Wang, F., & Muller, S. (2019). Lysosomes as a therapeutic target. *Nat Rev Drug Discov*, *18*(12), 923-948. https://doi.org/10.1038/s41573-019-0036-1

Borchelt, D. R., Davis, J., Fischer, M., Lee, M. K., Slunt, H. H., Ratovitsky, T., Regard, J., Copeland, N. G., Jenkins, N. A., Sisodia, S. S., & Price, D. L. (1996). A vector for expressing foreign genes in the brains and hearts of transgenic mice. *Genet Anal*, *13*(6), 159-163. https://doi.org/10.1016/s1050-3862(96)00167-2

Bourgognon, J. M., & Cavanagh, J. (2020). The role of cytokines in modulating learning and memory and brain plasticity. *Brain Neurosci Adv*, *4*, 2398212820979802. https://doi.org/10.1177/2398212820979802

Bowman, B. J., & Bowman, E. J. (2002). Mutations in subunit C of the vacuolar ATPase confer resistance to bafilomycin and identify a conserved antibiotic binding site. *J Biol Chem*, *277*(6), 3965-3972. https://doi.org/10.1074/jbc.M109756200

Bozzi, Y., Casarosa, S., & Caleo, M. (2012). Epilepsy as a neurodevelopmental disorder. *Front Psychiatry*, *3*, 19. https://doi.org/10.3389/fpsyt.2012.00019

Braida, D., Sacerdote, P., Panerai, A. E., Bianchi, M., Aloisi, A. M., Iosue, S., & Sala, M. (2004). Cognitive function in young and adult IL (interleukin)-6 deficient mice. *Behav Brain Res*, *153*(2), 423-429. https://doi.org/10.1016/j.bbr.2003.12.018

Brainstorm Consortium., Anttila, V., Bulik-Sullivan, B., Finucane, H. K., Walters, R. K., Bras, J., Duncan, L., Escott-Price, V., Falcone, G. J., Gormley, P., Malik, R., Patsopoulos, N. A., Ripke, S., Wei, Z., Yu, D., Lee, P. H., Turley, P., Grenier-Boley, B., Chouraki, V., . . . Murray, R. (2018). Analysis of shared heritability in common disorders of the brain. *Science*, *360*(6395). https://doi.org/10.1126/science.aap8757

Brandenstein, L., Schweizer, M., Sedlacik, J., Fiehler, J., & Storch, S. (2016). Lysosomal dysfunction and impaired autophagy in a novel mouse model deficient for the lysosomal membrane protein Cln7. *Hum Mol Genet*, *25*(4), 777-791. https://doi.org/10.1093/hmg/ddv615

Bressan, C., Pecora, A., Gagnon, D., Snapyan, M., Labrecque, S., De Koninck, P., Parent, M., & Saghatelyan, A. (2020). The dynamic interplay between ATP/ADP levels and autophagy sustain neuronal migration in vivo. *Elife*, *9*. https://doi.org/10.7554/eLife.56006

Brommage, R. (2003). Validation and calibration of DEXA body composition in mice. *Am J Physiol Endocrinol Metab*, *285*(3), E454-459. https://doi.org/10.1152/ajpendo.00470.2002

Brown, A. P., Dinger, N., & Levine, B. S. (2000). Stress produced by gavage administration in the rat. *Contemp Top Lab Anim Sci*, *39*(1), 17-21. https://www.ncbi.nlm.nih.gov/pubmed/11178310

Brown, J. W., Buell, A. K., Michaels, T. C., Meisl, G., Carozza, J., Flagmeier, P., Vendruscolo, M., Knowles, T. P., Dobson, C. M., & Galvagnion, C. (2016). beta-Synuclein suppresses both the initiation and amplification steps of alpha-synuclein aggregation via competitive binding to surfaces. *Sci Rep*, *6*, 36010. https://doi.org/10.1038/srep36010

Buckinx, A., De Bundel, D., Kooijman, R., & Smolders, I. (2021). Targeting the Ghrelin Receptor as a Novel Therapeutic Option for Epilepsy. *Biomedicines*, *10*(1). https://doi.org/10.3390/biomedicines10010053

Budzinski, K. L., Allen, R. W., Fujimoto, B. S., Kensel-Hammes, P., Belnap, D. M., Bajjalieh, S. M., & Chiu, D. T. (2009). Large structural change in isolated synaptic vesicles upon loading with neurotransmitter. *Biophys J*, *97*(9), 2577-2584. https://doi.org/10.1016/j.bpj.2009.08.032

Buendia, I., Michalska, P., Navarro, E., Gameiro, I., Egea, J., & Leon, R. (2016). Nrf2-ARE pathway: An emerging target against oxidative stress and neuroinflammation in neurodegenerative diseases. *Pharmacol Ther*, *157*, 84-104. https://doi.org/10.1016/j.pharmthera.2015.11.003

Bullitt, E. (1990). Expression of c-fos-like protein as a marker for neuronal activity following noxious stimulation in the rat. *J Comp Neurol*, *296*(4), 517-530. https://doi.org/10.1002/cne.902960402

Buxbaum, J. N., Ye, Z., Reixach, N., Friske, L., Levy, C., Das, P., Golde, T., Masliah, E., Roberts, A. R., & Bartfai, T. (2008). Transthyretin protects Alzheimer's mice from the behavioral and

biochemical effects of Abeta toxicity. *Proc Natl Acad Sci U S A*, *105*(7), 2681-2686. https://doi.org/10.1073/pnas.0712197105

Bygrave, A. M., Jahans-Price, T., Wolff, A. R., Sprengel, R., Kullmann, D. M., Bannerman, D. M., & Katzel, D. (2019). Hippocampal-prefrontal coherence mediates working memory and selective attention at distinct frequency bands and provides a causal link between schizophrenia and its risk gene GRIA1. *Transl Psychiatry*, *9*(1), 142. https://doi.org/10.1038/s41398-019-0471-0

Caberlotto, E., Michel, V., Foucher, I., Bahloul, A., Goodyear, R. J., Pepermans, E., Michalski, N., Perfettini, I., Alegria-Prevot, O., Chardenoux, S., Do Cruzeiro, M., Hardelin, J. P., Richardson, G. P., Avan, P., Weil, D., & Petit, C. (2011). Usher type 1G protein sans is a critical component of the tip-link complex, a structure controlling actin polymerization in stereocilia. *Proc Natl Acad Sci U S A*, *108*(14), 5825-5830. https://doi.org/10.1073/pnas.1017114108

Cahill, P. J., Rinella, A. S., & Bielski, R. J. (2007). Orthopaedic complications of myotubular myopathy. *J Pediatr Orthop*, *27*(1), 98-103. https://doi.org/10.1097/BPO.0b013e31802b6c73

Calcagnotto, M. E., Paredes, M. F., Tihan, T., Barbaro, N. M., & Baraban, S. C. (2005). Dysfunction of synaptic inhibition in epilepsy associated with focal cortical dysplasia. *J Neurosci*, *25*(42), 9649-9657. https://doi.org/10.1523/JNEUROSCI.2687-05.2005

Calderon, G. D., Juarez, O. H., Hernandez, G. E., Punzo, S. M., & De la Cruz, Z. D. (2017). Oxidative stress and diabetic retinopathy: development and treatment. *Eye (Lond)*, *31*(8), 1122-1130. https://doi.org/10.1038/eye.2017.64

Camby, I., Le Mercier, M., Lefranc, F., & Kiss, R. (2006). Galectin-1: a small protein with major functions. *Glycobiology*, *16*(11), 137R-157R. https://doi.org/10.1093/glycob/cwl025

Campbell, I. L., Abraham, C. R., Masliah, E., Kemper, P., Inglis, J. D., Oldstone, M. B., & Mucke, L. (1993). Neurologic disease induced in transgenic mice by cerebral overexpression of interleukin 6. *Proc Natl Acad Sci U S A*, *90*(21), 10061-10065. https://doi.org/10.1073/pnas.90.21.10061

Campeau, P. M., Kasperaviciute, D., Lu, J. T., Burrage, L. C., Kim, C., Hori, M., Powell, B. R., Stewart, F., Felix, T. M., van den Ende, J., Wisniewska, M., Kayserili, H., Rump, P., Nampoothiri, S., Aftimos, S., Mey, A., Nair, L. D., Begleiter, M. L., De Bie, I., . . . Sisodiya, S. M. (2014). The genetic basis of DOORS syndrome: an exome-sequencing study. *Lancet Neurol*, *13*(1), 44-58. https://doi.org/10.1016/S1474-4422(13)70265-5

Campochiaro, P. A., & Mir, T. A. (2018). The mechanism of cone cell death in Retinitis Pigmentosa. *Prog Retin Eye Res*, *62*, 24-37. https://doi.org/10.1016/j.preteyeres.2017.08.004

Cannata Serio, M., Graham, L. A., Ashikov, A., Larsen, L. E., Raymond, K., Timal, S., Le Meur, G., Ryan, M., Czarnowska, E., Jansen, J. C., He, M., Ficicioglu, C., Pichurin, P., Hasadsri, L., Minassian, B., Rugierri, A., Kalimo, H., Rios-Ocampo, W. A., Gilissen, C., . . . Lefeber, D. J. (2020). Mutations in the V-ATPase Assembly Factor VMA21 Cause a Congenital Disorder of Glycosylation With Autophagic Liver Disease. *Hepatology*, *72*(6), 1968-1986. https://doi.org/10.1002/hep.31218

Cantor, J. R., Stone, E. M., Chantranupong, L., & Georgiou, G. (2009). The human asparaginase-like protein 1 hASRGL1 is an Ntn hydrolase with beta-aspartyl peptidase activity. *Biochemistry*, *48*(46), 11026-11031. https://doi.org/10.1021/bi901397h

Capecci, M., Petrelli, M., Emanuelli, B., Millevolte, M., Nicolai, A., Provinciali, L., & Ceravolo, M. G. (2013). Rest energy expenditure in Parkinson's disease: role of disease progression and dopaminergic therapy. *Parkinsonism Relat Disord*, *19*(2), 238-241. https://doi.org/10.1016/j.parkreldis.2012.10.016

Cardoso-Moreira, M., Halbert, J., Valloton, D., Velten, B., Chen, C., Shao, Y., Liechti, A., Ascencao, K., Rummel, C., Ovchinnikova, S., Mazin, P. V., Xenarios, I., Harshman, K., Mort, M., Cooper, D. N., Sandi, C., Soares, M. J., Ferreira, P. G., Afonso, S., . . . Kaessmann, H. (2019). Gene expression across mammalian organ development. *Nature*, *571*(7766), 505-509. https://doi.org/10.1038/s41586-019-1338-5

Carling, P. J., Ryan, B. J., McGuinness, W., Kataria, S., Humble, S. W., Milde, S., Duce, J. A., Kapadia, N., Zuercher, W. J., Davis, J. B., Di Daniel, E., & Wade-Martins, R. (2022). Multiparameter phenotypic screening for endogenous TFEB and TFE3 translocation identifies novel chemical series modulating lysosome function. *Autophagy*, 1-14. https://doi.org/10.1080/15548627.2022.2095834

Carlson, D., & Carin, L. (2019). Continuing progress of spike sorting in the era of big data. *Curr Opin Neurobiol*, *55*, 90-96. https://doi.org/10.1016/j.conb.2019.02.007

Carlson, R. J., & Avraham, K. B. (2022). Emerging complexities of the mouse as a model for human hearing loss. *Proc Natl Acad Sci U S A*, *119*(35), e2211351119. https://doi.org/10.1073/pnas.2211351119

Casali, B. T., & Reed-Geaghan, E. G. (2021). Microglial Function and Regulation during Development, Homeostasis and Alzheimer's Disease. *Cells*, *10*(4). https://doi.org/10.3390/cells10040957

Caselli, A., Paoli, P., Santi, A., Mugnaioni, C., Toti, A., Camici, G., & Cirri, P. (2016). Low molecular weight protein tyrosine phosphatase: Multifaceted functions of an evolutionarily conserved enzyme. *Biochim Biophys Acta*, *1864*(10), 1339-1355. https://doi.org/10.1016/j.bbapap.2016.07.001

Castroflorio, E., den Hoed, J., Svistunova, D., Finelli, M. J., Cebrian-Serrano, A., Corrochano, S., Bassett, A. R., Davies, B., & Oliver, P. L. (2021). The Ncoa7 locus regulates V-ATPase formation and function, neurodevelopment and behaviour. *Cell Mol Life Sci*, *78*(7), 3503-3524. https://doi.org/10.1007/s00018-020-03721-6

Cavallero, A., Marte, A., & Fedele, E. (2009). L-aspartate as an amino acid neurotransmitter: mechanisms of the depolarization-induced release from cerebrocortical synaptosomes. *J Neurochem*, *110*(3), 924-934. https://doi.org/10.1111/j.1471-4159.2009.06187.x

Cesareni, G., Panni, S., Nardelli, G., & Castagnoli, L. (2002). Can we infer peptide recognition specificity mediated by SH3 domains? *FEBS Lett*, *513*(1), 38-44. https://doi.org/10.1016/s0014-5793(01)03307-5

Chabrol, E., Navarro, V., Provenzano, G., Cohen, I., Dinocourt, C., Rivaud-Pechoux, S., Fricker, D., Baulac, M., Miles, R., Leguern, E., & Baulac, S. (2010). Electroclinical characterization of epileptic seizures in leucine-rich, glioma-inactivated 1-deficient mice. *Brain*, *133*(9), 2749-2762. https://doi.org/10.1093/brain/awq171

Chakrabarti, L., Eng, J., Ivanov, N., Garden, G. A., & La Spada, A. R. (2009). Autophagy activation and enhanced mitophagy characterize the Purkinje cells of pcd mice prior to neuronal death. *Mol Brain*, *2*, 24. https://doi.org/10.1186/1756-6606-2-24

Champion, K. M., Cook, R. J., Tollaksen, S. L., & Giometti, C. S. (1994). Identification of a heritable deficiency of the folate-dependent enzyme 10-formyltetrahydrofolate dehydrogenase in mice. *Proc Natl Acad Sci U S A*, *91*(24), 11338-11342. https://doi.org/10.1073/pnas.91.24.11338

Chandler, R. J., Williams, I. M., Gibson, A. L., Davidson, C. D., Incao, A. A., Hubbard, B. T., Porter, F. D., Pavan, W. J., & Venditti, C. P. (2017). Systemic AAV9 gene therapy improves the lifespan of

mice with Niemann-Pick disease, type C1. *Hum Mol Genet*, *26*(1), 52-64. https://doi.org/10.1093/hmg/ddw367

Chandran, V., Gao, K., Swarup, V., Versano, R., Dong, H., Jordan, M. C., & Geschwind, D. H. (2017). Inducible and reversible phenotypes in a novel mouse model of Friedreich's Ataxia. *Elife*, *6*. https://doi.org/10.7554/eLife.30054

Chantranupong, L., Saulnier, J. L., Wang, W., Jones, D. R., Pacold, M. E., & Sabatini, B. L. (2020). Rapid purification and metabolomic profiling of synaptic vesicles from mammalian brain. *Elife*, *9*. https://doi.org/10.7554/eLife.59699

Charbaut, E., Curmi, P. A., Ozon, S., Lachkar, S., Redeker, V., & Sobel, A. (2001). Stathmin family proteins display specific molecular and tubulin binding properties. *J Biol Chem*, *276*(19), 16146-16154. https://doi.org/10.1074/jbc.M010637200

Chen, D., Wu, C. F., Shi, B., & Xu, Y. M. (2002). Tamoxifen and toremifene cause impairment of learning and memory function in mice. *Pharmacol Biochem Behav*, *71*(1-2), 269-276. https://doi.org/10.1016/s0091-3057(01)00656-6

Chen, X. S., Reader, R. H., Hoischen, A., Veltman, J. A., Simpson, N. H., Francks, C., Newbury, D. F., & Fisher, S. E. (2017). Next-generation DNA sequencing identifies novel gene variants and pathways involved in specific language impairment. *Sci Rep*, *7*, 46105. https://doi.org/10.1038/srep46105

Cheung, H., Kamp, D., & Harris, E. (1992). An in vitro investigation of the action of lamotrigine on neuronal voltage-activated sodium channels. *Epilepsy Res*, *13*(2), 107-112. https://doi.org/10.1016/0920-1211(92)90065-2

Chini, M., Gretenkord, S., Kostka, J. K., Popplau, J. A., Cornelissen, L., Berde, C. B., Hanganu-Opatz, I. L., & Bitzenhofer, S. H. (2019). Neural Correlates of Anesthesia in Newborn Mice and Humans. *Front Neural Circuits*, *13*, 38. https://doi.org/10.3389/fncir.2019.00038

Choi, C. I., Yoon, S. P., Choi, J. M., Kim, S. S., Lee, Y. D., Birnbaumer, L., & Suh-Kim, H. (2014). Simultaneous deletion of floxed genes mediated by CaMKIIalpha-Cre in the brain and in male germ cells: application to conditional and conventional disruption of Goalpha. *Exp Mol Med*, *46*, e93. https://doi.org/10.1038/emm.2014.14

Choi, S., Hill, D., Guo, L., Nicholas, R., Papadopoulos, D., & Cordeiro, M. F. (2022). Automated characterisation of microglia in ageing mice using image processing and supervised machine learning algorithms. *Sci Rep*, *12*(1), 1806. https://doi.org/10.1038/s41598-022-05815-6

Chowdhury, U. N., Ahmad, S., Islam, M. B., Alyami, S. A., Quinn, J. M. W., Eapen, V., & Moni, M. A. (2021). System biology and bioinformatics pipeline to identify comorbidities risk association: Neurodegenerative disorder case study. *PLoS One*, *16*(5), e0250660. https://doi.org/10.1371/journal.pone.0250660

Chui, A., Zhang, Q., Dai, Q., & Shi, S. H. (2020). Oxidative stress regulates progenitor behavior and cortical neurogenesis. *Development*, *147*(5). https://doi.org/10.1242/dev.184150

Cobley, J. N., Fiorello, M. L., & Bailey, D. M. (2018). 13 reasons why the brain is susceptible to oxidative stress. *Redox Biol*, *15*, 490-503. https://doi.org/10.1016/j.redox.2018.01.008

Colasante, G., Qiu, Y., Massimino, L., Di Berardino, C., Cornford, J. H., Snowball, A., Weston, M., Jones, S. P., Giannelli, S., Lieb, A., Schorge, S., Kullmann, D. M., Broccoli, V., & Lignani, G. (2020). In

vivo CRISPRa decreases seizures and rescues cognitive deficits in a rodent model of epilepsy. *Brain*, *143*(3), 891-905. https://doi.org/10.1093/brain/awaa045

Consalez, G. G., Goldowitz, D., Casoni, F., & Hawkes, R. (2020). Origins, Development, and Compartmentation of the Granule Cells of the Cerebellum. *Front Neural Circuits*, *14*, 611841. https://doi.org/10.3389/fncir.2020.611841

Consortium, S. L. I. (2002). A genomewide scan identifies two novel loci involved in specific language impairment. *Am J Hum Genet*, *70*(2), 384-398. https://doi.org/10.1086/338649

Cook, C. N., Wu, Y., Odeh, H. M., Gendron, T. F., Jansen-West, K., Del Rosso, G., Yue, M., Jiang, P., Gomes, E., Tong, J., Daughrity, L. M., Avendano, N. M., Castanedes-Casey, M., Shao, W., Oskarsson, B., Tomassy, G. S., McCampbell, A., Rigo, F., Dickson, D. W., . . . Petrucelli, L. (2020). C9orf72 poly(GR) aggregation induces TDP-43 proteinopathy. *Sci Transl Med*, *12*(559). https://doi.org/10.1126/scitranslmed.abb3774

Cougnoux, A., Yerger, J. C., Fellmeth, M., Serra-Vinardell, J., Martin, K., Navid, F., Iben, J., Wassif, C. A., Cawley, N. X., & Porter, F. D. (2020). Single Cell Transcriptome Analysis of Niemann-Pick Disease, Type C1 Cerebella. *Int J Mol Sci*, *21*(15). https://doi.org/10.3390/ijms21155368

Cunningham, F., Allen, J. E., Allen, J., Alvarez-Jarreta, J., Amode, M. R., Armean, I. M., Austine-Orimoloye, O., Azov, A. G., Barnes, I., Bennett, R., Berry, A., Bhai, J., Bignell, A., Billis, K., Boddu, S., Brooks, L., Charkhchi, M., Cummins, C., Da Rin Fioretto, L., . . . Flicek, P. (2022). Ensembl 2022. *Nucleic Acids Res*, *50*(D1), D988-D995. https://doi.org/10.1093/nar/gkab1049

da Costa, C. A., Masliah, E., & Checler, F. (2003). Beta-synuclein displays an antiapoptotic p53-dependent phenotype and protects neurons from 6-hydroxydopamine-induced caspase 3 activation: cross-talk with alpha-synuclein and implication for Parkinson's disease. *J Biol Chem*, *278*(39), 37330-37335. https://doi.org/10.1074/jbc.M306083200

Dagan, E., Schlesinger, I., Ayoub, M., Mory, A., Nassar, M., Kurolap, A., Peretz-Aharon, J., & Gershoni-Baruch, R. (2015). The contribution of Niemann-Pick SMPD1 mutations to Parkinson disease in Ashkenazi Jews. *Parkinsonism Relat Disord*, *21*(9), 1067-1071. https://doi.org/10.1016/j.parkreldis.2015.06.016

Damodaran, S., Wood, T. D., Nagarajan, P., & Rabin, R. A. (2007). Evaluating peptide mass fingerprinting-based protein identification. *Genomics Proteomics Bioinformatics*, *5*(3-4), 152-157. https://doi.org/10.1016/S1672-0229(08)60002-9

Daniels, R. W., Collins, C. A., Gelfand, M. V., Dant, J., Brooks, E. S., Krantz, D. E., & DiAntonio, A. (2004). Increased expression of the Drosophila vesicular glutamate transporter leads to excess glutamate release and a compensatory decrease in quantal content. *J Neurosci*, *24*(46), 10466-10474. https://doi.org/10.1523/JNEUROSCI.3001-04.2004

Dardiotis, E., Siokas, V., Sokratous, M., Tsouris, Z., Aloizou, A. M., Florou, D., Dastamani, M., Mentis, A. A., & Brotis, A. G. (2018). Body mass index and survival from amyotrophic lateral sclerosis: A meta-analysis. *Neurol Clin Pract*, *8*(5), 437-444. https://doi.org/10.1212/CPJ.0000000000000521

de Camp, N. V., Hense, F., Lecher, B., Scheu, H., & Bergeler, J. (2017). Models for Preterm Cortical Development Using Non Invasive Clinical EEG. *Transl Neurosci*, *8*, 211-224. https://doi.org/10.1515/tnsci-2017-0029

Demaria, M., & Poli, V. (2012). PKM2, STAT3 and HIF-1alpha: The Warburg's vicious circle. *JAKSTAT*, *1*(3), 194-196. https://doi.org/10.4161/jkst.20662

Dennery, P. A. (2007). Effects of oxidative stress on embryonic development. *Birth Defects Res C Embryo Today*, *81*(3), 155-162. https://doi.org/10.1002/bdrc.20098

Dequen, F., Filali, M., Lariviere, R. C., Perrot, R., Hisanaga, S., & Julien, J. P. (2010). Reversal of neuropathy phenotypes in conditional mouse model of Charcot-Marie-Tooth disease type 2E. *Hum Mol Genet*, *19*(13), 2616-2629. https://doi.org/10.1093/hmg/ddq149

Deshpande, D., Gupta, S. K., Sarma, A. S., Ranganath, P., Jain, S. J., Sheth, J., Mistri, M., Gupta, N., Kabra, M., Phadke, S. R., Girisha, K. M., Dua Puri, R., Aggarwal, S., Datar, C., Mandal, K., Tilak, P., Muranjan, M., Bijarnia-Mahay, S., Rama Devi, A. R., . . . Dalal, A. B. (2021). Functional characterization of novel variants in SMPD1 in Indian patients with acid sphingomyelinase deficiency. *Hum Mutat*, *42*(10), 1336-1350. https://doi.org/10.1002/humu.24263

Dias, V., Junn, E., & Mouradian, M. M. (2013). The role of oxidative stress in Parkinson's disease. *J Parkinsons Dis*, *3*(4), 461-491. https://doi.org/10.3233/JPD-130230

Doan, R. N., Lim, E. T., De Rubeis, S., Betancur, C., Cutler, D. J., Chiocchetti, A. G., Overman, L. M., Soucy, A., Goetze, S., Autism Sequencing, C., Freitag, C. M., Daly, M. J., Walsh, C. A., Buxbaum, J. D., & Yu, T. W. (2019). Recessive gene disruptions in autism spectrum disorder. *Nat Genet*, *51*(7), 1092-1098. https://doi.org/10.1038/s41588-019-0433-8

Doerks, T., Copley, R. R., Schultz, J., Ponting, C. P., & Bork, P. (2002). Systematic identification of novel protein domain families associated with nuclear functions. *Genome Res*, *12*(1), 47-56. https://doi.org/10.1101/gr.203201

Donocoff, R. S., Teteloshvili, N., Chung, H., Shoulson, R., & Creusot, R. J. (2020). Optimization of tamoxifen-induced Cre activity and its effect on immune cell populations. *Sci Rep*, *10*(1), 15244. https://doi.org/10.1038/s41598-020-72179-0

Dorrbaum, A. R., Kochen, L., Langer, J. D., & Schuman, E. M. (2018). Local and global influences on protein turnover in neurons and glia. *Elife*, *7*. https://doi.org/10.7554/eLife.34202

Doyle, T., Moncorge, O., Bonaventure, B., Pollpeter, D., Lussignol, M., Tauziet, M., Apolonia, L., Catanese, M. T., Goujon, C., & Malim, M. H. (2018). The interferon-inducible isoform of NCOA7 inhibits endosome-mediated viral entry. *Nat Microbiol*, *3*(12), 1369-1376. https://doi.org/10.1038/s41564-018-0273-9

Dragatsis, I., & Zeitlin, S. (2000). CaMKIIalpha-Cre transgene expression and recombination patterns in the mouse brain. *Genesis*, *26*(2), 133-135. https://doi.org/10.1002/(sici)1526-968x(200002)26:2<133::aid-gene10>3.0.co;2-v

Dunham, W. H., Mullin, M., & Gingras, A. C. (2012). Affinity-purification coupled to mass spectrometry: basic principles and strategies. *Proteomics*, *12*(10), 1576-1590. https://doi.org/10.1002/pmic.201100523

Durand, M., Kolpak, A., Farrell, T., Elliott, N. A., Shao, W., Brown, M., & Volkert, M. R. (2007). The OXR domain defines a conserved family of eukaryotic oxidation resistance proteins. *BMC Cell Biol*, *8*, 13. https://doi.org/10.1186/1471-2121-8-13

Eastman, C. L., D'Ambrosio, R., & Ganesh, T. (2020). Modulating neuroinflammation and oxidative stress to prevent epilepsy and improve outcomes after traumatic brain injury. *Neuropharmacology*, *172*, 107907. https://doi.org/10.1016/j.neuropharm.2019.107907

Eaton, A. F., Brown, D., & Merkulova, M. (2021). The evolutionary conserved TLDc domain defines a new class of (H(+))V-ATPase interacting proteins. *Sci Rep*, *11*(1), 22654. https://doi.org/10.1038/s41598-021-01809-y

Eaton, A. F., Merkulova, M., & Brown, D. (2021). The H(+)-ATPase (V-ATPase): from proton pump to signaling complex in health and disease. *Am J Physiol Cell Physiol*, *320*(3), C392-C414. https://doi.org/10.1152/ajpcell.00442.2020

Eden, E., Lipson, D., Yogev, S., & Yakhini, Z. (2007). Discovering motifs in ranked lists of DNA sequences. *PLoS Comput Biol*, *3*(3), e39. https://doi.org/10.1371/journal.pcbi.0030039

Eden, E., Navon, R., Steinfeld, I., Lipson, D., & Yakhini, Z. (2009). GOrilla: a tool for discovery and visualization of enriched GO terms in ranked gene lists. *BMC Bioinformatics*, *10*, 48. https://doi.org/10.1186/1471-2105-10-48

Elliott, N. A., & Volkert, M. R. (2004). Stress induction and mitochondrial localization of Oxr1 proteins in yeast and humans. *Mol Cell Biol*, *24*(8), 3180-3187. https://doi.org/10.1128/MCB.24.8.3180-3187.2004

Engel, J., Jr., Thompson, P. M., Stern, J. M., Staba, R. J., Bragin, A., & Mody, I. (2013). Connectomics and epilepsy. *Curr Opin Neurol*, *26*(2), 186-194. https://doi.org/10.1097/WCO.0b013e32835ee5b8

Escartin, C., Galea, E., Lakatos, A., O'Callaghan, J. P., Petzold, G. C., Serrano-Pozo, A., Steinhauser, C., Volterra, A., Carmignoto, G., Agarwal, A., Allen, N. J., Araque, A., Barbeito, L., Barzilai, A., Bergles, D. E., Bonvento, G., Butt, A. M., Chen, W. T., Cohen-Salmon, M., . . . Verkhratsky, A. (2021). Reactive astrocyte nomenclature, definitions, and future directions. *Nat Neurosci*, *24*(3), 312-325. https://doi.org/10.1038/s41593-020-00783-4

Ethemoglu, O., Ay, H., Koyuncu, I., & Gonel, A. (2018). Comparison of cytokines and prooxidants/antioxidants markers among adults with refractory versus well-controlled epilepsy: A cross-sectional study. *Seizure*, *60*, 105-109. https://doi.org/10.1016/j.seizure.2018.06.009

Evers, B. M., Rodriguez-Navas, C., Tesla, R. J., Prange-Kiel, J., Wasser, C. R., Yoo, K. S., McDonald, J., Cenik, B., Ravenscroft, T. A., Plattner, F., Rademakers, R., Yu, G., White, C. L., 3rd, & Herz, J. (2017). Lipidomic and Transcriptomic Basis of Lysosomal Dysfunction in Progranulin Deficiency. *Cell Rep*, *20*(11), 2565-2574. https://doi.org/10.1016/j.celrep.2017.08.056

Fabregat, A., Sidiropoulos, K., Viteri, G., Forner, O., Marin-Garcia, P., Arnau, V., D'Eustachio, P., Stein, L., & Hermjakob, H. (2017). Reactome pathway analysis: a high-performance in-memory approach. *BMC Bioinformatics*, *18*(1), 142. https://doi.org/10.1186/s12859-017-1559-2

Falace, A., Buhler, E., Fadda, M., Watrin, F., Lippiello, P., Pallesi-Pocachard, E., Baldelli, P., Benfenati, F., Zara, F., Represa, A., Fassio, A., & Cardoso, C. (2014). TBC1D24 regulates neuronal migration and maturation through modulation of the ARF6-dependent pathway. *Proc Natl Acad Sci U S A*, *111*(6), 2337-2342. https://doi.org/10.1073/pnas.1316294111

Falace, A., Filipello, F., La Padula, V., Vanni, N., Madia, F., De Pietri Tonelli, D., de Falco, F. A., Striano, P., Dagna Bricarelli, F., Minetti, C., Benfenati, F., Fassio, A., & Zara, F. (2010). TBC1D24, an ARF6-interacting protein, is mutated in familial infantile myoclonic epilepsy. *Am J Hum Genet*, *87*(3), 365-370. https://doi.org/10.1016/j.ajhg.2010.07.020

Fan, J., Fong, T., Chen, X., Chen, C., Luo, P., & Xie, H. (2018). Glia maturation factor-beta: a potential therapeutic target in neurodegeneration and neuroinflammation. *Neuropsychiatr Dis Treat*, *14*, 495-504. https://doi.org/10.2147/NDT.S157099

Fan, J., Thalody, G., Kwagh, J., Burnett, E., Shi, H., Lewen, G., Chen, S. J., & Levesque, P. (2019). Assessing seizure liability using multi-electrode arrays (MEA). *Toxicol In Vitro*, *55*, 93-100. https://doi.org/10.1016/j.tiv.2018.12.001

Fancello, T., Dardis, A., Rosano, C., Tarugi, P., Tappino, B., Zampieri, S., Pinotti, E., Corsolini, F., Fecarotta, S., D'Amico, A., Di Rocco, M., Uziel, G., Calandra, S., Bembi, B., & Filocamo, M. (2009). Molecular analysis of NPC1 and NPC2 gene in 34 Niemann-Pick C Italian patients: identification and structural modeling of novel mutations. *Neurogenetics*, *10*(3), 229-239. https://doi.org/10.1007/s10048-009-0175-3

Farmer, B. C., Walsh, A. E., Kluemper, J. C., & Johnson, L. A. (2020). Lipid Droplets in Neurodegenerative Disorders. *Front Neurosci*, *14*, 742. https://doi.org/10.3389/fnins.2020.00742

Fassio, A., Esposito, A., Kato, M., Saitsu, H., Mei, D., Marini, C., Conti, V., Nakashima, M., Okamoto, N., Olmez Turker, A., Albuz, B., Semerci Gunduz, C. N., Yanagihara, K., Belmonte, E., Maragliano, L., Ramsey, K., Balak, C., Siniard, A., Narayanan, V., . . . Guerrini, R. (2018). De novo mutations of the ATP6V1A gene cause developmental encephalopathy with epilepsy. *Brain*, *141*(6), 1703-1718. https://doi.org/10.1093/brain/awy092

Feigin, V. L., Vos, T., Nichols, E., Owolabi, M. O., Carroll, W. M., Dichgans, M., Deuschl, G., Parmar, P., Brainin, M., & Murray, C. (2020). The global burden of neurological disorders: translating evidence into policy. *Lancet Neurology*, *19*(3), 255-265. https://doi.org/10.1016/S1474-4422(19)30411-9

Feil, R., Wagner, J., Metzger, D., & Chambon, P. (1997). Regulation of Cre recombinase activity by mutated estrogen receptor ligand-binding domains. *Biochem Biophys Res Commun*, *237*(3), 752-757. https://doi.org/10.1006/bbrc.1997.7124

Finelli, M. J., Aprile, D., Castroflorio, E., Jeans, A., Moschetta, M., Chessum, L., Degiacomi, M. T., Grasegger, J., Lupien-Meilleur, A., Bassett, A., Rossignol, E., Campeau, P. M., Bowl, M. R., Benfenati, F., Fassio, A., & Oliver, P. L. (2019). The epilepsy-associated protein TBC1D24 is required for normal development, survival and vesicle trafficking in mammalian neurons. *Hum Mol Genet*, *28*(4), 584-597. https://doi.org/10.1093/hmg/ddy370

Finelli, M. J., Liu, K. X., Wu, Y., Oliver, P. L., & Davies, K. E. (2015). Oxr1 improves pathogenic cellular features of ALS-associated FUS and TDP-43 mutations. *Hum Mol Genet*, *24*(12), 3529-3544. https://doi.org/10.1093/hmg/ddv104

Finelli, M. J., & Oliver, P. L. (2017). TLDc proteins: new players in the oxidative stress response and neurological disease. *Mamm Genome*, *28*(9-10), 395-406. https://doi.org/10.1007/s00335-017-9706-7

Finelli, M. J., Paramo, T., Pires, E., Ryan, B. J., Wade-Martins, R., Biggin, P. C., McCullagh, J., & Oliver, P. L. (2019). Oxidation Resistance 1 Modulates Glycolytic Pathways in the Cerebellum via an Interaction with Glucose-6-Phosphate Isomerase. *Mol Neurobiol*, *56*(3), 1558-1577. https://doi.org/10.1007/s12035-018-1174-x

Finelli, M. J., Sanchez-Pulido, L., Liu, K. X., Davies, K. E., & Oliver, P. L. (2016). The Evolutionarily Conserved Tre2/Bub2/Cdc16 (TBC), Lysin Motif (LysM), Domain Catalytic (TLDc) Domain Is Neuroprotective against Oxidative Stress. *J Biol Chem*, *291*(6), 2751-2763. https://doi.org/10.1074/jbc.M115.685222

Fischer, H., Zhang, X. U., O'Brien, K. P., Kylsten, P., & Engvall, E. (2001). C7, a novel nucleolar protein, is the mouse homologue of the Drosophila late puff product L82 and an isoform of human OXR1. *Biochem Biophys Res Commun*, *281*(3), 795-803. https://doi.org/10.1006/bbrc.2001.4345

Forgac, M. (2007). Vacuolar ATPases: rotary proton pumps in physiology and pathophysiology. *Nat Rev Mol Cell Biol*, *8*(11), 917-929. https://doi.org/10.1038/nrm2272

Fornasiero, E. F., Mandad, S., Wildhagen, H., Alevra, M., Rammner, B., Keihani, S., Opazo, F., Urban, I., Ischebeck, T., Sakib, M. S., Fard, M. K., Kirli, K., Centeno, T. P., Vidal, R. O., Rahman, R. U., Benito, E., Fischer, A., Dennerlein, S., Rehling, P., . . . Rizzoli, S. O. (2018). Precisely measured protein lifetimes in the mouse brain reveal differences across tissues and subcellular fractions. *Nat Commun*, *9*(1), 4230. https://doi.org/10.1038/s41467-018-06519-0

Fouet, G., Bally, I., Signor, L., Haussermann, K., Thielens, N. M., Rossi, V., & Gaboriaud, C. (2021). Headless C1q: a new molecular tool to decipher its collagen-like functions. *FEBS J*, *288*(6), 2030-2041. https://doi.org/10.1111/febs.15543

Frankenfield, A. M., Ni, J., Ahmed, M., & Hao, L. (2022). Protein Contaminants Matter: Building Universal Protein Contaminant Libraries for DDA and DIA Proteomics. *J Proteome Res*. https://doi.org/10.1021/acs.jproteome.2c00145

Franklin, R. J., & Ffrench-Constant, C. (2008). Remyelination in the CNS: from biology to therapy. *Nat Rev Neurosci*, *9*(11), 839-855. https://doi.org/10.1038/nrn2480

Frega, M., Linda, K., Keller, J. M., Gumus-Akay, G., Mossink, B., van Rhijn, J. R., Negwer, M., Klein Gunnewiek, T., Foreman, K., Kompier, N., Schoenmaker, C., van den Akker, W., van der Werf, I., Oudakker, A., Zhou, H., Kleefstra, T., Schubert, D., van Bokhoven, H., & Nadif Kasri, N. (2019). Neuronal network dysfunction in a model for Kleefstra syndrome mediated by enhanced NMDAR signaling. *Nat Commun*, *10*(1), 4928. https://doi.org/10.1038/s41467-019-12947-3

Frost, L. S., Dhingra, A., Reyes-Reveles, J., & Boesze-Battaglia, K. (2017). The Use of DQ-BSA to Monitor the Turnover of Autophagy-Associated Cargo. *Methods Enzymol*, *587*, 43-54. https://doi.org/10.1016/bs.mie.2016.09.052

Fukuda, M., Yamauchi, H., Yamamoto, H., Aminaka, M., Murakami, H., Kamiyama, N., Miyamoto, Y., & Koitabashi, Y. (2008). The evaluation of oxidative DNA damage in children with brain damage using 8-hydroxydeoxyguanosine levels. *Brain Dev*, *30*(2), 131-136. https://doi.org/10.1016/j.braindev.2007.07.005

Garden, G. A., & La Spada, A. R. (2012). Intercellular (mis)communication in neurodegenerative disease. *Neuron*, *73*(5), 886-901. https://doi.org/10.1016/j.neuron.2012.02.017

Gataullina, S., Lemaire, E., Wendling, F., Kaminska, A., Watrin, F., Riquet, A., Ville, D., Moutard, M. L., de Saint Martin, A., Napuri, S., Pedespan, J. M., Eisermann, M., Bahi-Buisson, N., Nabbout, R., Chiron, C., Dulac, O., & Huberfeld, G. (2016). Epilepsy in young Tsc1(+/-) mice exhibits age-dependent expression that mimics that of human tuberous sclerosis complex. *Epilepsia*, *57*(4), 648-659. https://doi.org/10.1111/epi.13325

GBD Neurology Collaborators. (2019). Global, regional, and national burden of neurological disorders, 1990-2016: a systematic analysis for the Global Burden of Disease Study 2016. *Lancet Neurol*, *18*(5), 459-480. https://doi.org/10.1016/S1474-4422(18)30499-X

Geiser, J., Venken, K. J., De Lisle, R. C., & Andrews, G. K. (2012). A mouse model of acrodermatitis enteropathica: loss of intestine zinc transporter ZIP4 (Slc39a4) disrupts the stem cell niche and intestine integrity. *PLoS Genet*, *8*(6), e1002766. https://doi.org/10.1371/journal.pgen.1002766

Geloso, M. C., Corvino, V., Marchese, E., Serrano, A., Michetti, F., & D'Ambrosi, N. (2017). The Dual Role of Microglia in ALS: Mechanisms and Therapeutic Approaches. *Front Aging Neurosci*, *9*, 242. https://doi.org/10.3389/fnagi.2017.00242

Gerber, Y. N., Sabourin, J. C., Rabano, M., Vivanco, M., & Perrin, F. E. (2012). Early functional deficit and microglial disturbances in a mouse model of amyotrophic lateral sclerosis. *PLoS One*, *7*(4), e36000. https://doi.org/10.1371/journal.pone.0036000

Gerrits, E., Brouwer, N., Kooistra, S. M., Woodbury, M. E., Vermeiren, Y., Lambourne, M., Mulder, J., Kummer, M., Moller, T., Biber, K., Dunnen, W., De Deyn, P. P., Eggen, B. J. L., & Boddeke, E. (2021). Distinct amyloid-beta and tau-associated microglia profiles in Alzheimer's disease. *Acta Neuropathol*, *141*(5), 681-696. https://doi.org/10.1007/s00401-021-02263-w

Ghoshal, N., Dearborn, J. T., Wozniak, D. F., & Cairns, N. J. (2012). Core features of frontotemporal dementia recapitulated in progranulin knockout mice. *Neurobiol Dis*, *45*(1), 395-408. https://doi.org/10.1016/j.nbd.2011.08.029

Ghyselinck, N. B., Bavik, C., Sapin, V., Mark, M., Bonnier, D., Hindelang, C., Dierich, A., Nilsson, C. B., Hakansson, H., Sauvant, P., Azais-Braesco, V., Frasson, M., Picaud, S., & Chambon, P. (1999). Cellular retinol-binding protein I is essential for vitamin A homeostasis. *EMBO J*, *18*(18), 4903-4914. https://doi.org/10.1093/emboj/18.18.4903

Gmitterova, K., Heinemann, U., Gawinecka, J., Varges, D., Ciesielczyk, B., Valkovic, P., Benetin, J., & Zerr, I. (2009). 8-OHdG in cerebrospinal fluid as a marker of oxidative stress in various neurodegenerative diseases. *Neurodegener Dis*, *6*(5-6), 263-269. https://doi.org/10.1159/000237221

Goldberg, E. M., & Coulter, D. A. (2013). Mechanisms of epileptogenesis: a convergence on neural circuit dysfunction. *Nat Rev Neurosci*, *14*(5), 337-349. https://doi.org/10.1038/nrn3482

Golechha, M., Chaudhry, U., Bhatia, J., Saluja, D., & Arya, D. S. (2011). Naringin protects against kainic acid-induced status epilepticus in rats: evidence for an antioxidant, anti-inflammatory and neuroprotective intervention. *Biol Pharm Bull*, *34*(3), 360-365. https://doi.org/10.1248/bpb.34.360

Gonzalez-Lozano, M. A., Koopmans, F., Sullivan, P. F., Protze, J., Krause, G., Verhage, M., Li, K. W., Liu, F., & Smit, A. B. (2020). Stitching the synapse: Cross-linking mass spectrometry into resolving synaptic protein interactions. *Sci Adv*, *6*(8), eaax5783. https://doi.org/10.1126/sciadv.aax5783

Goodwin, L. O., Splinter, E., Davis, T. L., Urban, R., He, H., Braun, R. E., Chesler, E. J., Kumar, V., van Min, M., Ndukum, J., Philip, V. M., Reinholdt, L. G., Svenson, K., White, J. K., Sasner, M., Lutz, C., & Murray, S. A. (2019). Large-scale discovery of mouse transgenic integration sites reveals frequent structural variation and insertional mutagenesis. *Genome Res*, *29*(3), 494-505. https://doi.org/10.1101/gr.233866.117

Gorenberg, E. L., Massaro Tieze, S., Yucel, B., Zhao, H. R., Chou, V., Wirak, G. S., Tomita, S., Lam, T. T., & Chandra, S. S. (2022). Identification of substrates of palmitoyl protein thioesterase 1 highlights roles of depalmitoylation in disulfide bond formation and synaptic function. *PLoS Biol*, *20*(3), e3001590. https://doi.org/10.1371/journal.pbio.3001590

Govek, E. E., Newey, S. E., & Van Aelst, L. (2005). The role of the Rho GTPases in neuronal development. *Genes Dev*, *19*(1), 1-49. https://doi.org/10.1101/gad.1256405

Greenfield, L. J., Jr. (2013). Molecular mechanisms of antiseizure drug activity at GABAA receptors. *Seizure*, *22*(8), 589-600. https://doi.org/10.1016/j.seizure.2013.04.015

Grieco, F., Bernstein, B. J., Biemans, B., Bikovski, L., Burnett, C. J., Cushman, J. D., van Dam, E. A., Fry, S. A., Richmond-Hacham, B., Homberg, J. R., Kas, M. J. H., Kessels, H. W., Koopmans, B., Krashes, M. J., Krishnan, V., Logan, S., Loos, M., McCann, K. E., Parduzi, Q., . . . Noldus, L. (2021). Measuring Behavior in the Home Cage: Study Design, Applications, Challenges, and Perspectives. *Front Behav Neurosci*, *15*, 735387. https://doi.org/10.3389/fnbeh.2021.735387

Groft, S. C., Posada de la Paz, M., & Taruscio, D. (2017). *Rare Diseases Epidemiology: Update and Overview* (2nd ed.). Springer International Publishing : Imprint: Springer,. https://doi.org/10.1007/978-3-319-67144-4

Gu, F., Parada, I., Yang, T., Longo, F. M., & Prince, D. A. (2018). Partial TrkB receptor activation suppresses cortical epileptogenesis through actions on parvalbumin interneurons. *Neurobiol Dis*, *113*, 45-58. https://doi.org/10.1016/j.nbd.2018.01.018

Guedes-Dias, P., de Proenca, J., Soares, T. R., Leitao-Rocha, A., Pinho, B. R., Duchen, M. R., & Oliveira, J. M. (2015). HDAC6 inhibition induces mitochondrial fusion, autophagic flux and reduces diffuse mutant huntingtin in striatal neurons. *Biochim Biophys Acta*, *1852*(11), 2484-2493. https://doi.org/10.1016/j.bbadis.2015.08.012

Guerrini, R., Mei, D., Kerti-Szigeti, K., Pepe, S., Koenig, M. K., Von Allmen, G., Cho, M. T., McDonald, K., Baker, J., Bhambhani, V., Powis, Z., Rodan, L., Nabbout, R., Barcia, G., Rosenfeld, J. A., Bacino, C. A., Mignot, C., Power, L. H., Harris, C. J., . . . Fassio, A. (2022). Phenotypic and genetic spectrum of ATP6V1A encephalopathy: a disorder of lysosomal homeostasis. *Brain*, *145*(8), 2687-2703. https://doi.org/10.1093/brain/awac145

Guo, Y. L., Chakraborty, S., Rajan, S. S., Wang, R., & Huang, F. (2010). Effects of oxidative stress on mouse embryonic stem cell proliferation, apoptosis, senescence, and self-renewal. *Stem Cells Dev*, *19*(9), 1321-1331. https://doi.org/10.1089/scd.2009.0313

Gupta, P., Soyombo, A. A., Atashband, A., Wisniewski, K. E., Shelton, J. M., Richardson, J. A., Hammer, R. E., & Hofmann, S. L. (2001). Disruption of PPT1 or PPT2 causes neuronal ceroid lipofuscinosis in knockout mice. *Proc Natl Acad Sci U S A*, *98*(24), 13566-13571. https://doi.org/10.1073/pnas.251485198

Gur-Hartman, T., Berkowitz, O., Yosovich, K., Roubertie, A., Zanni, G., Macaya, A., Heimer, G., Duenas, B. P., Sival, D. A., Pode-Shakked, B., Lopez-Laso, E., Humbertclaude, V., Riant, F., Bosco, L., Cayron, L. B., Nissenkorn, A., Nicita, F., Bertini, E., Hassin, S., . . . Blumkin, L. (2021). Clinical phenotypes of infantile onset CACNA1A-related disorder. *Eur J Paediatr Neurol*, *30*, 144-154. https://doi.org/10.1016/j.ejpn.2020.10.004

Habib, N., McCabe, C., Medina, S., Varshavsky, M., Kitsberg, D., Dvir-Szternfeld, R., Green, G., Dionne, D., Nguyen, L., Marshall, J. L., Chen, F., Zhang, F., Kaplan, T., Regev, A., & Schwartz, M. (2020). Disease-associated astrocytes in Alzheimer's disease and aging. *Nat Neurosci*, *23*(6), 701-706. https://doi.org/10.1038/s41593-020-0624-8

Hahl, P., Hunt, R., Bjes, E. S., Skaff, A., Keightley, A., & Smith, A. (2017). Identification of oxidative modifications of hemopexin and their predicted physiological relevance. *J Biol Chem*, *292*(33), 13658-13671. https://doi.org/10.1074/jbc.M117.783951

Hajam, Y. A., Rani, R., Ganie, S. Y., Sheikh, T. A., Javaid, D., Qadri, S. S., Pramodh, S., Alsulimani, A., Alkhanani, M. F., Harakeh, S., Hussain, A., Haque, S., & Reshi, M. S. (2022). Oxidative Stress in Human Pathology and Aging: Molecular Mechanisms and Perspectives. *Cells*, *11*(3). https://doi.org/10.3390/cells11030552

Hara, T., Nakamura, K., Matsui, M., Yamamoto, A., Nakahara, Y., Suzuki-Migishima, R., Yokoyama, M., Mishima, K., Saito, I., Okano, H., & Mizushima, N. (2006). Suppression of basal autophagy in neural cells causes neurodegenerative disease in mice. *Nature*, *441*(7095), 885-889. https://doi.org/10.1038/nature04724

Hardisty-Hughes, R. E., Parker, A., & Brown, S. D. (2010). A hearing and vestibular phenotyping pipeline to identify mouse mutants with hearing impairment. *Nat Protoc*, *5*(1), 177-190. https://doi.org/10.1038/nprot.2009.204

Harrison, S. M., Biesecker, L. G., & Rehm, H. L. (2019). Overview of Specifications to the ACMG/AMP Variant Interpretation Guidelines. *Curr Protoc Hum Genet*, *103*(1), e93. https://doi.org/10.1002/cphg.93

Hasel, P., Rose, I. V. L., Sadick, J. S., Kim, R. D., & Liddelow, S. A. (2021). Neuroinflammatory astrocyte subtypes in the mouse brain. *Nat Neurosci*, *24*(10), 1475-1487. https://doi.org/10.1038/s41593-021-00905-6

Hashimoto, M., Rockenstein, E., Mante, M., Crews, L., Bar-On, P., Gage, F. H., Marr, R., & Masliah, E. (2004). An antiaggregation gene therapy strategy for Lewy body disease utilizing beta-synuclein lentivirus in a transgenic model. *Gene Ther*, *11*(23), 1713-1723. https://doi.org/10.1038/sj.gt.3302349

Hashimoto, M., Rockenstein, E., Mante, M., Mallory, M., & Masliah, E. (2001). beta-synuclein inhibits alpha-synuclein aggregation: A possible role as an anti-parkinsonian factor. *Neuron*, *32*(2), 213-223. https://doi.org/Doi 10.1016/S0896-6273(01)00462-7

Haure-Mirande, J. V., Wang, M., Audrain, M., Fanutza, T., Kim, S. H., Heja, S., Readhead, B., Dudley, J. T., Blitzer, R. D., Schadt, E. E., Zhang, B., Gandy, S., & Ehrlich, M. E. (2019). Integrative approach to sporadic Alzheimer's disease: deficiency of TYROBP in cerebral Abeta amyloidosis mouse normalizes clinical phenotype and complement subnetwork molecular pathology without reducing Abeta burden. *Mol Psychiatry*, *24*(3), 431-446. https://doi.org/10.1038/s41380-018-0255-6

Hayashi, J., & Carver, J. A. (2022). beta-Synuclein: An Enigmatic Protein with Diverse Functionality. *Biomolecules*, *12*(1). https://doi.org/10.3390/biom12010142

Hebert, A. S., Thoing, C., Riley, N. M., Kwiecien, N. W., Shiskova, E., Huguet, R., Cardasis, H. L., Kuehn, A., Eliuk, S., Zabrouskov, V., Westphall, M. S., McAlister, G. C., & Coon, J. J. (2018). Improved Precursor Characterization for Data-Dependent Mass Spectrometry. *Anal Chem*, *90*(3), 2333-2340. https://doi.org/10.1021/acs.analchem.7b04808

Heffner, C. S., Herbert Pratt, C., Babiuk, R. P., Sharma, Y., Rockwood, S. F., Donahue, L. R., Eppig, J. T., & Murray, S. A. (2012). Supporting conditional mouse mutagenesis with a comprehensive cre characterization resource. *Nat Commun*, *3*, 1218. https://doi.org/10.1038/ncomms2186

Heidari, A., Yazdanpanah, N., & Rezaei, N. (2022). The role of Toll-like receptors and neuroinflammation in Parkinson's disease. *J Neuroinflammation*, *19*(1), 135. https://doi.org/10.1186/s12974-022-02496-w

Herman, G. E., Kopacz, K., Zhao, W., Mills, P. L., Metzenberg, A., & Das, S. (2002). Characterization of mutations in fifty North American patients with X-linked myotubular myopathy. *Hum Mutat*, *19*(2), 114-121. https://doi.org/10.1002/humu.10033

Hersheson, J., Burke, D., Clayton, R., Anderson, G., Jacques, T. S., Mills, P., Wood, N. W., Gissen, P., Clayton, P., Fearnley, J., Mole, S. E., & Houlden, H. (2014). Cathepsin D deficiency causes juvenile-onset ataxia and distinctive muscle pathology. *Neurology*, *83*(20), 1873-1875. https://doi.org/10.1212/WNL.0000000000000981

Hester, M. S., Tulina, N., Brown, A., Barila, G., & Elovitz, M. A. (2018). Intrauterine inflammation reduces postnatal neurogenesis in the hippocampal subgranular zone and leads to accumulation of hilar ectopic granule cells. *Brain Res*, *1685*, 51-59. https://doi.org/10.1016/j.brainres.2018.02.005

Hewett, S. J., Jackman, N. A., & Claycomb, R. J. (2012). Interleukin-1beta in Central Nervous System Injury and Repair. *Eur J Neurodegener Dis*, *1*(2), 195-211. https://www.ncbi.nlm.nih.gov/pubmed/26082912

Hiemstra, T. F., Charles, P. D., Hester, S. S., Karet, F. E., & Lilley, K. S. (2011). Uromodulin exclusion list improves urinary exosomal protein identification. *J Biomol Tech*, *22*(4), 136-145. https://www.ncbi.nlm.nih.gov/pubmed/22131889

Hirohama, D., Kawarazaki, W., Nishimoto, M., Ayuzawa, N., Marumo, T., Shibata, S., & Fujita, T. (2020). PGI2 Analog Attenuates Salt-Induced Renal Injury through the Inhibition of Inflammation and Rac1-MR Activation. *Int J Mol Sci*, *21*(12). https://doi.org/10.3390/ijms21124433

Hodge, K., Have, S. T., Hutton, L., & Lamond, A. I. (2013). Cleaning up the masses: exclusion lists to reduce contamination with HPLC-MS/MS. *J Proteomics*, *88*, 92-103. https://doi.org/10.1016/j.jprot.2013.02.023

Hopperton, K. E., Mohammad, D., Trepanier, M. O., Giuliano, V., & Bazinet, R. P. (2018). Markers of microglia in post-mortem brain samples from patients with Alzheimer's disease: a systematic review. *Mol Psychiatry*, *23*(2), 177-198. https://doi.org/10.1038/mp.2017.246

Hou, Y., Dan, X., Babbar, M., Wei, Y., Hasselbalch, S. G., Croteau, D. L., & Bohr, V. A. (2019). Ageing as a risk factor for neurodegenerative disease. *Nat Rev Neurol*, *15*(10), 565-581. https://doi.org/10.1038/s41582-019-0244-7

Hu, H., Gan, J., & Jonas, P. (2014). Interneurons. Fast-spiking, parvalbumin(+) GABAergic interneurons: from cellular design to microcircuit function. *Science*, *345*(6196), 1255263. https://doi.org/10.1126/science.1255263

Huang, S., Henry, L., Ho, Y. K., Pownall, H. J., & Rudenko, G. (2010). Mechanism of LDL binding and release probed by structure-based mutagenesis of the LDL receptor. *J Lipid Res*, *51*(2), 297-308. https://doi.org/10.1194/jlr.M000422

Huang, S. L., Wu, L. S., Lee, M., Chang, C. W., Cheng, W. C., Fang, Y. S., Chen, Y. R., Cheng, P. L., & Shen, C. J. (2020). A robust TDP-43 knock-in mouse model of ALS. *Acta Neuropathol Commun*, *8*(1), 3. https://doi.org/10.1186/s40478-020-0881-5

Hudson, A. M., & Cooley, L. (2002). A subset of dynamic actin rearrangements in Drosophila requires the Arp2/3 complex. *J Cell Biol*, *156*(4), 677-687. https://doi.org/10.1083/jcb.200109065

Huttlin, E. L., Jedrychowski, M. P., Elias, J. E., Goswami, T., Rad, R., Beausoleil, S. A., Villen, J., Haas, W., Sowa, M. E., & Gygi, S. P. (2010). A tissue-specific atlas of mouse protein phosphorylation and expression. *Cell*, *143*(7), 1174-1189. https://doi.org/10.1016/j.cell.2010.12.001

Ichimura, Y., Waguri, S., Sou, Y. S., Kageyama, S., Hasegawa, J., Ishimura, R., Saito, T., Yang, Y., Kouno, T., Fukutomi, T., Hoshii, T., Hirao, A., Takagi, K., Mizushima, T., Motohashi, H., Lee, M. S., Yoshimori, T., Tanaka, K., Yamamoto, M., & Komatsu, M. (2013). Phosphorylation of p62 activates the Keap1-Nrf2 pathway during selective autophagy. *Mol Cell*, *51*(5), 618-631. https://doi.org/10.1016/j.molcel.2013.08.003

Inga Jacome, M. C., Morales Chacon, L. M., Vera Cuesta, H., Maragoto Rizo, C., Whilby Santiesteban, M., Ramos Hernandez, L., Noris Garcia, E., Gonzalez Fraguela, M. E., Fernandez Verdecia, C. I., Vegas Hurtado, Y., Siniscalco, D., Goncalves, C. A., & Robinson-Agramonte, M. L. (2016). Peripheral Inflammatory Markers Contributing to Comorbidities in Autism. *Behav Sci (Basel)*, *6*(4). https://doi.org/10.3390/bs6040029

Inuzuka, L. M., Macedo-Souza, L. I., Della-Rippa, B., Monteiro, F. P., Delgado, D. S., Godoy, L. F., Ramos, L., de Athayde Costa, L. S., Garzon, E., & Kok, F. (2020). ATP6V1B2-related epileptic encephalopathy. *Epileptic Disord*, *22*(3), 317-322. https://doi.org/10.1684/epd.2020.1166

Ioannou, M. S., Jackson, J., Sheu, S. H., Chang, C. L., Weigel, A. V., Liu, H., Pasolli, H. A., Xu, C. S., Pang, S., Matthies, D., Hess, H. F., Lippincott-Schwartz, J., & Liu, Z. (2019). Neuron-Astrocyte Metabolic Coupling Protects against Activity-Induced Fatty Acid Toxicity. *Cell*, *177*(6), 1522-1535 e1514. https://doi.org/10.1016/j.cell.2019.04.001

Issandou, M., Guillard, R., Boullay, A. B., Linhart, V., & Lopez-Perez, E. (2004). Up-regulation of low-density lipoprotein receptor in human hepatocytes is induced by sequestration of free cholesterol in the endosomal/lysosomal compartment. *Biochem Pharmacol*, *67*(12), 2281-2289. https://doi.org/10.1016/j.bcp.2004.03.006

Jacomin, A. C., Fauvarque, M. O., & Taillebourg, E. (2016). A functional endosomal pathway is necessary for lysosome biogenesis in Drosophila. *BMC Cell Biol*, *17*(1), 36. https://doi.org/10.1186/s12860-016-0115-7

Jain, A., Lamark, T., Sjottem, E., Larsen, K. B., Awuh, J. A., Overvatn, A., McMahon, M., Hayes, J. D., & Johansen, T. (2010). p62/SQSTM1 is a target gene for transcription factor NRF2 and creates a positive feedback loop by inducing antioxidant response element-driven gene transcription. *J Biol Chem*, *285*(29), 22576-22591. https://doi.org/10.1074/jbc.M110.118976

Jankovic, M. J., Kapadia, P. P., & Krishnan, V. (2019). Home-cage monitoring ascertains signatures of ictal and interictal behavior in mouse models of generalized seizures. *PLoS One*, *14*(11), e0224856. https://doi.org/10.1371/journal.pone.0224856

Janowska, M. K., Wu, K. P., & Baum, J. (2015). Unveiling transient protein-protein interactions that modulate inhibition of alpha-synuclein aggregation by beta-synuclein, a pre-synaptic protein that co-localizes with alpha-synuclein. *Sci Rep*, *5*, 15164. https://doi.org/10.1038/srep15164

Jaramillo-Gutierrez, G., Molina-Cruz, A., Kumar, S., & Barillas-Mury, C. (2010). The Anopheles gambiae oxidation resistance 1 (OXR1) gene regulates expression of enzymes that detoxify reactive oxygen species. *PLoS One*, *5*(6), e11168. https://doi.org/10.1371/journal.pone.0011168

Jessop, F., Hamilton, R. F., Jr., Rhoderick, J. F., Fletcher, P., & Holian, A. (2017). Phagolysosome acidification is required for silica and engineered nanoparticle-induced lysosome membrane permeabilization and resultant NLRP3 inflammasome activity. *Toxicol Appl Pharmacol*, *318*, 58-68. https://doi.org/10.1016/j.taap.2017.01.012

Jiang, Y., Liu, J., Chen, L., Jin, Y., Zhang, G., Lin, Z., Du, S., Fu, Z., Chen, T., Qin, Y., & Sun, X. (2019). Serum secreted miR-137-containing exosomes affects oxidative stress of neurons by regulating OXR1 in Parkinson's disease. *Brain Res*, *1722*, 146331. https://doi.org/10.1016/j.brainres.2019.146331

Jin, W., Chen, X., Kong, L., & Huang, C. (2022). Gene therapy targeting inflammatory pericytes corrects angiopathy during diabetic wound healing. *Front Immunol*, *13*, 960925. https://doi.org/10.3389/fimmu.2022.960925

Jones, C. P., Boyd, K. L., & Wallace, J. M. (2016). Evaluation of Mice Undergoing Serial Oral Gavage While Awake or Anesthetized. *J Am Assoc Lab Anim Sci*, *55*(6), 805-810. https://www.ncbi.nlm.nih.gov/pubmed/27931321

Juckel, G., Manitz, M. P., Brune, M., Friebe, A., Heneka, M. T., & Wolf, R. J. (2011). Microglial activation in a neuroinflammational animal model of schizophrenia--a pilot study. *Schizophr Res*, *131*(1-3), 96-100. https://doi.org/10.1016/j.schres.2011.06.018

Kaiser, T., & Feng, G. (2019). Tmem119-EGFP and Tmem119-CreERT2 Transgenic Mice for Labeling and Manipulating Microglia. *eNeuro*, *6*(4). https://doi.org/10.1523/ENEURO.0448-18.2019

Kalita, J., Misra, U. K., Singh, L. S., & Tiwari, A. (2019). Oxidative stress in status epilepticus: A clinical-radiological correlation. *Brain Res*, *1704*, 85-93. https://doi.org/10.1016/j.brainres.2018.09.038

Kanamoto, T., Mizuhashi, K., Terada, K., Minami, T., Yoshikawa, H., & Furukawa, T. (2009). Isolation and characterization of a novel plasma membrane protein, osteoblast induction factor (obif), associated with osteoblast differentiation. *BMC Dev Biol*, *9*, 70. https://doi.org/10.1186/1471-213X-9-70

Kanehisa, M., Furumichi, M., Tanabe, M., Sato, Y., & Morishima, K. (2017). KEGG: new perspectives on genomes, pathways, diseases and drugs. *Nucleic Acids Res*, *45*(D1), D353-D361. https://doi.org/10.1093/nar/gkw1092

Kang, B. S., Choi, B. Y., Kho, A. R., Lee, S. H., Hong, D. K., Park, M. K., Lee, S. H., Lee, C. J., Yang, H. W., Woo, S. Y., Park, S. W., Kim, D. Y., Park, J. B., Chung, W. S., & Suh, S. W. (2023). Effects of Pyruvate Kinase M2 (PKM2) Gene Deletion on Astrocyte-Specific Glycolysis and Global Cerebral Ischemia-Induced Neuronal Death. *Antioxidants (Basel)*, *12*(2). https://doi.org/10.3390/antiox12020491

Karlsson, M., Zhang, C., Mear, L., Zhong, W., Digre, A., Katona, B., Sjostedt, E., Butler, L., Odeberg, J., Dusart, P., Edfors, F., Oksvold, P., von Feilitzen, K., Zwahlen, M., Arif, M., Altay, O., Li, X., Ozcan, M., Mardinoglu, A., . . . Lindskog, C. (2021). A single-cell type transcriptomics map of human tissues. *Sci Adv*, *7*(31). https://doi.org/10.1126/sciadv.abh2169

Kaur, H., Patro, I., Tikoo, K., & Sandhir, R. (2015). Curcumin attenuates inflammatory response and cognitive deficits in experimental model of chronic epilepsy. *Neurochem Int*, *89*, 40-50. https://doi.org/10.1016/j.neuint.2015.07.009

Kawaguchi, T., Rollins, M. G., Moinpour, M., Morera, A. A., Ebmeier, C. C., Old, W. M., & Schwartz, J. C. (2020). Changes to the TDP-43 and FUS Interactomes Induced by DNA Damage. *J Proteome Res*, *19*(1), 360-370. https://doi.org/10.1021/acs.jproteome.9b00575

Keam, S. J. (2021). Elivaldogene Autotemcel: First Approval. *Mol Diagn Ther*, *25*(6), 803-809. https://doi.org/10.1007/s40291-021-00555-1

Kemaladewi, D. U., Bassi, P. S., Erwood, S., Al-Basha, D., Gawlik, K. I., Lindsay, K., Hyatt, E., Kember, R., Place, K. M., Marks, R. M., Durbeej, M., Prescott, S. A., Ivakine, E. A., & Cohn, R. D. (2019). A mutation-independent approach for muscular dystrophy via upregulation of a modifier gene. *Nature*, *572*(7767), 125-130. https://doi.org/10.1038/s41586-019-1430-x

Kemp, K. C., Cook, A. J., Redondo, J., Kurian, K. M., Scolding, N. J., & Wilkins, A. (2016). Purkinje cell injury, structural plasticity and fusion in patients with Friedreich's ataxia. *Acta Neuropathol Commun*, *4*(1), 53. https://doi.org/10.1186/s40478-016-0326-3

Kensler, T. W., Wakabayashi, N., & Biswal, S. (2007). Cell survival responses to environmental stresses via the Keap1-Nrf2-ARE pathway. *Annu Rev Pharmacol Toxicol*, *47*, 89-116. https://doi.org/10.1146/annurev.pharmtox.46.120604.141046

Keren-Shaul, H., Spinrad, A., Weiner, A., Matcovitch-Natan, O., Dvir-Szternfeld, R., Ulland, T. K., David, E., Baruch, K., Lara-Astaiso, D., Toth, B., Itzkovitz, S., Colonna, M., Schwartz, M., & Amit, I. (2017). A Unique Microglia Type Associated with Restricting Development of Alzheimer's Disease. *Cell*, *169*(7), 1276-1290 e1217. https://doi.org/10.1016/j.cell.2017.05.018

Khan, M. M., Lee, S., Couoh-Cardel, S., Oot, R. A., Kim, H., Wilkens, S., & Roh, S. H. (2022). Oxidative stress protein Oxr1 promotes V-ATPase holoenzyme disassembly in catalytic activity-independent manner. *EMBO J*, *41*(3), e109360. https://doi.org/10.15252/embj.2021109360

Khurshid, K., Crow, A. J. D., Rupert, P. E., Minniti, N. L., Carswell, M. A., Mechanic-Hamilton, D. J., Kamath, V., Doty, R. L., Moberg, P. J., & Roalf, D. R. (2019). A Quantitative Meta-analysis of Olfactory Dysfunction in Epilepsy. *Neuropsychol Rev*, *29*(3), 328-337. https://doi.org/10.1007/s11065-019-09406-7

Kim, I., Mlsna, L. M., Yoon, S., Le, B., Yu, S., Xu, D., & Koh, S. (2015). A postnatal peak in microglial development in the mouse hippocampus is correlated with heightened sensitivity to seizure triggers. *Brain Behav*, *5*(12), e00403. https://doi.org/10.1002/brb3.403

Kirchner, A., Dachet, F., & Loeb, J. A. (2020). Identifying targets for preventing epilepsy using systems biology of the human brain. *Neuropharmacology*, *168*, 107757. https://doi.org/10.1016/j.neuropharm.2019.107757

Klepac, N., Relja, M., Klepac, R., Hecimovic, S., Babic, T., & Trkulja, V. (2007). Oxidative stress parameters in plasma of Huntington's disease patients, asymptomatic Huntington's disease gene carriers and healthy subjects : a cross-sectional study. *J Neurol*, *254*(12), 1676-1683. https://doi.org/10.1007/s00415-007-0611-y

Klockgether, T. (2010). Sporadic ataxia with adult onset: classification and diagnostic criteria. *Lancet Neurol*, *9*(1), 94-104. https://doi.org/10.1016/S1474-4422(09)70305-9

Koh, Y. I., Oh, K. S., Kim, J. A., Noh, B., Choi, H. J., Joo, S. Y., Rim, J. H., Kim, H. Y., Kim, D. Y., Yu, S., Kim, D. H., Lee, S. G., Jung, J., Choi, J. Y., & Gee, H. Y. (2022). OSBPL2 mutations impair autophagy and lead to hearing loss, potentially remedied by rapamycin. *Autophagy*, *18*(11), 2593-2614. https://doi.org/10.1080/15548627.2022.2040891

Koldaeva, A., Zhang, C., Huang, Y. P., Reinert, J. K., Mizuno, S., Sugiyama, F., Takahashi, S., Soliman, T., Matsunami, H., & Fukunaga, I. (2021). Generation and Characterization of a Cell Type-Specific, Inducible Cre-Driver Line to Study Olfactory Processing. *J Neurosci*, *41*(30), 6449-6467. https://doi.org/10.1523/JNEUROSCI.3076-20.2021

Kole, A. J., Annis, R. P., & Deshmukh, M. (2013). Mature neurons: equipped for survival. *Cell Death Dis*, *4*, e689. https://doi.org/10.1038/cddis.2013.220

Koppel, J., Boutterin, M. C., Doye, V., Peyro-Saint-Paul, H., & Sobel, A. (1990). Developmental tissue expression and phylogenetic conservation of stathmin, a phosphoprotein associated with cell regulations. *J Biol Chem*, *265*(7), 3703-3707. https://www.ncbi.nlm.nih.gov/pubmed/2303475

Kowluru, R. A. (2020). Retinopathy in a Diet-Induced Type 2 Diabetic Rat Model and Role of Epigenetic Modifications. *Diabetes*, *69*(4), 689-698. https://doi.org/10.2337/db19-1009

Krabbe, G., Halle, A., Matyash, V., Rinnenthal, J. L., Eom, G. D., Bernhardt, U., Miller, K. R., Prokop, S., Kettenmann, H., & Heppner, F. L. (2013). Functional impairment of microglia coincides with Beta-amyloid deposition in mice with Alzheimer-like pathology. *PLoS One*, *8*(4), e60921. https://doi.org/10.1371/journal.pone.0060921

Kraeuter, A. K., Guest, P. C., & Sarnyai, Z. (2019). The Open Field Test for Measuring Locomotor Activity and Anxiety-Like Behavior. *Methods Mol Biol*, *1916*, 99-103. https://doi.org/10.1007/978-1-4939-8994-2_9

Krasemann, S., Madore, C., Cialic, R., Baufeld, C., Calcagno, N., El Fatimy, R., Beckers, L., O'Loughlin, E., Xu, Y., Fanek, Z., Greco, D. J., Smith, S. T., Tweet, G., Humulock, Z., Zrzavy, T., Conde-Sanroman, P., Gacias, M., Weng, Z., Chen, H., . . . Butovsky, O. (2017). The TREM2-APOE Pathway Drives the Transcriptional Phenotype of Dysfunctional Microglia in Neurodegenerative Diseases. *Immunity*, *47*(3), 566-581 e569. https://doi.org/10.1016/j.immuni.2017.08.008

Krassnig, S., Schweinzer, C., Taub, N., Havas, D., Auer, E., Flunkert, S., Schreibmayer, W., Hutter-Paier, B., & Windisch, M. (2015). Influence of Lentiviral beta-Synuclein Overexpression in the Hippocampus of a Transgenic Mouse Model of Alzheimer's Disease on Amyloid Precursor Protein Metabolism and Pathology. *Neurodegener Dis*, *15*(4), 243-257. https://doi.org/10.1159/000430952

Kregel, K. C., & Zhang, H. J. (2007). An integrated view of oxidative stress in aging: basic mechanisms, functional effects, and pathological considerations. *Am J Physiol Regul Integr Comp Physiol*, *292*(1), R18-36. https://doi.org/10.1152/ajpregu.00327.2006

Kreher, C., Favret, J., Maulik, M., & Shin, D. (2021). Lysosomal Functions in Glia Associated with Neurodegeneration. *Biomolecules*, *11*(3). https://doi.org/10.3390/biom11030400

Kristianto, J., Johnson, M. G., Zastrow, R. K., Radcliff, A. B., & Blank, R. D. (2017). Spontaneous recombinase activity of Cre-ERT2 in vivo. *Transgenic Res*, *26*(3), 411-417. https://doi.org/10.1007/s11248-017-0018-1

Kubisch, R., Frohlich, T., Arnold, G. J., Schreiner, L., von Schwarzenberg, K., Roidl, A., Vollmar, A. M., & Wagner, E. (2014). V-ATPase inhibition by archazolid leads to lysosomal dysfunction resulting in impaired cathepsin B activation in vivo. *Int J Cancer*, *134*(10), 2478-2488. https://doi.org/10.1002/ijc.28562

Kugler, E., Bravo, I., Durmishi, X., Marcotti, S., Beqiri, S., Carrington, A., Stramer, B., Mattar, P., & MacDonald, R. B. (2023). GliaMorph: a modular image analysis toolkit to quantify Muller glial cell morphology. *Development*, *150*(3). https://doi.org/10.1242/dev.201008

Kuil, L. E., Lopez Marti, A., Carreras Mascaro, A., van den Bosch, J. C., van den Berg, P., van der Linde, H. C., Schoonderwoerd, K., Ruijter, G. J. G., & van Ham, T. J. (2019). Hexb enzyme deficiency leads to lysosomal abnormalities in radial glia and microglia in zebrafish brain development. *Glia*, *67*(9), 1705-1718. https://doi.org/10.1002/glia.23641

Kumar, P., Kalonia, H., & Kumar, A. (2012). Possible GABAergic mechanism in the neuroprotective effect of gabapentin and lamotrigine against 3-nitropropionic acid induced neurotoxicity. *Eur J Pharmacol*, *674*(2-3), 265-274. https://doi.org/10.1016/j.ejphar.2011.11.030

Kumar, V., Sami, N., Kashav, T., Islam, A., Ahmad, F., & Hassan, M. I. (2016). Protein aggregation and neurodegenerative diseases: From theory to therapy. *Eur J Med Chem*, *124*, 1105-1120. https://doi.org/10.1016/j.ejmech.2016.07.054

Kwon, H. K., Choi, G. B., & Huh, J. R. (2022). Maternal inflammation and its ramifications on fetal neurodevelopment. *Trends Immunol*, *43*(3), 230-244. https://doi.org/10.1016/j.it.2022.01.007

Lacombe, M. L., Milon, L., Munier, A., Mehus, J. G., & Lambeth, D. O. (2000). The human Nm23/nucleoside diphosphate kinases. *J Bioenerg Biomembr*, *32*(3), 247-258. https://doi.org/10.1023/a:1005584929050

Lafon-Cazal, M., Perez, V., Bockaert, J., & Marin, P. (2002). Akt mediates the anti-apoptotic effect of NMDA but not that induced by potassium depolarization in cultured cerebellar granule cells. *Eur J Neurosci*, *16*(4), 575-583. https://doi.org/10.1046/j.1460-9568.2002.02124.x

Lafontaine, D. L., & Tollervey, D. (2001). The function and synthesis of ribosomes. *Nat Rev Mol Cell Biol*, *2*(7), 514-520. https://doi.org/10.1038/35080045

Lagier-Tourenne, C., Polymenidou, M., & Cleveland, D. W. (2010). TDP-43 and FUS/TLS: emerging roles in RNA processing and neurodegeneration. *Hum Mol Genet*, *19*(R1), R46-64. https://doi.org/10.1093/hmg/ddq137

Landgrave-Gomez, J., Mercado-Gomez, O., & Guevara-Guzman, R. (2015). Epigenetic mechanisms in neurological and neurodegenerative diseases. *Front Cell Neurosci*, *9*, 58. https://doi.org/10.3389/fncel.2015.00058

Laplante, M., & Sabatini, D. M. (2009). mTOR signaling at a glance. *J Cell Sci*, *122*(Pt 20), 3589-3594. https://doi.org/10.1242/jcs.051011

Laporte, M. H., Chatellard, C., Vauchez, V., Hemming, F. J., Deloulme, J. C., Vossier, F., Blot, B., Fraboulet, S., & Sadoul, R. (2017). Alix is required during development for normal growth of the mouse brain. *Sci Rep*, *7*, 44767. https://doi.org/10.1038/srep44767

Larkin, H. D. (2022). Autologous Gene Therapy Approved for Childhood CALD. *JAMA*, *328*(17), 1679-1680. https://doi.org/10.1001/jama.2022.19800

Lattanzi, S., Trinka, E., Russo, E., Striano, P., Citraro, R., Silvestrini, M., & Brigo, F. (2019). Cannabidiol as adjunctive treatment of seizures associated with Lennox-Gastaut syndrome and Dravet syndrome. *Drugs Today (Barc)*, *55*(3), 177-196. https://doi.org/10.1358/dot.2019.55.3.2909248

Law, H. L., Wright, R. D., Iqbal, A. J., Norling, L. V., & Cooper, D. (2020). A Pro-resolving Role for Galectin-1 in Acute Inflammation. *Front Pharmacol*, *11*, 274. https://doi.org/10.3389/fphar.2020.00274

Le Hir, H., Sauliere, J., & Wang, Z. (2016). The exon junction complex as a node of post-transcriptional networks. *Nat Rev Mol Cell Biol*, *17*(1), 41-54. https://doi.org/10.1038/nrm.2015.7

Lee, J. A. (2012). Neuronal autophagy: a housekeeper or a fighter in neuronal cell survival? *Exp Neurobiol*, *21*(1), 1-8. https://doi.org/10.5607/en.2012.21.1.1

Lee, J. K. H. (2021). *Investigating the Functional Requirement of Nedd4L for Mammalian Hearing* University of Oxford].

Lewicki, M. S. (1998). A review of methods for spike sorting: the detection and classification of neural action potentials. *Network*, *9*(4), R53-78. https://www.ncbi.nlm.nih.gov/pubmed/10221571

Leyh, J., Paeschke, S., Mages, B., Michalski, D., Nowicki, M., Bechmann, I., & Winter, K. (2021). Classification of Microglial Morphological Phenotypes Using Machine Learning. *Front Cell Neurosci*, *15*, 701673. https://doi.org/10.3389/fncel.2021.701673

Li, H. L., Lin, H. R., & Xia, J. H. (2017). Differential Gene Expression Profiles and Alternative Isoform Regulations in Gill of Nile Tilapia in Response to Acute Hypoxia. *Mar Biotechnol (NY)*, *19*(6), 551-562. https://doi.org/10.1007/s10126-017-9774-4

Li, J., Snyder, E. Y., Tang, F. H. F., Pasqualini, R., Arap, W., & Sidman, R. L. (2020). Nna1 gene deficiency triggers Purkinje neuron death by tubulin hyperglutamylation and ER dysfunction. *JCI Insight*, *5*(19). https://doi.org/10.1172/jci.insight.136078

Li, N., Pan, X., Zhang, J., Ma, A., Yang, S., Ma, J., & Xie, A. (2017). Plasma levels of miR-137 and miR-124 are associated with Parkinson's disease but not with Parkinson's disease with depression. *Neurol Sci*, *38*(5), 761-767. https://doi.org/10.1007/s10072-017-2841-9

Li, X., Du, Z. J., Chen, M. Q., Chen, J. J., Liang, Z. M., Ding, X. T., Zhou, M., Li, S. J., Li, X. W., Yang, J. M., & Gao, T. M. (2020). The effects of tamoxifen on mouse behavior. *Genes Brain Behav*, *19*(4), e12620. https://doi.org/10.1111/gbb.12620

Li, X., Rydzewski, N., Hider, A., Zhang, X., Yang, J., Wang, W., Gao, Q., Cheng, X., & Xu, H. (2016). A molecular mechanism to regulate lysosome motility for lysosome positioning and tubulation. *Nat Cell Biol*, *18*(4), 404-417. https://doi.org/10.1038/ncb3324

Li, Y., Choi, P. S., Casey, S. C., & Felsher, D. W. (2014). Activation of Cre recombinase alone can induce complete tumor regression. *PLoS One*, *9*(9), e107589. https://doi.org/10.1371/journal.pone.0107589

Li, Y., Li, W., Liu, C., Yan, M., Raman, I., Du, Y., Fang, X., Zhou, X. J., Mohan, C., & Li, Q. Z. (2014). Delivering Oxidation Resistance-1 (OXR1) to Mouse Kidney by Genetic Modified Mesenchymal Stem Cells Exhibited Enhanced Protection against Nephrotoxic Serum Induced Renal Injury and Lupus Nephritis. *J Stem Cell Res Ther*, *4*(9). https://doi.org/10.4172/2157-7633.1000231

Li, Y., Ning, G., Kang, B., Zhu, J., Wang, X. Y., Wang, Q., & Cai, T. (2022). A novel recessive mutation in OXR1 is identified in patient with hearing loss recapitulated by the knockdown zebrafish. *Hum Mol Genet*. https://doi.org/10.1093/hmg/ddac229

Liang, J., Xia, L., Oyang, L., Lin, J., Tan, S., Yi, P., Han, Y., Luo, X., Wang, H., Tang, L., Pan, Q., Tian, Y., Rao, S., Su, M., Shi, Y., Cao, D., Zhou, Y., & Liao, Q. (2020). The functions and mechanisms of prefoldin complex and prefoldin-subunits. *Cell Biosci*, *10*, 87. https://doi.org/10.1186/s13578-020-00446-8

Liang, L. P., Huang, J., Fulton, R., Day, B. J., & Patel, M. (2007). An orally active catalytic metalloporphyrin protects against 1-methyl-4-phenyl-1,2,3,6-tetrahydropyridine neurotoxicity in vivo. *J Neurosci*, *27*(16), 4326-4333. https://doi.org/10.1523/JNEUROSCI.0019-07.2007

Liddelow, S. A., Guttenplan, K. A., Clarke, L. E., Bennett, F. C., Bohlen, C. J., Schirmer, L., Bennett, M. L., Munch, A. E., Chung, W. S., Peterson, T. C., Wilton, D. K., Frouin, A., Napier, B. A., Panicker,

N., Kumar, M., Buckwalter, M. S., Rowitch, D. H., Dawson, V. L., Dawson, T. M., . . . Barres, B. A. (2017). Neurotoxic reactive astrocytes are induced by activated microglia. *Nature*, *541*(7638), 481-487. https://doi.org/10.1038/nature21029

Lie, P. P. Y., & Nixon, R. A. (2019). Lysosome trafficking and signaling in health and neurodegenerative diseases. *Neurobiol Dis*, *122*, 94-105. https://doi.org/10.1016/j.nbd.2018.05.015

Lin, L., Lyu, Q., Kwan, P. Y., Zhao, J., Fan, R., Chai, A., Lai, C. S. W., Chan, Y. S., Shen, X., & Lai, K. O. (2020). The epilepsy and intellectual disability-associated protein TBC1D24 regulates the maintenance of excitatory synapses and animal behaviors. *PLoS Genet*, *16*(1), e1008587. https://doi.org/10.1371/journal.pgen.1008587

Lin, P., Zhang, D., Xu, G., & Yan, C. (2018). Identification of IFRD1 variant in a Han Chinese family with autosomal dominant hereditary spastic paraplegia associated with peripheral neuropathy and ataxia. *J Hum Genet*, *63*(4), 521-524. https://doi.org/10.1038/s10038-017-0394-7

Lin, X., Wang, W., Yang, M., Damseh, N., de Sousa, M. M. L., Jacob, F., Lång, A., Kristiansen, E., Pannone, M., Kissova, M., Almaas, R., Kuśnierczyk, A., Siller, R., Shahrour, M., Al-Ashhab, M., Abu-Libdeh, B., Tang, W., Slupphaug, G., Elpeleg, O., . . . Bjørås, M. (2022). Loss-of-function mutation in human Oxidation Resistance gene 1 disrupts the spatial-temporal regulation of histone arginine methylation in early brain development. *bioRxiv*, 2022.2005.2024.493324. https://doi.org/10.1101/2022.05.24.493324

Linde, C. I., Feng, B., Wang, J. B., & Golovina, V. A. (2013). Histidine triad nucleotide-binding protein 1 (HINT1) regulates Ca(2+) signaling in mouse fibroblasts and neuronal cells via store-operated Ca(2+) entry pathway. *Am J Physiol Cell Physiol*, *304*(11), C1098-1104. https://doi.org/10.1152/ajpcell.00073.2013

Lise, S., Clarkson, Y., Perkins, E., Kwasniewska, A., Sadighi Akha, E., Schnekenberg, R. P., Suminaite, D., Hope, J., Baker, I., Gregory, L., Green, A., Allan, C., Lamble, S., Jayawant, S., Quaghebeur, G., Cader, M. Z., Hughes, S., Armstrong, R. J., Kanapin, A., . . . Nemeth, A. H. (2012). Recessive mutations in SPTBN2 implicate beta-III spectrin in both cognitive and motor development. *PLoS Genet*, *8*(12), e1003074. https://doi.org/10.1371/journal.pgen.1003074

Litt, M., Qiu, Y., & Huang, S. (2009). Histone arginine methylations: their roles in chromatin dynamics and transcriptional regulation. *Biosci Rep*, *29*(2), 131-141. https://doi.org/10.1042/BSR20080176

Liu, K. (2016). *Molecular mechanisms of OXR1 function* Oxford University, UK].

Liu, K. X. (2014). *Molecular mechanisms of OXR1 function* University of Oxford].

Liu, K. X., Edwards, B., Lee, S., Finelli, M. J., Davies, B., Davies, K. E., & Oliver, P. L. (2015). Neuron-specific antioxidant OXR1 extends survival of a mouse model of amyotrophic lateral sclerosis. *Brain*, *138*(Pt 5), 1167-1181. https://doi.org/10.1093/brain/awv039

Liu, L., Zou, P., Zheng, L., Linarelli, L. E., Amarell, S., Passaro, A., Liu, D., & Cheng, Z. (2015). Tamoxifen reduces fat mass by boosting reactive oxygen species. *Cell Death Dis*, *6*, e1586. https://doi.org/10.1038/cddis.2014.553

Lopez, I. P., Rodriguez-de la Rosa, L., Pais, R. S., Pineiro-Hermida, S., Torrens, R., Contreras, J., Varela-Nieto, I., & Pichel, J. G. (2015). Differential organ phenotypes after postnatal Igf1r gene conditional deletion induced by tamoxifen in UBC-CreERT2; Igf1r fl/fl double transgenic mice. *Transgenic Res*, *24*(2), 279-294. https://doi.org/10.1007/s11248-014-9837-5

Lopez, M. E., Klein, A. D., Dimbil, U. J., & Scott, M. P. (2011). Anatomically defined neuron-based rescue of neurodegenerative Niemann-Pick type C disorder. *J Neurosci*, *31*(12), 4367-4378. https://doi.org/10.1523/JNEUROSCI.5981-10.2011

Luthy, K., Mei, D., Fischer, B., De Fusco, M., Swerts, J., Paesmans, J., Parrini, E., Lubarr, N., Meijer, I. A., Mackenzie, K. M., Lee, W. T., Cittaro, D., Aridon, P., Schoovaerts, N., Versees, W., Verstreken, P., Casari, G., & Guerrini, R. (2019). TBC1D24-TLDc-related epilepsy exercise-induced dystonia: rescue by antioxidants in a disease model. *Brain*, *142*(8), 2319-2335. https://doi.org/10.1093/brain/awz175

Lynch, D. R., Farmer, J., Hauser, L., Blair, I. A., Wang, Q. Q., Mesaros, C., Snyder, N., Boesch, S., Chin, M., Delatycki, M. B., Giunti, P., Goldsberry, A., Hoyle, C., McBride, M. G., Nachbauer, W., O'Grady, M., Perlman, S., Subramony, S. H., Wilmot, G. R., . . . Meyer, C. (2019). Safety, pharmacodynamics, and potential benefit of omaveloxolone in Friedreich ataxia. *Ann Clin Transl Neurol*, *6*(1), 15-26. https://doi.org/10.1002/acn3.660

Lynch, D. R., Perlman, S. L., & Meier, T. (2010). A phase 3, double-blind, placebo-controlled trial of idebenone in friedreich ataxia. *Arch Neurol*, *67*(8), 941-947. https://doi.org/10.1001/archneurol.2010.168

Ma, C. Y., Li, C., Zhou, X., Zhang, Z., Jiang, H., Liu, H., Chen, H. J., Tse, H. F., Liao, C., & Lian, Q. (2021). Management of adrenoleukodystrophy: From pre-clinical studies to the development of new therapies. *Biomed Pharmacother*, *143*, 112214. https://doi.org/10.1016/j.biopha.2021.112214

Machado, V. H., Palmini, A., Bastos, F. A., & Rotert, R. (2011). Long-term control of epileptic drop attacks with the combination of valproate, lamotrigine, and a benzodiazepine: a 'proof of concept,' open label study. *Epilepsia*, *52*(7), 1303-1310. https://doi.org/10.1111/j.1528-1167.2011.03075.x

Macrotrends. (2022). *World Life Expectancy 1950-2022*. Retrieved 27.07.2022 from https://www.macrotrends.net/countries/WLD/worLd/life-expectancy'>WorLd Life Expectancy 1950-2022. www.macrotrends.net. Retrieved 2022-10-31.

Maguire, M. J., Jackson, C. F., Marson, A. G., & Nevitt, S. J. (2020). Treatments for the prevention of Sudden Unexpected Death in Epilepsy (SUDEP). *Cochrane Database Syst Rev*, *4*, CD011792. https://doi.org/10.1002/14651858.CD011792.pub3

Maheshwari, A. (2020). Rodent EEG: Expanding the Spectrum of Analysis. *Epilepsy Curr*, *20*(3), 149-153. https://doi.org/10.1177/1535759720921377

Mahfouz, A., Ziats, M. N., Rennert, O. M., Lelieveldt, B. P., & Reinders, M. J. (2015). Shared Pathways Among Autism Candidate Genes Determined by Co-expression Network Analysis of the Developing Human Brain Transcriptome. *J Mol Neurosci*, *57*(4), 580-594. https://doi.org/10.1007/s12031-015-0641-3

Mao, D., Lin, G., Tepe, B., Zuo, Z., Tan, K. L., Senturk, M., Zhang, S., Arenkiel, B. R., Sardiello, M., & Bellen, H. J. (2019). VAMP associated proteins are required for autophagic and lysosomal degradation by promoting a PtdIns4P-mediated endosomal pathway. *Autophagy*, *15*(7), 1214-1233. https://doi.org/10.1080/15548627.2019.1580103

Marcelo, A., Afonso, I. T., Afonso-Reis, R., Brito, D. V. C., Costa, R. G., Rosa, A., Alves-Cruzeiro, J., Ferreira, B., Henriques, C., Nobre, R. J., Matos, C. A., de Almeida, L. P., & Nobrega, C. (2021). Autophagy in Spinocerebellar ataxia type 2, a dysregulated pathway, and a target for therapy. *Cell Death Dis*, *12*(12), 1117. https://doi.org/10.1038/s41419-021-04404-1

Marcelo, A., Brito, F., Carmo-Silva, S., Matos, C. A., Alves-Cruzeiro, J., Vasconcelos-Ferreira, A., Koppenol, R., Mendonca, L., de Almeida, L. P., & Nobrega, C. (2019). Cordycepin activates autophagy through AMPK phosphorylation to reduce abnormalities in Machado-Joseph disease models. *Hum Mol Genet*, *28*(1), 51-63. https://doi.org/10.1093/hmg/ddy328

March, P. A. (1998). Seizures: classification, etiologies, and pathophysiology. *Clin Tech Small Anim Pract*, *13*(3), 119-131. https://doi.org/10.1016/S1096-2867(98)80033-9

Mark, M. D., Maejima, T., Kuckelsberg, D., Yoo, J. W., Hyde, R. A., Shah, V., Gutierrez, D., Moreno, R. L., Kruse, W., Noebels, J. L., & Herlitze, S. (2011). Delayed postnatal loss of P/Q-type calcium channels recapitulates the absence epilepsy, dyskinesia, and ataxia phenotypes of genomic Cacna1a mutations. *J Neurosci*, *31*(11), 4311-4326. https://doi.org/10.1523/JNEUROSCI.5342-10.2011

Marschallinger, J., Iram, T., Zardeneta, M., Lee, S. E., Lehallier, B., Haney, M. S., Pluvinage, J. V., Mathur, V., Hahn, O., Morgens, D. W., Kim, J., Tevini, J., Felder, T. K., Wolinski, H., Bertozzi, C. R., Bassik, M. C., Aigner, L., & Wyss-Coray, T. (2020). Lipid-droplet-accumulating microglia represent a dysfunctional and proinflammatory state in the aging brain. *Nat Neurosci*, *23*(2), 194-208. https://doi.org/10.1038/s41593-019-0566-1

Martinet, W., De Bie, M., Schrijvers, D. M., De Meyer, G. R., Herman, A. G., & Kockx, M. M. (2004). 7-ketocholesterol induces protein ubiquitination, myelin figure formation, and light chain 3 processing in vascular smooth muscle cells. *Arterioscler Thromb Vasc Biol*, *24*(12), 2296-2301. https://doi.org/10.1161/01.ATV.0000146266.65820.a1

Martinez-Monseny, A. F., Edo, A., Casas-Alba, D., Izquierdo-Serra, M., Bolasell, M., Conejo, D., Martorell, L., Muchart, J., Carrera, L., Ortez, C. I., Nascimento, A., Oliva, B., Fernandez-Fernandez, J. M., & Serrano, M. (2021). CACNA1A Mutations Causing Early Onset Ataxia: Profiling Clinical, Dysmorphic and Structural-Functional Findings. *Int J Mol Sci*, *22*(10). https://doi.org/10.3390/ijms22105180

Mary, S., Kulkarni, M. J., Malakar, D., Joshi, S. R., Mehendale, S. S., & Giri, A. P. (2017). Placental Proteomics Provides Insights into Pathophysiology of Pre-Eclampsia and Predicts Possible Markers in Plasma. *J Proteome Res*, *16*(2), 1050-1060. https://doi.org/10.1021/acs.jproteome.6b00955

Masse, K., Dabernat, S., Bourbon, P. M., Larou, M., Amrein, L., Barraud, P., Perel, Y., Camara, M., Landry, M., Lacombe, M. L., & Daniel, J. Y. (2002). Characterization of the nm23-M2, nm23-M3 and nm23-M4 mouse genes: comparison with their human orthologs. *Gene*, *296*(1-2), 87-97. https://doi.org/10.1016/s0378-1119(02)00836-3

Matsui, A., Hashiguchi, K., Suzuki, M., & Zhang-Akiyama, Q. M. (2020). Oxidation resistance 1 functions in the maintenance of cellular survival and genome stability in response to oxidative stress-independent DNA damage. *Genes Environ*, *42*(1), 29. https://doi.org/10.1186/s41021-020-00168-w

Maurer-Stroh, S., Eisenhaber, B., & Eisenhaber, F. (2002). N-terminal N-myristoylation of proteins: refinement of the sequence motif and its taxon-specific differences. *J Mol Biol*, *317*(4), 523-540. https://doi.org/10.1006/jmbi.2002.5425

Mayford, M., Bach, M. E., Huang, Y. Y., Wang, L., Hawkins, R. D., & Kandel, E. R. (1996). Control of memory formation through regulated expression of a CaMKII transgene. *Science*, *274*(5293), 1678-1683. https://doi.org/10.1126/science.274.5293.1678

McCready, F. P., Gordillo-Sampedro, S., Pradeepan, K., Martinez-Trujillo, J., & Ellis, J. (2022). Multielectrode Arrays for Functional Phenotyping of Neurons from Induced Pluripotent Stem Cell Models of Neurodevelopmental Disorders. *Biology (Basel)*, *11*(2). https://doi.org/10.3390/biology11020316

McEntagart, M., Parsons, G., Buj-Bello, A., Biancalana, V., Fenton, I., Little, M., Krawczak, M., Thomas, N., Herman, G., Clarke, A., & Wallgren-Pettersson, C. (2002). Genotype-phenotype correlations in X-linked myotubular myopathy. *Neuromuscul Disord*, *12*(10), 939-946. https://doi.org/10.1016/s0960-8966(02)00153-0

McGinty, R. K., & Tan, S. (2015). Nucleosome structure and function. *Chem Rev*, *115*(6), 2255-2273. https://doi.org/10.1021/cr500373h

McIlwain, K. L., Merriweather, M. Y., Yuva-Paylor, L. A., & Paylor, R. (2001). The use of behavioral test batteries: effects of training history. *Physiol Behav*, *73*(5), 705-717. https://doi.org/10.1016/s0031-9384(01)00528-5

Medvedeva, Y. V., Ji, S. G., Yin, H. Z., & Weiss, J. H. (2017). Differential Vulnerability of CA1 versus CA3 Pyramidal Neurons After Ischemia: Possible Relationship to Sources of Zn2+ Accumulation and Its Entry into and Prolonged Effects on Mitochondria. *J Neurosci*, *37*(3), 726-737. https://doi.org/10.1523/JNEUROSCI.3270-16.2016

Meikle, L., Talos, D. M., Onda, H., Pollizzi, K., Rotenberg, A., Sahin, M., Jensen, F. E., & Kwiatkowski, D. J. (2007). A mouse model of tuberous sclerosis: neuronal loss of Tsc1 causes dysplastic and ectopic neurons, reduced myelination, seizure activity, and limited survival. *J Neurosci*, *27*(21), 5546-5558. https://doi.org/10.1523/JNEUROSCI.5540-06.2007

Mellacheruvu, D., Wright, Z., Couzens, A. L., Lambert, J. P., St-Denis, N. A., Li, T., Miteva, Y. V., Hauri, S., Sardiu, M. E., Low, T. Y., Halim, V. A., Bagshaw, R. D., Hubner, N. C., Al-Hakim, A., Bouchard, A., Faubert, D., Fermin, D., Dunham, W. H., Goudreault, M., . . . Nesvizhskii, A. I. (2013). The CRAPome: a contaminant repository for affinity purification-mass spectrometry data. *Nat Methods*, *10*(8), 730-736. https://doi.org/10.1038/nmeth.2557

Mendiola, A. S., Ryu, J. K., Bardehle, S., Meyer-Franke, A., Ang, K. K., Wilson, C., Baeten, K. M., Hanspers, K., Merlini, M., Thomas, S., Petersen, M. A., Williams, A., Thomas, R., Rafalski, V. A., Meza-Acevedo, R., Tognatta, R., Yan, Z., Pfaff, S. J., Machado, M. R., . . . Akassoglou, K. (2020). Transcriptional profiling and therapeutic targeting of oxidative stress in neuroinflammation. *Nat Immunol*, *21*(5), 513-524. https://doi.org/10.1038/s41590-020-0654-0

Mendoza-Velasquez, J. J., Flores-Vazquez, J. F., Barron-Velazquez, E., Sosa-Ortiz, A. L., Illigens, B. W., & Siepmann, T. (2019). Autonomic Dysfunction in alpha-Synucleinopathies. *Front Neurol*, *10*, 363. https://doi.org/10.3389/fneur.2019.00363

Mercado-Ayon, E., Warren, N., Halawani, S., Rodden, L. N., Ngaba, L., Dong, Y. N., Chang, J. C., Fonck, C., Mavilio, F., Lynch, D. R., & Lin, H. (2022). Cerebellar Pathology in an Inducible Mouse Model of Friedreich Ataxia. *Front Neurosci*, *16*, 819569. https://doi.org/10.3389/fnins.2022.819569

Mercuri, E., Muntoni, F., Baranello, G., Masson, R., Boespflug-Tanguy, O., Bruno, C., Corti, S., Daron, A., Deconinck, N., Servais, L., Straub, V., Ouyang, H., Chand, D., Tauscher-Wisniewski, S., Mendonca, N., Lavrov, A., & group, S. V.-E. s. (2021). Onasemnogene abeparvovec gene therapy for symptomatic infantile-onset spinal muscular atrophy type 1 (STR1VE-EU): an open-label, single-arm, multicentre, phase 3 trial. *Lancet Neurol*, *20*(10), 832-841. https://doi.org/10.1016/S1474-4422(21)00251-9

Merkulova, M., Paunescu, T. G., Nair, A. V., Wang, C. Y., Capen, D. E., Oliver, P. L., Breton, S., & Brown, D. (2018). Targeted deletion of the Ncoa7 gene results in incomplete distal renal tubular acidosis in mice. *Am J Physiol Renal Physiol*, *315*(1), F173-F185. https://doi.org/10.1152/ajprenal.00407.2017

Miller, S. G., & Kennedy, M. B. (1986). Regulation of brain type II Ca2+/calmodulin-dependent protein kinase by autophosphorylation: a Ca2+-triggered molecular switch. *Cell*, *44*(6), 861-870. https://doi.org/10.1016/0092-8674(86)90008-5

Mindell, J. A. (2012). Lysosomal acidification mechanisms. *Annu Rev Physiol*, *74*, 69-86. https://doi.org/10.1146/annurev-physiol-012110-142317

Ming, G. L., & Song, H. (2011). Adult neurogenesis in the mammalian brain: significant answers and significant questions. *Neuron*, *70*(4), 687-702. https://doi.org/10.1016/j.neuron.2011.05.001

Mitchell, A. L., Attwood, T. K., Babbitt, P. C., Blum, M., Bork, P., Bridge, A., Brown, S. D., Chang, H. Y., El-Gebali, S., Fraser, M. I., Gough, J., Haft, D. R., Huang, H., Letunic, I., Lopez, R., Luciani, A., Madeira, F., Marchler-Bauer, A., Mi, H., . . . Finn, R. D. (2019). InterPro in 2019: improving coverage, classification and access to protein sequence annotations. *Nucleic Acids Res*, *47*(D1), D351-D360. https://doi.org/10.1093/nar/gky1100

Miyata, M., Oishi, A., Oishi, M., Hasegawa, T., Ikeda, H. O., & Tsujikawa, A. (2018). Long-term efficacy and safety of anti-VEGF therapy in retinitis pigmentosa: a case report. *BMC Ophthalmol*, *18*(1), 248. https://doi.org/10.1186/s12886-018-0914-z

Mo, J. L., Pan, Z. G., Chen, X., Lei, Y., Lv, L. L., Qian, C., & Sun, F. Y. (2019). MicroRNA-365 Knockdown Prevents Ischemic Neuronal Injury by Activating Oxidation Resistance 1-Mediated Antioxidant Signals. *Neurosci Bull*, *35*(5), 815-825. https://doi.org/10.1007/s12264-019-00371-y

Moezi, L., Ashjazadeh, N., Rezapanah, S., Pirsalami, F., Esmaeili, Z., SoukhakLari, R., & Moosavi, M. (2021). Anticonvulsant effect of acute curcumin nanoparticle on pentylenetetrazole-induced seizures in mice: non-involvement of JNK restoration. *Physiology and Pharmacology*, *25*(1), 36-46. https://doi.org/10.32598/ppj.25.1.80

Mohammadi, M., Guan, J., Khodagholi, F., Yans, A., Khalaj, S., Gholami, M., Taghizadeh, G. H., Aliaghaei, A., Abdollahi, M., Ghahremani, M. H., & Sharifzadeh, M. (2016). Reduction of autophagy markers mediated protective effects of JNK inhibitor and bucladesine on memory deficit induced by Abeta in rats. *Naunyn Schmiedebergs Arch Pharmacol*, *389*(5), 501-510. https://doi.org/10.1007/s00210-016-1222-x

Moller, M., Swanepoel, T., & Harvey, B. H. (2015). Neurodevelopmental Animal Models Reveal the Convergent Role of Neurotransmitter Systems, Inflammation, and Oxidative Stress as Biomarkers of Schizophrenia: Implications for Novel Drug Development. *ACS Chem Neurosci*, *6*(7), 987-1016. https://doi.org/10.1021/cn5003368

Morimoto, M., Hashimoto, T., Tsuda, Y., Nakatsu, T., Kitaoka, T., & Kyotani, S. (2020). Assessment of oxidative stress in autism spectrum disorder using reactive oxygen metabolites and biological antioxidant potential. *PLoS One*, *15*(5), e0233550. https://doi.org/10.1371/journal.pone.0233550

Morozov, A., Kellendonk, C., Simpson, E., & Tronche, F. (2003). Using conditional mutagenesis to study the brain. *Biol Psychiatry*, *54*(11), 1125-1133. https://doi.org/10.1016/s0006-3223(03)00467-0

Mucha, B. E., Hennekam, R. C. M., Sisodiya, S., & Campeau, P. M. (2017). TBC1D24-Related Disorders. In M. P. Adam, D. B. Everman, G. M. Mirzaa, R. A. Pagon, S. E. Wallace, L. J. H. Bean, K. W. Gripp, & A. Amemiya (Eds.), *GeneReviews((R))*. https://www.ncbi.nlm.nih.gov/pubmed/25719194

Mukherjee, S., Klaus, C., Pricop-Jeckstadt, M., Miller, J. A., & Struebing, F. L. (2019). A Microglial Signature Directing Human Aging and Neurodegeneration-Related Gene Networks. *Front Neurosci*, *13*, 2. https://doi.org/10.3389/fnins.2019.00002

Mullen, R. J., Buck, C. R., & Smith, A. M. (1992). NeuN, a neuronal specific nuclear protein in vertebrates. *Development*, *116*(1), 201-211. https://doi.org/10.1242/dev.116.1.201

Mullen, R. J., Eicher, E. M., & Sidman, R. L. (1976). Purkinje cell degeneration, a new neurological mutation in the mouse. *Proc Natl Acad Sci U S A*, *73*(1), 208-212. https://doi.org/10.1073/pnas.73.1.208

Mullins, R. D., Heuser, J. A., & Pollard, T. D. (1998). The interaction of Arp2/3 complex with actin: nucleation, high affinity pointed end capping, and formation of branching networks of filaments. *Proc Natl Acad Sci U S A*, *95*(11), 6181-6186. https://doi.org/10.1073/pnas.95.11.6181

Murphy, M. P., & LeVine, H., 3rd. (2010). Alzheimer's disease and the amyloid-beta peptide. *J Alzheimers Dis*, *19*(1), 311-323. https://doi.org/10.3233/JAD-2010-1221

Murphy, N. M., Samarasekera, T. S., Macaskill, L., Mullen, J., & Rombauts, L. J. F. (2020). Genome sequencing of human in vitro fertilisation embryos for pathogenic variation screening. *Sci Rep*, *10*(1), 3795. https://doi.org/10.1038/s41598-020-60704-0

Murphy, S. J., & Werring, D. J. (2020). Stroke: causes and clinical features. *Medicine (Abingdon)*, *48*(9), 561-566. https://doi.org/10.1016/j.mpmed.2020.06.002

Mystkowski, P., Shankland, E., Schreyer, S. A., LeBoeuf, R. C., Schwartz, R. S., Cummings, D. E., Kushmerick, M., & Schwartz, M. W. (2000). Validation of whole-body magnetic resonance spectroscopy as a tool to assess murine body composition. *Int J Obes Relat Metab Disord*, *24*(6), 719-724. https://doi.org/10.1038/sj.ijo.0801231

Nadadhur, A. G., Alsaqati, M., Gasparotto, L., Cornelissen-Steijger, P., van Hugte, E., Dooves, S., Harwood, A. J., & Heine, V. M. (2019). Neuron-Glia Interactions Increase Neuronal Phenotypes in Tuberous Sclerosis Complex Patient iPSC-Derived Models. *Stem Cell Reports*, *12*(1), 42-56. https://doi.org/10.1016/j.stemcr.2018.11.019

Nakajo, S., Tsukada, K., Omata, K., Nakamura, Y., & Nakaya, K. (1993). A new brain-specific 14-kDa protein is a phosphoprotein. Its complete amino acid sequence and evidence for phosphorylation. *Eur J Biochem*, *217*(3), 1057-1063. https://doi.org/10.1111/j.1432-1033.1993.tb18337.x

Nakazawa, K., Quirk, M. C., Chitwood, R. A., Watanabe, M., Yeckel, M. F., Sun, L. D., Kato, A., Carr, C. A., Johnston, D., Wilson, M. A., & Tonegawa, S. (2002). Requirement for hippocampal CA3 NMDA receptors in associative memory recall. *Science*, *297*(5579), 211-218. https://doi.org/10.1126/science.1071795

Natoli, R., Provis, J., Valter, K., & Stone, J. (2008). Expression and role of the early-response gene Oxr1 in the hyperoxia-challenged mouse retina. *Invest Ophthalmol Vis Sci*, *49*(10), 4561-4567. https://doi.org/10.1167/iovs.08-1722

Navarro, J. F., Croteau, D. L., Jurek, A., Andrusivova, Z., Yang, B., Wang, Y., Ogedegbe, B., Riaz, T., Stoen, M., Desler, C., Rasmussen, L. J., Tonjum, T., Galas, M. C., Lundeberg, J., & Bohr, V. A. (2020). Spatial Transcriptomics Reveals Genes Associated with Dysregulated Mitochondrial Functions and Stress Signaling in Alzheimer Disease. *iScience*, *23*(10), 101556. https://doi.org/10.1016/j.isci.2020.101556

Negri, J., Menon, V., & Young-Pearse, T. L. (2020). Assessment of Spontaneous Neuronal Activity In Vitro Using Multi-Well Multi-Electrode Arrays: Implications for Assay Development. *eNeuro*, *7*(1). https://doi.org/10.1523/ENEURO.0080-19.2019

Nehls, U., Friedrich, T., Schmiede, A., Ohnishi, T., & Weiss, H. (1992). Characterization of assembly intermediates of NADH:ubiquinone oxidoreductase (complex I) accumulated in Neurospora mitochondria by gene disruption. *J Mol Biol*, *227*(4), 1032-1042. https://doi.org/10.1016/0022-2836(92)90519-p

Nesvizhskii, A. I. (2012). Computational and informatics strategies for identification of specific protein interaction partners in affinity purification mass spectrometry experiments. *Proteomics*, *12*(10), 1639-1655. https://doi.org/10.1002/pmic.201100537

Neumann, M., Sampathu, D. M., Kwong, L. K., Truax, A. C., Micsenyi, M. C., Chou, T. T., Bruce, J., Schuck, T., Grossman, M., Clark, C. M., McCluskey, L. F., Miller, B. L., Masliah, E., Mackenzie, I. R., Feldman, H., Feiden, W., Kretzschmar, H. A., Trojanowski, J. Q., & Lee, V. M. (2006). Ubiquitinated TDP-43 in frontotemporal lobar degeneration and amyotrophic lateral sclerosis. *Science*, *314*(5796), 130-133. https://doi.org/10.1126/science.1134108

Ngoh, A., Bras, J., Guerreiro, R., McTague, A., Ng, J., Meyer, E., Chong, W. K., Boyd, S., MacLellan, L., Kirkpatrick, M., & Kurian, M. A. (2017). TBC1D24 Mutations in a Sibship with Multifocal Polymyoclonus. *Tremor Other Hyperkinet Mov (N Y)*, *7*, 452. https://doi.org/10.7916/D8Q52VBV

Nguyen, J. T., Ray, C., Fox, A. L., Mendonca, D. B., Kim, J. K., & Krebsbach, P. H. (2018). Mammalian EAK-7 activates alternative mTOR signaling to regulate cell proliferation and migration. *Sci Adv*, *4*(5), eaao5838. https://doi.org/10.1126/sciadv.aao5838

O'Neil, S. M., Hans, E. E., Jiang, S., Wangler, L. M., & Godbout, J. P. (2022). Astrocyte immunosenescence and deficits in interleukin 10 signaling in the aged brain disrupt the regulation of microglia following innate immune activation. *Glia*, *70*(5), 913-934. https://doi.org/10.1002/glia.24147

Odabaee, M., Tokariev, A., Layeghy, S., Mesbah, M., Colditz, P. B., Ramon, C., & Vanhatalo, S. (2014). Neonatal EEG at scalp is focal and implies high skull conductivity in realistic neonatal head models. *Neuroimage*, *96*, 73-80. https://doi.org/10.1016/j.neuroimage.2014.04.007

Oliver, P. L., Finelli, M. J., Edwards, B., Bitoun, E., Butts, D. L., Becker, E. B., Cheeseman, M. T., Davies, B., & Davies, K. E. (2011). Oxr1 is essential for protection against oxidative stress-induced neurodegeneration. *PLoS Genet*, *7*(10), e1002338. https://doi.org/10.1371/journal.pgen.1002338

Olsen, R. W. (2018). GABAA receptor: Positive and negative allosteric modulators. *Neuropharmacology*, *136*(Pt A), 10-22. https://doi.org/10.1016/j.neuropharm.2018.01.036

Orvis, J., Gottfried, B., Kancherla, J., Adkins, R. S., Song, Y., Dror, A. A., Olley, D., Rose, K., Chrysostomou, E., Kelly, M. C., Milon, B., Matern, M. S., Azaiez, H., Herb, B., Colantuoni, C., Carter, R. L., Ament, S. A., Kelley, M. W., White, O., . . . Hertzano, R. (2021). gEAR: Gene

Expression Analysis Resource portal for community-driven, multi-omic data exploration. *Nat Methods*, *18*(8), 843-844. https://doi.org/10.1038/s41592-021-01200-9

Otero, A. S. (2000). NM23/nucleoside diphosphate kinase and signal transduction. *J Bioenerg Biomembr*, *32*(3), 269-275. https://doi.org/10.1023/a:1005589029959

Pajares, M., Cuadrado, A., & Rojo, A. I. (2017). Modulation of proteostasis by transcription factor NRF2 and impact in neurodegenerative diseases. *Redox Biol*, *11*, 543-553. https://doi.org/10.1016/j.redox.2017.01.006

Pandya, N. J., Koopmans, F., Slotman, J. A., Paliukhovich, I., Houtsmuller, A. B., Smit, A. B., & Li, K. W. (2017). Correlation profiling of brain sub-cellular proteomes reveals co-assembly of synaptic proteins and subcellular distribution. *Sci Rep*, *7*(1), 12107. https://doi.org/10.1038/s41598-017-11690-3

Pankiv, S., Clausen, T. H., Lamark, T., Brech, A., Bruun, J. A., Outzen, H., Overvatn, A., Bjorkoy, G., & Johansen, T. (2007). p62/SQSTM1 binds directly to Atg8/LC3 to facilitate degradation of ubiquitinated protein aggregates by autophagy. *J Biol Chem*, *282*(33), 24131-24145. https://doi.org/10.1074/jbc.M702824200

Panov, A., Orynbayeva, Z., Vavilin, V., & Lyakhovich, V. (2014). Fatty acids in energy metabolism of the central nervous system. *Biomed Res Int*, *2014*, 472459. https://doi.org/10.1155/2014/472459

Papp, G., Witter, M. P., & Treves, A. (2007). The CA3 network as a memory store for spatial representations. *Learn Mem*, *14*(11), 732-744. https://doi.org/10.1101/lm.687407

Pardo, O. E., & Seckl, M. J. (2013). S6K2: The Neglected S6 Kinase Family Member. *Front Oncol*, *3*, 191. https://doi.org/10.3389/fonc.2013.00191

Parenti, R., & Cicirata, F. (2004). Retinoids and binding proteins in the cerebellum during lifetime. *Cerebellum*, *3*(1), 16-20. https://doi.org/10.1080/14734220310017186

Park, E. K., Warner, N., Mood, K., Pawson, T., & Daar, I. O. (2002). Low-molecular-weight protein tyrosine phosphatase is a positive component of the fibroblast growth factor receptor signaling pathway. *Mol Cell Biol*, *22*(10), 3404-3414. https://doi.org/10.1128/MCB.22.10.3404-3414.2002

Park, H. W., Park, C. G., Park, M., Lee, S. H., Park, H. R., Lim, J., Paek, S. H., & Choy, Y. B. (2020). Intrastriatal administration of coenzyme Q10 enhances neuroprotection in a Parkinson's disease rat model. *Sci Rep*, *10*(1), 9572. https://doi.org/10.1038/s41598-020-66493-w

Parsons, A. L. M., Bucknor, E. M. V., Castroflorio, E., Soares, T. R., Oliver, P. L., & Rial, D. (2022). The Interconnected Mechanisms of Oxidative Stress and Neuroinflammation in Epilepsy. *Antioxidants (Basel)*, *11*(1). https://doi.org/10.3390/antiox11010157

Parzefall, T., Frohne, A., Koenighofer, M., Neesen, J., Laccone, F., Eckl-Dorna, J., Waters, J. J., Schreiner, M., Amr, S. S., Ashton, E., Schoefer, C., Gstoettner, W., Frei, K., & Lucas, T. (2020). A Novel Variant in the TBC1D24 Lipid-Binding Pocket Causes Autosomal Dominant Hearing Loss: Evidence for a Genotype-Phenotype Correlation. *Front Cell Neurosci*, *14*, 585669. https://doi.org/10.3389/fncel.2020.585669

Peeters, K., Chamova, T., Tournev, I., & Jordanova, A. (2017). Axonal neuropathy with neuromyotonia: there is a HINT. *Brain*, *140*(4), 868-877. https://doi.org/10.1093/brain/aww301

Pelechano, V., & Alepuz, P. (2017). eIF5A facilitates translation termination globally and promotes the elongation of many non polyproline-specific tripeptide sequences. *Nucleic Acids Res*, *45*(12), 7326-7338. https://doi.org/10.1093/nar/gkx479

Pena, S. A., Iyengar, R., Eshraghi, R. S., Bencie, N., Mittal, J., Aljohani, A., Mittal, R., & Eshraghi, A. A. (2020). Gene therapy for neurological disorders: challenges and recent advancements. *J Drug Target*, *28*(2), 111-128. https://doi.org/10.1080/1061186X.2019.1630415

Peng, J., Sheng, A. L., Xiao, Q., Shen, L., Ju, X. C., Zhang, M., He, S. T., Wu, C., & Luo, Z. G. (2019). Single-cell transcriptomes reveal molecular specializations of neuronal cell types in the developing cerebellum. *J Mol Cell Biol*, *11*(8), 636-648. https://doi.org/10.1093/jmcb/mjy089

Perucca, P., Bahlo, M., & Berkovic, S. F. (2020). The Genetics of Epilepsy. *Annu Rev Genomics Hum Genet*, *21*, 205-230. https://doi.org/10.1146/annurev-genom-120219-074937

Pettas, S., Karagianni, K., Kanata, E., Chatziefstathiou, A., Christoudia, N., Xanthopoulos, K., Sklaviadis, T., & Dafou, D. (2022). Profiling Microglia through Single-Cell RNA Sequencing over the Course of Development, Aging, and Disease. *Cells*, *11*(15). https://doi.org/10.3390/cells11152383

Pfisterer, U., Petukhov, V., Demharter, S., Meichsner, J., Thompson, J. J., Batiuk, M. Y., Asenjo-Martinez, A., Vasistha, N. A., Thakur, A., Mikkelsen, J., Adorjan, I., Pinborg, L. H., Pers, T. H., von Engelhardt, J., Kharchenko, P. V., & Khodosevich, K. (2020). Identification of epilepsy-associated neuronal subtypes and gene expression underlying epileptogenesis. *Nat Commun*, *11*(1), 5038. https://doi.org/10.1038/s41467-020-18752-7

Piccinini, A. M., & Midwood, K. S. (2010). DAMPening inflammation by modulating TLR signalling. *Mediators Inflamm*, *2010*. https://doi.org/10.1155/2010/672395

Platt, F. M. (2014). Sphingolipid lysosomal storage disorders. *Nature*, *510*(7503), 68-75. https://doi.org/10.1038/nature13476

Poulos, R. C., Hains, P. G., Shah, R., Lucas, N., Xavier, D., Manda, S. S., Anees, A., Koh, J. M. S., Mahboob, S., Wittman, M., Williams, S. G., Sykes, E. K., Hecker, M., Dausmann, M., Wouters, M. A., Ashman, K., Yang, J., Wild, P. J., deFazio, A., . . . Zhong, Q. (2020). Strategies to enable large-scale proteomics for reproducible research. *Nat Commun*, *11*(1), 3793. https://doi.org/10.1038/s41467-020-17641-3

Prakash, P., Jethava, K. P., Korte, N., Izquierdo, P., Favuzzi, E., Rose, I. V. L., Guttenplan, K. A., Manchanda, P., Dutta, S., Rochet, J. C., Fishell, G., Liddelow, S. A., Attwell, D., & Chopra, G. (2021). Monitoring phagocytic uptake of amyloid beta into glial cell lysosomes in real time. *Chem Sci*, *12*(32), 10901-10918. https://doi.org/10.1039/d1sc03486c

Prasad, M., Krishnan, P. R., Sequeira, R., & Al-Roomi, K. (2014). Anticonvulsant therapy for status epilepticus. *Cochrane Database Syst Rev*(9), CD003723. https://doi.org/10.1002/14651858.CD003723.pub3

Qualmann, B., & Kessels, M. M. (2008). Actin nucleation: putting the brakes on Arp2/3. *Curr Biol*, *18*(10), R420-R423. https://doi.org/10.1016/j.cub.2008.04.014

Que, Z., Olivero-Acosta, M. I., Zhang, J., Eaton, M., Tukker, A. M., Chen, X., Wu, J., Xie, J., Xiao, T., Wettschurack, K., Yunis, L., Shafer, J. M., Schaber, J. A., Rochet, J. C., Bowman, A. B., Yuan, C., Huang, Z., Hu, C. D., Trader, D. J., . . . Yang, Y. (2021). Hyperexcitability and Pharmacological Responsiveness of Cortical Neurons Derived from Human iPSCs Carrying Epilepsy-Associated Sodium Channel Nav1.2-L1342P Genetic Variant. *J Neurosci*, *41*(49), 10194-10208. https://doi.org/10.1523/JNEUROSCI.0564-21.2021

Quraishi, I. H., Stern, S., Mangan, K. P., Zhang, Y., Ali, S. R., Mercier, M. R., Marchetto, M. C., McLachlan, M. J., Jones, E. M., Gage, F. H., & Kaczmarek, L. K. (2019). An Epilepsy-Associated KCNT1 Mutation Enhances Excitability of Human iPSC-Derived Neurons by Increasing Slack K(Na) Currents. *J Neurosci*, *39*(37), 7438-7449. https://doi.org/10.1523/JNEUROSCI.1628-18.2019

Racay, P., Gregory, P., & Schwaller, B. (2006). Parvalbumin deficiency in fast-twitch muscles leads to increased 'slow-twitch type' mitochondria, but does not affect the expression of fiber specific proteins. *FEBS J*, *273*(1), 96-108. https://doi.org/10.1111/j.1742-4658.2005.05046.x

Rains, M. E., Muncie, C. B., Pang, Y., Fan, L. W., Tien, L. T., & Ojeda, N. B. (2021). Oxidative Stress and Neurodevelopmental Outcomes in Rat Offspring with Intrauterine Growth Restriction Induced by Reduced Uterine Perfusion. *Brain Sci*, *11*(1). https://doi.org/10.3390/brainsci11010078

Rama Rao, K. V., & Kielian, T. (2015). Neuron-astrocyte interactions in neurodegenerative diseases: Role of neuroinflammation. *Clin Exp Neuroimmunol*, *6*(3), 245-263. https://doi.org/10.1111/cen3.12237

Ramachandran, N., Munteanu, I., Wang, P., Ruggieri, A., Rilstone, J. J., Israelian, N., Naranian, T., Paroutis, P., Guo, R., Ren, Z. P., Nishino, I., Chabrol, B., Pellissier, J. F., Minetti, C., Udd, B., Fardeau, M., Tailor, C. S., Mahuran, D. J., Kissel, J. T., . . . Minassian, B. A. (2013). VMA21 deficiency prevents vacuolar ATPase assembly and causes autophagic vacuolar myopathy. *Acta Neuropathol*, *125*(3), 439-457. https://doi.org/10.1007/s00401-012-1073-6

Rao, M. S., Van Vleet, T. R., Ciurlionis, R., Buck, W. R., Mittelstadt, S. W., Blomme, E. A. G., & Liguori, M. J. (2018). Comparison of RNA-Seq and Microarray Gene Expression Platforms for the Toxicogenomic Evaluation of Liver From Short-Term Rat Toxicity Studies. *Front Genet*, *9*, 636. https://doi.org/10.3389/fgene.2018.00636

Rawn, J. D., & Ouellette, R. J. (2018). *Organic chemistry : structure, mechanism, synthesis* (Second edition. ed.). Academic Press. http://library.ncl.ac.uk/openurl/?u.ignore_date_coverage=true&rft.mms_id=9912681217402411

Redmann, M., Benavides, G. A., Berryhill, T. F., Wani, W. Y., Ouyang, X., Johnson, M. S., Ravi, S., Barnes, S., Darley-Usmar, V. M., & Zhang, J. (2017). Inhibition of autophagy with bafilomycin and chloroquine decreases mitochondrial quality and bioenergetic function in primary neurons. *Redox Biol*, *11*, 73-81. https://doi.org/10.1016/j.redox.2016.11.004

Reiman, E. M., Arboleda-Velasquez, J. F., Quiroz, Y. T., Huentelman, M. J., Beach, T. G., Caselli, R. J., Chen, Y., Su, Y., Myers, A. J., Hardy, J., Paul Vonsattel, J., Younkin, S. G., Bennett, D. A., De Jager, P. L., Larson, E. B., Crane, P. K., Keene, C. D., Kamboh, M. I., Kofler, J. K., . . . Alzheimer's Disease Genetics, C. (2020). Exceptionally low likelihood of Alzheimer's dementia in APOE2 homozygotes from a 5,000-person neuropathological study. *Nat Commun*, *11*(1), 667. https://doi.org/10.1038/s41467-019-14279-8

Rensing, N., Moy, B., Friedman, J. L., Galindo, R., & Wong, M. (2018). Longitudinal analysis of developmental changes in electroencephalography patterns and sleep-wake states of the neonatal mouse. *PLoS One*, *13*(11), e0207031. https://doi.org/10.1371/journal.pone.0207031

Repnik, U., Cesen, M. H., & Turk, B. (2013). The endolysosomal system in cell death and survival. *Cold Spring Harb Perspect Biol*, *5*(1), a008755. https://doi.org/10.1101/cshperspect.a008755

Rial, D., Castro, A. A., Machado, N., Garcao, P., Goncalves, F. Q., Silva, H. B., Tome, A. R., Kofalvi, A., Corti, O., Raisman-Vozari, R., Cunha, R. A., & Prediger, R. D. (2014). Behavioral phenotyping of

Parkin-deficient mice: looking for early preclinical features of Parkinson's disease. *PLoS One*, *9*(12), e114216. https://doi.org/10.1371/journal.pone.0114216

Rice, D., & Barone, S., Jr. (2000). Critical periods of vulnerability for the developing nervous system: evidence from humans and animal models. *Environ Health Perspect*, *108 Suppl 3*, 511-533. https://doi.org/10.1289/ehp.00108s3511

Rivers, R. C., Kumita, J. R., Tartaglia, G. G., Dedmon, M. M., Pawar, A., Vendruscolo, M., Dobson, C. M., & Christodoulou, J. (2008). Molecular determinants of the aggregation behavior of alpha- and beta-synuclein. *Protein Sci*, *17*(5), 887-898. https://doi.org/10.1110/ps.073181508

Rojo, A. I., Pajares, M., Rada, P., Nunez, A., Nevado-Holgado, A. J., Killik, R., Van Leuven, F., Ribe, E., Lovestone, S., Yamamoto, M., & Cuadrado, A. (2017). NRF2 deficiency replicates transcriptomic changes in Alzheimer's patients and worsens APP and TAU pathology. *Redox Biol*, *13*, 444-451. https://doi.org/10.1016/j.redox.2017.07.006

Rossignol, E., Kruglikov, I., van den Maagdenberg, A. M., Rudy, B., & Fishell, G. (2013). CaV 2.1 ablation in cortical interneurons selectively impairs fast-spiking basket cells and causes generalized seizures. *Ann Neurol*, *74*(2), 209-222. https://doi.org/10.1002/ana.23913

Roy, M., Sorokina, O., McLean, C., Tapia-Gonzalez, S., DeFelipe, J., Armstrong, J. D., & Grant, S. G. N. (2018). Regional Diversity in the Postsynaptic Proteome of the Mouse Brain. *Proteomes*, *6*(3). https://doi.org/10.3390/proteomes6030031

Ruan, Y., Zheng, X. Y., Zhang, H. L., Zhu, W., & Zhu, J. (2012). Olfactory dysfunctions in neurodegenerative disorders. *J Neurosci Res*, *90*(9), 1693-1700. https://doi.org/10.1002/jnr.23054

Rudolph, U., Crestani, F., Benke, D., Brunig, I., Benson, J. A., Fritschy, J. M., Martin, J. R., Bluethmann, H., & Mohler, H. (1999). Benzodiazepine actions mediated by specific gamma-aminobutyric acid(A) receptor subtypes. *Nature*, *401*(6755), 796-800. https://doi.org/10.1038/44579

Ruiz, J., Kouiavskaia, D., Migliorini, M., Robinson, S., Saenko, E. L., Gorlatova, N., Li, D., Lawrence, D., Hyman, B. T., Weisgraber, K. H., & Strickland, D. K. (2005). The apoE isoform binding properties of the VLDL receptor reveal marked differences from LRP and the LDL receptor. *J Lipid Res*, *46*(8), 1721-1731. https://doi.org/10.1194/jlr.M500114-JLR200

Rujano, M. A., Cannata Serio, M., Panasyuk, G., Peanne, R., Reunert, J., Rymen, D., Hauser, V., Park, J. H., Freisinger, P., Souche, E., Guida, M. C., Maier, E. M., Wada, Y., Jager, S., Krogan, N. J., Kretz, O., Nobre, S., Garcia, P., Quelhas, D., . . . Simons, M. (2017). Mutations in the X-linked ATP6AP2 cause a glycosylation disorder with autophagic defects. *J Exp Med*, *214*(12), 3707-3729. https://doi.org/10.1084/jem.20170453

Ruzankina, Y., Pinzon-Guzman, C., Asare, A., Ong, T., Pontano, L., Cotsarelis, G., Zediak, V. P., Velez, M., Bhandoola, A., & Brown, E. J. (2007). Deletion of the developmentally essential gene ATR in adult mice leads to age-related phenotypes and stem cell loss. *Cell Stem Cell*, *1*(1), 113-126. https://doi.org/10.1016/j.stem.2007.03.002

Sahu, B., Leon, L. M., Zhang, W., Puranik, N., Periasamy, R., Khanna, H., & Volkert, M. (2021). Oxidative Stress Resistance 1 Gene Therapy Retards Neurodegeneration in the rd1 Mutant Mouse Model of Retinopathy. *Invest Ophthalmol Vis Sci*, *62*(12), 8. https://doi.org/10.1167/iovs.62.12.8

Sakamaki, J. I., & Ryan, K. M. (2017). Transcriptional regulation of autophagy and lysosomal function by bromodomain protein BRD4. *Autophagy*, *13*(11), 2006-2007. https://doi.org/10.1080/15548627.2017.1364822

Salman, M. S. (2018). Epidemiology of Cerebellar Diseases and Therapeutic Approaches. *Cerebellum*, *17*(1), 4-11. https://doi.org/10.1007/s12311-017-0885-2

Sapir, T., Segal, M., Grigoryan, G., Hansson, K. M., James, P., Segal, M., & Reiner, O. (2019). The Interactome of Palmitoyl-Protein Thioesterase 1 (PPT1) Affects Neuronal Morphology and Function. *Front Cell Neurosci*, *13*, 92. https://doi.org/10.3389/fncel.2019.00092

Sarna, J. R., Larouche, M., Marzban, H., Sillitoe, R. V., Rancourt, D. E., & Hawkes, R. (2003). Patterned Purkinje cell degeneration in mouse models of Niemann-Pick type C disease. *J Comp Neurol*, *456*(3), 279-291. https://doi.org/10.1002/cne.10522

Sarva, H., & Shanker, V. L. (2014). Treatment Options in Degenerative Cerebellar Ataxia: A Systematic Review. *Mov Disord Clin Pract*, *1*(4), 291-298. https://doi.org/10.1002/mdc3.12057

Satoh, J., Kino, Y., Asahina, N., Takitani, M., Miyoshi, J., Ishida, T., & Saito, Y. (2016). TMEM119 marks a subset of microglia in the human brain. *Neuropathology*, *36*(1), 39-49. https://doi.org/10.1111/neup.12235

Sayers, E. W., Bolton, E. E., Brister, J. R., Canese, K., Chan, J., Comeau, D. C., Connor, R., Funk, K., Kelly, C., Kim, S., Madej, T., Marchler-Bauer, A., Lanczycki, C., Lathrop, S., Lu, Z., Thibaud-Nissen, F., Murphy, T., Phan, L., Skripchenko, Y., . . . Sherry, S. T. (2022). Database resources of the national center for biotechnology information. *Nucleic Acids Res*, *50*(D1), D20-D26. https://doi.org/10.1093/nar/gkab1112

Scalise, S., Zannino, C., Lucchino, V., Lo Conte, M., Scaramuzzino, L., Cifelli, P., D'Andrea, T., Martinello, K., Fucile, S., Palma, E., Gambardella, A., Ruffolo, G., Cuda, G., & Parrotta, E. I. (2022). Human iPSC Modeling of Genetic Febrile Seizure Reveals Aberrant Molecular and Physiological Features Underlying an Impaired Neuronal Activity. *Biomedicines*, *10*(5). https://doi.org/10.3390/biomedicines10051075

Schartz, N. D., & Tenner, A. J. (2020). The good, the bad, and the opportunities of the complement system in neurodegenerative disease. *J Neuroinflammation*, *17*(1), 354. https://doi.org/10.1186/s12974-020-02024-8

Schaum, N., Lehallier, B., Hahn, O., Hosseinzadeh, S., Lee, S. E., Sit, R., Lee, D. P., Losada, P. M., Zardeneta, M. E., Pálovics, R., Fehlmann, T., Webber, J., McGeever, A., Zhang, H., Berdnik, D., Tan, W., Zee, A., Tan, M., Pisco, A., . . . Wyss-Coray, T. (2019). The murine transcriptome reveals global aging nodes with organ-specific phase and amplitude. *bioRxiv*, 662254. https://doi.org/10.1101/662254

Schauwecker, P. E. (2013). Microarray-assisted fine mapping of quantitative trait loci on chromosome 15 for susceptibility to seizure-induced cell death in mice. *Eur J Neurosci*, *38*(12), 3679-3690. https://doi.org/10.1111/ejn.12351

Schmidt-Supprian, M., & Rajewsky, K. (2007). Vagaries of conditional gene targeting. *Nat Immunol*, *8*(7), 665-668. https://doi.org/10.1038/ni0707-665

Schorpp, M., Jager, R., Schellander, K., Schenkel, J., Wagner, E. F., Weiher, H., & Angel, P. (1996). The human ubiquitin C promoter directs high ubiquitous expression of transgenes in mice. *Nucleic Acids Res*, *24*(9), 1787-1788. https://doi.org/10.1093/nar/24.9.1787

Seibenhener, M. L., & Wooten, M. C. (2015). Use of the Open Field Maze to measure locomotor and anxiety-like behavior in mice. *J Vis Exp*(96), e52434. https://doi.org/10.3791/52434

Sellgren, C. M., Gracias, J., Watmuff, B., Biag, J. D., Thanos, J. M., Whittredge, P. B., Fu, T., Worringer, K., Brown, H. E., Wang, J., Kaykas, A., Karmacharya, R., Goold, C. P., Sheridan, S. D., & Perlis, R. H. (2019). Increased synapse elimination by microglia in schizophrenia patient-derived models of synaptic pruning. *Nat Neurosci*, *22*(3), 374-385. https://doi.org/10.1038/s41593-018-0334-7

Sellgren, C. M., Sheridan, S. D., Gracias, J., Xuan, D., Fu, T., & Perlis, R. H. (2017). Patient-specific models of microglia-mediated engulfment of synapses and neural progenitors. *Mol Psychiatry*, *22*(2), 170-177. https://doi.org/10.1038/mp.2016.220

Sen, N., Hara, M. R., Ahmad, A. S., Cascio, M. B., Kamiya, A., Ehmsen, J. T., Agrawal, N., Hester, L., Dore, S., Snyder, S. H., & Sawa, A. (2009). GOSPEL: a neuroprotective protein that binds to GAPDH upon S-nitrosylation. *Neuron*, *63*(1), 81-91. https://doi.org/10.1016/j.neuron.2009.05.024

Sepp, M., Leiss, K., Sarropoulos, I., Murat, F., Okonechnikov, K., Joshi, P., Leushkin, E., Mbengue, N., Schneider, C., Schmidt, J., Trost, N., Spänig, L., Giere, P., Khaitovich, P., Lisgo, S., Palkovits, M., Kutscher, L. M., Anders, S., Cardoso-Moreira, M., . . . Kaessmann, H. (2021). Cellular development and evolution of the mammalian cerebellum. *bioRxiv*, 2021.2012.2020.473443. https://doi.org/10.1101/2021.12.20.473443

Shachar, T., Lo Bianco, C., Recchia, A., Wiessner, C., Raas-Rothschild, A., & Futerman, A. H. (2011). Lysosomal storage disorders and Parkinson's disease: Gaucher disease and beyond. *Mov Disord*, *26*(9), 1593-1604. https://doi.org/10.1002/mds.23774

Shao, W., Halachmi, S., & Brown, M. (2002). ERAP140, a conserved tissue-specific nuclear receptor coactivator. *Mol Cell Biol*, *22*(10), 3358-3372. https://doi.org/10.1128/MCB.22.10.3358-3372.2002

Sharma, L. K., Lu, J., & Bai, Y. (2009). Mitochondrial respiratory complex I: structure, function and implication in human diseases. *Curr Med Chem*, *16*(10), 1266-1277. https://doi.org/10.2174/092986709787846578

Sharma, M., Khan, S., Rahman, S., & Singh, L. R. (2019). The Extracellular Protein, Transthyretin Is an Oxidative Stress Biomarker. *Front Physiol*, *10*, 5. https://doi.org/10.3389/fphys.2019.00005

Shellhaas, R. A. (2015). Continuous long-term electroencephalography: the gold standard for neonatal seizure diagnosis. *Semin Fetal Neonatal Med*, *20*(3), 149-153. https://doi.org/10.1016/j.siny.2015.01.005

Shimizu, H., Kawamura, S., & Ozaki, K. (2003). An essential role of Rab5 in uniformity of synaptic vesicle size. *J Cell Sci*, *116*(Pt 17), 3583-3590. https://doi.org/10.1242/jcs.00676

Shin, J. Y., Fang, Z. H., Yu, Z. X., Wang, C. E., Li, S. H., & Li, X. J. (2005). Expression of mutant huntingtin in glial cells contributes to neuronal excitotoxicity. *J Cell Biol*, *171*(6), 1001-1012. https://doi.org/10.1083/jcb.200508072

Shkolnik, K., Ben-Dor, S., Galiani, D., Hourvitz, A., & Dekel, N. (2008). Molecular characterization and bioinformatics analysis of Ncoa7B, a novel ovulation-associated and reproduction system-specific Ncoa7 isoform. *Reproduction*, *135*(3), 321-333. https://doi.org/10.1530/REP-07-0402

Siintola, E., Partanen, S., Stromme, P., Haapanen, A., Haltia, M., Maehlen, J., Lehesjoki, A. E., & Tyynela, J. (2006). Cathepsin D deficiency underlies congenital human neuronal ceroid-lipofuscinosis. *Brain*, *129*(Pt 6), 1438-1445. https://doi.org/10.1093/brain/awl107

Silver, D. L., Watkins-Chow, D. E., Schreck, K. C., Pierfelice, T. J., Larson, D. M., Burnetti, A. J., Liaw, H. J., Myung, K., Walsh, C. A., Gaiano, N., & Pavan, W. J. (2010). The exon junction complex component Magoh controls brain size by regulating neural stem cell division. *Nat Neurosci*, *13*(5), 551-558. https://doi.org/10.1038/nn.2527

Silverman, J. L., Babineau, B. A., Oliver, C. F., Karras, M. N., & Crawley, J. N. (2013). Influence of stimulant-induced hyperactivity on social approach in the BTBR mouse model of autism. *Neuropharmacology*, *68*, 210-222. https://doi.org/10.1016/j.neuropharm.2012.07.042

Simpson, D. S. A., & Oliver, P. L. (2020). ROS Generation in Microglia: Understanding Oxidative Stress and Inflammation in Neurodegenerative Disease. *Antioxidants (Basel)*, *9*(8). https://doi.org/10.3390/antiox9080743

Singh, K. K., Wachsmuth, L., Kulozik, A. E., & Gehring, N. H. (2013). Two mammalian MAGOH genes contribute to exon junction complex composition and nonsense-mediated decay. *RNA Biol*, *10*(8), 1291-1298. https://doi.org/10.4161/rna.25827

Skarnes, W. C., Rosen, B., West, A. P., Koutsourakis, M., Bushell, W., Iyer, V., Mujica, A. O., Thomas, M., Harrow, J., Cox, T., Jackson, D., Severin, J., Biggs, P., Fu, J., Nefedov, M., de Jong, P. J., Stewart, A. F., & Bradley, A. (2011). A conditional knockout resource for the genome-wide study of mouse gene function. *Nature*, *474*(7351), 337-342. https://doi.org/10.1038/nature10163

Snyder, H., Mensah, K., Hsu, C., Hashimoto, M., Surgucheva, I. G., Festoff, B., Surguchov, A., Masliah, E., Matouschek, A., & Wolozin, B. (2005). beta-Synuclein reduces proteasomal inhibition by alpha-synuclein but not gamma-synuclein. *J Biol Chem*, *280*(9), 7562-7569. https://doi.org/10.1074/jbc.M412887200

Sobue, A., Komine, O., Hara, Y., Endo, F., Mizoguchi, H., Watanabe, S., Murayama, S., Saito, T., Saido, T. C., Sahara, N., Higuchi, M., Ogi, T., & Yamanaka, K. (2021). Microglial gene signature reveals loss of homeostatic microglia associated with neurodegeneration of Alzheimer's disease. *Acta Neuropathol Commun*, *9*(1), 1. https://doi.org/10.1186/s40478-020-01099-x

Sofroniew, M. V., & Vinters, H. V. (2010). Astrocytes: biology and pathology. *Acta Neuropathol*, *119*(1), 7-35. https://doi.org/10.1007/s00401-009-0619-8

Soriano, P. (1999). Generalized lacZ expression with the ROSA26 Cre reporter strain. *Nat Genet*, *21*(1), 70-71. https://doi.org/10.1038/5007

Soukup, S. F., Kuenen, S., Vanhauwaert, R., Manetsberger, J., Hernandez-Diaz, S., Swerts, J., Schoovaerts, N., Vilain, S., Gounko, N. V., Vints, K., Geens, A., De Strooper, B., & Verstreken, P. (2016). A LRRK2-Dependent EndophilinA Phosphoswitch Is Critical for Macroautophagy at Presynaptic Terminals. *Neuron*, *92*(4), 829-844. https://doi.org/10.1016/j.neuron.2016.09.037

Sperk, G., Furtinger, S., Schwarzer, C., & Pirker, S. (2004). GABA and its receptors in epilepsy. *Adv Exp Med Biol*, *548*, 92-103. https://doi.org/10.1007/978-1-4757-6376-8_7

Squadrone, S., Brizio, P., Mancini, C., Abete, M. C., & Brusco, A. (2018). Altered homeostasis of trace elements in the blood of SCA2 patients. *J Trace Elem Med Biol*, *47*, 111-114. https://doi.org/10.1016/j.jtemb.2018.02.011

Srinivasan, R., Lu, T. Y., Chai, H., Xu, J., Huang, B. S., Golshani, P., Coppola, G., & Khakh, B. S. (2016). New Transgenic Mouse Lines for Selectively Targeting Astrocytes and Studying Calcium Signals in Astrocyte Processes In Situ and In Vivo. *Neuron*, *92*(6), 1181-1195. https://doi.org/10.1016/j.neuron.2016.11.030

Srinivasan, R., & Nunez, P. L. (2012). *Encyclopedia of human behavior* (2nd ed.). Academic Press. https://www.sciencedirect.com/science/referenceworks/9780080961804

Stamper, C., Siegel, A., Liang, W. S., Pearson, J. V., Stephan, D. A., Shill, H., Connor, D., Caviness, J. N., Sabbagh, M., Beach, T. G., Adler, C. H., & Dunckley, T. (2008). Neuronal gene expression correlates of Parkinson's disease with dementia. *Mov Disord*, *23*(11), 1588-1595. https://doi.org/10.1002/mds.22184

Steinfeld, R., Reinhardt, K., Schreiber, K., Hillebrand, M., Kraetzner, R., Bruck, W., Saftig, P., & Gartner, J. (2006). Cathepsin D deficiency is associated with a human neurodegenerative disorder. *Am J Hum Genet*, *78*(6), 988-998. https://doi.org/10.1086/504159

Steyer, B., Cory, E., & Saha, K. (2018). Developing precision medicine using scarless genome editing of human pluripotent stem cells. *Drug Discov Today Technol*, *28*, 3-12. https://doi.org/10.1016/j.ddtec.2018.02.001

Sturner, T., Tatarnikova, A., Mueller, J., Schaffran, B., Cuntz, H., Zhang, Y., Nemethova, M., Bogdan, S., Small, V., & Tavosanis, G. (2019). Transient localization of the Arp2/3 complex initiates neuronal dendrite branching in vivo. *Development*, *146*(7). https://doi.org/10.1242/dev.171397

Su, L. D., Zhang, Q. L., & Lu, Z. (2017). Oxidation resistance 1 (OXR1) participates in silkworm defense against bacterial infection through the JNK pathway. *Insect Sci*, *24*(1), 17-26. https://doi.org/10.1111/1744-7917.12285

Sultana, B., Panzini, M. A., Veilleux Carpentier, A., Comtois, J., Rioux, B., Gore, G., Bauer, P. R., Kwon, C. S., Jette, N., Josephson, C. B., & Keezer, M. R. (2021). Incidence and Prevalence of Drug-Resistant Epilepsy: A Systematic Review and Meta-analysis. *Neurology*, *96*(17), 805-817. https://doi.org/10.1212/WNL.0000000000011839

Sun, X., Fu, X., Li, J., Xing, C., Martin, D. W., Zhang, H. H., Chen, Z., & Dong, J. T. (2012). Heterozygous deletion of Atbf1 by the Cre-loxP system in mice causes preweaning mortality. *Genesis*, *50*(11), 819-827. https://doi.org/10.1002/dvg.22041

Svistunova, D. (2020). *Investigating the neuroprotective function of TLDc proteins* University of Oxford].

Svistunova, D. M., Simon, J. N., Rembeza, E., Crabtree, M., Yue, W. W., Oliver, P. L., & Finelli, M. J. (2019). Oxidation resistance 1 regulates post-translational modifications of peroxiredoxin 2 in the cerebellum. *Free Radic Biol Med*, *130*, 151-162. https://doi.org/10.1016/j.freeradbiomed.2018.10.447

Tahmaz, I., Shahmoradi Ghahe, S., & Topf, U. (2021). Prefoldin Function in Cellular Protein Homeostasis and Human Diseases. *Front Cell Dev Biol*, *9*, 816214. https://doi.org/10.3389/fcell.2021.816214

Takamori, S., Holt, M., Stenius, K., Lemke, E. A., Gronborg, M., Riedel, D., Urlaub, H., Schenck, S., Brugger, B., Ringler, P., Muller, S. A., Rammner, B., Grater, F., Hub, J. S., De Groot, B. L., Mieskes, G., Moriyama, Y., Klingauf, J., Grubmuller, H., . . . Jahn, R. (2006). Molecular anatomy of a trafficking organelle. *Cell*, *127*(4), 831-846. https://doi.org/10.1016/j.cell.2006.10.030

Tam, O. H., Rozhkov, N. V., Shaw, R., Kim, D., Hubbard, I., Fennessey, S., Propp, N., Consortium, N. A., Fagegaltier, D., Harris, B. T., Ostrow, L. W., Phatnani, H., Ravits, J., Dubnau, J., & Gale Hammell, M. (2019). Postmortem Cortex Samples Identify Distinct Molecular Subtypes of ALS: Retrotransposon Activation, Oxidative Stress, and Activated Glia. *Cell Rep*, *29*(5), 1164-1177 e1165. https://doi.org/10.1016/j.celrep.2019.09.066

Tammineni, P., Ye, X., Feng, T., Aikal, D., & Cai, Q. (2017). Impaired retrograde transport of axonal autophagosomes contributes to autophagic stress in Alzheimer's disease neurons. *Elife*, *6*. https://doi.org/10.7554/eLife.21776

Tan, Y. Z., Abbas, Y. M., Wu, J. Z., Wu, D., Keon, K. A., Hesketh, G. G., Bueler, S. A., Gingras, A. C., Robinson, C. V., Grinstein, S., & Rubinstein, J. L. (2022). CryoEM of endogenous mammalian V-ATPase interacting with the TLDc protein mEAK-7. *Life Sci Alliance*, *5*(11). https://doi.org/10.26508/lsa.202201527

Tang, Q., Liu, H., Shi, X. J., & Cheng, Y. (2020). Blood Oxidative Stress Marker Aberrations in Patients with Huntington's Disease: A Meta-Analysis Study. *Oxid Med Cell Longev*, *2020*, 9187195. https://doi.org/10.1155/2020/9187195

Tasaki, S., Xu, J., Avey, D. R., Johnson, L., Petyuk, V. A., Dawe, R. J., Bennett, D. A., Wang, Y., & Gaiteri, C. (2022). Inferring protein expression changes from mRNA in Alzheimer's dementia using deep neural networks. *Nat Commun*, *13*(1), 655. https://doi.org/10.1038/s41467-022-28280-1

Tauc, M., Cougnon, M., Carcy, R., Melis, N., Hauet, T., Pellerin, L., Blondeau, N., & Pisani, D. F. (2021). The eukaryotic initiation factor 5A (eIF5A1), the molecule, mechanisms and recent insights into the pathophysiological roles. *Cell Biosci*, *11*(1), 219. https://doi.org/10.1186/s13578-021-00733-y

Tebar, F., Chavero, A., Agell, N., Lu, A., Rentero, C., Enrich, C., & Grewal, T. (2020). Pleiotropic Roles of Calmodulin in the Regulation of KRas and Rac1 GTPases: Functional Diversity in Health and Disease. *Int J Mol Sci*, *21*(10). https://doi.org/10.3390/ijms21103680

Terrone, G., Balosso, S., Pauletti, A., Ravizza, T., & Vezzani, A. (2020). Inflammation and reactive oxygen species as disease modifiers in epilepsy. *Neuropharmacology*, *167*, 107742. https://doi.org/10.1016/j.neuropharm.2019.107742

Tersar, K., Boentert, M., Berger, P., Bonneick, S., Wessig, C., Toyka, K. V., Young, P., & Suter, U. (2007). Mtmr13/Sbf2-deficient mice: an animal model for CMT4B2. *Hum Mol Genet*, *16*(24), 2991-3001. https://doi.org/10.1093/hmg/ddm257

Thiele, E. A., Bebin, E. M., Bhathal, H., Jansen, F. E., Kotulska, K., Lawson, J. A., O'Callaghan, F. J., Wong, M., Sahebkar, F., Checketts, D., Knappertz, V., & Group, G. S. (2021). Add-on Cannabidiol Treatment for Drug-Resistant Seizures in Tuberous Sclerosis Complex: A Placebo-Controlled Randomized Clinical Trial. *JAMA Neurol*, *78*(3), 285-292. https://doi.org/10.1001/jamaneurol.2020.4607

Thompson, A. D., Dugan, A., Gestwicki, J. E., & Mapp, A. K. (2012). Fine-tuning multiprotein complexes using small molecules. *ACS Chem Biol*, *7*(8), 1311-1320. https://doi.org/10.1021/cb300255p

Tolosano, E., & Altruda, F. (2002). Hemopexin: structure, function, and regulation. *DNA Cell Biol*, *21*(4), 297-306. https://doi.org/10.1089/104454902753759717

Tona, R., Chen, W., Nakano, Y., Reyes, L. D., Petralia, R. S., Wang, Y. X., Starost, M. F., Wafa, T. T., Morell, R. J., Cravedi, K. D., du Hoffmann, J., Miyoshi, T., Munasinghe, J. P., Fitzgerald, T. S.,

Chudasama, Y., Omori, K., Pierpaoli, C., Banfi, B., Dong, L., . . . Friedman, T. B. (2019). The phenotypic landscape of a Tbc1d24 mutant mouse includes convulsive seizures resembling human early infantile epileptic encephalopathy. *Hum Mol Genet*, *28*(9), 1530-1547. https://doi.org/10.1093/hmg/ddy445

Tona, R., Lopez, I. A., Fenollar-Ferrer, C., Faridi, R., Anselmi, C., Khan, A. A., Shahzad, M., Morell, R. J., Gu, S., Hoa, M., Dong, L., Ishiyama, A., Belyantseva, I. A., Riazuddin, S., & Friedman, T. B. (2020). Mouse Models of Human Pathogenic Variants of TBC1D24 Associated with Non-Syndromic Deafness DFNB86 and DFNA65 and Syndromes Involving Deafness. *Genes (Basel)*, *11*(10). https://doi.org/10.3390/genes11101122

Tong, F., Zhang, M., Guo, X., Shi, H., Li, L., Guan, W., Wang, H., & Yang, S. (2016). Expression patterns of SH3BGR family members in zebrafish development. *Dev Genes Evol*, *226*(4), 287-295. https://doi.org/10.1007/s00427-016-0552-5

Townley, R. A., Boeve, B. F., & Benarroch, E. E. (2018). Progranulin: Functions and neurologic correlations. *Neurology*, *90*(3), 118-125. https://doi.org/10.1212/WNL.0000000000004840

Tsatmali, M., Walcott, E. C., Makarenkova, H., & Crossin, K. L. (2006). Reactive oxygen species modulate the differentiation of neurons in clonal cortical cultures. *Mol Cell Neurosci*, *33*(4), 345-357. https://doi.org/10.1016/j.mcn.2006.08.005

Tsien, J. Z., Chen, D. F., Gerber, D., Tom, C., Mercer, E. H., Anderson, D. J., Mayford, M., Kandel, E. R., & Tonegawa, S. (1996). Subregion- and cell type-restricted gene knockout in mouse brain. *Cell*, *87*(7), 1317-1326. https://doi.org/10.1016/s0092-8674(00)81826-7

Tsirikos, A. I., & Smith, G. (2012). Scoliosis in patients with Friedreich's ataxia. *J Bone Joint Surg Br*, *94*(5), 684-689. https://doi.org/10.1302/0301-620X.94B5.28391

Turner, P. V., Brabb, T., Pekow, C., & Vasbinder, M. A. (2011). Administration of substances to laboratory animals: routes of administration and factors to consider. *J Am Assoc Lab Anim Sci*, *50*(5), 600-613. https://www.ncbi.nlm.nih.gov/pubmed/22330705

Ulrich, H. D., & Jentsch, S. (2000). Two RING finger proteins mediate cooperation between ubiquitin-conjugating enzymes in DNA repair. *EMBO J*, *19*(13), 3388-3397. https://doi.org/10.1093/emboj/19.13.3388

Uusi-Rauva, K., Kyttala, A., van der Kant, R., Vesa, J., Tanhuanpaa, K., Neefjes, J., Olkkonen, V. M., & Jalanko, A. (2012). Neuronal ceroid lipofuscinosis protein CLN3 interacts with motor proteins and modifies location of late endosomal compartments. *Cell Mol Life Sci*, *69*(12), 2075-2089. https://doi.org/10.1007/s00018-011-0913-1

Uytterhoeven, V., Kuenen, S., Kasprowicz, J., Miskiewicz, K., & Verstreken, P. (2011). Loss of skywalker reveals synaptic endosomes as sorting stations for synaptic vesicle proteins. *Cell*, *145*(1), 117-132. https://doi.org/10.1016/j.cell.2011.02.039

Vainchtein, I. D., & Molofsky, A. V. (2020). Astrocytes and Microglia: In Sickness and in Health. *Trends Neurosci*, *43*(3), 144-154. https://doi.org/10.1016/j.tins.2020.01.003

Valassina, N., Brusco, S., Salamone, A., Serra, L., Luoni, M., Giannelli, S., Bido, S., Massimino, L., Ungaro, F., Mazzara, P. G., D'Adamo, P., Lignani, G., Broccoli, V., & Colasante, G. (2022). Scn1a gene reactivation after symptom onset rescues pathological phenotypes in a mouse model of Dravet syndrome. *Nat Commun*, *13*(1), 161. https://doi.org/10.1038/s41467-021-27837-w

Van Deerlin, V. M., Leverenz, J. B., Bekris, L. M., Bird, T. D., Yuan, W., Elman, L. B., Clay, D., Wood, E. M., Chen-Plotkin, A. S., Martinez-Lage, M., Steinbart, E., McCluskey, L., Grossman, M., Neumann, M., Wu, I. L., Yang, W. S., Kalb, R., Galasko, D. R., Montine, T. J., . . . Yu, C. E. (2008). TARDBP mutations in amyotrophic lateral sclerosis with TDP-43 neuropathology: a genetic and histopathological analysis. *Lancet Neurol*, *7*(5), 409-416. https://doi.org/10.1016/S1474-4422(08)70071-1

Van Harten, A. C. M., Phatnani, H., & Przedborski, S. (2021). Non-cell-autonomous pathogenic mechanisms in amyotrophic lateral sclerosis. *Trends Neurosci*, *44*(8), 658-668. https://doi.org/10.1016/j.tins.2021.04.008

Vance, C., Rogelj, B., Hortobagyi, T., De Vos, K. J., Nishimura, A. L., Sreedharan, J., Hu, X., Smith, B., Ruddy, D., Wright, P., Ganesalingam, J., Williams, K. L., Tripathi, V., Al-Saraj, S., Al-Chalabi, A., Leigh, P. N., Blair, I. P., Nicholson, G., de Belleroche, J., . . . Shaw, C. E. (2009). Mutations in FUS, an RNA processing protein, cause familial amyotrophic lateral sclerosis type 6. *Science*, *323*(5918), 1208-1211. https://doi.org/10.1126/science.1165942

Vanlandingham, P. A., & Ceresa, B. P. (2009). Rab7 regulates late endocytic trafficking downstream of multivesicular body biogenesis and cargo sequestration. *J Biol Chem*, *284*(18), 12110-12124. https://doi.org/10.1074/jbc.M809277200

Varvagiannis, K., Hanquinet, S., Billieux, M. H., De Luca, R., Rimensberger, P., Lidgren, M., Guipponi, M., Makrythanasis, P., Blouin, J. L., Antonarakis, S. E., Steinfeld, R., Kern, I., Poretti, A., Fluss, J., & Fokstuen, S. (2018). Congenital Neuronal Ceroid Lipofuscinosis with a Novel CTSD Gene Mutation: A Rare Cause of Neonatal-Onset Neurodegenerative Disorder. *Neuropediatrics*, *49*(2), 150-153. https://doi.org/10.1055/s-0037-1613681

Vezzani, A., & Granata, T. (2005). Brain inflammation in epilepsy: experimental and clinical evidence. *Epilepsia*, *46*(11), 1724-1743. https://doi.org/10.1111/j.1528-1167.2005.00298.x

Vogler, E. C., Flynn, D. T., Busciglio, F., Bohannan, R. C., Tran, A., Mahavongtrakul, M., & Busciglio, J. A. (2017). Low Cost Electrode Assembly for EEG Recordings in Mice. *Front Neurosci*, *11*, 629. https://doi.org/10.3389/fnins.2017.00629

Vogt, D. L., Thomas, D., Galvan, V., Bredesen, D. E., Lamb, B. T., & Pimplikar, S. W. (2011). Abnormal neuronal networks and seizure susceptibility in mice overexpressing the APP intracellular domain. *Neurobiol Aging*, *32*(9), 1725-1729. https://doi.org/10.1016/j.neurobiolaging.2009.09.002

Volkert, M. R., & Crowley, D. J. (2020). Preventing Neurodegeneration by Controlling Oxidative Stress: The Role of OXR1. *Front Neurosci*, *14*, 611904. https://doi.org/10.3389/fnins.2020.611904

Volkert, M. R., Elliott, N. A., & Housman, D. E. (2000). Functional genomics reveals a family of eukaryotic oxidation protection genes. *Proc Natl Acad Sci U S A*, *97*(26), 14530-14535. https://doi.org/10.1073/pnas.260495897

Vooijs, M., Jonkers, J., & Berns, A. (2001). A highly efficient ligand-regulated Cre recombinase mouse line shows that LoxP recombination is position dependent. *EMBO Rep*, *2*(4), 292-297. https://doi.org/10.1093/embo-reports/kve064

Walsh, R. N., & Cummins, R. A. (1976). The Open-Field Test: a critical review. *Psychol Bull*, *83*(3), 482-504. https://www.ncbi.nlm.nih.gov/pubmed/17582919

Wang, J., Al-Ouran, R., Hu, Y., Kim, S. Y., Wan, Y. W., Wangler, M. F., Yamamoto, S., Chao, H. T., Comjean, A., Mohr, S. E., Udn, Perrimon, N., Liu, Z., & Bellen, H. J. (2017). MARRVEL:

Integration of Human and Model Organism Genetic Resources to Facilitate Functional Annotation of the Human Genome. *Am J Hum Genet*, *100*(6), 843-853. https://doi.org/10.1016/j.ajhg.2017.04.010

Wang, J., Rousseau, J., Kim, E., Ehresmann, S., Cheng, Y. T., Duraine, L., Zuo, Z., Park, Y. J., Li-Kroeger, D., Bi, W., Wong, L. J., Rosenfeld, J., Gleeson, J., Faqeih, E., Alkuraya, F. S., Wierenga, K. J., Chen, J., Afenjar, A., Nava, C., . . . Campeau, P. M. (2019). Loss of Oxidation Resistance 1, OXR1, Is Associated with an Autosomal-Recessive Neurological Disease with Cerebellar Atrophy and Lysosomal Dysfunction. *Am J Hum Genet*, *105*(6), 1237-1253. https://doi.org/10.1016/j.ajhg.2019.11.002

Wang, X., & Michaelis, E. K. (2010). Selective neuronal vulnerability to oxidative stress in the brain. *Front Aging Neurosci*, *2*, 12. https://doi.org/10.3389/fnagi.2010.00012

Wang, X., Zaidi, A., Pal, R., Garrett, A. S., Braceras, R., Chen, X. W., Michaelis, M. L., & Michaelis, E. K. (2009). Genomic and biochemical approaches in the discovery of mechanisms for selective neuronal vulnerability to oxidative stress. *BMC Neurosci*, *10*, 12. https://doi.org/10.1186/1471-2202-10-12

Wang, Y., Hersheson, J., Lopez, D., Hammer, M., Liu, Y., Lee, K. H., Pinto, V., Seinfeld, J., Wiethoff, S., Sun, J., Amouri, R., Hentati, F., Baudry, N., Tran, J., Singleton, A. B., Coutelier, M., Brice, A., Stevanin, G., Durr, A., . . . Baudry, M. (2016). Defects in the CAPN1 Gene Result in Alterations in Cerebellar Development and Cerebellar Ataxia in Mice and Humans. *Cell Rep*, *16*(1), 79-91. https://doi.org/10.1016/j.celrep.2016.05.044

Wang, Y., Zhang, Y., Wei, Z., Li, H., Zhou, H., Zhang, Z., & Zhang, Z. (2009). JNK inhibitor protects dopaminergic neurons by reducing COX-2 expression in the MPTP mouse model of subacute Parkinson's disease. *J Neurol Sci*, *285*(1-2), 172-177. https://doi.org/10.1016/j.jns.2009.06.034

Wang, Z., Berkey, C. D., & Watnick, P. I. (2012). The Drosophila protein mustard tailors the innate immune response activated by the immune deficiency pathway. *J Immunol*, *188*(8), 3993-4000. https://doi.org/10.4049/jimmunol.1103301

Watts, C. (2022). Lysosomes and lysosome-related organelles in immune responses. *FEBS Open Bio*, *12*(4), 678-693. https://doi.org/10.1002/2211-5463.13388

Wegiel, J., Kaczmarski, W., Flory, M., Martinez-Cerdeno, V., Wisniewski, T., Nowicki, K., Kuchna, I., & Wegiel, J. (2018). Deficit of corpus callosum axons, reduced axon diameter and decreased area are markers of abnormal development of interhemispheric connections in autistic subjects. *Acta Neuropathol Commun*, *6*(1), 143. https://doi.org/10.1186/s40478-018-0645-7

Wendimu, M. Y., & Hooks, S. B. (2022). Microglia Phenotypes in Aging and Neurodegenerative Diseases. *Cells*, *11*(13). https://doi.org/10.3390/cells11132091

Westenbroek, R. E., Sakurai, T., Elliott, E. M., Hell, J. W., Starr, T. V., Snutch, T. P., & Catterall, W. A. (1995). Immunochemical identification and subcellular distribution of the alpha 1A subunits of brain calcium channels. *J Neurosci*, *15*(10), 6403-6418. https://doi.org/10.1523/JNEUROSCI.15-10-06403.1995

Whitfield, J., Littlewood, T., & Soucek, L. (2015). Tamoxifen administration to mice. *Cold Spring Harb Protoc*, *2015*(3), 269-271. https://doi.org/10.1101/pdb.prot077966

WHO, W. H. O. (2022). *Epilepsy*. World Health Organisation. Retrieved 05.11.2022 from www.who.int/news-room/fact-sheets/detail/epilepsy

Wilcox, A. (2019). *Circadian characterisation of the transcription factor Zfhx3 utilising a conditional mutagenesis approach* University of Oxford].

Wilcox, A. G., Vizor, L., Parsons, M. J., Banks, G., & Nolan, P. M. (2017). Inducible Knockout of Mouse Zfhx3 Emphasizes Its Key Role in Setting the Pace and Amplitude of the Adult Circadian Clock. *J Biol Rhythms*, *32*(5), 433-443. https://doi.org/10.1177/0748730417722631

Wilde, G. J., Pringle, A. K., Wright, P., & Iannotti, F. (1997). Differential vulnerability of the CA1 and CA3 subfields of the hippocampus to superoxide and hydroxyl radicals in vitro. *J Neurochem*, *69*(2), 883-886. https://doi.org/10.1046/j.1471-4159.1997.69020883.x

Williams, I. M., Wallom, K. L., Smith, D. A., Al Eisa, N., Smith, C., & Platt, F. M. (2014). Improved neuroprotection using miglustat, curcumin and ibuprofen as a triple combination therapy in Niemann-Pick disease type C1 mice. *Neurobiol Dis*, *67*, 9-17. https://doi.org/10.1016/j.nbd.2014.03.001

Williams, T. W., Dumas, K. J., & Hu, P. J. (2010). EAK proteins: novel conserved regulators of C. elegans lifespan. *Aging (Albany NY)*, *2*(10), 742-747. https://doi.org/10.18632/aging.100214

Williamson, M. (2019). *The protective function of the oxidation resistance 1 gene in ALS* University of Oxford].

Williamson, M. G., Finelli, M. J., Sleigh, J. N., Reddington, A., Gordon, D., Talbot, K., Davies, K. E., & Oliver, P. L. (2019). Neuronal over-expression of Oxr1 is protective against ALS-associated mutant TDP-43 mislocalisation in motor neurons and neuromuscular defects in vivo. *Hum Mol Genet*, *28*(21), 3584-3599. https://doi.org/10.1093/hmg/ddz190

Winnubst, J., Cheyne, J. E., Niculescu, D., & Lohmann, C. (2015). Spontaneous Activity Drives Local Synaptic Plasticity In Vivo. *Neuron*, *87*(2), 399-410. https://doi.org/10.1016/j.neuron.2015.06.029

Wittig, S., Ganzella, M., Barth, M., Kostmann, S., Riedel, D., Perez-Lara, A., Jahn, R., & Schmidt, C. (2021). Cross-linking mass spectrometry uncovers protein interactions and functional assemblies in synaptic vesicle membranes. *Nat Commun*, *12*(1), 858. https://doi.org/10.1038/s41467-021-21102-w

World Health Organization. (2006). *Neurological disorders : public health challenges*. World Health Organization.

Xia, L., Pan, S.-Q., Zhang, Q.-M., Zhou, Q., Xia, L., & Lu, Z.-N. (2018). Elevated IL-6 and IL-1β are associated with temporal lobe epilepsy: A study in Chinese patients. *European Journal of Inflammation*, *16*, 2058739218778934. https://doi.org/10.1177/2058739218778934

Xiao, W., Chow, B. L., Broomfield, S., & Hanna, M. (2000). The Saccharomyces cerevisiae RAD6 group is composed of an error-prone and two error-free postreplication repair pathways. *Genetics*, *155*(4), 1633-1641. https://doi.org/10.1093/genetics/155.4.1633

Xu, H., Jiang, Y., Li, S., Xie, L., Tao, Y. X., & Li, Y. (2020). Zebrafish Oxr1a Knockout Reveals Its Role in Regulating Antioxidant Defenses and Aging. *Genes (Basel)*, *11*(10). https://doi.org/10.3390/genes11101118

Xu, H., Wang, G., Chi, Y. Y., Kou, Y. X., & Li, Y. (2021). Expression profiling and functional characterization of the duplicated Oxr1b gene in zebrafish. *Comp Biochem Physiol Part D Genomics Proteomics*, *39*, 100857. https://doi.org/10.1016/j.cbd.2021.100857

Yang, L., Shen, Q., Xia, Y., Lei, X., & Peng, J. (2018). Sevoflurane-induced neurotoxicity is driven by OXR1 post-transcriptional downregulation involving hsa-miR-302e. *Mol Med Rep*, *18*(5), 4657-4665. https://doi.org/10.3892/mmr.2018.9442

Yang, M., & Crawley, J. N. (2009). Simple behavioral assessment of mouse olfaction. *Curr Protoc Neurosci*, *Chapter 8*, Unit 8 24. https://doi.org/10.1002/0471142301.ns0824s48

Yang, M., Lin, X., Rowe, A., Rognes, T., Eide, L., & Bjoras, M. (2015). Transcriptome analysis of human OXR1 depleted cells reveals its role in regulating the p53 signaling pathway. *Sci Rep*, *5*, 17409. https://doi.org/10.1038/srep17409

Yang, M., Lin, X., Segers, F., Suganthan, R., Hildrestrand, G. A., Rinholm, J. E., Aas, P. A., Sousa, M. M. L., Holm, S., Bolstad, N., Warren, D., Berge, R. K., Johansen, R. F., Yndestad, A., Kristiansen, E., Klungland, A., Luna, L., Eide, L., Halvorsen, B., . . . Bjoras, M. (2020). OXR1A, a Coactivator of PRMT5 Regulating Histone Arginine Methylation. *Cell Rep*, *30*(12), 4165-4178 e4167. https://doi.org/10.1016/j.celrep.2020.02.063

Yang, M., Luna, L., Sorbo, J. G., Alseth, I., Johansen, R. F., Backe, P. H., Danbolt, N. C., Eide, L., & Bjoras, M. (2014). Human OXR1 maintains mitochondrial DNA integrity and counteracts hydrogen peroxide-induced oxidative stress by regulating antioxidant pathways involving p21. *Free Radic Biol Med*, *77*, 41-48. https://doi.org/10.1016/j.freeradbiomed.2014.09.003

Yang, W., & Lu, Z. (2015). Pyruvate kinase M2 at a glance. *J Cell Sci*, *128*(9), 1655-1660. https://doi.org/10.1242/jcs.166629

Yang, Y., Vidensky, S., Jin, L., Jie, C., Lorenzini, I., Frankl, M., & Rothstein, J. D. (2011). Molecular comparison of GLT1+ and ALDH1L1+ astrocytes in vivo in astroglial reporter mice. *Glia*, *59*(2), 200-207. https://doi.org/10.1002/glia.21089

Ye, R., Wang, Q. A., Tao, C., Vishvanath, L., Shao, M., McDonald, J. G., Gupta, R. K., & Scherer, P. E. (2015). Impact of tamoxifen on adipocyte lineage tracing: Inducer of adipogenesis and prolonged nuclear translocation of Cre recombinase. *Mol Metab*, *4*(11), 771-778. https://doi.org/10.1016/j.molmet.2015.08.004

Yeh, F. L., Wang, Y., Tom, I., Gonzalez, L. C., & Sheng, M. (2016). TREM2 Binds to Apolipoproteins, Including APOE and CLU/APOJ, and Thereby Facilitates Uptake of Amyloid-Beta by Microglia. *Neuron*, *91*(2), 328-340. https://doi.org/10.1016/j.neuron.2016.06.015

Yoshii, S. R., & Mizushima, N. (2017). Monitoring and Measuring Autophagy. *Int J Mol Sci*, *18*(9). https://doi.org/10.3390/ijms18091865

Yu, L., Croze, E., Yamaguchi, K. D., Tran, T., Reder, A. T., Litvak, V., & Volkert, M. R. (2015). Induction of a unique isoform of the NCOA7 oxidation resistance gene by interferon beta-1b. *J Interferon Cytokine Res*, *35*(3), 186-199. https://doi.org/10.1089/jir.2014.0115

Zaheer, A., Zaheer, S., Thangavel, R., Wu, Y., Sahu, S. K., & Yang, B. (2008). Glia maturation factor modulates beta-amyloid-induced glial activation, inflammatory cytokine/chemokine production and neuronal damage. *Brain Res*, *1208*, 192-203. https://doi.org/10.1016/j.brainres.2008.02.093

Zallen, J. A., Cohen, Y., Hudson, A. M., Cooley, L., Wieschaus, E., & Schejter, E. D. (2002). SCAR is a primary regulator of Arp2/3-dependent morphological events in Drosophila. *J Cell Biol*, *156*(4), 689-701. https://doi.org/10.1083/jcb.200109057

Zampieri, S., Filocamo, M., Pianta, A., Lualdi, S., Gort, L., Coll, M. J., Sinnott, R., Geberhiwot, T., Bembi, B., & Dardis, A. (2016). SMPD1 Mutation Update: Database and Comprehensive Analysis of Published and Novel Variants. *Hum Mutat*, *37*(2), 139-147. https://doi.org/10.1002/humu.22923

Zanelli, C. F., Maragno, A. L., Gregio, A. P., Komili, S., Pandolfi, J. R., Mestriner, C. A., Lustri, W. R., & Valentini, S. R. (2006). eIF5A binds to translational machinery components and affects translation in yeast. *Biochem Biophys Res Commun*, *348*(4), 1358-1366. https://doi.org/10.1016/j.bbrc.2006.07.195

Zanelli, S., Goodkin, H. P., Kowalski, S., & Kapur, J. (2014). Impact of transient acute hypoxia on the developing mouse EEG. *Neurobiol Dis*, *68*, 37-46. https://doi.org/10.1016/j.nbd.2014.03.005

Zareba-Koziol, M., Figiel, I., Bartkowiak-Kaczmarek, A., & Wlodarczyk, J. (2018). Insights Into Protein S-Palmitoylation in Synaptic Plasticity and Neurological Disorders: Potential and Limitations of Methods for Detection and Analysis. *Front Mol Neurosci*, *11*, 175. https://doi.org/10.3389/fnmol.2018.00175

Zenuni, H., Grillo, P., Sancesario, G. M., Bernardini, S., Mercuri, N. B., & Schirinzi, T. (2021). How Comorbidity Reflects on Cerebrospinal Fluid Biomarkers of Neurodegeneration in Aging. *J Alzheimers Dis Rep*, *5*(1), 87-92. https://doi.org/10.3233/ADR-200280

Zhang, B., Zou, J., Han, L., Beeler, B., Friedman, J. L., Griffin, E., Piao, Y. S., Rensing, N. R., & Wong, M. (2018). The specificity and role of microglia in epileptogenesis in mouse models of tuberous sclerosis complex. *Epilepsia*, *59*(9), 1796-1806. https://doi.org/10.1111/epi.14526

Zhang, J., Li, Y., Xiong, J., Xu, H., Xiang, G., Fan, M., Zhou, K., Lin, Y., Chen, X., Xie, L., Zhang, H., Wang, J., & Xiao, J. (2021). Delivery of pOXR1 through an injectable liposomal nanoparticle enhances spinal cord injury regeneration by alleviating oxidative stress. *Bioact Mater*, *6*(10), 3177-3191. https://doi.org/10.1016/j.bioactmat.2021.03.001

Zhang, X., Zhang, S., Liu, X., Wang, Y., Chang, J., Zhang, X., Mackintosh, S. G., Tackett, A. J., He, Y., Lv, D., Laberge, R. M., Campisi, J., Wang, J., Zheng, G., & Zhou, D. (2018). Oxidation resistance 1 is a novel senolytic target. *Aging Cell*, *17*(4), e12780. https://doi.org/10.1111/acel.12780

Zhang, Y., Chen, K., Sloan, S. A., Bennett, M. L., Scholze, A. R., O'Keeffe, S., Phatnani, H. P., Guarnieri, P., Caneda, C., Ruderisch, N., Deng, S., Liddelow, S. A., Zhang, C., Daneman, R., Maniatis, T., Barres, B. A., & Wu, J. Q. (2014). An RNA-sequencing transcriptome and splicing database of glia, neurons, and vascular cells of the cerebral cortex. *J Neurosci*, *34*(36), 11929-11947. https://doi.org/10.1523/JNEUROSCI.1860-14.2014

Zhang, Y., James, M., Middleton, F. A., & Davis, R. L. (2005). Transcriptional analysis of multiple brain regions in Parkinson's disease supports the involvement of specific protein processing, energy metabolism, and signaling pathways, and suggests novel disease mechanisms. *Am J Med Genet B Neuropsychiatr Genet*, *137B*(1), 5-16. https://doi.org/10.1002/ajmg.b.30195

Zhang, Y., Sloan, S. A., Clarke, L. E., Caneda, C., Plaza, C. A., Blumenthal, P. D., Vogel, H., Steinberg, G. K., Edwards, M. S., Li, G., Duncan, J. A., 3rd, Cheshier, S. H., Shuer, L. M., Chang, E. F., Grant, G. A., Gephart, M. G., & Barres, B. A. (2016). Purification and Characterization of Progenitor and Mature Human Astrocytes Reveals Transcriptional and Functional Differences with Mouse. *Neuron*, *89*(1), 37-53. https://doi.org/10.1016/j.neuron.2015.11.013

Zhao, X., Liao, Y., Morgan, S., Mathur, R., Feustel, P., Mazurkiewicz, J., Qian, J., Chang, J., Mathern, G. W., Adamo, M. A., Ritaccio, A. L., Gruenthal, M., Zhu, X., & Huang, Y. (2018). Noninflammatory

Changes of Microglia Are Sufficient to Cause Epilepsy. *Cell Rep*, *22*(8), 2080-2093. https://doi.org/10.1016/j.celrep.2018.02.004

Zhu, G., Wang, X., Chen, L., Lenahan, C., Fu, Z., Fang, Y., & Yu, W. (2022). Crosstalk Between the Oxidative Stress and Glia Cells After Stroke: From Mechanism to Therapies. *Front Immunol*, *13*, 852416. https://doi.org/10.3389/fimmu.2022.852416

Ziegler-Waldkirch, S., & Meyer-Luehmann, M. (2018). The Role of Glial Cells and Synapse Loss in Mouse Models of Alzheimer's Disease. *Front Cell Neurosci*, *12*, 473. https://doi.org/10.3389/fncel.2018.00473

Zou, J., Zhang, B., Gutmann, D. H., & Wong, M. (2017). Postnatal reduction of tuberous sclerosis complex 1 expression in astrocytes and neurons causes seizures in an age-dependent manner. *Epilepsia*, *58*(12), 2053-2063. https://doi.org/10.1111/epi.13923